

**A RAPID, RELIABLE METHODOLOGY FOR RADIONUCLIDE  
CHARACTERIZATION OF WET OR DRY STORED USED NUCLEAR FUEL  
VIA THE APPLICATION OF ALGORITHM-ENHANCED SCINTILLATOR  
SURVEY SPECTRA**

A Dissertation  
Presented to  
The Academic Faculty

by

Jessica N. Paul

In Partial Fulfillment  
of the Requirements for the Degree  
Doctor of Philosophy in Nuclear and Radiological Engineering

Georgia Institute of Technology  
August 2015

**COPYRIGHT 2015 BY JESSICA N. PAUL**

**A RAPID, RELIABLE METHODOLOGY FOR RADIONUCLIDE  
CHARACTERIZATION OF WET OR DRY STORED USED NUCLEAR FUEL  
VIA THE APPLICATION OF ALGORITHM-ENHANCED SCINTILLATOR  
SURVEY SPECTRA**

Approved by:

Dr. Chaitanya S. Deo, Advisor  
George W. Woodruff School  
*Georgia Institute of Technology*

Dr. Farzad Rahnema  
George W. Woodruff School  
*Georgia Institute of Technology*

Dr. Ce Yi  
George W. Woodruff School  
*Georgia Institute of Technology*

Dr. Glenn E. Sjoden  
Chief Scientist  
*Air Force Technical Applications Center*

Dr. Chad Pope  
Department of Nuclear Engineering and  
Health Physics  
*Idaho State University*

Date Approved: April, 24, 2015

## **DEDICATION**

*To my fiancé and family.*

## ACKNOWLEDGEMENTS

There are many extraordinary individuals I have met and worked with who I would like to thank.

I would first like to thank my PhD reading committee members: Dr. Chaitanya Deo, Dr. Glenn Sjoden, Dr. Farzad Rahnema, Dr. Ce Yi, and Dr. Chad Pope. I am lucky to have such a talented committee, and I really appreciate their participation in reviewing and critiquing my work, so that I can produce a quality dissertation.

I have had the privilege to work with a great group of students and faculty members at the Georgia Institute of Technology. I would like to thank Kevin Manalo, Christopher Edgar, and Michael Chin for welcoming me into the CRiTCEL group when I first began my graduate education.

I would especially like to thank Dr. Glenn Sjoden for seeing potential in me and motivating me to pursue an advanced education. His courses at the University of Florida helped me realize that I wanted to change my original plan of pursuing medical physics to pursuing a career safeguarding and supporting peaceful nuclear technology. I am grateful for him inviting me into his research group at the Georgia Institute of Technology, and motivating me to tackle difficult challenges. When he left his faculty position to take on a new career position, he continued to support my work and push me to complete my degree. I am forever grateful to have had such a dedicated and motivational mentor.

I would like to thank Mr. Hague for introducing me to the field of radiochemistry. I believe this education has helped broaden my understanding of nuclear science, and has made a lasting impact on my career goals.

I would like to thank my family, Cindy, Robert, and Christie for their ongoing support. They have always pushed me to further my education.

I would also like to thank Evan Redd and Daniel Lago for listening to my thoughts on my research and helping me in my editing processes. I am lucky to have them as good friends to help me stay focused and not let the stress of the doctoral program become overwhelming.

I would like to thank Dr. Anna Erikson for allowing me to use her lab space for collecting NaI(Tl) spectra from calibration sources. Paul Rose was a great help in providing me access to the laboratory and helped set up equipment for spectrum collection.

I would like to thank my PhD advisor, Dr. Chaitanya Deo, for taking me on as one of his students.

I would like to thank the Nuclear Forensics Graduate Fellowship for supporting me financially for my entire graduate career. I should note that the material in this dissertation is based upon work supported by the U.S. Department of Homeland Security under Grant Award Number, 2012-DN-130-NF0001. The views and conclusions contained in this document are those of the authors and should not be interpreted as representing the official policies, either expressed or implied, of the U.S. Department of Homeland Security.

Lastly, I would like to thank my fiancé, Christopher Johnson, for his support while I completed my graduate education. It has not been easy living 2,000 miles apart for the past four years, but you have always been supportive and found every possible

way to be a major part of my life, especially when it was difficult for me to travel and leave Atlanta.

# TABLE OF CONTENTS

	Page
ACKNOWLEDGEMENTS	iv
LIST OF TABLES	x
LIST OF FIGURES	xii
LIST OF SYMBOLS AND ABBREVIATIONS	xx
SUMMARY	xxi
 <u>CHAPTER</u>	
1 INTRODUCTION	1
1.1 Background	1
1.2 Objectives	2
1.3 Current Technologies and Methodologies	3
1.3.1 Limitations	5
1.4 Challenges	9
1.5 References	16
2 SMARTID	19
2.1 Background	19
2.1.1 Peak Finding	19
2.1.2 Nuclide Scoring	26
2.2 Enhancements for Water Stored Fuel	31
2.2.1 Running SmartID	37
2.3 References	41
3 LABORATORY EXPERIMENTS	43
3.1 Calibration Source Experiment	43

3.2 Irradiated Fuel Pin Experiment	59
3.2.1 Spectra collection during irradiation	63
3.2.2 Spectra collection post irradiation	67
3.3 References	81
4 SIMULATED SPECTRAL ANALYSIS	82
4.1 Origen Source	82
4.2 MCNP Models	87
4.3 SmartID Analysis	91
4.3.1 319 Emissions from 15 Isotopes Case	92
4.3.2 130 Emissions from 10 Isotopes Case	98
4.3.3 1,024 Emissions Case from Top Contributing Nuclides	107
4.3.4 12 Emissions Case	115
4.4 Final Thoughts	121
4.5 References	121
5 ADJOINT COUPLING	122
5.1 Radiation Transport Methods	122
5.1.1 Discrete Ordinates ( $S_N$ )	122
5.1.2 PENTRAN	125
5.1.3 Application of Adjoint	126
5.2 Adjoint Models	129
5.3 Forward Models	134
5.4 SmartID with Adjoint Coupling	139
5.4.1 Individual Pin Adjoint Importances	139
5.4.2 SmartID Procedure	151
5.4.2.1 $^{137}\text{Cs}$ Example	153



5.4.2.2 $^{106}\text{Rh}$ Example	157
5.4.2.3 $^{134}\text{Cs}$ Example	161
5.4.3 Fuel Pin Diversion	164
5.5 Fuel Burnup Analysis	166
5.6 References	182
6 CONCLUSION	184
6.1 Final Design	186
6.2 Future Work and Recommendations	186
6.3 Nuclear Forensics Impact	188
6.4 References	189
APPENDIX A: MCNP DRF Example Input File	190
APPENDIX B: SmartID Experiment FWHM and Energy Files	194
APPENDIX C: SmartID Experiment Input Files	195
APPENDIX D: SmartID Experiment Output Files	296
APPENDIX E: New SmartID Library for Spent Fuel Attribution	233
APPENDIX F: Adjoint Importances per Fuel Pin	264
APPENDIX G: Code for Determining Adjoint Importances per Fuel Pin	276
APPENDIX E: Calculating Burnup from $^{137}\text{Cs}$ Activity	289
VITA	292

## LIST OF TABLES

	Page
Table 1.1: Principle gamma-ray signatures for plutonium isotopes.	6
Table 1.2: Comparison of specifications for different types of detectors	10
Table 3.1: Calibration gamma peak data for a 2 in. x 2 in. NaI(Tl) detector in air.	40
Table 4.1: Top 15 gamma emitting isotopes from PWR fuel assembly burned to 33,000 MWD 1 day since removal from reactor.	74
Table 4.2: FWHM values from Gaussian Energy Broadening setting in MCNP.	78
Table 4.3: Identified Peaks for the 15 nuclides in air included in the MCNP simulation.	94
Table 4.4: Identified Peaks for 15 nuclides in water included in the MCNP simulation.	86
Table 4.5: 10 gamma emitting isotopes from PWR fuel assembly burned to 33,000 MWD 1 day since removal from reactor.	87
Table 4.6: Identified Peaks for the 10 nuclides in air included in the MCNP simulation.	91
Table 4.7: Identified Peaks for the 10 nuclides in water included in the MCNP simulation.	95
Table 4.8: 24 12 gamma source emissions chosen for MCNP simulation.	106
Table 4.9: SmartID peaks identified and corresponding gamma emissions.	106
Table 5.1: 24 group structure for Gamma emissions.	131
Table 5.2: Key radionuclide gamma emissions organized by energy group for adjoint importance evaluation.	142
Table 5.3: Change in count rate due to fuel pin removal.	165
Table 5.4: Cumulative Thermal Fission Yields for strong gamma emitting nuclides in spent PWR fuel after 1 day since removal from reactor core.	168
Table 5.5: Fuel assembly burnup estimated from $^{137}\text{Cs}$ activity.	173
Table 5.6: Percent differences computed for selected nuclide's activities at various fuel assembly burnups for initial enrichment of 2.6 w% $^{235}\text{U}$ .	179
Table 5.7: Fuel assembly burnup estimated from $^{106}\text{Ru}$ activity.	182

## LIST OF FIGURES

	Page
Figure 1.1: A high resolution gamma-ray spectrum of a PWR fuel assembly burned to 32 GWd/tU and cooled for 9 months.	7
Figure 1.2: Mass distribution of fission products for the thermal fission of $^{235}\text{U}$ and $^{239}\text{Pu}$ .	8
Figure 1.3: Change in fuel composition versus neutron fluence for Pu, U, and fission products. Neutron fluence is directly related to burnup.	9
Figure 1.4: Correctly identified shielded WGPu spectrum in air by SmartID post processing algorithm. The measured spectrum is shown in blue and the background is shown in yellow. Gamma emissions are identified by the red vertical lines.	14
Figure 2.1: Collected spectrum before (yellow points) and after (blue lin) the ACHIP denoising procedure.	21
Figure 2.2: SmartID “FWHM.txt” file.	24
Figure 2.3: Paradigm of the SmartID peak identification algorithm.	25
Figure 2.4: Detectability for a typical detector with shielding.	28
Figure 2.5: MCNP model geometry for a Westinghouse 17x17 PWR fuel assembly in water (yellow) with a NaI(Tl) detector (green) collimated by tungsten shielding (pink) in front of a concrete wall (orange). The left image shows a cross section along the y-axis, and the right image shows a cross section along the z-axis.	31
Figure 2.6: Compton scattering interaction.	32
Figure 2.7: 3.0 MeV incident gamma MCNP pulse height spectrum with detector 40 cm from source in water. Average and maximum 1-sigma errors were 1.71% and 3.82%, respectively for $1 \times 10^{12}$ particle histories.	33
Figure 2.8: 2.25 MeV incident gamma MCNP pulse height spectrum with detector 40 cm from source in water. Average and maximum 1 sigma errors were 1.57% and 3.05% respectively for $1 \times 10^{12}$ particle histories.	34
Figure 2.9: 1.50 MeV incident gamma MCNP pulse height spectrum with detector 40 cm from source in water. Average and maximum 1 sigma errors were 1.50% and 2.74% respectively for $1 \times 10^{12}$ particle histories.	34

Figure 2.10: 0.55 MeV incident gamma MCNP pulse height spectrum with detector 40 cm from source in water. Average and maximum 1 sigma errors were 1.98% and 3.66% respectively for $1 \times 10^{12}$ particle histories.	35
Figure 2.11: Input file, “smartid.inp,” SmartID utilizes for post-processing. Each line numbered for description	38
Figure 3.1: Experimental setup of NaI detector facing source stand.	43
Figure 3.2: $^{137}\text{Cs}$ spectrum in air shown in blue. $^{137}\text{Cs}$ spectrum in water shown in pink. Background spectrum shown in yellow.	45
Figure 3.3: $^{137}\text{Cs}$ spectrum in air shown in blue. Background was not subtracted. All identified peaks are shown by the red vertical lines.	46
Figure 3.4: Scored nuclides identified by SmartID for the $^{137}\text{Cs}$ spectrum without background subtraction.	48
Figure 3.5: $^{137}\text{Cs}$ spectrum in air shown in blue. Background shown in yellow. All identified peaks are shown by the red vertical lines.	49
Figure 3.6: $^{137}\text{Cs}$ spectrum in water with peaks identified by SmartID. Background shown in yellow. All identified peaks are shown by the red vertical lines.	50
Figure 3.7: SmartID partial output file for $^{137}\text{Cs}$ through water.	51
Figure 3.8: $^{60}\text{Co}$ spectra through 40 cm of air in blue with background in yellow.	52
Figure 3.9: $^{60}\text{Co}$ spectrum in air shown in blue. Background was not subtracted. All identified peaks are shown by the red vertical lines.	53
Figure 3.10: Scored nuclides identified by SmartID for the $^{60}\text{Co}$ spectrum without background subtraction.	54
Figure 3.11: $^{60}\text{Co}$ spectrum in air with peaks identified by SmartID. Background shown in yellow. All identified peaks are shown by the red vertical lines.	55
Figure 3.12: SmartID score summary for the $^{60}\text{Co}$ source through air.	56
Figure 3.13: $^{60}\text{Co}$ raw spectra through 40 cm of water.	57
Figure 3.14: Peaks identified for a $^{60}\text{Co}$ spectrum (blue) through 40 cm of water. The background is shown in yellow.	57
Figure 3.15: SmartID output file for $^{60}\text{Co}$ spectrum through water.	58
Figure 3.16: MCNP model of the experiment setup sliced along the x-axis.	59

Figure 3.17: Neutron interactions for the MCNP model of the experiment setup along the x-axis.	60
Figure 3.18: Actual experimental setup. Left: Sources in place. Right: Detector with Pb sheilding.	61
Figure 3.19: $^{155}\text{Eu}/^{22}\text{Na}$ calibration source spectra with identified gamma peaks. The yellow counts are from a background count; the blue counts are the gross counts.	62
Figure 3.20: $^{137}\text{Cs}$ calibration source spectra with identified gamma peaks. The yellow counts are the background and the blue counts are the gross counts.	63
Figure 3.21: First 8 hr and last 8hr spectra measured during irradiation of fuel element.	64
Figure 3.22: First 8 hr and last 8hr spectra measured durring irradiation of fuel element scaled linearly and plotted between 600 and 1400 keV.	65
Figure 3.23: Identified peaks from last 8 hour spectrum accumulation during irradiation.	66
Figure 3.24: Identified peak energies for the last 8 hour accumulated spectrum during irradiation.	66
Figure 3.25: SmartID nuclide score summary of the last 8 hour spectrum accumulation during irradiation.	67
Figure 3.26: Counts per minute for a NaI(Tl) detector minus the background. Each line represents a different 5 minute counting interval, where 1 <sup>st</sup> represents the first 5 minute count, and 21 <sup>st</sup> represents the last 5 minute count taken.	68
Figure 3.27: 1 <sup>st</sup> 5 min spectrum collected immediately following irradiation.	69
Figure 3.28: SmartID identified isotopes from a 5 minute spectra collected immediately following irradiation of a natural uranium fuel rod.	71
Figure 3.29: Peaks identified for the 20 <sup>th</sup> 5 min spectrum using the water DRF option.	73
Figure 3.30: Peaks identified for the 20 <sup>th</sup> 5 min spectra using the air DRF option and scattered counts scaling factor of 1.2.	74
Figure 3.31: Isotopes identified by SmartID using the water DRF option from a 5 minute spectra collected 1 hour and 35 minutes following irradiation.	75
Figure 3.32: SmartID identified isotopes with scores greater than 99.6 using the air DRF and scattered counts scaling option from a 5 minute spectra collected 1 hour and 35 minutes following irradiation of a natural uranium fuel rod.	78

Figure 3.33: Photopeak attribution for $^{234}\text{Pa}$ using the air DRF and scattered counts scaling option from a 5 minute spectra collected 1 hour and 35 minutes following irradiation of a natural uranium fuel rod.	79
Figure 3.34: Photopeak attribution for $^{140}\text{La}$ using the air DRF and scattered counts scaling option from a 5 minute spectra collected 1 hour and 35 minutes following irradiation of a natural uranium fuel rod.	80
Figure 4.1: Identified gamma line emissions from a Westinghouse 17x17 PWR fuel assembly burned to 33,000 MWD and cooled for 1 day, representing emissions from 73 nuclides.	84
Figure 4.2: 319 gamma emissions identified from 15 major isotopes found in spent fuel after 1 day of cooling.	86
Figure 4.3: 130 gamma emissions identified from 10 major isotopes found in spent fuel after 1 day of cooling.	87
Figure 4.4: Gaussian distributions for a mean energy of 660 keV.	89
Figure 4.5: MCNP simulated spectra for 319 gamma emissions from spent fuel in both air and water. The spectrum in air is shown in blue and the spectrum in water is shown in pink. Emissions are depicted by the vertical lines.	90
Figure 4.6: MCNP 1 sigma errors for 319 gamma emissions from spent fuel assembly gamma spectrum through water and air.	91
Figure 4.7: Peaks identified from a NaI(Tl) spectrum measuring 319 gamma emissions from a burned PWR fuel assembly in air.	93
Figure 4.8: Peaks identified from a NaI(Tl) spectrum measuring 319 gamma emissions from 15 nuclides in a burned PWR fuel assembly in water.	96
Figure 4.9: MCNP simulated spectra for 130 gamma emissions from spent fuel in both air and water. The spectrum in air is shown in blue and the spectrum in water is shown in pink. Emissions are depicted by the vertical lines.	99
Figure 4.10: MCNP 1 sigma errors for 130 gamma emissions from spent fuel assembly gamma spectrum through water and air.	100
Figure 4.11: Peaks identified from a NaI(Tl) spectrum measuring 130 gamma emissions in air from a burned PWR fuel assembly in air.	101
Figure 4.12: Top scored nuclides identified for the 130 gamma emissions source in air from a PWR spent fuel assembly after 1 day from removal from the reactor core.	104

Figure 4.13: Peaks identified from a NaI(Tl) spectrum measuring 10 isotope emissions from a burned PWR fuel assembly in water.	105
Figure 4.14: Peaks identified for the 130 gamma emissions source in water from a PWR spent fuel assembly after 1 day from removal from the reactor core.	105
Figure 4.15: Top scored nuclides identified for the 130 gamma emissions source in water from a PWR spent fuel assembly after 1 day from removal from the reactor core.	107
Figure 4.16: MCNP simulated spectrum of 1,024 gamma emissions for spent PWR fuel assembly in air.	108
Figure 4.17: MCNP 1 sigma errors for 1,024 gamma emissions from a spent PWR fuel assembly gamma spectrum through water and air.	108
Figure 4.18: Peaks identified from a NaI(Tl) spectrum measuring 1,024 emissions from a burned PWR fuel assembly in air.	109
Figure 4.19: Nuclides identified for a PWR spent fuel assembly after 1 day from removal from the reactor core with a 2% energy window for peak attribution.	111
Figure 4.20: Nuclides identified for a PWR spent fuel assembly after 1 day from removal from the reactor core with a 1% energy window for peak attribution.	112
Figure 4.21: SmartID emission attribution for scored nuclide, $^{140}\text{La}$ .	114
Figure 4.22: SmartID emission attribution for scored nuclide, $^{137}\text{Cs}$ .	115
Figure 4.23: Simulated spectrum from 12 gamma emissions along with SmartID identified peaks.	117
Figure 4.24: The relationship between the Gaussian Energy Broadened spectrum produced through f8 tallies in MCNP for the 12 emissions case and the corresponding 1 sigma errors	119
Figure 4.25: SmartID nuclide scoring and emission attribution of $^{134}\text{Cs}$ for the 12 emission case.	120
Figure 5.1: $S_6$ level symmetric discrete ordinates set.	123
Figure 5.2: 2-D top-down view PENTRAN model of NaI(Tl) detector underwater “looking” at a used fuel assembly.	130
Figure 5.3: $S_{90}$ adjoint importances mapped for 6 out of 24 adjoint energy groups. Each group is scaled individually for better visualization.	132
Figure 5.4: $S_{90}$ adjoint importances mapped for 6 out of 24 adjoint energy groups. Scaling is equal across all groups.	133

Figure 5.5: Normalized forward source by energy group.	134
Figure 5.6: $S_{90}$ forward flux mapped for 6 out of 24 forward energy groups. Each group is scaled individually for better visualization.	136
Figure 5.7: $S_{90}$ forward importances mapped for 6 out of 24 adjoint energy groups. Scaling is equal across all groups.	137
Figure 5.8: Fuel assembly pin numbering system. The front face of the detector will be located to the right of the fuel assembly such that the first row is the row of pins closest to the detector.	140
Figure 5.9: Adjoint importance values across the fuel assembly for forward energy group 23 (0.3 – 0.741MeV).	141
Figure 5.10: Adjoint group 6 (0.767- 0.954 MeV) adjoint importances per fuel pin in a Westinghouse 17x17 PWR fuel assembly.	144
Figure 5.11: Adjoint group 14 (1.26- 1.5 MeV) adjoint importances per fuel pin in a Westinghouse 17x17 PWR fuel assembly.	145
Figure 5.12: Adjoint group 23 (2.25- 2.75 MeV) adjoint importances per fuel pin in a Westinghouse 17x17 PWR fuel assembly.	145
Figure 5.13: Average adjoint importances plotted at the center of each energy group for 90%, 95%, and 99% of the total counts in the detector. The best fit correlation is also shown for each case.	147
Figure 5.14: Number of pins plotted at the center of each energy group for 90%, 95%, and 99% of the total counts in the detector. The best fit correlation is also shown for each case.	148
Figure 5.15: Paradigm of the activity estimation from identified peaks in SmartID.	153
Figure 5.16: Cross section of MCNP model for $^{137}\text{Cs}$ spectrum simulation.	154
Figure 5.17: Identified peaks for MCNP simulated $^{137}\text{Cs}$ spectrum in water.	155
Figure 5.18: SmartID output for a $^{137}\text{Cs}$ spectrum in water.	156
Figure 5.19: Estimated activities for SmartID scored nuclides from a $^{137}\text{Cs}$ spectrum in water.	156
Figure 5.20: Identified peaks for MCNP simulated $^{106}\text{Rh}$ spectrum in water.	158
Figure 5.21: Peaks identified by SmartID for the $^{106}\text{Ru}$ test case.	159
Figure 5.22: Details of the $^{106}\text{Ru}$ test case emissions identified.	160



Figure 5.23: Activity estimate for $^{106}\text{Ru}$ test case by employing the adjoint methodology discussed in this chapter.	160
Figure 5.24: Identified peaks for MCNP simulated $^{134}\text{Cs}$ spectrum in water.	161
Figure 5.25: Peaks identified by SmartID for the $^{134}\text{Cs}$ test case.	162
Figure 5.26: Details of the $^{134}\text{Cs}$ test case emissions identified.	163
Figure 5.27: Activity estimate for $^{134}\text{Cs}$ test case by employing the adjoint methodology discussed in this chapter.	164
Figure 5.28: Fuel pin locations selected for diversion analysis.	165
Figure 5.29: Mass distribution of fission products for the thermal fission of $^{235}\text{U}$ and $^{239}\text{Pu}$ .	167
Figure 5.30: Total activity of $^{140}\text{La}$ in a Westinghouse 17x17 fuel assembly at various fuel burnups.	170
Figure 5.31: Total activity of $^{140}\text{Ba}$ in a Westinghouse 17x17 fuel assembly at various fuel burnups.	171
Figure 5.32: Total activity of $^{99}\text{Mo}$ in a Westinghouse 17x17 fuel assembly at various fuel burnups.	171
Figure 5.33: Total activity of $^{137}\text{Cs}$ in a Westinghouse 17x17 fuel assembly at various fuel burnups.	172
Figure 5.34: Total activity of $^{134}\text{Cs}$ in a Westinghouse 17x17 fuel assembly at various fuel burnups.	174
Figure 5.35: Total activity of $^{154}\text{Eu}$ in a Westinghouse 17x17 fuel assembly at various fuel burnups.	175
Figure 5.36: Total activity of $^{106}\text{Ru}$ in a Westinghouse 17x17 fuel assembly at various fuel burnups.	176
Figure 5.37: Total activity of $^{95}\text{Zr}$ in a Westinghouse 17x17 fuel assembly at various fuel burnups.	177
Figure 5.38: Total activity of $^{91}\text{Sr}$ in a Westinghouse 17x17 fuel assembly at various fuel burnups.	178
Figure 5.39: Plutonium isotopic content in a Westinghouse 17x17 PWR fuel assembly enriched to 2.6 w% $^{235}\text{U}$ at various burnup levels.	180
Figure 5.40: Total plutonium content in fuel assembly for various burnup levels.	180

Figure 6.1: Underwater fuel assembly detection system.	186
Figure 6.2: PWR Spent Fuel Cooling Systems. A potential area for detection is located for individual assembly detection.	187
Figure B.1: “FWHM.txt” file for irradiated fuel rod experiment spectra	194
Figure B.2: Energy calibration file, “Energy.txt” for irradiated fuel rod experiment spectra	194
Figure C.1: SmartID input file for 20 <sup>th</sup> 5 minute spectrum collected after fuel rod irradiated for 2 weeks. Options chosen included an aliasing factor of 0.5, chi threshold of 0.01, DRF representing the fuel assembly in water, and shielding search	195
Figure D.1: (Below) SmartID output file for 20 <sup>th</sup> 5min count spectrum with aliasing factor of 0.5, chi threshold of 0.01, DRF representing the fuel assembly in water, and shielding search. Only top scoring shielding scenario included	196
Figure D.2: (Below) SmartID output file for 20 <sup>th</sup> 5min count spectrum with aliasing factor of 0.5, chi threshold of 0.01, DRF representing the fuel assembly in water, scattering counts set to 1.85 and shielding search. Only top scoring shielding scenario included	207
Figure F.1: Adjoint group 1 (0 – 0.3 MeV) adjoint importances per fuel pin in a Westinghouse 17x17 PWR fuel assembly	264
Figure F.2: Adjoint group 2 (0.3 – 0.741 MeV) adjoint importances per fuel pin in a Westinghouse 17x17 PWR fuel assembly	264
Figure F.3: Adjoint group 3 (0.741 – 0.743 MeV) adjoint importances per fuel pin in a Westinghouse 17x17 PWR fuel assembly	265
Figure F.4: Adjoint group 4 (0.743 – 0.765 MeV) adjoint importances per fuel pin in a Westinghouse 17x17 PWR fuel assembly	265
Figure F.5: Adjoint group 5 (0.765 – 0.767 MeV) adjoint importances per fuel pin in a Westinghouse 17x17 PWR fuel assembly	266
Figure F.6: Adjoint group 6 (0.767 – 0.954 MeV) adjoint importances per fuel pin in a Westinghouse 17x17 PWR fuel assembly	266
Figure F.7: Adjoint group 7 (0.954 – 0.956 MeV) adjoint importances per fuel pin in a Westinghouse 17x17 PWR fuel assembly	267
Figure F.8: Adjoint group 8 (0.956 – 0.999 MeV) adjoint importances per fuel pin in a Westinghouse 17x17 PWR fuel assembly	267

Figure F.9: Adjoint group 9 (0.999 – 1.002 MeV) adjoint importances per fuel pin in a Westinghouse 17x17 PWR fuel assembly	268
Figure F.10: Adjoint group 10 (1.002 – 1.18 MeV) adjoint importances per fuel pin in a Westinghouse 17x17 PWR fuel assembly	268
Figure F.11: Adjoint group 11 (1.18 – 1.2 MeV) adjoint importances per fuel pin in a Westinghouse 17x17 PWR fuel assembly	269
Figure F.12: Adjoint group 12 (1.2 – 1.24 MeV) adjoint importances per fuel pin in a Westinghouse 17x17 PWR fuel assembly	269
Figure F.13: Adjoint group 13 (1.24 – 1.26 MeV) adjoint importances per fuel pin in a Westinghouse 17x17 PWR fuel assembly	270
Figure F.14: Adjoint group 14 (1.26 – 1.5 MeV) adjoint importances per fuel pin in a Westinghouse 17x17 PWR fuel assembly	270
Figure F.15: Adjoint group 15 (1.5 – 1.52 MeV) adjoint importances per fuel pin in a Westinghouse 17x17 PWR fuel assembly	271
Figure F.16: Adjoint group 16 (1.52 – 1.736 MeV) adjoint importances per fuel pin in a Westinghouse 17x17 PWR fuel assembly	271
Figure F.17: Adjoint group 17 (1.736 – 1.74 MeV) adjoint importances per fuel pin in a Westinghouse 17x17 PWR fuel assembly	272
Figure F.18: Adjoint group 1 (1.74 – 1.76 MeV) adjoint importances per fuel pin in a Westinghouse 17x17 PWR fuel assembly	272
Figure F.19: Adjoint group 19 (1.76 – 1.83 MeV) adjoint importances per fuel pin in a Westinghouse 17x17 PWR fuel assembly	273
Figure F.20: Adjoint group 20 (1.83 – 1.832 MeV) adjoint importances per fuel pin in a Westinghouse 17x17 PWR fuel assembly	273
Figure F.21: Adjoint group 21 (1.832 – 2.21 MeV) adjoint importances per fuel pin in a Westinghouse 17x17 PWR fuel assembly	274
Figure F.22: Adjoint group 22 (2.21 – 2.25 MeV) adjoint importances per fuel pin in a Westinghouse 17x17 PWR fuel assembly	274
Figure F.23: Adjoint group 23 (2.25 – 2.749 MeV) adjoint importances per fuel pin in a Westinghouse 17x17 PWR fuel assembly	275
Figure F.24: Adjoint group 24 (2.749 – 3 MeV) adjoint importances per fuel pin in a Westinghouse 17x17 PWR fuel assembly	275

## LIST OF SYMBOLS AND ABBREVIATIONS

CZT	Cadmium Zinc Telluride
DHS	Department of Homeland Security
DOE	Department of Energy
DRF	Detector Response Function
FWHM	Full Width Half Maximum
GEB	Gaussian Energy Broadening
HPGe	High Purity Germanium
HPXe	High Purity Xenon
IAEA	International Atomic Energy Agency
LWR	Light Water Reactor
NDA	Non Destructive Assay
PWR	Pressurized Water Reactor
RSEL	Radiological Science and Engineering Laboratory
SNM	Special Nuclear Material
WGPu	Weapons Grade Plutonium

## SUMMARY

The growing concern regarding regulation and accountability of plutonium and SNM produced in commercial and research nuclear reactor fuel has driven the need for new spent nuclear fuel characterization methods to enable quantification and qualification of radioisotopes contained in used fuel in a reliable, quick, and inexpensive manner, with little to no impact on normal reactor operating procedures. This research aims to meet these objectives by employing advanced computational radiation transport methods incorporated into an algorithm to post process scintillator detector data gathered from used nuclear fuel in a spent fuel pool or in air. An existing, novel post processing algorithm, SmartID, has been updated to extract and identify unique photopeaks represented in the underwater environment for pool cooled used fuel. The resulting spectral data will be post-processed using an updated SmartID algorithm folded with deterministic adjoint results to render both qualitative and quantitative fuel content and irradiation estimates. This work has much significance to the nuclear power industry, safeguards, and forensics communities, since it yields this information at room temperature for a relatively low cost.

# **CHAPTER 1**

## **INTRODUCTION**

The growing concern regarding regulation and accountability of plutonium and SNM produced in commercial and research nuclear reactor fuel has prompted the need for rapid, low cost characterization and attribution of fuel materials and mixed radioisotopes for forensics purposes, and has driven the need for new spent nuclear fuel characterization methods. Moreover, any new methods must also enable quantification in addition to traditional qualification of radioisotopes contained in used fuel in a reliable, quick, and inexpensive manner, with little to no impact on normal reactor operations. Achieving this with low cost detectors augmented by advanced algorithms, as outlined in this work, will not only aid in strengthening weaknesses in the current safeguards protocols, but also will yield a capability for rapid, cost effective identification of radionuclide content supporting a variety of nuclear forensics applications.

### **1.1 Background**

The IAEA estimates that by the year 2020, approximately 445,000 tons of heavy metal will have been discharged from the world's commercial nuclear power plants [1]. One quarter of this amount (111,250 tons) is expected to be sent to fuel reprocessing facilities. Given this large amount of material, the risk for undetected diversion or tampering through loss of continuity of knowledge is real. Additional safeguards measures are important and necessary to mitigate this risk by providing low cost methods to quickly account for and confirm relative isotopic content of spent fuel rods in order to flag discrepancies and enable forensics assessments of SNM where needed.

Additionally, the DOE Radiological Assistance Program (RAP) team currently utilizes gamma data collected from NaI detectors in both ground-based and airborne

platforms as part of their mission. This requires forensic analysis of the data to determine whether or not one can identify a potential nuclear threat. A real-time data analysis method optimized for this type of detection equipment is necessary for the detection of a nuclear threat if a spent fuel pin or assembly was stolen and configured into a radiological dispersal device (RDD). The RAP team typically flies on the order of 100-1000 feet above the ground to take gamma spectra data. From a Compton Scattering mass integral perspective, gamma spectra behave similarly for sources at thousands of feet from the detector in air and sources about 40 cm from the detector in water. Therefore, the techniques and detector response functions developed for analyzing gamma spectra in water from spent fuel are similar to analyzing gamma spectra collected from an aircraft from a possible RDD.

## **1.2 Objectives**

This research aims to meet the needs discussed by employing advanced computational radiation transport methods incorporated into an algorithm to post-process scintillator detector data gathered from used nuclear fuel in a spent fuel pool or in air. An existing, novel post-processing algorithm, SmartID, will be modified to extract and identify unique photopeaks represented in the underwater environment for pool-cooled used fuel. Because of the manner in which SmartID processes the spectrum through unfolding using interpolated transport theory detector response functions, it removes all artifacts of scattering to yield the collective of photopeaks, even in regions where these are normally masked due to severe Compton pileup in a typically low cost room temperature scintillator. The resulting spectral data in this work will be post-processed using the SmartID algorithm modified for water based operations, folded with deterministic radiation transport adjoint computations to render both qualitative and quantitative fuel content and irradiation estimates. As already noted, this work has much significance to the nuclear power, safeguards, and forensics communities, since it yields

this information at room temperature for very low cost. The proposed work is subdivided into five key goals, as follows:

- 1.) To employ computational radiation transport methods to model how a scintillator detector responds to the radiation from a spent fuel assembly in water.
- 2.) To determine how Compton scattering in water affects the gamma spectrum at singular discrete energies.
- 3.) To update an existing post processing algorithm for the characterization of gamma peaks in order to extract radionuclide information important to determining plutonium content and fuel burnup.
- 4.) To test the algorithm by irradiating a natural uranium metal fuel rod and measuring the emitted gamma radiation transported through water during active irradiation, and as a function of cool-down time, with particular attention to short term irradiation products.
- 5.) To integrate adjoint transport computations with the radionuclide information extracted from the post processed spectral data for plutonium content from fuel burnup.

### **1.3 Current Technologies and Methodologies**

A great deal of work has been accomplished using passive gamma signatures and integrated gamma counts to determine burnup and cooling time of spent fuel assemblies in pools; however, no work has been done leveraging the algorithm post-processing of low cost “pool temperature” scintillators as proposed here. The “Fork” detector is currently used at power plants, along with MOX python (SMOPY), and Cherenkov viewing devices [2]. The Fork detector consists of cadmium-zinc-telluride (CZT) gamma detectors along with a cadmium covered fission chamber to measure epithermal neutrons, and an uncovered fission chamber to measure thermal neutrons [3]. These detectors can produce the data to determine burnup, cooling time and assembly declarations, but they do not have the capability to do so independently, or determine initial enrichment. Early models only included ionization and fission chambers to measure gross gamma and



neutron yields, rather than considering spectral information, but these models were improved by adding CZT detectors to gather spectral information.

The Fork detector is designed to focus on three key radionuclide signatures:  $^{137}\text{Cs}$  peak at 662 keV,  $^{134}\text{Cs}$  peaks, and the  $^{106}\text{Ru}$  peaks. It has long been studied and validated that the burnup value of spent fuel has a nearly linear relationship with the  $^{137}\text{Cs}$  content in the fuel.  $^{137}\text{Cs}$  is a proven indicator of burnup due to its negligible neutron absorption cross section, approximately equal yields from fission of  $^{235}\text{U}$  and  $^{239}\text{Pu}$ , and a long 30 year half-life [1]. The combination of these three attributes removes the necessity to correct for reactor power history [1].

Furthermore, ratios of fission products will also result in linear relationships with burnup for limited burnup ranges. The  $^{134}\text{Cs}/^{137}\text{Cs}$  activity ratio and the  $^{154}\text{Eu}/^{137}\text{Cs}$  activity ratio are valid for low and medium burnup (<50GWd/t), while the  $^{134}\text{Cs}/^{154}\text{Eu}$  ratio is valid at high burnups (>50GWd/t) [4]. However, it is important to note that after approximately 12 years of cooling, the entire  $^{134}\text{Cs}$  signal is practically lost due to  $^{134}\text{Cs}$  decay (half-life of 2.0652 years). As mentioned,  $^{137}\text{Cs}$  has a relatively linear relationship with burnup, but this linear relationship must be corrected for short cooling times due to indicators from  $^{134}\text{Cs}$  and  $^{106}\text{Ru}/^{103}\text{Rh}$  causing deviations from linearity [3]. Therefore, it has been shown that corrections must be made to the gross gamma signal to determine an “adjusted”  $^{137}\text{Cs}$  count. This adjustment is shown by the following equation,

$$G_{37} = \frac{G}{1 + 2.620R_{34} + 0.324R_{06}} \quad (1)$$

where  $G_{37}$  is the adjusted  $^{137}\text{Cs}$  count rate,  $G$  is the gross gamma emission rate,  $R_{34}$  is the measured activity ratio of  $^{134}\text{Cs}/^{137}\text{Cs}$ , and  $R_{06}$  is the measured activity ratio of  $^{106}\text{Ru}/^{103}\text{Rh}$  [3]. This correction has been shown to greatly improve results for a linear

trend of  $^{137}\text{Cs}$  with burnup in the experiments performed at the TVO KPA Store in 1999 [3].

The Safeguards MOX Python (SMOPY) is an underwater detection system that is designed to distinguish between MOX and LEU fuel. It consists of a CZT gamma detector and a fission chamber to measure neutron emission and determine the  $^{134}\text{Cs}/^{137}\text{Cs}$  ratio. Similar to the Fork detector, this device must use operator data to determine burnup, and it cannot detect fuel pin diversions [5].

Cherenkov viewing devices are used to observe the intensity of the visible blue Cherenkov glow from used fuel assemblies in a spent fuel pool. They do not typically provide any quantifiable information in relation to fuel burnup, but can indicate whether or not a “dummy” fuel element is present. The user must be well trained to be able to discern if an element has Cherenkov glow, or it is being illuminated by a near-neighbor spent fuel element [6]. In some cases, the glow intensity can be utilized to estimate burnup by comparing it to a known reference spent fuel assembly that has been measured in the same storage pool [7].

### **2.3.1 Limitations**

The desire of the IAEA is to find a low-cost, non-destructive method to quantify plutonium content in spent fuel assemblies and detect the diversion of fuel pins. This is not possible with current passive gamma methodologies discussed. Current passive gamma measurements are also unable to detect pin diversions. In this work, I determine how post-processing of room temperature scintillator spectra (from NaI) impacts this IAEA requirement.

Many researchers have expressed in the literature that any gamma spectral information from low energy gamma emitters such as plutonium is “washed out” due to the substantial count rates and Compton pileup from the numerous fission products in the source term. After fuel rods are removed from the reactor for one year, fission products

produce a total gamma-ray intensity of approximately  $2 \times 10^{10}$  gamma/g-s, but major plutonium gamma rays only have intensities in the range of  $10^3$  to  $10^4$  gammas/g-s [8]. With the addition of Compton pileup effects in the detector, plutonium gammas are completely hidden in the spectra. According to the PANDA manual, the principle gamma signatures emitted by plutonium isotopes are listed in Table 1.1.

**Table 1.1:** Principle gamma-ray signatures for plutonium isotopes [9].

Isotope	Half-Life (y)	Energy (keV)	Branching Ratio	Activity( gamma/g-s)
$^{238}\text{Pu}$	87.74	152.7	$9.37 \times 10^{-6}$	$5.90 \times 10^6$
		766.4	$2.20 \times 10^{-7}$	$1.387 \times 10^5$
$^{239}\text{Pu}$	24,119	129.3	$6.31 \times 10^{-5}$	$1.436 \times 10^5$
		413.7	$1.47 \times 10^{-5}$	$3.416 \times 10^4$
$^{240}\text{Pu}$	6564	45.2	$4.50 \times 10^{-4}$	$3.80 \times 10^6$
		642.5	$1.30 \times 10^{-7}$	$1.044 \times 10^3$
$^{241}\text{Pu}$	14.348	148.6	$1.85 \times 10^{-6}$	$7.15 \times 10^6$
		208.0 <sup>1</sup>	$2.12 \times 10^{-1}$	$2.041 \times 10^7$
$^{241}\text{Am}$	432	59.5	$3.59 \times 10^{-1}$	$4.54 \times 10^{10}$
		125.3	$4.08 \times 10^{-5}$	$5.16 \times 10^6$

It is seen that the majority of plutonium gamma lines emit with energies less than 400 keV, which can be problematic to detect in cooling pools, although several key lines are observed at 413.7 keV, 652.5 keV, and 766.4 keV. A sample spectrum of a used PWR assembly, as shown in Figure 1.1, depicts how these key gamma peaks are lost in the overabundance of high activity fission product gamma sources. The lowest energy peaks visible are from  $^{106}\text{Rh}$  and  $^{134}\text{Cs}$ , and no plutonium peaks are visible.

<sup>1</sup> This is from  $^{241}\text{Pu}$  daughter product  $^{237}\text{U}$ .

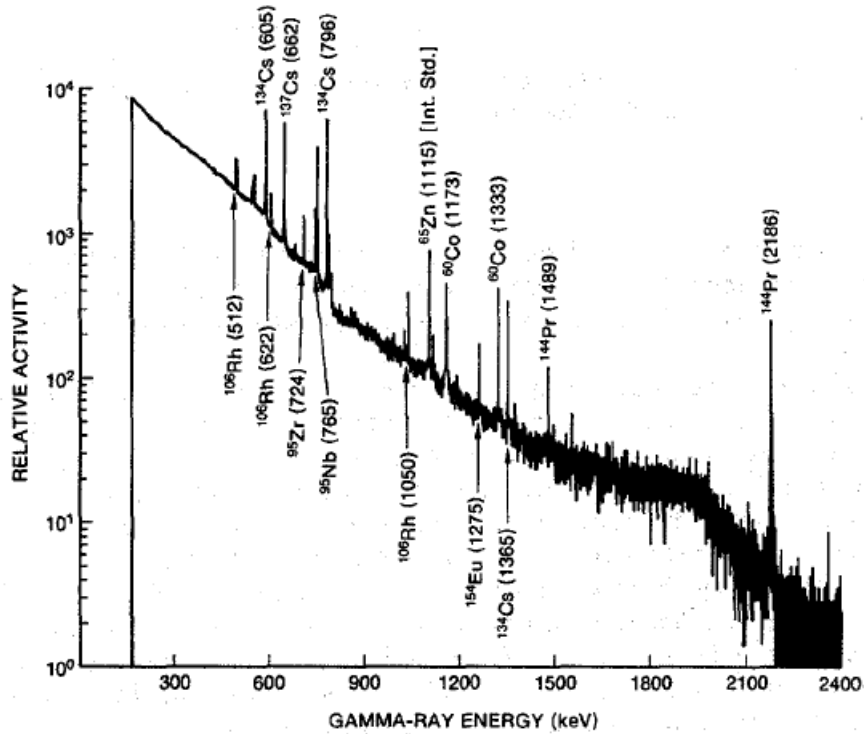


**Figure 1.1:** A high resolution gamma-ray spectrum of a PWR fuel assembly burned to 32 GWd/tU and cooled for 9 months [9].

There are currently 99 commercial nuclear reactors operating in the United States [10]. Like any other nonrenewable fuel source, nuclear fuel has a finite lifetime; therefore as the fuel diminishes, it must be replaced with new fresh fuel. In the case of nuclear fuel, this process is not as basic as simply replacing old rods with new rods and throwing out the old. The basis of a nuclear fission reaction is when an atomic nucleus splits into two new lighter nuclei plus additional neutrons. The nuclei produced will depend on the isotope undergoing fission. Different fission nuclei have differing yields depending on the original heavy isotope shown by Figure 1.2.

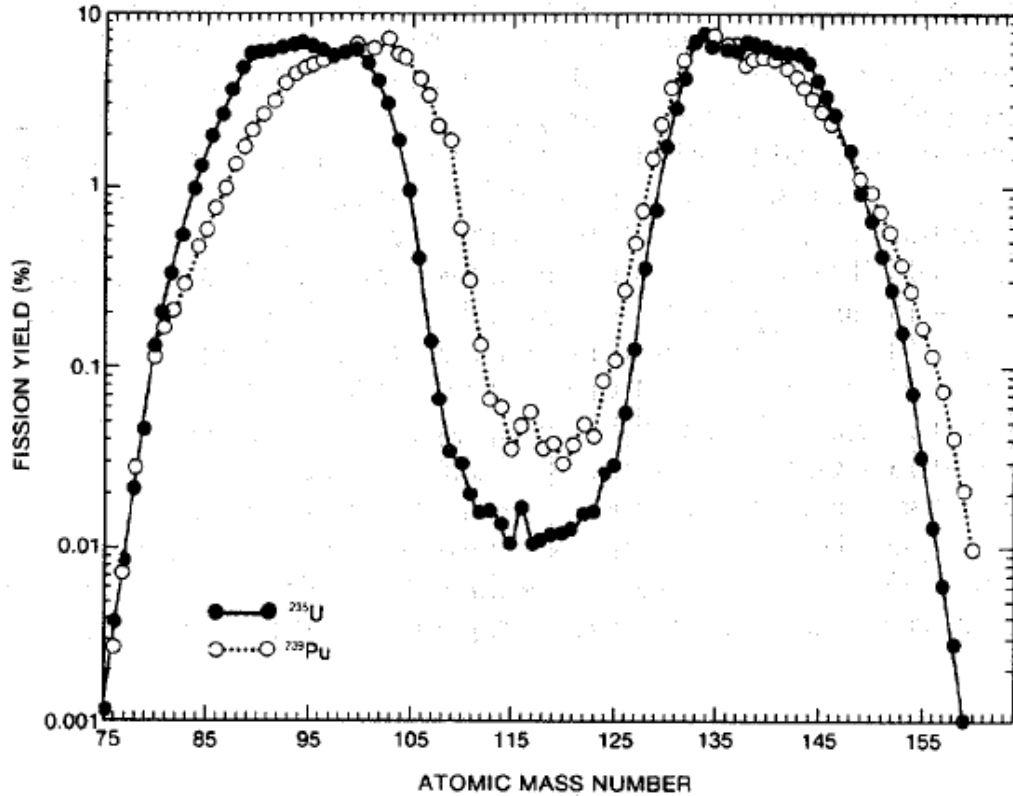


**Figure 1.2:** Mass distribution of fission products for the thermal fission of  $^{235}\text{U}$  and  $^{239}\text{Pu}$  [9].

These new nuclei are in an unstable state and go through many radioactive decay processes before finding a more stable configuration (most often they are neutron heavy and undergo beta decay to new daughter products). These daughter products have intense radioactivity resulting in heat generation and harmful gamma radiation. Because of this, spent fuel rods must be placed into temporary storage until they cool down enough, e.g. 5 – 10 years, to be placed in more permanent storage configurations. Additionally neutron absorption reactions also take place in the fuel creating additional isotopes such as  $^{239}\text{Pu}$ ,  $^{240}\text{Pu}$ ,  $^{241}\text{Pu}$ , and  $^{242}\text{Pu}$ . These isotopes are of sufficient mass and lead to non-proliferation and safeguards concerns. Figure 1.2 shows how these isotopes grow into the fuel assembly along with other U isotopes and fission products.

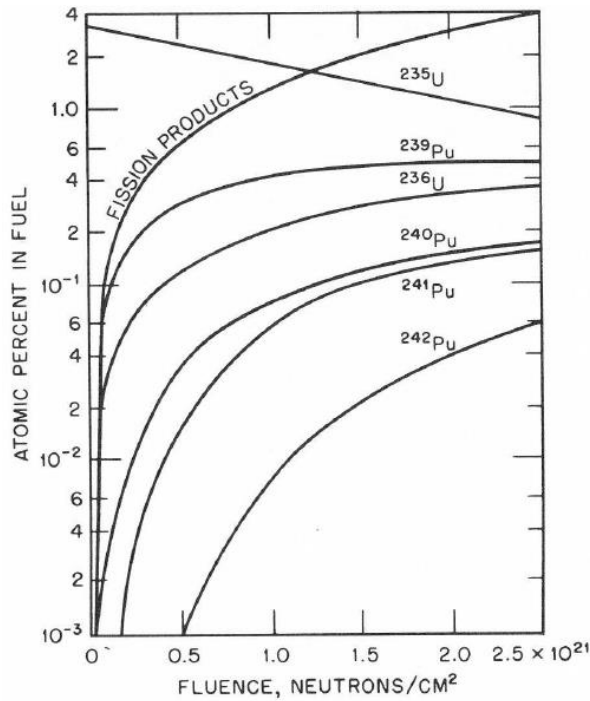


**Figure 1.3:** Change in fuel composition versus neutron fluence for Pu, U, and fission products. Neutron fluence is directly related to burnup [11].

### 1.4 Challenges

One of the key challenges is finding a detector that will be capable of resolving spectral peaks while keeping costs at a minimum. I considered three types of detector materials for use in this project: solid-state, gas, and scintillator. Each type has certain advantages and disadvantages, and there are many different material compositions within each type. HPGc and CZT are the most talked about in spent fuel measurements above water and below, NaI, and CsI are commonly used for their ruggedness and integrated activity, but are often relied on for individual gamma ray assay, and HPXe is a newer type that shows promise for spent fuel applications. In order to narrow down these detector choices to only one for experimentation, one can compare the most common and relevant detectors available commercially. At sufficiently low burnup levels, less than 1,000 MWD/MTU, the concentrations of plutonium are consistent with weapons grade

plutonium (WGPu). WGPu is defined as having a  $^{239}\text{Pu}$  concentration greater than 90% of the total plutonium content [12]. It is important that a detection system can distinguish this level of burnup.

**Table 1.2:** Comparison of specifications for different types of detectors.

	HPGe	CZT	HPXe	LaBr <sub>3</sub>	NaI(Tl)	CsI(Na)(Tl) (undoped)
<b>Type</b>	Solid-state	Solid-state	Gas	Scintillator	Scintillator	Scintillator
<b>Shape</b>	Planar	Rectangular			Cylindrical	
<b>xsec area depth</b>	5 cm 1.5 cm	2.3 cm <sup>2</sup> 1.5 cm [13]			5 cm <sup>2</sup> 5 cm [13]	
<b>Density</b>	5.3 g/cc	6.0 g/cc	0.4-0.5 g/cc		3.7 g/cc	4.5 g/cc
<b>Intrinsic Efficiency</b>	• 1.4% at 662keV • 81% at 122keV [13]	• 8% at 662keV • 100% at 122keV [13]	• 3% at 662keV • 1% at 1.332MeV • Small photo-peak efficiency	Better than NaI(Tl) [14]	• 15% at 662keV • 100% at 122keV [13]	• 35% at 1MeV[15]
<b>Resolution</b>	• 0.15% at 1.332MeV • 0.2% at 662keV • 0.4% at 122keV	• 3.2% at 662keV • 6.3% at 122keV [13]	• 2-2.5% at 662keV • 1.5-2% at 1.332MeV • 7% at 122keV	• 2.8-3.5% at 662keV • Better than NaI at 122keV	• 7.5-8.5% at 662keV • 12% at 122keV [16]	• 5.8-6% at 662keV • 15% at 122keV
<b>Operating Temperature Range I</b>	Need cryogenic cooling	For resistive type, the resolution significantly changes at T>10C For a schottky type, changes T>33C [17]	15-200[9] Superior temperature stability [13]	4-43 degree C [Canberra] Gain change at high temperature changes	Change in gain with temp. Some commercial systems track gain drift and compensate, widening the temp range [13]	
<b>Lifetime Cost</b>	Expensive	Expensive	Not as expensive as HPGe	Moderate costs relative to NaI	Inexpensive	Inexpensive

**Table 1.2 Continued**

<b>Operational mode</b>			Ionization and scintillation (2ns decay time)			
<b>Contamination</b>				<sup>227</sup> Ac and <sup>138</sup> La impurities		
<b>Radiation exposure effects</b>	Conventional Ge detector show resolution change after 10 <sup>7</sup> n/cm <sup>2</sup> [18] but gamma-x detector claims show little change up to 10 <sup>10</sup> n/cm <sup>2</sup> [22]	Significant resolution losses after 7x10 <sup>10</sup> n/cm <sup>2</sup> but resolution largely recovered after 12 weeks of annealing at room temp. [19]	Resistant to radiation damage [13]	Significant change of yield and E resolution after 1 <sup>st</sup> irradiation with 0.1kGy dose. As much as 22% of yield lost and res inc from 2.8% to 4.6%	Susceptible to radiation damage. Prolonged exposures degrades performance [20]	Only undoped CsI is radiation hard. No substantial changes up to 10 <sup>5</sup> rad. Doped versions are susceptible to radiation damage [21]
<b>Availability</b>		1yr after order	Constellation Technology Not mass produced	4-8 wks after order	2 wks after order	

Table 1.2 shows which detectors have potential in my proposed application, and which ones do not. High Purity Germanium (HPGe) detectors are ideal for high resolution spectra, but they suffer from many drawbacks for an underwater system. These detectors will become severely damaged or non-functioning without proper cryogenic cooling, either from liquid nitrogen or an electronic cooling system. They are also extremely expensive, typically more than twenty times the cost of a single NaI crystal; therefore, utilities or inspection agencies are often unwilling to subject them to harmful radiation in wet/hostile environments, where they have a greater likelihood of being damaged. Because of this, HPGe detectors cannot be a viable low cost option for underwater spent fuel NDA.



Scintillators are known to have low energy resolutions, but make up for that in their efficiency, ruggedness and low cost. NaI has the lowest energy resolution out of all of the detectors listed, and a high intrinsic efficiency which would result in this type of detector needing sufficient shielding to mitigate detector deadtime. Although it is rugged in many applications, it is susceptible to radiation damage after prolonged exposures that will degrade its performance. CsI (doped with Na, Tl, or undoped) is similar to NaI in that it is also a scintillator, is relatively inexpensive, and has low energy resolution. This detector material has slight modifications to its operating specifications depending on whether or not it has been doped with Na or Tl. Doping does help with energy resolution, but it also makes the detector much more susceptible to radiation damage. Undoped CsI detectors are “radiation hard,” meaning they are relatively immune to changes in resolution due to high radiation exposures. These undoped detectors see no substantial changes up to a dose of  $10^3$  rad [21]. This should not be a concerning issue since a background measurement must be taken with the detector and subtracted out for proper analysis. Therefore, CsI is a better candidate for spent fuel detection than a NaI detector.

The third scintillator under consideration is a LaBr<sub>3</sub> detector. These detectors have a much better energy resolution than both NaI and CsI, but they also may experience significant gain change with increasing temperature, and have a natural radioactivity inherent in the material. These detectors are more expensive than NaI, but are still much less expensive than HPGe detectors. LaBr<sub>3</sub> detectors experience gamma ray contamination from <sup>227</sup>Ac, and <sup>138</sup>La impurities. They also suffer from significant radiation damage effects after 0.1 kGy dose.

The final detector considered, HPXe, is a relatively new detector that has shown a lot of promise for applications in spent fuel pools. HPXe detectors are very rugged allowing them to be able to operate for years without maintenance and servicing [13]. One of the most beneficial attributes of an HPXe detector is that its high energy

resolution stays stable over a wide temperature operating range of 15 to 200°C. This detector is also the most resistant to radiation damage out of the group since it is a gas and not a plastic scintillator or solid-state detector. Its intrinsic efficiency is much lower than the other detectors considered, a quality desired for high activity sources such as spent fuel. Therefore, less rigorous shielding will be necessary for protection and dead time optimization. There are, however, some downfalls to this detector. It is subject to electronic noise caused by the high-voltage power supply, acoustic/microphone noise and the geometry of the electrodes causing excessive electrical capacitance [13]. Brookhaven National Lab is working to overcome these problems by using a better high-voltage power supply, and using a new multi-anode design to help improve the energy resolution and reduce the sensitivity to acoustic/microphonic noise of large volume HPXe ionization chambers [13]. Some researchers claim that the high-purity xenon needed for HPXe detectors is a lot lower than that of HPGe and CZT, at \$1/g as opposed to \$50/g for HPGe and \$300/g for CZT [23]. However, they are not currently mass produced, making it much more difficult to procure which would drive up production costs.

Although I showed that NaI(Tl) is potentially not the best ideal detector for measuring gamma radiation from a spent fuel assembly, it is the easiest detector system to acquire, most cost effective, and is not susceptible to large electronic noise interferences. By choosing this detector, my work will also essentially eliminate the limitations of HPGe systems in water based environments. Although NaI detectors produce much lower resolution spectra in comparison to HPGe detectors, this issue will be largely solved through the use of a novel post-processing algorithm, SmartID. The SmartID algorithm is designed to extract detailed spectral information from a low resolution detector spectrum such as one from CsI or NaI. Using transport results adapted to the data, it enables one to screen out all Compton and other spectral interference features with an optimized analysis to unveil gamma photopeaks across the energy spectrum. Figure 2.3 shows an example NaI(Tl) gross spectrum of shielded

weapons grade plutonium (WGPu) and the background spectrum for the measurement; note how the resulting photopeaks are rendered from the region. The background was subtracted out, and SmartID subsequently extracted each photopeak to reveal the many red photopeak lines representing full energy peaks normally masked by Compton pileup. The spectra gathered from the irradiated fuel experiment will be similarly processed in a few seconds by SmartID to determine the key fission products discerned with nuclide attribution in an underwater environment.

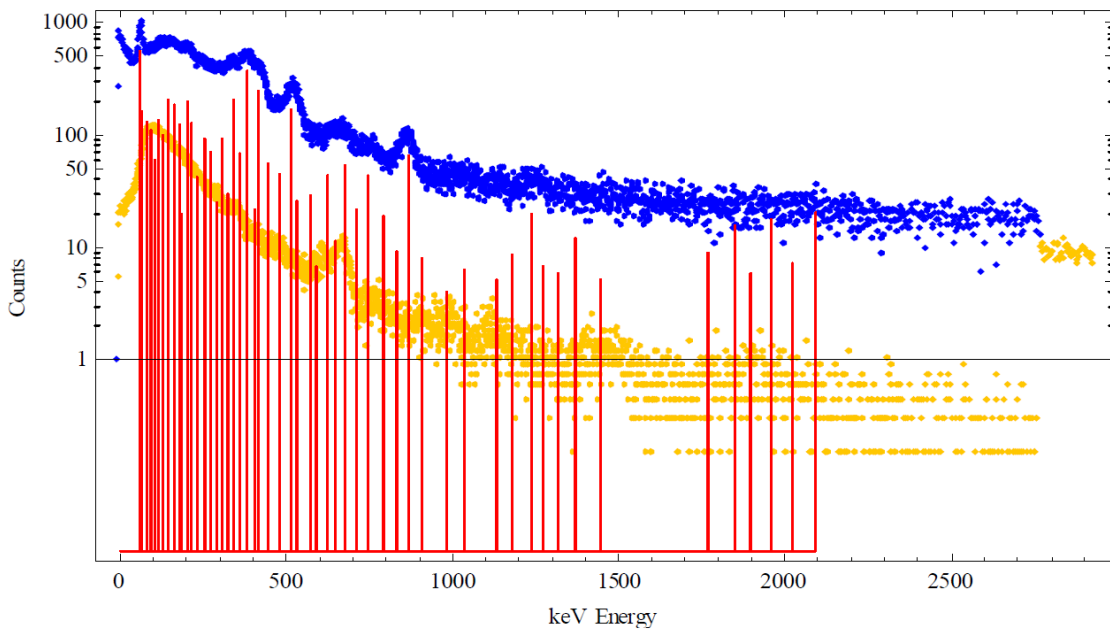


**Figure 1.4:** Correctly identified shielded WGPu spectrum in air by SmartID post processing algorithm. The measured spectrum is shown in blue and the background is shown in yellow. Gamma emissions are identified by the red vertical lines. [24]

A second challenge I faced in this work was to profile a system that will provide limited disruption to normal plant refueling operations for forensics, safeguards, or simple burnup assessment purposes. Power plants must pay attention to minimizing costs, meaning any time they spend not producing power and conducting normal plant

operations, they are losing money. If a detector system is built that can determine relative isotopic content but significantly inhibits refueling operations, utilities and governments will not see this as an acceptable option that is cost effective with enough benefit. Therefore, my work follows a detector design that will ensure there will be a relatively small impact to plant operations while still providing additional cost saving benefits. The spectrum from a fuel bundle can be collected while fuel is being removed from the reactor core to be placed into the spent fuel pool.

Further challenges arise in measuring the gamma spectrum for spent fuel assemblies with short cooling times. Detector dead time is a prominent issue when trying to make reasonable measurements. Collimator material, size, and geometry depend on detector efficiency and radiation exposure limitations. It is important to make sure a detector system is not heavily weighed down by shielding/collimation. A proper support structure is necessary to hold the detector and collimation in place. I considered collimation constructed from tungsten with a 1 mm pin hole in order to stop a majority of the high energy gammas, and limit detector dose and field of view.

The greatest challenge of this dissertation effort was the analysis of data produced by SmartID and coupling that with deterministic transport adjoint importances to estimate fuel content, specifically relating to plutonium. This is a difficult task that has not been demonstrated previously, but I have been successful in developing a method to alias scintillator detected SNM photon peaks identified in SmartID to the actual activity for each nuclide identified at specific locations in the 3-D fuel assembly.

This dissertation outlines the many integral parts to meeting this challenge. In Chapter 2 I discuss in detail the theory behind the SmartID post-processing algorithm, how this algorithm has been updated to consider an underwater spent fuel scenario. In Chapter 3 I present how SmartID performed with experimental spectra data, and in Chapter 4 I show MCNP simulations developed for a complicated spent nuclear fuel assembly. Chapter 5 details the deterministic transport models generated, and how I can

use the adjoint to estimate burnup from key gamma emissions. All of these parts are fully integrated to show how I can achieve an estimate of plutonium in the spent nuclear fuel. This research has the potential to greatly contribute to the many needs of nuclear forensics, safeguards, and facility operations as specified earlier.

### 1.5 References

- [1]. BORELLA, A., VAN DER MEER, K., FLACHET, F., CAUWENBERGH, K., and DELPORTE, R., "Towards an improved burnup measurement equipment for spent fuel assemblies in Belgian nuclear power plants," INMM 54<sup>th</sup> Annual Meeting Proceedings, Presented at the INMM Annual Meeting, Palm Desert, CA, 2013.
- [2] CHEATHAM, J., and WAGNER, J., "Review and ranking of NDA techniques to determine plutonium content in spent fuel," UT-Battelle, LLC. Contract DE-AC05-00OR22725.
- [3] TIITTA, J., HAUTAMÄKI, A., TURUNEN, R., ARLT, J., CARRASCO, K., ESMAILPOUR-KAZEROUNI, and SCHWALBACK, P., "Spent BWR fuel characterization combining a fork detector with gamma spectrometry," Report on Task JNT A 1071 FIN of the Finnish Support Programme to IAEA Safeguards. STUK.STUK-YTO-TR175. 2001
- [4] CARUSO, S., MURPHY, M., JATUFF, F., and CHAWLA, R., "Validation of <sup>134</sup>Cs, <sup>137</sup>Cs and <sup>154</sup>Eu single ratios as burnup monitors for ultra-high burnup UO<sub>2</sub> fuel," Annals of Nuclear Energy, vol.34, 2007.
- [5] LEBRUN, A., MERELLI, M., SZABO, J-L., HUVER, M., ARLT, R., and ARENAS-CARRASCO, J., "SMOPY a New NDA Tool for Safeguards of LEU and MOX Spent Fuel." IAEA-SM-367/14/03
- [6] DOYLE, J. Nuclear Safeguards, Security and Nonproliferation: Achieving Security with Technology and Policy. Butterworth-Heinemann., 1<sup>st</sup> Edition. (2008).
- [7] KURIBARA, M. "Spent Fuel Burnup Estimation by Cerenkov Glow Intensity Measurement." IEEE Transactions on Nuclear Science. vol. 41, no 5. 1994.

- [8] REILLY, D., ENSSLIN, N., SMITH, H., and KREINER, S., "Passive Nondestructive Assay Manual," Office of Nuclear Regulatory Research. U.S. Nuclear Regulatory Commission. NUREG/CR-5550. 1991.
- [9] Office of Nuclear Research, Passive Nondestructive Assay of Nuclear Materials (PANDA). U.S. Nuclear Regulatory Commission, NUREG/CR-5550, Washington, March, 1991.
- [10] Nuclear Regulatory Commission, "Operating reactors- what we regulate," <http://www.nrc.gov/reactors/operating.html> (Accessed March 20, 2015).
- [11] BELL, G., and GLASSTONE, S., Nuclear Reactor Theory. Krieger Publishing Co., Malabar, 1985.
- [12] International Atomic Energy Agency, "Safe handling and storage of plutonium," Safety Reports Series, no. 9, Vienna, 1998.
- [13] RUSSO, P.A., and VO, D.T., "Gamma-ray Detectors for Nondestructive Analysis," Los Alamos Technical Report. LA-UR-05-3813. Los Alamos, NM. 2005.
- [14] Canberra, LABR-1.5x1.5-LaBr<sub>3</sub>(Ce) Scintillation Detector. <http://www.canberra.com/products/detectors/pdf/LABR-SS-C38657.pdf> (Accessed March 20, 2015).
- [15] WEISSHAAR, D., "An introduction: gamma rays, detectors, spectrometers," Exotic Beams Summer School, slide 41. MSU, 2011.
- [16] Canberra. "Gamma and X-Ray detection," <http://www.canberra.com/literature/fundamental-principles/pdf/Gamma-Xray-Detection.pdf> (Accessed March 20, 2015).
- [17] PARK, S.H., HA, J.H., LEE, J.H., KIM, H.S., and CHO, Y.H., "Effect of Temperature on the Performance of a CZT Radiation Detector," Journal of the Korean Physical Society, vol. 56, no. 4, pp. 1070-1082. April 2010.
- [18] ZHANG, J., FU, C., MO, X, ZHANG, Z., LI D., and WANG, B., "Effects due to a Pu-C source on a HPGe detector and the corresponding neutron shielding," Chinese Physics C. vol. 35. no.7. Jul. 2011.

- [19] FRANKS, L., and JAMES, R., “Status of Radiation Damage Measurements in Room Temperature Semiconductor Radiation Detectors,” Sandia Report. SAND98-8237. SNL. Albuquerque, NM. April 1998.
- [20] Saint-Gobain. “NaI(Tl) and Polyscin NaI(Tl) Sodium Iodide Scintillation Material,” [http://www.crystals.saint-gobain.com/uploadedFiles/SG-Crystals/Documents/NaI\(Tl\)%20Data%20Sheet.pdf](http://www.crystals.saint-gobain.com/uploadedFiles/SG-Crystals/Documents/NaI(Tl)%20Data%20Sheet.pdf) (Accessed March 20, 2015).
- [21] Saint-Gobain. “CsI(pure) cesium iodide scintillation material,” <http://www.crystals.saint-gobain.com/uploadedFiles/SG-Crystals/Documents/CsI%20Pure%20Data%20Sheet.pdf> (Accessed March 20, 2015).
- [22] ORTEC, “GMX Series coaxial HPGe detector product configuration guide,” <file:///C:/Users/jessicanp/Downloads/GAMMA-X.pdf> (Accessed March 20, 2015).
- [23] GHOSH, V.J., BOLOTNIKOV, A., and ROHATGI, U.S., “A feasibility study exploring the use of high-pressure xenon (HPXe) detectors for the characterization of spent fuel bundles,” Brookhaven National Laboratory, BNL-98177-2012-IR. June 2012.
- [24] YI, C., and SJODEN, G., “SmartID-XP: synthetic scoring scheme for isotope identification,” SmartID-XP manual.

## CHAPTER 2

### SMARTID

#### 2.1 Background

SmartID is a post processing algorithm designed to reveal detailed spectral information from low resolution detectors such as NaI, CsI, or LaBr<sub>3</sub>. This algorithm at its current state is the result of almost a decade of development. It has been rigorously tested and verified for identifying radioactive sources in air, but has not yet been applied to highly complex fuel characterization applications in water. The logic behind extracting photonuclear peaks and aliasing them to specific nuclides is continued and extended here from previous work, however, many challenges arise with changing the detection environment from air to water. Compton scattering has a much more dominant role in the particle transport, significantly altering the gamma spectrum. Additionally, a strong 2.2 MeV gamma peak resulting from (n,  $\gamma$ ) hydrogen interactions with the fission neutrons arises, further complicating nuclide identification. Therefore, I must develop an entirely new detector response function (DRF) database in order to properly enable the algorithm to extract photopeaks in a Compton-rich environment and identify nuclides in water.

##### 2.1.1 Peak Finding

SmartID employs a systematic procedure for discovering and identifying individual energy peaks in a CsI or NaI detector spectrum. It begins by removing noise in the measured spectrum through an adaptive Chi-square called 'ACHIP' smoothing algorithm [1]. This is especially important for short counting times or low count spectra. The Chi-square analysis was selected over a weighted average analysis in order to limit



further spectral resolution reduction. This method determines whether or not the differences between counts in neighboring channels are statistically significant or if they are electronic noise. SmartID conducts this analysis based on a user-specified test parameter,  $\alpha$ , which is a significance value spanning from 0.005 to 0.995. This value provides the limit at which the differences in counts between neighboring channels are considered significant. The process begins by looking at three channels; the center channel is the channel of interest for noise removal. A least squares fit is utilized to create a parabolic model fitting the 3 points [1]. Once these 3 points are fit, additional points are considered and Chi-square values are computed. If the Chi value is greater than the Chi value for the specified  $\alpha$  statistical significance parameter and corresponding degrees of freedom, the previous Chi-square satisfying model is applied [1]. This ensures that an apparent “peak” in the spectrum is a “true feature” while mitigating resolution degradation [1]. Additionally, a smooth parabolic least squares approach is also implemented in order to mitigate “chopping” effects [2]. Figure 2.1 depicts a NaI(Tl) spectrum before denoising and after denoising. Note how the peak resolution remains unchanged.

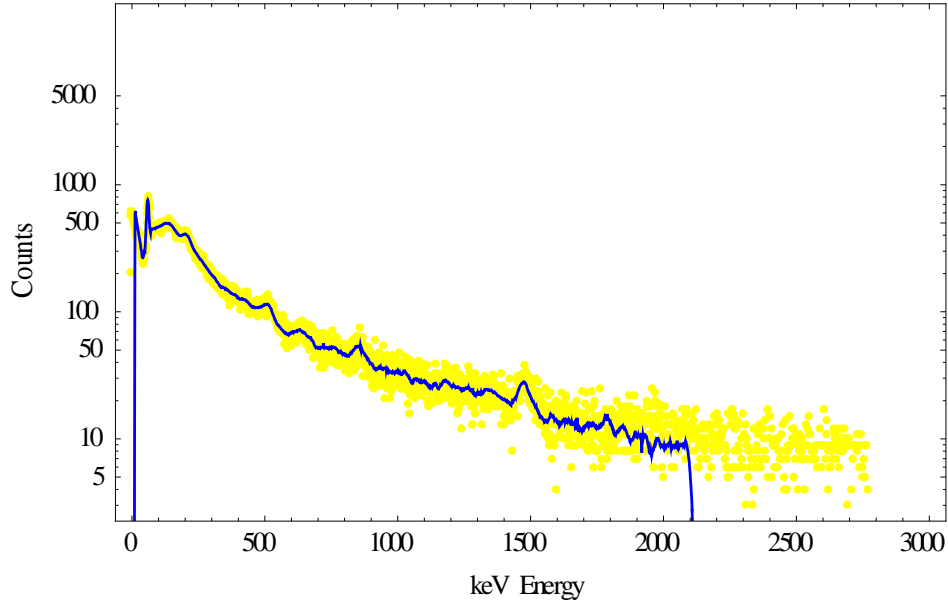


**Figure 2.1:** Collected spectrum before (yellow points) and after (blue line) the ACHIP denoising procedure.

Once both the raw collected spectrum and background spectrum have been denoised, the time scaled and denoised background spectrum is subtracted from the gross collected spectrum. Included in SmartID is the option to weight the background spectrum by a *Background Significance Factor* in order to increase or decrease the effect background has on the subtracted spectrum. The effect shown by this factor on the signal spectrum is shown by

$$S_s = S_t - F_b S_b \frac{T_s}{T_b} \quad (2.1)$$

Where  $S_s$  is the signal spectrum,  $S_t$  is the total, measured spectrum,  $S_b$  is the background spectrum,  $T_s$  is the signal spectrum counting time,  $T_b$  is the background spectrum counting time, and  $F_b$  is the background significance factor. By default,  $F_b$  is set equal to one. This allows the user to adjust the background in order to see what information can

still be discerned from the spectrum if the location for measurement were to change to an area with greater background, such as at a higher altitude.

Once the signal spectrum is computed, the search for photopeaks commences. SmartID searches for gamma peaks between the energies 20 keV and 3 MeV. The peak search begins at 3 MeV and scans progressively lower energies. Once a photopeak is located, SmartID determines the corresponding detector response, accounting for the various physics effects taking place. The detector responses are precomputed by Monte Carlo simulations, and are included in a data library for the SmartID code. MCNP5 was the selected Monte Carlo code for the simulations.

The Monte Carlo computational method as implemented in the MCNP code is currently the most extensively used, straight forward technique for particle transport. It has been widely demonstrated as being capable of representing very complex geometries in a rigorous manner using robust particle physics by statistically tracking the outcome of individual particle histories [3]. MCNP can be used in several transport modes, and was developed with over 500 person-years of effort at Los Alamos National Laboratory. It operates in neutron only, photon only, electron only, and combined neutron-photon transport problems where the photons are produced by neutron interactions, neutron-photon-electron interactions, photon-electron, or electron-photon interactions.

The detector response simulations, now referred to as Detector Response Functions (DRFs), were generated using photon only mode in MCNP. They are included in the SmartID package for multiple types of detectors and shielding configurations, including, but not limited to 2" x 2" NaI(Tl) detector in air, 4" x 4" NaI(Tl) detector in air, and a CsI detector in air. For each detector scenario, 61 DRFs were generated for individual gamma emissions. The energy emissions were chosen at 50 keV intervals starting at 50 keV and ending at 3 MeV, with an additional emission at 20 keV. However, it is important to note that the peaks identified in SmartID will fall in between many of these intervals and will have a response somewhere in between that of the

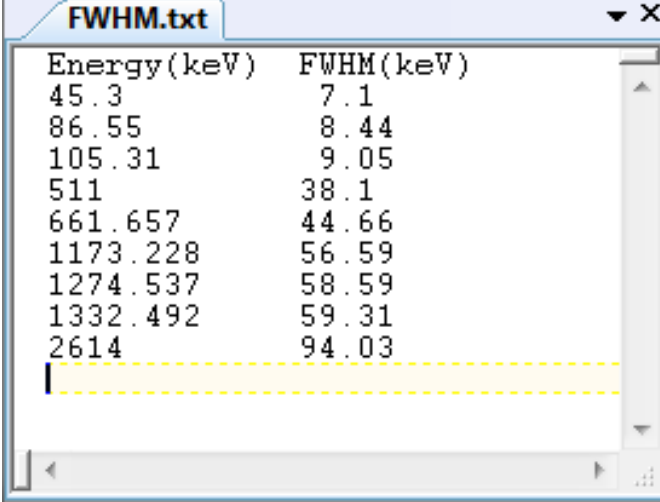
nearest two DRFs. Instead of computing many more DRFs to account for every keV gamma emission, a special interpolation procedure is incorporated to generate the expected response. A simple interpolation is not sufficient to accurately portray every physics interaction taking place, and the algorithm must conserve these interactions. Depending on the incident gamma emissions energy, different features will arise. For example, single escape peaks and double escape peaks only occur when the incident gamma is greater than 1.022 MeV. Details on these types of interactions and features will be described in more detail later on in the Section 2.2.

Spectral information occurring near these features is linearly interpolated based on how far from the feature the point of interest is. For example, consider a gamma emission with an energy of 460 keV. The two closest DRFs in SmartID's library are for 450 keV and 500 keV. Arbitrarily choosing an energy in the spectrum, 180 keV, it is seen that this occurs 116 keV from the Compton edge. Therefore, the detector responses compared for the 450 keV and 500 keV are also predicted to occur also at energies 116 keV from their respective Compton edge. These resulting energies are 181 keV and 175 keV respectively. Now that the comparison energies are determined, a simple linear interpolation can be applied to determine the response,  $f$ , at 180 keV for a 460 keV gamma emission shown by

$$f_{460}(180 \text{ keV}) = \left( \frac{f_{500}(181 \text{ keV}) - f_{450}(175 \text{ keV})}{500 \text{ keV} - 450 \text{ keV}} \right) (460 \text{ keV} - 450 \text{ keV}) \quad (2.2)$$

where  $f_{460}(180 \text{ keV})$  is the number of counts per second at 180 keV for a 460 keV gamma emission. Similarly,  $f_{500}(181 \text{ keV})$  is the number of counts per second at 181 keV for a 500 keV gamma emission, and  $f_{450}(175 \text{ keV})$  is the number of counts per second at 175 keV for a 450 keV gamma emission. Once an identified energy peak's full detector response is determined, Gaussian broadening is applied to account for electronic

“detector” broadening. The relative amount of broadening applied for each energy is determined from FWHM data incorporated in a file to be read by SmartID. The “FWHM.txt” file properly accounts for the specific detector properties, and a new file must be created for every new spectrum collected when the energy calibration has changed. This file contains full width half maximum (FWHM) data that can be determined from known calibration sources. Figure 2.2 shows how this file is organized.



Energy (keV)	FWHM (keV)
45.3	7.1
86.55	8.44
105.31	9.05
511	38.1
661.657	44.66
1173.228	56.59
1274.537	58.59
1332.492	59.31
2614	94.03

**Figure 2.2:** SmartID “FWHM.txt” file.

This information is applied in the following equation to determine the Gaussian distribution,

$$G(E; \mu, \sigma) = \frac{1}{\sigma\sqrt{2\pi}} e^{-\frac{(E-\mu)^2}{2\sigma^2}} = \frac{2.35}{FWHM\sqrt{2\pi}} e^{-\frac{2.35^2(E-\mu)^2}{2FWHM^2}} \quad (2.3)$$

where  $\mu$  is the mean or energy of the peak,  $\sigma^2$  is the variance,  $E$  is the energy, and  $G$  is the probability density. To determine the appropriate counts at an energy,  $E$ , the following is applied,

$$C_{new}(E) = \sum_i C_{old}(i)G(E; i, \sigma_i) \quad (2.4)$$

where  $C_{new}$  is the new number of counts at energy  $E$ , and  $C_{old}$  is the old number of counts at energy  $i$  [4].

After the full detector response is transformed, it can be subtracted from the measured spectrum to unveil additional hidden photopeaks. This process is repeated for the remaining counts until no more peaks are found in the spectrum. Figure 2.3 summarizes the procedure of how SmartID identifies energy peak information from an initial raw spectrum.

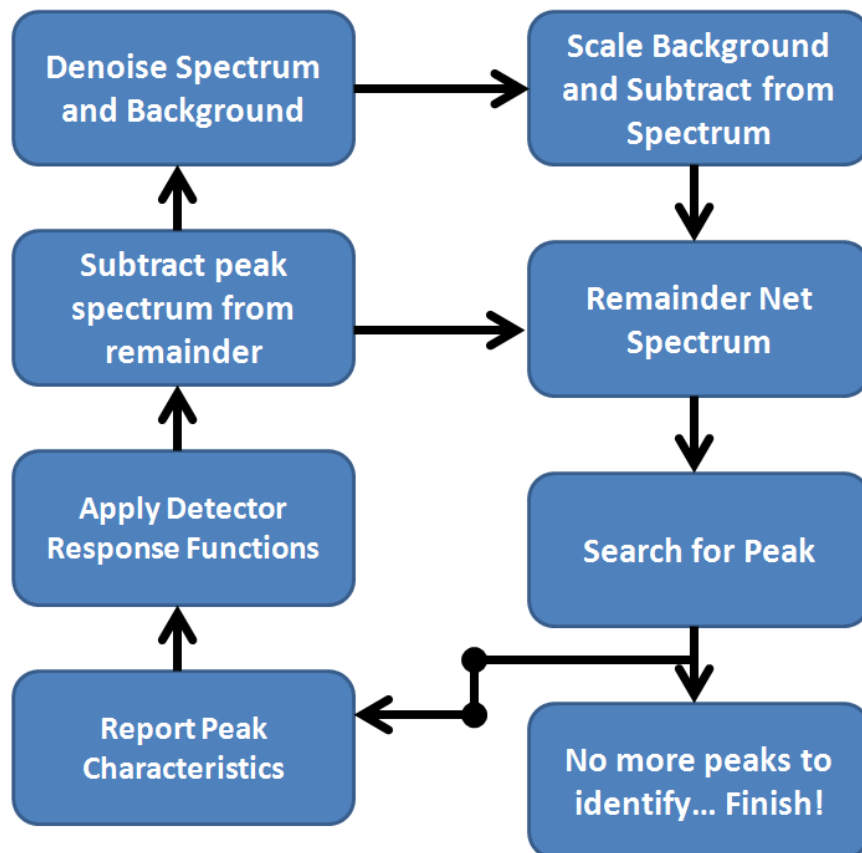


**Figure 2.3:** Paradigm of the ASEDRA peak identification algorithm [4].

Once all peaks are identified, additional options selected or adjusted in the SmartID input will determine how isotope energy emissions will be matched to these peaks. Emissions within a specified tolerance of an identified peak are considered a match for the peak. This tolerance is determined by the SmartID user and can be set such that any emission within the tolerance is considered a match, or set to determine the most likely scenario within a maximum set tolerance. In the latter method, a search begins with a tolerance of 0.01 (1% energy window), and gradually increases by given step size (0.005 by default) until the maximum tolerance is reached or an isotope is scored greater than the specified high correlation threshold, or the highest scored isotope does not change when increasing tolerance. Details on how nuclides are scored are described later on in the following section. On occasion, one peak may be identified as two peaks. In order to resolve this scenario, a *blur coefficient* is specified to determine whether or not two peaks should actually be combined into one. This coefficient is by default set to 0.15, which essentially combines gamma lines that are within the energy window of the energy's FWHM multiplied by the blur coefficient. The higher the coefficient, the greater the energy range for combining peaks.

### **2.1.2 Nuclide Scoring**

Once the algorithm has completed its search for peaks, it compares the peaks identified with emission energies from various isotopes in a database. The SmartID isotope database consists of 204 nuclides plus gamma emissions from (n, $\gamma$ ) interactions with hydrogen, Ge-Kesc, and W-Kalpha. The isotopes are listed in the library along with their emissions, probabilities of decay, half-life, and classification. Isotopes are classified by fission product, special nuclear material, medical isotope, daughter product, or parent of important nuclides, such as  $^{239}\text{Pu}$ .

SmartID identifies the peaks through a synthetic scoring scheme designed by a combination of a base score and bonus scores. Equation 2.5 shows how these scores

contribute to an overall total score which identifies the most likely nuclides present in a spectrum.

$$S_t = A_0 + A_1 + A_2 + A_3 = S_b + \alpha_1 S_1 + \alpha_2 S_2 + \alpha_3 S_3 \quad (2.5)$$

where  $S_b$  is the base score with  $0 \leq S_b \leq 1$ ,  $S_{\#}$ 's are bonus scores,  $\alpha_{\#}$ 's are bonus score weights, and  $S_t$  is the total score [4]. Additionally, the total score is multiplied by a scaling factor of 100 to achieve the final score for nuclide identification.

The base score is computed from an equation relating the number of peaks matched to the number of emissions of a given isotope shown by,

$$S_b = \frac{\tan^{-1} \frac{\# \text{ of matched peaks}}{\# \text{ of emissions}}}{\frac{\pi}{4}} \quad (2.6)$$

This equation is further developed by taking into account how the emissions from a given nuclide are actually released. For example a  $^{60}\text{Co}$  nuclide emits two gammas at the same rate, but a  $^{95}\text{Nb}$  nuclide emits three gammas at different fractions of yield of decay. For example the 765.81 keV emissions for  $^{95}\text{Nb}$  only account for 99.8% of the total decay rate of the nuclide. Equation 2.7 shows how these branching ratios are taken into consideration when computing the base score,

$$S_b = \frac{\tan^{-1} \frac{\sum BR_j D_j M_j}{\sum BR_i D_i}}{\frac{\pi}{4}} \quad (2.7)$$



where  $B_i$  is the branching ratio (yield) for the  $i^{\text{th}}$  gamma emission, and  $D_i$  is the detectability for the  $i^{\text{th}}$  emission [4].  $M_j$  is the matching factor for the peak matching emission.

*Detectability* is based purely on the properties of the detector and possible shield in place, and is calculated for each energy emission. The intensity of a gamma emission will exponentially decrease as it passes through the detector in a similar manner as it decreases through a shield. This is depicted in Figure 2.4.

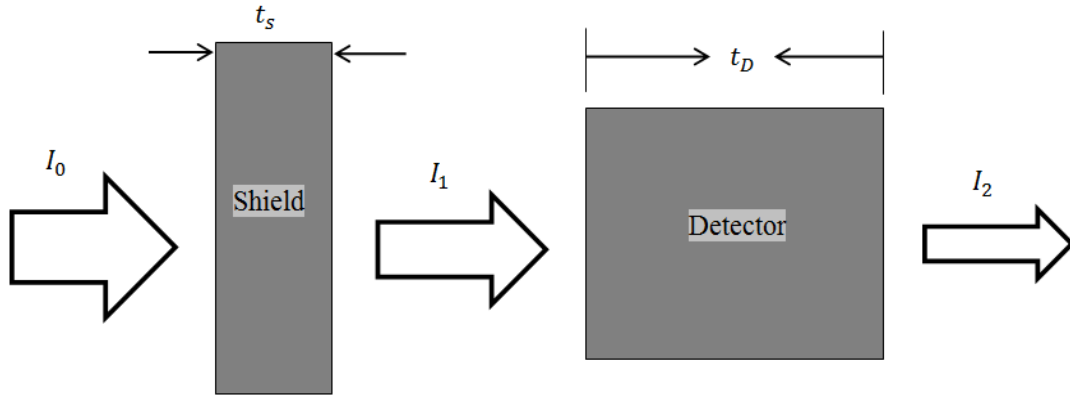


**Figure 2.4:** Detectability for a typical detector with shielding [4].

Equation 2.8 shows how the detectability is calculated as an estimate of the detector and possible shield attenuation properties.

$$D(E_i) = \left( \frac{\mu_{D,i}}{\sigma_{D,i}} \right) \exp(-\sigma_{S,i}t_S) [1 - \exp(-\sigma_{D,i}t_D)] \quad (2.8)$$

where  $E_i$  is the  $i^{\text{th}}$  emission energy;  $\mu_{D,i}$  is the  $i^{\text{th}}$  detector photoelectric attenuation coefficient at energy  $E_i$ ;  $\sigma_{D,i}$  is the  $i^{\text{th}}$  detector total macroscopic cross section at energy  $E_i$ ;  $\sigma_{S,i}$  is the shielding total cross section at energy  $E_i$ ;  $t_D$  and  $t_S$  are the detector characteristic size and shielding size, respectively [4].

The final variable,  $M$ , in Equation 2.9 relates how much the emission energy is aligned with the peak energy found in the spectrum. This is computed by

$$M_j = \begin{cases} A + (1 - A) \left(1 - \frac{\delta}{\varepsilon}\right), & \delta < \varepsilon \\ 0, & \delta \geq \varepsilon \end{cases} \quad (2.9)$$

where  $\delta = \frac{|E_{emission} - E_{peak}|}{E_{peak}}$ , and  $\delta$  is the relative difference between the emission  $j$  energy and a given peak energy,  $A$  is a pre-defined constant (by default,  $A=0.85$ ), and  $\varepsilon$  is a user-defined tolerance to identify matching peaks [4]. This tolerance refers to the energy window. For example, if  $\varepsilon = 0.02$ , then the energy window spans from  $0.02 \times E$  to  $1.02 \times E$ .

In addition to the base score, three bonus scores are computed to account for the number of matched peaks, peak height score, and an emission/peak height distribution preference. The first bonus score, similar to the base score, relates the number of peaks identified to the total number of emissions a given nuclide. The relationship is shown by

$$A_1 = \alpha_1 S_1 = \alpha_1 (N_m^k - 1) \left(1 + \frac{N_m}{N_e}\right) \quad (2.10)$$

where  $N_m$  is the *number of matched emissions*,  $N_e$  is the *total number of emissions*, and  $\alpha_1$  is a fixed factor to adjust the contribution of the bonus score to the total score [4]. The power coefficient,  $k$ , is designated constant set by the user. The default setting is  $k=1.8$ , which gives increasing score emphasis as the number of matched peaks increases. This scoring method helps to identify high emission nuclides such as fission products. For example,  $^{132}\text{I}$  has 173 emissions listed in SmartID's nuclide library. It is nearly impossible for SmartID to identify every emission in a spectrum, especially at the lower

energies. Therefore, this scoring technique helps compensate for number of missing emissions when a nuclide has a large number of matched emissions.

The second bonus score accounts for the number of counts expected in the full energy peak for each emission. There are many cases where multiple nuclides have emissions within the window energy range of the identified peak, but this does not necessarily mean every nuclide is present. Introducing a scoring technique to account for the peak height helps identify which isotopes are more likely present. The bonus score is calculated by

$$A_2 = \alpha_2 S_2 = \alpha_2 \frac{\sum F_j}{\sum F_k} \quad (2.11)$$

where  $\alpha_2$  is a fixed multiplier to adjust the contribution of this bonus score relative to the total score, and  $F$  is defined as the adjusted peak height

$$F_k = \frac{f_k}{D_k} \quad (2.12)$$

where again,  $D$  is the detectability, and  $f$  is the number of counts attributed to an identified peak,  $k$  [4].

The final bonus score takes into account the emission to peak height distribution preference. Much like the second bonus score, where detectability of a peak is considered, the emission branch distribution is considered to determine how well a nuclide is matched to an identified energy peak. This is calculated by

$$A_3 = D_{KL} = \sum \hat{F}_i \ln\left(\frac{\hat{F}_i}{\hat{B}_i}\right) \quad (2.13)$$

where  $\hat{F}_i$  and  $\hat{B}_i$  are the normalized adjusted peak height and branch ratio value, respectively. This bonus score is a function of the Kullback–Leibler divergence of the two normalized distributions ( $\hat{B}$  and  $\hat{F}$ ) [4]. The lower the divergence (meaning the distributions agree with each other better), the higher the bonus score.

## 2.2 Enhancements for Water Stored Fuel

In order to properly capture the complex interactions taking place in an underwater fuel storage scenario, I employed computational modeling. I developed MCNP simulations to show the behavior of photons emitted from a spent fuel assembly when they reach and interact with a NaI(Tl) detector submerged in water. The MCNP models were created for a NaI(Tl) detector placed 40 cm distal from a Westinghouse PWR fuel assembly. Figure 2.5 shows the MCNP model geometry created for the DRF simulations.

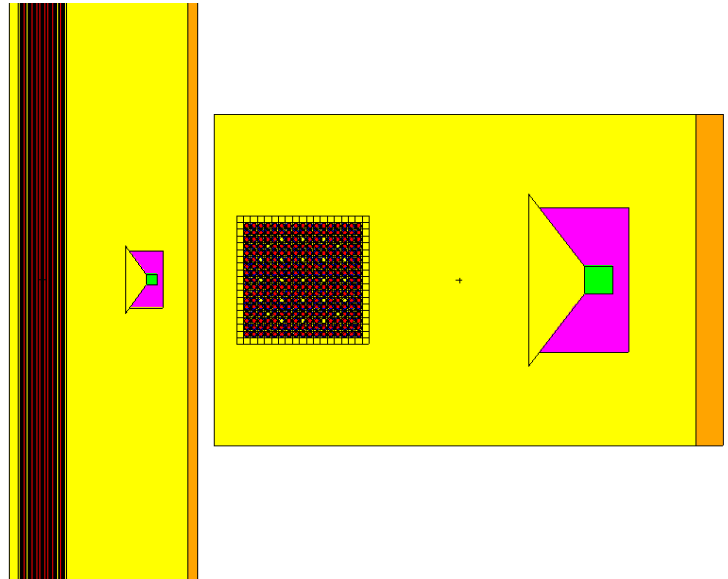


**Figure 2.5:** MCNP model geometry for a Westinghouse 17x17 PWR fuel assembly in water (yellow) with a NaI(Tl) detector (green) collimated by tungsten shielding (pink) in front of a concrete wall (orange). The left image shows a cross section along the y-axis, and the right image shows a cross section along the z-axis.

DRFs were generated from pulse height simulations in MCNP. In a real spent fuel scenario, the detector would need to be highly shielded. The original design simulated was to completely surround the detector with tungsten shielding collimated by a small, 1 mm in diameter, pinhole. However, in order to achieve reasonably good counting statistics for the Monte Carlo simulations (regarding model efficiency), the tungsten collimation was adjusted to allow for a wider field of view. The collimation was opened up at an angle equal to the average Compton scattering angle for a 1 MeV photon. This required the calculation of the average scattering angle for 1 MeV photons, determined to be  $53.2424^\circ$ . Details regarding Compton scattering for this application are shown by Figure 2.6.

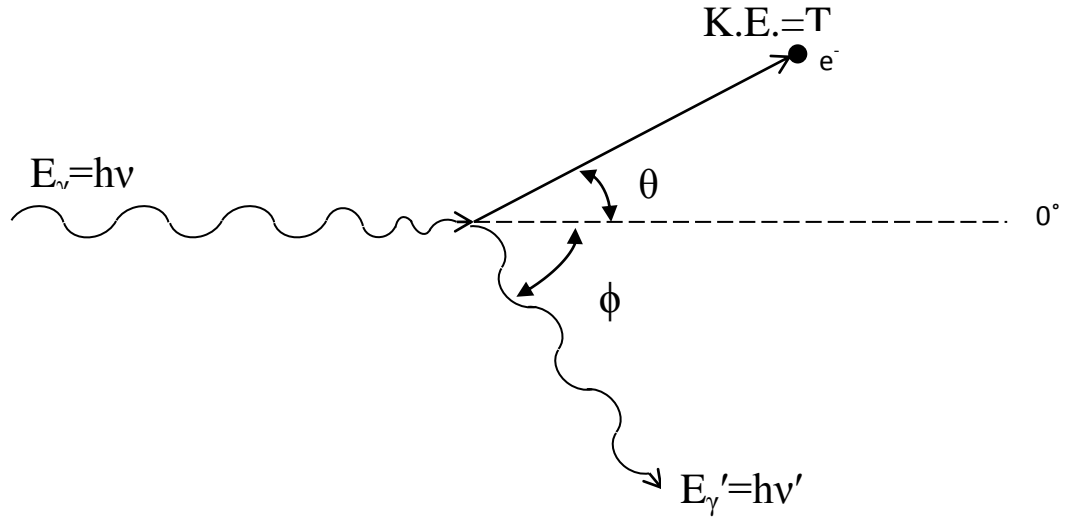


**Figure 2.6:** Compton scattering interaction.

The new photon energy can be solved for by

$$E_\gamma' = \frac{E_\gamma}{1 + \frac{E_\gamma}{511}(1 - \cos \phi)} \quad (2.14)$$

Where  $E'_\gamma$  is the Compton energy of the photon,  $E_\gamma$ , is the incident energy of the photon, and  $\varphi$  is the Compton scattering angle [4].

The source definition is set up to show the detector response from a single gamma emission. Appendix A shows the MCNP input for a 200 keV gamma emission. As described in Chapter 2.1.1, DRFs were generated for individual gamma emissions at 50 keV intervals. However, since the medium for gamma transport has changed from air to water, the gamma emissions with low energies are much less likely to reach the detector. Therefore, I only included gamma emission intervals starting at 100 keV and ending at 3 MeV for a total of 59 DRF cases. Figures 2.7, 2.8, 2.9 and 2.10 show four gamma energies chosen to represent the typical gamma spectrums detected by NaI(Tl) in the configuration discussed for producing the DRFs.

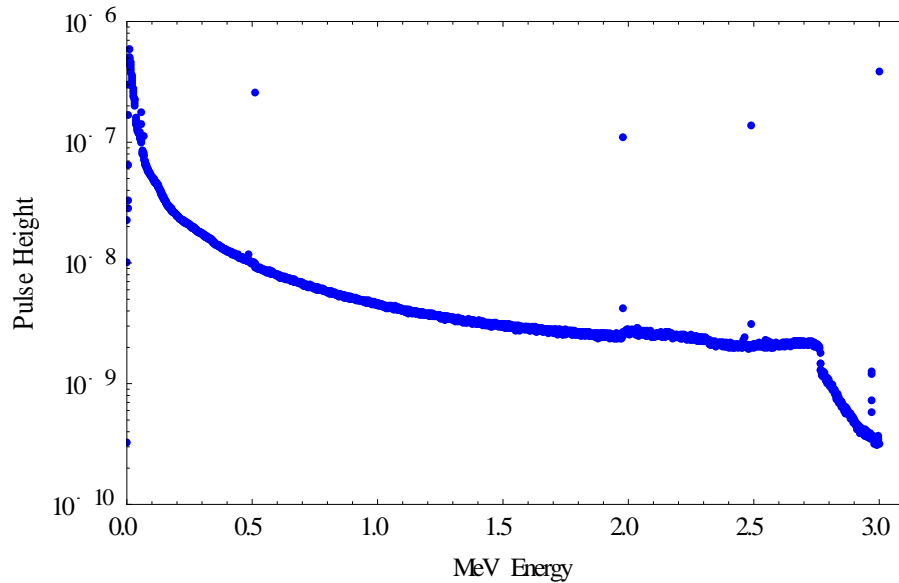


**Figure 2.7:** 3.0 MeV incident gamma MCNP pulse height spectrum with detector 40 cm from source in water. Average and maximum 1-sigma errors were 1.71% and 3.82%, respectively for  $1 \times 10^{12}$  particle histories.

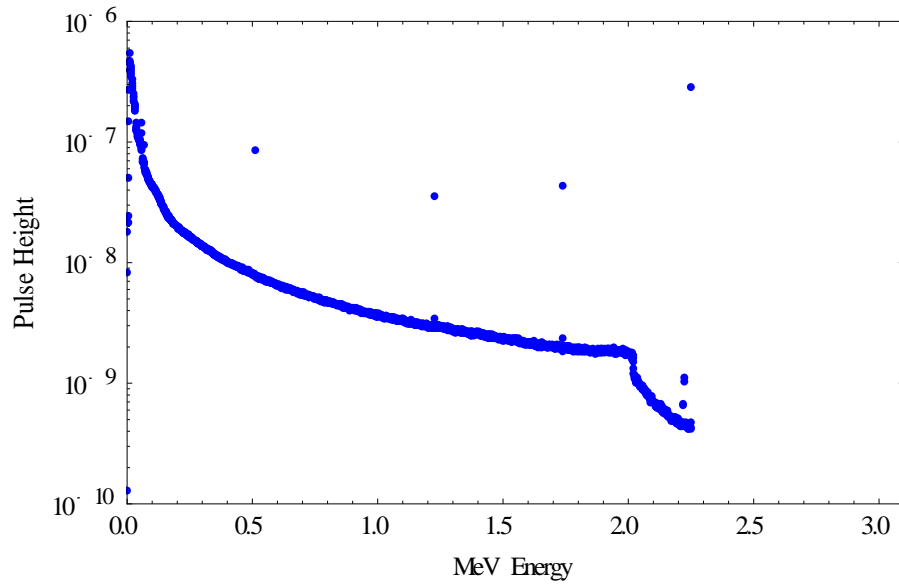


**Figure 2.8:** 2.25 MeV incident gamma MCNP pulse height spectrum with detector 40 cm from source in water. Average and maximum 1 sigma errors were 1.57% and 3.05%, respectively for  $1 \times 10^{12}$  particle histories.

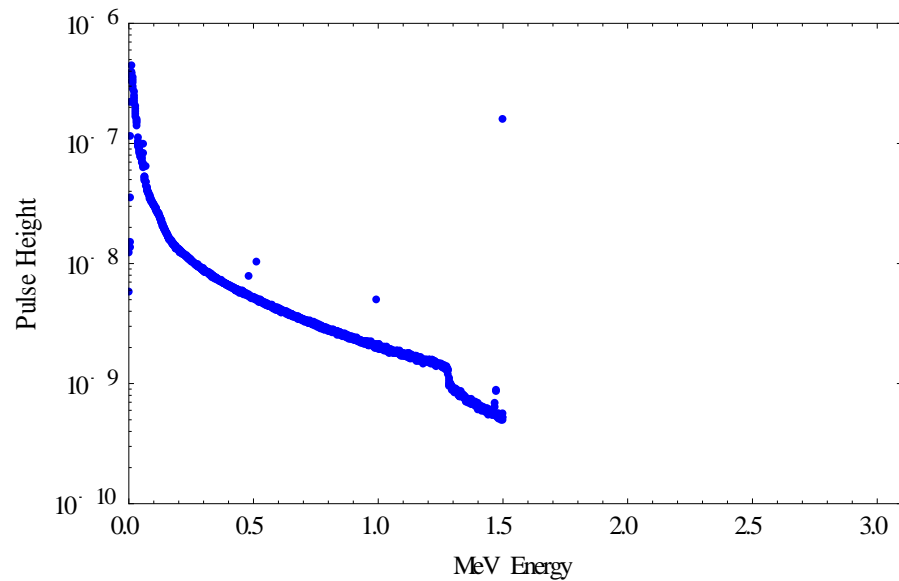


**Figure 2.9:** 1.50 MeV incident gamma MCNP pulse height spectrum with detector 40cm from source in water. Average and maximum 1 sigma errors were 1.50% and 2.74%, respectively for  $1 \times 10^{12}$  particle histories.

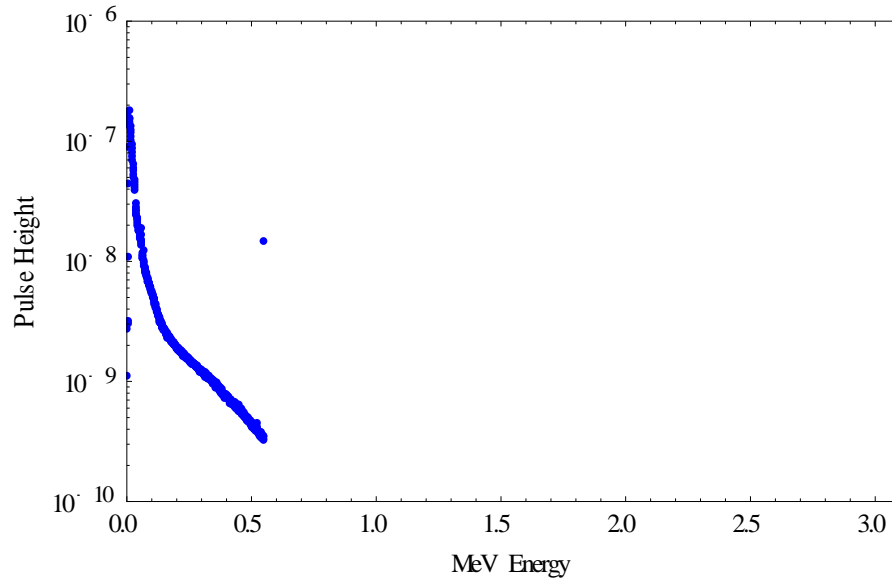


**Figure 2.10:** 0.55 MeV incident gamma MCNP pulse height spectrum with detector 40 cm from source in water. Average and maximum 1 sigma errors were 1.98% and 3.66%, respectively for  $1 \times 10^{12}$  particle histories.

These four energies were selected to illustrate how with increasing photon energy, additional peaks with respect to the energy of interest show up in the energy spectrum. These additional peaks are a result of different interactions taking place with the high energy photons and the low  $Z$  material. Although it is much less likely than Compton scattering, pair production can occur when the incident photon energy is sufficiently high ( $>1.02$  MeV). This reaction results in the complete disappearance of the photon, while at the same time, the creation of an electron-positron pair. The electron and positron are only able to travel a few millimeters before losing all of their kinetic energy; therefore, they never leave the detector and the energy deposited in the detector is the  $2m_0c^2$  less than the energy of the incident photon [5]. This is evident in Figure 2.9, where the 1500 keV incident photon occasionally undergoes pair production resulting in a peak in the spectrum at 480 keV, and in Figure 2.8 where the 2250 keV incident photon produces an additional peak in the detector at 1230 keV. This is referred to as the *double escape peak*



since both annihilation photons escape from the detector. A *single escape peak* can also occur when only one annihilation photon escapes while the other is absorbed in the detector [5]. This results in a peak at  $m_0c^2$  less than the energy of the incident photon. A third phenomenon that is apparent with incident gamma energies greater than 1.02 MeV is annihilation or combination with a normal electron of the positron in the detector. If this occurs, both electron and positron disappear, and are replaced by two annihilation photons with an energy of  $m_0c^2$  (0.511 MeV) [5]. Equations 2.14 to 2.18 summarize these effects.

$$E_{peak} = E_{emission} \quad (2.15)$$

$$E_{S.E.} = E_{emission} - 511, \text{ for } E_{emission} > 1.022 \text{ MeV} \quad (2.16)$$

$$E_{D.E.} = E_{emission} - 1,022, \text{ for } E_{emission} > 1.022 \text{ MeV} \quad (2.17)$$

$$E_{backscatter} = \frac{511}{2 + \frac{511}{E_{emission}}} \quad (2.18)$$

$$E_{ComptonEdge} = E_{emission} - E_{backscatter} \quad (2.19)$$

where  $E_{peak}$  refers to the incident gamma emission,  $E_{emission}$ , from a source.  $E_{S.E.}$  is the energy of the single escape peak,  $E_{D.E.}$  is the energy of the double escape peak.

$E_{backscatter}$  is the energy of the incident gamma emission when it is backscattered. This is derived from equation 2.14 when  $\varphi$  is  $180^\circ$ .  $E_{ComptonEdge}$  refers to the gamma energy where the Compton edge begins [4].

Referring back to Figures 2.7 to 2.10, the MCNP models with pulse height tallies show the DRFs are consistent with all necessary nuclear physics and interactions. These models will be used to update the SmartID algorithm so that the Compton effects, along with other radiation physics events in the water will be removed, leaving only the key peak photoelectric related information to remain, as is consistent with the SmartID algorithm.

### **2.2.1. Running SmartID**

Post-processing spectra with SmartID is a relatively simple task. Only five files are needed. These include a spectrum file in “.Spe” form, a FWHM file “FWHM.txt”, an energy calibration file “Energy.txt”, a background spectrum file in “.Spe” form, and an input file “smartid.inp”. The “Energy.txt” file is setup with the channel number in the first column followed by the corresponding energy in units of keV in the second column. The “FWHM.txt” file is set up in a similar manner. The first column lists the energy in units of keV for a peak, and the second column lists the corresponding width of the FWHM in units of keV. Figure 2.11 shows the “smartid.inp” input file needed to run the program.

```

1 Spectrum File
2 "spectrum.Spe"
3 Background File
4 "bkgd.Spe"
5 Background Significance Factor
6 1.0
7 Max Energy FWHM calibration table
8 ".FWHM.txt"
9 Low energy tailing: height ratio, FWHM in keV
10 0.2500000 23
11 Aliasing Factor (-1 diablse, >0 elim pk w/in fract FWHM)
12 -1
13 Energy Calibration Tabl
14 "Energy.txt"
15 Chi-squared threshold
16 -1
17 AlphaI for adaptive chi
18 0.005
19 Dector response function (DRF) type (0-5=NaI, 6=HPGe, 7-8=CsI, 9=Water)
20 9
21 Rejection Threshold (minimum peak height)
22 3
23 Relative channel threshold percent of total spectrum in a channel
24 1
25 Scattered counts scale factor
26 1.0
27 smartid paramethers: low energy cutoff (MeV)
28 0.100
29 high energy cutoff (MeV)
30 3.0
31 min halflife unit (ignore smaller than s=second m=minute h=hour d=day y=year)
32 s
33 detector material (3=NaI, 4=CsI 5=LaBr3 6=SrI2)
34 3
35 mean detector thickness (cm)
36 5.080
37 shield material (1=Fe, 2=Pb, 0=uncertain--iterate)
38 0
39 shield thickness (cm,<0:iteratively search for optimum thickness <absolute value)
40 -5
41 tolerance ratio (pk vs emiss E; <0:fixed value; >0:adaptive up to val)
42 0.01
43 blur coefficient (combine gamma lines if closer than FWHM*blur)
44 0.01
45 energy mismatch weight
46 1.0
47 output file
48 "spectrum.out"
49 correlation threshold (high/moderate/low setpoints)
50 108 99 50
51 tol_start, tol_step, iso_range (iterate tol ratio)
52 0.001 0.005, 3

```

**Figure 2.11:** Input file, “smartid.inp,” SmartID utilizes for post-processing. Each line numbered for description.

Many of the lines are self-explanatory, however, each line will be explained along with options for clarification. Lines 1 and 2 point to the location of the spectrum file in “.Spe” format to be post-processed. Lines 3 and 4 refer to the background spectrum and points to its location. Lines 5 and 6 refer to the background significance factor which is used to increase or decrease the contribution from the background spectrum when subtracting from the gross count spectrum. Lines 7 and 8 point to the location of the

“FWHM.txt” file. Low energy tailing, as listed in lines 9 and 10, refers to low energy regions in the spectrum where the right side of the photopeak has a larger FWHM than the left. The first parameter is the weight of the Gaussian with the larger FWHM, and the second parameter is the larger FWHM in units of keV [6].

Lines 11 and 12 refer to peak aliasing which aliases peaks too close to dominant peaks. This will eliminate these minor incidental peaks and add to the dominant peak. This option helps with the accuracy by decreasing sensitivity to a specific DRF model [6].

The energy calibration is determined from the “Energy.txt” file which is pointed to in lines 13 and 14. Lines 15 and 16 introduce the chi-square threshold option. It is recommended that this option be set to -1 since this refers to the adaptive chi-processed denoising explained in Chapter 2.1.1. If this is chosen, the following lines, 17 and 18, must be included. The alpha setting refers to the rejection criteria used in denoising. The minimum value is 0.005. This can be increased to 0.995. Increasing this value decreases the amount of denoising taking place, but also decreases the risk of removing real features [6].

I introduced the new DRFs into SmartID in lines 19 and 20. Option “9” refers to these new DRFs modeled specifically for a PWR fuel assembly in water. Options 0-5 refer to a NaI detector, but in different configurations and size. Option 0 is for a 2” × 2” NaI detector point source with no shield. Option 1 is similar to option 0 with an added thin iron shield [6]. Option 3 is a 4” × 4” × 16” NaI bottom portal monitor with a small source and no shield. The source is located 140 cm off of the ground and 140 cm from the steel portal monitor box [6]. Option 3 is similar to option 2, but the portal monitor box is located above the lower box assembly. Option 4 is similar to option 2 with an added steel shield. Option 5 is similar to Option 3 with an added steel shield. Option 6 refers to a 3” in diameter by 1” Portable HPGe detector as an option with a point source

and concrete floor [6]. Options 7 and 8 consider a 2" × 2" CsI detector with a point source. Option 8 also includes a small cast-iron scattering plane [6].

The rejection threshold in lines 21 and 22 gives the minimum number of counts that will be accepted as a peak. Peaks found that do not meet the minimum number of counts will be rejected. The relative channel threshold option in lines 23 and 24 helps prevent "leftover" subtracted counts from leading to "false" peaks [6]. This setting has the user input a minimum percentage of the original spectrum at that point that a synthetic peak must represent. It is recommended that this value is set to at least 5% [6].

The scattered counts scaling factor in lines 25 and 26 lets the user input the degree upon which scattered counts are associated with a full energy photopeak. For example, inputting a value of 2 would double the amount of scattered counts [6].

Lines 27 and 28 give the user the option for the user to input the lowest energy SmartID will consider for peak identification, whereas lines 29 and 30 show the option for the highest energy considered. The maximum is currently 3.0 MeV. The nuclides SmartID will consider for peak attribution are selected by the minimum highlife unit considered which is inputted in line 32. The detector material is selected in lines 33 and 34. This should match with the detector response function chosen in line 20. The corresponding detector thickness is referred to and inputted in lines 35 and 36. A thickness of 5.080 cm refers to a typical 2" × 2" detector.

SmartID is also unique in that it has the ability to determine the most likely shielding scenario that a source may be placed behind. Lines 37 and 38 refer to the selected shield material. This could be chosen as either iron or lead, or it can be uncertain. In the latter case, the code iterates between the different shielding scenarios and scores each. In a similar manner, the thickness of the shield can be either set at a specific thickness or can be unspecified in lines 39 and 40. If unspecified, the code will iterate up to the maximum specified thickness in units of cm.

Identified peaks are attributed to gamma emissions by the options specified in lines 41 to 46, and lines 49 to 52. The tolerance ratio in lines 41 and 42 refer to the energy range in which a peak will be matched to an emission. This is described in more detail in chapter 2.1.1. This value can either be set as a maximum or be used in an iterative scenario for best attribution [7]. Lines 43 and 44 refer to a blur coefficient. If two identified peaks fall within the energy determined by this coefficient, the 2 peaks will be combined. The energy mismatch weight is set in lines 45 and 46, and is typically set to 1 [7].

The location and name of the resulting output file compiled by SmartID can be established by the user in lines 47 and 48. It is best to make the name as descriptive as possible in order to remember which spectrum was analyzed.

Lines 49 and 50 let the user set the scoring parameters for the correlation thresholds of how well a nuclide is matched. Typical values are set as 110 for highly matched, 90 for moderately matched, and 60 for low matched nuclides [7]. The final 2 lines, 51 and 52, include the parameters for determining the best tolerance value for nuclide identification. The first value represents the starting tolerance; the second value represents the increasing tolerance step size; and the third value represents the minimum number of highly scored nuclides (score set in line 50). The maximum tolerance value was set by the user in line 42.

Now that all options have been described in detail, I'll apply SmartID in post-processing real and simulated source scenarios to determine if the algorithm is performing well, and which options must be included or altered to achieve the most reliable results.

## 2.3 References

- [1] SJODEN, G.E., DETWILER, R., LAVIGNE, E., and BACIAK, J.E, "Positive SNM Gamma Detection Achieved Through Synthetic Enhancement of Sodium Iodide Detector Spectra." IEEE Transactions on Nuclear Science. vol. 56, no.3., June 2009.

- [2] LAVIGNE, E. "Advanced Synthetically Enhanced Detector Resolution Algorithm: A System for Extracting Photopeaks From a Sodium Iodide Scintillation Detector Spectrum." MS Thesis. University of Florida. Gainesville. 2007
  
- [3] Los Alamos National Laboratory, "MCNP5: Monte Carlo N-Particle Transport Code Including MCNP5 1.60 and MCNPX 2.7.0 & Data Libraries," *RSICC Data Library Collection*, C00740 MNYCP 08, 5.0 ed., Los Alamos, New Mexico (2011).
  
- [4] YI, C., PAUL, J., and SJODEN, G. "Synthetic Scoring Scheme for Isotope Identification in SmartID." INMM Annual Meeting Conference Proceedings. Indian Wells, CA. 2013.
  
- [5] KRANE, K. *Introductory Nuclear Physics*. John Wiley & Sons, Inc., 1988.
  
- [6] LAVIGNE, E., SJODEN, G., BACIAK, J., and DETWILER, R. "Advanced Synthetically Enhanced Detector Resolution Algorithm (ASEDRA) Users Guide." Rev 1.8. HSW Technologies LLC. Copyright 2010.
  
- [7] YI, C., and SJODEN G., "SmartID-XP: Synthetic Scoring Scheme for Isotope Identification." User manual.

## CHAPTER 3

### LABORATORY EXPERIMENTS

#### 3.1 Calibration Source Experiment

Real world experiments with SmartID were required to establish the code for the fuel assessment application for the project. Therefore, I designed an experiment to verify SmartID's ability to identify radionuclides in an air medium, and to determine if SmartID is capable of correctly identifying radionuclides through a water medium. The spectra were collected by a Canberra 2 in. x 2 in. NaI(Tl) scintillator detector.

I created a simple experimental setup to minimize any external interference. On a free standing table in the center of a detection laboratory, I aligned a NaI(Tl) detector 40 cm away from a stand to hold various radiation sources, as shown in Figure 3.1.



**Figure 3.1:** Experimental setup of NaI detector facing source stand.



Additionally, I purchased a 40 cm long plastic tub and filled it with water. This was later placed between the detector and source stand for the water medium spectra collections. I collected spectra of sources in this configuration through air, and also collected spectra for the same sources after adding a container of water in between the detector and sources. My two radionuclides of initial interest were  $^{137}\text{Cs}$  and  $^{60}\text{Co}$ . The  $^{137}\text{Cs}$  calibration source had an activity of 262.8  $\mu\text{Ci}$ . This source was dated February 1, 1999. Taking into account a half-life of 30 years, the current activity of the source was calculated to be 180  $\mu\text{Ci}$ . The  $^{60}\text{Co}$  sources were much weaker (each 1  $\mu\text{Ci}$  on January 28, 2008 and 0.4  $\mu\text{Ci}$  on date of measure); therefore I placed two of these sources on the source stand for data acquisition.

I calibrated the detector using both of these sources, plus a natural thorium glass source (that included a  $^{208}\text{Tl}$  source) and a  $^{22}\text{Na}$  calibration source through air. From the calibration spectra, I calculated the FWHM values for various energy peaks for use in the SmartID analysis of the collected spectra. Table 3.1 lists the calibration data for use in the “Energy.txt” and “FWHM.txt” files needed to properly run SmartID.

**Table 3.1:** Calibration gamma peak data for a 2 in. x 2 in. NaI(Tl) detector in air.

Energy (keV)	Channel	FWHM (keV)
511	243	37.85
661.657	311	46.526
1173.23	542	55.365
1332.49	614	66.36
2614	1191	86.618

As previously stated, the  $^{137}\text{Cs}$  source was much stronger than the  $^{60}\text{Co}$  sources. Figure 3.2 shows the spectrum collected with air between the detector and source, and with water between the detector and source.  $^{137}\text{Cs}$  has only one major gamma energy

emission at 662 keV. Due to its strength, its peak was still easily discernable in the water spectrum, but it is noteworthy to see how significantly the signal drops off for the number of counts collected over 30 minutes from an air environment to a water environment. The peak in the air case is 20 times greater than the peak for the water case.

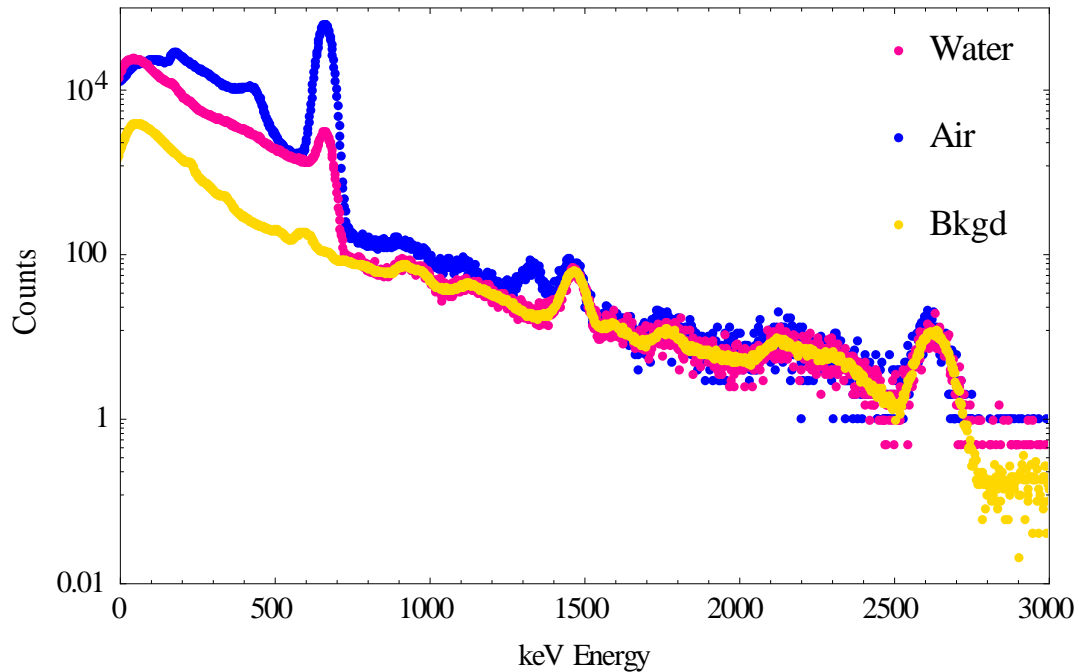


**Figure 3.2:**  $^{137}\text{Cs}$  spectrum in air shown in blue.  $^{137}\text{Cs}$  spectrum in water shown in pink. Background spectrum shown in yellow.

The measurements were taken in a laboratory located on the top floor of the Boggs building at Georgia Tech. This laboratory stores many types of calibration sources for radiation detection research. The storage of these radioactive sources contributes to a noisy, elevated background shown in yellow in Figure 3.2. Identifiable peaks are visible at energies near 2600 keV (relating to  $^{208}\text{Tl}$ ), and 1400 keV (relating to  $^{40}\text{K}$ ). It is also evident that this background contributes to the overall shape of the spectra collected for the  $^{137}\text{Cs}$  sample. It is important to verify that SmartID is able to perform well in noisy

environments by removing all background effects without removing important features of the measured source. I verified this by employing the SmartID algorithm with the  $^{137}\text{Cs}$  in air spectrum with the background spectrum subtracted and without the background subtracted. Figure 3.3 shows the identified  $^{137}\text{Cs}$  in air spectrum without background subtraction, and Figure 3.4 shows the corresponding nuclides identified by SmartID.

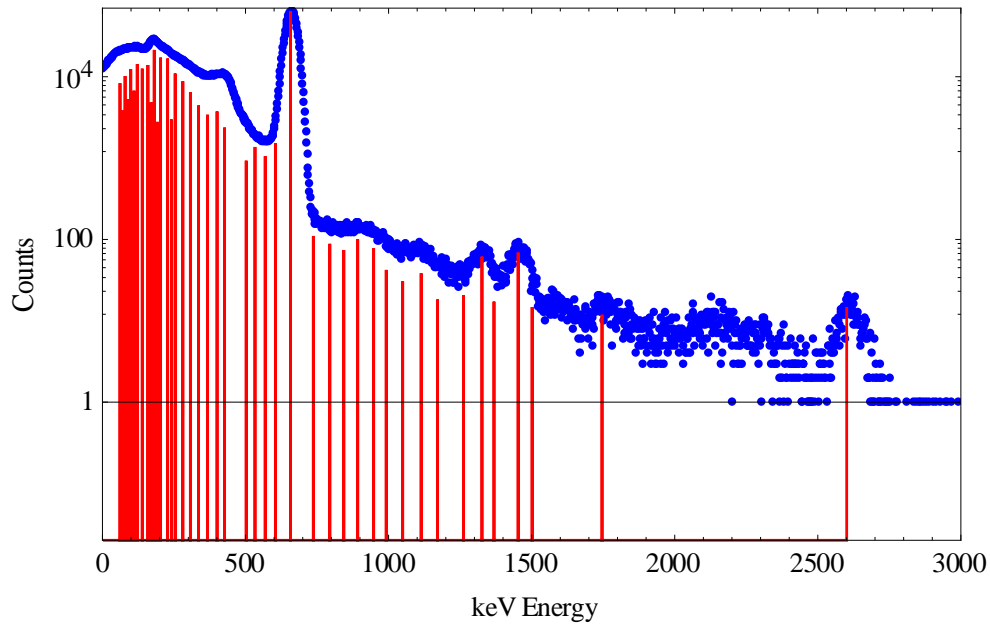


**Figure 3.3:**  $^{137}\text{Cs}$  spectrum in air shown in blue. Background was not subtracted. All identified peaks are shown by the red vertical lines.

I included a shielding search in my “smartid.inp” file since many of the sources contributing to the overall background are most likely stored and shielded. The most likely shielding scenario scored was 3 cm of lead. This resulted in  $^{137}\text{Cs}$  as the most likely nuclide. This is actually highly likely since I know that  $^{137}\text{Cs}$  was the source used for spectrum collection.  $^{60}\text{Co}$  was also identified, and I find this to be likely since I know that this source was in the vicinity of the detector, for later use. The remaining nuclides scored present a unique background. There is a natural thorium glass source present in

the laboratory; however, its exact nuclide content is unknown. The background suggests that this is not a pure source, and might have at one time been subjected to irradiation or been in the presence of a neutron source. In order to be sure that SmartID would best match nuclides present, I set the tolerance ratio, or energy window, to 1%. Looking closely at the individual nuclide's emission attributions, I see that it is unlikely that both  $^{231}\text{Pa}$  and  $^{227}\text{Th}$  are present. Both have 2 very similar gamma emissions, and the 302.74 keV photopeak and 331.54 keV photopeak are attributed to both nuclides. The 302.74 keV photopeak is also attributed to  $^{212}\text{Pb}$ , a daughter product of natural Th. Therefore, this is actually the nuclide present. The 2600.7 keV photopeak identified is clearly shown, and is most likely from the 2614 keV emission attributed to  $^{208}\text{Tl}$ . In fact, SmartID attributes 3 out of the 4  $^{208}\text{Tl}$  emissions. It is also likely that  $^{22}\text{Na}$  is present in the background, since the spectrum collection took place on the top floor of the Boggs building at Georgia tech. Both emissions for this nuclide are attributed by SmartID. Since I believe this nuclide,  $^{22}\text{Na}$ , is present, it is unlikely that  $^{65}\text{Zn}$  is present. This nuclide shares an emission at 511 keV with  $^{22}\text{Na}$ , and its second emission is double counted by  $^{46}\text{Sc}$ , and  $^{214}\text{Bi}$ , which is a daughter product of  $^{238}\text{U}$ . I determined that it is more likely that  $^{238}\text{U}$  is present rather than  $^{46}\text{Sc}$  since  $^{226}\text{Ra}$ , also a  $^{238}\text{U}$  daughter product is scored, along with  $^{238}\text{U}$  itself.

Score Details for Shielding Options:							
-----							
Possible Shielding Setting: 1 Total Score: 2037.46							
Shielding Material: Pb Thickness (cm): 3.00							
Note:							
base score : fuction of (#matched/#emissions), weighted by yield,detectability							
bonus I : bonus from number of matched peaks							
bonus II : bonus from relative peak height							
bonus III : bonus from alignment between peakheights and emission yields							
Score Summary:							
-----							
Nuclide	Total	(base + bonus I, II, III)				Comment	Correlation
137Cs	125.63	( 98.2	0.0	27.4	0.0 )	Fiss_Prod	High
110mAg	114.32	( 79.5	6.8	28.1	0.0 )	Fiss_Prod	High
231Pa	109.60	( 98.6	1.0	5.0	5.0 )	U-235_Dau+Irr_T	High
227Th	105.10	( 99.1	1.0	5.0	0.0 )	U-235_Daughter	Moderate
60Co	105.03	( 99.0	1.0	0.0	5.0 )	c	Moderate
46Sc	104.61	( 98.6	1.0	0.1	5.0 )	c	Moderate
212Pb	100.69	( 97.8	0.0	2.9	0.0 )	Th-232_Daughter	Moderate
65Zn	100.59	( 99.1	1.0	0.5	0.0 )	Fiss_Prod	Moderate
22Na	100.39	( 98.9	1.0	0.5	0.0 )	Cosmic_spall_pr	Moderate
40K	98.39	( 98.4	0.0	0.0	0.0 )	NORM	Low
241Am	98.38	( 62.4	1.7	29.3	5.0 )	SNM	Low
58Co	98.11	( 98.1	0.0	0.0	0.0 )	c	Low
226Ra	89.69	( 89.0	0.0	0.7	0.0 )	U-238_Daughter	Low
124Sb	84.08	( 51.8	1.6	0.7	30.0 )	Fiss_Prod	Low
238U	76.74	( 76.7	0.0	0.0	0.0 )	SNM	Low
208Tl	74.51	( 71.8	2.2	0.5	0.0 )	Th-232_Daughter	Low
166mHo	71.26	( 60.5	6.6	4.1	0.0 )	Fiss_Prod	Low
239Pu	69.33	( 24.7	8.2	36.3	0.0 )	SNM	Low
134Cs	68.34	( 45.6	2.0	0.7	20.0 )	Fiss_Prod	Low
214Bi	67.43	( 60.3	6.4	0.7	0.0 )	U-238_Daughter	Low
95Zr	65.70	( 65.6	0.0	0.1	0.0 )	Fiss_Prod	Low
125Sb	59.13	( 58.4	0.0	0.7	0.0 )	Fiss_Prod	Low
192Ir	50.42	( 49.7	0.0	0.7	0.0 )	medical_RDD	Low

**Figure 3.4:** Scored nuclides identified by SmartID for the  $^{137}\text{Cs}$  spectrum without background subtraction.

I repeated analyzing the  $^{137}\text{Cs}$  spectrum in air with SmartID, this time taking into account background subtraction. Figure 3.5 shows the resulting identified peaks. Multiple peaks still are identified, but they no longer hold as much significance to the overall gross count rate. SmartID was able to accurately identify  $^{137}\text{Cs}$  as the most likely nuclide present.

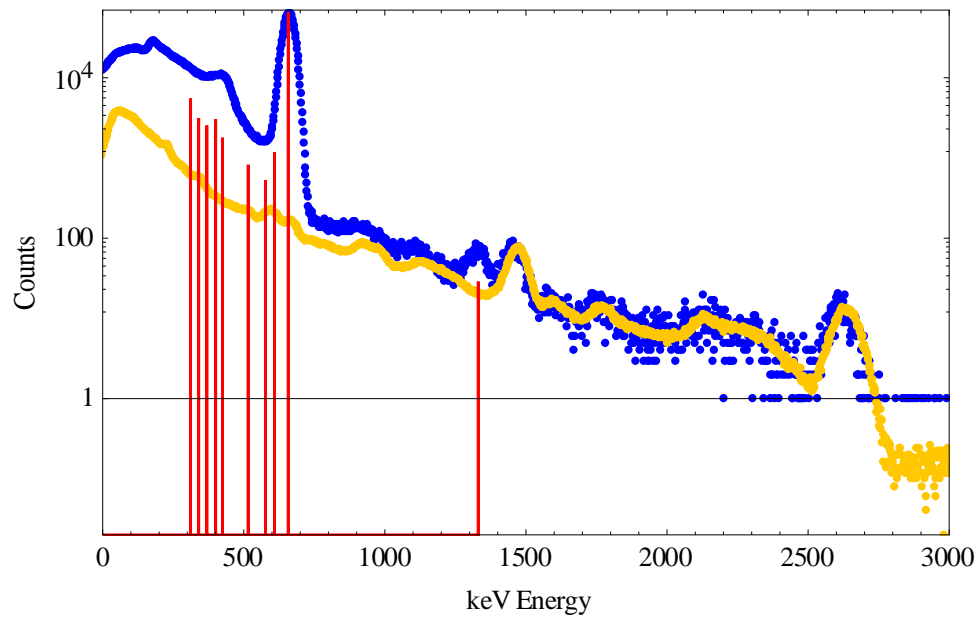


**Figure 3.5:**  $^{137}\text{Cs}$  spectrum in air shown in blue. Background shown in yellow. All identified peaks are shown by the red vertical lines.

I processed the water case spectrum through SmartID, which successfully scored  $^{137}\text{Cs}$  as the most likely isotope. SmartIDFigure 3.6 shows the identified peaks of the water spectrum with background subtraction.

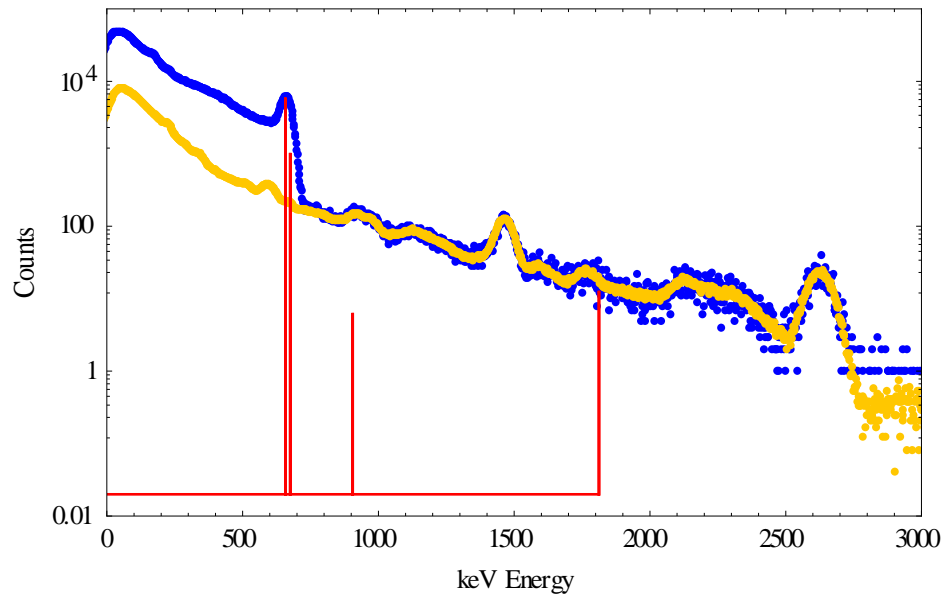


**Figure 3.6:**  $^{137}\text{Cs}$  spectrum in water with peaks identified by SmartID. Background shown in yellow. All identified peaks are shown by the red vertical lines.

Although less pronounced, the 662 keV peak is clearly identified by SmartID, and  $^{137}\text{Cs}$  is the top scoring nuclide. Figure 3.7 shows the identified peaks, and resulting nuclides scored for this case. The identified 657.23 keV peak is attributed to the 662 keV emission associated with  $^{137}\text{Cs}$ .

```

-----
SmartID-XP
Extended Protocol Synthetic Resolution Identifier
Ver 2.5J
By
G. Sjoden, C. Yi, E. LaVigne, J. Paul
Georgia Institute of Technology
June 2014

Contact: sjoden@gatech.edu
-----

Spectrum Name: ./SmallExp/Cs137.Spe

4 Peak(s) Identified - Sort by Energy
-----
keV          Counts          Norm% Cts   Peak Id
657.23      5.9867E+03      85.09786    3
674.94      1.0291E+03      14.62813    4
905.26      6.3920E+00      0.09086     2
1812.20     1.2885E+01      0.18315     1

Possible Shielding Setting: 1 Total Score: 472.93
Shielding Material: Fe Thickness (cm): 0.00

Note:
base score : fuction of (#matched/#emissions), weighted by yield,detectability
bonus I : bonus from number of matched peaks
bonus II : bonus from relative peak height
bonus III : bonus from alignment between peakheights and emission yields

Score Summary:
-----
Nuclide      Total  (base + bonus I, II, III)      Comment      Correlation
137Cs       131.60 ( 98.2  0.0 33.4  0.0 )      Fiss_Prod    High
240Pu       126.62 ( 94.9  0.0 31.7  0.0 )              SNM          High
110mAg      114.84 ( 72.5  2.8 39.5  0.0 )      Fiss_Prod    High
57Co        99.87 ( 94.5  0.0 5.4  0.0 )              c           Moderate

```

**Figure 3.7:** SmartID partial output file for  $^{137}\text{Cs}$  through water.

Although the spectrum shown in Figure 3.6 was greatly altered through the water, I wanted further validation that a more complicated or weaker source could still be correctly identified in this type of very noisy background medium. The isotope  $^{60}\text{Co}$  has two gamma peaks; one at 1173.228 keV and one at 1332.490 keV. Figure 3.8 shows these peaks when the spectrum was taken in air.



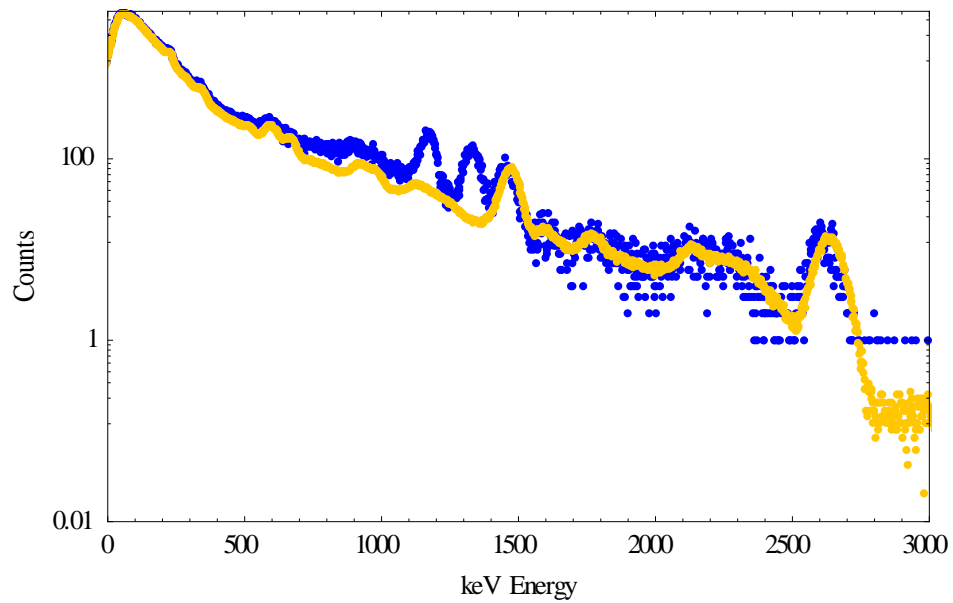


**Figure 3.8:**  $^{60}\text{Co}$  spectra through 40 cm of air in blue with background in yellow.

In a similar manner to the  $^{137}\text{Cs}$  cases just presented, the background spectrum has a noticeable effect on the raw collected spectrum for the  $^{60}\text{Co}$  source. However, in this case, the  $^{60}\text{Co}$  sources are much weaker, and the background produces a more complicated spectrum with multiple energy peaks not associated with or expected to be seen for a  $^{60}\text{Co}$  source. Again, I utilized SmartID to identify energy peaks for the  $^{60}\text{Co}$  spectrum in air without subtracting background. Figure 3.9 shows the identified peaks. A total of 40 peaks are identified when the only source to be directly measured was the  $^{60}\text{Co}$ .

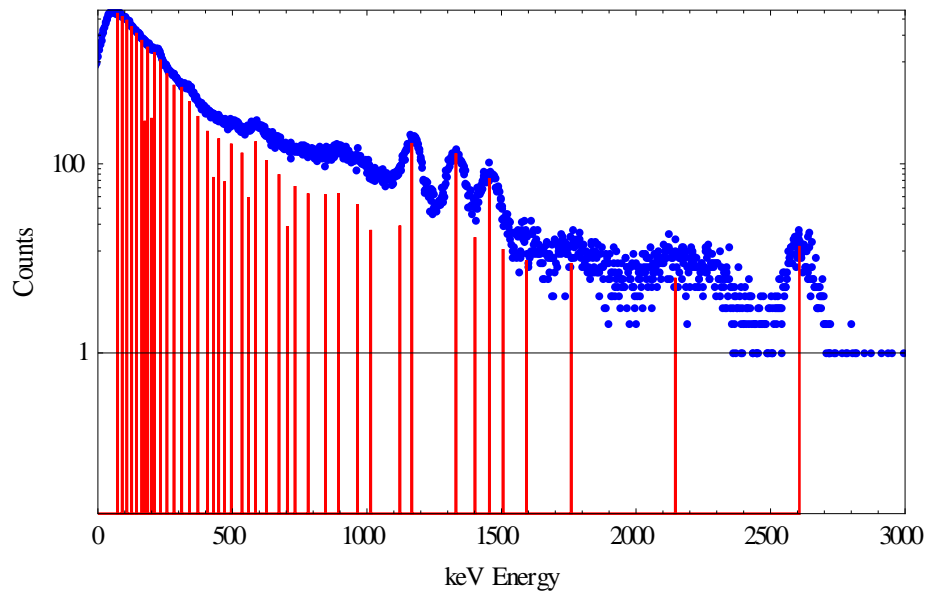


**Figure 3.9:**  $^{60}\text{Co}$  spectrum in air shown in blue. Background was not subtracted. All identified peaks are shown by the red vertical lines.

The laboratory environment produced a highly complicated low radiation area. Figure 3.10 shows the identified nuclides from the SmartID output file. I see high correlations for many fission products and nuclides associated with  $^{232}\text{Th}$ . At first, it seems that SmartID is inaccurately identifying nuclides, but the thorium source located in the laboratory is actually highly complicated with numerous daughter products. Like the previous  $^{137}\text{Cs}$  plus background analysis, the natural thorium source is creating this unique spectrum. This source is in glass form, and was found left behind in another laboratory at Georgia Tech. The history of the source is unknown, but I have confirmed that it contains natural thorium. I have previously employed SmartID to try and identify this source and found that it likely is not pure thorium. Although, its visual energy peak features show the key energy peaks linked to  $^{232}\text{Th}$ , I believe it may also contain some natural uranium. Figure 3.10 shows the complicated nuclide identification. In addition to the daughter products and nuclides associated with Th,  $^{40}\text{K}$ , and  $^{22}\text{Na}$  are identified. The key identifying nuclide for the presence of Th is  $^{208}\text{Tl}$ . Two out of four peaks were

identified by SmartID, and the peak heights follow the branching ratio and detectability patterns of the emissions. Two additional  $^{232}\text{Th}$  daughter nuclides,  $^{212}\text{Bi}$  and  $^{228}\text{Ac}$ , were also identified. In addition to the many fission products discovered by SmartID, The  $^{40}\text{K}$  peak is clearly visible in the spectrum. It has a gamma emission at 1460.83 keV and attributed the peak identified at 1454.6 keV. The higher energy peak for  $^{22}\text{Na}$  was identified 1263.9 keV for the 1274.5 emission. Again, I do not believe that  $^{46}\text{Sc}$  is actually present due to double counting of attributed gamma emissions from  $^{214}\text{Bi}$  and  $^{234}\text{Pa}$ .

Score Details for Shielding Options:								
=====								
Possible Shielding Setting: 1		Total Score: 1720.21						
Shielding Material: Pb		Thickness (cm): 4.00						
Note:								
base score : fuction of (#matched/#emissions), weighted by yield,detectability a								
bonus I : bonus from number of matched peaks								
bonus II : bonus from relative peak height								
bonus III : bonus from alignment between peakheights and emission yields								
Score Summary:								
-----								
Nuclide	Total	(base + bonus I, II, III)					Comment	Correlation
60Co	124.69	( 98.8	1.0	4.9	20.0	)	c	High
46Sc	106.00	( 98.8	1.0	1.2	5.0	)	c	Moderate
223Ra	100.84	( 97.8	0.0	3.1	0.0	)	U-235_Daughter	Moderate
56Mn	99.97	( 99.2	0.0	0.8	0.0	)	c	Moderate
40K	99.79	( 98.6	0.0	1.1	0.0	)	NORM	Moderate
214Pb	99.13	( 98.3	0.0	0.8	0.0	)	U-238_Daughter	Moderate
65Zn	98.33	( 98.0	0.0	0.4	0.0	)	Fiss_Prod	Low
208Tl	94.34	( 90.5	0.7	3.1	0.0	)	Th-232_Daughter	Low
152Eu	93.12	( 81.1	7.9	2.1	2.0	)	Fiss_Prod	Low
22Na	88.22	( 88.1	0.0	0.1	0.0	)	Cosmic_spall_pr	Low
212Bi	86.04	( 78.5	0.8	1.8	5.0	)	Th-232_Daughter	Low
160Tb	79.20	( 72.1	3.2	3.9	0.0	)	Fiss_Prod	Low
106Ru	74.96	( 73.1	0.0	1.8	0.0	)	Fiss_Prod	Low
56Co	70.02	( 61.1	5.0	3.9	0.0	)	c	Low
214Bi	64.73	( 56.7	4.3	3.7	0.0	)	U-238_Daughter	Low
124Sb	63.67	( 59.3	1.6	2.8	0.0	)	Fiss_Prod	Low
154Eu	60.55	( 53.9	3.2	3.5	0.0	)	Fiss_Prod	Low
192Ir	58.49	( 51.8	0.7	4.0	2.0	)	medical_RDD	Low
228Ac	54.49	( 47.8	1.5	5.2	0.0	)	Th-232_Daughter	Low
106Rh	53.51	( 51.7	0.0	1.8	0.0	)	Fiss_Prod	Low
234Pa	50.10	( 24.0	15.0	11.1	0.0	)	U-238_Daughter	Low

**Figure 3.10:** Scored nuclides identified by SmartID for the  $^{60}\text{Co}$  spectrum without background subtraction.

Although it is impressive that the SmartID algorithm was able to pull out many hidden energy peaks relating to Th, it is more impressive that the majority of these peaks

are removed when background removal is applied. Figure 3.11 shows the same collected raw spectrum for  $^{60}\text{Co}$  in air with the background. The background was subtracted from the raw spectrum and SmartID identified far fewer energy peaks. Figure 3.12 shows the new results which are much more limited in comparison to Figure 3.10. Some of the background nuclides bleed through to the new net spectrum, but  $^{60}\text{Co}$  is overwhelmingly identified as the most likely nuclide present.

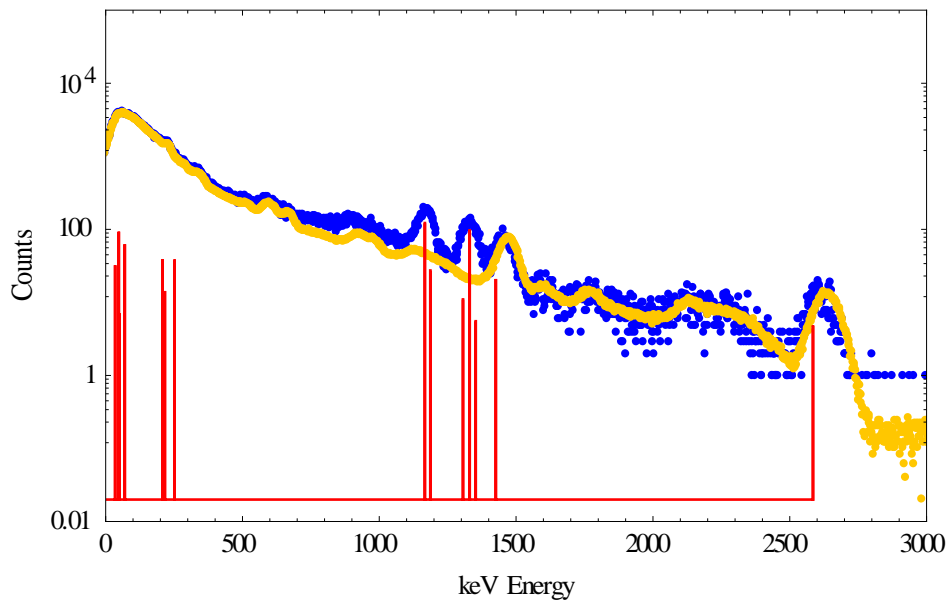


**Figure 3.11:**  $^{60}\text{Co}$  spectrum in air with peaks identified by SmartID. Background shown in yellow. All identified peaks are shown by the red vertical lines

Score Summary:							
Nuclide	Total	(base +	bonus I,	II,	III)	Comment	Correlation
$^{60}\text{Co}$	159.85	( 98.8	1.0	30.1	30.0 )	c	High
40K	97.39	( 94.7	0.0	2.7	0.0 )	NORM	Moderate
$^{160}\text{Tb}$	60.48	( 22.3	3.1	5.1	30.0 )	Fiss_Prod	Moderate
$^{214}\text{Bi}$	36.24	( 6.7	6.2	21.3	2.0 )	U-238_Daughter	Low
$^{234}\text{Pa}$	26.21	( 1.4	1.3	3.5	20.0 )	U-238_Daughter	Low
$^{124}\text{Sb}$	25.03	( 1.5	2.9	20.6	0.0 )	Fiss_Prod	Low
$^{56}\text{Co}$	22.19	( 2.8	1.6	17.8	0.0 )	c	Low
$^{154}\text{Eu}$	22.10	( 20.7	0.0	1.4	0.0 )	Fiss_Prod	Low
$^{134}\text{Cs}$	19.10	( 1.0	0.7	17.4	0.0 )	Fiss_Prod	Low
$^{152}\text{Eu}$	16.30	( 5.5	3.1	7.7	0.0 )	Fiss_Prod	Low
$^{22}\text{Na}$	12.23	( 10.8	0.0	1.4	0.0 )	Cosmic_spall_pr	Low

**Figure 3.12:** SmartID score summary for the  $^{60}\text{Co}$  source through air.

Changing the medium of travel for the gamma emissions from air to water significantly alters the spectrum's appearance. These two peaks become nearly indiscernible, as shown in Figure 3.13, due to the low resolution in a NaI(Tl) detector, the noisy background, the Compton scattering effects from the water, and the close proximity between the peaks. I analyzed this spectrum with SmartID, accounting for the background. If the DRFs were computed correctly, and SmartID is properly tuned, these two peaks will be identified and the output will compute a high likelihood of  $^{60}\text{Co}$  in the sample. Figure 3.14 shows the identified peaks for this spectrum.

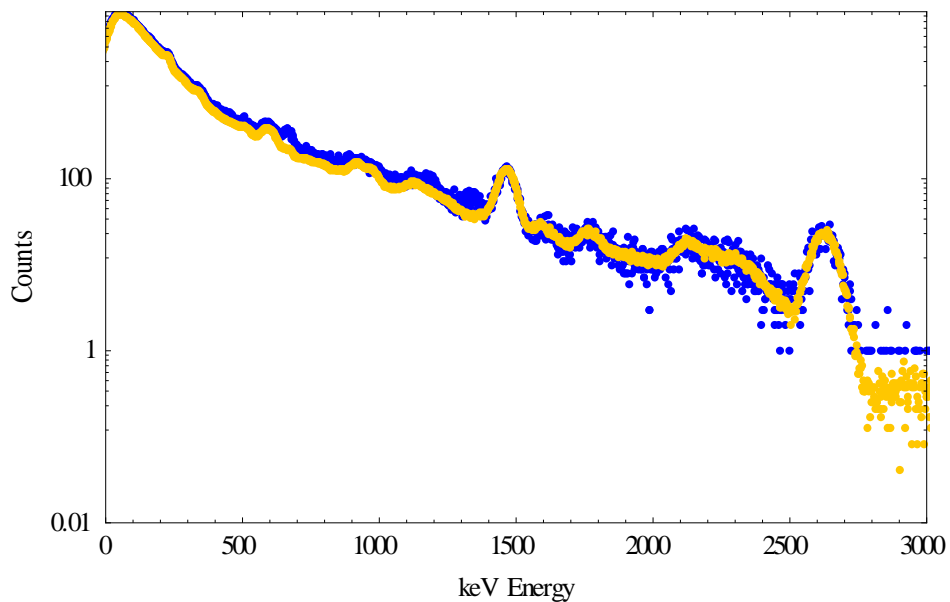


**Figure 3.13:**  $^{60}\text{Co}$  raw spectra through 40 cm of water.

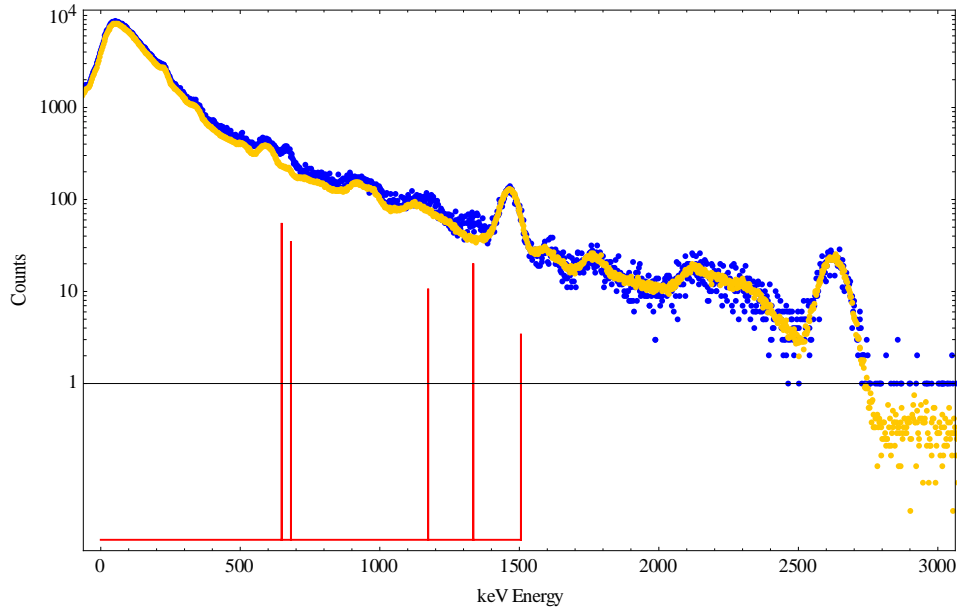


**Figure 3.14:** Peaks identified for a  $^{60}\text{Co}$  spectrum (blue) through 40 cm of water. The background is shown in yellow.

The SmartID results show that the two peaks can be accurately identified. Figure 3.15 shows the output file describing the results.

```

=====
SmartID-XP
Extended Protocol Synthetic Resolution Identifier
Ver 2.5J
By
G. Sjoden, C. Yi, E. LaVigne, J. Paul
Georgia Institute of Technology
June 2014

Contact: sjoden@gatech.edu
=====

Spectrum Name: ./SmallExp/Co60.Spe

5 Peak(s) Identified - Sort by Energy
=====
keV          Counts          Norm% Cts    Peak Id
648.36      6.5992E+01      45.62806     4
681.59      4.2154E+01      29.14604     5
1171.00     1.2629E+01      8.73192      3
1334.70     2.0381E+01     14.09179     2
1505.70     3.4743E+00      2.40219     1

Possible Shielding Setting: 1 Total Score: 157.37
Shielding Material: Fe Thickness (cm): 0.00

Note:
base score : fuction of (#matched/#emissions), weighted by yield,detectability and matching factor
bonus I : bonus from number of matched peaks
bonus II : bonus from relative peak height
bonus III : bonus from alignment between peakheights and emission yields

Score Summary:
-----
Nuclide      Total  (base + bonus I, II, III)      Comment      Correlation
60Co        114.23 ( 99.2  1.0  9.1  5.0 )      c            High
124Sb       24.39 ( 6.3  0.0 18.0  0.0 )      Fiss_Prod    Low
239Pu       18.75 ( 0.1  0.5 18.1  0.0 )      SNM          Low

Scored nuclides details:
-----
Nuclide      Score      T1/2      T1/2_unit  #EmissionInRange  #Matched      Correlation      Comment
60Co        114.23     5.2700E+00  y           2                  2              High             c

Emission(KeV)  Prob/DK      Detectability      0.50% Energy Window      Peak(KeV)      Norm%_cts
+ 1173.23      1.0000E+00    3.0135E-02      ( 1167.36 to 1179.10 )    1171.00         8.7319
+ 1332.51      1.0000E+00    2.4321E-02      ( 1325.85 to 1339.17 )    1334.70        14.0918

```

**Figure 3.15:** SmartID output file for  $^{60}\text{Co}$  spectrum through water.

The most likely nuclide by far, identified by SmartID is  $^{60}\text{Co}$  with a very tight energy window. This is very impressive considering the complex background and how weak the  $^{60}\text{Co}$  sources considered were. It does appear from the peaks near 662 keV that the strong  $^{137}\text{Cs}$  located in the laboratory is influencing the spectrum, but does not interfere enough to significantly alter the scoring. From these studies, I have found that SmartID has proven to work well in noisy laboratory environment, making it appropriate for use in further studies.

### 3.2 Irradiated Fuel Pin Experiment

In addition to the  $^{137}\text{Cs}$  and  $^{60}\text{Co}$  calibration source experiment, I designed an experiment to replicate a simplified spent fuel pool environment. I did this in order to verify that key spectral information from irradiated fuel submerged in water can be determined. The Radiological Science and Engineering Laboratory (RSEL) at Georgia Tech has the facilities and sources available that allow a natural uranium metal fuel rod to be irradiated by strong neutron sources, in order to produce fission products normally seen in used nuclear fuel. The fission products' gamma radiation will be measured with a low cost scintillator detector, NaI(Tl).

To support the actual experiment setup and irradiation, I produced MCNP models to profile the experimental outcome prior to running the experiment, and determine the dose rates involved. The experiment was designed to take place in the D-T neutron vault of the RSEL for this reason. Figure 3.16 shows the basic experimental setup. The light pink area represents the concrete walls and floor of the lab, the purple represents the lab space air. The fuel rod is the long vertical cylinder, the green is the water filled tub, and the orange is lead shielding surrounding the detector, which is represented by the color pink.

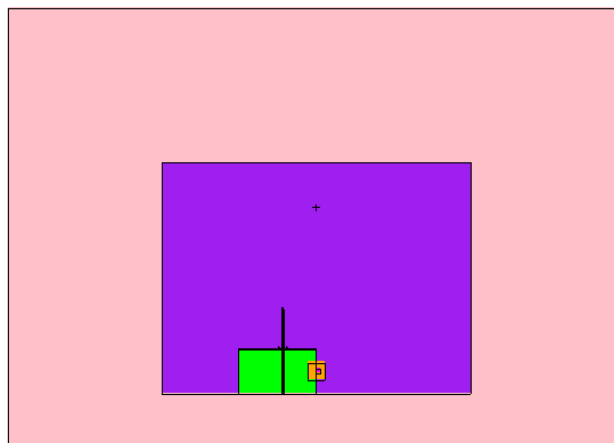


**Figure 3.16:** MCNP model of the experiment setup sliced along the x-axis.



Water is an excellent neutron moderator due to its abundance of hydrogen, which is nearly identical in mass to neutrons, greatly slowing down and thermalizing fast neutrons. This thermalization is ideal, since most neutron induced fissions of natural uranium result from thermal neutrons. The placement of the neutron sources allow the emitted neutrons to travel through the container of water and scatter down to thermal energies before interacting with the uranium fuel pin. This ideally induces fission reactions in the uranium fuel which produce key fission products for detection. Figure 3.17 shows a close up view of the neutron interactions taking place near the natural uranium fuel rod.

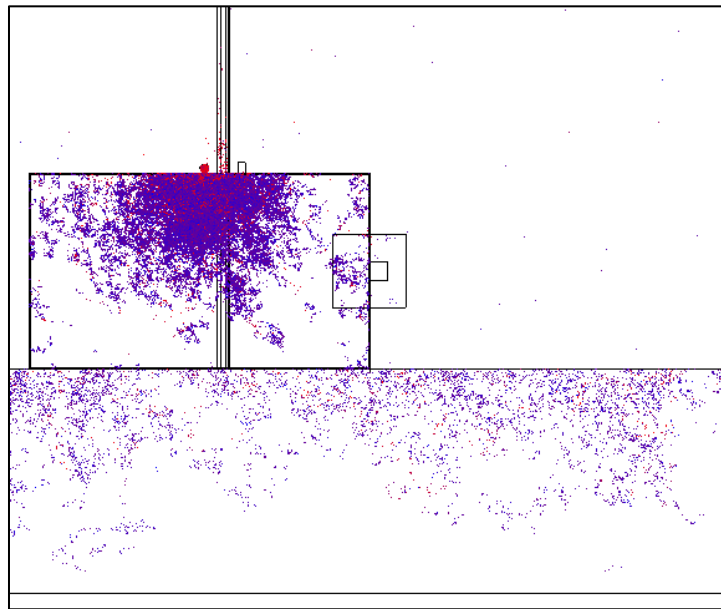


**Figure 3.17:** Neutron interactions for the MCNP model of the experiment setup along the x-axis.

Once the computational modeling of the experiment was complete, the actual experiment was set up in the RSEL neutron vault. Figure 3.18 shows the actual experiment setup. The image on the left shows the 3 1-Ci PuBe sources and the  $1.2 \times 10^8$

neutrons per second emitting AmBe source. These were held in place by small plastic containers. The right image shows how the detector will be pointed at the fuel rod and shielded by lead. The irradiation of the fuel rod continued for approximately 2 weeks. For the first week of irradiation, the detector was removed from the vault, and it was added after the sources were removed to take a 5 min and 1 hour gamma spectrum. Once the spectra collection was complete, the neutron sources were added back to the experiment. In the next sequence, the detector was left in place and fuel rod was irradiated for an additional week. During this second week of irradiation, the detector was set to collect, remotely, gamma spectra information at 8 hour time increments in order to assess if the detector was able to detect a set of both short lived and long lived fission products growing in the fuel pin with time. This culminated in a total of 21 eight hour spectra over the course of one week. The sources were removed again, and 21 consecutive 5 minute spectra were taken in order to see how the short lived fission products die out.



**Figure 3.18:** Actual experimental setup. Left: Sources in place. Right: Detector with Pb sheilding.

Before irradiation began, initial energy calibration and FWHM measurements were acquired. Figure 3.19 shows a sample energy calibration for an  $^{155}\text{Eu}/^{22}\text{Na}$ . Figure 3.20 shows a  $^{137}\text{Cs}$  source spectrum. The peaks were correctly identified by SmartID. A total of four sources,  $^{155}\text{Eu}/^{22}\text{Na}$ ,  $^{137}\text{Cs}$ ,  $^{232}\text{Th}$ , and  $^{60}\text{Co}$  were used to calibrate spectra from 45 keV to 2614 keV.

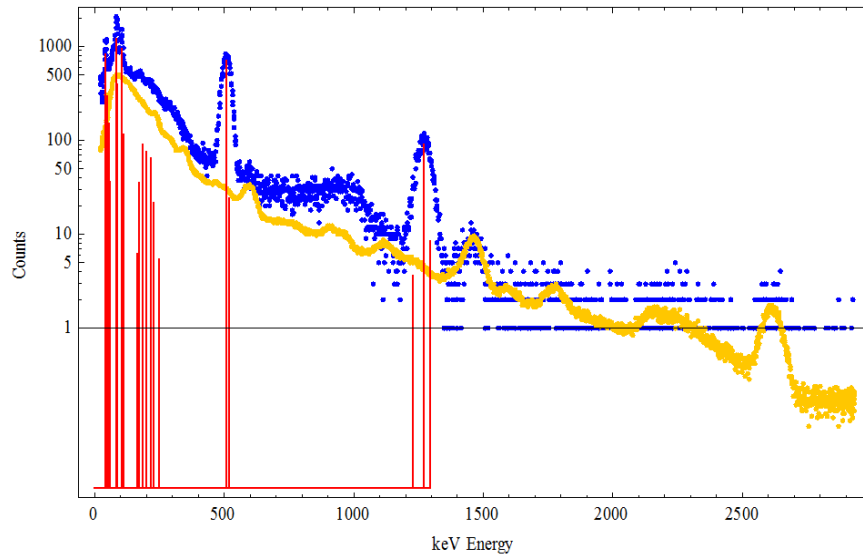


**Figure 3.19:**  $^{155}\text{Eu}/^{22}\text{Na}$  calibration source spectra with identified gamma peaks. The yellow counts are from a background count; the blue counts are the gross counts.

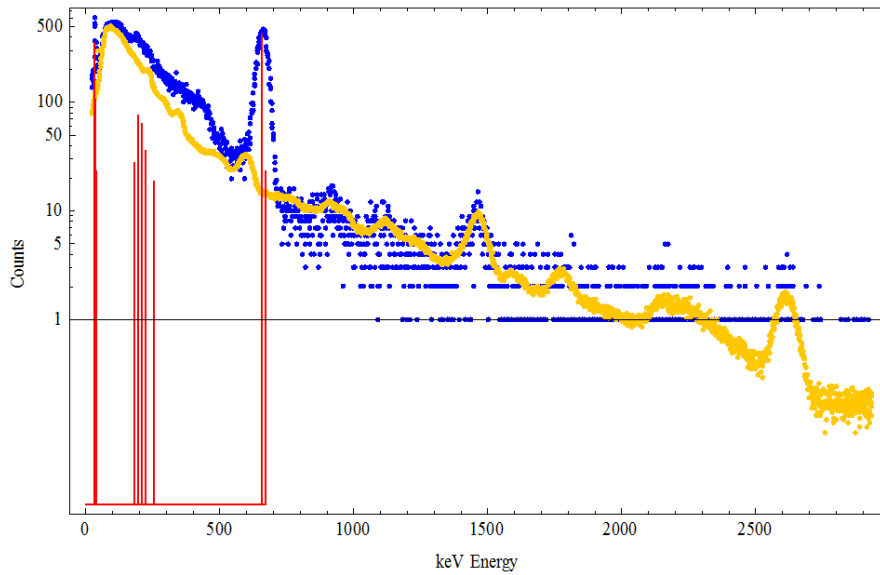


**Figure 3.20:**  $^{137}\text{Cs}$  calibration source spectra with identified gamma peaks. The yellow counts are the background and the blue counts are the gross counts.

### 3.2.1 Spectra collection during irradiation

The initial and final 8 hr spectra gathered from the irradiation experiment are shown by Figure 3.21. Since this spectrum was acquired during the irradiation period, a clear 2.2 MeV gamma peak from  $(n,\gamma)$  interactions with the hydrogen in the water is observed at 2.21 MeV. The additional peaks visible are from the neutron sources themselves and not from the irradiated fuel. The first and last 8 hour spectra collected were compared to determine whether or not significant observable changes in resolution due to detector radiation damage occurred. A change in the FWHM of the visible peaks are not apparent in Figure 3.21, indicating the detector did not incur significant damage due to the presence of the neutron sources. Although difficult to observe from Figure 3.21, close examination shows that the last 8 hour spectra has an overall greater count rate, indicating the buildup of fission products in the fuel. This differentiation between the first 8 hour and last 8 hour spectra is difficult to distinguish due to the neutron sources

combined gamma strength being much stronger than the fission product's gamma strength. Figure 3.22 shows a closer view of the difference between counts over the 8 hour collection period. The last case has an overall increased count rate from the first case of 204.23 counts per second.

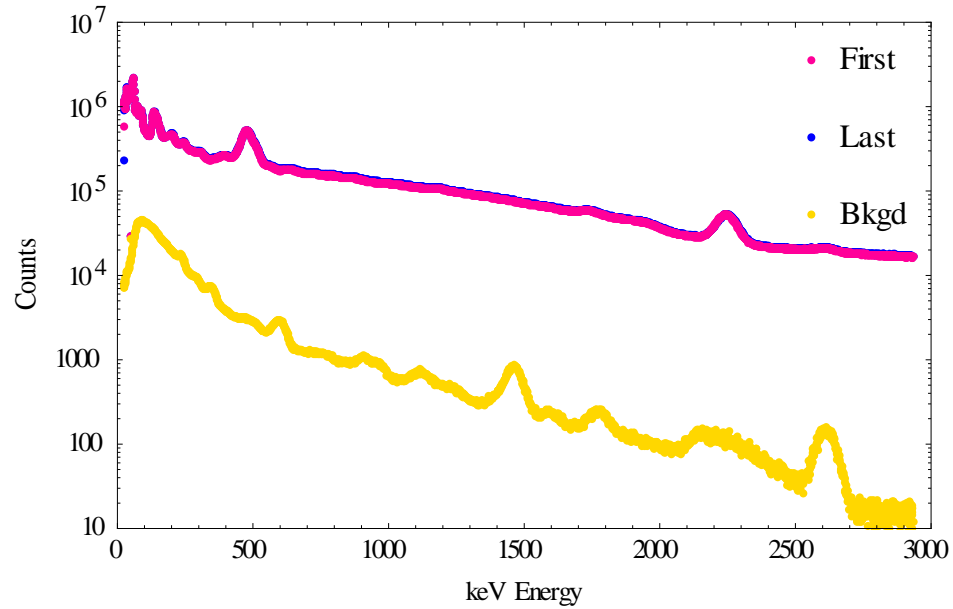


**Figure 3.21:** First 8 hour and last 8 hour spectra measured during irradiation of fuel element.

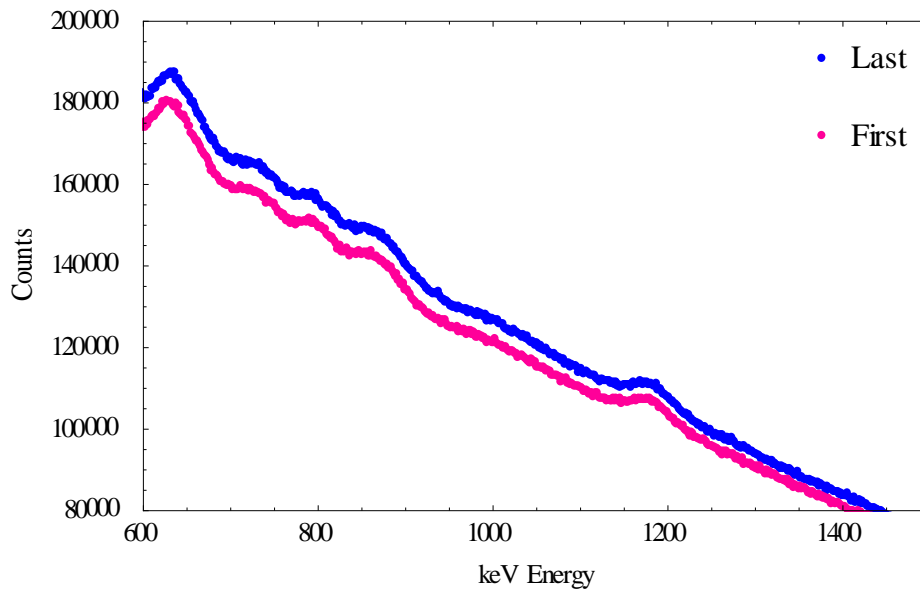


**Figure 3.22:** First 8 hour and last 8 hour spectra measured during irradiation of fuel element scaled linearly and plotted between 600 and 1400 keV.

Using SmartID, I analyzed the last 8 hour counting spectrum to identify peaks and possible nuclides. The identified peaks are shown by Figure 3.23 and listed in Figure 3.24. These peaks are matched to gamma emissions to produce the results shown in Figure 3.25. Although it does not appear that many peaks are identified, the SmartID nuclide scoring techniques are robust and take many factors into account as described in detail in Chapter 2.1.2. It is important to take a close look at the scoring break down of the nuclides identified. The *High*, *Moderate*, and *Low* correlation descriptors represent how much emphasis is placed on the points scored for each isotope. These threshold values are decided upon by the SmartID user and can be changed in the SmartID input file. Sometimes these overall high scores actually have instances of very low base or bonus scores in comparison to some moderately correlated nuclides. The long list of short lived fission products, and the presence of  $(n,\gamma)$  interactions appearing in the spectrum are expected from this irradiation period.

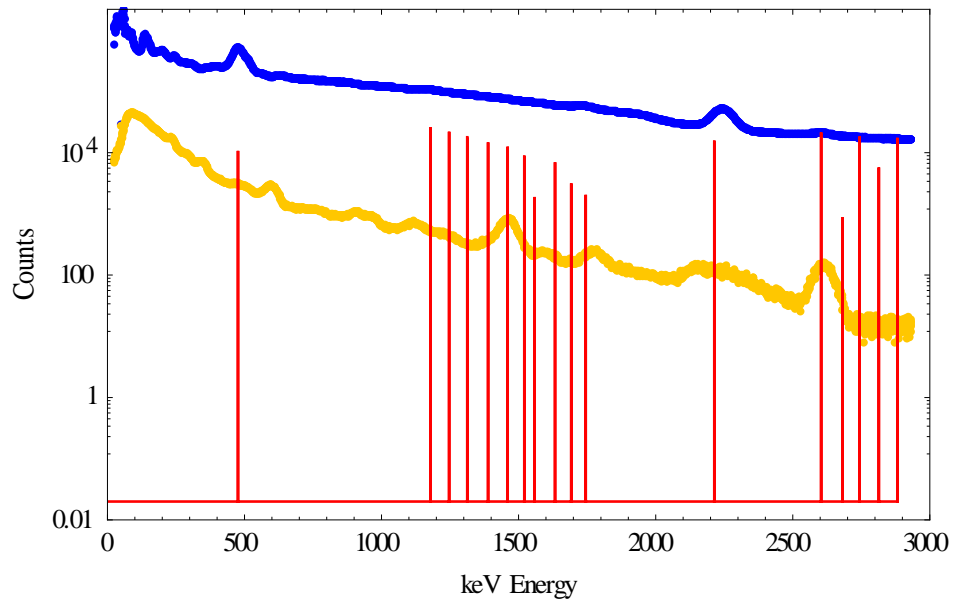


**Figure 3.23:** Identified peaks from last 8 hour spectrum accumulation during irradiation.

17 Peak(s) Identified - Sort by Energy			
keV	Counts	Norm% Cts	Peak Id
476.10	1.0734E+04	5.18365	17
1177.90	2.6120E+04	12.61383	10
1246.50	2.2040E+04	10.64352	11
1312.70	1.7864E+04	8.62686	12
1388.60	1.4808E+04	7.15106	13
1459.90	1.2577E+04	6.07367	14
1520.50	8.9817E+03	4.33743	15
1558.50	1.8903E+03	0.91286	16
1632.80	6.9870E+03	3.37415	7
1691.90	3.1637E+03	1.52781	8
1745.00	2.0494E+03	0.98969	9
2213.60	1.5779E+04	7.61997	6
2603.40	2.1456E+04	10.36150	1
2681.30	8.8786E+02	0.42876	5
2744.00	1.8448E+04	8.90888	2
2814.30	5.7513E+03	2.77741	4
2881.50	1.7537E+04	8.46894	3

**Figure 3.24:** Identified peak energies for the last 8 hour accumulated spectrum during irradiation.

Score Summary:							
Nuclide	Total	(base +	bonus I,	II,	III)	Comment	Correlation
60Co	137.06	( 97.8	1.0	8.3	30.0 )	c	High
47Ca	124.07	( 88.0	0.8	5.2	30.0 )	c	High
209Tl	118.53	( 95.3	1.0	2.3	20.0 )	Np-237_Daughter	High
24Na	109.43	( 97.2	1.0	6.3	5.0 )	n_activ_prod	High
135I	106.39	( 31.9	50.0	24.5	0.0 )	Fiss_Prod	High
40K	101.77	( 99.3	0.0	2.4	0.0 )	NORM	High
H-1_n-g	101.57	( 98.6	0.0	3.0	0.0 )	n_irrad=SNM	High
7Be	100.93	( 98.9	0.0	2.1	0.0 )	c	High
138Cs	100.14	( 69.2	10.5	20.4	0.0 )	Fiss_Prod	High
90Y	100.09	( 98.1	0.0	2.0	0.0 )	Fiss_Prod	High
41Ar	99.90	( 96.6	0.0	3.3	0.0 )	n_activ_prod	Moderate
223Fr	99.07	( 97.1	0.0	2.0	0.0 )	U-235_Daughter	Moderate
143La	97.35	( 97.0	0.0	0.4	0.0 )	Fiss_Prod	Moderate
141La	97.12	( 94.5	0.0	2.6	0.0 )	Fiss_Prod	Moderate
132I	88.24	( 4.0	50.0	34.3	0.0 )	Fiss_Prod	Low
92Sr	86.64	( 78.5	0.7	7.4	0.0 )	Fiss_Prod	Low
42K	83.20	( 81.5	0.0	1.7	0.0 )	c	Low
140La	77.92	( 53.3	8.1	16.5	0.0 )	Fiss_Prod	Low
156Eu	59.84	( 32.1	8.5	14.2	5.0 )	Fiss_Prod	Low
187W	57.49	( 55.5	0.0	2.0	0.0 )	c	Low
214Bi	57.22	( 17.0	19.0	21.3	0.0 )	U-238_Daughter	Low
154Eu	56.96	( 22.0	0.6	4.3	30.0 )	Fiss_Prod	Low
93Y	56.24	( 14.7	21.8	19.7	0.0 )	Fiss_Prod	Low
89Rb	55.78	( 35.6	5.1	13.0	2.0 )	Fiss_Prod	Low
88Kr	52.92	( 26.8	9.9	16.2	0.0 )	Fiss_Prod	Low

**Figure 3.25:** SmartID nuclide score summary of the last 8 hour spectrum accumulation during irradiation.

Since this spectra was taken during the irradiation of the fuel rod, activation products are expected to be identified. SmartID identifies activation products  $^{24}\text{Na}$  and  $^{41}\text{Ar}$ , as highly and moderately correlated. It also accurately identifies the 2.2 MeV gamma emission from neutron interactions with the hydrogen in the water with the peak identified at 2213.6 keV. The water used in the experiment was tap water which contains calcium. The  $^{47}\text{Ca}$  nuclide likely results from the calcium in the water being subjected to high neutron radiation.

### 3.2.2 Spectra collection post irradiation

Although some fission products were identified by SmartID for the during irradiation case, the neutron sources were much stronger in activity than the fission products, making it difficult to resolve many of the fine details. Therefore, I decided to collect spectra after irradiation without the neutron sources present.



Immediately following irradiation, the neutron sources were removed from the experiment and stored in their respective proper storage locations. 21 consecutive 5 minute spectra were then measured. Figure 3.26 shows the 1<sup>st</sup>, 5<sup>th</sup>, 10<sup>th</sup>, 15<sup>th</sup>, and 21<sup>st</sup> 5 minute accumulated spectra for comparison. It is promising that fission products will be identified since there appears to be a clear die away of counts in the detector with each 5 minute count.

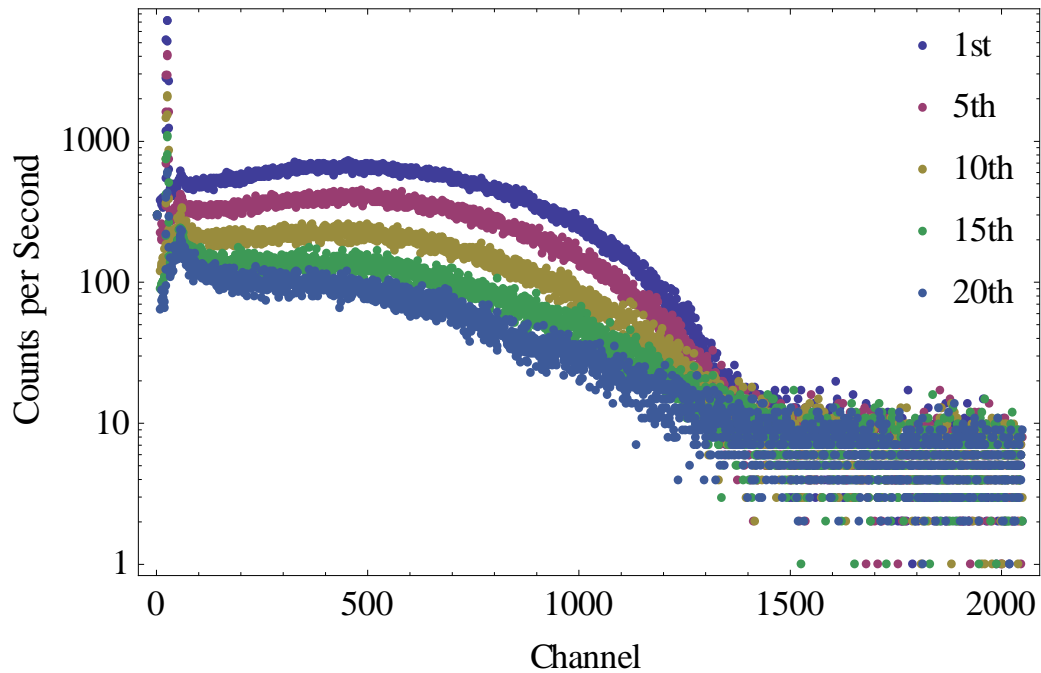


**Figure 3.26:** Counts per minute for a NaI(Tl) detector minus the background. Each line represents a different 5 minute counting interval, where 1<sup>st</sup> represents the first 5 minute count, and 21<sup>st</sup> represents the last 5 minute count taken.

I post-processed each case with SmartID, and noticed that the greatest number of peaks were identified in the first 5 minute count spectra. As spectra were collected later and later after irradiation, less and less peaks were identified along with isotopes. This is consistent with fission product behavior, since many of the fission products produced during irradiation are very short lived with half-lives on the order of seconds. Since this

experiment only utilized PuBe and AmBe irradiation sources over a week's period of time, I expected to see significantly less of the fission products typically seen in a reactor. Figure 3.27 shows the 1<sup>st</sup> 5 minute count case collected 1 hour and 35 minutes after irradiation, and Figure 3.28 shows the corresponding scoring of the identified nuclides for the first 5 minute count case collected immediately after irradiation.

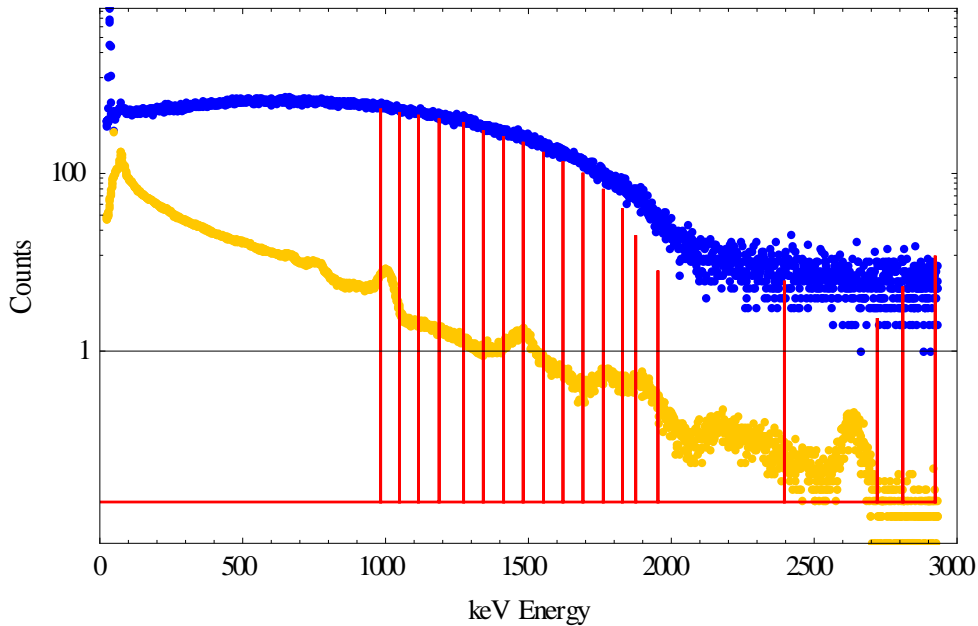


**Figure 3.27:** 1<sup>st</sup> 5 minute spectrum collected immediately following irradiation.

A significant challenge for nuclide identification took place in determining the optimal options for the “smartid.inp” file. In Chapter 2.2.1, I described each option that could be tailored to identify the peaks present and match the most likely isotopes from the identified photopeaks. Since the experimental setup was not identical to the modeled DRF cases for an assembly in water, I turned on the shielding option so that it would iterate between shielding cases of iron or lead, and also allowed iteration of shield thickness up to 10 cm. I expected to see one of the shielding options, especially the lead, to be scored higher than an unshielded case due to the large amount of lead shielding

surrounding the detector assembly. I also set the Aliasing Factor to 0.75, in order to remove possible incidental peaks. This feature helps in cases where the actual measurement geometry is not an exact model matched by the DRFs. Since this was a real experiment, I expected noise from electronics to be a real contributing phenomenon. In order to mitigate the noise effects, I set the alpha parameter for chi-square analysis to 0.01. I risk losing key spectral information if I set this value too low, but I also do not want to miss true spectral changes due to closely lying photopeaks. The next setting I changed was to have SmartID utilize the new water DRFs, so I set this option to "9". I kept my rejection threshold low since the overall counts in the spectrum were low due to the quick collection time (5min). I set my low energy cutoff value to 0.3 MeV, since I know that my DRFs lose accuracy along with my calibration at low energies. I also set the minimum half-life unit to seconds in order to account for the very short lived isotopes characteristic to uranium that has undergone fissions. I tried keeping a tight tolerance ratio since many fission product emissions fall very close to one another, and I wanted to minimize the effects of double counting peaks. Employing these settings provided the results shown by Figure 3.28.

I spent significant time adjusting these parameters to determine the optimal settings that I believe best represent what is truly present. When I changed some parameters, such as the alpha value, I noticed significant changes in the scored nuclides. I decided on the 0.1 value since the top scored nuclides matched the expected top gamma emitters from fission. When my set parameters differed from the optimal settings I discovered, I would see either very few nuclides scored, or nuclides scored that I knew were very unlikely to be present in the highest distinguishable amounts such as  $^{58}\text{Co}$  and  $^{48}\text{Sc}$ .

Score Summary:							
Nuclide	Total	(base +	bonus I,	II,	III)	Comment	Correlation
135I	182.46	( 94.1	50.0	38.4	0.0 )	Fiss_Prod	High
132I	144.08	( 55.7	50.0	38.4	0.0 )	Fiss_Prod	High
59Fe	126.44	( 96.7	1.0	8.8	20.0 )	c	High
88Rb	125.08	( 93.8	0.8	0.5	30.0 )	Fiss_Prod	High
238Np	124.69	( 83.0	0.7	10.9	30.0 )	SNM	High
124Sb	124.06	( 91.9	9.9	22.3	0.0 )	Fiss_Prod	High
140La	121.98	( 90.9	10.6	20.5	0.0 )	Fiss_Prod	High
93Y	113.77	( 71.1	25.3	17.3	0.0 )	Fiss_Prod	High
133Te	113.68	( 87.5	6.9	19.2	0.0 )	Fiss_Prod	High
60Co	111.40	( 97.7	1.0	7.7	5.0 )	c	High
65Ni	109.68	( 99.4	0.8	7.5	2.0 )	c	High
160Tb	106.82	( 77.6	5.1	19.1	5.0 )	Fiss_Prod	Moderate
82Br	106.40	( 88.9	1.6	10.9	5.0 )	Fiss_Prod	Moderate
141Ba	105.86	( 89.9	1.5	9.5	5.0 )	Fiss_Prod	Moderate
106Rh	104.50	( 99.1	0.0	5.4	0.0 )	Fiss_Prod	Moderate
106Ru	104.50	( 99.1	0.0	5.4	0.0 )	Fiss_Prod	Moderate
65Zn	104.33	( 99.3	0.0	5.0	0.0 )	Fiss_Prod	Moderate
214Bi	103.48	( 72.4	14.6	16.4	0.0 )	U-238_Daughter	Moderate
22Na	103.36	( 99.2	0.0	4.1	0.0 )	Cosmic_spall_pr	Moderate
154Eu	101.82	( 85.6	3.0	11.2	2.0 )	Fiss_Prod	Moderate
141La	100.87	( 97.6	0.0	3.2	0.0 )	Fiss_Prod	Moderate
24Na	100.58	( 96.4	1.0	3.2	0.0 )	n_activ_prod	Moderate
41Ar	100.29	( 96.4	0.0	3.9	0.0 )	n_activ_prod	Moderate
209Tl	99.53	( 97.7	0.0	1.9	0.0 )	Np-237_Daughter	Moderate
52mMn	99.34	( 96.6	0.0	2.8	0.0 )	c	Moderate
47Ca	99.15	( 95.2	0.0	3.9	0.0 )	c	Moderate
40K	99.14	( 96.8	0.0	2.4	0.0 )	NORM	Moderate
152Eu	99.11	( 82.7	3.1	13.4	0.0 )	Fiss_Prod	Moderate
61Cu	98.10	( 93.6	0.0	4.5	0.0 )	c	Low
42K	97.72	( 95.9	0.0	1.8	0.0 )	c	Low
238U	96.85	( 91.3	0.0	5.6	0.0 )	SNM	Low
143La	96.82	( 95.8	0.0	1.1	0.0 )	Fiss_Prod	Low
148Pm	94.35	( 92.0	0.0	2.4	0.0 )	Fiss_Prod	Low
212Bi	92.63	( 91.1	0.0	1.5	0.0 )	Th-232_Daughter	Low
89Rb	89.90	( 68.8	5.1	11.0	5.0 )	Fiss_Prod	Low
52Mn	89.32	( 82.6	0.6	6.0	0.0 )	c	Low
240Np	87.94	( 71.4	1.5	10.1	5.0 )	SNM	Low
142Ba	87.23	( 65.9	4.6	14.8	2.0 )	Fiss_Prod	Low
142La	86.99	( 64.2	11.2	11.5	0.0 )	Fiss_Prod	Low
46Sc	86.83	( 81.9	0.0	4.9	0.0 )	c	Low
131mTe	86.82	( 63.3	2.6	15.9	5.0 )	Fiss_Prod	Low
134I	86.66	( 55.1	10.9	20.7	0.0 )	Fiss_Prod	Low
88Kr	83.40	( 67.4	4.6	11.4	0.0 )	Fiss_Prod	Low
48Sc	82.09	( 50.3	0.7	11.1	20.0 )	c	Low
138Cs	81.05	( 71.9	1.6	7.6	0.0 )	Fiss_Prod	Low
228Ac	77.77	( 49.1	1.5	7.1	20.0 )	Th-232_Daughter	Low
234Pa	75.97	( 45.9	9.7	15.3	5.0 )	U-238_Daughter	Low
133mTe	74.58	( 44.0	12.6	18.0	0.0 )	Fiss_Prod	Low
136Cs	70.60	( 65.2	0.0	5.4	0.0 )	Fiss_Prod	Low
92Y	70.15	( 67.3	0.0	2.8	0.0 )	Fiss_Prod	Low
84Br	68.14	( 60.1	4.6	3.4	0.0 )	Fiss_Prod	Low
143Ce	66.72	( 47.8	5.5	13.4	0.0 )	Fiss_Prod	Low

**Figure 3.28:** SmartID identified isotopes from a 5 minute spectra collected immediately following irradiation of a natural uranium fuel rod.

Although peaks less than 982.7 keV were not identified, SmartID was still able to score the most active gamma emitters in spent fuel. The lack of peak identification in the lower energy region was most likely due to the very high emission rates of the short lived

fission products creating a large pileup effect. However, the higher energy emissions provide key identifying information. Figure 3.28 shows the SmartID output listing the most highly correlated nuclides to the peaks identified. The nuclides appearing in the *High* correlated list are nuclides that are expected to be in high concentration immediately following irradiation. Additionally, since the neutron sources were removed very soon before the spectra were collected, it is highly likely that activation products would be present which is confirmed by SmartID.

The top scoring nuclides for the top scoring shielding scenario (10 cm of lead) are made up of highly active fission products,  $^{135}\text{I}$  and  $^{132}\text{I}$ , along with other isotopes not commonly acknowledged with spent fuel.  $^{59}\text{Fe}$  is the third highest scoring nuclide, but this is most likely not from fission. The lab space has many metal objects, including the detector stand, made up of iron.  $^{58}\text{Fe}$  is a naturally occurring isotope of Fe, and although in small concentration, it can capture a neutron to become  $^{59}\text{Fe}$ .  $^{88}\text{Rb}$ ,  $^{238}\text{Np}$ ,  $^{124}\text{Sb}$ ,  $^{140}\text{La}$ ,  $^{93}\text{Y}$  are high gamma emitting nuclides, but some peaks are attributed multiple times. I decreased the tolerance to only allow a 1.5% energy window for peak attribution, to find the order of scored nuclides to change slightly.  $^{135}\text{I}$ ,  $^{59}\text{Fe}$ , and  $^{132}\text{I}$  were still the highest correlated nuclides, but  $^{60}\text{Co}$ ,  $^{65}\text{Ni}$ , and  $^{106}\text{Rh}$  followed. These nuclides could be present due to neutron capture interactions in many of the surrounding materials in the laboratory. Nickel is naturally in steel, and cobalt is produced by neutron activation of iron isotopes.

Utilizing the same parameters as the 1<sup>st</sup> 5 minute case, I post-processed the 20<sup>th</sup> 5 minute case through SmartID. Not only did this case show less counts per second in the detector, but it also showed a change in the spectrum shape due to the short lived isotopes dying out. I saw a decrease in the number of peaks identified using the water DRFs. Figure 3.29 shows the spectrum with peaks identified.

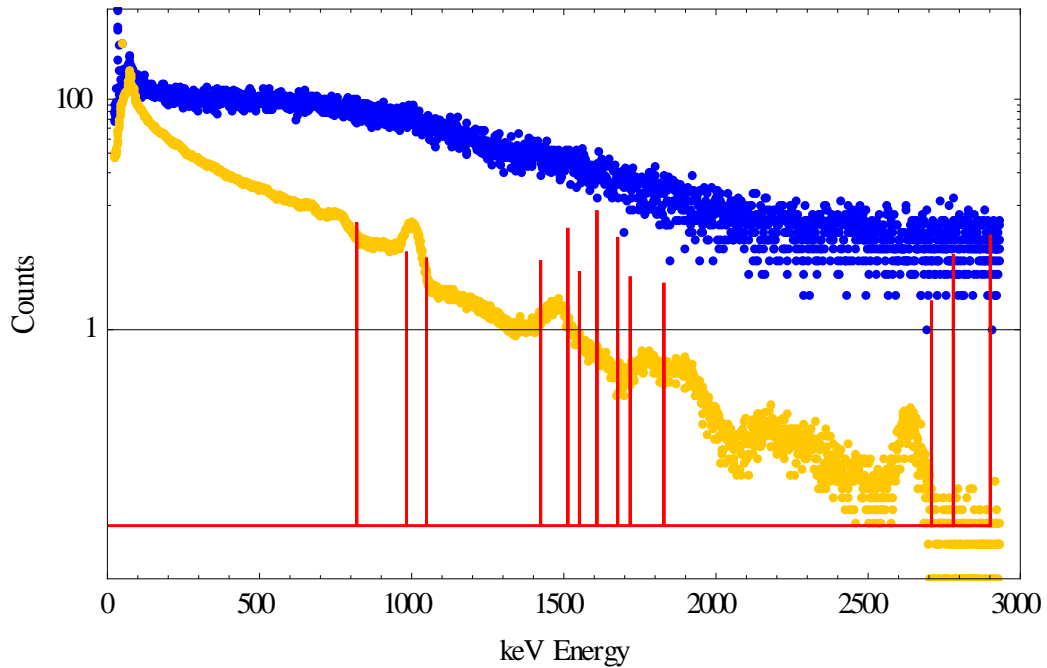


**Figure 3.29:** Peaks identified for the 20<sup>th</sup> 5 minute spectrum using the water DRF option.

The same, 10 cm thick lead, shielding scenario was scored the highest, and the resulting nuclide scoring is shown in Figure 3.30. The order of some nuclides change, but the top 4, highly correlated, nuclides all represent some of the highest gamma emitting nuclides for irradiated fuel. Key identifying peaks for  $^{140}\text{La}$  are clear, especially since many of  $^{140}\text{La}$ 's gamma emissions lie in the upper energies.  $^{42}\text{K}$  is also highly correlated, but I do not believe this nuclide is actually present in a discernable concentration. SmartID only identifies one possible emission out of 2 for this nuclide. Additionally, the photopeak attributed, 1513 keV, is already attributed to emissions of  $^{135}\text{I}$ , which is a much more likely nuclide to be present.

Score Summary:							
Nuclide	Total	(base + bonus I, II, III)				Comment	Correlation
140La	121.88	( 93.5	5.9	22.5	0.0 )	Fiss_Prod	High
132I	119.91	( 35.1	50.0	34.8	0.0 )	Fiss_Prod	High
238Np	118.89	( 83.0	0.7	5.1	30.0 )	SNM	High
135I	109.65	( 33.7	44.4	31.5	0.0 )	Fiss_Prod	High
42K	102.39	( 98.0	0.0	4.4	0.0 )	c	Moderate
58Co	102.34	( 97.5	0.0	4.9	0.0 )	c	Moderate
88Rb	102.18	( 93.9	0.8	2.5	5.0 )	Fiss_Prod	Moderate
106Rh	101.60	( 99.1	0.0	2.5	0.0 )	Fiss_Prod	Moderate
106Ru	101.60	( 99.1	0.0	2.5	0.0 )	Fiss_Prod	Moderate
211Pb	101.27	( 96.5	0.0	4.8	0.0 )	U-235_Daughter	Moderate
143La	100.57	( 98.9	0.0	1.7	0.0 )	Fiss_Prod	Moderate
54Mn	100.54	( 95.8	0.0	4.8	0.0 )	c	Moderate
52mMn	100.33	( 98.0	0.0	2.3	0.0 )	c	Moderate
124Sb	100.12	( 86.2	2.9	11.0	0.0 )	Fiss_Prod	Moderate
209Tl	99.31	( 97.5	0.0	1.8	0.0 )	Np-237_Daughter	Moderate
212Bi	95.94	( 89.7	0.0	6.2	0.0 )	Th-232_Daughter	Low
238U	93.94	( 91.3	0.0	2.6	0.0 )	SNM	Low
228Ac	91.31	( 71.1	4.6	13.5	2.0 )	Th-232_Daughter	Low
136Cs	90.11	( 79.9	0.7	7.5	2.0 )	Fiss_Prod	Low
52Mn	83.64	( 81.4	0.0	2.3	0.0 )	c	Low
138Cs	81.63	( 72.4	0.6	8.6	0.0 )	Fiss_Prod	Low
166mHo	80.38	( 75.0	0.6	4.8	0.0 )	Fiss_Prod	Low
48Sc	76.20	( 50.3	0.7	5.2	20.0 )	c	Low
152Eu	74.87	( 67.4	0.6	4.9	2.0 )	Fiss_Prod	Low
92Y	68.28	( 66.0	0.0	2.3	0.0 )	Fiss_Prod	Low
24Na	64.77	( 62.2	0.0	2.6	0.0 )	n_activ_prod	Low
56Mn	61.97	( 60.5	0.0	1.5	0.0 )	c	Low
134I	58.39	( 37.7	4.1	14.5	2.0 )	Fiss_Prod	Low
234Pa	58.10	( 29.6	12.3	11.2	5.0 )	U-238_Daughter	Low
240Np	57.85	( 54.5	0.6	2.8	0.0 )	SNM	Low
125Sn	56.70	( 48.7	0.6	7.3	0.0 )	Fiss_Prod	Low
214Bi	55.28	( 26.4	8.6	18.3	2.0 )	U-238_Daughter	Low
133Te	52.14	( 41.9	1.5	6.7	2.0 )	Fiss_Prod	Low

**Figure 3.30:** Isotopes identified by SmartID using the water DRF option from a 5 minute spectra collected 1 hour and 35 minutes following irradiation.

In order to see if the nuclide scoring would change significantly if I decreased the tolerance (energy window), I post-processed this spectrum with a maximum 1.5% energy window for photopeak attribution. The resulting nuclide scoring showed <sup>140</sup>La and <sup>135</sup>I as the most likely nuclides followed by <sup>42</sup>K, <sup>58</sup>Co, <sup>88</sup>Rb, <sup>106</sup>Rh, and <sup>106</sup>Ru. As I described previously, I do not believe <sup>42</sup>K to actually be present for the same reasons, but I do find it promising that a cobalt isotope, along with <sup>88</sup>Rb and <sup>106</sup>Rh to be identified. These latter two nuclides were also identified in the 1<sup>st</sup> 5 minute case, and <sup>106</sup>Rh can be directly correlated to fission, especially fissions of <sup>239</sup>Pu.

Since this experiment configuration did differ from the water DRF models, I thought it would be useful to also to process the spectrum using the air DRF model while

utilizing the scattering option. It is recommended that when using this option, it be set initially to 1.25 [1]. I reprocessed the spectrum, each time increasing the scattering option by .1, until I started losing key nuclides I knew should be present, but still maintained a high score for the lead shielding option. I found that I needed to set the scattering parameter to 1.85 for this to occur. Figure 3.31 shows the resulting peaks identified in the spectrum. As noticed, many more peaks are identified in the lower energy ranges than for the previous cases with the water DRFs.

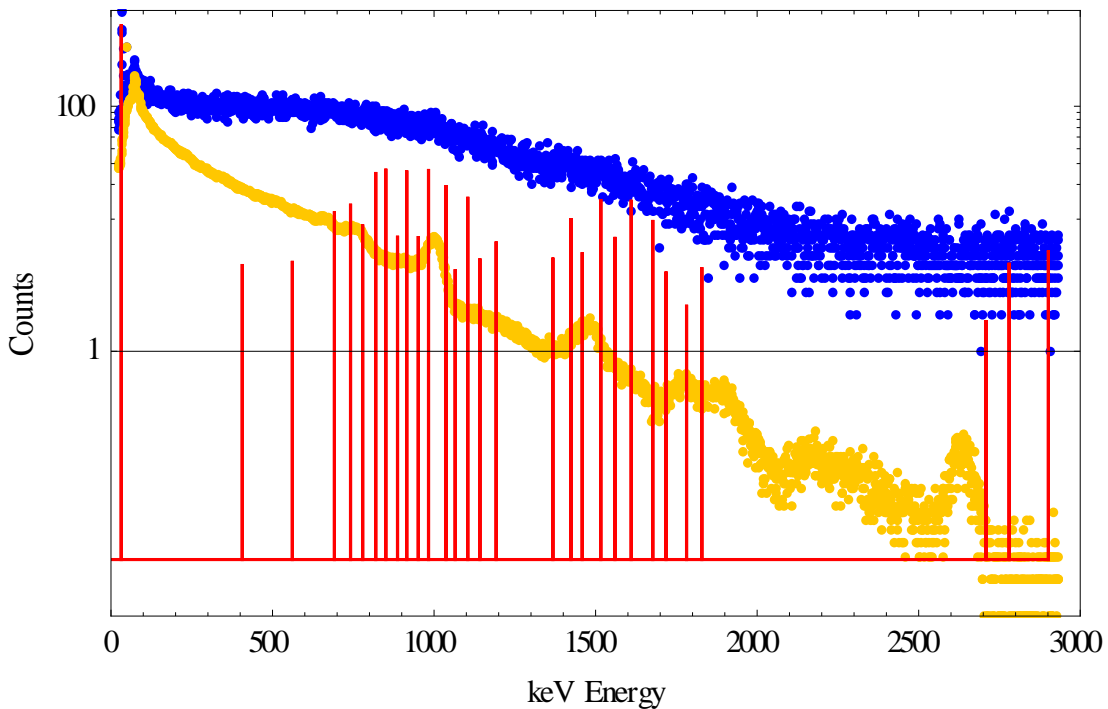


**Figure 3.31:** Peaks identified for the 20<sup>th</sup> 5 minute spectra using the air DRF option and scattered counts scaling factor of 1.85.

The difference between peak identification results shown in Figures 3.29 and 3.31 is most likely a result of the experimental environment. Unlike a spent fuel pool scenario as modeled for the water DRFs, the experiment had greatly decreased the amount of water surrounding the fuel rod and detector. Due to material constraints, the detector was



not submerged underwater. Instead, the detector was pushed against the side of the water tub and the remaining sides were surrounded by air. The irradiated fuel rod was also not fully submerged, allowing some fission products to reach the detector without any interaction with the water. The detector was surrounded by lead shielding, but due to the configuration of the detector and stand, the lead shielding arrangement contained small gaps, allowing gammas scattered off the walls and flooring to enter the detector, and potentially allowing gammas directly from the exposed fuel rod to enter the detector without ever interacting with the water. Referring back to Figure 3.18, it is easy to identify gaps in shielding coverage.

The corresponding nuclides scored from the peaks identified in Figure 3.32. Since the fuel rod is natural uranium, I would expect SmartID to identify the presence of  $^{238}\text{U}$ . For this case, this was confirmed true through the attribution of  $^{234}\text{Pa}$ , a daughter product of  $^{238}\text{U}$ . Figure 3.33 shows the details of the individual gamma attribution for this isotope. It is likely that this is only determined in this case since much of the uranium fuel rod is exposed and out of the water. Many of the gamma emissions from this isotope are most likely not scattered through the water, therefore more emissions have the opportunity to interact with the detector, especially at lower energies.

It is promising to see the fission products scored in Figure 3.30 also scored in Figure 3.32. Investigating further shows nuclides with a higher *bonus score II* match up more closely with those scored in the water DRF case. Recalling Chapter 2, the base score takes into account the overall number of emissions of and isotope and the number of matched peaks with respect to detectability. The second *bonus score* takes into account the number of counts expected to be observed in the full energy peak for each emission. For this spectrum, since only a finite number of peaks are identified, *bonus score II* is a better measure of how likely an isotope is present in the spectrum. Now looking back at Figure 3.31 with this perspective, I see that some of the highest scoring nuclides in the scattering option case are likely not present. For example,  $^{187}\text{W}$  is not a

likely nuclide. When looking closer at its peak attribution, I also see that the peaks attributed have already been attributed to other, higher scored nuclides. I also do not see  $^{46}\text{Sc}$  as a highly likely nuclide do to similar reasoning. I believe  $^{140}\text{La}$  to be present due to the specific emissions attributed.  $^{140}\text{La}$  is unique in that it has high emitting gammas in the MeV range of energies. Looking closely at the peak attribution, Figure 3.34, it is shown that the highest energy emission, 2899.61 keV is attributed, along with its high probability of decay emission at 1596.21 keV. Although, it does attribute some other photopeaks to its lower energy emission, I believe these are actually falsely attributed due to the low probability per decay. I do not see this as an issue in determining the presence of  $^{140}\text{La}$ , since the high energy gammas are relatively unique to this nuclide, and the emissions in question have already been attributed to other nuclides such as  $^{132}\text{I}$  and  $^{238}\text{Np}$ . Overall, the top nuclides scored also correspond to many of the most active nuclides found in spent PWR fuel soon after removal from the reactor core and can be correlated to burnup.

Score Summary:							
Nuclide	Total	(base +	bonus I,	II,	III)	Comment	Correlation
234Pa	159.63	( 90.1	50.0	19.5	0.0 )	U-238_Daughter	High
134I	151.91	( 97.4	35.8	18.7	0.0 )	Fiss_Prod	High
132I	149.29	( 64.4	50.0	34.9	0.0 )	Fiss_Prod	High
135I	148.04	( 70.7	50.0	27.3	0.0 )	Fiss_Prod	High
140La	136.98	( 94.6	20.6	21.8	0.0 )	Fiss_Prod	High
151Fm	132.47	( 62.2	50.0	20.3	0.0 )	Fiss_Prod	High
46Sc	131.35	( 97.3	1.0	3.0	30.0 )	c	High
24Na	130.78	( 98.5	1.0	1.3	30.0 )	n_activ_prod	High
99Mo	126.22	( 98.9	10.7	16.6	0.0 )	medical_FP	High
133mTe	123.77	( 80.6	26.7	16.5	0.0 )	Fiss_Prod	High
131mTe	123.57	( 85.9	22.2	15.5	0.0 )	Fiss_Prod	High
110mAg	121.82	( 92.3	16.4	13.2	0.0 )	Fiss_Prod	High
228Ac	120.30	( 94.6	9.7	11.0	5.0 )	Th-232_Daughter	High
142Ba	117.57	( 90.9	16.4	10.3	0.0 )	Fiss_Prod	High
187W	116.52	( 93.0	0.7	2.8	20.0 )	c	High
238Np	114.33	( 98.3	4.5	9.5	2.0 )	SNM	High
97Zr	112.14	( 85.9	3.0	3.2	20.0 )	Fiss_Prod	High
214Bi	110.61	( 77.5	22.5	10.6	0.0 )	U-238_Daughter	High
240Np	108.86	( 81.0	15.4	12.5	0.0 )	SNM	High
91Sr	108.50	( 96.0	3.5	9.0	0.0 )	Fiss_Prod	High
134Te	108.46	( 93.5	5.0	10.0	0.0 )	Fiss_Prod	High
152Eu	106.45	( 83.5	12.2	5.7	5.0 )	Fiss_Prod	Moderate
124Sb	105.23	( 87.9	7.1	10.3	0.0 )	Fiss_Prod	Moderate
148Pm	103.62	( 98.7	0.7	4.2	0.0 )	Fiss_Prod	Moderate
143Ce	103.07	( 55.7	30.1	17.3	0.0 )	Fiss_Prod	Moderate
88Rb	102.61	( 98.4	2.5	1.7	0.0 )	Fiss_Prod	Moderate
92Sr	101.74	( 97.2	2.2	2.3	0.0 )	Fiss_Prod	Moderate
57Co	100.87	( 99.3	0.0	1.6	0.0 )	c	Moderate
166mHo	100.80	( 83.2	6.6	8.9	2.0 )	Fiss_Prod	Moderate
233Pa	100.79	( 99.2	0.0	1.6	0.0 )	Np-237_Daughter	Moderate
97mNb	100.75	( 98.9	0.0	1.8	0.0 )	Fiss_Prod	Moderate
58Co	100.73	( 97.5	0.0	3.3	0.0 )	c	Moderate
42K	100.37	( 98.4	0.0	2.0	0.0 )	c	Moderate
101Tc	100.22	( 98.6	0.0	1.6	0.0 )	Fiss_Prod	Moderate
40K	99.90	( 99.1	0.0	0.7	0.0 )	NORM	Moderate
129mTe	99.89	( 98.3	0.0	1.6	0.0 )	Fiss_Prod	Moderate
209Tl	99.59	( 98.6	0.0	1.0	0.0 )	Np-237_Daughter	Moderate
65Zn	99.55	( 97.5	0.0	2.1	0.0 )	Fiss_Prod	Moderate
52mMn	99.43	( 98.0	0.0	1.4	0.0 )	c	Moderate
143La	99.41	( 98.9	0.0	0.5	0.0 )	Fiss_Prod	Moderate
214Pb	98.92	( 97.7	0.0	1.2	0.0 )	U-238_Daughter	Low
140Ba	98.74	( 97.2	0.0	1.6	0.0 )	Fiss_Prod	Low
141La	98.28	( 97.6	0.0	0.7	0.0 )	Fiss_Prod	Low
90Y	98.19	( 96.6	0.0	1.5	0.0 )	Fiss_Prod	Low
44Sc	97.53	( 96.9	0.0	0.6	0.0 )	c	Low
61Cu	96.71	( 91.7	0.7	4.3	0.0 )	c	Low
125Sn	96.68	( 83.8	3.5	9.4	0.0 )	Fiss_Prod	Low
136Cs	94.38	( 82.7	0.7	5.9	5.0 )	Fiss_Prod	Low
57Ni	93.08	( 86.4	0.7	0.9	5.0 )	c	Low
212Bi	92.61	( 83.6	0.8	3.2	5.0 )	Th-232_Daughter	Low
147Nd	91.89	( 90.3	0.0	1.6	0.0 )	Fiss_Prod	Low

**Figure 3.32:** SmartID identified isotopes with scores greater than 91.89 using the air DRF and scattered counts scaling option from a 5 minute spectra collected 1 hour and 35 minutes following irradiation of a natural uranium fuel rod.

Scored nuclides details:							
Nuclide	Score	T1/2	T1/2_unit	#EmissionInRange	#Matched	Correlation	
<sup>234</sup> Pa	159.63	7.6500E-04	y	44	29	High	
Emission(KeV)	Prob/DK	Detectability	1.50%	Energy Window	Peak(KeV)	Norm%_cts	
369.80	2.9600E-02	2.6450E-01	(	364.25 to 375.35 )			
372.40	1.3300E-02	2.6102E-01	(	366.81 to 377.99 )			
458.80	1.5300E-02	1.7609E-01	(	451.92 to 465.68 )			
506.80	1.6300E-02	1.4364E-01	(	499.20 to 514.40 )			
513.70	1.3300E-02	1.4017E-01	(	505.99 to 521.41 )			
+ 565.90	1.4300E-02	1.1634E-01	(	557.41 to 574.39 )	561.22		1.5470
+ 568.70	3.0600E-02	1.1517E-01	(	560.17 to 577.23 )	561.22		1.5470
+ 569.50	1.0900E-01	1.1484E-01	(	560.96 to 578.04 )	561.22		1.5470
574.00	2.0400E-02	1.1300E-01	(	565.39 to 582.61 )			
664.80	1.3300E-02	8.6177E-02	(	654.83 to 674.77 )			
666.70	1.6300E-02	8.5728E-02	(	656.70 to 676.70 )			
669.90	1.4300E-02	8.4978E-02	(	659.85 to 679.95 )			
+ 699.00	4.6900E-02	7.8434E-02	(	688.52 to 709.49 )	691.66		3.9224
706.10	3.1600E-02	7.6912E-02	(	695.51 to 716.69 )			
+ 733.00	8.7700E-02	7.1395E-02	(	722.01 to 744.00 )	741.17		4.5257
+ 738.00	1.0200E-02	7.0412E-02	(	726.93 to 749.07 )	741.17		4.5257
+ 742.81	2.4500E-02	6.9479E-02	(	731.67 to 753.95 )	741.17		4.5257
755.60	1.4300E-02	6.7053E-02	(	744.27 to 766.93 )			
+ 780.70	1.1200E-02	6.2526E-02	(	768.99 to 792.41 )	778.67		3.0712
+ 786.27	1.4300E-02	6.1561E-02	(	774.48 to 798.06 )	778.67		3.0712
793.60	1.5300E-02	6.0314E-02	(	781.70 to 805.50 )			
796.30	3.8800E-02	5.9860E-02	(	784.36 to 808.24 )			
805.60	3.3700E-02	5.8583E-02	(	793.52 to 817.68 )			
+ 819.60	2.6500E-02	5.6959E-02	(	807.31 to 831.89 )	819.18		8.2070
+ 826.30	4.0800E-02	5.6197E-02	(	813.91 to 838.69 )	819.18		8.2070
+ 831.60	5.6100E-02	5.5602E-02	(	819.13 to 844.07 )	819.18		8.2070
+ 876.40	4.0800E-02	5.0803E-02	(	863.25 to 889.55 )	886.69		2.4800
+ 880.51	1.3220E-01	5.0383E-02	(	867.30 to 893.72 )	886.69		2.4800
+ 883.24	1.2200E-01	5.0106E-02	(	869.99 to 896.49 )	886.69		2.4800
+ 899.00	4.1800E-02	4.8535E-02	(	885.52 to 912.48 )	886.69		2.4800
+ 925.00	2.9600E-02	4.6045E-02	(	911.13 to 938.87 )	915.19		8.4563
+ 926.00	1.1200E-01	4.5952E-02	(	912.11 to 939.89 )	915.19		8.4563
+ 926.72	9.1800E-02	4.5885E-02	(	912.82 to 940.62 )	915.19		8.4563
+ 946.00	1.2200E-01	4.4124E-02	(	931.81 to 960.19 )	951.20		2.4658
+ 949.00	8.1600E-02	4.3856E-02	(	934.77 to 963.23 )	951.20		2.4658
+ 955.59	1.0100E-02	4.3273E-02	(	941.26 to 969.92 )	951.20		2.4658
+ 978.80	1.4300E-02	4.1276E-02	(	964.12 to 993.48 )	982.70		8.6883
+ 980.50	5.1000E-02	4.1134E-02	(	965.79 to 995.21 )	982.70		8.6883
+ 984.00	1.9400E-02	4.0841E-02	(	969.24 to 998.76 )	982.70		8.6883
+ 1353.30	1.7300E-02	2.3728E-02	(	1333.00 to 1373.60 )	1367.40		1.6446
1394.10	3.0600E-02	2.2604E-02	(	1373.19 to 1415.01 )			
+ 1452.70	1.0200E-02	2.1081E-02	(	1430.91 to 1474.49 )	1458.40		1.8213
+ 1668.50	1.2200E-02	1.7114E-02	(	1643.47 to 1693.53 )	1676.80		3.3360
+ 1694.60	1.2200E-02	1.6715E-02	(	1669.18 to 1720.02 )	1676.80		3.3360

**Figure 3.33:** Photopeak attribution for <sup>234</sup>Pa using the air DRF and scattered counts scaling option from a 5 minute spectra collected 1 hour and 35 minutes following irradiation of a natural uranium fuel rod.

Nuclide	Score	T1/2	T1/2_unit	#EmissionInRange	#Matched	Correlation
<sup>140</sup> La	136.98	4.0300E+01	h	28	11	High
Emission(KeV)	Prob/DK	Detectability	1.50%	Energy Window	Peak(KeV)	Norm%_cts
306.90	2.4800E-04	3.6098E-01	(	302.30 to 311.50 )		
328.76	2.0300E-01	3.2465E-01	(	323.83 to 333.69 )		
397.52	7.3500E-04	2.2929E-01	(	391.56 to 403.48 )		
432.49	2.9000E-02	1.9717E-01	(	426.00 to 438.98 )		
438.50	3.9100E-04	1.9216E-01	(	431.92 to 445.08 )		
445.50	2.8600E-05	1.8648E-01	(	438.82 to 452.18 )		
487.02	4.5500E-01	1.5575E-01	(	479.71 to 494.33 )		
618.12	3.7200E-04	9.7921E-02	(	608.85 to 627.39 )		
+ 751.64	4.3300E-02	6.7795E-02	(	740.37 to 762.91 )	741.17	4.5257
+ 815.77	2.3300E-01	5.7399E-02	(	803.53 to 828.01 )	819.18	8.2070
867.85	5.5000E-02	5.1687E-02	(	854.83 to 880.87 )		
+ 919.55	2.6600E-02	4.6557E-02	(	905.76 to 933.34 )	915.19	8.4563
+ 925.19	6.9000E-02	4.6027E-02	(	911.31 to 939.07 )	915.19	8.4563
+ 950.99	5.1900E-03	4.3679E-02	(	936.73 to 965.25 )	951.20	2.4658
+ 992.90	1.3400E-04	4.0107E-02	(	978.01 to 1007.79 )	982.70	8.6883
+ 1045.05	2.4800E-04	3.6570E-02	(	1029.37 to 1060.73 )	1036.70	6.4133
+ 1097.20	2.2900E-04	3.3807E-02	(	1080.74 to 1113.66 )	1104.20	5.1494
1303.50	4.2000E-04	2.5172E-02	(	1283.95 to 1323.05 )		
+ 1405.20	5.9100E-04	2.2308E-02	(	1384.12 to 1426.28 )	1423.50	3.4563
+ 1596.21	9.5400E-01	1.8269E-02	(	1572.27 to 1620.15 )	1610.00	4.8766
1877.29	4.1000E-04	1.4166E-02	(	1849.13 to 1905.45 )		
1924.62	1.3400E-04	1.3570E-02	(	1895.75 to 1953.49 )		
2083.20	1.1500E-04	1.1978E-02	(	2051.95 to 2114.45 )		
2347.88	8.4900E-03	1.0254E-02	(	2312.66 to 2383.10 )		
2464.10	1.1400E-04	9.5771E-03	(	2427.14 to 2501.06 )		
2521.40	3.4600E-02	9.2597E-03	(	2483.58 to 2559.22 )		
2547.34	1.0100E-03	9.1195E-03	(	2509.13 to 2585.55 )		
+ 2899.61	6.6800E-04	7.4109E-03	(	2856.12 to 2943.10 )	2901.00	1.8885

**Figure 3.34:** Photopeak attribution for <sup>140</sup>La using the air DRF and scattered counts scaling option from a 5 minute spectra collected 1 hour and 35 minutes following irradiation of a natural uranium fuel rod.

The results shown by Figure 3.32 from the air DRFs with scattered counts scaling factor similarly emphasize the presence of fission products in the spectrum. But this time with the additional energy peaks identified, the *base score* and *bonus score I* are represented better. I mentioned that <sup>132</sup>I would actually be one of the most likely fission products seen for the water DRF case if I looked at *bonus score II*. *Bonus score II* examines the emission rates instead of the other scores due to the lack of peaks identified. This is shown to be true in the Figure 3.22 case. Many more emissions are identified, and the highest scoring nuclide is <sup>132</sup>I.

I have shown in this chapter that SmartID appears to perform very well under highly complicated backgrounds, and irradiated fuel scenarios. The next chapter will build upon this concept with simulated spectrums I developed from modeling a PWR fuel assembly.

### 3.3 References

- [1] LAVIGNE, E., SJODEN, G., BACIAK, J., and DETWILER, R. “Advanced Synthetically Enhanced Detector Resolution Algorithm (ASEDRA) Users Guide.” Rev 1.8. HSW Technologies LLC. Copyright 2010.

## CHAPTER 4

### SIMULATED SPECTRAL ANALYSIS

#### 4.1 Origen Source

In the preceding chapter, I collected real spectra of known calibration sources and also of an irradiated fuel rod. SmartID performed well for each case, but in order to justify and demonstrate that SmartID can identify with a high level of accuracy nuclides in a complicated fuel assembly, I need to analyze a spectrum representing a Westinghouse 17x17 PWR spent fuel assembly after 1 day since removal from the reactor core. I considered simulated spectral information instead of collected data in order to have clear comparison to the actual material present in the fuel assembly. Since I am modeling a source with a known material composition, I will be able to compare the results from SmartID and the original emissions modeled directly. For the purposes of this dissertation, and the ideas explored, a collected spectrum is not needed.

In order to develop a representative burned PWR fuel assembly model in water, I determined the individual gamma emissions expected from such a source. This was completed by employing the ORIGEN/ORIGEN-ARP modules that are isotopic depletion and decay analysis tools part of the Oak Ridge National Laboratory SCALE6 code system [1]. This code system is used worldwide to provide fuel depletion analyses as a much faster alternative to traditional burnup analyses [1]. The cross sections used for analysis are pre-computed from a reactor physics transport code modeling the fuel assembly design and reactor type. For the purposes of my evaluation of spent fuel, I have considered a Westinghouse PWR 17x17 fuel assembly. ORIGEN allows the user to define the fuel type, enrichment, and irradiation conditions, for which it interpolates from

the pre-computed cross sections. This significantly reduces the computational time without altering the accuracy of the solution.

All nuclides included in the ORIGEN-S library are analyzed, and ORIGEN determines the isotopic compositions of the spent fuel materials as a function of time in order to determine decay heat generation and the resulting radiation source terms [1]. Therefore, it produces a detailed output file accounting for all decay daughter products and their radiation contributions based on mass yield. It also provides the unique gamma and neutron spectra as a function of decay time per energy group for the material in question. It has been validated extensively for light water reactor (LWR) spent fuel, and many benchmarking studies have been completed for MOX fuel calculations [1].

For the Westinghouse 17x17 PWR fuel assembly, I set the initial enrichment to 2.6 weight percent  $^{235}\text{U}$ , with the total amount of uranium in the assembly set to 1 Metric Ton. I chose the 238 energy group SCALE neutron library group structure, and constructed my gamma energy group structure equal to the 24 group structure outlined in previous chapters. I considered three burnup cycles with continuous 37.8 MW/MTU at 95% power, resulting in a total burnup of 33,000 MWD/MTU. I set my decay cases for 0.01, 0.03, 0.1, 0.3, 1, 3, 10, 30, 100, and 130 days after the last burn cycle. These cases show the activities and masses for the fission products and actinides at the determined times after the burn cycle concludes. For my analyses, I only considered the 1 day decay case in order to determine the key gamma information that can be gathered by a NaI(Tl) detector when a fuel assembly is moved from the reactor core to a spent fuel pool for cooling.

The resulting ORIGEN output provides a list of the individual radionuclides produced and their corresponding activities in Curies and concentrations in grams. Additionally, gamma contributions, in photons/s/basis, from each energy group were printed, providing a sense of how the overall gamma spectrum would behave. From this information, the individual gamma emission contributions for each isotope were



determined. The individual emission lines are plotted in Figure 4.1. There are over 3,000 gamma emissions present between energy range of 0.3 to 3.0 MeV. The rate of gamma emission is for the total emission contribution from the entire fuel assembly.

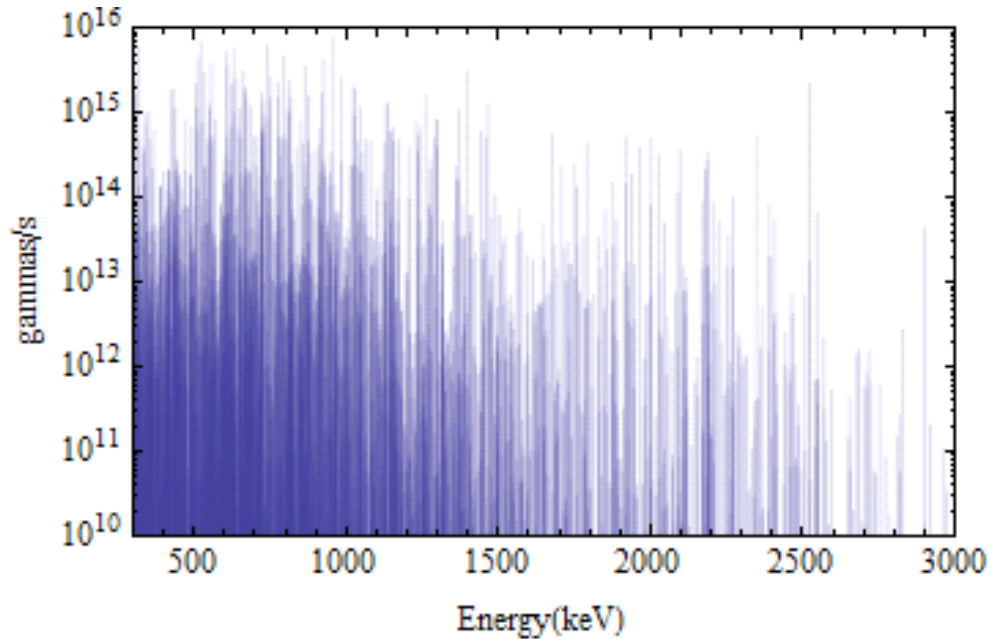


**Figure 4.1:** Identified gamma line emissions from a Westinghouse 17x17 PWR fuel assembly burned to 33,000 MWD and cooled for 1 day, representing emissions from 73 nuclides.

The majority of gamma emissions originate in the lower energy range, with the average photon emission from both x-rays and gammas at 0.7519 MeV. The large quantity of gamma emissions, especially those with energies less than 1 MeV, pose a challenge for SmartID to accurately account for every single emission. However, this is not the intended scope of this study. I restrict my interest to be key radionuclides which contribute the greatest emission rate to the spectrum, while also providing informative data on the burnup to aid in estimating plutonium content. Therefore, I decreased the number of fission products considered to fifteen, analyzing those with the greatest

gamma peak contributions. Table 4.1 shows the considered nuclides, along with their greatest contributing gamma emission. Details on the thermal fission yields from these nuclides can be found in Chapter 5.5, Table 5.4.

**Table 4.1:** Top 15 gamma emitting isotopes from PWR fuel assembly burned to 33,000 MWD 1 day since removal from reactor.

Isotope	T <sub>1/2</sub>	Energy (MeV)	Emission rate (gamma/s)
<sup>140</sup> La	1.6781 d	1.5962	6.3082 10 <sup>16</sup>
<sup>103</sup> Ru	39.26 d	0.49709	5.9303 10 <sup>16</sup>
<sup>95</sup> Nb	34.975 d	0.7658	5.5422 10 <sup>16</sup>
<sup>132</sup> I	1.387 h	0.66771	4.4540 10 <sup>16</sup>
<sup>95</sup> Zr	64.02 d	0.75673	3.0665 10 <sup>16</sup>
<sup>97</sup> Nb	72.1 m	0.65794	2.2804 10 <sup>16</sup>
<sup>97m</sup> Nb	52.7 s	0.74336	2.1928 10 <sup>16</sup>
<sup>97</sup> Zr	16.9 h	0.74336	2.1690 10 <sup>16</sup>
<sup>140</sup> Ba	12.752 d	0.53726	1.4779 10 <sup>16</sup>
<sup>99</sup> Mo	65.94 h	0.73950	6.5565 10 <sup>15</sup>
<sup>134</sup> Cs	2.0648 y	0.60472	5.4602 10 <sup>15</sup>
<sup>106</sup> Rh	29.8 s	0.51186	4.5767 10 <sup>15</sup>
<sup>137</sup> Cs <sup>2</sup>	30.07 y	0.66166	3.3296 10 <sup>15</sup>
<sup>238</sup> Np	2.117 d	0.98445	2.6747 10 <sup>15</sup>
<sup>91</sup> Sr	9.63 h	1.0243	2.1567 10 <sup>15</sup>

Removing the remaining gamma emissions from isotopes not included in this list results in a more manageable emission profile shown by Figure 4.2. However, there are still many very close emission lines that would make computational modeling difficult in order to produce a simulated spectrum. Reducing the number of nuclides considered

<sup>2</sup> This emission is actually from <sup>137m</sup>Ba, a decay daughter of <sup>137</sup>Cs

from 15 to 10 reduces the number of gamma emissions considered from 319 to 130. I did this by removing the isotopes  $^{91}\text{Sr}$ ,  $^{132}\text{I}$ ,  $^{99}\text{Mo}$ ,  $^{95}\text{Nb}$ , and  $^{97\text{m}}\text{Nb}$ .  $^{132}\text{I}$  has many emissions, and removing this isotope from the source list greatly reduces the number of emissions by 137. The gamma emission from  $^{91}\text{Sr}$ 's highest emitting gamma energy had the lowest gamma emission strength in comparison to the other top 15 isotopes, and  $^{95}\text{Nb}$  only had two gamma emissions, both less than 0.766 MeV. Figure 4.3 shows the remaining emissions. Comparing Figure 4.3 to Figure 4.2 shows a thinning out of gamma emissions, but the overall emission profile is not significantly altered.

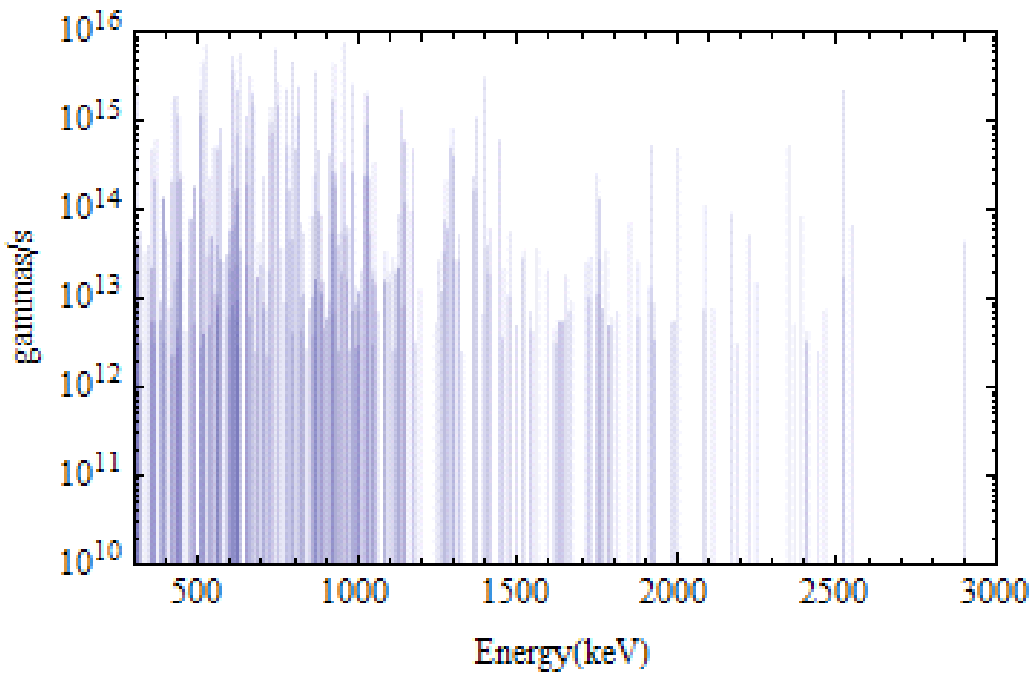


**Figure 4.2:** 319 gamma emissions identified from 15 major isotopes found in spent fuel after 1 day of cooling.

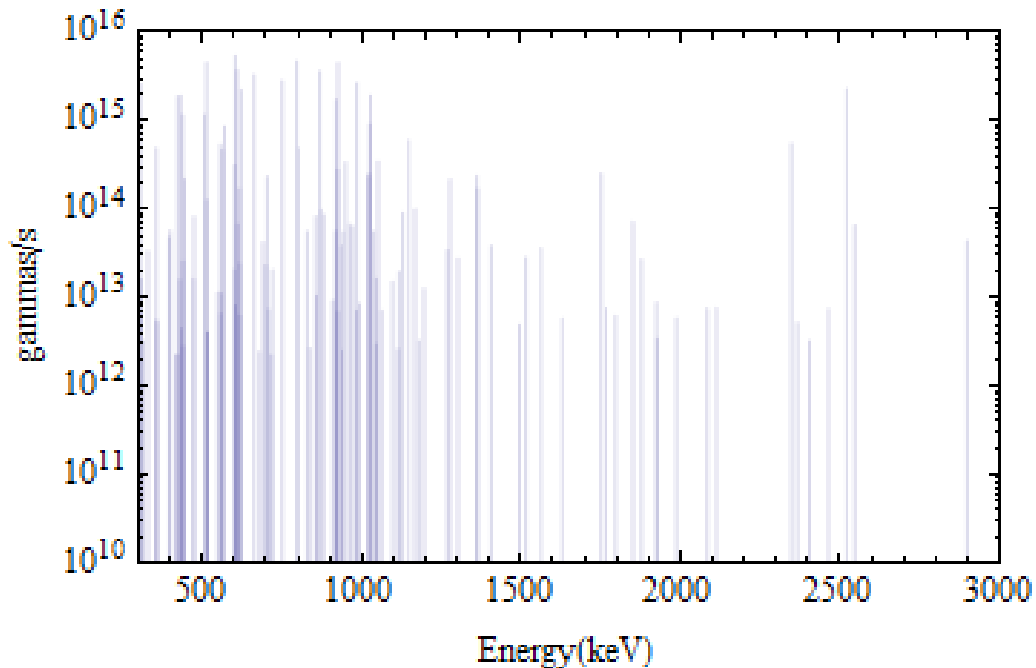


**Figure 4.3:** 130 gamma emissions identified from 10 major isotopes found in spent fuel after 1 day of cooling.

## 4.2 MCNP models

The MCNP models developed for the burned fuel assembly simulation were developed from the models generated for the DRF computations. Therefore, it is expected that SmartID can identify the gamma emissions included in the MCNP source definitions for burnup analysis test cases.

Just as I created three gamma emission profiles, I created three MCNP source models based on these profiles. For the 319 and 130 gamma emission source models, I simulated spectra for both water and air as the gamma transport medium. Instead of developing a model with all 3,000+ possible gamma emissions, I only considered the strongest 1,022 emissions. In order to simulate the detector response for a NaI(Tl) detector, I employed the Gaussian energy broadening (GEB) option for an F8 pulse height tally [2]. Equation 4.1 shows how MCNP incorporates this option by utilizing 3

user specified constants. Table 4.2 shows the resulting FWHM values computed from the GEB setting employed in the models.

$$FWHM = a + b\sqrt{E + cE^2} \quad (4.1)$$

where  $a$ ,  $b$  and  $c$  are user defined constants, and  $E$  is the energy of the emission in units of MeV. For my model, I set  $a = -7.25 \times 10^{-3}$ ,  $b = 0.073219$ , and  $c = 0.313286$ . Including a GEB option for the MCNP simulations is necessary in order to best represent a true detector spectrum. Scintillator detectors accumulate counts correlating to specific gamma energies, but this does not mean all counts will be the exact energy emission. Counts seen in a detector follow a Gaussian (or Normal) distribution [3]. The counts can be represented by

$$G(E) = \frac{1}{\sqrt{2\pi}\sigma} e^{\left(-\frac{1}{2}\left(\frac{E-E_{peak}}{\sigma}\right)^2\right)} \quad (4.2)$$

Where from the mathematical definition for a Gaussian distribution relating the FWHM to  $\sigma$ .

$$\sigma = \frac{FWHM}{2\sqrt{2\ln(2)}} \quad (4.3)$$

$E$  is energy, and  $E_{peak}$  is the energy of the peak or emission [3]. Figure 4.4 shows a Gaussian distribution and how the FWHM is determined.

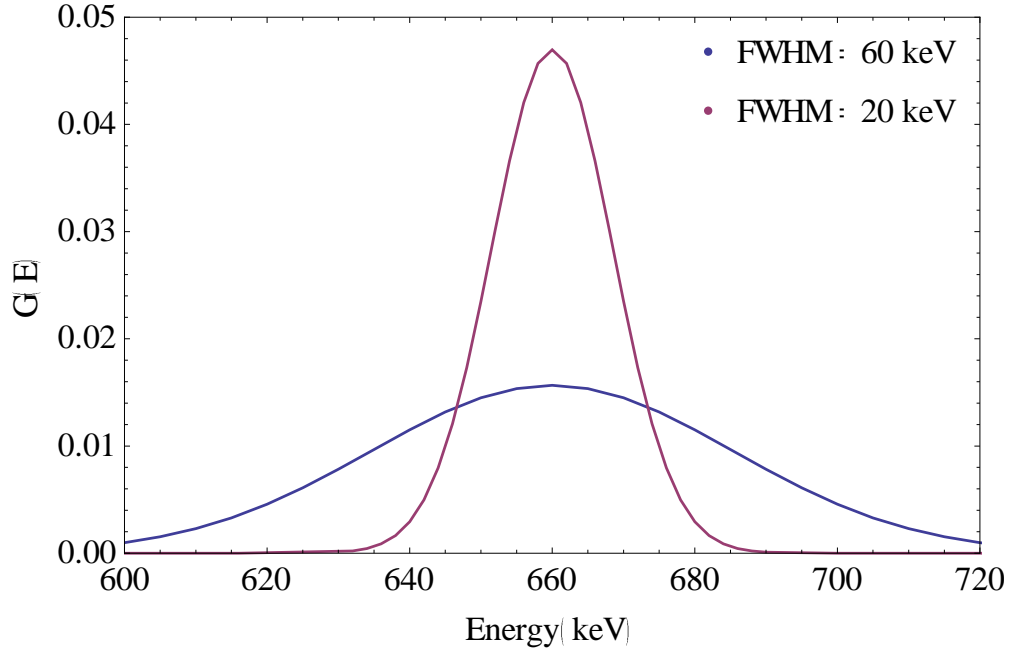


**Figure 4.4:** Gaussian distributions for a mean energy of 660 keV.

**Table 4.2:** FWHM values from Gaussian Energy Broadening setting in MCNP.

Peak Energy (keV)	FWHM (keV)
81	13.85
121.8	18.78
356	38.80
661.7	58.19
1173.2	85.49
1274.5	90.52
1332.5	93.37
2614.5	152.42

The 319 emissions and 1,022 emissions models were executed for  $10^{12}$  particle histories, and the 130 gamma emission water case was executed for  $2 \times 10^{12}$  particle histories in order to minimize errors. All cases were executed in parallel on 100 processors. Computational time and demand was one of the greatest challenges for these

simulations; MCNP requires significant time for particle transport through large absorbing and scattering mediums such as water. I employed variance reduction techniques and reduced the size of my model to decrease computation time, but the models still required approximately 4 to 5 days to run on 100 processors.

Figure 4.5 shows both the water and air cases for the 15 isotope source. As expected, the air model shows more defined peaks and valleys whereas the water model seems relatively blurred due to the increased Compton interactions. Figure 4.6 shows how much more error is introduced in the water MCNP model in comparison to the air model.

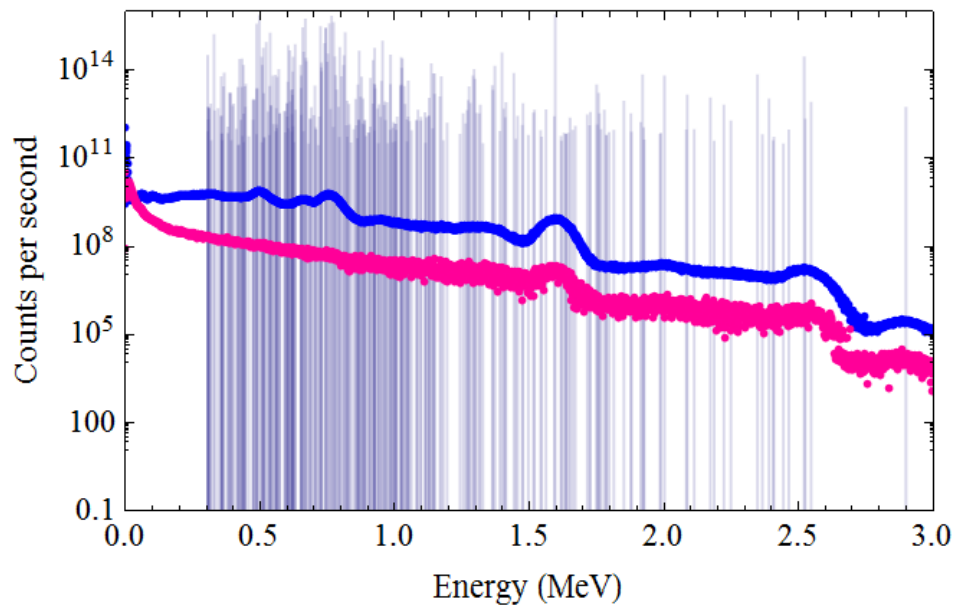


**Figure 4.5:** MCNP simulated spectra for 319 gamma emissions from spent fuel in both air and water. The spectrum in air is shown in blue and the spectrum in water is shown in pink. Emissions are depicted by the vertical lines.

The blurry condition of the water case is not entirely an attribute of gamma transport through water, but a result of increased statistical error from the Monte Carlo calculations. Figure 4.6 shows how the 1 sigma errors differ for the air and water cases

with the same number of particle histories. The significant errors due to the water serving as a shield are observed in the water case, and this can cause large errors when analyzing the spectrum for gamma emissions and the relative contributions of counts to each emission. This should be taken into consideration when processing the spectrum with SmartID.

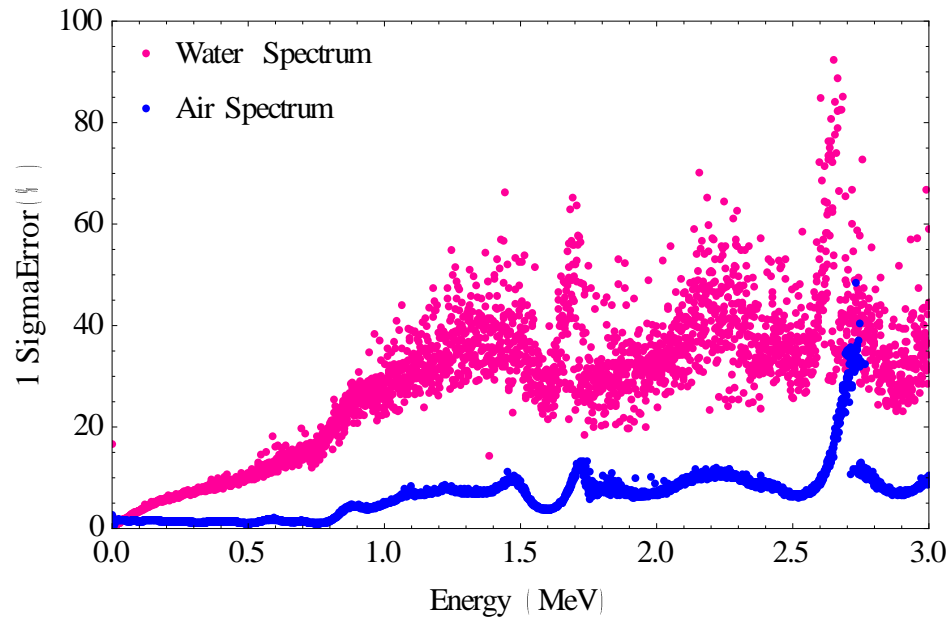


**Figure 4.6:** MCNP 1 sigma errors for 319 gamma emissions from spent fuel assembly gamma spectrum through water and air.

### 4.3 SmartID Analysis

The simulated spectra are unique in the fact that no background is introduced into each case. SmartID still requires a background .Spe file, so I created one with zero counts in every bin. The detector “channels” are essentially the 1keV bin structure implemented in my f8 MCNP tallies making the “Energy.txt” a list of channels corresponding to the energy in keV [2]. The “FWHM.txt” file is no longer derived from calibration spectra, but from the calculated GEB setting used for the f8 tally. Appendix B



contains the “.Spe”, “Energy.txt”, and “FWHM.txt” files used for SmartID isotope identification from each case.

#### **4.3.1. 319 Emissions from 15 Isotopes Case**

I continued to examine the 319 gamma emissions from the top 15 isotopes case spectra shown by Figure 4.5. Both the in air and in water spectra were post processed by the SmartID algorithm to extract peak information and predict the most likely nuclides present. The results were intriguing. Although only emissions from 15 isotopes were included in the models, SmartID scored additional fission products higher than many of the isotopes actually present due to the number of isotopes with similar energies, and due to the highly complex emission profile. Many of the emissions for fission products lie within tight energy and magnitude ranges of other fission product emissions. Therefore, it is important to incorporate only the most substantial gamma emitters in order to best determine which peaks are actually correlated to certain emissions. I determined that for spent fuel analysis, it would be important to develop a nuclide library specifically tailored to short cooled spent fuel measurements. Including too many low yield and low gamma emitting nuclides can result in many peaks being double counted and potentially falsely attributed. Considering the greatest emitting nuclides release gammas on the order of  $10^{16}$ , I only included nuclides in the library that had at least one gamma emission greater than  $1 \times 10^{13}$  gammas per second for the total fuel assembly. Appendix C shows the new gamma library.

Processing the 319 gamma emissions in air case with SmartID resulted in the identification of 46 peaks. Figure 4.7 shows the air case with identified emissions.

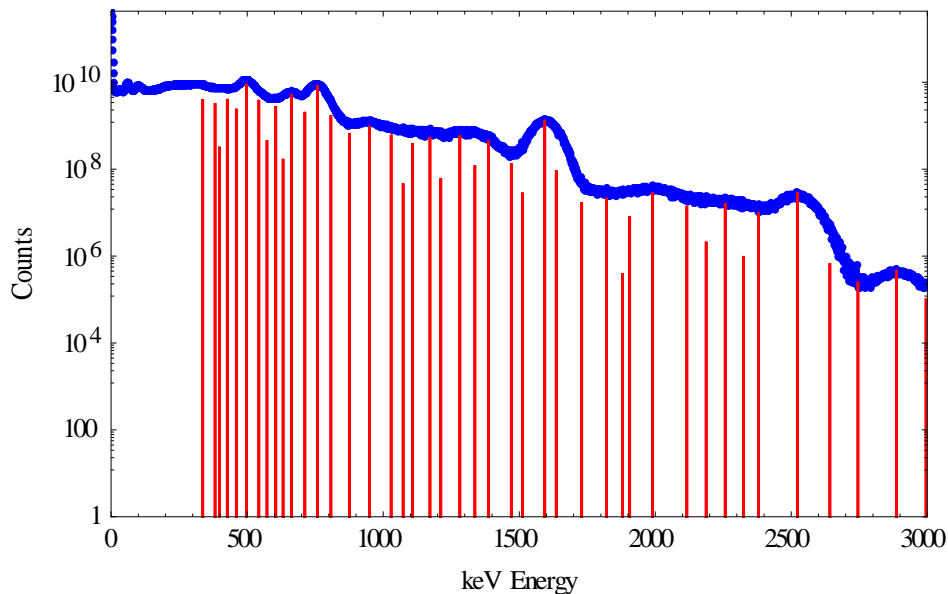


**Figure 4.7:** Peaks identified from a NaI(Tl) spectrum measuring 319 gamma emissions from a burned PWR fuel assembly in air.

SmartID does a great job of identifying energy peaks that were included in the original MCNP models. With a narrow energy window of 0.5%, SmartID identified 10 out of the 15 included nuclides in the simulated spectrum. The top 3 nuclides,  $^{103}\text{Ru}$ ,  $^{137}\text{mBa}$ , and  $^{137}\text{Cs}$  were the highest scored and can all be attributed to the original MCNP model. SmartID can score many nuclides not actually present in the spectrum. This is due to the peak tolerance,  $\epsilon$ . The energy window is selected for determining whether an emission lies within  $\epsilon E < \text{peak} < (1+\epsilon E)$ . At especially high gamma energies, this range can cause very large energy windows. For example, a 1596.21 keV emission with  $\epsilon = 1\%$  will match peaks identified at energies between 1554.71 and 1637.71 keV. Since many of the peaks identified fall in this upper energy range, it is best to tighten the energy window so that I can best correlate the identified peaks. Table 4.3 shows the identified energy peaks for the 15 nuclides included in the MCNP model that were matched within an energy window of  $\epsilon = 0.5\%$ .

**Table 4.3:** Identified Peaks for the 15 nuclides in air included in the MCNP simulation.

Identified Peak (keV)	Counts	Nuclide	Attributed Emission (keV)	Probability of Decay	Detectability
304	$5.09 \times 10^8$	$^{140}\text{Ba}$	304.85	$4.29 \times 10^{-2}$	$3.65 \times 10^{-1}$
337	$2.39 \times 10^9$				
362	$4.14 \times 10^8$	$^{132}\text{I}$	363.34	$4.94 \times 10^{-3}$	$2.73 \times 10^{-1}$
386	$1.87 \times 10^9$	$^{132}\text{I}$	387.9	$8.88 \times 10^{-3}$	$2.41 \times 10^{-1}$
408	$3.32 \times 10^8$				
433	$2.70 \times 10^9$	$^{140}\text{La}$	432.49	$2.90 \times 10^{-2}$	$1.97 \times 10^{-1}$
		$^{132}\text{I}$	431.8	$4.74 \times 10^{-3}$	$1.98 \times 10^{-1}$
465	$1.25 \times 10^9$				
497	$8.55 \times 10^9$	$^{103}\text{Ru}$	497.08	$8.89 \times 10^{-1}$	$1.49 \times 10^{-1}$
543	$3.29 \times 10^9$				
573	$2.29 \times 10^8$	$^{132}\text{I}$	572.5	$5.92 \times 10^{-4}$	$1.14 \times 10^{-1}$
605	$2.19 \times 10^9$	$^{97}\text{Zr}$	602.37	$1.38 \times 10^{-2}$	$1.02 \times 10^{-1}$
		$^{134}\text{Cs}$	604.7	$9.76 \times 10^{-1}$	$1.02 \times 10^{-1}$
632	$1.23 \times 10^8$	$^{132}\text{I}$	630.19	$1.33 \times 10^{-1}$	$9.47 \times 10^{-2}$
663	$4.86 \times 10^9$	$^{137\text{m}}\text{Ba}$	661.65	$9.00 \times 10^{-1}$	$8.69 \times 10^{-2}$
712	$1.86 \times 10^9$				
758	$8.40 \times 10^9$	$^{95}\text{Zr}$	756.73	$5.45 \times 10^{-1}$	$6.68 \times 10^{-2}$
808	$1.73 \times 10^9$	$^{132}\text{I}$	809.5	$2.57 \times 10^{-2}$	$5.81 \times 10^{-2}$
		$^{132}\text{I}$	812	$5.53 \times 10^{-2}$	$5.81 \times 10^{-2}$
876	$5.84 \times 10^8$	$^{132}\text{I}$	876.6	$1.04 \times 10^{-2}$	$5.08 \times 10^{-2}$
949	$9.34 \times 10^8$	$^{140}\text{La}$	950.99	$5.19 \times 10^{-3}$	$4.37 \times 10^{-2}$
		$^{132}\text{I}$	947.2	$4.44 \times 10^{-4}$	$4.40 \times 10^{-2}$
1029	$5.69 \times 10^8$	$^{238}\text{Np}$	1025.9	$8.21 \times 10^{-2}$	$3.76 \times 10^{-2}$
		$^{238}\text{Np}$	1028.5	$1.74 \times 10^{-1}$	$3.74 \times 10^{-2}$
		$^{91}\text{Sr}$	1024.3	$3.25 \times 10^{-1}$	$3.77 \times 10^{-2}$
1073	$4.15 \times 10^7$				
1108	$3.58 \times 10^8$	$^{132}\text{I}$	1112.4	$6.51 \times 10^{-4}$	$3.30 \times 10^{-2}$
1172	$5.05 \times 10^8$	$^{134}\text{Cs}$	1167.9	$1.80 \times 10^{-2}$	$3.04 \times 10^{-2}$
		$^{132}\text{I}$	1172.9	$1.09 \times 10^{-2}$	$3.02 \times 10^{-2}$
1212	$5.67 \times 10^7$	$^{132}\text{I}$	1212.3	$1.18 \times 10^{-4}$	$2.84 \times 10^{-2}$
1282	$5.66 \times 10^8$	$^{97}\text{Zr}$	1276.07	$9.40 \times 10^{-3}$	$2.60 \times 10^{-2}$
1337	$1.21 \times 10^8$				
1387	$4.34 \times 10^8$	$^{132}\text{I}$	1390.7	$1.48 \times 10^{-4}$	$2.27 \times 10^{-2}$

**Table 4.3 Continued**

1471	$1.25 \times 10^8$	$^{132}\text{I}$	1476.7	$1.30 \times 10^{-3}$	$2.05 \times 10^{-2}$
1512	$2.88 \times 10^7$	close to $^{132}\text{I}$	1519.6	$7.90 \times 10^{-4}$	$1.96 \times 10^{-2}$
1594	$1.36 \times 10^9$	$^{140}\text{La}$	1596.21	$9.54 \times 10^{-1}$	$1.83 \times 10^{-2}$
		$^{132}\text{I}$	1592.9	$4.74 \times 10^{-4}$	$1.83 \times 10^{-2}$
1636	$1.04 \times 10^8$	$^{132}\text{I}$	1636.5	$2.36 \times 10^{-4}$	$1.76 \times 10^{-2}$
		$^{132}\text{I}$	1639.1	$7.90 \times 10^{-5}$	$1.76 \times 10^{-2}$
		$^{132}\text{I}$	1644	$1.28 \times 10^{-4}$	$1.75 \times 10^{-2}$
1659	$6.84 \times 10^6$	$^{132}\text{I}$	1661.4	$1.58 \times 10^{-4}$	$1.72 \times 10^{-2}$
1730	$1.73 \times 10^7$	$^{132}\text{I}$	1727.2	$6.71 \times 10^{-4}$	$1.62 \times 10^{-2}$
1821	$2.09 \times 10^7$	$^{132}\text{I}$	1814	$1.58 \times 10^{-4}$	$1.50 \times 10^{-2}$
		$^{132}\text{I}$	1830.1	$2.76 \times 10^{-4}$	$1.48 \times 10^{-2}$
1880	$4.24 \times 10^5$	$^{140}\text{La}$	1877.29	$4.10 \times 10^{-4}$	$1.42 \times 10^{-2}$
		$^{132}\text{I}$	1879.2	$1.38 \times 10^{-4}$	$1.41 \times 10^{-2}$
1906	$8.15 \times 10^6$	$^{132}\text{I}$	1913.7	$2.96 \times 10^{-4}$	$1.37 \times 10^{-2}$
1989	$2.93 \times 10^7$	$^{132}\text{I}$	1985.64	$1.18 \times 10^{-4}$	$1.28 \times 10^{-2}$
2116	$1.40 \times 10^7$				
2187	$2.22 \times 10^6$	$^{132}\text{I}$	2187	$6.91 \times 10^{-5}$	$1.13 \times 10^{-2}$
2257	$1.64 \times 10^7$	$^{132}\text{I}$	2249.1	$3.36 \times 10^{-4}$	$1.09 \times 10^{-2}$
2324	$1.07 \times 10^6$				
2380	$1.00 \times 10^7$	$^{132}\text{I}$	2390.48	$1.88 \times 10^{-3}$	$1.00 \times 10^{-2}$
2522	$2.90 \times 10^7$	$^{140}\text{La}$	2521.4	$3.46 \times 10^{-2}$	$9.26 \times 10^{-3}$
		$^{132}\text{I}$	2525.14	$3.95 \times 10^{-4}$	$9.24 \times 10^{-3}$
2642	$8.61 \times 10^5$	$^{132}\text{I}$	2653.8	$9.87 \times 10^{-6}$	$8.57 \times 10^{-3}$
2745	$2.21 \times 10^5$	$^{132}\text{I}$	2757.8	$1.28 \times 10^{-5}$	$8.06 \times 10^{-3}$
2887	$4.85 \times 10^5$	$^{140}\text{La}$	2899.61	$6.68 \times 10^{-4}$	$7.41 \times 10^{-3}$
2994	$1.04 \times 10^5$				

The water case is more challenging not only due to the increased Compton scattering interactions, but also the poor statistics as shown in Figure 5.5. However, even with these challenges, SmartID was successful in identifying 20 peaks and attributing them to the greatest gamma emitters for spent nuclear fuel. Fission products often have

many gamma emissions within the energy window SmartID uses to determine whether or not a peak is correlated to an emission. This causes complications when a single peak may be correlated to many different emissions. This can be mitigated by narrowing the energy window; however, careful attention to the energy and FWHM calibration is important for proper identification. The energy window was minimized to 0.05% for the simulation spectra since I know the exact energy calibration. Figure 4.8 shows the peaks identified, and Table 4.4 shows which peaks were contributed to the nuclides included in the MCNP simulation.

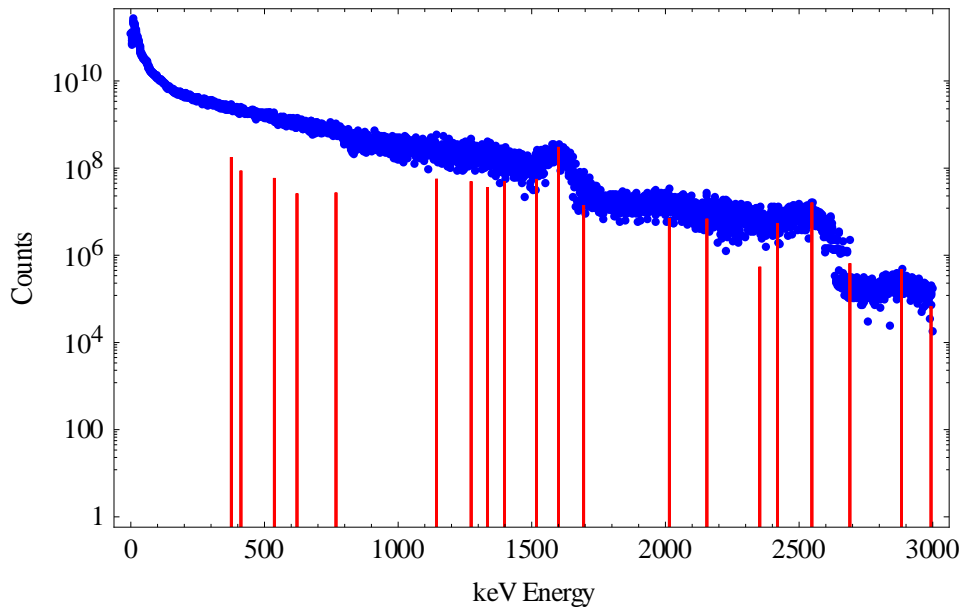


**Figure 4.8:** Peaks identified from a NaI(Tl) spectrum measuring 319 gamma emissions from 15 nuclides in a burned PWR fuel assembly in water.

**Table 4.4:** Identified Peaks for 15 nuclides in water included in the MCNP simulation.

Identified Peak (keV)	Counts	Nuclide	Attributed Emission (keV)	Probability of Decay	Detectability
377	$1.78 \times 10^8$				
413	$8.70 \times 10^7$	$^{99}\text{Mo}$	411.49	$1.46 \times 10^{-4}$	$2.16 \times 10^{-1}$
538	$6.09 \times 10^7$	$^{132}\text{I}$	535.4	$5.13 \times 10^{-3}$	$1.30 \times 10^{-1}$
		$^{140}\text{Ba}$	537.26	$2.44 \times 10^{-1}$	$1.29 \times 10^{-1}$
		$^{99}\text{Mo}$	537.79	$3.28 \times 10^{-5}$	$1.29 \times 10^{-1}$
623	$2.79 \times 10^7$	$^{132}\text{I}$	620.9	$3.95 \times 10^{-3}$	$9.72 \times 10^{-2}$
		$^{106}\text{Rh}$	621.84	$9.81 \times 10^{-2}$	$9.69 \times 10^{-2}$
		$^{99}\text{Mo}$	620.03	$2.30 \times 10^{-5}$	$9.74 \times 10^{-2}$
		$^{99}\text{Mo}$	621.77	$2.58 \times 10^{-4}$	$9.70 \times 10^{-2}$
769	$2.89 \times 10^7$	$^{132}\text{I}$	771.7	$1.97 \times 10^{-4}$	$6.41 \times 10^{-2}$
1145	$5.75 \times 10^7$	$^{132}\text{I}$	1143.3	$1.35 \times 10^{-2}$	$3.15 \times 10^{-2}$
		$^{132}\text{I}$	1147.8	$2.66 \times 10^{-3}$	$3.13 \times 10^{-2}$
		$^{97}\text{Zr}$	1147.97	$2.62 \times 10^{-2}$	$3.13 \times 10^{-2}$
1274	$5.01 \times 10^7$	$^{132}\text{I}$	1272.8	$1.68 \times 10^{-3}$	$2.61 \times 10^{-2}$
1336	$3.71 \times 10^7$				
1399	$4.99 \times 10^7$	$^{132}\text{I}$	1398.57	$7.01 \times 10^{-2}$	$2.25 \times 10^{-2}$
		$^{140}\text{La}$	1405.2	$5.91 \times 10^{-4}$	$2.23 \times 10^{-2}$
1519	$5.84 \times 10^7$	$^{132}\text{I}$	1519.6	$7.90 \times 10^{-4}$	$1.96 \times 10^{-2}$
1601	$3.08 \times 10^8$	$^{140}\text{La}$	1596.21	$9.54 \times 10^{-1}$	$1.83 \times 10^{-2}$
1695	$1.56 \times 10^7$				
2015	$7.15 \times 10^6$				
2156	$6.96 \times 10^6$				
2354	$5.66 \times 10^5$	$^{140}\text{La}$	2347.88	$8.49 \times 10^{-3}$	$1.03 \times 10^{-2}$
2420	$5.57 \times 10^6$	$^{132}\text{I}$	2408.6	$9.38 \times 10^{-5}$	$9.89 \times 10^{-3}$
		$^{132}\text{I}$	2416.9	$1.38 \times 10^{-5}$	$9.85 \times 10^{-3}$
2549	$1.62 \times 10^7$	$^{132}\text{I}$	2546.5	$1.58 \times 10^{-5}$	$9.12 \times 10^{-3}$
		$^{140}\text{La}$	2547.34	$1.01 \times 10^{-3}$	$9.12 \times 10^{-3}$
2691	$7.17 \times 10^5$	$^{132}\text{I}$	2690.8	$9.87 \times 10^{-6}$	$8.38 \times 10^{-3}$
2884	$4.80 \times 10^5$	close to $^{140}\text{La}$	2899.61	$6.68 \times 10^{-4}$	$7.41 \times 10^{-3}$
2994	$7.08 \times 10^4$				

### 4.3.2. 130 Emissions from 10 Isotopes Case

The simulated spectra for the 319 and 130 gamma emissions cases are similar, but more differentiation is seen between energy peaks for the 130 emissions case. Table 4.5 lists the nuclides considered in this case. Figure 4.9 shows the comparison between the water and air case spectra for the 130 gamma emissions. More differentiation is observed in the higher energy ranges. This should help show that the nuclides matched to the peaks found in this region are correctly identified.

**Table 4.5:** 10 gamma emitting isotopes from PWR fuel assembly burned to 33,000 MWD 1 day since removal from reactor.

Isotope	T <sub>1/2</sub>	Energy (MeV)	Emission rate (gamma/s)
<sup>140</sup> La	1.6781 d	1.5962	6.3082 10 <sup>16</sup>
<sup>103</sup> Ru	39.26 d	0.49709	5.9303 10 <sup>16</sup>
<sup>95</sup> Zr	64.02 d	0.75673	3.0665 10 <sup>16</sup>
<sup>97</sup> Nb	72.1 m	0.65794	2.2804 10 <sup>16</sup>
<sup>97</sup> Zr	16.9 h	0.74336	2.1690 10 <sup>16</sup>
<sup>140</sup> Ba	12.752 d	0.53726	1.4779 10 <sup>16</sup>
<sup>134</sup> Cs	2.0648 y	0.60472	5.4602 10 <sup>15</sup>
<sup>106</sup> Rh	29.8 s	0.51186	4.5767 10 <sup>15</sup>
<sup>137</sup> Cs <sup>3</sup>	30.07 y	0.66166	3.3296 10 <sup>15</sup>
<sup>238</sup> Np	2.117 d	0.98445	2.6747 10 <sup>15</sup>

<sup>3</sup> This emission is actually from <sup>137m</sup>Ba, a decay daughter of <sup>137</sup>Cs

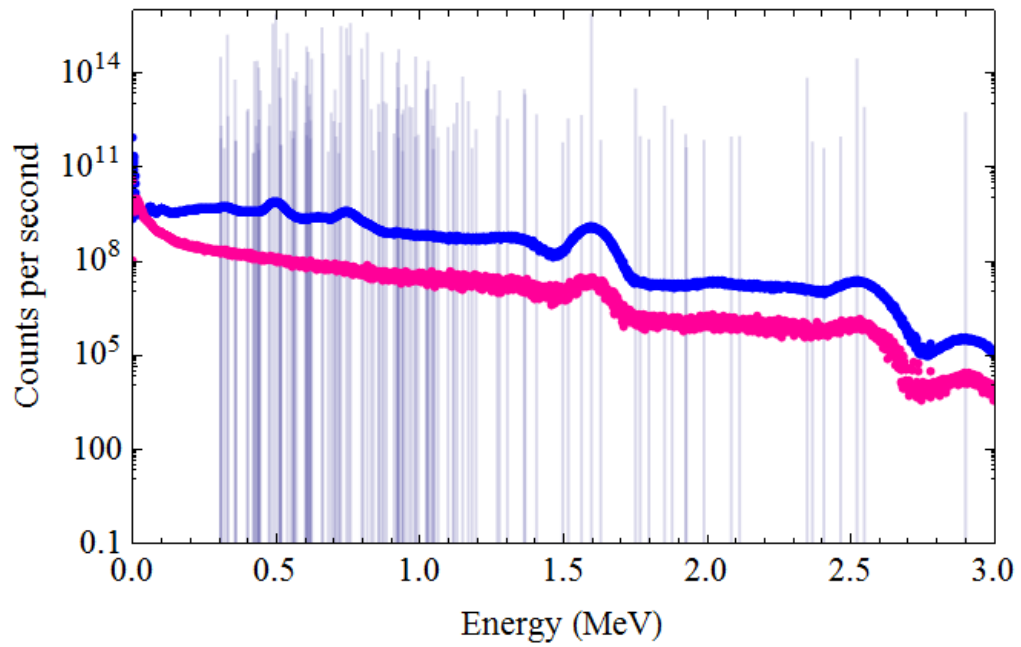


**Figure 4.9:** MCNP simulated spectra for 130 gamma emissions from spent fuel in both air and water. The spectrum in air is shown in blue and the spectrum in water is shown in pink. Emissions are depicted by the vertical lines.

The 1 sigma errors in Figure 4.10 for the 130 gamma emissions in water spectrum continue to be much greater than the errors for the air case.



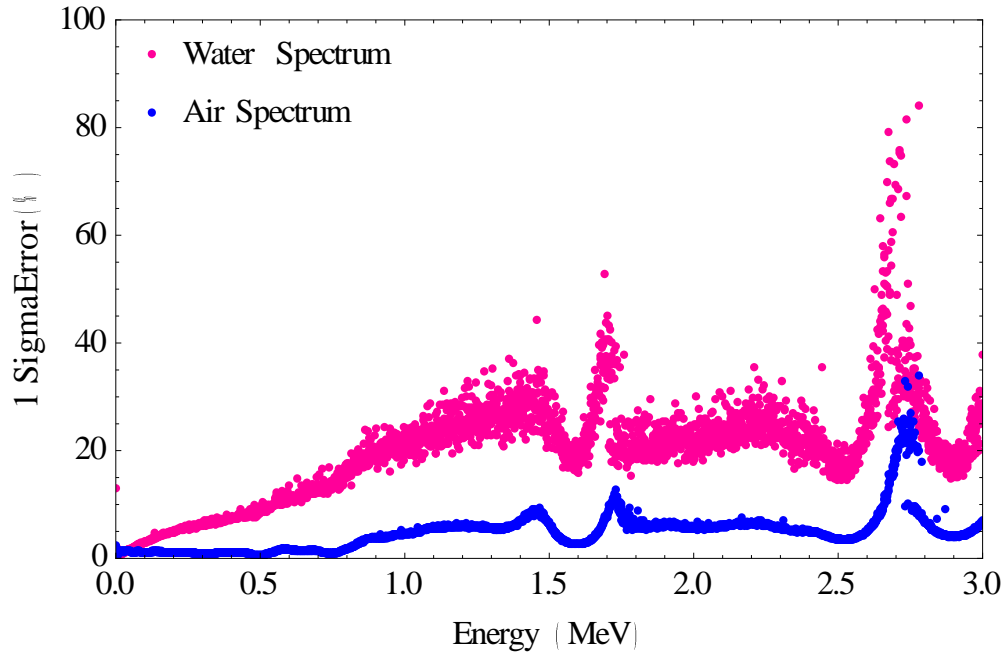


**Figure 4.10:** MCNP 1 sigma errors for 130 gamma emissions from spent fuel assembly gamma spectrum through water and air.

Figure 4.11 shows the air case with 35 peaks identified after processing the spectrum with SmartID. Table 4.6 lists the identified energy peaks and the attributed nuclides that were included in the MCNP models. Many peaks appear listed without nuclide attribution. This is due to the small energy window applied in order to determine that these peaks could be identified clearly. I noted that the peaks attributed also tend to have the largest counts associated with them. These are the most prominent peaks, and therefore are correctly attributed to the greatest emitting fission products as noted in Table 4.6.

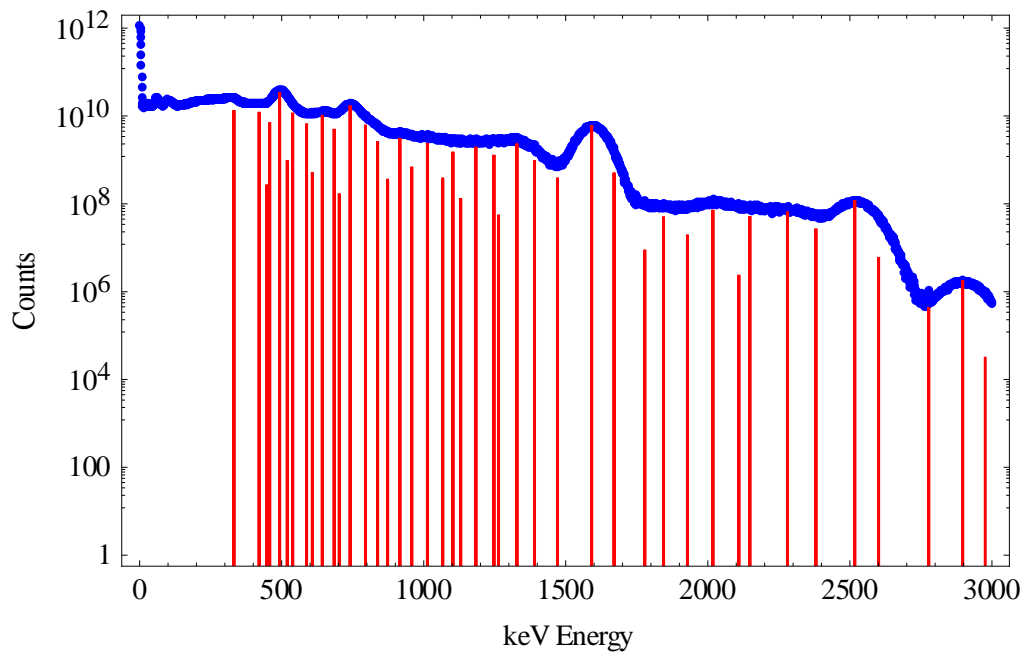


**Figure 4.11:** Peaks identified from a NaI(Tl) spectrum measuring 130 gamma emissions in air from a burned PWR fuel assembly in air.

**Table 4.6:** Identified Peaks for the 10 nuclides in air included in the MCNP simulation.

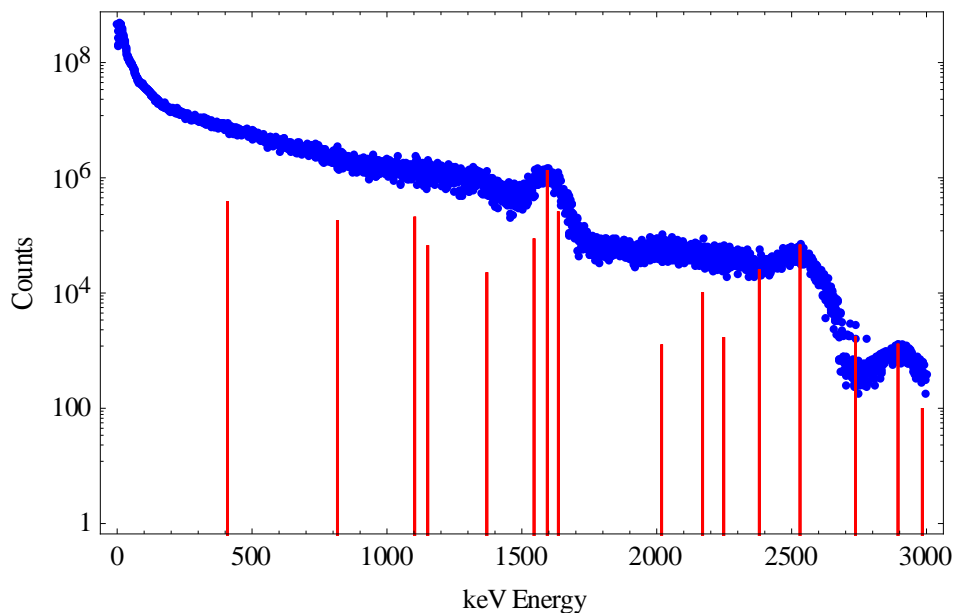
Identified Peak (keV)	Counts	Nuclide	Attributed Emission (keV)	Probability of Decay	Detectability
333	1.71E+09				
422	1.71E+09	<sup>140</sup> Ba	423.72	3.15E-02	2.05E-01
459	4.02E+09				
476	9.15E+08	<sup>134</sup> Cs	475.35	1.46E-02	1.64E-01
499	2.85E+10	<sup>103</sup> Ru	497.08	8.89E-01	1.49E-01
543	5.38E+09				
596	3.27E+09				
644	7.96E+09				
686	3.73E+09				
742	1.59E+10	<sup>97</sup> Zr	743.36	9.31E-01	6.94E-02
796	5.30E+09	<sup>134</sup> Cs	795.84	8.54E-01	5.99E-02
839	1.91E+09				
874	1.22E+08				
917	1.99E+09	<sup>140</sup> La	919.55	2.66E-02	4.66E-02
959	3.83E+08				
1014	1.25E+09				
1075	2.09E+08				
1131	3.29E+08				
1185	3.69E+08				
1248	1.69E+08				
1329	3.18E+08				
1391	5.90E+08				
1490	1.89E+08				
1592	6.08E+09	<sup>140</sup> La	1596.21	9.54E-01	1.83E-02
1671	5.43E+08				
1845	1.61E+07				
2019	5.69E+06				
2163	6.21E+06				
2328	3.78E+07				
2403	6.77E+06				
2518	1.21E+08	<sup>140</sup> La	2521.4	3.46E-02	9.26E-03
2602	6.80E+06				
2778	3.17E+05				
2898	1.83E+06	<sup>140</sup> La	2899.61	6.68E-04	7.41E-03
2977	4.76E+04				

Figure 4.12 shows the details of the 35 peaks identified from the SmartID output file. I know from Table 4.6 that  $^{140}\text{La}$  should be one of the highest scored isotopes, especially with its strong high energy gamma emissions. This is validated by the peaks identified by SmartID. I see many of the most prominent peaks match the emissions of this isotope, and the score summary in Figure 4.12 shows  $^{140}\text{La}$  as most likely. Many isotopes other than those included are listed as highly correlated with this spectrum, but examining the SmartID performance further, I notice that much of the scoring can be due to a few of the peaks matching many different emissions. As Table 4.6 highlighted, it is important to understand the emissions that are correlated to the most important isotopes and determine how close the peaks found are to these.

Score Summary:							
Nuclide	Total	(base +	bonus I,	II,	III)	Comment	Correlation
140La	161.03	( 90.6	50.0	18.4	2.0 )	Fiss_Prod	High
135I	159.05	( 89.0	50.0	20.0	0.0 )	Fiss_Prod	High
133mTe	149.30	( 81.9	49.9	17.5	0.0 )	Fiss_Prod	High
99Mo	144.31	( 84.5	36.9	22.9	0.0 )	medical_FP	High
134I	141.76	( 78.7	41.6	21.5	0.0 )	Fiss_Prod	High
234Pa	135.49	( 73.9	50.0	11.6	0.0 )	U-238_Daughter	High
227Th	134.85	( 97.9	2.5	4.4	30.0 )	U-235_Daughter	High
142La	128.65	( 88.3	31.9	3.4	5.0 )	Fiss_Prod	High
103Ru	127.07	( 98.0	1.0	8.1	20.0 )	Fiss_Prod	High
93Y	121.59	( 87.9	31.4	2.3	0.0 )	Fiss_Prod	High
60Co	120.21	( 98.2	1.0	1.0	20.0 )	c	High
214Bi	115.12	( 89.6	23.3	2.2	0.0 )	U-238_Daughter	High
160Tb	113.76	( 96.0	15.6	2.2	0.0 )	Fiss_Prod	High
140Ba	111.50	( 94.0	5.6	6.9	5.0 )	Fiss_Prod	High
156Eu	111.47	( 64.2	43.7	3.6	0.0 )	Fiss_Prod	High
131Te	110.78	( 94.2	8.1	8.6	0.0 )	Fiss_Prod	High
84Br	110.38	( 91.1	13.0	6.3	0.0 )	Fiss_Prod	High
237U	109.82	( 98.7	0.7	5.4	5.0 )	237Np_Parent	High
91Sr	109.50	( 93.3	3.7	7.5	5.0 )	Fiss_Prod	High
129Te	109.11	( 98.6	1.0	9.5	0.0 )	Fiss_Prod	High
65Ni	107.40	( 97.3	2.5	2.6	5.0 )	c	High
67Ga	106.79	( 98.8	1.0	2.0	5.0 )	Fiss_Prod	High
124Sb	106.30	( 92.7	10.2	3.4	0.0 )	Fiss_Prod	High
239Pu	106.03	( 61.7	30.1	14.2	0.0 )	SNM	High
231Pa	104.55	( 99.1	1.0	4.5	0.0 )	U-235_Dau+Irr_T	High
97mNb	102.88	( 98.9	0.0	4.0	0.0 )	Fiss_Prod	High
141Ba	101.84	( 73.6	17.3	10.9	0.0 )	Fiss_Prod	High
240Pu	101.77	( 99.3	0.0	2.5	0.0 )	SNM	High
131mTe	101.64	( 57.0	31.9	12.7	0.0 )	Fiss_Prod	High
132I	101.51	( 24.1	50.0	27.4	0.0 )	Fiss_Prod	High
241Am	101.11	( 86.5	3.2	6.4	5.0 )	SNM	High
97Zr	100.98	( 86.1	5.1	4.7	5.0 )	Fiss_Prod	High
130I	100.84	( 80.8	5.9	12.2	2.0 )	Fiss_Prod	High
75Se	100.64	( 97.7	1.0	1.9	0.0 )	Fiss_Prod	High
151Pm	100.44	( 14.8	50.0	35.6	0.0 )	Fiss_Prod	High
138Cs	100.33	( 79.3	14.2	6.8	0.0 )	Fiss_Prod	High
87Kr	100.32	( 95.2	3.5	1.7	0.0 )	Fiss_Prod	High
212Pb	100.27	( 98.9	0.0	1.4	0.0 )	Th-232_Daughter	High
232U	100.01	( 97.0	0.0	3.0	0.0 )	Irrad_Th-230_23	High

**Figure 4.12:** Top scored nuclides identified for the 130 gamma emissions source in air from a PWR spent fuel assembly after 1 day from removal from the reactor core.

Figure 4.13 shows the water case with 16 peaks identified. As was the instance with 319 gamma emissions through water case, this case also suffered from significant MCNP errors. However, even with these errors, SmartID is able to discern a number of emissions even when significantly fewer emissions are included in the 10 isotope case from the 15 isotope case. Figure 4.14 lists the 16 peaks identified and their relative contributions to the counts seen in the detector.



**Figure 4.13:** Peaks identified from a NaI(Tl) spectrum measuring 10 isotope emissions from a burned PWR fuel assembly in water.

16 Peak(s) Identified - Sort by Energy			
keV	Counts	Norm% Cts	Peak Id
409.00	3.9358E+05	14.49937	16
816.00	1.8517E+05	6.82161	15
1103.00	2.1270E+05	7.83581	14
1151.00	6.7737E+04	2.49541	13
1370.00	2.2829E+04	0.84101	12
1545.00	9.6554E+04	3.55702	11
1594.00	1.3545E+06	49.89939	9
1635.00	2.6848E+05	9.89073	10
2018.00	1.3879E+03	0.05113	8
2170.00	1.0505E+04	0.38700	7
2248.00	2.0817E+03	0.07669	6
2380.00	2.6260E+04	0.96741	5
2531.00	6.9408E+04	2.55697	3
2736.00	1.8337E+03	0.06755	4
2894.00	1.3258E+03	0.04884	1
2984.00	1.1018E+02	0.00406	2

**Figure 4.14:** Peaks identified for the 130 gamma emissions source in water from a PWR spent fuel assembly after 1 day from removal from the reactor core.

**Table 4.7:** Identified Peaks for the 10 nuclides in water included in the MCNP simulation.

Identified Peak (keV)	Counts	Nuclide	Attributed Emission (keV)	Probability of Decay	Detectability
410	4.03E+05				
817	1.88E+05	<sup>140</sup> La	815.77	2.33E-01	5.74E-02
1104	2.12E+05	<sup>140</sup> La	1097.2	2.29E-04	3.38E-02
1152	6.85E+04	<sup>97</sup> Zr	1147.97	2.62E-02	3.13E-02
1371	2.35E+04	<sup>97</sup> Zr	1362.68	1.02E-02	2.35E-02
		<sup>97</sup> Zr	1361	6.51E-03	2.35E-02
1546	9.66E+04				
1595	1.35E+06	<sup>140</sup> La	1596.21	9.54E-01	1.83E-02
1636	2.68E+05				
2019	1.07E+03				
2171	1.05E+04				
2249	2.08E+03				
2381	2.63E+04				
2532	6.94E+04	<sup>140</sup> La	2521.4	3.46E-02	9.26E-03
		<sup>140</sup> La	2547.34	1.01E-03	9.12E-03
2737	1.83E+03				
2895	1.33E+03	<sup>140</sup> La	2899.61	6.68E-04	7.41E-03
2985	1.10E+02				

It is misleading to look at the nuclides scored by SmartID in Figure 4.15 due to the low number of emissions identified; however, it is important to note that high emitters <sup>140</sup>La, along with <sup>97</sup>Zr are correctly identified. When I decreased the number of emissions from 329 to 130, I removed some of the most active emissions in the upper energy ranges. <sup>140</sup>La and <sup>97</sup>Zr are significant gamma emitters in the MeV range, and combining this along with poor MCNP errors, many of the lower energy gamma emissions are difficult to identify.

Score Summary:								
Nuclide	Total	(base + bonus I, II, III)					Comment	Correlation
132I	87.05	( 3.3	50.0	33.7	0.0	)	Fiss_Prod	Moderate
156Eu	62.27	( 38.8	14.1	7.3	2.0	)	Fiss_Prod	Moderate
140La	55.58	( 21.1	5.9	26.6	2.0	)	Fiss_Prod	Moderate
151Pm	42.97	( 0.8	3.5	8.6	30.0	)	Fiss_Prod	Low
136Cs	32.07	( 29.3	0.0	2.7	0.0	)	Fiss_Prod	Low
97Zr	24.75	( 1.8	1.6	1.3	20.0	)	Fiss_Prod	Low
135I	21.91	( 1.9	14.0	6.0	0.0	)	Fiss_Prod	Low
154Eu	21.67	( 1.3	0.6	19.8	0.0	)	Fiss_Prod	Low
148mPm	20.37	( 14.6	0.0	5.7	0.0	)	Fiss_Prod	Low
99Mo	15.87	( 0.9	1.4	8.5	5.0	)	medical_FP	Low
131mTe	15.03	( 4.8	2.6	7.6	0.0	)	Fiss_Prod	Low
93Y	12.49	( 3.5	4.1	5.0	0.0	)	Fiss_Prod	Low
143Ce	12.38	( 0.8	2.4	7.1	2.0	)	Fiss_Prod	Low

**Figure 4.15:** Top scored nuclides identified for the 130 gamma emissions source in water from a PWR spent fuel assembly after 1 day from removal from the reactor core.

It may seem that SmartID is not performing well, but the algorithm is performing on a low resolution detector processing a complicated and spectra with statistical errors that are large. This is important to know for real detection scenarios. If a spectrum is collected with poor counting statistics, the user needs to understand how the algorithm performs and what information can still be gained for burnup analysis and calculations. The fact that SmartID can correctly attribute key spectral data in less than ideal situations is promising for real measurement applications.

#### 4.3.3. 1,024 Emissions from Major Contributing Nuclides Case

The final case I modeled in MCNP was a much more complex source in air. Since a true PWR fuel assembly burned at 33,000 MWD has over 3,000 emissions, I reduced my large model to include the top 76 emitting isotopes accounting for the top 1,024 emissions. Figure 4.16 shows the simulated spectrum from MCNP, and Figure 4.17 shows the corresponding 1 sigma errors. This spectrum was run for a total of  $2 \times 10^{12}$  particle histories.



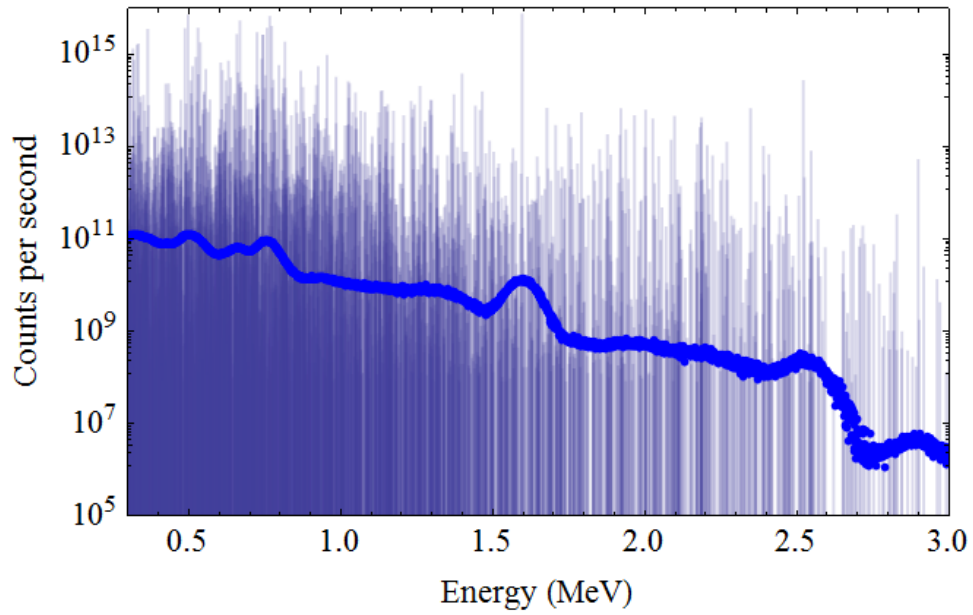


**Figure 4.16:** MCNP simulated spectrum of 1,024 gamma emissions for spent PWR fuel assembly in air.

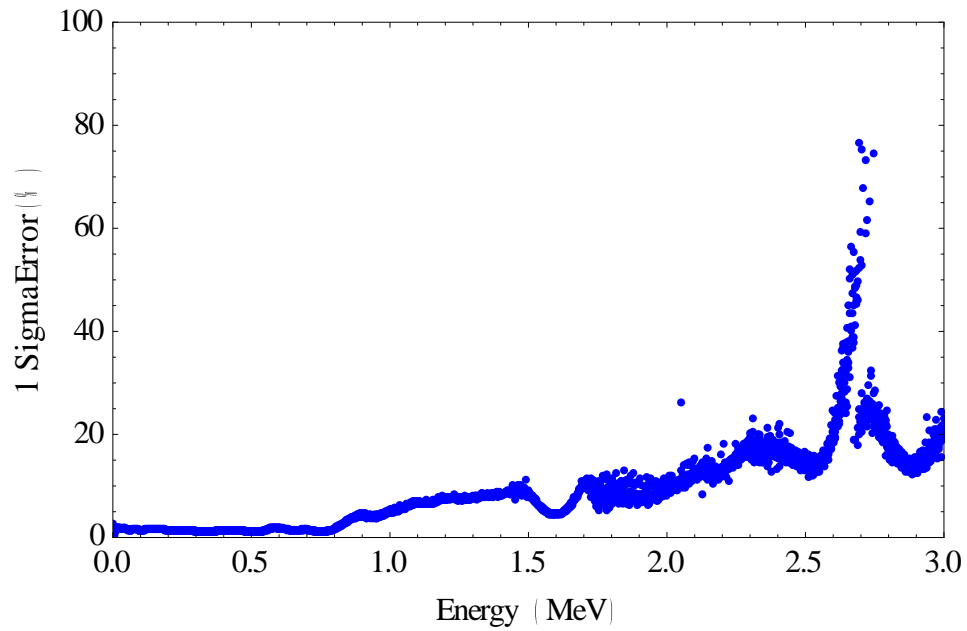


**Figure 4.17:** MCNP 1 sigma errors for 1,024 gamma emissions from a spent PWR fuel assembly gamma spectrum through water and air.

Peaks were identified by SmartID for this case, and are shown by Figure 4.18. SmartID identified a total of 39 peaks, which is significantly less than the number of emissions included in the MCNP model. However, even though SmartID subtracts out peak by peak to unveil hidden peaks, it is difficult to reveal every weak emission. Referring back to Figures 4.1, 4.2 and 4.3, I see that many of the weaker emissions are up to 4 orders of magnitude weaker than the strongest emissions. When these weak emissions lie within a few keV or less to the strongest emissions, they are easily lost within the FWHM of surrounding peaks. This should not be major issue, as long as I keep in mind what nuclides are responsible for the strongest emissions and where in the spectrum they occur in relation to other strong gamma emitting nuclides. The most important understanding is that the major emissions are identified, and the attributed nuclides identified match the key nuclides included in the MCNP model.

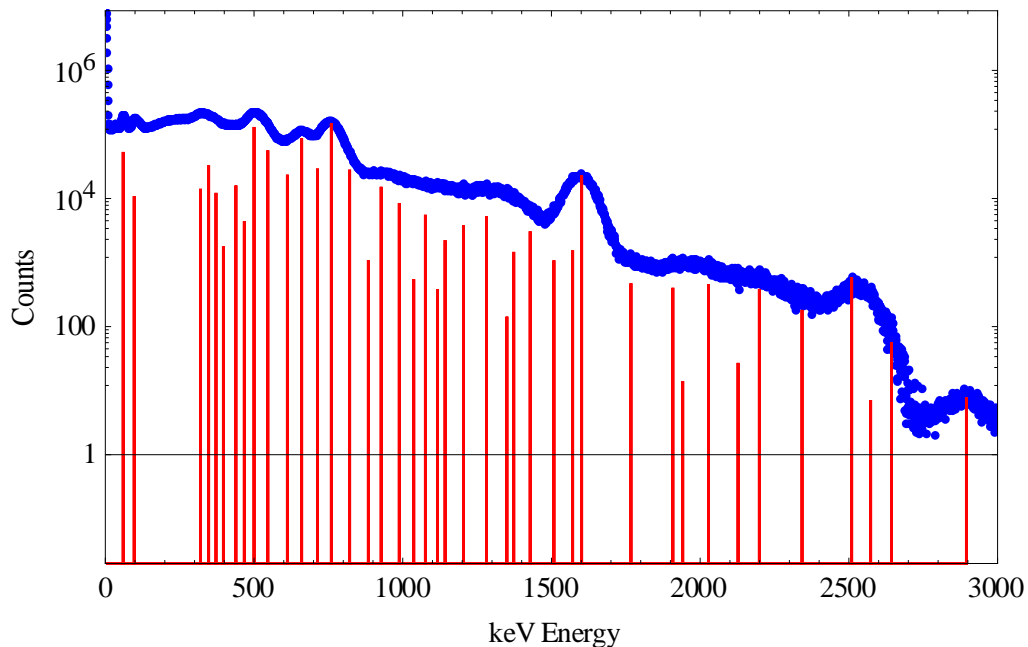


**Figure 4.18:** Peaks identified from a NaI(Tl) spectrum measuring 1,024 emissions from a burned PWR fuel assembly in air.

The resulting nuclides identified are shown in Figure 4.19. As evident previously, SmartID identifies other nuclides that are not present due to library aliasing, but it does identify the nuclides I expect to be characterized. It performs well scoring the greatest gamma emitting nuclides present in the MCNP model relative to the weaker emission nuclides. I included the shielding search option in post-processing this model, since the spent fuel assembly does not exactly match the air DRFs utilized in SmartID. There will be a large contribution to how the spectrum is represented due to self-shielding from the rows of fuel pins in the fuel assembly. Including this shielding search will help better account for these shielding effects. The highest scored shielding scenario is 3 cm of lead shielding. This is closely followed by 2 cm, 4 cm, and 5 cm thick lead shielding. The score drops off after this point at 1 cm thick lead, and decreases as the shielding case decreases in thickness or is represented by iron. I find this to be a good representation of the fuel assembly model since the shielding accounts for much of the source emitting in rows furthest from the detector being shielded by fuel pins in rows closest to the detector. The energy window considered for this first case was 2%. Figure 4.19 shows a large list of potential nuclides present in the fuel assembly. However, due to the limited number of peaks identified, I cannot have confidence that all are actually represented. Since many of these nuclides have emissions falling within very close intervals, a smaller energy window is ideal. I reprocessed the spectrum with an energy window of 1%. Figure 4.20 shows the resulting scored nuclides from this new scoring condition.

Score Details for Shielding Options:							
-----							
Possible Shielding Setting: 1 Total Score: 10994.20							
Shielding Material: Pb Thickness (cm): 3.00							
Note:							
base score : fuction of (#matched/#emissions), weighted by yield,detectability and matching facto							
bonus I : bonus from number of matched peaks							
bonus II : bonus from relative peak height							
bonus III : bonus from alignment between peakheights and emission yields							
Score Summary:							
-----							
Nuclide	Total	(base + bonus I, II, III)				Comment	Correlation
143Ce	181.82	( 96.6	50.0	35.3	0.0 )	Fiss_Prod	High
132I	172.74	( 85.1	50.0	37.6	0.0 )	Fiss_Prod	High
151Pm	164.28	( 79.2	50.0	35.1	0.0 )	Fiss_Prod	High
140La	160.31	( 94.0	50.0	16.3	0.0 )	Fiss_Prod	High
214Bi	158.51	( 89.9	50.0	18.6	0.0 )	U-238_Daughter	High
135I	152.34	( 82.2	50.0	20.2	0.0 )	Fiss_Prod	High
234Pa	148.73	( 71.1	50.0	27.6	0.0 )	U-238_Daughter	High
133mTe	145.33	( 82.5	50.0	12.8	0.0 )	Fiss_Prod	High
110mAg	140.32	( 93.7	25.6	21.0	0.0 )	Fiss_Prod	High
103Ru	138.60	( 98.4	1.0	9.2	30.0 )	Fiss_Prod	High
97Nb	135.03	( 98.8	1.0	5.2	30.0 )	Fiss_Prod	High
156Eu	132.67	( 77.4	50.0	5.2	0.0 )	Fiss_Prod	High
105Ru	131.13	( 83.2	29.5	18.4	0.0 )	Fiss_Prod	High
211Pb	127.33	( 94.8	0.8	1.7	30.0 )	U-235_Daughter	High
154Eu	125.54	( 95.4	17.3	12.9	0.0 )	Fiss_Prod	High
166mHo	122.34	( 91.3	11.5	19.5	0.0 )	Fiss_Prod	High
91Sr	118.04	( 96.1	5.9	16.0	0.0 )	Fiss_Prod	High
131mTe	117.98	( 68.6	29.7	19.7	0.0 )	Fiss_Prod	High
241Am	116.92	( 94.6	8.4	9.0	5.0 )	SNM	High
152Eu	114.40	( 73.2	37.2	4.0	0.0 )	Fiss_Prod	High
95Zr	114.30	( 97.7	1.0	10.6	5.0 )	Fiss_Prod	High
239Pu	114.12	( 40.8	50.0	23.3	0.0 )	SNM	High
240Np	113.67	( 77.3	25.6	10.7	0.0 )	SNM	High
125Sn	109.85	( 97.7	9.0	3.2	0.0 )	Fiss_Prod	High
134I	109.58	( 57.5	34.8	17.3	0.0 )	Fiss_Prod	High
92Y	109.25	( 87.5	0.7	1.1	20.0 )	Fiss_Prod	High
228Ac	106.86	( 81.8	11.9	13.2	0.0 )	Th-232_Daughter	Moderate
95Nb	106.82	( 98.0	0.0	8.8	0.0 )	Fiss_Prod	Moderate
238Pu	106.65	( 97.8	0.0	8.8	0.0 )	SNM	Moderate
138Xe	106.15	( 92.1	13.0	1.1	0.0 )	Fiss_Prod	Moderate
140Ba	105.59	( 94.7	4.6	6.2	0.0 )	Fiss_Prod	Moderate
46Sc	104.69	( 98.6	1.0	0.1	5.0 )	c	Moderate
138Cs	104.64	( 81.9	17.3	5.4	0.0 )	Fiss_Prod	Moderate
137Cs	104.20	( 99.0	0.0	5.2	0.0 )	Fiss_Prod	Moderate
137mBa	104.18	( 99.0	0.0	5.2	0.0 )	Fiss_Prod	Moderate
238Np	104.16	( 98.3	4.5	1.5	0.0 )	SNM	Moderate
110Ag	103.99	( 98.8	0.0	5.2	0.0 )	Fiss_Prod	Moderate
84Br	103.67	( 85.0	16.8	1.8	0.0 )	Fiss_Prod	Moderate
142Ba	103.14	( 85.0	11.9	1.2	5.0 )	Fiss_Prod	Moderate
88Kr	101.49	( 74.1	24.9	2.5	0.0 )	Fiss_Prod	Moderate
238U	101.46	( 91.4	0.7	9.3	0.0 )	SNM	Moderate
106Ru	100.80	( 96.4	1.0	1.4	2.0 )	Fiss_Prod	Moderate
65Ni	100.62	( 97.3	2.5	0.8	0.0 )	c	Moderate
134Te	100.59	( 68.4	9.4	17.8	5.0 )	Fiss_Prod	Moderate
131Te	100.33	( 77.9	7.7	14.7	0.0 )	Fiss_Prod	Moderate
51Cr	100.28	( 99.4	0.0	0.9	0.0 )	medical	Moderate
209Tl	100.12	( 98.9	0.8	0.4	0.0 )	Np-237_Daughter	Moderate
213Bi	99.81	( 98.8	0.0	1.0	0.0 )	U-233_Daughter	Moderate
233U	99.75	( 98.3	0.6	0.9	0.0 )	Np-237_Daughter	Moderate
135Xe	99.66	( 98.3	0.0	1.4	0.0 )	Fiss_Prod	Moderate
247Cm	99.53	( 96.8	0.7	2.1	0.0 )	SNM	Moderate
211Bi	99.13	( 97.2	0.0	1.9	0.0 )	U-235_Daughter	Moderate
115mCd	98.96	( 98.1	0.0	0.9	0.0 )	Fiss_Prod	Low
43K	98.91	( 90.9	3.7	2.3	2.0 )	c	Low
141La	98.84	( 98.8	0.0	0.0	0.0 )	Fiss_Prod	Low
47Ca	98.70	( 95.9	0.8	1.9	0.0 )	c	Low
58Co	98.66	( 97.0	0.0	1.6	0.0 )	c	Low
92Sr	98.63	( 95.5	2.0	1.1	0.0 )	Fiss_Prod	Low
111Ag	98.59	( 96.7	0.0	1.9	0.0 )	Fiss_Prod	Low
65Zn	98.36	( 98.3	0.0	0.0	0.0 )	Fiss_Prod	Low
142La	98.25	( 54.0	43.7	0.5	0.0 )	Fiss_Prod	Low
59Fe	98.06	( 97.0	0.7	0.3	0.0 )	c	Low
41Ar	97.89	( 97.6	0.0	0.3	0.0 )	n_activ_prod	Low
54Mn	97.85	( 96.2	0.0	1.6	0.0 )	c	Low
75Se	97.74	( 97.6	0.0	0.1	0.0 )	Fiss_Prod	Low
92Ru	97.60	( 96.8	0.0	0.8	0.0 )	Fiss_Prod	Low

**Figure 4.19:** Nuclides identified for a PWR spent fuel assembly after 1 day from removal from the reactor core with a 2% energy window for peak attribution.

Possible Shielding Setting: 1 Total Score: 5408.62							
Shielding Material: Pb Thickness (cm): 3.00							
Note:							
base score : fuction of (#matched/#emissions), weighted by yield,detectability and matching facto							
bonus I : bonus from number of matched peaks							
bonus II : bonus from relative peak height							
bonus III : bonus from alignment between peakheights and emission yields							
Score Summary:							
Nuclide	Total	(base +	bonus I.	II.	III)	Comment	Correlation
151Pm	138.62	( 52.8	50.0	35.8	0.0 )	Fiss_Prod	High
103Ru	138.60	( 98.4	1.0	9.2	30.0 )	Fiss_Prod	High
140La	124.39	( 89.5	27.9	7.0	0.0 )	Fiss_Prod	High
234Pa	116.37	( 59.0	37.7	19.6	0.0 )	U-238_Daughter	High
110mAg	114.14	( 83.7	12.6	17.8	0.0 )	Fiss_Prod	High
135I	109.04	( 44.5	50.0	14.5	0.0 )	Fiss_Prod	High
95Nb	106.82	( 98.0	0.0	8.8	0.0 )	Fiss_Prod	Moderate
238Pu	106.65	( 97.8	0.0	8.8	0.0 )	SNM	Moderate
214Bi	104.74	( 78.4	18.3	8.0	0.0 )	U-238_Daughter	Moderate
46Sc	104.69	( 98.6	1.0	0.1	5.0 )	c	Moderate
137Cs	104.20	( 99.0	0.0	5.2	0.0 )	Fiss_Prod	Moderate
137mBa	104.18	( 99.0	0.0	5.2	0.0 )	Fiss_Prod	Moderate
110Ag	103.99	( 98.8	0.0	5.2	0.0 )	Fiss_Prod	Moderate
97Nb	102.89	( 97.7	0.0	5.2	0.0 )	Fiss_Prod	Moderate
51Cr	100.28	( 99.4	0.0	0.9	0.0 )	medical	Moderate
209Tl	100.12	( 98.9	0.8	0.4	0.0 )	Np-237_Daughter	Moderate
213Bi	99.81	( 98.8	0.0	1.0	0.0 )	U-233_Daughter	Moderate
233U	99.75	( 98.3	0.6	0.9	0.0 )	Np-237_Daughter	Moderate
135Xe	99.66	( 98.3	0.0	1.4	0.0 )	Fiss_Prod	Moderate
115mCd	98.96	( 98.1	0.0	0.9	0.0 )	Fiss_Prod	Low
141La	98.84	( 98.8	0.0	0.0	0.0 )	Fiss_Prod	Low
65Zn	98.36	( 98.3	0.0	0.0	0.0 )	Fiss_Prod	Low
41Ar	97.89	( 97.6	0.0	0.3	0.0 )	n_activ_prod	Low
75Se	97.74	( 97.6	0.0	0.1	0.0 )	Fiss_Prod	Low
138Cs	97.71	( 79.0	13.3	5.4	0.0 )	Fiss_Prod	Low
92Sr	96.25	( 95.3	0.7	0.2	0.0 )	Fiss_Prod	Low
67Ga	95.69	( 95.6	0.0	0.1	0.0 )	Fiss_Prod	Low
134Te	95.62	( 66.1	6.8	17.8	5.0 )	Fiss_Prod	Low
43K	94.46	( 88.4	1.9	2.2	2.0 )	c	Low
143Ce	93.73	( 54.3	21.4	18.0	0.0 )	Fiss_Prod	Low
57Ni	93.09	( 86.0	2.0	0.1	5.0 )	c	Low
105Rh	92.28	( 91.4	0.0	0.8	0.0 )	Fiss_Prod	Low
238Np	91.12	( 87.5	2.2	1.5	0.0 )	SNM	Low
138Xe	85.48	( 80.6	4.6	0.2	0.0 )	Fiss_Prod	Low
84Br	83.18	( 78.2	4.6	0.4	0.0 )	Fiss_Prod	Low
154Eu	80.68	( 60.8	7.1	12.9	0.0 )	Fiss_Prod	Low
52Mn	79.09	( 72.4	0.6	1.1	5.0 )	c	Low
48Sc	77.14	( 74.4	2.0	0.8	0.0 )	c	Low
89Rb	76.32	( 66.1	5.0	5.2	0.0 )	Fiss_Prod	Low
126Sb	76.18	( 37.6	2.7	5.8	30.0 )	Fiss_Prod	Low
22Na	75.30	( 75.0	0.0	0.3	0.0 )	Cosmic_spall_pr	Low
101Tc	75.29	( 71.9	0.0	3.4	0.0 )	Fiss_Prod	Low
95Zr	73.87	( 65.0	0.0	8.9	0.0 )	Fiss_Prod	Low
24Na	73.65	( 73.6	0.0	0.1	0.0 )	n_activ_prod	Low
134I	72.66	( 50.5	8.1	14.0	0.0 )	Fiss_Prod	Low
52mMn	72.46	( 72.3	0.0	0.2	0.0 )	c	Low
92Y	71.48	( 70.6	0.0	0.9	0.0 )	Fiss_Prod	Low
241Am	70.79	( 58.5	1.4	5.9	5.0 )	SNM	Low
132I	70.66	( 7.9	50.0	12.7	0.0 )	Fiss_Prod	Low
192Ir	68.66	( 66.4	0.6	1.7	0.0 )	medical_RDD	Low
125Sn	68.63	( 64.6	1.8	2.3	0.0 )	Fiss_Prod	Low
142Ba	68.45	( 58.4	4.4	0.7	5.0 )	Fiss_Prod	Low
239Pu	66.95	( 29.1	17.1	20.8	0.0 )	SNM	Low
160Tb	65.73	( 51.4	4.9	9.5	0.0 )	Fiss_Prod	Low
131Te	65.26	( 57.9	1.6	5.7	0.0 )	Fiss_Prod	Low
136Cs	56.75	( 55.1	0.0	1.7	0.0 )	Fiss_Prod	Low
131mTe	56.35	( 35.5	10.7	10.1	0.0 )	Fiss_Prod	Low
93Y	53.26	( 42.5	8.0	2.7	0.0 )	Fiss_Prod	Low
48V	51.71	( 51.2	0.0	0.5	0.0 )	medical_from_Ti	Low
141Ba	50.95	( 45.7	2.8	2.5	0.0 )	Fiss_Prod	Low
87Kr	50.77	( 49.0	1.7	0.0	0.0 )	Fiss_Prod	Low
59Fe	50.22	( 49.9	0.0	0.3	0.0 )	c	Low

**Figure 4.20:** Nuclides identified for a PWR spent fuel assembly after 1 day from removal from the reactor core with a 1% energy window for peak attribution.

The number of nuclides scored drops dramatically from 209 to 61, and the order in which nuclides are scored changes when the energy window is decreased to 1%. Figure 4.19 showed a number of nuclides scored high which were not actually included in the MCNP model due to library aliasing. Figure 4.20 shows a better representation of the original source definition. The top three scored nuclides are actually present in the source definition, and have a relatively high contribution to the overall gamma emission profile.  $^{234}\text{Pa}$ , although highly scored, is falsely attributed due to double counting of many of the identified peaks.  $^{110\text{m}}\text{Ag}$  and  $^{135}\text{I}$  are also high gamma emitters included in the model, and properly identified.  $^{95}\text{Nb}$  is accurately identified for its 765.81 keV emission; however, the double counting of this same peak causes  $^{238}\text{Pu}$  to be inaccurately identified. In a similar manner,  $^{214}\text{Bi}$  and  $^{45}\text{Sc}$  are falsely identified.

$^{137}\text{Cs}$  is the scored nuclide along with  $^{137\text{m}}\text{Ba}$ , which is the daughter product of  $^{137}\text{Cs}$ . Therefore, it is not actually a mistaken double counted emission since the 662 keV emission from  $^{137}\text{Cs}$  really refers to the 662 keV emission from  $^{137\text{m}}\text{Ba}$ . The following scored nuclide,  $^{110}\text{Ag}$  (ground state) is often mistakenly scored when  $^{137}\text{Cs}$  is shown to be present. This is due to  $^{110}\text{Ag}$  also only having one gamma emission at 657.76 keV, which is very close to the 661.6 keV emission from  $^{137}\text{Cs}$ . Figure 4.21 shows the details from this scoring. I observe the same gamma emission attributed to both  $^{137}\text{Cs}$  and  $^{110}\text{Ag}$ . At this point, the uniquely attributable scoring begins to diminish, and remaining attributed emissions are double counted due to library aliasing. Many of these lower scored nuclides were included in the original source definition; however, I find that I can't show with enough certainty these nuclides are present due to the limited number of emissions identified.

To gain a better understanding of how some of the key identifying nuclides are attributed to the peaks identified, I examined the emission attributions for  $^{140}\text{La}$  and  $^{137}\text{Cs}$ . Figures 4.21 and 4.22 shows the emissions identified for these nuclides. I see that SmartID is accurately attributing the key gamma emissions to  $^{140}\text{La}$  with respect to the

number of counts in the spectrum to the probability of decay and detectability of each emission.

Nuclide	Score	T1/2	T1/2_unit	#EmissionInRange	#Matched	Correlation	Comment
<sup>140</sup> La	124.39	4.0300E+01	h	33	13	High	Fiss_Prod
Emission(KeV)	Prob/DK	Detectability	1.00% Energy Window		Peak(KeV)	Norm%_cts	
109.42	2.1900E-03	8.5100E-01	(	108.33 to 110.51)			
131.12	4.6700E-03	7.9615E-01	(	129.81 to 132.43)			
173.54	1.2700E-03	6.8339E-01	(	171.80 to 175.28)			
241.93	4.1400E-03	5.0326E-01	(	239.51 to 244.35)			
266.54	4.6600E-03	4.4546E-01	(	263.87 to 269.21)			
306.90	2.4800E-04	3.6098E-01	(	303.83 to 309.97)			
328.76	2.0300E-01	3.2465E-01	(	325.47 to 332.05)			
+ 397.52	7.3500E-04	2.2929E-01	(	393.54 to 401.50)	397.00	0.2713	
432.49	2.9000E-02	1.9717E-01	(	428.17 to 436.81)			
+ 438.50	3.9100E-04	1.9216E-01	(	434.12 to 442.89)	439.00	2.4206	
445.50	2.8600E-05	1.8648E-01	(	441.05 to 449.96)			
487.02	4.5500E-01	1.5575E-01	(	482.15 to 491.89)			
+ 618.12	3.7200E-04	9.7921E-02	(	611.94 to 624.30)	612.00	3.5649	
751.64	4.3300E-02	6.7795E-02	(	744.12 to 759.16)			
+ 815.77	2.3300E-01	5.7399E-02	(	807.61 to 823.93)	821.00	4.2716	
867.85	5.5000E-02	5.1687E-02	(	859.17 to 876.53)			
+ 919.55	2.6600E-02	4.6557E-02	(	910.35 to 928.75)	927.00	2.3077	
+ 925.19	6.9000E-02	4.6027E-02	(	915.94 to 934.44)	927.00	2.3077	
950.99	5.1900E-03	4.3679E-02	(	941.48 to 960.50)			
+ 992.90	1.3400E-04	4.0107E-02	(	982.97 to 1002.83)	988.00	1.2809	
+ 1045.05	2.4800E-04	3.6570E-02	(	1034.60 to 1055.50)	1037.00	0.0831	
1097.20	2.2900E-04	3.3807E-02	(	1086.23 to 1108.17)			
1303.50	4.2000E-04	2.5172E-02	(	1290.47 to 1316.54)			
1405.20	5.9100E-04	2.2308E-02	(	1391.15 to 1419.25)			
+ 1596.21	9.5400E-01	1.8269E-02	(	1580.25 to 1612.17)	1601.00	3.4706	
1877.29	4.1000E-04	1.4166E-02	(	1858.52 to 1896.06)			
+ 1924.62	1.3400E-04	1.3570E-02	(	1905.37 to 1943.87)	1941.00	0.0021	
2083.20	1.1500E-04	1.1978E-02	(	2062.37 to 2104.03)			
+ 2347.88	8.4900E-03	1.0254E-02	(	2324.40 to 2371.36)	2342.00	0.0276	
2464.10	1.1400E-04	9.5771E-03	(	2439.46 to 2488.74)			
+ 2521.40	3.4600E-02	9.2597E-03	(	2496.19 to 2546.61)	2509.00	0.0885	
2547.34	1.0100E-03	9.1195E-03	(	2521.87 to 2572.81)			
+ 2899.61	6.6800E-04	7.4109E-03	(	2870.61 to 2928.61)	2895.00	0.0012	

Figure 4.21: SmartID emission attribution for scored nuclide, <sup>140</sup>La.

The emission attributed to <sup>137</sup>Cs is very well matched to the peak identified, and the significant number of counts attributed to this peak matches what would be expected from a high activity nuclide with only a single emission. As I previously stated, the additional nuclides attributed to this peak are most likely not present. <sup>110</sup>Ag happens to also have a single gamma emission within the energy window of the identified peak, but this is a commonly misidentified nuclide. <sup>97</sup>Nb has 2 emissions, but the only one that shows a match is the 660 keV peak, which has already been attributed to <sup>137</sup>Cs.

Nuclide	Score	T1/2	T1/2_unit	#EmissionInRange	#Matched	Correlation	Comment
137Cs	104.20	3.0200E+01	y	1	1	Moderate	Fiss_Prod
Emission(KeV)	Prob/DK	Detectability	1.00%	Energy Window	Peak(KeV)	Norm%_cts	
+ 661.60	8.5100E-01	8.6937E-02	(	654.98 to 668.22 )	660.00	13.0811	
Nuclide	Score	T1/2	T1/2_unit	#EmissionInRange	#Matched	Correlation	Comment
137mBa	104.18	2.5500E+00	m	1	1	Moderate	Fiss_Prod
Emission(KeV)	Prob/DK	Detectability	1.00%	Energy Window	Peak(KeV)	Norm%_cts	
+ 661.65	9.0000E-01	8.6925E-02	(	655.03 to 668.27 )	660.00	13.0811	
Nuclide	Score	T1/2	T1/2_unit	#EmissionInRange	#Matched	Correlation	Comment
110Ag	103.99	2.4600E+01	s	1	1	Moderate	Fiss_Prod
Emission(KeV)	Prob/DK	Detectability	1.00%	Energy Window	Peak(KeV)	Norm%_cts	
+ 657.75	4.4900E-02	8.7860E-02	(	651.17 to 664.33 )	660.00	13.0811	
Nuclide	Score	T1/2	T1/2_unit	#EmissionInRange	#Matched	Correlation	Comment
97Nb	102.89	7.2100E+01	m	2	1	Moderate	Fiss_Prod
Emission(KeV)	Prob/DK	Detectability	1.00%	Energy Window	Peak(KeV)	Norm%_cts	
+ 657.90	9.8100E-01	8.7824E-02	(	651.32 to 664.48 )	660.00	13.0811	
1024.50	1.0800E-02	3.7718E-02	(	1014.26 to 1034.75 )			

**Figure 4.22:** SmartID emission attribution for scored nuclide, <sup>137</sup>Cs.

#### 4.3.4. 12 Emissions in Water

In order to further prove that SmartID can correctly identify key identifying emissions for spent nuclear fuel, I developed a simplified, 12 emissions case to show have many, if all, could be identified and correlated to the correct nuclides. Table 4.8 shows the gamma emissions I chose to include in the model, along with each corresponding nuclide.



**Table 4.8:** 12 gamma source emissions chosen for MCNP simulation.

<b>Emission Energy (keV)</b>	<b>Nuclide</b>	<b>Emission rate for entire assembly (gamma/s)</b>
511.86	<sup>106</sup> Rh	$4.58 \times 10^{15}$
604.72	<sup>134</sup> Cs	$2.18 \times 10^{15}$
621.93	<sup>106</sup> Rh	$2.23 \times 10^{15}$
652.9	<sup>91</sup> Sr	$5.18 \times 10^{14}$
661.66	<sup>137</sup> Cs	$3.33 \times 10^{15}$
723.3	<sup>154</sup> Eu	$4.75 \times 10^{13}$
749.8	<sup>91</sup> Sr	$1.52 \times 10^{15}$
795.86	<sup>134</sup> Cs	$4.78 \times 10^{15}$
1004.8	<sup>154</sup> Eu	$4.27 \times 10^{13}$
1024.3	<sup>91</sup> Sr	$2.16 \times 10^{15}$
1050.4	<sup>106</sup> Rh	$3.50 \times 10^{14}$
1274.4	<sup>154</sup> Eu	$8.25 \times 10^{13}$

I incorporated these emissions in the MCNP model which produced the spectrum shown by Figure 4.23. I executed the MCNP models for enough particle histories ( $5 \times 10^{11}$  histories) to reduce my average 1 sigma errors to less than 10%. I then created a “.Spe” file from the resulting spectrum and post-processed with SmartID. The red lines in Figure 4.23 show the identified peaks. Rather than all 12 emissions identified, SmartID only extracted 7 peaks.

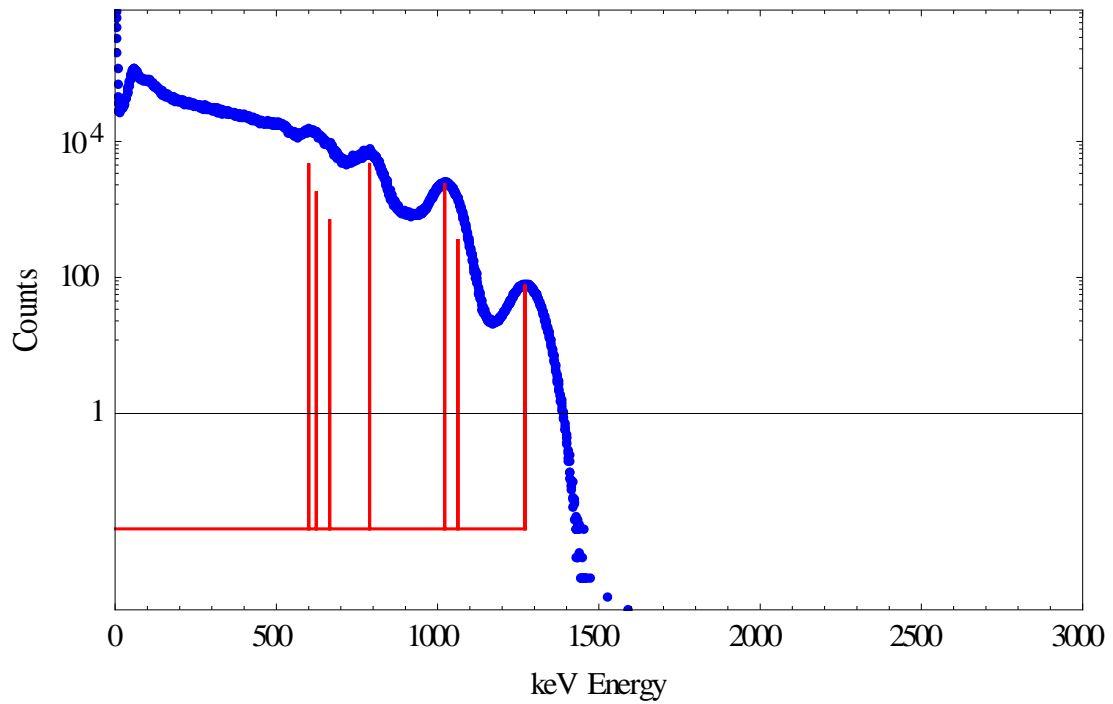


**Figure 4.23:** Simulated spectrum from 12 gamma emissions along with SmartID identified peaks.

I matched the identified peaks to the emissions included in the model. I noted that each of the 7 peaks identified matched one of the 12 energy peaks modeled. Table 4.9 shows each individual identified photopeak along with the matched emission.

**Table 4.9:** SmartID peaks identified and corresponding gamma emissions.

<b>Emission (keV)</b>	<b>Nuclide</b>	<b>Identified Peak</b>	<b>Counts</b>
511.86	<sup>106</sup> Rh	Not matched	
604.72	<sup>134</sup> Cs	600	4.8016×10 <sup>3</sup>
621.93	<sup>106</sup> Rh	624	1.8580×10 <sup>3</sup>
652.9	<sup>91</sup> Sr	Not matched	
661.66	<sup>137</sup> Cs	665	7.1746×10 <sup>2</sup>
723.3	<sup>154</sup> Eu	Not matched	
749.8	<sup>91</sup> Sr	Not matched	
795.86	<sup>134</sup> Cs	789	4.8495×10 <sup>3</sup>
1004.8	<sup>154</sup> Eu	Not matched	
1024.3	<sup>91</sup> Sr	1022	2.4277×10 <sup>3</sup>
1050.4	<sup>106</sup> Rh	1061	3.6683×10 <sup>2</sup>
1274.4	<sup>154</sup> Eu	1271	7.8835×10 <sup>1</sup>

I tried a variety of settings on the “smartid.inp” file to see if any significant changes in peak identification would take place. I slowly increased the Chi-square threshold from 0.005 up to 0.995. Once I had a Chi-square value of 0.9, an additional peak was identified at 820 keV. This peak does not match any peaks introduced into the MCNP source definition in the model. I investigated why this was occurring. I noticed was that the non-matching peak existed to the right of a major peak. It seemed that the entire Gaussian broadened peak was not subtracted out, leaving a false elevation in counts within the major peak’s FWHM, but when I increased the aliasing factor, this peak was still identified. Therefore, something else was at play. I compared the 1 sigma errors to the spectrum shape as energy increasing, and observed an interesting pattern. Looking at Figure 4.24, I see that the MCNP errors increase to a peak at approximately 820 keV. The spectrum shown is normalized to fit within the bounds of the plotted MCNP 1 sigma errors. The increase in error at this energy possibly created a “false” peak which was not rejected during the smoothing process. The chi-square test was not rigorous enough to reject this spectral change. This shows the great importance of

implementing noise reduction. Even in a simulated spectrum, where noise is reduced, even small modeling errors can play into how peaks are identified.

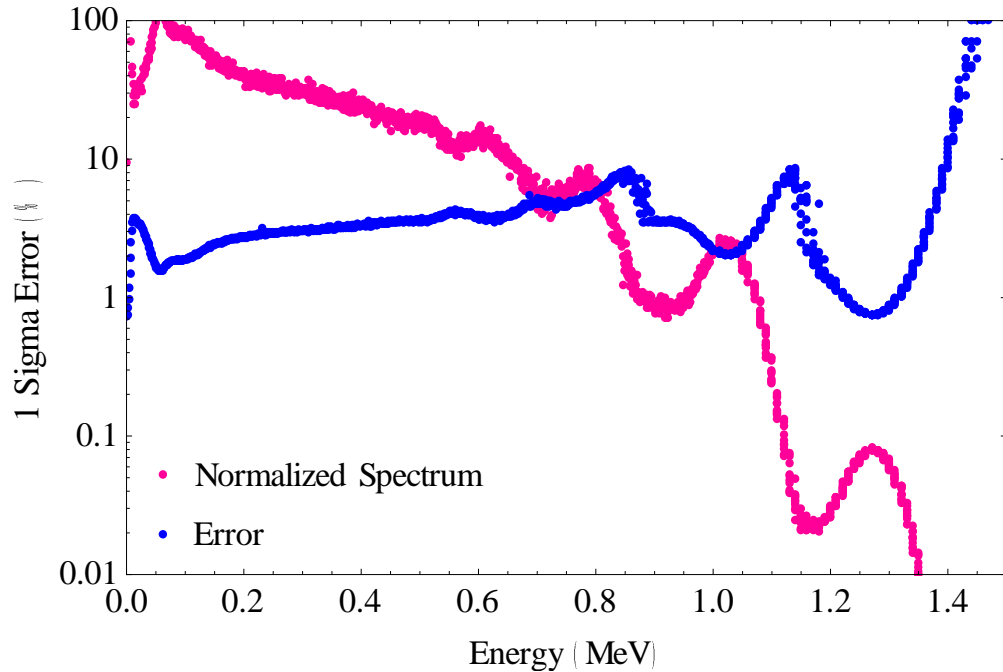


**Figure 4.24:** The relationship between the Gaussian Energy Broadened spectrum produced through f8 tallies in MCNP for the 12 emissions case and the corresponding 1 sigma errors.

This example identifies a key issue when simulating spectra rather than collecting real, known spectra in a spent fuel pool environment. However, considering the limitations placed on this study, the peak identification performs very well. The SmartID nuclide matching is not expected to be reliable for this case since I only chose to include a few emissions from nuclides that may have many additional characteristic gamma emissions. However, even with this limiting condition,  $^{134}\text{Cs}$  was highly correlated, followed closely by  $^{137}\text{Cs}$  and  $^{106}\text{Ru}$ , proving the robustness of the nuclide scoring feature.

Score Summary:							
Nuclide	Total	(base +	bonus I,	II,	III)	Comment	Correlation
134Cs	114.81	( 84.3	0.6	24.9	5.0 )	Fiss_Prod	High
132I	100.60	( 55.0	13.3	32.3	0.0 )	Fiss_Prod	Moderate
137mBa	100.41	( 98.5	0.0	1.9	0.0 )	Fiss_Prod	Moderate
137Cs	100.39	( 98.5	0.0	1.9	0.0 )	Fiss_Prod	Moderate
106Ru	100.17	( 95.3	0.0	4.9	0.0 )	Fiss_Prod	Moderate
124Sb	94.94	( 82.4	0.0	12.5	0.0 )	Fiss_Prod	Low
143Ce	70.11	( 26.2	9.7	34.2	0.0 )	Fiss_Prod	Low
151Pm	65.02	( 2.0	25.2	37.8	0.0 )	Fiss_Prod	Low
148mPm	63.11	( 37.8	1.6	23.8	0.0 )	Fiss_Prod	Low
238Np	61.75	( 54.7	0.7	6.3	0.0 )	SNM	Low
91Sr	57.39	( 40.5	0.6	11.2	5.0 )	Fiss_Prod	Low
131mTe	57.24	( 19.1	2.6	15.5	20.0 )	Fiss_Prod	Low
89Rb	57.15	( 50.9	0.0	6.2	0.0 )	Fiss_Prod	Low
125Sb	56.44	( 21.3	0.6	14.5	20.0 )	Fiss_Prod	Low
226Ra	53.70	( 41.0	0.0	12.7	0.0 )	U-238_Daughter	Low

Scored nuclides details:							
Nuclide	Score	T1/2	T1/2_unit	#EmissionInRange	#Matched	Correlation	
134Cs	114.81	2.0600E+00	y	9	2	High	
Emission(KeV)	Prob/DK	Detectability	1.00% Energy Window		Peak(KeV)	Norm%_cts	
475.35	1.4600E-02	1.6389E-01	( 470.60 to 480.10 )				
563.23	8.3800E-02	1.1746E-01	( 557.60 to 568.86 )				
569.32	1.5400E-01	1.1492E-01	( 563.63 to 575.01 )				
+ 604.70	9.7600E-01	1.0157E-01	( 598.65 to 610.75 )		600.00	31.7988	
+ 795.84	8.5400E-01	5.9937E-02	( 787.88 to 803.80 )		789.00	32.1161	
801.93	8.7300E-02	5.9015E-02	( 793.91 to 809.95 )				
1038.60	1.0000E-02	3.6927E-02	( 1028.21 to 1048.99 )				
1167.90	1.8000E-02	3.0380E-02	( 1156.22 to 1179.58 )				
1365.20	3.0400E-02	2.3395E-02	( 1351.55 to 1378.85 )				

**Figure 4.25:** SmartID nuclide scoring and emission attribution of  $^{134}\text{Cs}$  for the 12 emission case.

$^{132}\text{I}$  was identified as the second most likely nuclide present, but I easily determine this not to be the case, since only 10 out of 145 emissions were matched. Additionally, when I look closer at the emissions matched, I see that these are also matched aliasing with other nuclides. For example, the highly correlated  $^{134}\text{Cs}$  nuclide matches the 600 keV and 789 keV photopeak. These same two emissions are matched in the  $^{132}\text{I}$  case. Knowing that  $^{134}\text{Cs}$  is much more likely to be present, I can eliminate these peaks from the  $^{132}\text{I}$  attribution and see that many less emissions are matched. This proves that although many nuclides emit a large number of emissions, only a few may be needed to provide attribution.

I believe the matching of nuclides for the few emissions is even more impressive due to me keeping a large nuclide library available for matching. I did condense the

library down from the many nuclides not associated with spent fuel or SNM, but I set my half-life option to seconds so that I would not be ruling out any fission products.

#### **4.4. Final Thoughts**

Overall, SmartID worked very well for the MCNP simulated spectra. The most prominent peaks were correctly attributed to the most active fission products. However, special attention to the fine details of how the emissions are attributed to an energy peak continues to be important for analysis of the burned fuel assembly. The limiting factors of this technology are dependent on the detector specifications provided by the user. It is imperative that energy calibrations are accurate, and the FWHM data is carefully measured. Without proper calibration, many fission products could be mistakenly attributed.

#### **4.5. References**

- [1] Oak Ridge National Laboratory, "SCALE6: A Comprehensive Modeling and Simulation Suite for Nuclear Safety Analysis and Design; Includes ORIGEN (Source & Executables)," RSICC Data Library Collection, C00785-MNYCP-00, 6.0 ed., (2009).
- [2] Los Alamos National Laboratory, "MCNP5: Monte Carlo N-Particle Transport Code Including MCNP5 1.60 and MCNPX 2.7.0 & Data Libraries," *RSICC Data Library Collection*, C00740 MNYCP 08, 5.0 ed., Los Alamos, New Mexico (2011).
- [3] KNOLL, G.E., Radiation Detection and Measurement. 3<sup>rd</sup> Ed. John Wiley & Sons, Inc., 2000.

# CHAPTER 5

## ADJOINT COUPLING

### 5.1. Radiation Transport Methods

Understanding how gamma rays emitted from a fuel assembly will interact with a highly collimated detector is important for predicting the composition of isotopes in that assembly from a spectrum collected by the detector. The radiation transport equation carefully accounts for the various interactions that can take place in a system and is an important fundamental tool in determining the information available in the detector. This equation for a time independent fixed source is shown by

$$\begin{aligned} \widehat{\Omega} \cdot \nabla \psi(\vec{r}, \widehat{\Omega}, E) + \sigma(\vec{r}, E)\psi(\vec{r}, \widehat{\Omega}, E) = \\ \int_{\forall E} \int_{4\pi} dE' d\Omega' \sigma_s(\vec{r}, \widehat{\Omega}' \cdot \widehat{\Omega}, E' \rightarrow E)\psi(\vec{r}, \widehat{\Omega}, E') + q(\vec{r}, \widehat{\Omega}, E), \end{aligned} \quad (5.1)$$

where  $\widehat{\Omega}$  is the solid angle of particle direction,  $\vec{r}$  is the spatial coordinate of particle position,  $E$  is the particle's energy,  $\psi(\vec{r}, \widehat{\Omega}, E)$  is the angular particle flux,  $\sigma(\vec{r}, E)$  is the total macroscopic cross section,  $\sigma_s(\vec{r}, \widehat{\Omega}' \cdot \widehat{\Omega}, E' \rightarrow E)$  is the macroscopic scattering cross section, and  $q(\vec{r}, \widehat{\Omega}, E)$  is the fixed source term.

#### 5.1.1 Discrete Ordinates ( $S_N$ )

Equation 5.1 can be solved by discretizing the variables for energy, angle, and space. Energy is discretized by spectrally averaging over energy groups. Energy groups are ordered from  $g=1$  to  $g=G$ , where  $g=1$  is the highest energies, and  $G$  represents the lowest. The new multigroup transport equation is represented by

$$\begin{aligned}
& \widehat{\Omega} \cdot \nabla \psi_g(\vec{r}, \widehat{\Omega}) + \sigma_g(\vec{r}) \psi_g(\vec{r}, \widehat{\Omega}) \\
&= \sum_{g'=1}^g \int_{4\pi} d\Omega' \sigma_{s,g' \rightarrow g}(\vec{r}, \widehat{\Omega}' \cdot \widehat{\Omega}) \psi_g(\vec{r}, \widehat{\Omega}) + q_g(\vec{r}, \widehat{\Omega})
\end{aligned} \tag{5.2}$$

Angle is discretized by  $\mu$ ,  $\eta$ , and  $\xi$ , which are the direction cosines along the x, y, and z axes [1]. In order to specify the direction  $\widehat{\Omega}$  of particle travel, two angles are required. A set of direction cosines must satisfy the condition,  $\mu_n^2 + \eta_n^2 + \xi_n^2 = 1$ .  $S_N$  quadratures refer to quadratures in the  $\frac{N}{2}$  positive  $\mu_n$ . The number of ordinates in a quadrant is given by  $\frac{N(N+2)}{8}$ . Figure 5.1 shows how these directions are discretized for an  $S_6$  level symmetric discrete ordinates set.

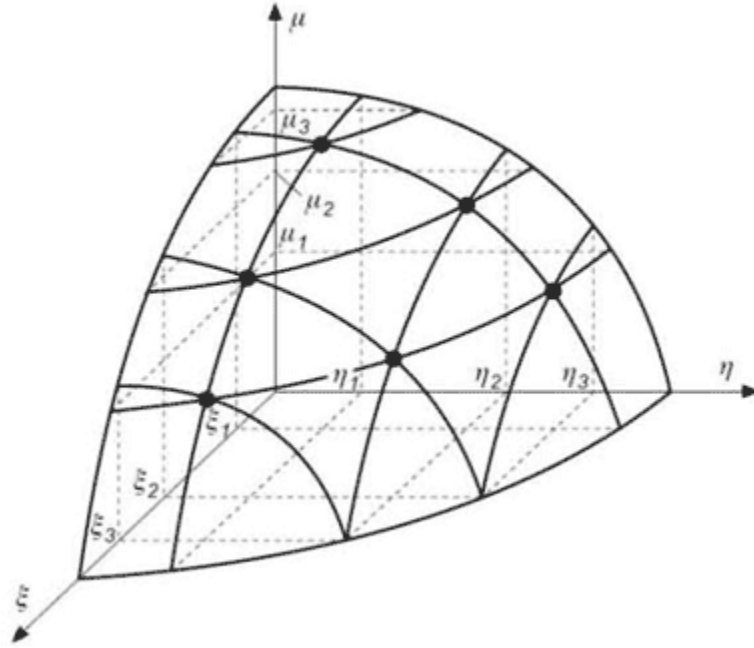


**Figure 5.1:**  $S_6$  level symmetric discrete ordinates set.



Finally, after applying energy, angle, and space discretization, the 3-D Cartesian Boltmann Transport Equation for photons is represented by

$$\begin{aligned}
& \left( \mu \frac{\partial}{\partial x} + \eta \frac{\partial}{\partial y} + \xi \frac{\partial}{\partial z} \right) \psi_g(x, y, z, \mu, \varphi) + \sigma_g(x, y, z) \psi_g(x, y, z, \mu, \varphi) \\
& = \sum_{g'=1}^g \sum_{l=0}^L (2l+1) \sigma_{s,g' \rightarrow g,l}(x, y, z) \left\{ P_l(\mu) \phi_{g',l}(x, y, z) \right. \\
& + 2 \sum_{k=1}^l \frac{(l-k)!}{(l+k)!} P_l^k(\mu) \left[ \phi_{c,g',l}^k(x, y, z) \cos(k\phi) \right. \\
& \left. \left. + \phi_{s,g',l}^k(x, y, z) \sin(k\phi) \right] \right\} + q_g(\vec{r}, \hat{\Omega})
\end{aligned} \tag{5.3}$$

where the new term  $l$  is the Legendre expansion index,  $\sigma_{s,g' \rightarrow g,l}$  is the  $l^{\text{th}}$  Legendre moment of the macroscopic differential scattering cross section,  $P_l$  is the  $l^{\text{th}}$  Legendre polynomial,  $\phi_{g',l}$  is the  $l^{\text{th}}$  Legendre scalar flux moment for group  $g$ ,  $P_l^k(\mu)$  is the  $l^{\text{th}}$   $k^{\text{th}}$  associated Legendre polynomial,  $\phi_{c,g',l}^k$  is the  $l^{\text{th}}$ ,  $k^{\text{th}}$  cosine associated Legendre scalar flux moment for group  $g$ , and  $\phi_{s,g',l}^k$  is the  $l^{\text{th}}$ ,  $k^{\text{th}}$  sine associated Legendre scalar flux moment for group  $g$  [2].

Computational modeling is necessary for conducting these types of calculations and, in typical form, models look at how radiation emanating from a point will interact with surroundings. This makes it difficult, however, to determine how source strengths and compositions will be computed in a detector if these source conditions change, because a new model will need to be developed and executed for each specified case. However, instead of creating multiple forward transport models of PWR fuel assemblies with various source strengths and radionuclide compositions, only one adjoint transport model needs to be created to show how gamma radiation originating in the fuel pins

interacts with a NaI detector at a 40 cm distance away. The adjoint transport equation essentially reverses the forward transport equation. Instead of a radiation source term,  $q$ , the detector's absorption cross section is treated as the "source," and the streaming direction is reversed along with the energy group structure. Instead of the flux variable,  $\phi$ , a new variable called the adjoint importance,  $\phi^*$ , is introduced. Unlike flux, the adjoint importance does not have units; instead, it is a measure of how likely a particle located at any location distal from the detector is to create an event in the detector. Determining the adjoint importances at all locations around a detector in one transport model is a very powerful tool. The code system, PENTRAN, has this capability and was chosen to calculate these adjoint importances.

### 5.1.2 PENTRAN

The PENTRAN code system, developed by Sjoden and Haghghat, can be used for 3-D multigroup forward or adjoint discrete ordinates ( $S_n$ ) simulations. The  $S_n$  method is a deterministic approach that discretizes the angular, energy, and physical spatial variables into a finite number of discrete angular ordinates, energy groups, and spatial grids over the entire phase space system. The PENTRAN system is actually a suite of codes that allows one to readily generate mesh geometries, solve 3-D transport models, and automatically collates parallel data. PENTRAN is a multi-group, anisotropic  $S_n$  code for 3-D Cartesian geometries; it has been specifically designed for distributed memory, scalable parallel computer architectures using the Message Passing Interface library [3]. Automatic domain decomposition of the phase space among the angular, energy, and spatial variables with an adaptive differencing algorithm and other numerical enhancements make PENTRAN an extremely robust solver with a 0.996 parallel code fraction (based on Amdahl's law). Numerous simulations have been performed using the PENTRAN code system, including many international benchmark computations [3,4]. The many advanced numerical features in PENTRAN, including adaptive differencing

with a two-level parallel angular memory structure in a scalable architecture, are well-suited for deterministic work in this research.

### 5.1.3 Application of Adjoint

As previously mentioned, the adjoint efficiencies calculated in the PENTRAN models can be used to estimate the forward source strength of the fission products and actinides in the PWR fuel assembly. The forward and adjoint detector response rates are derived from the forward transport equation which was given by equation 5.1. The forward transport equation is written in operator form as

$$\begin{aligned} H\varphi &= q_{fwd} \\ \varphi &= 0 \text{ on } dV, \quad \hat{n} \cdot \hat{\Omega} < 0 \end{aligned} \tag{5.4}$$

where  $H$  is the forward operator,  $\varphi$  is the angular flux variable,  $q_{fwd}$  is the forward source density ( $\text{n cm}^{-3} \text{ s}^{-1}$ ),  $\hat{n}$  is the outward normal, and  $dV$  is the surface of the spatial domain,  $V$ , so that the boundary condition represents a vacuum boundary meeting the condition that no particles enter the region. The forward operator is given by

$$H = \hat{\Omega} \cdot \nabla + \sigma_g(\vec{r}) - \sum_{g'=1}^G \int_{4\pi} \sigma_{s,g' \rightarrow g}(\vec{r}, \hat{\Omega}' \cdot \hat{\Omega}) d\Omega' \tag{5.5}$$

The operator is non-self-adjoint, therefore the adjoint operator must be solved for. In order to do so, equation 5.5 must be multiplied by the adjoint variable  $\varphi^+$ , which is referred to as the adjoint importance. The resulting adjoint transport equation is written as

$$\begin{aligned}
H^+ \varphi^+ &= \sigma_d \\
\varphi^+ &= 0 \text{ on } dV, \hat{n} \cdot \hat{\Omega} > 0,
\end{aligned} \tag{5.6}$$

where  $H^+$  is the adjoint operator,  $\varphi^+$  is the adjoint importance variable,  $\sigma_d$  is the detector cross section ( $\text{cm}^{-1}$ ),  $\hat{n}$  is the outward normal, and  $dV$  is the surface of the spatial domain,  $V$ , so that the boundary condition represents a vacuum boundary condition in that no particles leave the region. The adjoint operator is given by

$$H^+ = -\hat{\Omega} \cdot \nabla + \sigma_g(\vec{r}) - \sum_{g'=1}^G \int_{4\pi} \sigma_{s,g \rightarrow g'}(\vec{r}, \hat{\Omega}' \cdot \hat{\Omega}) d\hat{\Omega}'. \tag{5.7}$$

The response of a detector with a total cross section,  $\sigma_d$ , a volume,  $V_d$ , and scalar flux  $\phi(\vec{r}_d, E)$  can be determined by the reaction rate at  $\vec{r}_d$ ,

$$R = V_d \int dE \sigma_d(E) \phi(\vec{r}_d, E). \tag{5.8}$$

This reaction rate can be rewritten as

$$R = \langle \varphi \sigma_d \rangle, \tag{5.9}$$

and by applying the adjoint identity, the adjoint response is

$$R = \langle \varphi^+ q_{fwd} \rangle. \tag{5.10}$$

The forward and adjoint calculations were computed using a finite 24-group energy structure and in space using a PENTRAN's coarse mesh structure, therefore, the forward response can be rewritten as

$$\begin{aligned}
R_{fwd} &= \int_{V_d, \forall E} \phi(x, y, z, E) \sigma_d(x, y, z, E) dx dy dz dE \\
&\approx \sum_{g=1}^G \sum_{i=1}^{CM} \phi_{g,i} \sigma_{d,g,i} \Delta V_i
\end{aligned} \tag{5.11}$$

Where  $R_{fwd}$  is the forward response rate,  $\phi(x, y, z, E)$  is the spatial energy dependent scalar flux ( $\text{n cm}^{-2} \text{s}^{-1}$ ),  $\sigma_d(x, y, z, E)$  is the spatial energy dependent detector cross section ( $\text{cm}^{-1}$ ),  $(x, y, z)$  is the spatial location of the detector,  $\phi_{g,i}$  is the  $i^{\text{th}}$  cell scalar flux for group  $g$ ,  $\sigma_{d,g,i}$  is the  $i^{\text{th}}$  cell detector cross section for group  $g$  ( $\text{cm}^{-1}$ ), and  $\Delta V_i$  is the  $i^{\text{th}}$  cell volume ( $\text{cm}^3$ ). The adjoint response can be rewritten as

$$\begin{aligned}
R_{adj} &= \int_{V_s, \forall E} \phi^+(x', y', z', E) q(x', y', z', E) dx' dy' dz' dE \\
&\approx \sum_{i=1}^{CM} \sum_{g=1}^G \Delta V_i q_{g,i} \phi_{g,i}^+
\end{aligned} \tag{5.12}$$

where  $R_{adj}$  is the adjoint response rate,  $\phi^+(x', y', z', E)$  is the spatial energy dependent scalar adjoint function ( $\text{n cm}^{-2} \text{s}^{-1}$ ),  $q(x', y', z', E)$  is the spatial energy dependent source ( $\text{n cm}^{-3} \text{s}^{-1}$ ),  $(x', y', z')$  is the spatial location of non-zero source cells,  $\phi_{g,i}^+$  is the  $i^{\text{th}}$  cell scalar adjoint function for detector  $d$  and group  $g$ ,  $q_{g,i}$  is the  $i^{\text{th}}$  cell source density for group  $g$  ( $\text{n cm}^{-3} \text{s}^{-1}$ ), and  $\Delta V_i$  is the  $i^{\text{th}}$  cell volume ( $\text{cm}^3$ ).

The forward source can be solved for from equation 5.8 and used to determine the activity which then can be utilized to determine the number of particles from a specific nuclide present in the material.

$$\begin{aligned}
R_{adj} = & \Delta V_1 [q_{1,1} \phi_{1,1}^+ + q_{2,1} \phi_{2,1}^+ + \dots + q_{G,1} \phi_{G,1}^+] \\
& + \Delta V_2 [q_{1,2} \phi_{1,2}^+ + q_{2,2} \phi_{2,2}^+ + \dots + q_{G,2} \phi_{G,2}^+] + \dots \\
& + \Delta V_{CM} [q_{1,CM} \phi_{1,CM}^+ + q_{2,CM} \phi_{2,CM}^+ + \dots + q_{G,CM} \phi_{G,CM}^+].
\end{aligned} \tag{5.13}$$

The detector response can be grouped by energy if assuming a homogenous source across course meshes.

$$R_{adj,g} = q_g \sum_{i=1}^{CM} \phi_{g,i}^+ \Delta V_i. \tag{5.14}$$

## 5.2 Adjoint Models

As discussed, adjoint efficiencies essentially show how important a particle originating at a location  $\vec{r}$  is to the detector response. This information can be used to solve for the relative contribution of fission product gammas emitted from different areas of the fuel assembly. Combining this information along with nuclide identification will provide the basis for estimating the relative concentrations of key radionuclides. SmartID will be updated to account for the specified geometry of a spent fuel pool NDA examination and correct for detector efficiencies along the energy spectrum in order to rapidly reveal a predicted fuel mass characterization. A model of a NaI(Tl) detector, shown in Figure 5.2, “looking” at a spent fuel assembly underwater was created using the PENTRAN 3-D deterministic code to determine the adjoint efficiencies at all locations in the fuel assembly.

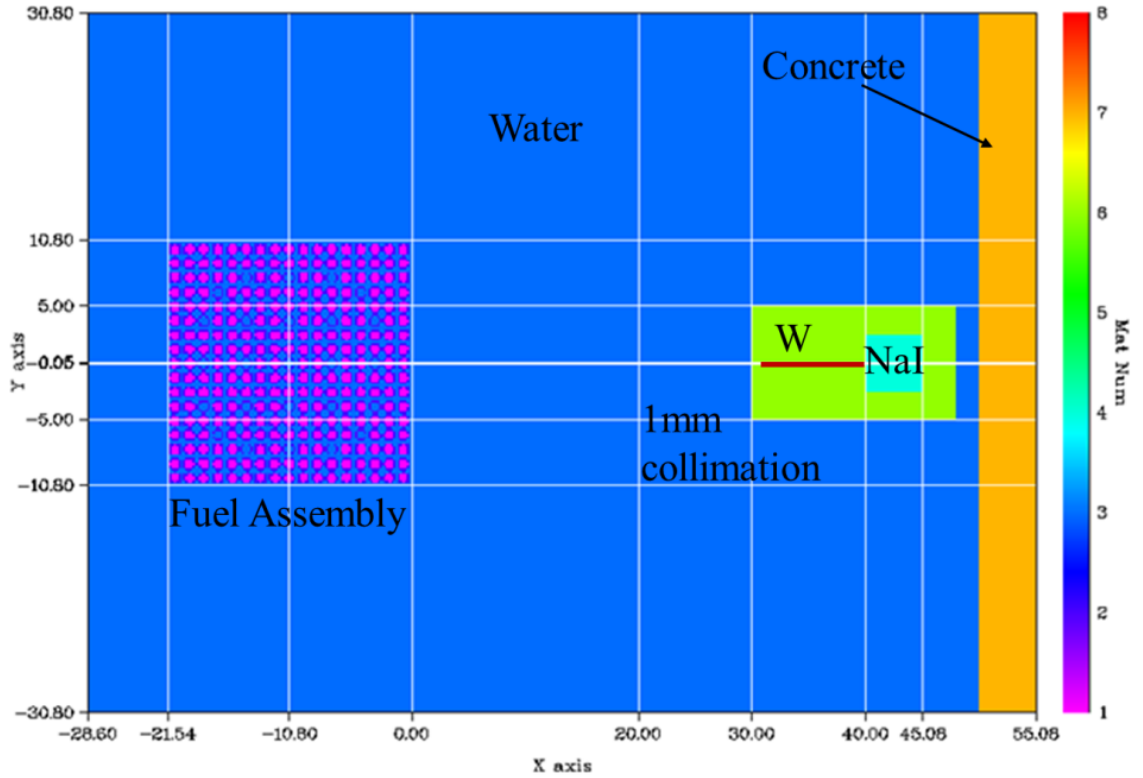


**Figure 5.2:** 2-D top-down view PENTRAN model of NaI(Tl) detector underwater “looking” at a used fuel assembly.

The energy groups were defined as a 24-group structure and the energy bounds are shown in Table 5.1. This structure was designed for uranium and plutonium detection, and has performed well in previous research efforts [5, 6]. It is important to keep in mind that these are forward energy groups. The adjoint groups will be numbered in reverse order. From now on, I will refer to energy groups as either adjoint or forward groups for clarification.

**Table 5.1:** 24-group structure for Gamma emissions.

<b>Group</b>	<b>Upper Energy Bound (keV)</b>	<b>Group</b>	<b>Upper Energy Bound (keV)</b>
1	3000	13	1240
2	2749	14	1200
3	2250	15	1180
4	2210	16	1002
5	1832	17	999
6	1830	18	956
7	1760	19	954
8	1740	20	767
9	1736	21	765
10	1520	22	743
11	1500	23	741
12	1260	24	300

Figure 5.2 shows an  $S_{90}$  calculation (8,280 directions per mesh) of the adjoint importances in the model depicted in Figure 5.2. The model consisted of 85,165 fine meshes and ran on 112 processors with a maximum memory of 4,096 Mb for approximately 2 days. A 1 mm diameter pinhole with a length of 10 cm collimates the very high activity fuel assembly to prevent oversaturation of the detector, but this collimation still allows the detector to interact with low energy gamma radiation emitted from the first few rows of pins in the assembly. Upon closer examination of the location of the fuel assembly in Figure 5.3, the individual pins can still be distinguished, and gamma importances are only 4 to 5 orders of magnitude less than if they originated close to the detector for high energy gammas, and 5 to 6 orders of magnitude less for lower energy gammas. It is important to note that Figure 5.3 depicts each energy group with a different adjoint importance scaling in order to show in more detail how the importances change with location. Figure 5.4 was added to show a better representation of how the importances relate to gamma energy. The strongest gammas also show the highest



importances across the entire system. It will be important to identify a key region in the fuel, consistent with what can be seen at the lowest energy ranges, in order to properly compare nuclide content ratios and mass.

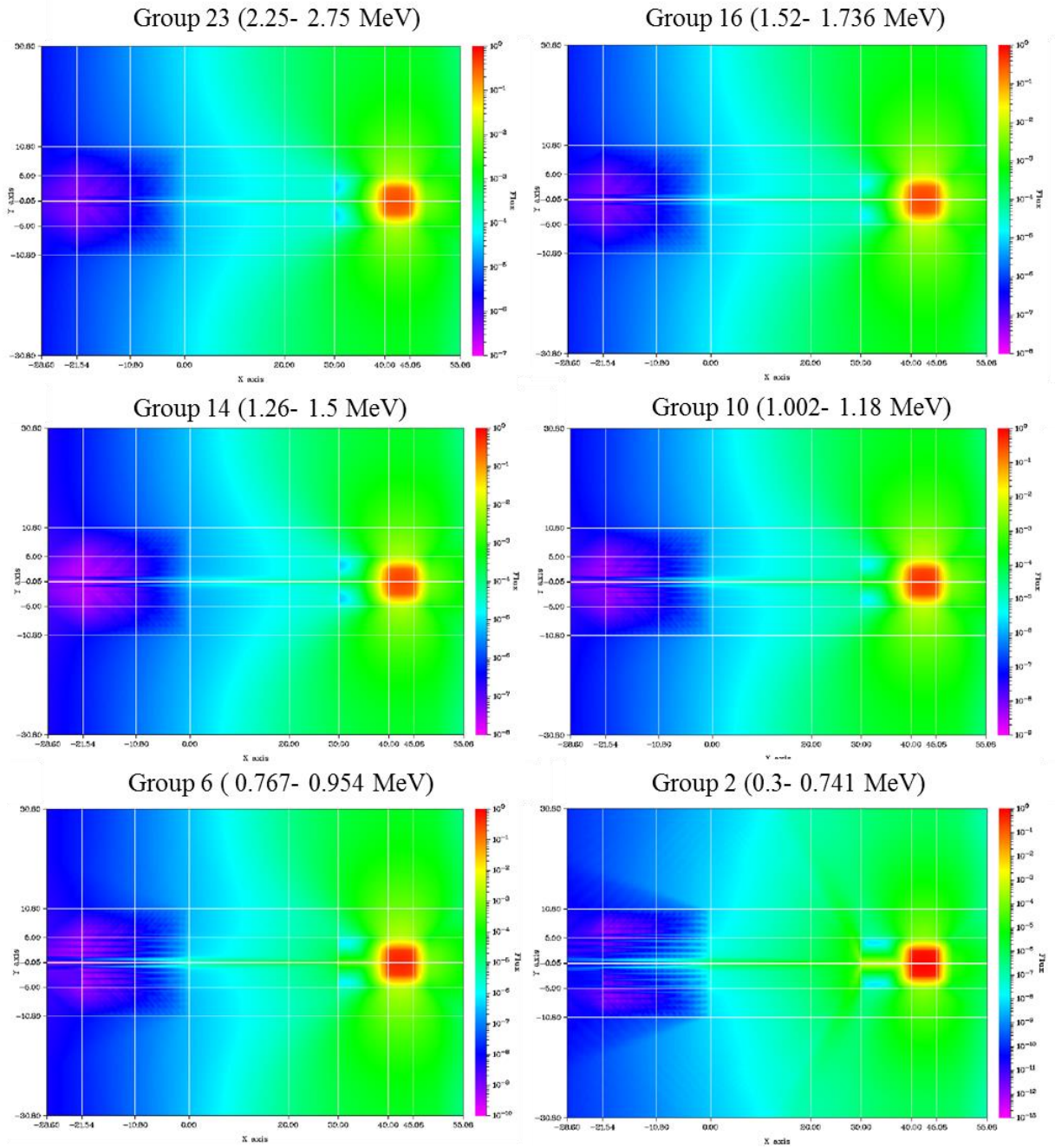


**Figure 5.3:**  $S_{90}$  adjoint importances mapped for 6 out of 24 adjoint energy groups. Each group is scaled individually for better visualization.

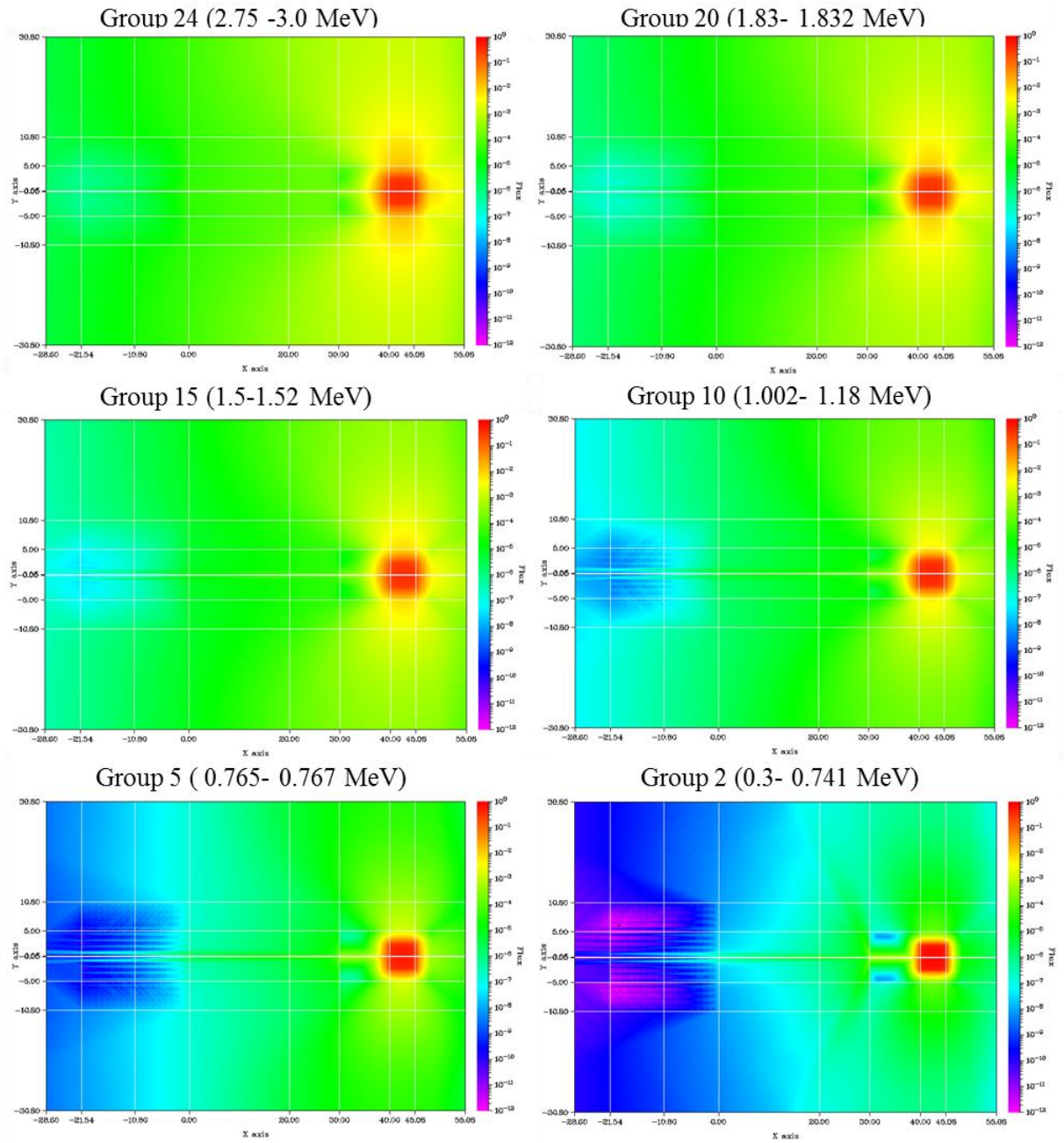


**Figure 5.4:**  $S_{90}$  adjoint importances mapped for 6 out of 24 adjoint energy groups.

Scaling is equal across all groups.

### 5.3 Forward Models

To gain a better understanding of how the gamma emissions interact near the fuel and behave near the detector, I created 2-D forward transport models in PENTRAN. The model geometry is identical to the adjoint model case, but instead of using the detector absorption cross section as the source, I developed a simple source based on a Westinghouse 17x17 PWR fuel assembly burned in a reactor and cooled for approximately 1 day. The energy group structure remains identical to adjoint energy structure; however, the group ordering is reversed. Figure 5.5 shows the normalized forward source used in the model calculations.

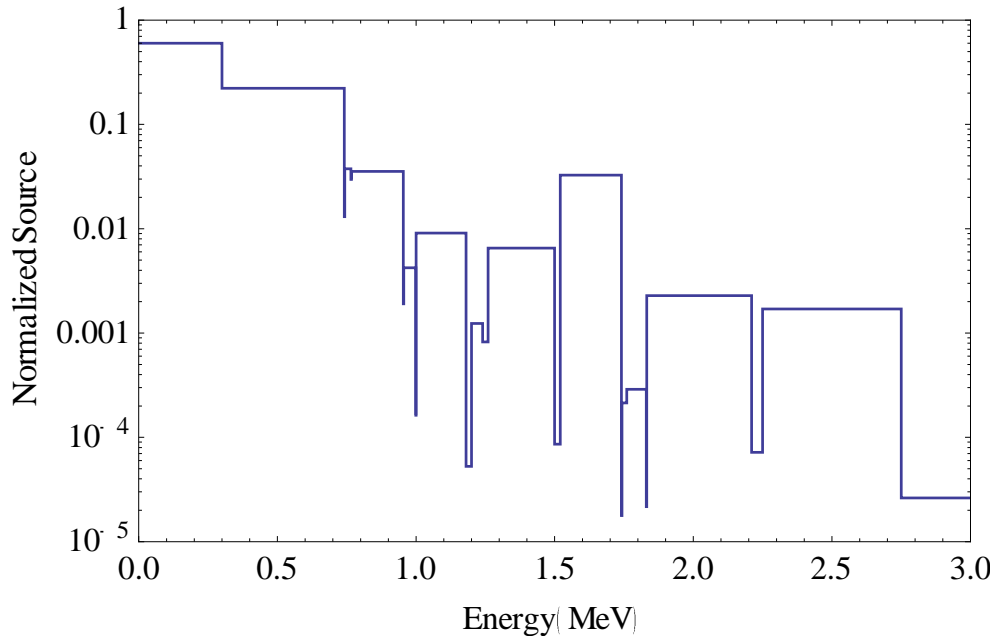


**Figure 5.5:** Normalized forward source by energy group.

Figure 5.6 shows the flux profiles for six different forward energy groups. Notice that forward group 1 has the same energy range as adjoint group 24; forward group 5 has the same energy range as adjoint group 20, with this pattern continuing through all groups.

Instead of showing how likely a particle within a certain energy range will interact with the detector, the forward flux gives an idea of the quantity of particles within an energy range that will show up in the detector for a single source composition. These flux profiles will vary with each change in the spent fuel assembly investigated because the energy profile of spent fuel is unique for each burnup case and fuel assembly.

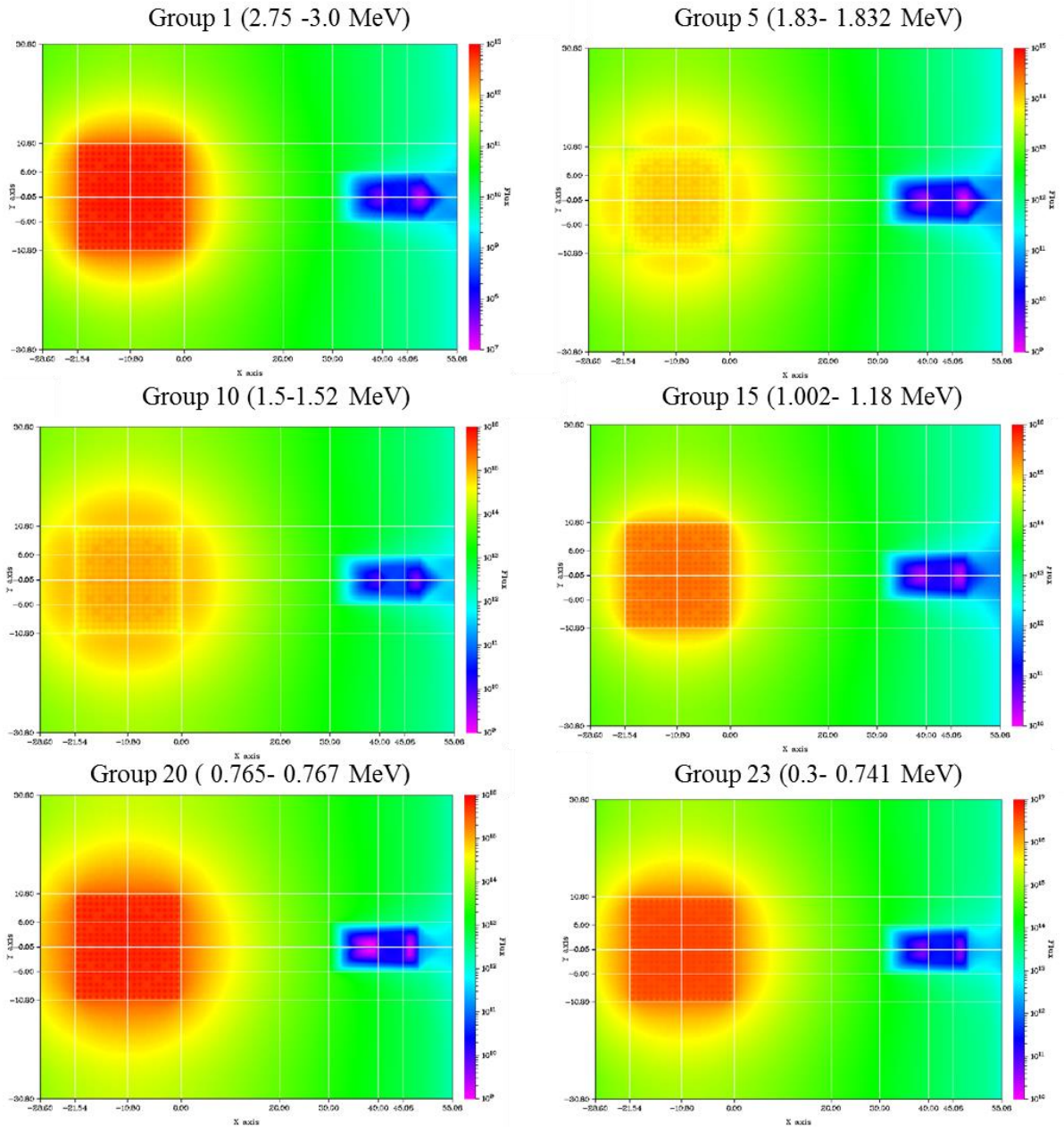


**Figure 5.6:**  $S_{90}$  forward flux mapped for 6 out of 24 forward energy groups. Each group is scaled individually for better visualization.

Forward transport models show how much gamma flux is reaching the detector from a full 2-D slice of a PWR fuel assembly. Figure 4.6 gives a better understanding how the source behaves. Even though it is expected that high energy gammas will

interact with the detector much more frequently, much of the spent fuel assembly's gamma emissions originate in energies less than 1.5 MeV.

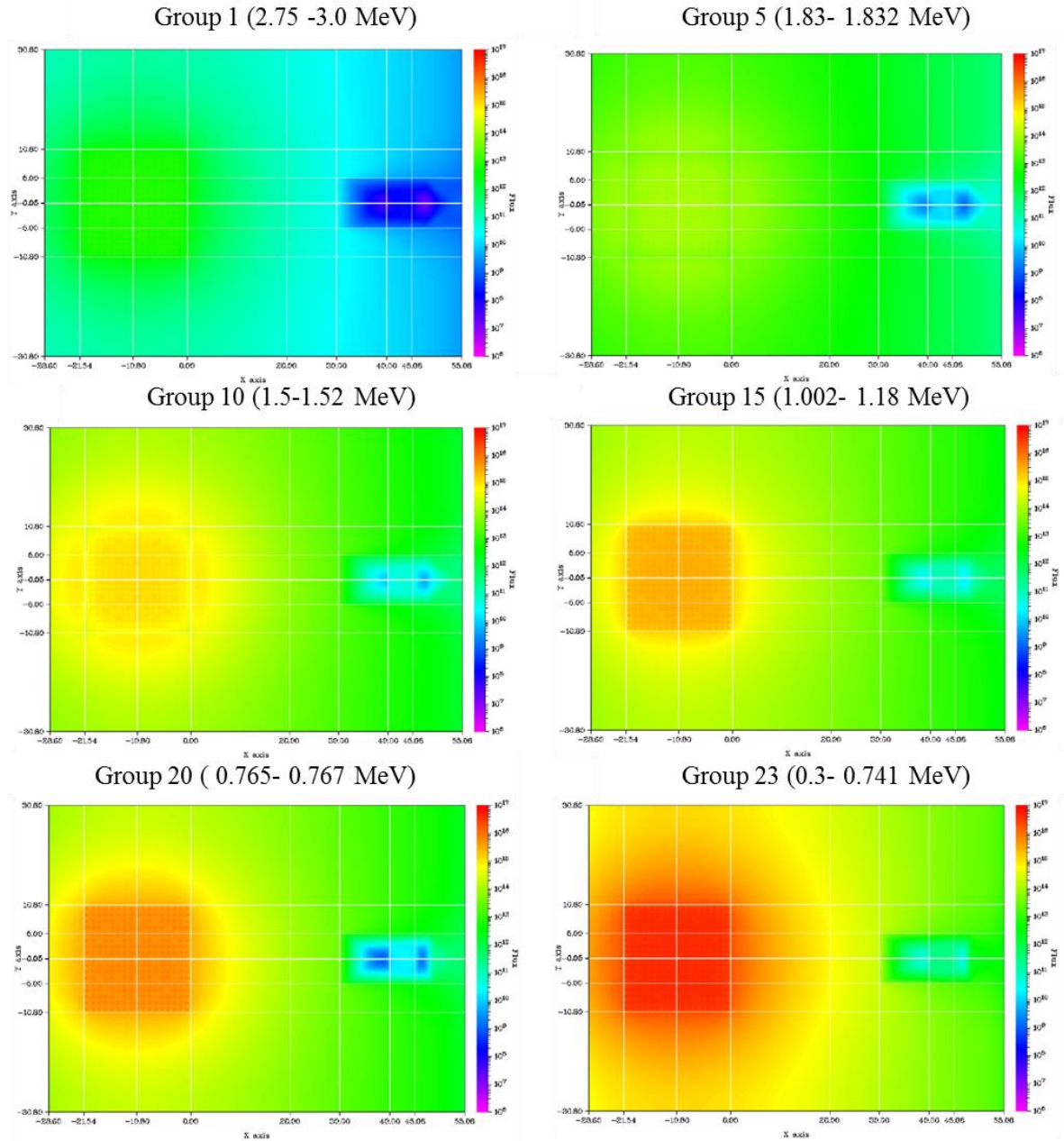


**Figure 5.6:**  $S_{90}$  forward importances mapped for 6 out of 24 adjoint energy groups.

Scaling is equal across all groups.

My models also do not show observable ray effects indicating my angular quadrature and fine mesh structure was well suited for the deterministic transport calculations. The ray effect phenomenon refers to unphysical oscillations in the solution [1]. The small ratio of the scattering cross section to the total cross section, and small dimensions of the model make it possible that a particle will pass through boundaries without scattering. This inaccurately peaks the distribution. Photon transport suffers most from this phenomenon since these particles are highly anisotropic and do not have many significant scattering interactions with materials such as air. These effects can be mitigated by increasing the quadrature and decreasing the mesh size. However, determining the proper quadrature and corresponding mesh structure is not a straight forward task, since increasing quadrature and meshes can significantly increase necessary computational resources, but it becomes more intuitive the more one becomes familiar with modeling. For my models, I needed at least an  $S_{90}$  quadrature to achieve good results. This quadrature represents a total of 8,280 directions per mesh or 1,035 directions per octant. My forward and adjoint models had 85,165 fine meshes and ran on 112 processors each with a maximum memory of 4,096 Mb for approximately 2 days.

Additionally, the models can be determined to show good convergence if both the detector responses for the adjoint and forwards cases match. I computed the detector response from both the adjoint case and forward case to determine if my models showed good convergence. The adjoint detector response was calculated from the importances located in the fuel from Equation 5.12. Rather than a coarse mesh basis, the volumes were computed per fine mesh, along with the corresponding importances. The total adjoint detector response was calculated to be  $1.56 \times 10^{11}$  counts per second. In a similar manner, the forward detector response was computed from Equation 5.11 using a fine mesh basis. The forward detector response was determined to be  $1.78 \times 10^{11}$  counts per second. Comparing the detector response between the forward and adjoint cases, I found

that the relative difference was 13.2%. This corresponds to reasonable model convergence, considering the nature of photon transport.

#### **5.4. SmartID with Adjoint Coupling**

As noted earlier in this chapter, the adjoint importances for a PWR assembly in water will be coupled to the detector response for radionuclide characterization efforts in SmartID. Individual gamma energy peaks and the corresponding number of counts per second for each peak are identified by the SmartID algorithm. These values are essentially the forward detector response for a given gamma energy; therefore, since the adjoint equation is linear, I can use superposition to match the adjoint importances at an identified gamma energy to solve for the source strength of the corresponding radionuclide.

##### **5.4.1. Individual Pin Adjoint Importances**

Before I can examine a real or simulated spectrum of a fuel assembly, I must determine how best to utilize the adjoint importances computed. The adjoint importance information can be extracted from the PENTRAN outputs either by a coarse mesh or fine mesh basis. Due to the nature of how the importance significantly decreases moving further away from the detector and into the fuel, the fine mesh data is the most beneficial value to operate with. From this data, I created a program to read in the fine mesh information and extract the data from only the fuel pins in order to compute the average adjoint importance per pin. Figure 5.8 shows how I labeled each pin with respect to row and location within the row. For example the pin located at the far right of the front row facing the detector is labeled (1,1) for row 1, pin position 1. Each individual pin's adjoint importance was determined by the following logic



$$\varphi_{pin(i,j)}^+ = \frac{\sum_{k=1}^{FM} \varphi_k^+ V_k}{\sum_k^{FM} V_k} \quad (5.15)$$

where  $\varphi_{pin(i,j)}^+$  is the adjoint importance for an individual pin at location (i, j),  $\varphi_k^+$  is the adjoint importance computed by PENTRAN for a fine mesh location within the pin of interest, and  $V_k$  is the volume of the fine mesh within the pin of interest.

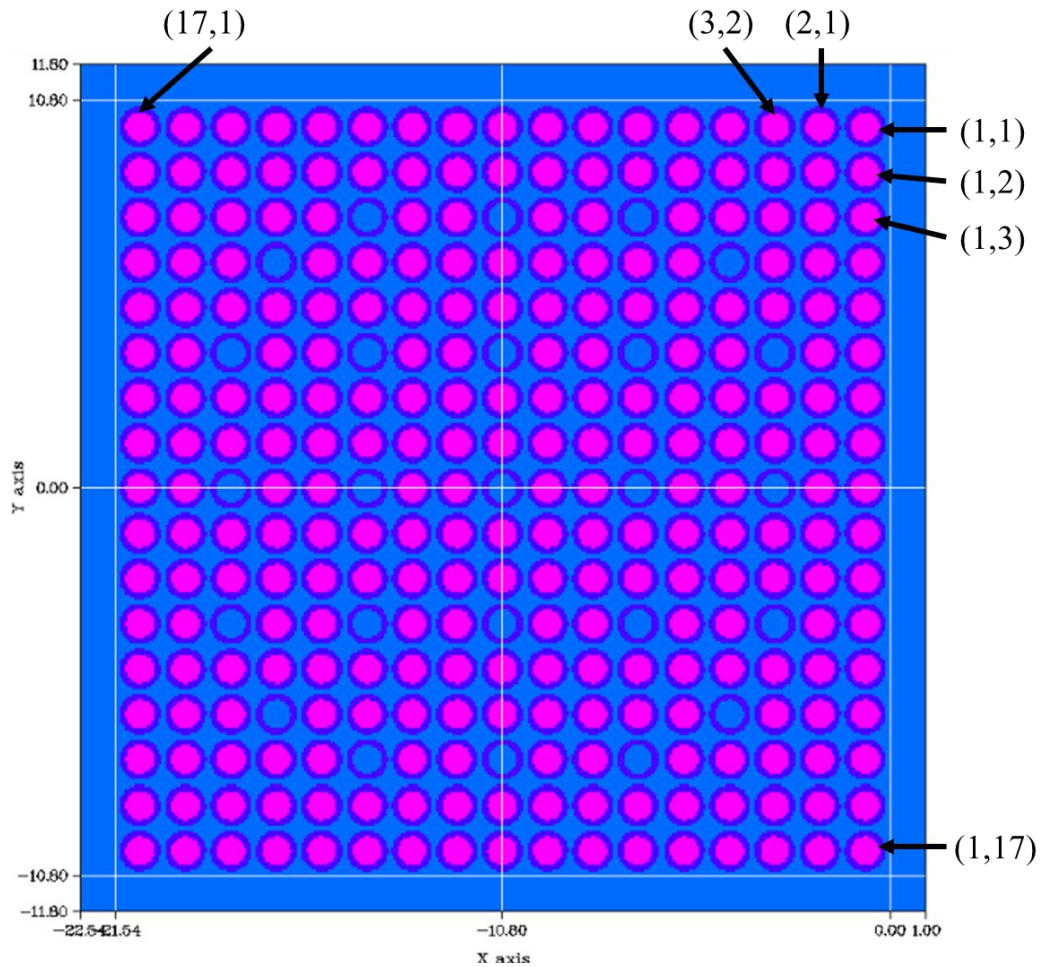


**Figure 5.8:** Fuel assembly pin numbering system. The front face of the detector will be located to the right of the fuel assembly such that the first row is the row of pins closest to the detector.

The adjoint importances drop off significantly moving further away from the detector. Figure 5.9 shows how the importances change with distance along the front face of the fuel assembly, and it also shows how the adjoint falls as you move row by row away from the detector. The x-axis values represent the pin position across the side of the assembly facing the detector, while each linked group represents importances from a different row. The lines linking each marker do not represent adjoint importances; they are only in place to see individual rows of pins more clearly. The locations of discontinuity represent a control rod location. It is also important to note that this figure shows the importances for forward energy group 23, which spans energies 0.3 to 0.741 MeV.

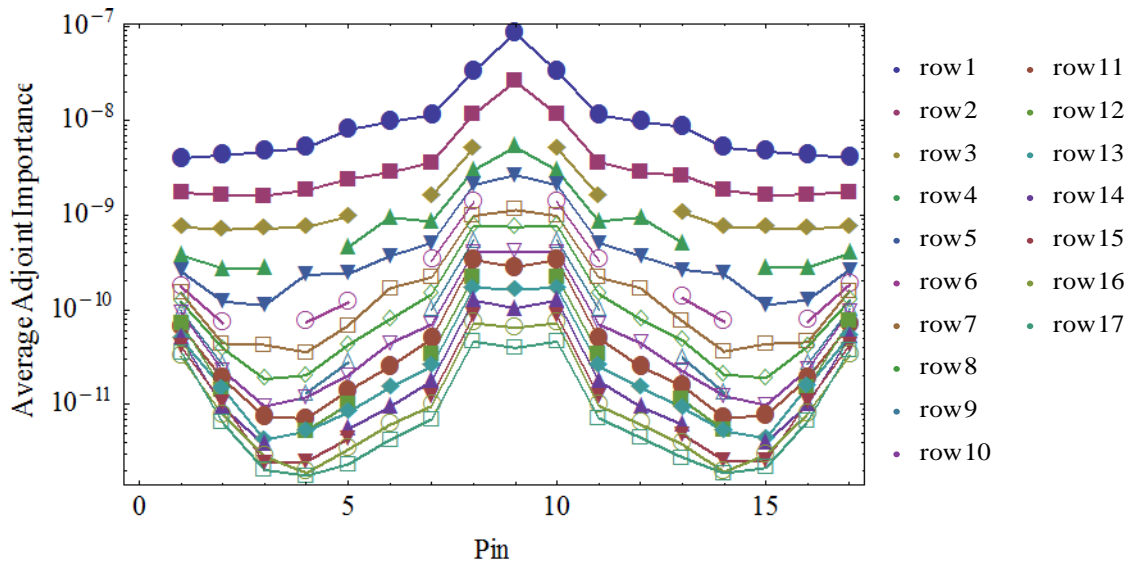


**Figure 5.9:** Adjoint importance values across the fuel assembly for forward energy group 23 (0.3 – 0.741MeV).

In order to achieve the best estimate for the true number of gammas emitted from each fuel pin, I only considered the most important pins - those with the greatest adjoint importances. I identified how many pins would be necessary to achieve 90%, 95%, and 99% of the count rate seen in the detector. Table 5.2 shows some of the nuclides and

their corresponding gamma lines, along with the adjoint importances seen in the energy groups for the fuel assembly.

**Table 5.2:** Key radionuclide gamma emissions organized by energy group for adjoint importance evaluation.

Grp	Upper E bound (MeV)	Key Nuclide gamma energy (MeV)	Photons/s for nuclide after 1d decay	Threshold importance	%	#of pin	Rows	Avg photon/s/keV per pin	Max photons/s/keV per pin
1	0.3			1e-34		1	1	5.72e9	1.51e11
2	0.741	La40: 0.48702 Rh106: 0.512 Sb124: 0.6027 Cs134: 0.605 Rh106: 0.622 Pu240: 0.652 Cs137: 0.662	1.24e10 3.76e9 3.32e8 4.45e9 2.42e9 1.17e5 2.71e9	1.61e-9 7.22e-10 1.01e-10	90% 95% 99%	43 64 123	4 8 14	7.86e8	4.82e10
3	0.743			5.42e-9 2.81e-9 6.35e-10	90% 95% 99%	69 101 173		9.07e5	1.8e6
4	0.765	Zr95: 0.75673 Nb95: 0.7658	2.5e10 4.51e10	9.81e-9 4.52e-9 1.08e-9	90% 95% 99%	72 105 176		2.14e9	2.5e10
5	0.767	Pu238: 0.766	4.36e4	1.37e-8 6.79e-9 1.67e-9	90% 95% 99%	77 109 179		4.36e4	4.36e4
6	0.954	Cs134: 0.796 La40: 0.81578 Tc96: 0.84986 La40: 0.95099	3.90e9 1.25e10 1.08e7 1.40e8	2.37e-8 1.16e-8 3.42e-9	90% 95% 99%	90 125 193		3.89e8	2.79e10
7	0.956			4.20e-8 2.23e-8 6.90e-9	90% 95% 99%	99 135 202		3.24e9	6.48e9
8	0.999			5.83e-8 3.19e-8 9.64e-9	90% 95% 99%	101 137 204		6.96e7	2.39e9
9	1.002			7.23e-8 3.96e-8 1.33e-8	90% 95% 99%	104 140 205		7.14e7	1.09e8
10	1.18	Rh106: 1.05 Co60: 1.173	1.15e9 4.01e8	1.02e-7 5.91e-8 1.85e-8	90% 95% 99%	110 146 210		8.13e7	1.99e9
11	1.2			1.57e-7 9.06e-8 2.83e-8	90% 95% 99%	116 152 215		3.74e6	5.13e7

**Table 5.2 Continued**

12	1.24			1.97e-7	90%	118	4.79e7	6.53e8
				1.16e-7	95%	154		
				3.78e-8	99%	217		
13	1.26			2.54e-7	90%	121	3.13e7	5.44e8
				1.51e-7	95%	156		
				4.81e-8	99%	218		
14	1.5	Eu154: 1.275	6.72e7	3.45e-7	90%	125	4.60e7	2.59e9
		Co60: 1.333	1.97e6	2.17e-7	95%	161		
		Cs134: 1.365	1.37e8	7.30e-8	99%	222		
15	1.52			4.93e-7	90%	130	7.24e6	5.14e7
				2.83e-7	95%	166		
				1.1e-7	99%	226		
16	1.736	La40: 1.5962	5.13e10	6.2e-7	90%	134	2.43e8	5.13e10
		Sb124: 1.69097	6.05e6	3.96e-7	95%	170		
				1.57e-7	99%	228		
17	1.74			8.51e-7	90%	137	6.76e6	2.69e7
				5.19e-7	95%	173		
				2.16e-7	99%	230		
18	1.76			1.01e-6	90%	138	1.61e7	2.05e8
				6.20e-7	95%	173		
				2.53e-7	99%	231		
19	1.83			1.20e-6	90%	139	6.67e6	3.68e8
				7.25e-7	95%	175		
				2.99e-7	99%	231		
20	1.832			1.34e-6	90%	140	1.40e7	2.79e7
				8.4e-7	95%	175		
				3.43e-7	99%	232		
21	2.21	Pr144: 2.186	2.86e8	1.72e-6	90%	143	9.56e6	4.55e8
				1.05e-6	95%	179		
				4.62e-6	99%	234		
22	2.25			2.24e-6	90%	146	1.71e6	4.37e7
				1.34e-6	95%	182		
				5.79e-7	99%	236		
23	2.749	La140: 2.5213	1.86e9	2.86e-6	90%	149	5.44e6	1.86e9
				1.77e-6	95%	185		
				7.85e-7	99%	238		
24	3.0			4.09e-6	90%	153	1.65e5	3.59e7
				2.47e-6	95%	189		
				1.17e-6	99%	240		

Recalling that the adjoint importances relate the counts seen in the detector to the source strength, I determined how the count rate seen in the detector is attributed to each pin. I determined that for adjoint energy group 2 (0.3 MeV to 0.741 MeV), the front

center pin (1,9) contributes 21.29% of the count rate in the detector for a gamma energy of 662 keV. The per pin contribution to the detector response drops off significantly moving away from the front center pin.

For forward energy group 16, 0.999 MeV to 1.002 MeV, the importances peak at the central fuel pins, but moving further back in the rows, the importances increase towards the outer pins. This is due to the effects of distance and self-shielding. It is of interest that as the gamma energies increase, the adjoint importances seem to flatten across the pin rows. This results in each pin having less of an individual direct effect on the detector response and more of equal effect as its neighboring pins causing an increase in the total number of pins to account for approximately 90% or so of the detector count rate. Figures 5.10, 5.11 and 5.12 show the adjoint importances per pin for adjoint energy groups 6, 14, and 23. These groups were selected due to key isotope emissions falling within these groups as shown in Table 5.2. Appendix E shows the adjoint importance per pin mapping for all 24 energy groups.

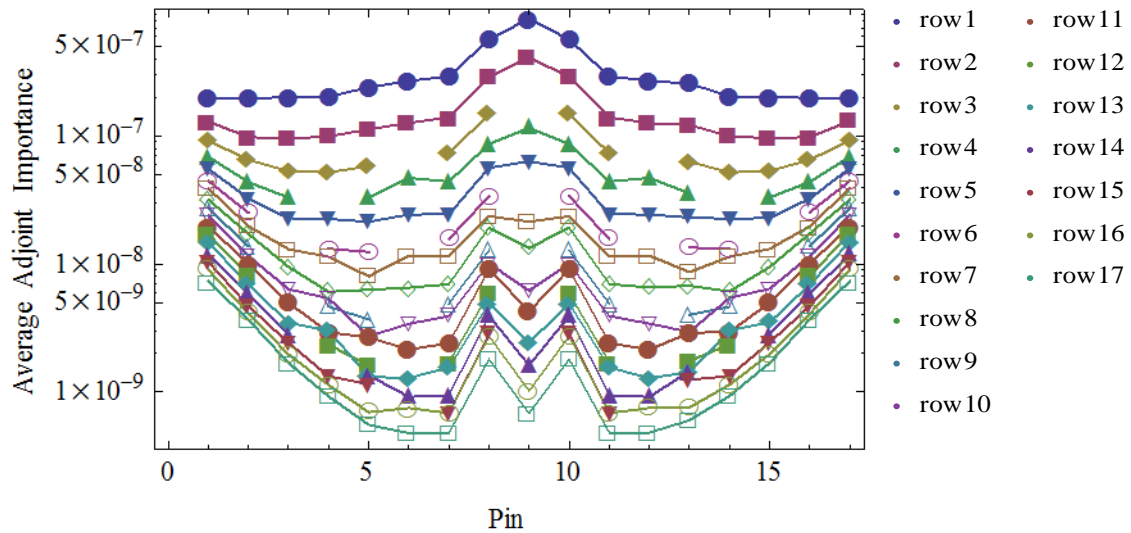


**Figure 5.10:** Adjoint group 6 (0.767- 0.954 MeV) adjoint importances per fuel pin in a Westinghouse 17x17 PWR fuel assembly.

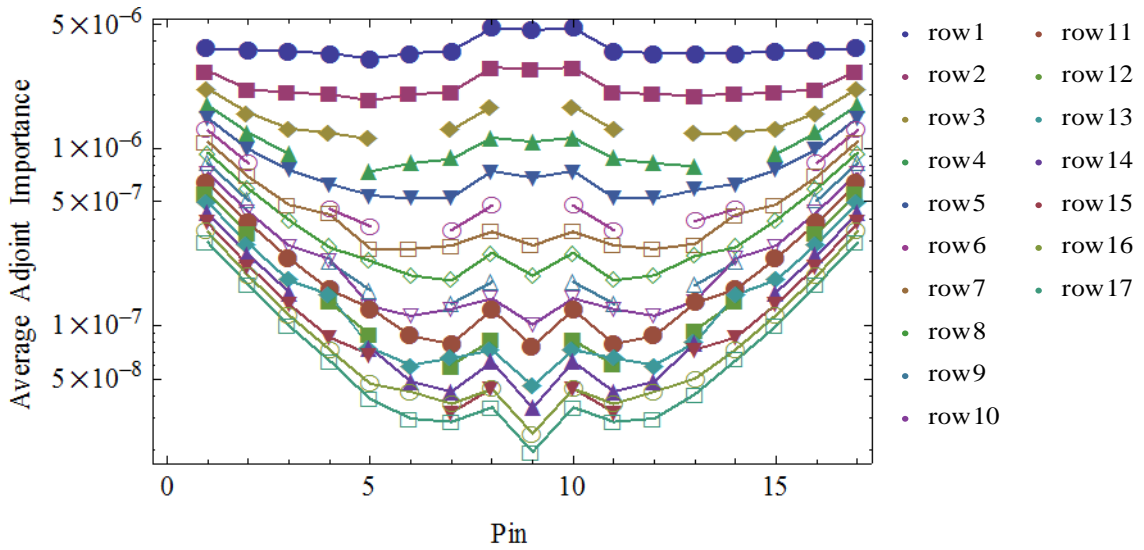


**Figure 5.11:** Adjoint group 14 (1.26- 1.5 MeV) adjoint importances per fuel pin in a Westinghouse 17x17 PWR fuel assembly.

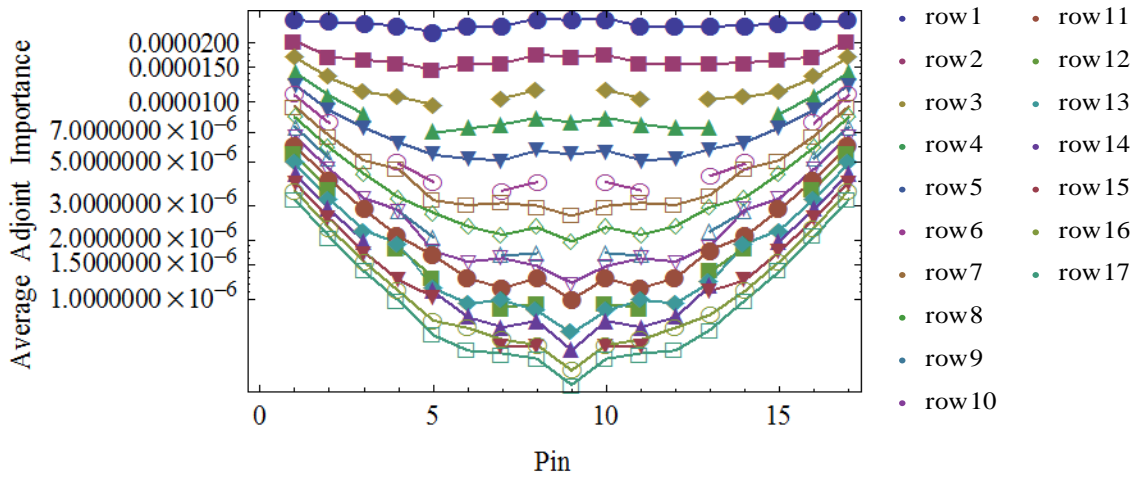


**Figure 5.12:** Adjoint group 23 (2.25- 2.75 MeV) adjoint importances per fuel pin in a Westinghouse 17x17 PWR fuel assembly.

Noting that the importance of a pin can change dramatically moving through the assembly, I inferred that the majority of the counts seen in the detector originated from only a few or a fraction of the pins in the assembly. I chose to set a threshold value for

importance that would only consider the fuel pins that contribute to 90%, 95%, and 99% of the counts seen in the detector. I then averaged the importance across these pins in order to estimate an adjoint group importance relating the detector to the entire fuel assembly. I plotted these averages at the central energy value for each energy group, and saw that there was a strong relationship between importance and energy. I then applied adjoint importances to determine an empirical correlation for each case in order to best predict the importance of every possible gamma energy, and plotted these correlations along with the averaged importances in Figure 5.13. I noticed that for each fuel pin contribution case, there is a noticeable change in the relationship between energy and importance that occurs approximately between 1 MeV and 1.1 MeV. This is due to the different physical effects taking place at this energy range. As described in Chapter 2, incident gamma energies 1.02 MeV and greater can undergo pair production resulting in additional gamma energy peaks, including a peak at 0.511 MeV due to annihilation, a single escape peak, and a double escape peak.

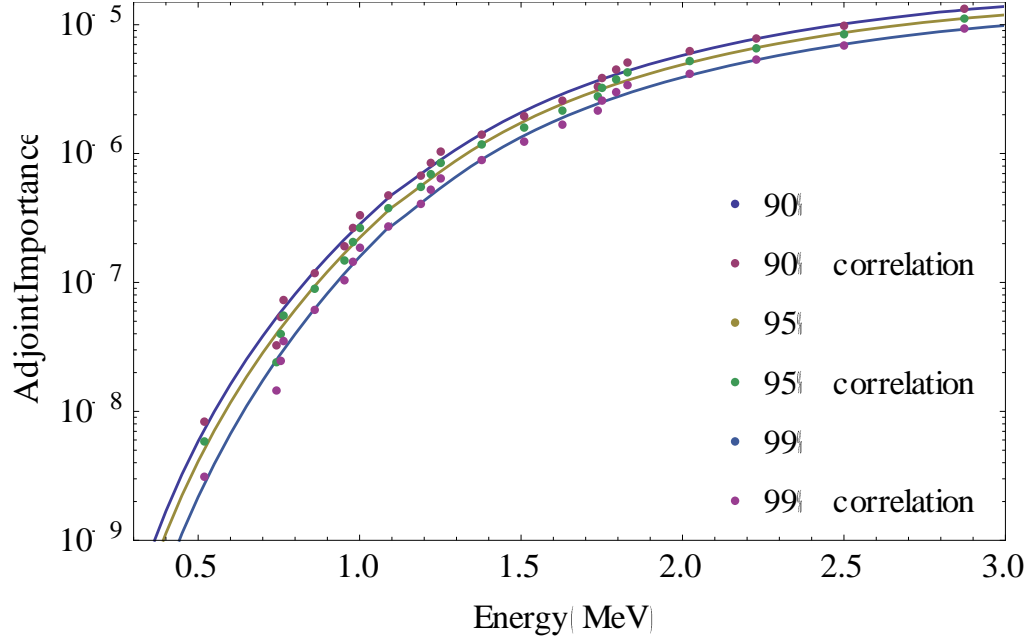


**Figure 5.13:** Average adjoint importances plotted at the center of each energy group for 90%, 95%, and 99% of the total counts in the detector. The best fit correlation is also shown for each case.

The adjoint importance predicted for the number of pins contributing to 90% of the counts seen in the detector is given by

$$Importance = \begin{cases} 2.8228 \times 10^{-7} E^{5.91}, & E < 1.095 \\ 8.1077 \times 10^{-6} - 1.7859 \times 10^{-5} E + \\ 1.1867 \times 10^{-5} E^2 - 1.7594 \times 10^{-6} E^3, & E \geq 1.095 \end{cases} \quad (5.16)$$

where  $E$  is the gamma energy in MeV. This correlation has an  $r^2$  value of 0.982 for  $E < 1.095$  MeV, and an  $r^2$  value of 0.995 for  $E \geq 1.0951$  MeV.

The correlation for 95% of the counts in the detector is given by



$$Importance = \begin{cases} 2.2194 \times 10^{-7} E^{5.76}, & E < 1.095 \\ 6.9956 \times 10^{-6} - 1.5362 \times 10^{-5} E + \\ 1.0141 \times 10^{-5} E^2 - 1.4919 \times 10^{-6} E^3, & E \geq 1.095 \end{cases} \quad (5.17)$$

where  $r^2$  has a value of 0.979 for  $E < 1.095$  MeV, and 0.995 for  $E \geq 1.0951$  MeV.

Lastly, the correlation for 99% of the counts in the detector is given by

$$Importance = \begin{cases} 1.5792 \times 10^{-7} E^{6.186}, & E < 1.095 \\ 5.6992 \times 10^{-6} - 1.2407 \times 10^{-5} E + \\ 8.0693 \times 10^{-6} E^2 - 1.1569 \times 10^{-6} E^3, & E \geq 1.095 \end{cases} \quad (5.18)$$

where  $r^2$  has a value of 0.970 for  $E < 1.095$  MeV, and 0.996 for  $E \geq 1.0951$  MeV.

I also found it necessary to plot the number of pins represented by 90%, 95%, and 99% of the counts. Figure 5.14 shows this relationship.

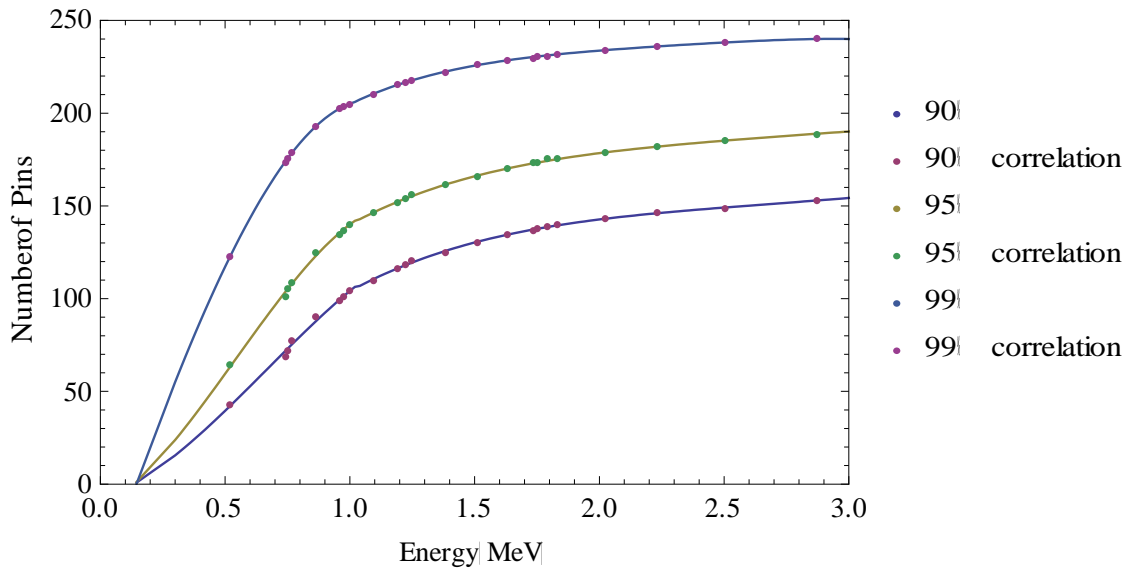


**Figure 5.14:** Number of pins plotted at the center of each energy group for 90%, 95%, and 99% of the total counts in the detector. The best fit correlation is also shown for each case.

Again, the correlation for each case changes at approximately 1.02 MeV. These correlations will be utilized along with the information gathered by SmartID to best predict where the counts in the detector are originating from and how this relates to the entire fuel assembly. Each correlation for predicting the number of pins is very well fit with  $r^2$  values all greater than 0.9975.

The number of pins predicted to account for 90% of the counts seen in the detector is given by

$$Pins = \begin{cases} -8.1792 + 44.0168E + 137.2431E^2 - 68.9146E^3, & E < 1.095 \\ -35.9819 + 227.5443E - 109.9411E^2 + \\ \quad 24.4343E^3 - 2.0076E^4, & E \geq 1.095 \end{cases} \quad (5.19)$$

where  $E$  is the gamma energy in MeV. This correlation has an  $r^2$  value of 0.9975 for  $E < 1.095$  MeV, and an  $r^2$  value of 0.9987 for  $E \geq 1.0951$  MeV. The correlation for 95% of the counts in the detector is given by

$$Pins = \begin{cases} -13.1542 + 69.7568E + 218.4472E^2 - 135.025E^3, & E < 1.095 \\ -1.804 + 223.973E - 117.3454E^2 + \\ \quad 27.6828E^3 - 2.4856E^4, & E \geq 1.095 \end{cases} \quad (5.20)$$

where  $r^2$  has a value of 0.999 for  $E < 1.095$  MeV, and 0.9995 for  $E \geq 1.0951$  MeV.

Lastly, the correlation for 99% of the counts in the detector is given by

$$Pins = \begin{cases} -54.7303 + 387.0015E + 45.7433E^2 - 81.4123E^3, & E < 1.095 \\ -51.7545 + 279.9656E - 169.2952E^2 + \\ \quad 47.6161E^3 - 5.1065E^4, & E \geq 1.095 \end{cases} \quad (5.21)$$

where  $r^2$  has a value of 0.9999 for  $E < 1.095$  MeV, and 0.9992 for  $E \geq 1.0951$  MeV.

Remembering that the adjoint importance essentially shows how likely a particle with energy,  $E$ , will interact with the detector, I can apply the adjoint importance to determine the decay activity for an emission for a given nuclide. Activity is defined by,

$$A = \lambda N = qV = \frac{R}{\phi^+}, \quad (5.22)$$

where  $A$  is the activity in units of number of decays per second,  $\lambda$  is the probability of decay for a given nuclide,  $N$  is the number of particles of the given nuclide,  $R$  is the detector response in units of counts per second, and  $\phi^+$  is the adjoint importance. From equations 5.10 and 5.11,  $N$  is solved for and is shown as

$$N = \frac{A}{\lambda} = \frac{qV}{\lambda} = \frac{R}{\lambda\phi^+} \quad (5.23)$$

As previously mentioned, in order to solve for the number of particles for a given nuclide, the detector response must be known. This can be determined from actual detector measurements. The response is essentially the number of counts per second in the detector divided by some intrinsic efficiency relating to the electronics of the system. Therefore, the equation for the number of particles is

$$N = \frac{\text{Counts in det/s}}{\lambda\phi^+ \varepsilon_{electronics}}, \quad (5.24)$$

again noting that  $\varepsilon_{electronics}$  can be ignored in computational modeling. It is important to point out that nuclides often do not produce gamma emissions at the same rate as their rate of decay. In order to account for an individual gamma emissions relationship to the

nuclide's activity, a branching ratio,  $BR$ , is applied. Incorporating this into Equation 5.15 leaves me with an activity calculation based on a single emission at energy as

$$A = \frac{R}{\phi^+ BR} \quad (5.25)$$

This equation shows the basis of how I will determine nuclide activity from the peaks identified by SmartID.

In order to compute an estimate for the amount of a given isotope present in the fuel assembly, I will refer to equation 5.25. For each case (90%, 95%, and 99%), I assume these are accounting for the entire signal seen in the detector. Since the adjoint values are an average across a determined number of pins, I must scale to the entire fuel assembly. This further changes equation 5.25 to

$$A = \frac{R}{\phi_{avg}^+ BR} \left( \frac{264 \text{ pins}}{N_{avg}} \right) \quad (5.26)$$

where  $A$  is the activity of the nuclide associated with the identified photopeak at an energy  $E$ ,  $R$  is the detector response in terms of counts in the detector per second for the identified photopeak,  $BR$  is the branching ratio of the energy emission for the nuclide of interest at energy  $E$ ,  $N_{avg}$  is the number of pins correlated to  $E$  determined from equations 5.18, 5.19, and 5.20, and  $\phi_{avg}^+$  is the average adjoint importance correlated to  $E$  determined by equations 5.15, 5.16, and 5.17.

#### 5.4.2. SmartID procedure

Once I determined the appropriate adjoint efficiencies for mass evaluation, I developed and implemented a new procedure to add onto the SmartID post processing algorithm following the calculation of activity from Equation 5.26. This addition gives

the user the option to estimate the amount of key radionuclides in a PWR assembly which then can lead to an estimate of burnup. For the intentions of this dissertation, no other source configurations will be considered or included. If there was further interest in alternate source geometries, such as a 14 x 14 assembly or 15 x15 assembly, additional computational models can be developed and added as long as the adjoint calculation work described earlier in the chapter is repeated for the new geometry. Therefore, this work could be greatly expanded for various PWR fuel assembly configurations and BWR fuel assemblies along with other unique and complicated sources.

I incorporated all of the relevant information computed and needed in order to calculate an estimate of the source activity by creating a Fortran code to process the SmartID output file and the “.Spe” file for mass estimation. This program pulls the peak and count information from the output file and the time of measurement from the “.Spe” file and uses that information along with the calculated adjoint importances to produce a separate output file for radionuclide mass estimates.

The flow of the program is illustrated by Figure 5.15. The output from the program for the  $^{137}\text{Cs}$  case is shown in Figure 5.16. The source code showing how the calculations were employed is included in Appendix F.

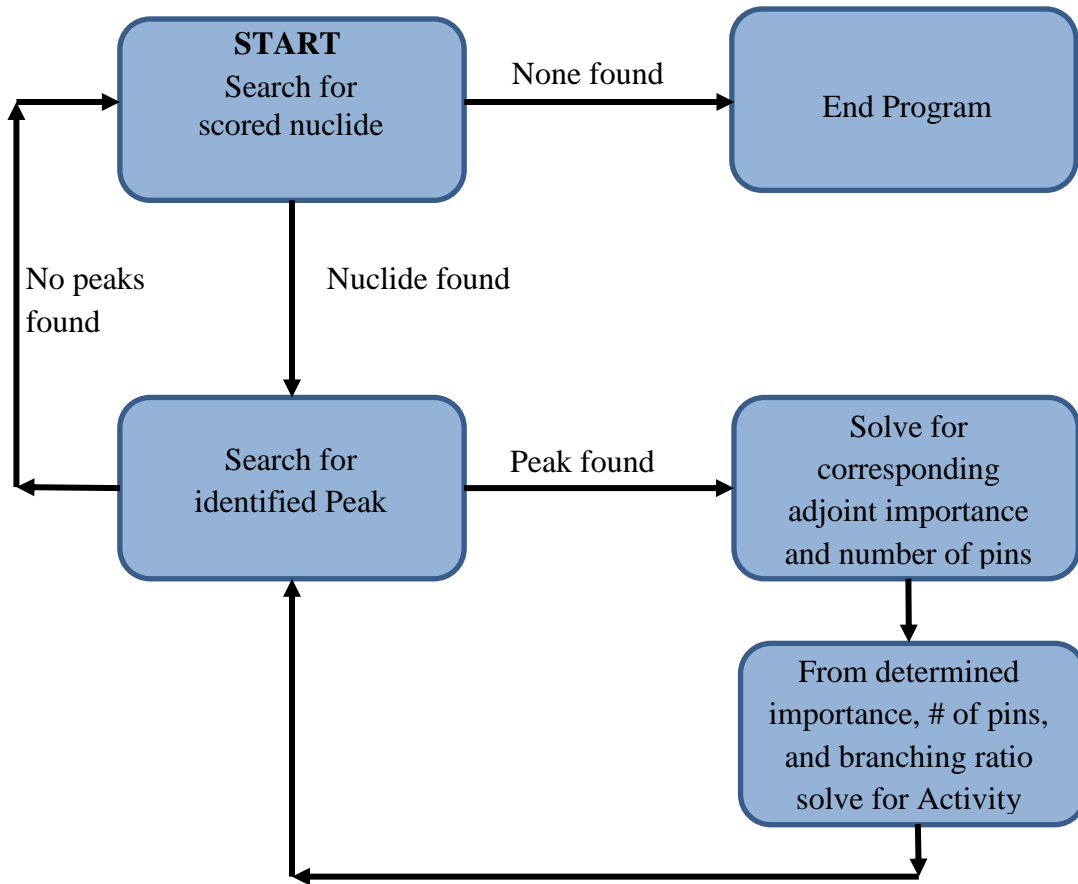


**Figure 5.15:** Paradigm of the activity estimation from identified peaks in SmartID.

#### 5.4.2.1. <sup>137</sup>Cs Example

In order to determine whether or not, my methodology for estimating the source strength from a fuel assembly is acceptable, I created a test problem. I created an MCNP model for a Westinghouse PWR assembly and only included the source for the 662 keV gamma emissions from <sup>137</sup>Cs for an overall modeled activity of  $1.06 \times 10^5$  Ci. Figure 5.16 shows a cross section view of this model. The distances from the detector and fuel assembly are consistent with the PENTRAN models; however, as was done with the MCNP DRF models, the collimation was opened at the average Compton scattering angle

to decrease computational errors. I used an f8 pulse height tally along with the Gaussian Energy Broadening option to simulate a real spectrum minus background.

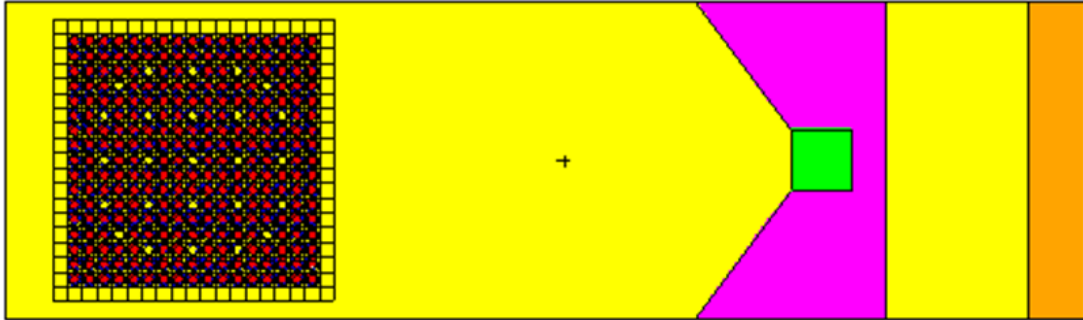


**Figure 5.16:** Cross section of MCNP model for  $^{137}\text{Cs}$  spectrum simulation.

The resulting MCNP spectrum is shown by Figure 5.17. Since the source nuclide is known, and there are no additional nuclides present, the detector response can be determined without running SmartID. The response is the number of counts per second under the 662 keV gamma peak. After gaining this information, it is relatively easy to determine the source strength from the adjoint activity equation 5.21. In this case, only the adjoint importances from forward energy group 23 will be utilized.

This example is complicated when multiple gamma energies or radionuclides are introduced into the source, but the same procedure can be applied. Instead of counting the counts per second under a known peak, SmartID can be utilized to pull out the individual gamma peaks; therefore, the individual detector responses for all gamma energies are known.

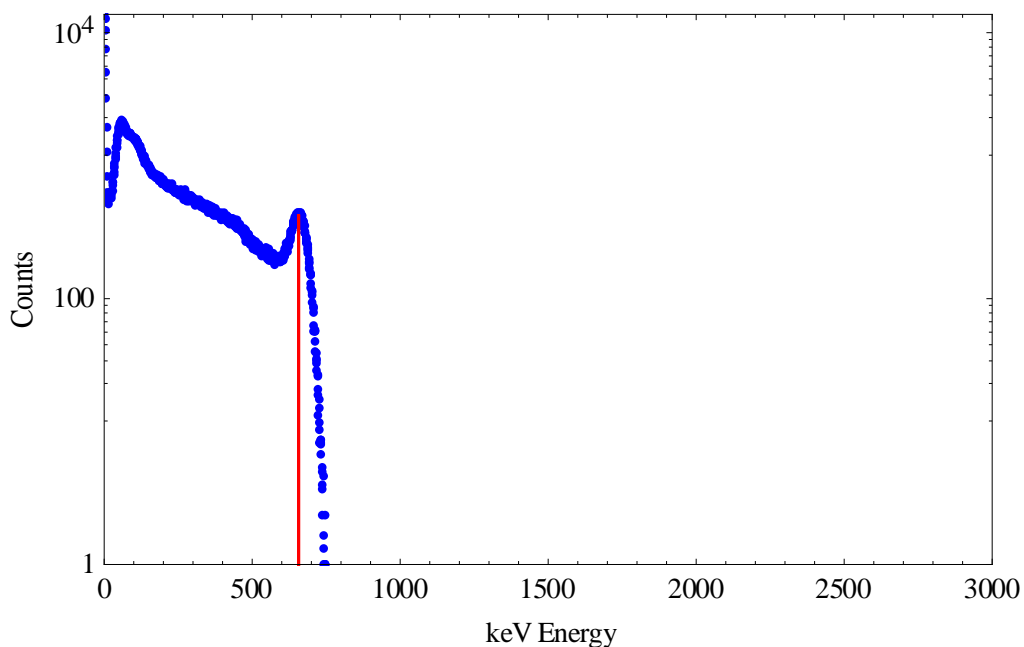


**Figure 5.17:** Identified peaks for MCNP simulated  $^{137}\text{Cs}$  spectrum in water.

Looking at a SmartID output before a mass estimate component was added shows identified peak and the corresponding counts Figure 5.18 shows the top portion of an output from a strong  $^{137}\text{Cs}$  source through water. The gamma peak at 657.00 keV was correctly identified as the 662 keV peak characteristic of  $^{137}\text{Cs}$ . The output file also shows  $4.3004 \times 10^2$  counts are attributed to this energy peak. It is from these counts that adjoint importances will be applied to quantitatively predict the amount of radionuclide identified.  $^{110\text{m}}\text{Ag}$  is also identified as a possible nuclide, but I can easily rule this out as a possibility. The scoring is significantly less and only one out of 15 emissions for  $^{110\text{m}}\text{Ag}$  fits within the window of attribution for the identified peak. I also employed the shielding search option to see if SmartID would correctly identify my shielding case. It identified no shielding as the most probable scenario, which is the correct shielding configuration. The resulting activity computed from this identified emission is listed in Figure 4.19.



```

SmartID-XP
Extended Protocol Synthetic Resolution Identifier
Ver 2.5J
By
G. Sjoden, C. Yi, E. LaVigne, J. Paul
Georgia Institute of Technology
June 2014

Contact: sjoden@gatech.edu
=====
Spectrum Name: ./MCNPtest/Cs137/CsW.Spe

1 Peak(s) Identified - Sort by Energy
=====
keV          Counts      Norm% Cts   Peak Id
657.00       4.3004E+02  100.00000   1

Most Probable Shielding Settings:
=====
Shielding material  shielding size(cm)  score
Fe                 0.000              226.3
Pb                 0.000              226.3

Score Correlation Threshold:
=====
High correlation:  score > 108.0
Moderate correlation:  score in between: [ 99.0, 108.0]
Low correlation:  score < 99.0 with a cutoff at 50.0

Overall Mean Nuclide Scores (total_scored=2):
[based on integral average of score from each nuclide for all shielding options]
=====
Nuclide      Score      Comment      Correlation
137Cs       137.33     Fiss_Prod    High
110mAg      88.98      Fiss_Prod    Low

Score Details for Shielding Options:
=====
Possible Shielding Setting: 1 Total Score: 226.31
Shielding Material: Fe      Thickness (cm): 0.00

Note:
base score : fuction of (#matched/#emissions), weighted by yield,detectability and matching
bonus I    : bonus from number of matched peaks
bonus II   : bonus from relative peak height
bonus III  : bonus from alignment between peakheights and emission yields

Score Summary:
=====
Nuclide      Total      (base + bonus I, II, III)      Comment      Correlation
137Cs       137.33     ( 98.2  0.0 39.2  0.0 )      Fiss_Prod    High
110mAg      88.98      ( 49.1  0.0 39.9  0.0 )      Fiss_Prod    Low

Scored nuclides details:
=====
Nuclide      Score      T1/2      T1/2_unit  #EmissionInRange  #Matched  Correlation
137Cs       137.33     3.0200E+01  y           1                1          High

Emission(KeV)  Prob/DK      Detectability      1.00% Energy Window      Peak(KeV)      Norm%_cts
+ 661.60       8.5100E-01  8.6937E-02      ( 654.98 to 668.22 )      657.00         100.0000

```

Figure 5.18: SmartID output for a <sup>137</sup>Cs spectrum in water.

```

Files read: CsW.out
% for number of pins contributing to signal: 99
Nuclide      Emission(MeV)  half life (s)      Activity (Ci)
137Cs        0.6616000     9.5303949E+08     6.8177981E+05
110mAg       0.6577500     2.1585398E+07     7.1177006E+05

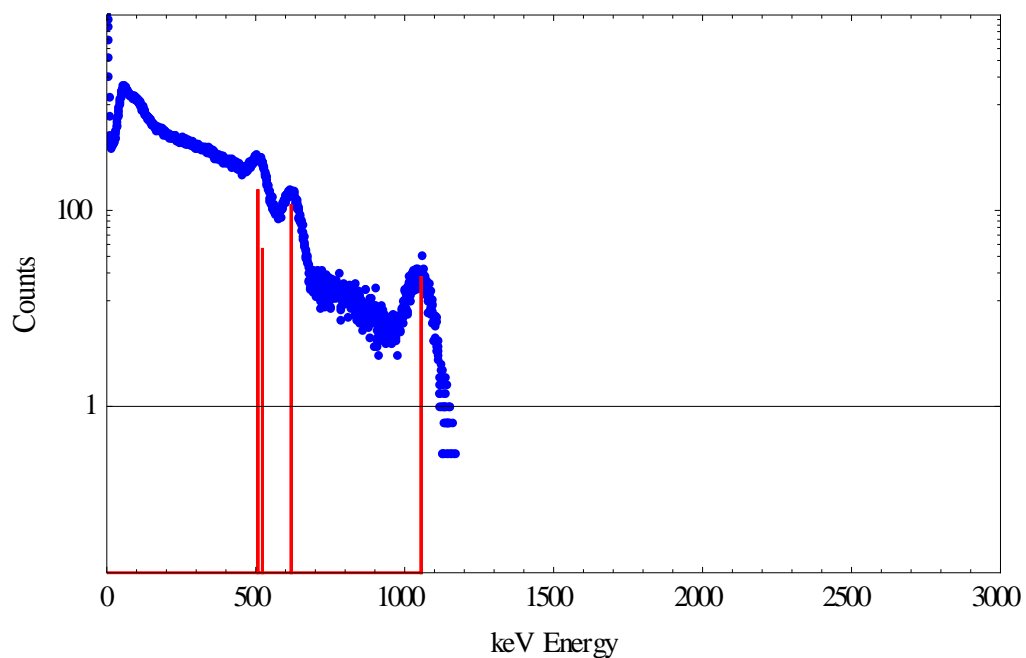
```

Figure 5.19: Estimated activities for SmartID scored nuclides from a <sup>137</sup>Cs spectrum in water.

The resulting activity calculation shows a larger activity than what was implemented in the MCNP model and “.Spe” spectrum file. As I previously mentioned, the modeled activity for the assembly was  $1.06 \times 10^5$  Ci. This is due to the increased detector field of view needed in order to minimize errors in the MCNP modeling. For a more highly collimated scenario, the “.Spe” file will show an overall decrease in count rate, which would result in a decrease in the computed activity. Even with this slight geometry modification, I can determine that I am achieving a significant result. The highly collimated models essentially showed that for a low energy emission, the front center pin would be the most dominant source seen by the detector. Since this is a low energy emission, I still would not expect to see very far into the assembly, but I would expect to have an increased count rate from the front row of pins. Referring back to Figure 5.15, the detector face is open and shows about 3-5 pins directly facing the detector. The percent difference between the modeled activity ( $1.06 \times 10^5$  Ci) and the calculated activity ( $6.82 \times 10^5$  Ci) is 146%, and the percent difference between the 1mm pinhole collimation and front face of the detector is 199%. This further shows that the greatest contributing factor to this activity calculation for the low energy emission is due to a much increased view of the assembly. To further test this, I applied the same methodology to a model with multiple emissions, including a strong emission from  $^{106}\text{Rh}$  at 1050 keV.

#### 5.4.2.2. $^{106}\text{Rh}$ Example

SmartID was successful in identifying peaks for  $^{106}\text{Rh}$  as shown by Figure 5.20. The counts and counting times were scaled accordingly to the emission rate and number of particle histories conducted for the “.Spe” file needed by SmartID to account for a total modeled assembly activity of  $6.121 \times 10^5$  Ci.



**Figure 5.20.** Identified peaks for MCNP simulated  $^{106}\text{Rh}$  spectrum in water.

Figure 5.21 shows the counts associated with the peaks SmartID identified, and accurately determined that this model most likely did not include shielding. Since this was a simulated spectrum, I was able to score nuclides within a tight 1% energy window. The scoring shows  $^{106}\text{Rh}$  and  $^{106}\text{Ru}$  as the most likely nuclides present.

```

=====
SmartID-XP
Extended Protocol Synthetic Resolution Identifier
Ver 2.5J
By
G. Sjoden, C. Yi, E. LaVigne, J. Paul
Georgia Institute of Technology
June 2014

Contact: sjoden@gatech.edu
=====

Spectrum Name: ./MCNPtest/Rh106/RhW.Spe

4 Peak(s) Identified - Sort by Energy
=====
keV          Counts          Norm% Cts    Peak Id
507.00       1.6430E+02      47.99224    3
522.00       4.1492E+01      12.11987    4
619.00       1.1522E+02      33.65591    2
1055.00      2.1335E+01      6.23198     1

Most Probable Shielding Settings:
=====
Shielding material  shielding size(cm)  score
Fe                 0.000              451.1
Pb                 0.000              451.1
Fe                 0.100              450.5
Pb                 0.100              448.3

Score Correlation Threshold:
=====
High correlation:  score > 108.0
Moderate correlation:  score in between: [ 99.0, 108.0]
Low correlation:  score < 99.0 with a cutoff at 50.0

Overall Mean Nuclide Scores (total_scored=4):
[based on integral average of score from each nuclide for all shielding options]
=====
Nuclide          Score          Comment          Correlation
106Rh            139.72         Fiss_Prod        High
106Ru            135.20         Fiss_Prod        High
22Na             110.48         Cosmic_spall_pro High
56Co             64.86          c                Low

```

**Figure 5.21:** Peaks identified by SmartID for the  $^{106}\text{Ru}$  test case.

Although I set out to model emissions from  $^{106}\text{Rh}$ ,  $^{106}\text{Ru}$  is identified with about equal probability. This is not a mistake in the code, or error by SmartID's nuclide attribution.  $^{106}\text{Ru}$  decays by beta emissions to  $^{106}\text{Rh}$ .  $^{106}\text{Ru}$  actually does not emit gamma emissions, rather  $^{106}\text{Rh}$  emits gammas. These two nuclides are said to be in secular equilibrium, meaning that the daughter product's half-life is much smaller than the parent's. Therefore, a sign of  $^{106}\text{Rh}$  can be directly attributed to  $^{106}\text{Ru}$ . Figure 5.22 shows the emissions identified and attributed to these nuclides. It is shown that the

SmartID library includes some key gamma emissions from  $^{106}\text{Rh}$  as identifying emissions for  $^{106}\text{Ru}$ .

Scored nuclides details:							
Nuclide	Score	T1/2	T1/2_unit	#EmissionInRange	#Matched	Correlation	
$^{106}\text{Rh}$	139.72	1.0000E+00	y	3	3	High	
Emission(KeV)	Prob/DK	Detectability	1.00% Energy Window		Peak(KeV)	Norm%_cts	
+ 512.00	2.0600E-01	1.4101E-01	( 506.88 to 517.12 )		507.00	47.9922	
+ 621.84	9.8100E-02	9.6932E-02	( 615.62 to 628.06 )		619.00	33.6559	
+ 1050.50	1.7300E-02	3.6272E-02	( 1040.00 to 1061.01 )		1055.00	6.2320	
Nuclide	Score	T1/2	T1/2_unit	#EmissionInRange	#Matched	Correlation	
$^{106}\text{Ru}$	135.20	1.0000E+00	y	2	2	High	
Emission(KeV)	Prob/DK	Detectability	1.00% Energy Window		Peak(KeV)	Norm%_cts	
+ 622.20	9.9500E-02	9.6837E-02	( 615.98 to 628.42 )		619.00	33.6559	
+ 1050.50	1.5600E-02	3.6272E-02	( 1040.00 to 1061.01 )		1055.00	6.2320	

**Figure 5.22:** Details of the  $^{106}\text{Ru}$  test case emissions identified.

Once I had the output file from SmartID, I was able to run the results through my new code for activity calculation. Figure 5.23 highlights the calculated activity for identified  $^{106}\text{Ru}$  emissions. I know from my peak analysis that this is in fact the nuclide that can be attributed to the identified emission, and this is the activity I can refer to.

Files read: RhW.out			
% for number of pins contributing to signal: 95			
Nuclide	Emission(MeV)	half life (s)	Activity (Ci)
$^{106}\text{Rh}$	0.5120000	3.1557600E+07	1.7610263E+06
$^{106}\text{Rh}$	0.6218401	3.1557600E+07	2.8886931E+05
$^{106}\text{Rh}$	1.0505000	3.1557600E+07	1.2255724E+03
$^{106}\text{Ru}$	0.6222000	3.1557600E+07	2.8763253E+05
$^{106}\text{Ru}$	1.0505000	3.1557600E+07	1.2255724E+03
$^{22}\text{Na}$	0.5110000	8.8361280E+07	1.7871603E+06
$^{56}\text{Co}$	0.5110000	6.6902110E+06	1.7871603E+06

**Figure 5.23:** Activity estimate for  $^{106}\text{Ru}$  test case by employing the adjoint methodology discussed in this chapter.

I averaged the computed activities across all identified emissions to determine an overall activity attributed to this nuclide. The resulting activity is  $6.84 \times 10^5$  Ci.

Knowing that for 33 GWD/MTU burned fuel I should see an activity of  $6.121 \times 10^5$  Ci, I see that my results come much closer than for the  $^{137}\text{Cs}$  case. This is due to the addition of emissions with increased energy from the  $^{137}\text{Cs}$  case. These emissions are more penetrating so an increase in the field of view does not have as great of an effect as it did for the lower energy emission case. The computed activity is only 11% different from the modeled activity. This is also within the error I calculated (13.2%) and showed for the detector response between the adjoint and forward transport models in Chapter 5.3.

#### 5.4.2.3. $^{134}\text{Cs}$ Example

The last fission product that relates well to burnup I modeled was  $^{134}\text{Cs}$ . Figure 5.24 shows the resulting spectrum simulated from MCNP and the peaks identified by SmartID.

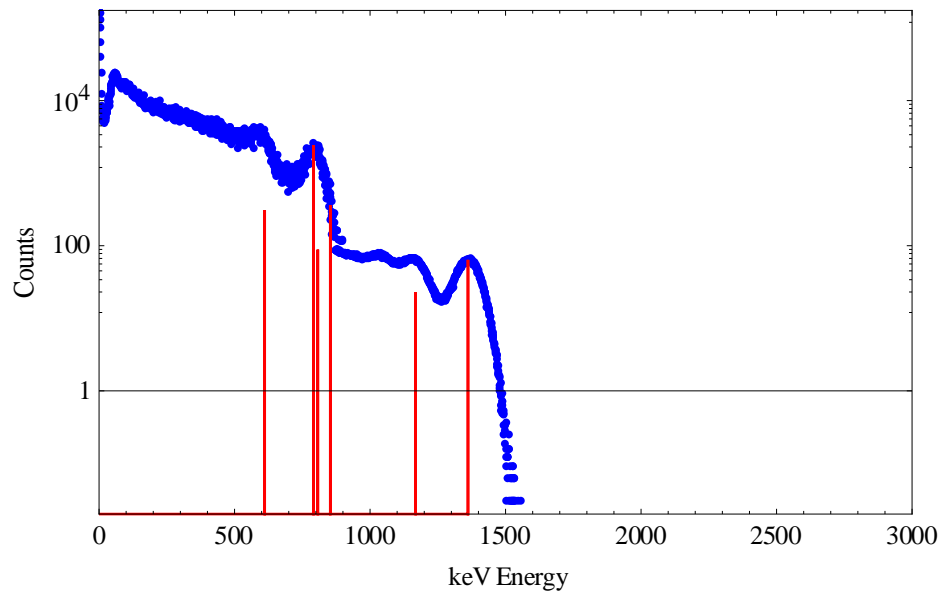


**Figure 5.24.** Identified peaks for MCNP simulated  $^{134}\text{Cs}$  spectrum in water.

As was the case with the  $^{137}\text{Cs}$  and  $^{106}\text{Rh}$  examples, employing the shielding search option correctly showed that no additional shielding was introduced into the

models. Figure 5.25 shows the peaks identified and the corresponding scored nuclides.  $^{134}\text{Cs}$  is scored substantially higher than any other nuclide, clearly indicating its presence. The other nuclides scored are determined not to be present due to their lack of many key identifying emissions and double counting of the  $^{134}\text{Cs}$  emissions.

```

=====
SmartID-XP
Extended Protocol Synthetic Resolution Identifier
Ver 2.5J
By
G. Sjoden, C. Yi, E. LaVigne, J. Paul
Georgia Institute of Technology
June 2014

Contact: sjoden@gatech.edu
=====

Spectrum Name: ./MCNPtest/Cs134/Cs134W.Spe

6 Peak(s) Identified - Sort by Energy
=====
keV          Counts          Norm% Cts    Peak Id
-----
611.00      3.9577E+02      11.38386     6
791.00      2.4530E+03      70.55764     3
807.00      9.6364E+01      2.77180     5
853.00      4.4161E+02      12.70239     4
1168.00     2.5975E+01      0.74714     2
1361.00     6.3871E+01      1.83717     1

Most Probable Shielding Settings:
=====
Shielding material  shielding size(cm)  score
-----
Fe                  0.000                650.2
Pb                  0.000                650.2

Score Correlation Threshold:
=====
High correlation:  score > 108.0
Moderate correlation:  score in between: [ 99.0, 108.0]
Low correlation:  score < 99.0 with a cutoff at 50.0

Overall Mean Nuclide Scores (total_scored=7):
[based on integral average of score from each nuclide for all shielding options]
=====
Nuclide      Score      Comment      Correlation
-----
134Cs        138.21     Fiss_Prod    High
56Mn         103.04     c            Moderate
58Co         99.70      c            Moderate
214Bi        94.88      U-238_Daughter  Low
124Sb        91.68      Fiss_Prod    Low
60Co         63.50      c            Low
56Co         59.22      c            Low

```

**Figure 5.25.** Peaks identified by SmartID for the  $^{134}\text{Cs}$  test case.

Upon further inspection of the  $^{134}\text{Cs}$  emissions identified, I discover that all emissions other than the emission with the lowest probability of decay are attributed. The additional peaks identified but not attributed can be explained by the MCNP

simulation errors. When employing the GEB card for an f8 tally, the pulse heights computed on the high energy side of the Gaussian curve increase substantially in error. I've noticed that the pulse heights are usually skewed higher than what is expected from a true Gaussian, therefore, when SmartID subtracts out the computed attributed counts from the peak, many are left behind to the right side of the peak. These remainder counts are falsely identified as an additional peak, and can distort the lower energy counts in the spectrum. This can be mitigated by increasing the FWHM values in the "FWHM.txt" file for SmartID, but even with this correction, poor errors from MCNP have a noticeable effect on peak identification.

Scored nuclides details:						
Nuclide	Score	T1/2	T1/2_unit	#EmissionInRange	#Matched	Correlation
<sup>134</sup> Cs	138.21	2.0600E+00	y	6	5	High
Emission(KeV)	Prob/DK	Detectability	1.50% Energy Window		Peak(KeV)	Norm%_cts
+ 604.70	9.7600E-01	1.0157E-01	( 595.63 to 613.77 )		611.00	11.3839
+ 795.84	8.5400E-01	5.9937E-02	( 783.90 to 807.78 )		791.00	70.5576
+ 801.93	8.7300E-02	5.9015E-02	( 789.90 to 813.96 )		807.00	2.7718
1038.60	1.0000E-02	3.6927E-02	( 1023.02 to 1054.18 )			
+ 1167.90	1.8000E-02	3.0380E-02	( 1150.38 to 1185.42 )		1168.00	0.7471
+ 1365.20	3.0400E-02	2.3395E-02	( 1344.72 to 1385.68 )		1361.00	1.8372

**Figure 5.26.** Details of the <sup>134</sup>Cs test case emissions identified.

Once again, I ran the results from SmartID through my adjoint activity calculator. Figure 5.27 shows the resulting emission activities.



Files read: Cs134W.out			
% for number of pins contributing to signal: 90			
Nuclide	Emission(MeV)	half life (s)	Activity (Ci)
134Cs	0.6047000	6.5008656E+07	2.1593088E+05
134Cs	0.7958401	6.5008656E+07	1.9903355E+05
134Cs	0.8019300	6.5008656E+07	7.4482508E+04
134Cs	1.1679001	6.5008656E+07	8.0362070E+03
134Cs	1.3652000	6.5008656E+07	4.9293325E+03
56Mn	0.8467500	6.6902110E+06	2.0158863E+04
58Co	0.8107600	6.1221745E+06	6.0440996E+03
214Bi	0.6093100	1.1960331E+03	4.3020641E+05
214Bi	0.8061700	1.1960331E+03	5.0888088E+05
214Bi	1.1552000	1.1960331E+03	9.0324922E+03
214Bi	1.1580001	1.1960331E+03	4.3175059E+03
214Bi	1.3777000	1.1960331E+03	3.4788684E+03
124Sb	0.6027101	5.2070045E+06	2.2060895E+05
124Sb	1.3682001	5.2070045E+06	5.9028506E+03
60Co	1.1732301	1.6630854E+08	1.4107423E+02
56Co	0.8467500	6.6902110E+06	1.9937117E+04
56Co	1.1751001	6.6902110E+06	6.1333672E+03
56Co	1.3602000	6.6902110E+06	3.5601182E+03

**Figure 5.27.** Activity estimate for  $^{134}\text{Cs}$  test case by employing the adjoint methodology discussed in this chapter.

Again, I averaged these values and achieve an overall activity attribution to  $^{134}\text{Cs}$  to be  $1.0 \times 10^5$  Ci. This result is only 33% less than the modeled activity of  $1.51 \times 10^5$  Ci. This decreased activity could be due to the false attribution of a peak at 853 keV. This would cause counts to be subtracted from other real peaks that ordinarily should not have been subtracted. Even though this is the case, I find that I am still remaining relatively close to the desired activity.

### 5.4.3. Fuel Pin Diversions

Identifying possible fuel pin diversions is a major concern for safeguards. Typically, detecting diversions from passive gamma spectroscopy techniques is a nearly impossible feat, but if the concept of adjoint transport is considered, possible applications could exist to help flag a missing fuel pin. Referring back to earlier in the chapter, it was shown that as the detector faces one side of the fuel assembly it only effectively “sees” gamma emissions from a limited number of fuel pins. For example, if the overall count

rate between energies 0.3 MeV and 0.741 MeV is lower than expected by approximately 21.3%, then it is likely a pin is missing from pin position (1,9) in relation to the detector face. However, if the pin missing in a row further back, higher energy emissions must be considered. Table 5.3 shows the relative effect on the count rate in the detector positioned at every side face of the fuel assembly if a fuel pin is diverted from either location (6,5) or (4,11). The pin positions refer to the positions defined by Figure 5.28.

**Table 5.3:** Change in count rate due to fuel pin removal.

Adjoint Group	Pin location (6,5)					Pin location (4,11)				
	2	6	14	16	23	2	6	14	16	23
	(%)	(%)	(%)	(%)	(%)	(%)	(%)	(%)	(%)	(%)
<b>Right</b>	-0.03	-0.1	-0.18	-0.21	-0.24	-0.22	-0.37	-0.44	-0.46	-0.47
<b>Left</b>	-0.0	-0.01	-0.05	-0.06	-0.09	-0.0	-0.01	-0.02	-0.03	-0.04
<b>Top</b>	-0.09	-0.21	-0.26	-0.29	-0.32	-0.0	-0.02	-0.08	-0.1	-0.13
<b>Bottom</b>	-0.0	-0.01	-0.03	-0.04	-0.06	-0.0	-0.1	-0.21	-0.24	-0.28

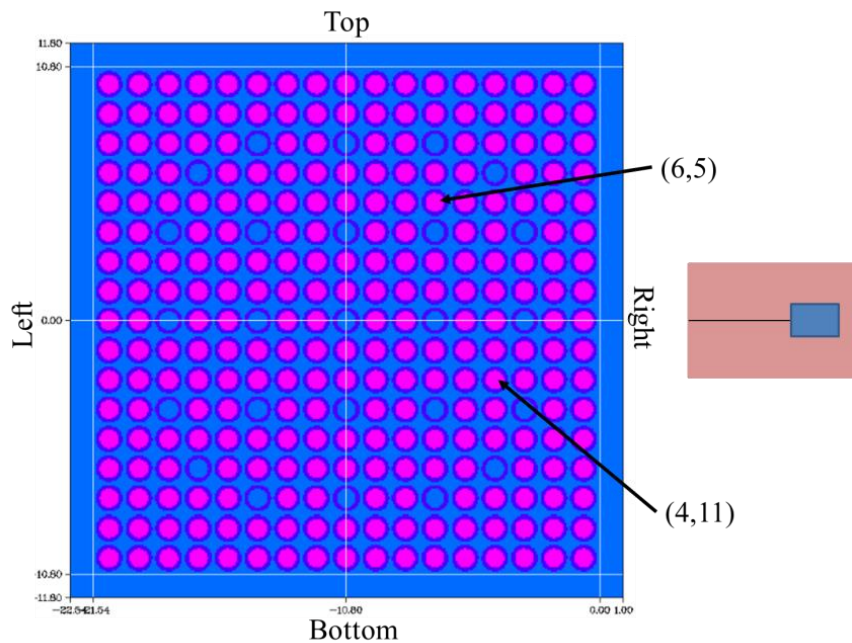


**Figure 5.28:** Fuel pin locations selected for diversion analysis.

The very small changes in count rate due to the diversion of pins located within the fuel assembly poses an issue when trying to detect this diversion using passive gamma techniques. The errors in counting are often larger than these changes can show. The detector's view of the individual fuel pins becomes less differentiated as the emissions increase in energy, allowing the detector to see almost equally further into the assembly. This can still make it difficult to identify if and where a pin diversion has taken place. Most of the fuel pins only affect the overall count rate by a small fraction which may not be enough to determine a significant difference from the expected count rate. Additionally, if the detector only views the fuel assembly from one side, a possible fuel diversion could appear as different burnup estimations. In order to better examine the fuel assembly the count rates must be measured from each side of the fuel assembly, and determined if there are any significant differentiations between sides.

## **5.5 Fuel Burnup Analysis**

It has long been known that the buildup of certain fission products in a fuel assembly over a reactor cycle can provide key identifying information for fuel burnup measurements and calculations. The gamma ray activity from some of these fission products can give a direct quantitative measurement of the fuel burnup. From my adjoint calculations, I have been able to determine a protocol for determining the activities of individual nuclides identified by SmartID. This information can be directly applied to burnup estimation, but it is important to understand which nuclide activities are of most importance and which emissions should be selected for calculating activity.

Since many of the isotopes identified have emissions falling within the same energy windows as other identified isotopes, only those most likely to be present with source strengths that would make their emissions identifiable will be considered for best approximating plutonium content. Certain nuclides are better indicators of fission of  $^{235}\text{U}$  or  $^{239}\text{Pu}$ , and others are good indicators of the total number of fissions taking place.

Figure 5.22 shows the fission yields per atomic mass number for  $^{239}\text{Pu}$  and  $^{235}\text{U}$ . Some mass regions show a strong differentiation between yields from these two nuclides, while other mass regions show very similar yields. This allows me to determine approximately the number of fissions resulting from  $^{239}\text{Pu}$  and the total number of fission taking place from the two main thermal fission nuclides,  $^{239}\text{Pu}$  and  $^{235}\text{U}$ . I added vertical lines to Figure 5.29 to show where these regions occur. For example, at atomic mass number 106, there is a large difference between the fission yields, but at atomic mass number 140, the yields are almost identical. Table 5.3 identifies key nuclides in these atomic mass regions that have strong fission yields, and are also seen as strong gamma emitters.

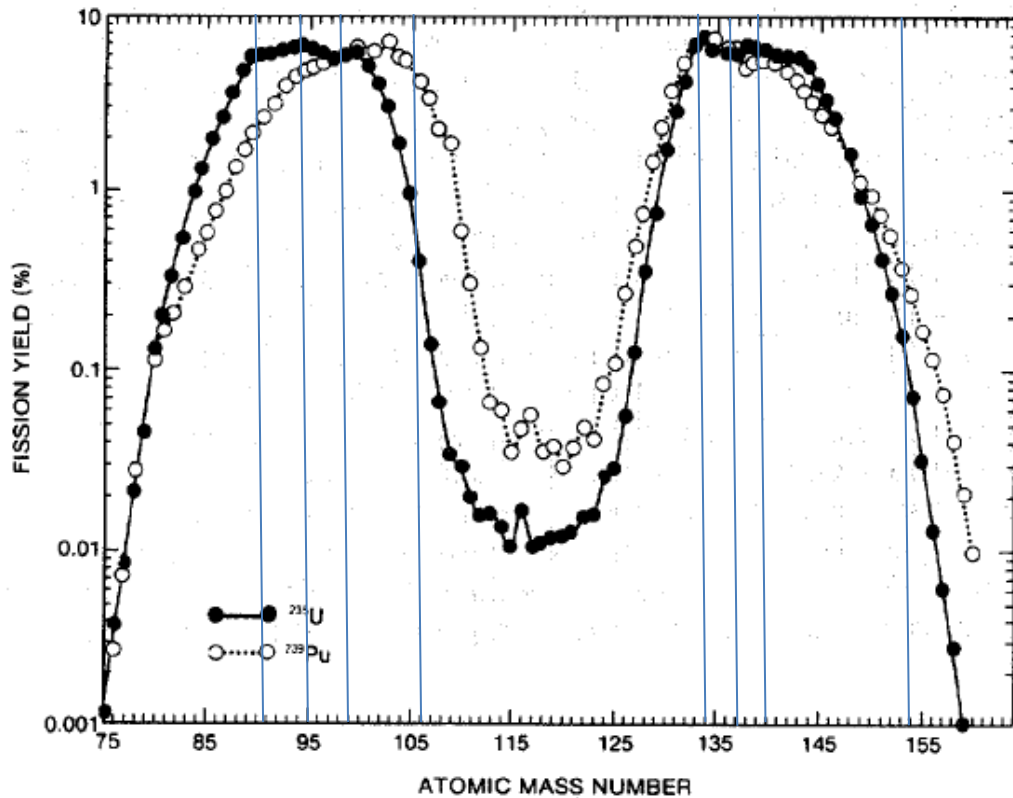


**Figure 5.29:** Mass distribution of fission products for the thermal fission of  $^{235}\text{U}$  and  $^{239}\text{Pu}$  [2].

**Table 5.4:** Cumulative Thermal Fission Yields for strong gamma emitting nuclides in spent PWR fuel after 1 day since removal from reactor core [7].

Nuclide	Cumulative Thermal Fission Yield from $^{235}\text{U}$ (% per fission)	Cumulative Thermal Fission Yield from $^{239}\text{Pu}$ (% per fission)
$^{91}\text{Sr}$	$5.82 \times 10^{-2} \pm 5.95 \times 10^{-4}$	$2.48 \times 10^{-2} \pm 4.968 \times 10^{-4}$
$^{95}\text{Zr}$	$6.502 \pm 0.072$	$4.949 \pm 0.099$
$^{99}\text{Mo}$	$6.132 \pm 0.092$	$6.185 \pm 0.056$
$^{106}\text{Ru}$	$0.41 \pm 0.011$	$4.188 \pm 0.092$
$^{134}\text{Cs}$	$1.21 \times 10^{-5} \pm 3.2 \times 10^{-6}$	$6.7 \times 10^{-4} \pm 1.8 \times 10^{-4}$
$^{137}\text{Cs}$	$6.221 \pm 0.069$	$6.588 \pm 0.08$
$^{140}\text{La}$	$6.315 \pm 0.095$	$5.333 \pm 0.059$
$^{154}\text{Eu}$	$1.95 \times 10^{-7} \pm 6.4 \times 10^{-8}$	$4.9 \times 10^{-5} \pm 1.2 \times 10^{-5}$

Fuel assembly burnup can be calculated from the relationship between fission product activity and the fission yield for a given fission product. Equation 5.22 shows the definition of burnup as

$$\begin{aligned}
 \text{Burnup}[MWd] \cdot 86400 \frac{s}{d} &= \overline{\phi_T} \overline{\Sigma_f} V_{Fuel} t \cdot 200 \frac{MeV}{fiss} \cdot 6.022 \times 10^{-13} \frac{J}{MeV} \\
 &= N_{fiss} \cdot 200 \frac{MeV}{fiss} \cdot 6.022 \times 10^{-13} \frac{J}{MeV} = Pt
 \end{aligned} \tag{5.27}$$

where  $\overline{\phi_T}$  is the average thermal flux in the assembly,  $\overline{\Sigma_f}$  is the average macroscopic fission cross section in the fuel,  $V_{Fuel}$  is the volume of the fuel in the assembly, and  $N_{fiss}$  is the number of fissions that took place in the assembly.  $N_{fiss}$  for a given isotope that has a fission yield that is similar across all fissile isotopes can be calculated by

$$N_{fiss} = \frac{A}{\text{yield} \cdot \lambda} \tag{5.28}$$

where  $A$  is the activity of the given nuclide,  $f_{yield}$  is the fission yield for the given nuclide, and  $\lambda$  is the decay probability for the given nuclide.

Knowing the activities of key burnup indicating fission products, such as  $^{137}\text{Cs}$  and  $^{134}\text{Cs}$ , an estimate of the total fuel assembly burnup can be computed. If the average thermal flux is known, or if the average power in the assembly during irradiation is known, then the time that the assembly was in the reactor can be predicted. This information is useful for understanding whether the reactor operators are following their operating declarations. For burnups less than 500 MWD/MTU, the plutonium content is considered to be weapons usable material. It is important to be able to discern that this is not the case when the fuel is removed from the reactor core.

From the gamma nuclide identification with SmartID,  $^{140}\text{La}$  is a suitable isotope for total fission determination;  $^{91}\text{Sr}$  indicates fissions from  $^{235}\text{U}$ , while  $^{106}\text{Ru}$  and  $^{154}\text{Eu}$  are good indicators of plutonium fissions taking place in the reactor. These isotopes can be used for a burnup estimate of the fuel assembly and will allow a prediction of the total amount of plutonium content in the fuel assembly.

Similar to the ORIGEN source modeling for the 33 GWD /MTU fuel assembly burnup simulations in Chapter 4, I created new ORIGEN models to show the emissions for a range of burnups and fuel enrichments. I determined the nuclide contents for each burnup and enrichment case in terms of activity. Plotting the activities of the nuclides after 1 day since removal from the reactor versus burnup shows how these signatures can be utilized to predict how much plutonium is produced in the fuel assembly. Figure 5.30 shows how  $^{140}\text{La}$  activity decreases as the fuel assembly is burned in the reactor. It is interesting to see the activity increases between 15 GWD/MTU and 20 GWD/MTU. This is likely due to the competing neutron capture interactions with  $^{139}\text{La}$  and  $^{140}\text{La}$ , the decay of  $^{140}\text{Ba}$  to  $^{140}\text{La}$ , and the decay of  $^{140}\text{La}$ . Overall, this does not make a difference when analyzing the fuel for burnup. The activity changes very slightly, such that the errors involved with determining the measured activity are too large for an accurate

determination of burnup from  $^{140}\text{La}$  alone. Another issue with  $^{140}\text{La}$  as an indicator of burnup results from its very short half-life of 40.22 hrs. The amount of  $^{140}\text{La}$  does not accumulate much over the burnup cycle, so the  $^{140}\text{La}$  activity is relatively stable across burnup levels once it reaches a threshold level. Further analyses of other strong gamma emitting nuclides are necessary in moving closer to a burnup estimate.

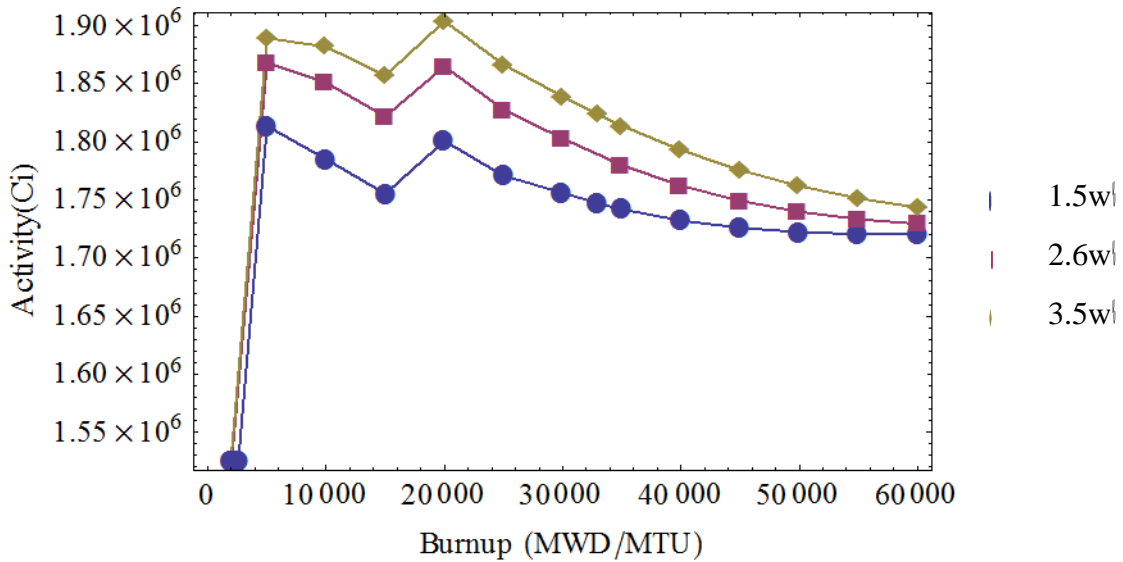


**Figure 5.30:** Total activity of  $^{140}\text{La}$  in a Westinghouse 17x17 fuel assembly at various fuel burnups.

The relationship between activity and burnup for  $^{140}\text{Ba}$  and  $^{99}\text{Mo}$  is that activity slowly decreases as fuel burnup increases, but, as was the case with  $^{140}\text{La}$ , this decrease is not a significant change. This is again mostly due to their short half-lives. The half-life of  $^{140}\text{Ba}$  is 12.8 days and the half-life of  $^{99}\text{Mo}$  is 66 hours. Figures 5.31 and 5.32 show these relationships. The reason there is a slight decrease is the destruction of  $^{235}\text{U}$ . Although small, this fissionable nuclide produces a slightly higher fission yield for  $^{140}\text{Ba}$  and  $^{99}\text{Mo}$  than some of the other bred fissionable nuclides.

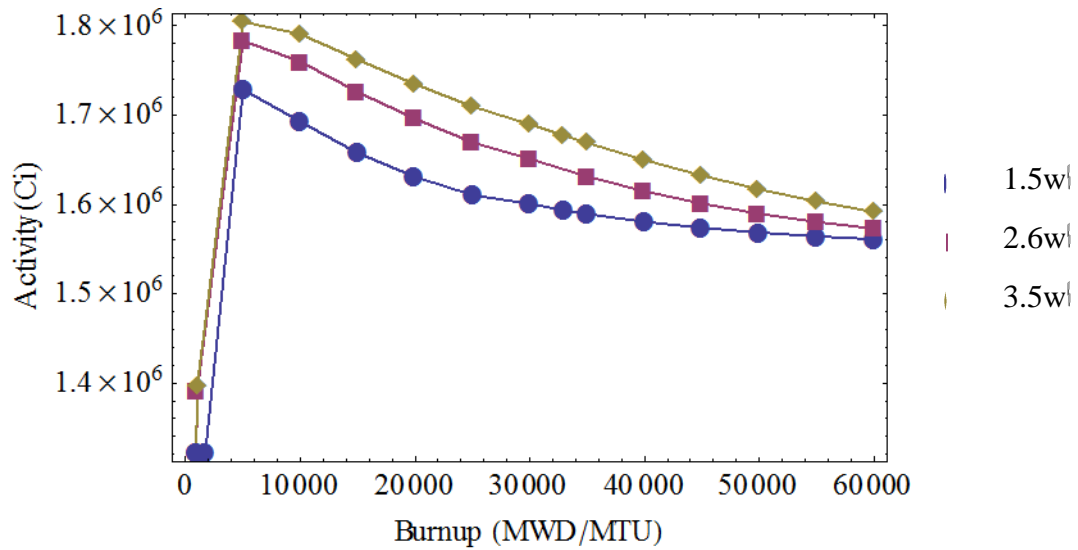


**Figure 5.31:** Total activity of  $^{140}\text{Ba}$  in a Westinghouse 17x17 fuel assembly at various fuel burnups.

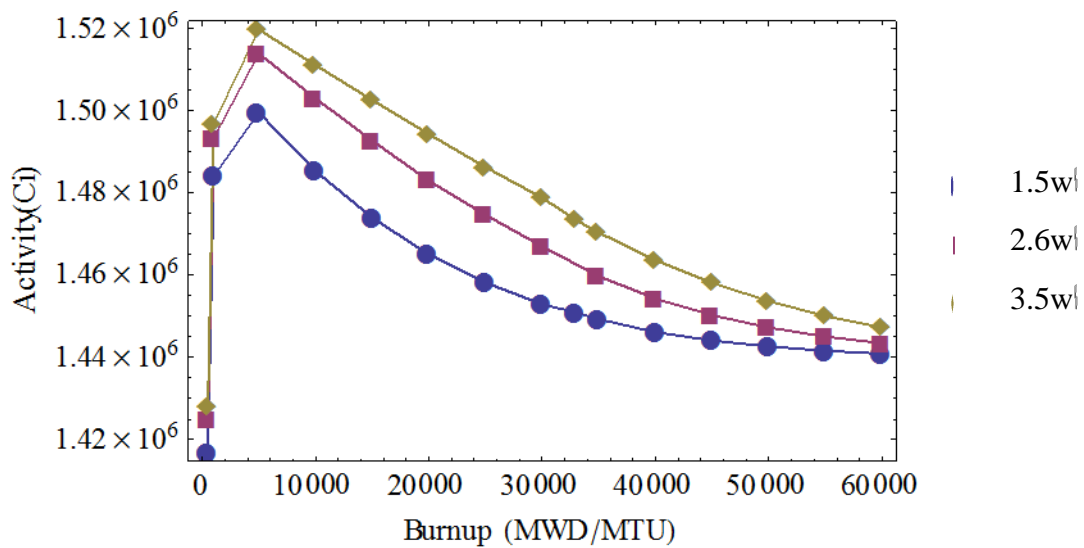


**Figure 5.32:** Total activity of  $^{99}\text{Mo}$  in a Westinghouse 17x17 fuel assembly at various fuel burnups.

Mentioned previously in Chapter 1,  $^{137}\text{Cs}$  is a commonly favored signature for burnup prediction. Figure 5.33 shows a relatively linear relationship between the activity and burnup for this nuclide, which is also nearly identical for each  $^{235}\text{U}$  enrichment case.



Unlike the previous nuclides I analyzed,  $^{137}\text{Cs}$  has a long half-life of 30 years. This, along with its small thermal neutron absorption cross section and its fission yield being approximately equal for all fissile materials, provides a strong relationship between the amount of  $^{137}\text{Cs}$  present in the fuel and how much the fuel assembly has been burned. However, for very short cooling times, its gamma emissions are much weaker than the gamma emissions from the other fission products considered. Consequently, the  $^{137}\text{Cs}$  signature is much more likely to be washed out or detected with high counting error. It is difficult to find another nuclide that varies linearly with burnup while maintaining a minimal dependency on enrichment.

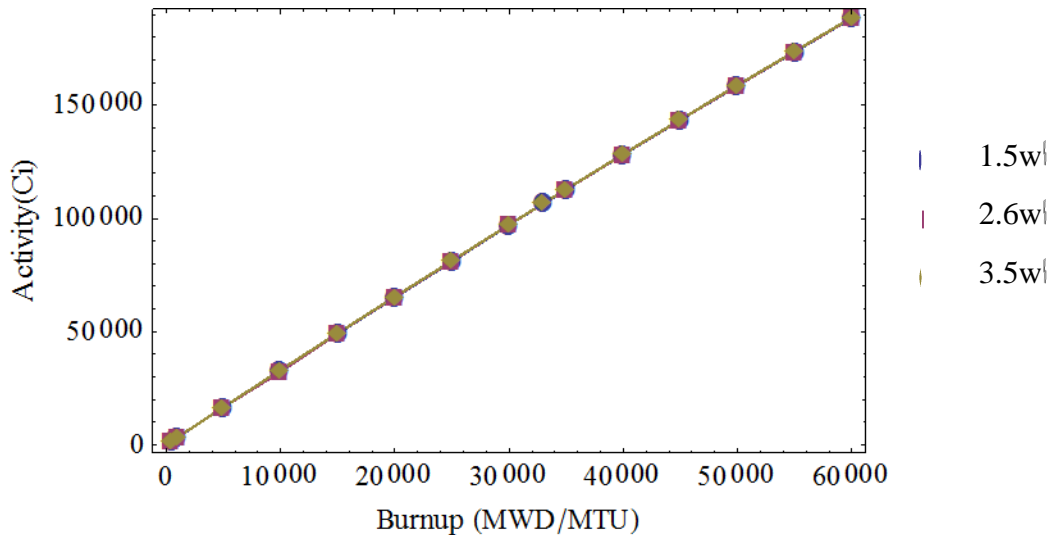


**Figure 5.33:** Total activity of  $^{137}\text{Cs}$  in a Westinghouse 17x17 fuel assembly at various fuel burnups.

Referring to Equation 5.22, the burnup values can be computed from the activity of  $^{137}\text{Cs}$  in the fuel assembly. For example, I calculated the number of fissions that took place in the assembly. First I calculated the  $^{137}\text{Cs}$  activity once the fuel was discharged from the reactor core from the activity after 1 day since removal. The activity was computed to be  $1.0605 \times 10^5$  Ci. From this, I solved for the number of fissions from

Equation 5.23, and determined that approximately  $8.624 \times 10^{25}$  fissions took place. Solving for burnup, I computed that this number of fissions related to a burnup of 32,000 GWD/MTU. The expected burnup for this activity as predicted by the SCALE/ORIGEN code was 33,000 MWD/MTU. This relatively simplistic burnup calculation is only 3.08% from the expected burnup. I repeated these calculations for additional desired burnup values from ORIGEN and included the results in Table 5.5. Appendix G shows the details of the calculations

**Table 5.5:** Fuel assembly burnup estimated from  $^{137}\text{Cs}$  activity.

ORIGEN		Calculated			
Burnup (MWD/MTU)	Activity at t = 1 day (Ci)	Activity at t = 0 day (Ci)	Number of fissions	Burnup (MWD/MTU)	% change
500	$1.6601 \times 10^3$	$1.6602 \times 10^3$	$1.35 \times 10^{24}$	500.7	0.13
15,000	$4.9184 \times 10^4$	$4.9187 \times 10^4$	$4.00 \times 10^{25}$	14,834	-1.11
33,000	$1.0604 \times 10^5$	$1.0605 \times 10^5$	$8.62 \times 10^{25}$	31,982	-3.08
45,000	$1.4364 \times 10^5$	$1.4365 \times 10^5$	$1.17 \times 10^{26}$	43,323	-3.73
60,000	$1.8865 \times 10^5$	$1.8866 \times 10^5$	$1.53 \times 10^{26}$	56,895	-5.17

Another member of the cesium family,  $^{134}\text{Cs}$ , also behaves as a good predictor of fuel burnup. This nuclide is a strong gamma emitter, with a wide range of energy emissions. Its strongest emissions are at 604.7 keV, 795.84 keV, and 801.93 keV, but it also emits gammas with higher energies such as 1167.9 keV, and 1365.2 keV. This makes it suitable for detection and adjoint analysis. Figure 5.34 shows the relationship between activity and burnup for  $^{134}\text{Cs}$ .

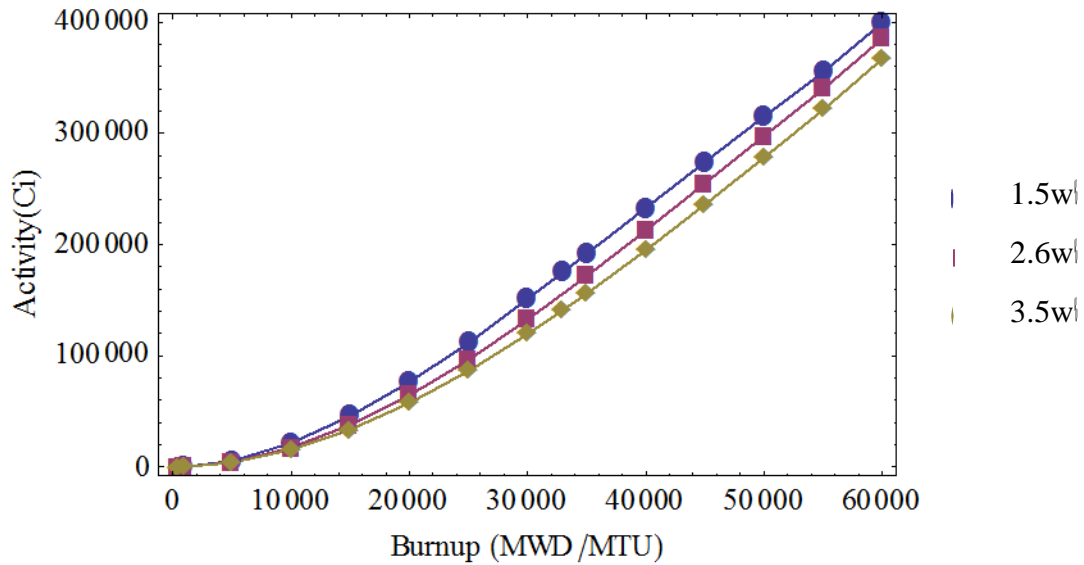


**Figure 5.34:** Total activity of  $^{134}\text{Cs}$  in a Westinghouse 17x17 fuel assembly at various fuel burnups.

$^{154}\text{Eu}$  is another fission product with a high activity yield from a burned PWR fuel assembly. It has high energy gamma emissions and has a long half-life of 16 years in comparison to many of the short lived fission products produced. Therefore, it is able to accumulate in the fuel as the fuel assembly is burned. Figure 5.35 shows how the activity of  $^{154}\text{Eu}$  in a fuel assembly increases almost linearly with respect to burnup in a similar manner to  $^{137}\text{Cs}$ . The identification and activity determination from SmartID for this nuclide can help predict the burnup of the fuel assembly in question. Referring back to Table 5.4, it is seen that  $^{154}\text{Eu}$  has 2 orders of magnitude greater fission yield from  $^{239}\text{Pu}$  than from  $^{235}\text{U}$ . This leads to the slight changes in activity dependent on original fuel enrichment, but this also shows that  $^{154}\text{Eu}$  has a strong relationship with how much plutonium is produced in the fuel assembly.

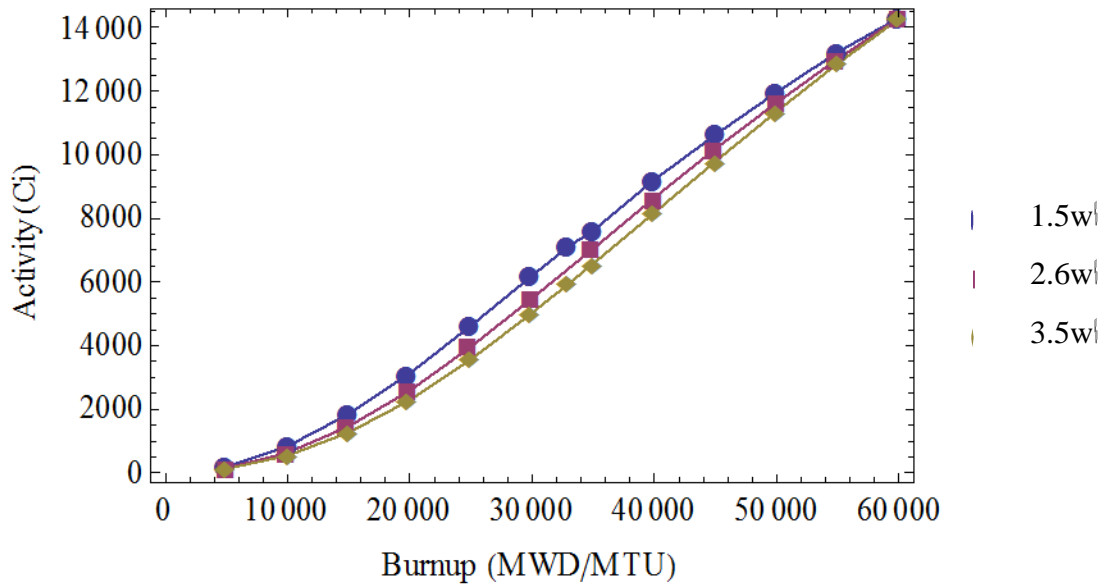


**Figure 5.35:** Total activity of  $^{154}\text{Eu}$  in a Westinghouse 17x17 fuel assembly at various fuel burnups.

The final nuclide I considered with a stronger yield from  $^{239}\text{Pu}$  than  $^{235}\text{U}$  was  $^{106}\text{Ru}$ . This nuclide's activity also has a strong dependence on assembly burnup as shown in Figure 5.36. As the plutonium content increases in the assembly, the  $^{106}\text{Ru}$  content increases as well, but the level at which the activity reaches can also indicate the most likely initial fuel enrichment. Using multiple isotopes as predictors of burnup can help identify which enrichment curve the  $^{106}\text{Ru}$  activity falls under. If the  $^{134}\text{Cs}$ ,  $^{137}\text{Cs}$ , and  $^{154}\text{Eu}$  signal a most likely burnup, then the  $^{106}\text{Ru}$  activity can be verified to see if this burnup is consistent, and its activity can also tell which enrichment condition is most favorable for the predicted burnup.

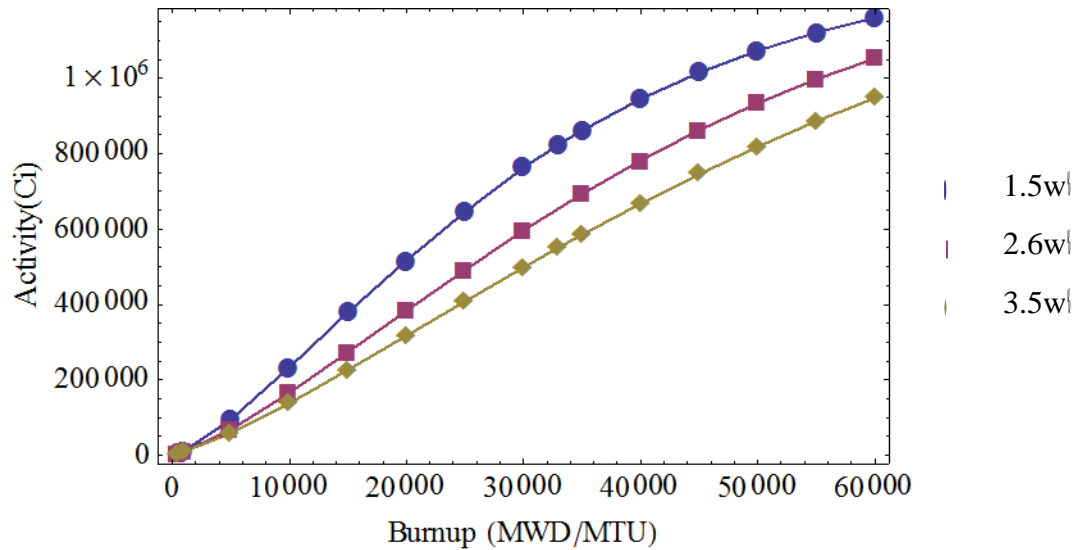


**Figure 5.36:** Total activity of  $^{106}\text{Ru}$  in a Westinghouse 17x17 fuel assembly at various fuel burnups.

The  $^{106}\text{Ru}$  activity is actually determined from gamma emissions from its daughter product,  $^{106}\text{Rh}$ . These isotopes are considered to be in secular equilibrium, since the half-life of  $^{106}\text{Rh}$  (on the order of seconds) is much shorter than the half-life of  $^{106}\text{Ru}$  (approximately 1 year) [8]. This means that both isotopes are essentially decaying at the same rate, and  $^{106}\text{Rh}$  is decaying at the same rate at which it is formed.

Alternatively, fission products related more directly to  $^{235}\text{U}$  than  $^{239}\text{Pu}$  are helpful for narrowing down the predicted burnup condition of the fuel assembly. If electronics or other conditions result in an elevated prediction of isotopic activity, the burnup could be predicted too high, or possibly too low if the activity is under calculated. Fission products dependent on uranium fissions will decrease in contribution to overall activity. The fission product  $^{95}\text{Zr}$  is one such case. It has a half-life of 65.5 days, and can also be produced by neutron capture with  $^{94}\text{Zr}$ . For low burnups,  $^{95}\text{Zr}$  has not had much time to decay away while it is still being produced by fission and neutron capture; however, once it reaches a certain burnup level, it isn't being produced fast enough by neutron capture to

keep up with its decay and decreasing fission production from  $^{235}\text{U}$ . Therefore, burnup prediction from this nuclide is difficult.

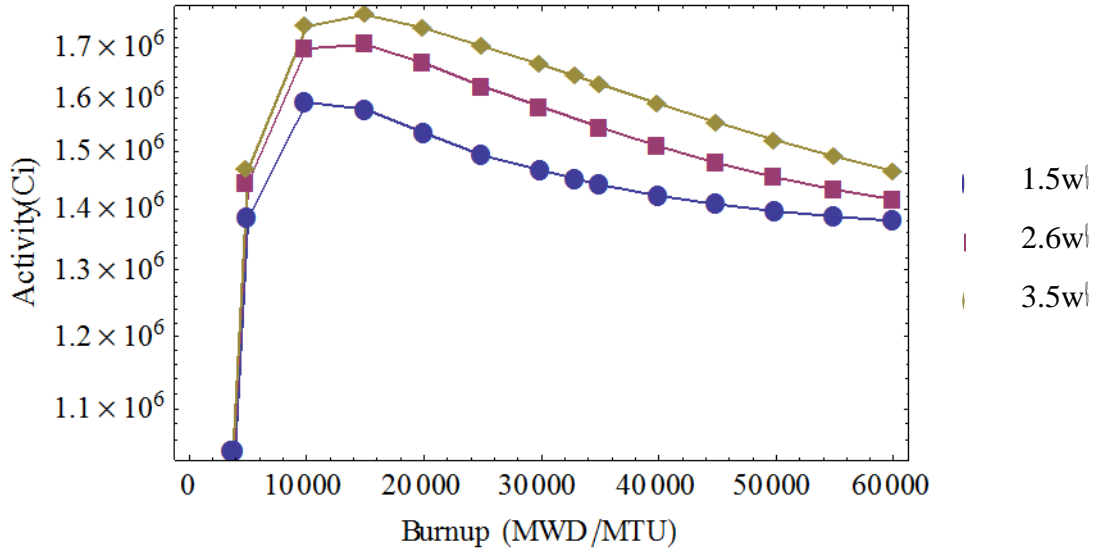


**Figure 5.37:** Total activity of  $^{95}\text{Zr}$  in a Westinghouse 17x17 fuel assembly at various fuel burnups.

Another nuclide with higher fission yield from  $^{235}\text{U}$  than  $^{239}\text{Pu}$  is  $^{90}\text{Sr}$ . This isotope has a half-life of 9.63 hours; therefore, the activity seen after irradiation can be directly attributed to the amount of  $^{235}\text{U}$  left in the assembly. Since  $^{235}\text{U}$  is burned, thereby decreasing the  $^{235}\text{U}$  content, the amount of  $^{91}\text{Sr}$  produced by fission is also decreasing. Figure 5.25 shows this relationship. For each burnup plotted in Figure 5.38, the activity has on average a 25% difference between a fuel assembly originally enriched with 1.5 weight percent  $^{235}\text{U}$  and a fuel assembly enriched to 3.5 weight percent  $^{235}\text{U}$ .

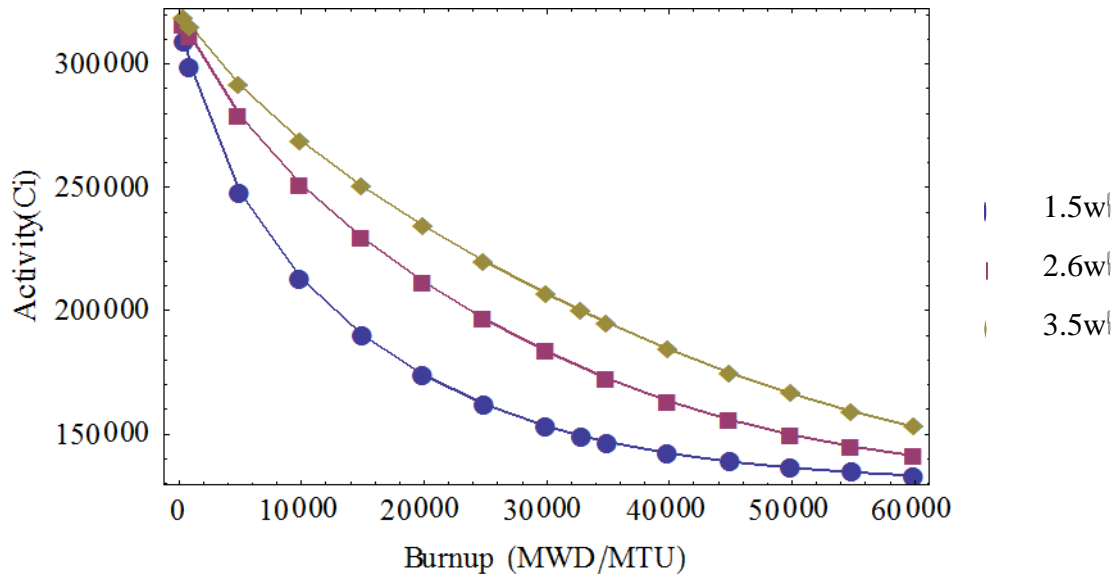


**Figure 5.38:** Total activity of  $^{91}\text{Sr}$  in a Westinghouse 17x17 fuel assembly at various fuel burnups.

For each nuclide there is a relationship between burnup and its activity, but there are differences in how significant the changes are in terms of activity as burnup changes. I quantified how the activities changed with increasing burnup by using a percent difference relationship shown in Equation 5.22,

$$\% \text{ Difference} = \frac{100|A_1 - A_2|}{\frac{1}{2}(A_1 + A_2)} \quad (5.29)$$

where  $A_1$  is the activity at burnup 1, and  $A_2$  is the activity at burnup 2. This method shows how the two activities compare while taking into account the overall strength of the activities. Table 5.6 shows the calculated percent differences from equation 5.22 between the activities at two different fuel burnup levels. The last row shows the percent difference between a low and high burnup assembly for each nuclide considered.

**Table 5.6:** Percent differences computed for selected nuclide's activities at various fuel assembly burnups for initial enrichment of 2.6 w% <sup>235</sup>U.

<b>Burnup Comparison (GWD/MTU)</b>	<sup>91</sup> Sr % diff	<sup>95</sup> Zr % diff	<sup>99</sup> Mo % diff	<sup>106</sup> Ru % diff	<sup>134</sup> Cs % diff	<sup>137</sup> Cs % diff	<sup>140</sup> Ba % diff	<sup>140</sup> La % diff	<sup>154</sup> Eu % diff
0.5 & 1	1.68	59.71	4.68	73.18	147.4	66.62	37.85	43.95	--
1 & 5	10.87	97.17	1.37	151.2	190.0	133.2	24.73	28.14	--
5 & 10	10.53	16.14	0.72	83.41	120.6	64.22	1.31	0.92	122.6
10 & 15	8.99	0.49	0.69	49.22	73.97	41.76	1.95	1.59	78.48
15 & 20	8.11	2.27	0.65	33.51	51.99	28.09	1.75	2.34	55.15
20 & 25	7.44	2.79	0.56	24.64	39.47	21.73	1.58	2.02	41.92
25 & 30	6.80	2.44	0.52	19.43	31.87	17.99	1.11	1.36	32.25
30 & 35	6.22	2.50	0.49	14.99	25.61	14.89	1.20	1.29	24.86
35 & 40	5.47	2.29	0.38	12.06	21.37	12.83	1.02	0.99	20.38
40 & 45	4.71	2.01	0.28	9.79	18.10	11.26	0.86	0.75	16.35
45 & 50	3.95	1.73	0.21	7.99	15.43	10.02	0.71	0.54	13.22
50 & 55	3.24	1.46	0.15	6.54	13.26	9.02	0.58	0.37	11.15
55 & 60	2.60	1.20	0.11	5.35	12.50	8.19	0.47	0.23	9.43
5 & 60	60.22	2.03	4.76	175.7	195.6	167.8	12.53	7.70	195.7

These values help identify which nuclides would show the largest changes over the burnup levels which is important for predicting the plutonium content of the assembly. It is difficult to predict burnup with any certainty if the counting errors are just as large as or larger than the percent differences between fuel burnups. Therefore, nuclides such as <sup>106</sup>Ru, <sup>134</sup>Cs, <sup>137</sup>Cs, and <sup>154</sup>Eu have the best activity-to-burnup relationships for burnup prediction.

It is interesting to see how these different plutonium isotopes grow into the assembly as burnup increases. Figure 5.39 shows how <sup>239</sup>Pu initially grows at a fast rate before slowing, where the other isotopes grow more consistently. This creates some concern if fuel is not burned to an appropriate level since at low burnups the <sup>239</sup>Pu content is high while the <sup>240</sup>Pu content is very low. Figure 5.40 shows the total plutonium content



in the assembly after 1 day of removal from the reactor. It is clear that the  $^{239}\text{Pu}$  content has the greatest contribution to the total plutonium.

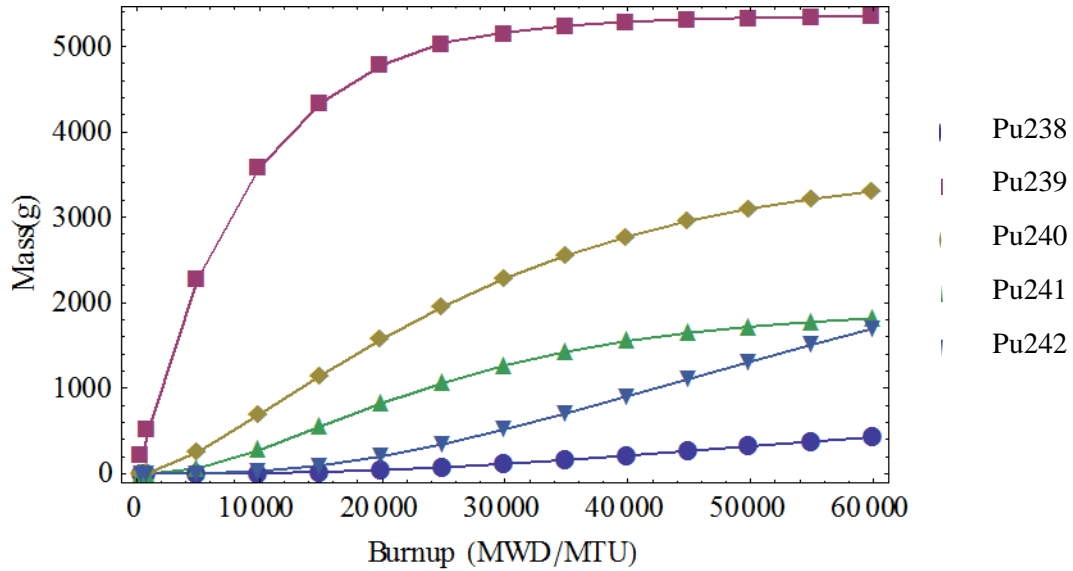


**Figure 5.39:** Plutonium isotopic content in a Westinghouse 17x17 PWR fuel assembly enriched to 2.6 w%  $^{235}\text{U}$  at various burnup levels.

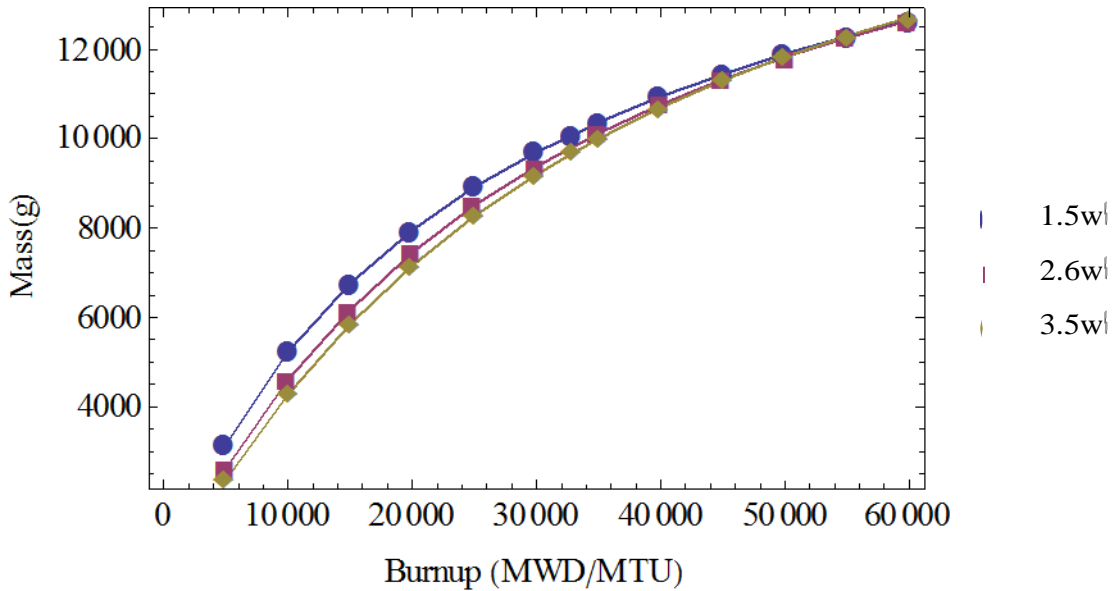


**Figure 5.40:** Total plutonium content in fuel assembly for various burnup levels.

As the various enriched fuel assemblies reach greater burnups, the total plutonium content depends less and less on the fuel enrichment. The percent difference between the 1.5 weight percent  $^{235}\text{U}$  fuel and 3.5 weight percent  $^{235}\text{U}$  fuel is 28.41% at 5 GWD/MTU, and decreases to 0.085% at 60 GWD/MTU. Matching the predicted burnup value from SmartID calculated activities for the various fission products discussed in this chapter to the plutonium content shown by Figures 5.29 and 5.30 will give an investigator a unique view of very short cooled spent nuclear fuel.

Recalling the  $^{106}\text{Ru}$  case presented at the end of Chapter 5.4.2.2, I found that the activity predicted from my activity estimation code was  $6.84 \times 10^5$  Ci. Looking at Figure 5.28, I see this matches up with a burnup level around 33 GWD/MTU, and a total plutonium mass of approximately 9.5 to 10 kg. The real value for total Pu from 2.6 w% enriched 33,000 MWD fuel assembly is 9.8 kg total plutonium. I can also directly relate the number of fissions from calculated activity for  $^{106}\text{Rh}$ .  $^{106}\text{Ru}$  can be directly correlated to the  $^{106}\text{Rh}$  activity. Its fission yield is strongly dependent on  $^{239}\text{Pu}$  at 4.19%, while its fission yield from  $^{235}\text{U}$  is substantially weaker at 0.41%. There is a direct correlation between the number of fissions and ingrowth of plutonium in the fuel assembly. Solving the burnup equation (Equation 5.2) in the same manner burnup was solved for  $^{137}\text{Cs}$ ; I found that burnup can be strongly related for the  $^{106}\text{Ru}$  case. Table 5.7 shows the calculated burnup values from direct ORIGEN activity values. There is a slight bias towards higher burnup once actual burnup surpasses 10,000MWD, but overall the percent change above this level is on the average of 8.82%.

**Table 5.7:** Fuel assembly burnup estimated from  $^{106}\text{Ru}$  activity.

ORIGEN		Calculated			
Burnup (MWD/MTU)	Activity at t = 1 day (Ci)	Activity at t = 0 day (Ci)	Number of fissions	Burnup (MWD/MTU)	% change
500	$4.3884 \times 10^3$	$4.3965 \times 10^3$	$1.81 \times 10^{23}$	252.1	-49.57
15,000	$2.7322 \times 10^5$	$2.7373 \times 10^5$	$1.13 \times 10^{24}$	15,698	4.66
33,000	$6.1210 \times 10^5$	$6.1324 \times 10^5$	$2.52 \times 10^{25}$	35,169	6.57
45,000	$8.6259 \times 10^5$	$8.6419 \times 10^5$	$3.55 \times 10^{25}$	49,562	10.14
60,000	$1.0524 \times 10^6$	$1.0544 \times 10^6$	$4.34 \times 10^{25}$	60,469	0.78

I now proceed and calculate burnup from this simplified method for the SmartID identified and adjoint calculated activity to determine if I can achieve a reasonable estimate of burnup. From this activity, I found that approximately  $2.82 \times 10^{25}$  fissions took place resulting in a fuel burnup value of 39,300 MWD. This is 19% greater than the actual burnup modeled, and 11.7% greater than the burnup calculated from the ORIGEN activity for this case. However, it is important to note the geometry conditions biased the results towards a slightly higher activity calculation.

This performs well given all of the moving parts required in this type of analysis along with the low resolution detector system being utilized. Therefore, this shows a lot of promise for future work in this area, especially with higher resolution detection systems such as CZT, which are already used in underwater spent fuel applications. Knowing that nuclide attribution along with activity and burnup determination can be possible with a low resolution system in NaI(Tl), this approach would pave the way for future work examining fuel discharged from the reactor core.

## 5.6 References

- [1] LEWIS, E.E., AND MILLER, W.F., Computational Methods of Neutron Transport. American Nuclear Society, Inc., 1993.

- [2] WALKER, S., "Spectrally-Matched Neutron Detectors Designed Using Computational Adjoint SN for Plug-In Replacement of Helium-3," Dissertation. Georgia Institute of Technology. August 2013.
- [3] SJODEN, G., AND HAGHIGHAT, A., "PENTRAN - A 3-D Cartesian Parallel SN Code with Angular, Energy, and Spatial Decomposition", Proceedings of the Joint International Conference on Mathematical Methods and Supercomputing for Nuclear Applications, p. 553, Saratoga Springs, NY, October 5-10, 1997.
- [4] HAGHIGHAT, A., SJODEN, G., KUCUBOYACI, V., "Effectiveness of PENTRAN's Unique Numerics for Simulation of the Kobayashi Benchmarks", Special Issue, Progress in Nuclear Energy Journal, 3D Radiation Transport Benchmarks for Simple Geometries with Void Region, 39, 2, (2001), ISSN 0149-1970.
- [5] CHIN, M., PAUL, J., SJODEN, G., "Mobile pit verification system (MPVS) design phase I," Final Report Prepared for U.S. Department of State. September 2012
- [6] EDGAR, C., MOLINAR, M., MANALO, K., WALKER, S., HUANG, M., APPLGATE, J., ROVETO, J., BARRON, B., YI, CI., and SJODEN, G., "Transport simulation & validation of a synthetic aperture SNM detection system," Final Report Prepared for National Nuclear Security Administration. June 2013.
- [7] NICHOLS, A.L., ALDAMA, D.L., and VERPELLI, M., "Handbook of nuclear data for safeguards: database extensions, august 2008," INDC International Nuclear Data Committee. International Atomic Energy Agency. INDC(NDS)-0534. Vienna, Austria, August, 2008.
- [8] KRANE, K. Introductory Nuclear Physics. John Wiley & Sons, Inc., 1988.

# CHAPTER 6

## CONCLUSION

### 6.1 Final Design

The final design for an underwater system to rapidly characterize spent nuclear fuel from a PWR after removal from the reactor core incorporates a robust 2 in. × 2 in. NaI(Tl) scintillator detector encased in highly attenuating tungsten shielding. A 1 mm in diameter pinhole collimates the field of view such that only a portion of the fuel assembly is measured during a given detector counting time. The detector system must pass by each side face of the assembly in order to spatially determine if fuel pins may be missing. The adjoint importance calculations can lead the investigator to determine whether or not there should be concern for tampering of the fuel assembly or if the reactor operators are following their declarations.

The work presented in this dissertation showcased a multi-faceted, approach to solving the issue of underwater spent fuel characterization with low resolution detection systems. I detailed the theory behind the SmartID post-processing algorithm, how this algorithm had been updated to consider an underwater spent fuel scenario, how SmartID performed with experimental spectra data, MCNP simulations developed for a complicated spent nuclear fuel assembly, and the deterministic transport models generated. All of these parts were fully integrated to show how it is possible to estimate burnup and plutonium content in the spent nuclear fuel from low resolution detection systems.

My work demonstrated basic estimations for the activities of SmartID identified highly scored nuclides can be determined from adjoint importance computations combined with the detector count rate outputs from the correlated identified peaks. Due

to the simplification of energy dependency, the importance calculations lead only to an estimation of the assembly's source strength. Due to the highly complex emission profile for spent nuclear fuel, nuclides with strong gamma emissions that are relatively isolated from other strong gamma emissions make the best candidates for fuel characterization efforts. The nuclides  $^{106}\text{Ru}$ ,  $^{134}\text{Cs}$ ,  $^{137}\text{Cs}$ , and  $^{154}\text{Eu}$  are the best candidates for burnup analysis due to their strong activity dependency on burnup. Typically, investigators like to analyze the  $^{137}\text{Cs}$  peak for burnup predictions, but this is not necessarily the best option when the fuel assembly is measured shortly after removal from the reactor due to many of the short lived gamma emissions washing out the  $^{137}\text{Cs}$ 's corresponding photopeak. The other nuclides considered have much greater energy emissions easier for SmartID to identify, therefore these nuclides have been deemed best suited for this type of application.

I presented experimental data collected which showed SmartID was successful in identifying the nuclides of interest in highly complicated background scenarios. The weak  $^{60}\text{Co}$  sources were identified by SmartID even though the peaks attributed to this nuclide could not be identified by looking at the spectrum due to the elevated Compton effects and attenuation. Additionally, SmartID was able to identify key nuclides involved with fissions and neutron sources during the irradiation of a natural uranium fuel rod. I further tested this algorithm with MCNP spent fuel assembly simulations to determine that SmartID was in fact identifying the key gamma emitters. Due to the energy windows necessary for peak attribution, some other nuclides were identified in error, but if the investigator is trained and knowledgeable on which peaks are double counted and should actually be attributed, then this tool can be effective for spent fuel monitoring. That said, this tool may not be appropriate for use by an inexperienced user or by someone with little background in spent nuclear fuel characterization.

I tested my adjoint mass estimation methodology with simplified MCNP models in order to achieve better statistics within the models. I was able to come close to

matching the activity for  $^{137}\text{Cs}$  peak, and I was able to match the activity for a  $^{106}\text{Ru}$  peak within 19% of the modeled activity proving that this tool can be effective for spent fuel burnup characterization estimation. This resulted in the predicted burnup to be computed to be 39,300 MWD corresponding to a total plutonium estimate of 10 kg. This burnup estimate also has a 19% difference from the modeled burnup of 33,000 MWD, and the 9.8 kg of plutonium calculated for a 33,000 MWD burnup in ORIGEN falls within the estimated plutonium content range predicted.

## 6.2 Future Work and Recommendations

The work presented in this dissertation is just the beginning of a whole wide range of applications and future work. NaI(Tl) showed great promise for use in underwater spent fuel applications, but I believe the same methodologies applied here could be applied to higher resolution detectors already used in spent fuel scenarios such as CZT. A detector with a higher resolution will potentially have better results in the lower end of the spectrum in comparison to NaI(Tl) thereby giving the investigator more information about the composition of the fuel assembly. In addition, the better resolution will improve the counts attributed to closely aligned peaks. This may help investigators with less experience and knowledge since it will be easier to see peak differentiation in the spectra recorded.

Additionally, in order to fully show how this type of system can provide detailed information from short cooled spent fuel, a full experimental evaluation should be performed. In order to do that, access to a spent fuel pool, and funding for all materials needed for fabrication would be necessary. I created a concept design based off of my detector model surrounded by Tungsten shielding, facing a side of a fuel assembly. Figure 1.4 shows a concept design of how the detector will scan across the fuel assembly. This system would be capable of measuring the fuel after the upending device rotates the fuel assembly once it passes through the fuel transfer canal.

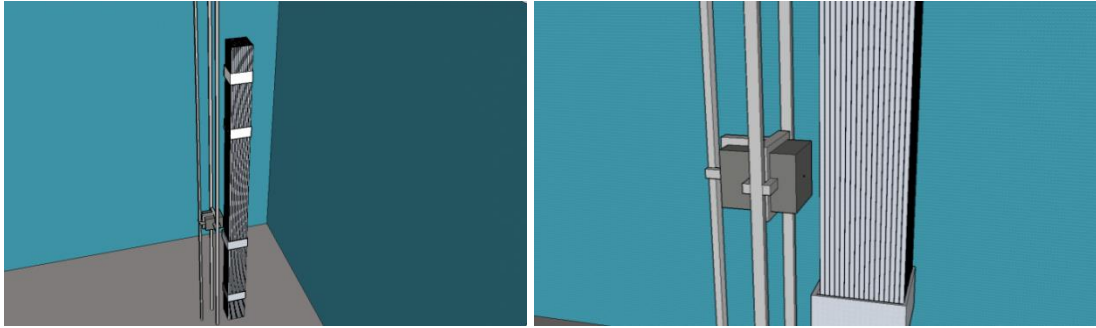


**Figure 6.1:** Underwater fuel assembly detection system.

Figure 1.5 shows a schematic of a typical pressurized water reactor (PWR) which is a type of light water reactor (LWR). These types of reactors utilize low enriched uranium (LEU) with  $^{235}\text{U}$  content between 2.1 and 3.1 weight percent [1]. The fuel is typically burned to 33,000 MWD/MTU which results in high fission product production while minimizing the  $^{239}\text{Pu}$  content in relationship to the overall Pu content. Due to the high nuclide activity following irradiation, the detector scan would be rapid with minimal impact on refueling operations. Such a system could also be used in the spent fuel pool to look at individual fuel assemblies.



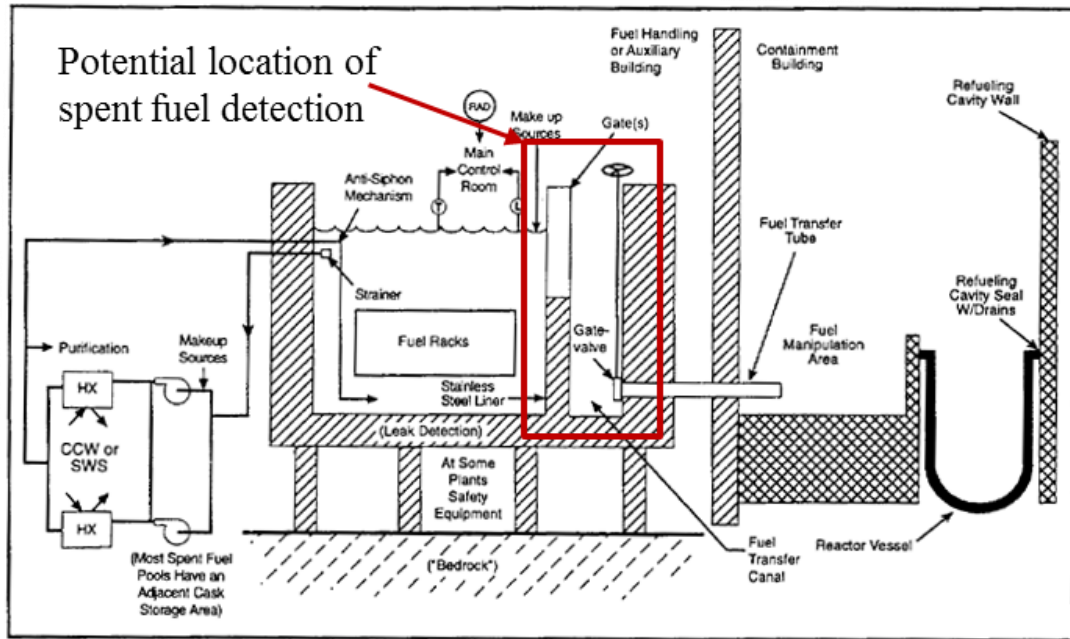


**Figure 6.2:** PWR Spent Fuel Cooling Systems. A potential area for detection is located for individual assembly detection. [2]

### 6.3 Potential Impact on Nuclear Forensic Capabilities

The work presented in this dissertation has the potential to positively impact nuclear forensics efforts by allowing immediate access to key radionuclide characterization for unknown source compositions through the use of inexpensive and readily available NaI(Tl) detector systems. The IAEA desires low-cost, non-destructive methods for plutonium quantification, and this work helps meet those conditions through the post-processing of NaI(Tl) scintillator spectra. The idea of nuclide characterization for spent nuclear fuel in an underwater environment significantly improves real time estimation of potential operator declarations, and helps identify any potential diversions of material.

The work I completed provides a strong basis for potentially wide ranging applications from airborne radionuclide platforms to portal monitoring. Short-cooled,

high burnup spent nuclear fuel produces some of the most complex gamma emission profiles known to researchers. Achieving peak identification for this type of source in a highly scattering and absorbing medium, and being able to utilize this information to produce an estimate of significant nuclide activities is a considerable achievement.

This work paves the way for future analysis on low cost, transportable systems for any possible in-field scenario a nuclear forensics investigator could face. The methodologies present here could be applied to newer and higher resolution scintillator detectors types, which would only increase the reliability and functionality of this type of system analysis.

#### **6.4 References**

- [1] DUDERSTADT, J., and HAMILTON, L., Nuclear Reactor Analysis. John Wiley & Sons, Inc., 1976.
- [2] IBARRA, J.G., JONES, W.R., LANIK, G.F., ORNSTEIN, H.L., and PULLANI, S.V., "Operating Experience Feedback Report." Assessment of Spent Fuel Cooling. U.S. Nuclear Regulatory Commission. NUREG-1275. Vol. 12. 1997.



```

c CsI detector
18  cx    2.54
19  px   40.83
20  px   45.91
c 21  p   -66.9395 -39.6181 -89.6181 -3492.03
c 22  p   89.6181 66.9395 -0.0001 -4675.11
c 23  p   89.6181 -0.0001 -66.9395 -4675.11
c 24  p   -66.9395 89.6181 -39.6181 -3492.03
21  p   30.83 -15.1779 15.1779
      30.83 15.1779 15.1779
      40.83 -1.79 1.79
22  p   35.83 8.48396 -1.79
      40.83 1.79 -1.79
      30.83 15.1779 -15.1779
23  p   40.83 -1.79 -1.79
      35.83 -1.79 -8.48396
      30.83 -15.1779 -15.1779
24  p   30.83 -15.1779 15.1779
      40.83 -1.79 -1.79
      30.83 -15.1779 -15.1779
25  X   30.83 15.9279 40.83 2.54
c Air Pin Hole
31  px   41.03
32  cx    0.05
c Tungsten Collimator
33  px   30.83
34  px   48.91
35  py  -13.3929
36  py   13.3929
37  pz  -13.3929
38  pz   13.3929
c Concrete
39  px   65.91
40  pz   -40
41  pz    40

c DATA CARDS
c -----
c material cards
mode p
m1  92000.04p  1          $U- Fuel
m2  40000.04p -0.982     $Zr- Cladding
      50000.04p -0.015     $Sn
      26000.04p -0.002     $Fe
      24000.04p -0.001     $Cr
m3  1000.04p  2          $H- Water
      8000.04p  1          $O
m4  11000.04p 0.0147471 $Na- NaI
      53000.04p 0.0147471 $I
      81000.04p 1.47471e-5 $Tl
c      material 5 is an CsI(Tl) detector
m5  55000 0.0147471
      53000 0.0147471
      81000 1.47471e-5

c
m6  74000.04p 1.0        $W- Tungsten
c      material 7 is Concrete density: 2.300E+00 g/cc
m7  1001.      1.3741E-02
      14028.    1.6620E-02
      8016.     4.6056E-02
      13027.    1.7454E-03
      11023.    1.7472E-03
      20040.    1.5206E-03
      26054.    2.0851E-05
      26056.    3.1825E-04
      26057.    7.1522E-06
      26058.    1.0042E-06
c      material 8 is air rho=0.00120282 80% r.h. 25C 1.5 w pct water vapor
m8  7014.50c -0.769 8016.50c -0.2293 1001.50c -0.0017
c m8  6000.04p -0.000124 $C- Air
c      7000.04p -0.755268 $N
c      8000.04p -0.231781 $O
c      18000.04p -0.012827 $Ar
c -----

```

c source cards  
 SDEF PAR=2 ERG=D1 CELL 1:2:3 EXT D2 RAD=D3 EFF=0.01 AXS 0 0 1  
 POS=0 0 0

c -----  
 c Source Energy Dist #1 w/sampling bias wgts  
 c -----

#	sil h	sp1 d	sb1 d
c	0.01	0.0	0.0
	0.05	0.0	0.0
	0.10	0.0	0.0
	0.15	0.0	0.0
	0.199	0.0	0.0
	0.200	1.0	1.0
	0.201	0.0	0.0
	0.25	0.0	0.0
	0.30	0.0	0.0
	0.35	0.0	0.0
	0.40	0.0	0.0
	0.45	0.0	0.0
	0.50	0.0	0.0
	0.55	0.0	0.0
	0.60	0.0	0.0
	0.65	0.0	0.0
	0.70	0.0	0.0
	0.75	0.0	0.0
	0.80	0.0	0.0
	0.85	0.0	0.0
	0.90	0.0	0.0
	0.95	0.0	0.0
	1.00	0.0	0.0
	1.05	0.0	0.0
	1.10	0.0	0.0
	1.15	0.0	0.0
	1.20	0.0	0.0
	1.25	0.0	0.0
	1.30	0.0	0.0
	1.35	0.0	0.0
	1.40	0.0	0.0
	1.45	0.0	0.0
	1.50	0.0	0.0
	1.55	0.0	0.0
	1.60	0.0	0.0
	1.65	0.0	0.0
	1.70	0.0	0.0
	1.75	0.0	0.0
	1.80	0.0	0.0
	1.85	0.0	0.0
	1.90	0.0	0.0
	1.95	0.0	0.0
	2.00	0.0	0.0
	2.05	0.0	0.0
	2.10	0.0	0.0
	2.15	0.0	0.0
	2.20	0.0	0.0
	2.25	0.0	0.0
	2.30	0.0	0.0
	2.35	0.0	0.0
	2.40	0.0	0.0
	2.45	0.0	0.0
	2.50	0.0	0.0
	2.55	0.0	0.0
	2.60	0.0	0.0
	2.65	0.0	0.0
	2.70	0.0	0.0
	2.75	0.0	0.0
	2.80	0.0	0.0
	2.85	0.0	0.0
	2.90	0.0	0.0
	2.95	0.0	0.0
	3.00	0.0	0.0

c  
 SI2 -182.87 182.87  
 SP2 0 1  
 SI3 0.3 0.4  
 SP3 -21 1

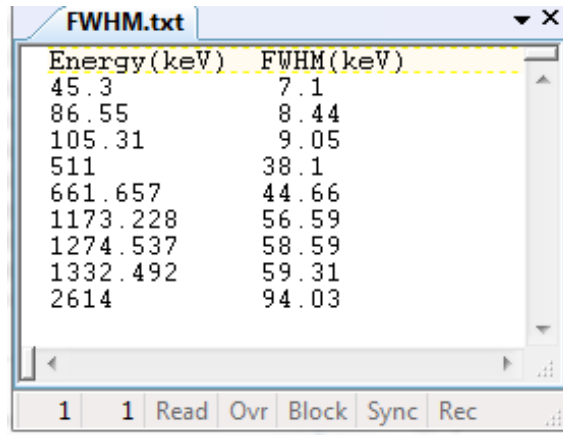
```

c -----
c tally cards
c -----
c
c fc11 Hemisphere Current w/ directions normal to -x, +x, 8 keV bins
c (x-normal vector ref for top (dir normal to surf)), delE=8 keV
f11:p 19
c11 0 1
c Energy Bins
e11 0.00 1.e-5 0.001 400i 3.209 3.30
c
c
c fc28 CsI Pulse Height, Shielded, 1 keV bins
f28:p ( 9 )
c zero bin eps bin energy bins
e28 0.00 1.e-5 0.001 3198i 3.200 3.30
c
c
c fc38 CsI(Tl) Pulse Height, 1 keV bins
f38:P ( 9 )
ft38 GEB -7.25e-3 0.0732219233 0.3132861 $Gaussian Energy Broadening a b c
e38 0.00 1.0e-5 0.001 3198i 3.200 3.30
c
c
c fc44 CsI(Tl) Flux in detector
c f44:P ( 9 )
c fm44 2.4878e18
c
c
print
Rand GEN=2
CTME 92160

```

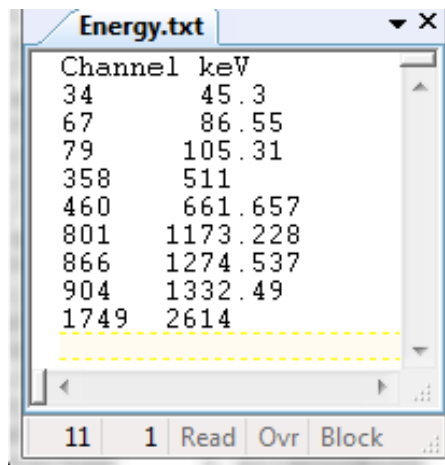
## APPENDIX B

### SMARTID EXPERIMENT FWHM AND ENERGY FILES



Energy(keV)	FWHM(keV)
45.3	7.1
86.55	8.44
105.31	9.05
511	38.1
661.657	44.66
1173.228	56.59
1274.537	58.59
1332.492	59.31
2614	94.03

**Figure B.1:** “FWHM.txt” file for irradiated fuel rod experiment spectra.



Channel	keV
34	45.3
67	86.55
79	105.31
358	511
460	661.657
801	1173.228
866	1274.537
904	1332.49
1749	2614

**Figure B.2:** Energy calibration file, “Energy.txt” for irradiated fuel rod experiment spectra.

## APPENDIX C

### SMARTID EXPERIMENT INPUT FILES

```
Spectrum File
"/IrradExp/5minSpec/20th5min/20th5min.Spe"
Background File
"/IrradExp/5minSpec/4-30-14BkgdwRod.Spe"
Background Significance Factor
1.0
MaxI Energy FWHM calibration table
"/IrradExp/FWHM.txt"
Low energy tailing: height ratio, FWHM in keV
0.2500000 25
Aliasing Factor (-1 diablises, >0 elim pk w/in fract FWHM)
0.5
Energy Calibration Tabl
"/IrradExp/Energy.txt"
Chi-squared threshold
-1
AlphaI for adaptive chi
0.01
Detector response function (DRF) type (0-5=NaI, 6=HPGe, 7-8=CsI, 9=Water)
9
Rejection Threshold (minimum peak height)
1
Relative channel threshold percent of total spectrum in a channel
5
Scattered counts scale factor
1.0
smartid parameters: low energy cutoff (MeV)
0.300
high energy cutoff (MeV)
3.0
min halflife unit (ignore smaller than s=second m=minute h=hour d=day y=year)
s
detector material (3=NaI, 4=CsI 5=LaBr3 6=SrI2)
3
mean detector thickness (cm)
5.080
shield material (1=Fe, 2=Pb, 0=uncertain--iterate)
0
shield thickness (cm,<0:iteratively search for optimum thickness <absolute value)
-10
tolerance ratio (pk vs emiss E; <0:fixed value; >0:adaptive up to val)
0.015
blur coefficient (combine gamma lines if closer than FWHM*blur)
0.01
energy mismatch weight
1.0
output file
"/IrradExp/5minSpec/20th5min/20th5min.out"
correlation threshold (high/moderate/low setpoints)
108 99 50
tol_start, tol_step, iso_range (iterate tol ratio)
0.001 0.005, 3
```

**Figure C.1:** SmartID input file for 20<sup>th</sup> 5 minute spectrum collected after fuel rod irradiated for 2 weeks. Options chosen included an aliasing factor of 0.5, chi threshold of 0.01, DRF representing the fuel assembly in water, and shielding search.



# APPENDIX D

## SMARTID EXPERIMENT OUTPUT FILES

20<sup>th</sup> 5min count with water DRF

SmartID-XP  
Extended Protocol Synthetic Resolution Identifier  
Ver 2.5J

By  
G. Sjoden, C. Yi, E. LaVigne, J. Paul  
Georgia Institute of Technology  
June 2014

Contact: sjoden@gatech.edu

Spectrum Name: ../IrradExp/5minSpec/20th5min/20th5min.Spe

13 Peak(s) Identified - Sort by Energy

keV	Counts	Norm% Cts	Peak Id
819.18	8.5750E+00	12.59805	13
982.70	4.7650E+00	7.00055	12
1048.70	4.2127E+00	6.18913	11
1423.50	3.9833E+00	5.85211	10
1513.00	7.6644E+00	11.26023	8
1550.90	3.2297E+00	4.74495	9
1608.50	1.0851E+01	15.94186	5
1676.80	6.3377E+00	9.31110	6
1717.70	2.8936E+00	4.25116	7
1828.40	2.5529E+00	3.75062	4
2708.20	1.7901E+00	2.62994	3
2779.90	4.5216E+00	6.64295	2
2901.00	6.6891E+00	9.82736	1

Most Probable Shielding Settings:

Shielding material	shielding size(cm)	score
Pb	10.000	2884.1
Pb	8.000	2745.2
Fe	10.000	2001.7
Pb	6.000	1939.6
Pb	5.000	1763.6
Pb	3.000	1628.8
Pb	4.000	1614.7
Pb	2.000	1327.9
Fe	8.000	1234.6
Pb	1.000	1032.9
Fe	6.000	1027.6
Fe	5.000	959.9
Fe	4.000	954.2
Fe	3.000	936.8
Fe	2.000	907.9

Score Correlation Threshold:

High correlation: score > 108.0  
Moderate correlation: score in between: [ 99.0, 108.0]  
Low correlation: score < 99.0 with a cutoff at 50.0

Overall Mean Nuclide Scores (total\_scored=38):

[based on integral average of score from each nuclide for all shielding options]

Nuclide	Score	Comment	Correlation
48Sc	109.25	c	High
58Co	102.35	c	Moderate
136Cs	100.89	Fiss_Prod	Moderate
143La	100.57	Fiss_Prod	Moderate
42K	97.06	c	Low
135I	94.66	Fiss_Prod	Low
132I	92.28	Fiss_Prod	Low
140La	75.89	Fiss_Prod	Low
238Np	65.95	SNM	Low
88Rb	49.54	Fiss_Prod	Low

156Eu	43.60	Fiss_Prod
211Pb	39.06	U-235_Daughter
209Tl	36.13	Np-237_Daughter
138Cs	32.48	Fiss_Prod
52Mn	28.09	c
124Sb	25.81	Fiss_Prod
166mHo	24.01	Fiss_Prod
228Ac	20.98	Th-232_Daughter
52Mn	15.21	c
106Ru	14.41	Fiss_Prod
54Mn	13.71	c
212Bi	13.42	Th-232_Daughter
24Na	13.14	n_activ_prod
238U	11.91	SNM
106Rh	11.71	Fiss_Prod
48V	9.59	medical_from_Ti-
152Eu	9.36	Fiss_Prod
125Sn	8.50	Fiss_Prod
240Np	7.54	SNM
92Y	5.71	Fiss_Prod
56Mn	5.28	c
234Pa	5.15	U-238_Daughter
214Bi	4.96	U-238_Daughter
133Te	4.76	Fiss_Prod
134I	2.65	Fiss_Prod
88Kr	2.51	Fiss_Prod
89Rb	2.50	Fiss_Prod
141Ba	2.39	Fiss_Prod

Score Details for Shielding Options:

-----  
Possible Shielding Setting: 1 Total Score: 2884.07  
Shielding Material: Pb Thickness (cm): 10.00

Note:

base score : fuction of (#matched/#emissions), weighted by yield,detectability and matching factor  
bonus I : bonus from number of matched peaks  
bonus II : bonus from relative peak height  
bonus III : bonus from alignment between peakheights and emission yields

Score Summary:

Nuclide	Total	(base + bonus I, II, III)	Comment	Correlation
140La	121.88	( 93.5 5.9 22.5 0.0 )	Fiss_Prod	High
132I	119.91	( 35.1 50.0 34.8 0.0 )	Fiss_Prod	High
238Np	118.89	( 83.0 0.7 5.1 30.0 )	SNM	High
135I	109.65	( 33.7 44.4 31.5 0.0 )	Fiss_Prod	High
42K	102.39	( 98.0 0.0 4.4 0.0 )	c	Moderate
58Co	102.34	( 97.5 0.0 4.9 0.0 )	c	Moderate
88Rb	102.18	( 93.9 0.8 2.5 5.0 )	Fiss_Prod	Moderate
106Rh	101.60	( 99.1 0.0 2.5 0.0 )	Fiss_Prod	Moderate
106Ru	101.60	( 99.1 0.0 2.5 0.0 )	Fiss_Prod	Moderate
211Pb	101.27	( 96.5 0.0 4.8 0.0 )	U-235_Daughter	Moderate
143La	100.57	( 98.9 0.0 1.7 0.0 )	Fiss_Prod	Moderate
54Mn	100.54	( 95.8 0.0 4.8 0.0 )	c	Moderate
52Mn	100.33	( 98.0 0.0 2.3 0.0 )	c	Moderate
124Sb	100.12	( 86.2 2.9 11.0 0.0 )	Fiss_Prod	Moderate
209Tl	99.31	( 97.5 0.0 1.8 0.0 )	Np-237_Daughter	Moderate
212Bi	95.94	( 89.7 0.0 6.2 0.0 )	Th-232_Daughter	Low
238U	93.94	( 91.3 0.0 2.6 0.0 )	SNM	Low
228Ac	91.31	( 71.1 4.6 13.5 2.0 )	Th-232_Daughter	Low
136Cs	90.11	( 79.9 0.7 7.5 2.0 )	Fiss_Prod	Low
52Mn	83.64	( 81.4 0.0 2.3 0.0 )	c	Low
138Cs	81.63	( 72.4 0.6 8.6 0.0 )	Fiss_Prod	Low
166mHo	80.38	( 75.0 0.6 4.8 0.0 )	Fiss_Prod	Low
48Sc	76.20	( 50.3 0.7 5.2 20.0 )	c	Low
152Eu	74.87	( 67.4 0.6 4.9 2.0 )	Fiss_Prod	Low
92Y	68.28	( 66.0 0.0 2.3 0.0 )	Fiss_Prod	Low

24Na	64.77	( 62.2	0.0	2.6	0.0 )	n_activ_prod	Low
56Mn	61.97	( 60.5	0.0	1.5	0.0 )	c	Low
134I	58.39	( 37.7	4.1	14.5	2.0 )	Fiss_Prod	Low
234Pa	58.10	( 29.6	12.3	11.2	5.0 )	U-238_Daughter	Low
240Np	57.85	( 54.5	0.6	2.8	0.0 )	SNM	Low
125Sn	56.70	( 48.7	0.6	7.3	0.0 )	Fiss_Prod	Low
214Bi	55.28	( 26.4	8.6	18.3	2.0 )	U-238_Daughter	Low
133Te	52.14	( 41.9	1.5	6.7	2.0 )	Fiss_Prod	Low

Scored nuclides details:

Nuclide	Score	T1/2	T1/2_unit	#EmissionInRange	#Matched	Correlation	Comment
140La	121.88	4.0300E+01	h	28	6	High	Fiss_Prod
Emission(KeV)	Prob/DK	Detectability	2.00% Energy Window		Peak(KeV)	Norm%_cts	
306.90	2.4800E-04	3.6098E-01	( 300.76 to 313.04 )				
328.76	2.0300E-01	3.2465E-01	( 322.18 to 335.34 )				
397.52	7.3500E-04	2.2929E-01	( 389.57 to 405.47 )				
432.49	2.9000E-02	1.9717E-01	( 423.84 to 441.14 )				
438.50	3.9100E-04	1.9216E-01	( 429.73 to 447.27 )				
445.50	2.8600E-05	1.8648E-01	( 436.59 to 454.41 )				
487.02	4.5500E-01	1.5575E-01	( 477.28 to 496.76 )				
618.12	3.7200E-04	9.7921E-02	( 605.76 to 630.48 )				
751.64	4.3300E-02	6.7795E-02	( 736.61 to 766.67 )				
+ 815.77	2.3300E-01	5.7399E-02	( 799.45 to 832.09 )		819.18	12.5980	
867.85	5.5000E-02	5.1687E-02	( 850.49 to 885.21 )				
919.55	2.6600E-02	4.6557E-02	( 901.16 to 937.94 )				
925.19	6.9000E-02	4.6027E-02	( 906.69 to 943.69 )				
950.99	5.1900E-03	4.3679E-02	( 931.97 to 970.01 )				
+ 992.90	1.3400E-04	4.0107E-02	( 973.04 to 1012.76 )		982.70	7.0005	
+ 1045.05	2.4800E-04	3.6570E-02	( 1024.15 to 1065.95 )		1048.70	6.1891	
1097.20	2.2900E-04	3.3807E-02	( 1075.26 to 1119.14 )				
1303.50	4.2000E-04	2.5172E-02	( 1277.43 to 1329.57 )				
+ 1405.20	5.9100E-04	2.2308E-02	( 1377.10 to 1433.30 )		1423.50	5.8521	
+ 1596.21	9.5400E-01	1.8269E-02	( 1564.29 to 1628.13 )		1608.50	15.9419	
1877.29	4.1000E-04	1.4166E-02	( 1839.74 to 1914.84 )				
1924.62	1.3400E-04	1.3570E-02	( 1886.13 to 1963.11 )				
2083.20	1.1500E-04	1.1978E-02	( 2041.54 to 2124.86 )				
2347.88	8.4900E-03	1.0254E-02	( 2300.92 to 2394.84 )				
2464.10	1.1400E-04	9.5771E-03	( 2414.82 to 2513.38 )				
2521.40	3.4600E-02	9.2597E-03	( 2470.97 to 2571.83 )				
2547.34	1.0100E-03	9.1195E-03	( 2496.39 to 2598.29 )				
+ 2899.61	6.6800E-04	7.4109E-03	( 2841.62 to 2957.60 )		2901.00	9.8274	

Nuclide	Score	T1/2	T1/2_unit	#EmissionInRange	#Matched	Correlation	Comment
132I	119.91	2.3000E+00	h	147	35	High	Fiss_Prod
Emission(KeV)	Prob/DK	Detectability	2.00% Energy Window		Peak(KeV)	Norm%_cts	
302.00	1.9700E-04	3.6957E-01	( 295.96 to 308.04 )				
306.70	1.9740E-03	3.6133E-01	( 300.57 to 312.83 )				
310.10	8.8800E-04	3.5547E-01	( 303.90 to 316.30 )				
310.40	8.8800E-04	3.5495E-01	( 304.19 to 316.61 )				
316.70	1.2800E-03	3.4430E-01	( 310.37 to 323.03 )				
343.70	8.8800E-04	3.0158E-01	( 336.83 to 350.57 )				
351.80	7.9000E-04	2.8964E-01	( 344.76 to 358.84 )				
363.34	4.9400E-03	2.7331E-01	( 356.07 to 370.61 )				
387.90	8.8800E-03	2.4105E-01	( 380.14 to 395.66 )				
416.80	4.7400E-03	2.1080E-01	( 408.46 to 425.14 )				
431.80	4.7400E-03	1.9775E-01	( 423.16 to 440.44 )				
445.00	9.8700E-04	1.8688E-01	( 436.10 to 453.90 )				
446.20	6.0200E-03	1.8592E-01	( 437.28 to 455.12 )				
473.60	1.6800E-03	1.6514E-01	( 464.13 to 483.07 )				
478.20	1.6800E-03	1.6187E-01	( 468.64 to 487.76 )				
488.00	8.3000E-03	1.5509E-01	( 478.24 to 497.76 )				
505.79	4.9400E-02	1.4415E-01	( 495.67 to 515.91 )				
522.65	1.6000E-01	1.3578E-01	( 512.20 to 533.10 )				
535.40	5.1300E-03	1.2975E-01	( 524.69 to 546.11 )				
547.20	1.1400E-02	1.2440E-01	( 536.26 to 558.14 )				
559.70	8.8800E-04	1.1895E-01	( 548.51 to 570.89 )				

572.50	5.9200E-04	1.1361E-01	(	561.05	to	583.95	)		
591.10	1.3820E-03	1.0624E-01	(	579.28	to	602.92	)		
600.00	2.5600E-03	1.0288E-01	(	588.00	to	612.00	)		
609.80	3.9500E-04	1.0017E-01	(	597.60	to	622.00	)		
621.14	1.9750E-02	9.7118E-02	(	608.72	to	633.56	)		
630.19	1.3300E-01	9.4747E-02	(	617.59	to	642.79	)		
642.20	3.9500E-04	9.1685E-02	(	629.36	to	655.04	)		
650.50	2.5700E-02	8.9624E-02	(	637.49	to	663.51	)		
667.72	9.8700E-01	8.5488E-02	(	654.37	to	681.07	)		
669.80	4.6400E-02	8.5001E-02	(	656.40	to	683.20	)		
671.40	3.4500E-02	8.4628E-02	(	657.97	to	684.83	)		
684.40	7.9000E-04	8.1655E-02	(	670.71	to	698.09	)		
687.80	3.9500E-04	8.0894E-02	(	674.04	to	701.56	)		
706.40	1.9700E-04	7.6848E-02	(	692.27	to	720.53	)		
727.12	5.3300E-02	7.2568E-02	(	712.58	to	741.66	)		
728.40	1.5800E-02	7.2311E-02	(	713.83	to	742.97	)		
771.70	1.9700E-04	6.4115E-02	(	756.27	to	787.13	)		
772.60	7.5600E-01	6.3954E-02	(	757.15	to	788.05	)		
780.00	1.1800E-02	6.2648E-02	(	764.40	to	795.60	)		
784.40	3.8500E-03	6.1884E-02	(	768.71	to	800.09	)		
791.20	9.8700E-04	6.0720E-02	(	775.38	to	807.02	)		
+ 809.50	2.5700E-02	5.8126E-02	(	793.31	to	825.69	)	819.18	12.5980
+ 812.00	5.5300E-02	5.7835E-02	(	795.76	to	828.24	)	819.18	12.5980
+ 831.30	2.4700E-04	5.5635E-02	(	814.67	to	847.93	)	819.18	12.5980
847.90	1.6800E-04	5.3808E-02	(	830.94	to	864.86	)		
863.00	5.6300E-03	5.2195E-02	(	845.74	to	880.26	)		
866.00	7.1000E-04	5.1880E-02	(	848.68	to	883.32	)		
876.60	1.0400E-02	5.0782E-02	(	859.07	to	894.13	)		
886.10	2.4700E-04	4.9817E-02	(	868.38	to	903.82	)		
888.70	6.9000E-04	4.9556E-02	(	870.93	to	906.47	)		
904.40	1.2800E-04	4.8007E-02	(	886.31	to	922.49	)		
910.10	9.2800E-03	4.7456E-02	(	891.90	to	928.30	)		
927.40	4.1500E-03	4.5822E-02	(	908.85	to	945.95	)		
947.20	4.4400E-04	4.4017E-02	(	928.26	to	966.14	)		
954.55	1.7600E-01	4.3364E-02	(	935.46	to	973.64	)		
+ 965.80	3.4500E-04	4.2383E-02	(	946.48	to	985.12	)	982.70	7.0005
+ 984.20	5.9200E-03	4.0825E-02	(	964.52	to	1003.88	)	982.70	7.0005
+ 995.80	2.9600E-04	3.9871E-02	(	975.88	to	1015.72	)	982.70	7.0005
+ 1002.50	5.1400E-04	3.9337E-02	(	982.45	to	1022.55	)	982.70	7.0005
1005.40	1.5800E-04	3.9114E-02	(	985.29	to	1025.51	)		
1009.00	4.6400E-04	3.8839E-02	(	988.82	to	1029.18	)		
+ 1035.00	5.1300E-03	3.7127E-02	(	1014.30	to	1055.70	)	1048.70	6.1891
+ 1049.60	4.6400E-04	3.6321E-02	(	1028.61	to	1070.59	)	1048.70	6.1891
1081.80	3.4500E-04	3.4602E-02	(	1060.16	to	1103.44	)		
1086.20	7.9000E-04	3.4373E-02	(	1064.48	to	1107.92	)		
1096.90	4.4400E-04	3.3823E-02	(	1074.96	to	1118.84	)		
1112.40	6.5100E-04	3.3040E-02	(	1090.15	to	1134.65	)		
1126.50	9.8800E-04	3.2344E-02	(	1103.97	to	1149.03	)		
1136.00	3.0100E-02	3.1883E-02	(	1113.28	to	1158.72	)		
1143.30	1.3500E-02	3.1533E-02	(	1120.43	to	1166.17	)		
1147.80	2.6600E-03	3.1319E-02	(	1124.84	to	1170.76	)		
1172.90	1.0900E-02	3.0150E-02	(	1149.44	to	1196.36	)		
1212.30	1.1800E-04	2.8401E-02	(	1188.05	to	1236.55	)		
1242.60	8.8800E-05	2.7122E-02	(	1217.75	to	1267.45	)		
1254.10	5.9200E-04	2.6689E-02	(	1229.02	to	1279.18	)		
1263.60	2.6600E-04	2.6390E-02	(	1238.33	to	1288.87	)		
1272.80	1.6800E-03	2.6104E-02	(	1247.34	to	1298.26	)		
1290.80	1.1300E-02	2.5554E-02	(	1264.98	to	1316.62	)		
1295.10	1.8800E-02	2.5424E-02	(	1269.20	to	1321.00	)		
1297.91	8.8800E-03	2.5339E-02	(	1271.95	to	1323.87	)		
1314.00	5.9200E-04	2.4861E-02	(	1287.72	to	1340.28	)		
1317.93	1.1800E-03	2.4745E-02	(	1291.57	to	1344.29	)		
1360.00	5.9200E-05	2.3540E-02	(	1332.80	to	1387.20	)		
1372.07	2.4700E-02	2.3204E-02	(	1344.63	to	1399.51	)		
1390.70	1.4800E-04	2.2696E-02	(	1362.89	to	1418.51	)		
+ 1398.57	7.0100E-02	2.2484E-02	(	1370.60	to	1426.54	)	1423.50	5.8521
+ 1410.60	4.3400E-04	2.2165E-02	(	1382.39	to	1438.81	)	1423.50	5.8521
+ 1442.56	1.4000E-02	2.1337E-02	(	1413.71	to	1471.41	)	1423.50	5.8521
+ 1450.00	7.9000E-05	2.1149E-02	(	1421.00	to	1479.00	)	1423.50	5.8521
1456.50	4.9400E-04	2.0985E-02	(	1427.37	to	1485.63	)		

1476.70	1.3000E-03	2.0486E-02	( 1447.17 to 1506.23 )				
+ 1519.60	7.9000E-04	1.9575E-02	( 1489.21 to 1549.99 )	1513.00		11.2602	
+ 1531.90	5.9200E-05	1.9359E-02	( 1501.26 to 1562.54 )	1513.00		11.2602	
+ 1542.30	1.5800E-04	1.9179E-02	( 1511.45 to 1573.15 )	1550.90		4.7449	
+ 1559.00	8.8800E-05	1.8892E-02	( 1527.82 to 1590.18 )	1550.90		4.7449	
+ 1592.90	4.7400E-04	1.8323E-02	( 1561.04 to 1624.76 )	1608.50		15.9419	
+ 1617.90	9.8700E-05	1.7915E-02	( 1585.54 to 1650.26 )	1608.50		15.9419	
+ 1618.90	6.9100E-05	1.7898E-02	( 1586.52 to 1651.28 )	1608.50		15.9419	
+ 1636.50	2.3600E-04	1.7616E-02	( 1603.77 to 1669.23 )	1608.50		15.9419	
+ 1639.10	7.9000E-05	1.7575E-02	( 1606.32 to 1671.88 )	1608.50		15.9419	
+ 1644.00	1.2800E-04	1.7497E-02	( 1611.12 to 1676.88 )	1676.80		9.3111	
+ 1661.40	1.5800E-04	1.7225E-02	( 1628.17 to 1694.63 )	1676.80		9.3111	
+ 1671.30	2.1700E-04	1.7071E-02	( 1637.87 to 1704.73 )	1676.80		9.3111	
+ 1679.30	5.9200E-05	1.6948E-02	( 1645.71 to 1712.89 )	1676.80		9.3111	
+ 1715.40	5.5300E-04	1.6404E-02	( 1681.09 to 1749.71 )	1717.70		4.2512	
+ 1720.60	5.4300E-04	1.6327E-02	( 1686.19 to 1755.01 )	1717.70		4.2512	
+ 1727.20	6.7100E-04	1.6230E-02	( 1692.66 to 1761.74 )	1717.70		4.2512	
+ 1752.30	2.4700E-04	1.5865E-02	( 1717.25 to 1787.35 )	1717.70		4.2512	
1757.40	2.9600E-03	1.5792E-02	( 1722.25 to 1792.55 )				
1760.40	5.9200E-04	1.5749E-02	( 1725.19 to 1795.61 )				
1768.50	2.4700E-04	1.5634E-02	( 1733.13 to 1803.87 )				
1778.50	7.9000E-04	1.5493E-02	( 1742.93 to 1814.07 )				
1786.50	2.1800E-04	1.5381E-02	( 1750.77 to 1822.23 )				
+ 1814.00	1.5800E-04	1.5003E-02	( 1777.72 to 1850.28 )	1828.40		3.7506	
+ 1830.10	2.7600E-04	1.4786E-02	( 1793.50 to 1866.70 )	1828.40		3.7506	
1879.20	1.3800E-04	1.4142E-02	( 1841.62 to 1916.78 )				
1913.70	2.9600E-04	1.3705E-02	( 1875.43 to 1951.97 )				
1921.08	1.2300E-02	1.3614E-02	( 1882.66 to 1959.50 )				
1925.70	1.9700E-05	1.3557E-02	( 1887.19 to 1964.21 )				
1939.50	4.9400E-05	1.3388E-02	( 1900.71 to 1978.29 )				
1985.64	1.1800E-04	1.2838E-02	( 1945.93 to 2025.35 )				
2002.20	1.1400E-02	1.2650E-02	( 1962.16 to 2042.24 )				
2086.82	2.5700E-03	1.1952E-02	( 2045.08 to 2128.56 )				
2172.68	2.0700E-03	1.1365E-02	( 2129.23 to 2216.13 )				
2187.00	6.9100E-05	1.1270E-02	( 2143.26 to 2230.74 )				
2204.20	2.9600E-05	1.1157E-02	( 2160.12 to 2248.28 )				
2223.17	1.1800E-03	1.1033E-02	( 2178.71 to 2267.63 )				
2249.10	3.3600E-04	1.0867E-02	( 2204.12 to 2294.08 )				
2290.60	3.5500E-05	1.0605E-02	( 2244.79 to 2336.41 )				
2390.48	1.8800E-03	1.0001E-02	( 2342.67 to 2438.29 )				
2408.60	9.3800E-05	9.8947E-03	( 2360.43 to 2456.77 )				
2416.90	1.3800E-05	9.8465E-03	( 2368.56 to 2465.24 )				
2444.00	5.6300E-05	9.6909E-03	( 2395.12 to 2492.88 )				
2454.80	2.0700E-05	9.6296E-03	( 2405.70 to 2503.90 )				
2487.80	7.9000E-06	9.4445E-03	( 2438.04 to 2537.56 )				
2525.14	3.9500E-04	9.2394E-03	( 2474.64 to 2575.64 )				
2546.50	1.5800E-05	9.1240E-03	( 2495.57 to 2597.43 )				
2569.80	4.9400E-05	8.9998E-03	( 2518.40 to 2621.20 )				
2593.80	1.1800E-05	8.8736E-03	( 2541.92 to 2645.68 )				
2603.20	1.4800E-05	8.8247E-03	( 2551.14 to 2655.26 )				
2607.20	9.8700E-06	8.8039E-03	( 2555.06 to 2659.34 )				
2614.50	3.5500E-05	8.7662E-03	( 2562.21 to 2666.79 )				
2653.80	9.8700E-06	8.5657E-03	( 2600.72 to 2706.88 )				
+ 2690.80	9.8700E-06	8.3811E-03	( 2636.98 to 2744.62 )	2708.20		2.6299	
+ 2717.50	3.4500E-05	8.2504E-03	( 2663.15 to 2771.85 )	2708.20		2.6299	
+ 2757.80	1.2800E-05	8.0569E-03	( 2702.64 to 2812.96 )	2779.90		6.6430	

Nuclide	Score	T1/2	T1/2_unit	#EmissionInRange	#Matched	Correlation	Comment
<sup>238</sup> Np	118.89	2.1200E+00	d	4	2	High	SNM
Emission(KeV)	Prob/DK	Detectability	2.00% Energy Window	Peak(KeV)	Norm%_cts		
923.98	2.4800E-02	4.6140E-02	( 905.50 to 942.46 )				
+ 984.45	2.3800E-01	4.0804E-02	( 964.76 to 1004.14 )	982.70	7.0005		
1025.90	8.2100E-02	3.7638E-02	( 1005.38 to 1046.42 )				
+ 1028.50	1.7400E-01	3.7492E-02	( 1007.93 to 1049.07 )	1048.70	6.1891		

Nuclide	Score	T1/2	T1/2_unit	#EmissionInRange	#Matched	Correlation	Comment
<sup>135</sup> I	109.65	6.5900E+00	h	79	18	High	Fiss_Prod

Emission(KeV)	Prob/DK	Detectability	2.00% Energy Window	Peak(KeV)	Norm%_cts
304.91	3.1600E-04	3.6445E-01	( 298.81 to 311.01 )		
305.83	9.5000E-04	3.6285E-01	( 299.71 to 311.95 )		
326.00	2.3000E-05	3.2906E-01	( 319.48 to 332.52 )		
333.60	3.7300E-04	3.1702E-01	( 326.93 to 340.27 )		
342.52	8.6100E-06	3.0335E-01	( 335.67 to 349.37 )		
361.85	1.8700E-03	2.7538E-01	( 354.61 to 369.09 )		
403.03	2.3200E-03	2.2346E-01	( 394.97 to 411.09 )		
414.83	3.0100E-03	2.1257E-01	( 406.53 to 423.13 )		
417.63	3.5300E-02	2.1006E-01	( 409.28 to 425.98 )		
429.93	3.0400E-03	1.9934E-01	( 421.33 to 438.53 )		
433.74	5.5400E-03	1.9612E-01	( 425.07 to 442.41 )		
451.63	3.1600E-03	1.8162E-01	( 442.60 to 460.66 )		
530.80	3.1600E-04	1.3190E-01	( 520.18 to 541.42 )		
546.56	7.1500E-02	1.2469E-01	( 535.63 to 557.49 )		
575.97	1.2900E-03	1.1220E-01	( 564.45 to 587.49 )		
588.28	5.1700E-04	1.0733E-01	( 576.51 to 600.05 )		
616.90	3.7300E-04	9.8248E-02	( 604.56 to 629.24 )		
649.85	4.5600E-03	8.9784E-02	( 636.85 to 662.85 )		
656.09	7.4600E-04	8.8261E-02	( 642.97 to 669.21 )		
679.22	5.4500E-04	8.2827E-02	( 665.64 to 692.80 )		
684.60	2.3000E-04	8.1610E-02	( 670.91 to 698.29 )		
690.13	1.2900E-03	8.0376E-02	( 676.33 to 703.93 )		
707.92	6.6000E-03	7.6526E-02	( 693.76 to 722.08 )		
785.48	1.5200E-03	6.1697E-02	( 769.77 to 801.19 )		
795.50	2.3000E-04	5.9994E-02	( 779.59 to 811.41 )		
797.71	1.7200E-03	5.9625E-02	( 781.76 to 813.66 )		
+ 807.20	4.5900E-04	5.8395E-02	( 791.06 to 823.34 )	819.18	12.5980
836.80	6.6900E-02	5.5023E-02	( 820.06 to 853.54 )		
960.29	3.4400E-04	4.2861E-02	( 941.08 to 979.50 )		
961.43	1.4600E-03	4.2762E-02	( 942.20 to 980.66 )		
+ 971.96	8.9000E-03	4.1855E-02	( 952.52 to 991.40 )	982.70	7.0005
+ 972.62	1.2100E-02	4.1799E-02	( 953.17 to 992.07 )	982.70	7.0005
+ 995.09	1.5500E-03	3.9928E-02	( 975.19 to 1014.99 )	982.70	7.0005
+ 1038.76	7.9500E-02	3.6918E-02	( 1017.98 to 1059.54 )	1048.70	6.1891
1096.86	8.9000E-04	3.3825E-02	( 1074.92 to 1118.80 )		
1101.58	1.6100E-02	3.3585E-02	( 1079.55 to 1123.61 )		
1124.00	3.6200E-02	3.2466E-02	( 1101.52 to 1146.48 )		
1131.51	2.2600E-01	3.2100E-02	( 1108.88 to 1154.14 )		
1151.51	2.8700E-05	3.1143E-02	( 1128.48 to 1174.54 )		
1159.90	1.0300E-03	3.0750E-02	( 1136.70 to 1183.10 )		
1169.04	8.7500E-03	3.0327E-02	( 1145.66 to 1192.42 )		
1180.46	6.3100E-04	2.9807E-02	( 1156.85 to 1204.07 )		
1225.60	4.3100E-04	2.7833E-02	( 1201.09 to 1250.11 )		
1240.47	9.0400E-03	2.7210E-02	( 1215.66 to 1265.28 )		
1254.80	1.1480E-04	2.6666E-02	( 1229.70 to 1279.90 )		
1260.41	2.8700E-01	2.6490E-02	( 1235.20 to 1285.62 )		
1277.83	5.7400E-04	2.5949E-02	( 1252.27 to 1303.39 )		
1308.70	3.4400E-04	2.5017E-02	( 1282.53 to 1334.87 )		
1315.77	6.6000E-04	2.4808E-02	( 1289.45 to 1342.09 )		
1334.80	3.1600E-04	2.4255E-02	( 1308.10 to 1361.50 )		
1343.66	7.7500E-04	2.4001E-02	( 1316.79 to 1370.53 )		
1367.89	6.0800E-03	2.3320E-02	( 1340.53 to 1395.25 )		
+ 1416.30	3.1600E-04	2.2015E-02	( 1387.97 to 1444.63 )	1423.50	5.8521
+ 1441.80	1.7200E-04	2.1356E-02	( 1412.96 to 1470.64 )	1423.50	5.8521
+ 1448.35	3.1600E-03	2.1190E-02	( 1419.38 to 1477.32 )	1423.50	5.8521
1457.56	8.6700E-02	2.0959E-02	( 1428.41 to 1486.71 )		
+ 1502.79	1.0800E-02	1.9874E-02	( 1472.73 to 1532.85 )	1513.00	11.2602
+ 1521.99	3.7300E-04	1.9533E-02	( 1491.55 to 1552.43 )	1513.00	11.2602
+ 1543.70	2.5800E-04	1.9155E-02	( 1512.83 to 1574.57 )	1550.90	4.7449
+ 1566.41	1.2900E-02	1.8766E-02	( 1535.08 to 1597.74 )	1550.90	4.7449
+ 1613.75	2.5800E-04	1.7982E-02	( 1581.48 to 1646.03 )	1608.50	15.9419
+ 1678.03	9.5600E-02	1.6968E-02	( 1644.47 to 1711.59 )	1676.80	9.3111
+ 1706.46	4.1000E-02	1.6537E-02	( 1672.33 to 1740.59 )	1717.70	4.2512
+ 1742.00	1.7200E-04	1.6014E-02	( 1707.16 to 1776.84 )	1717.70	4.2512
1791.20	7.7200E-02	1.5316E-02	( 1755.38 to 1827.02 )		
+ 1830.69	5.8000E-03	1.4778E-02	( 1794.08 to 1867.30 )	1828.40	3.7506
+ 1845.30	5.7400E-05	1.4583E-02	( 1808.39 to 1882.21 )	1828.40	3.7506
1927.30	2.9600E-03	1.3537E-02	( 1888.75 to 1965.85 )		

1948.49	6.3100E-04	1.3279E-02	(	1909.52	to	1987.46	)
2045.88	8.7200E-03	1.2243E-02	(	2004.96	to	2086.80	)
2112.40	6.8900E-04	1.1774E-02	(	2070.15	to	2154.65	)
2151.50	2.2400E-04	1.1507E-02	(	2108.47	to	2194.53	)
2179.70	4.0200E-05	1.1318E-02	(	2136.11	to	2223.29	)
2189.40	1.2900E-04	1.1254E-02	(	2145.61	to	2233.19	)
2255.46	6.1400E-03	1.0826E-02	(	2210.35	to	2300.57	)
2408.65	9.5600E-03	9.8944E-03	(	2360.48	to	2456.82	)
2452.80	8.6100E-05	9.6409E-03	(	2403.74	to	2501.86	)
2466.07	7.1800E-04	9.5660E-03	(	2416.75	to	2515.39	)
2477.10	1.4400E-05	9.5041E-03	(	2427.56	to	2526.64	)

Nuclide	Score	T1/2	T1/2_unit	#EmissionInRange	#Matched	Correlation	Comment
42K	102.39	1.2400E+01	h	2	1	Moderate	c
Emission(KeV)	Prob/DK	Detectability		2.00% Energy Window	Peak(KeV)	Norm%_cts	
312.70	3.1900E-03	3.5103E-01	(	306.45 to 318.95	)		
+ 1524.70	1.7900E-01	1.9485E-02	(	1494.21 to 1555.19	)	1513.00	11.2602

Nuclide	Score	T1/2	T1/2_unit	#EmissionInRange	#Matched	Correlation	Comment
58Co	102.34	1.9400E-01	y	1	1	Moderate	c
Emission(KeV)	Prob/DK	Detectability		2.00% Energy Window	Peak(KeV)	Norm%_cts	
+ 810.76	9.9400E-01	5.7979E-02	(	794.54 to 826.98	)	819.18	12.5980

Nuclide	Score	T1/2	T1/2_unit	#EmissionInRange	#Matched	Correlation	Comment
88Rb	102.18	1.7800E+01	m	3	2	Moderate	Fiss_Prod
Emission(KeV)	Prob/DK	Detectability		2.00% Energy Window	Peak(KeV)	Norm%_cts	
898.02	1.4000E-01	4.8631E-02	(	880.06 to 915.98	)		
+ 1836.00	2.1400E-01	1.4707E-02	(	1799.28 to 1872.72	)	1828.40	3.7506
+ 2677.90	1.9600E-02	8.4450E-03	(	2624.34 to 2731.46	)	2708.20	2.6299

Nuclide	Score	T1/2	T1/2_unit	#EmissionInRange	#Matched	Correlation	Comment
106Rh	101.60	1.0000E+00	y	3	1	Moderate	Fiss_Prod
Emission(KeV)	Prob/DK	Detectability		2.00% Energy Window	Peak(KeV)	Norm%_cts	
512.00	2.0600E-01	1.4101E-01	(	501.76 to 522.24	)		
621.84	9.8100E-02	9.6932E-02	(	609.40 to 634.28	)		
+ 1050.50	1.7300E-02	3.6272E-02	(	1029.49 to 1071.51	)	1048.70	6.1891

Nuclide	Score	T1/2	T1/2_unit	#EmissionInRange	#Matched	Correlation	Comment
106Ru	101.60	1.0000E+00	y	2	1	Moderate	Fiss_Prod
Emission(KeV)	Prob/DK	Detectability		2.00% Energy Window	Peak(KeV)	Norm%_cts	
622.20	9.9500E-02	9.6837E-02	(	609.76 to 634.64	)		
+ 1050.50	1.5600E-02	3.6272E-02	(	1029.49 to 1071.51	)	1048.70	6.1891

Nuclide	Score	T1/2	T1/2_unit	#EmissionInRange	#Matched	Correlation	Comment
211Pb	101.27	6.8700E-05	y	3	1	Moderate	U-235_Daughter
Emission(KeV)	Prob/DK	Detectability		2.00% Energy Window	Peak(KeV)	Norm%_cts	
404.84	2.9400E-02	2.2176E-01	(	396.74 to 412.94	)		
427.08	1.3200E-02	2.0178E-01	(	418.54 to 435.62	)		
+ 831.96	2.8600E-02	5.5562E-02	(	815.32 to 848.60	)	819.18	12.5980

Nuclide	Score	T1/2	T1/2_unit	#EmissionInRange	#Matched	Correlation	Comment
143La	100.57	1.4200E+01	m	1	1	Moderate	Fiss_Prod
Emission(KeV)	Prob/DK	Detectability		2.00% Energy Window	Peak(KeV)	Norm%_cts	
+ 1722.90	1.6800E-02	1.6293E-02	(	1688.44 to 1757.36	)	1717.70	4.2512

Nuclide	Score	T1/2	T1/2_unit	#EmissionInRange	#Matched	Correlation	Comment
54Mn	100.54	8.5500E-01	y	1	1	Moderate	c
Emission(KeV)	Prob/DK	Detectability	2.00% Energy Window	Peak(KeV)	Norm%_cts		
+ 834.83	1.0000E+00	5.5242E-02	( 818.13 to 851.53 )	819.18	12.5980		
Nuclide	Score	T1/2	T1/2_unit	#EmissionInRange	#Matched	Correlation	Comment
52Mn	100.33	2.1100E+01	m	3	1	Moderate	c
Emission(KeV)	Prob/DK	Detectability	2.00% Energy Window	Peak(KeV)	Norm%_cts		
377.74	1.6800E-02	2.5399E-01	( 370.19 to 385.29 )				
511.00	1.9300E+00	1.4151E-01	( 500.78 to 521.22 )				
+ 1434.10	9.8200E-01	2.1553E-02	( 1405.42 to 1462.78 )	1423.50	5.8521		
Nuclide	Score	T1/2	T1/2_unit	#EmissionInRange	#Matched	Correlation	Comment
124Sb	100.12	1.6500E-01	y	13	4	Moderate	Fiss_Prod
Emission(KeV)	Prob/DK	Detectability	2.00% Energy Window	Peak(KeV)	Norm%_cts		
602.71	9.7900E-01	1.0212E-01	( 590.66 to 614.76 )				
645.85	7.2600E-02	9.0773E-02	( 632.93 to 658.77 )				
709.31	1.4200E-02	7.6233E-02	( 695.12 to 723.50 )				
713.82	2.3800E-02	7.5288E-02	( 699.54 to 728.10 )				
722.78	1.1100E-01	7.3445E-02	( 708.32 to 737.24 )				
+ 968.20	1.9200E-02	4.2177E-02	( 948.84 to 987.56 )	982.70	7.0005		
+ 1045.20	1.8600E-02	3.6562E-02	( 1024.30 to 1066.10 )	1048.70	6.1891		
1208.30	1.3400E-02	2.8574E-02	( 1184.13 to 1232.47 )				
1325.50	1.5000E-02	2.4524E-02	( 1298.99 to 1352.01 )				
1368.20	2.5100E-02	2.3311E-02	( 1340.84 to 1395.56 )				
+ 1436.60	1.1400E-02	2.1489E-02	( 1407.87 to 1465.33 )	1423.50	5.8521		
+ 1691.00	4.9000E-01	1.6770E-02	( 1657.18 to 1724.82 )	1676.80	9.3111		
2091.00	5.7300E-02	1.1923E-02	( 2049.18 to 2132.82 )				
Nuclide	Score	T1/2	T1/2_unit	#EmissionInRange	#Matched	Correlation	Comment
209Tl	99.31	4.1900E-06	y	2	1	Moderate	Np-237_Daughter
Emission(KeV)	Prob/DK	Detectability	2.00% Energy Window	Peak(KeV)	Norm%_cts		
465.07	9.6600E-01	1.7137E-01	( 455.77 to 474.37 )				
+ 1567.00	9.9700E-01	1.8756E-02	( 1535.66 to 1598.34 )	1550.90	4.7449		
Nuclide	Score	T1/2	T1/2_unit	#EmissionInRange	#Matched	Correlation	Comment
212Bi	95.94	1.1500E-04	y	3	1	Low	Th-232_Daughter
Emission(KeV)	Prob/DK	Detectability	2.00% Energy Window	Peak(KeV)	Norm%_cts		
727.17	1.1800E-01	7.2558E-02	( 712.63 to 741.71 )				
785.46	1.9700E-02	6.1701E-02	( 769.75 to 801.17 )				
+ 1620.60	2.7500E-02	1.7871E-02	( 1588.19 to 1653.01 )	1608.50	15.9419		
Nuclide	Score	T1/2	T1/2_unit	#EmissionInRange	#Matched	Correlation	Comment
238U	93.94	4.4700E+09	y	4	1	Low	SNM
Emission(KeV)	Prob/DK	Detectability	2.00% Energy Window	Peak(KeV)	Norm%_cts		
742.78	5.7600E-04	6.9484E-02	( 727.92 to 757.64 )				
766.37	2.1100E-03	6.5074E-02	( 751.04 to 781.70 )				
786.26	3.4900E-04	6.1563E-02	( 770.53 to 801.99 )				
+ 1001.04	6.0900E-03	3.9450E-02	( 981.02 to 1021.06 )	982.70	7.0005		
Nuclide	Score	T1/2	T1/2_unit	#EmissionInRange	#Matched	Correlation	Comment
228Ac	91.31	7.0000E-04	y	14	5	Low	Th-232_Daughter
Emission(KeV)	Prob/DK	Detectability	2.00% Energy Window	Peak(KeV)	Norm%_cts		
327.64	3.2100E-02	3.2643E-01	( 321.09 to 334.19 )				
338.32	1.1400E-01	3.0973E-01	( 331.55 to 345.09 )				
409.51	2.1300E-02	2.1742E-01	( 401.32 to 417.70 )				
463.00	4.4300E-02	1.7291E-01	( 453.74 to 472.26 )				



	772.17	1.5500E-02	6.4031E-02	( 756.73 to 787.61 )				
	794.70	4.6300E-02	6.0129E-02	( 778.81 to 810.59 )				
+	835.50	1.7500E-02	5.5167E-02	( 818.79 to 852.21 )	819.18	12.5980		
	911.07	2.7700E-01	4.7363E-02	( 892.85 to 929.29 )				
	947.77	4.1200E-02	4.3966E-02	( 928.81 to 966.73 )				
+	964.60	5.2100E-02	4.2487E-02	( 945.31 to 983.89 )	982.70	7.0005		
+	969.11	1.6600E-01	4.2099E-02	( 949.73 to 988.49 )	982.70	7.0005		
+	1588.00	3.5500E-02	1.8405E-02	( 1556.24 to 1619.76 )	1608.50	15.9419		
+	1630.40	1.8600E-02	1.7714E-02	( 1597.79 to 1663.01 )	1608.50	15.9419		
-----								
Nuclide	Score	T1/2	T1/2_unit	#EmissionInRange	#Matched	Correlation	Comment	
<sup>136</sup> Cs	90.11	1.3100E+01	d	4	2	Low	Fiss_Prod	
Emission(KeV)	Prob/DK	Detectability	2.00% Energy Window		Peak(KeV)	Norm%_cts		
	340.57	4.8500E-01	3.0630E-01	( 333.76 to 347.38 )				
+	818.50	9.9700E-01	5.7085E-02	( 802.13 to 834.87 )	819.18	12.5980		
+	1048.10	7.9600E-01	3.6403E-02	( 1027.14 to 1069.06 )	1048.70	6.1891		
	1235.30	1.9700E-01	2.7425E-02	( 1210.59 to 1260.01 )				
-----								
Nuclide	Score	T1/2	T1/2_unit	#EmissionInRange	#Matched	Correlation	Comment	
<sup>52</sup> Mn	83.64	5.5900E+00	d	7	1	Low	c	
Emission(KeV)	Prob/DK	Detectability	2.00% Energy Window		Peak(KeV)	Norm%_cts		
	511.00	5.8800E-01	1.4151E-01	( 500.78 to 521.22 )				
	744.21	9.0000E-01	6.9209E-02	( 729.33 to 759.09 )				
	848.13	3.3200E-02	5.3783E-02	( 831.17 to 865.09 )				
	935.52	9.4500E-01	4.5073E-02	( 916.81 to 954.23 )				
	1246.20	4.2100E-02	2.6974E-02	( 1221.28 to 1271.12 )				
	1333.60	5.0700E-02	2.4289E-02	( 1306.93 to 1360.27 )				
+	1434.10	1.0000E+00	2.1553E-02	( 1405.42 to 1462.78 )	1423.50	5.8521		
-----								
Nuclide	Score	T1/2	T1/2_unit	#EmissionInRange	#Matched	Correlation	Comment	
<sup>138</sup> Cs	81.63	3.3400E+01	m	11	2	Low	Fiss_Prod	
Emission(KeV)	Prob/DK	Detectability	2.00% Energy Window		Peak(KeV)	Norm%_cts		
	408.98	4.6600E-02	2.1791E-01	( 400.80 to 417.16 )				
	462.79	3.0800E-01	1.7307E-01	( 453.53 to 472.05 )				
	546.94	1.0800E-01	1.2452E-01	( 536.00 to 557.88 )				
	871.80	5.1100E-02	5.1277E-02	( 854.36 to 889.24 )				
	1009.80	2.9800E-01	3.8778E-02	( 989.60 to 1030.00 )				
	1147.20	1.2400E-02	3.1347E-02	( 1124.26 to 1170.14 )				
	1343.60	1.1500E-02	2.4003E-02	( 1316.73 to 1370.47 )				
+	1435.90	7.6300E-01	2.1507E-02	( 1407.18 to 1464.62 )	1423.50	5.8521		
+	1613.20	1.6200E-02	1.7991E-02	( 1580.94 to 1645.46 )	1608.50	15.9419		
	2218.00	1.5200E-01	1.1067E-02	( 2173.64 to 2262.36 )				
	2639.60	7.6300E-02	8.6376E-03	( 2586.81 to 2692.39 )				
-----								
Nuclide	Score	T1/2	T1/2_unit	#EmissionInRange	#Matched	Correlation	Comment	
<sup>166</sup> Ho	80.38	1.2000E+03	y	16	2	Low	Fiss_Prod	
Emission(KeV)	Prob/DK	Detectability	2.00% Energy Window		Peak(KeV)	Norm%_cts		
	300.74	3.7200E-02	3.7181E-01	( 294.73 to 306.75 )				
	365.78	2.4200E-02	2.6995E-01	( 358.46 to 373.10 )				
	410.94	1.1100E-01	2.1611E-01	( 402.72 to 419.16 )				
	451.52	2.9200E-02	1.8171E-01	( 442.49 to 460.55 )				
	464.83	1.2000E-02	1.7155E-01	( 455.53 to 474.13 )				
	529.81	9.5100E-02	1.3236E-01	( 519.21 to 540.41 )				
	571.00	5.4700E-02	1.1422E-01	( 559.58 to 582.42 )				
	611.52	1.4200E-02	9.9699E-02	( 599.29 to 623.75 )				
	670.51	5.3500E-02	8.4835E-02	( 657.10 to 683.92 )				
	691.21	1.3600E-02	8.0137E-02	( 677.39 to 705.03 )				
	711.69	5.4100E-01	7.5733E-02	( 697.46 to 725.92 )				
	752.27	1.2100E-01	6.7677E-02	( 737.22 to 767.32 )				
	778.82	3.0300E-02	6.2855E-02	( 763.24 to 794.40 )				
+	810.31	5.7100E-01	5.8032E-02	( 794.10 to 826.52 )	819.18	12.5980		
+	830.56	9.6600E-02	5.5718E-02	( 813.95 to 847.17 )	819.18	12.5980		

950.94 2.6900E-02 4.3683E-02 ( 931.92 to 969.96 )

Nuclide	Score	T1/2	T1/2_unit	#EmissionInRange	#Matched	Correlation	Comment
48Sc	76.20	4.3700E+01	h	4	2	Low	c

Emission(KeV)	Prob/DK	Detectability	2.00% Energy Window	Peak(KeV)	Norm%_cts
+ 983.50	1.0000E+00	4.0883E-02	( 963.83 to 1003.17 )	982.70	7.0005
+ 1037.50	9.7500E-01	3.6988E-02	( 1016.75 to 1058.25 )	1048.70	6.1891
1212.80	2.3800E-02	2.8379E-02	( 1188.54 to 1237.06 )		
1312.10	1.0000E+00	2.4917E-02	( 1285.86 to 1338.34 )		

Nuclide	Score	T1/2	T1/2_unit	#EmissionInRange	#Matched	Correlation	Comment
152Eu	74.87	1.3400E+01	y	12	2	Low	Fiss_Prod

Emission(KeV)	Prob/DK	Detectability	2.00% Energy Window	Peak(KeV)	Norm%_cts
344.27	2.6500E-01	3.0073E-01	( 337.38 to 351.16 )		
411.11	2.2100E-02	2.1595E-01	( 402.89 to 419.33 )		
443.98	2.8100E-02	1.8770E-01	( 435.10 to 452.86 )		
778.89	1.2700E-01	6.2842E-02	( 763.31 to 794.47 )		
867.32	4.1600E-02	5.1742E-02	( 849.97 to 884.67 )		
+ 964.01	1.4400E-01	4.2538E-02	( 944.73 to 983.29 )	982.70	7.0005
1085.80	9.9600E-02	3.4394E-02	( 1064.08 to 1107.52 )		
1089.70	1.6800E-02	3.4192E-02	( 1067.91 to 1111.49 )		
1112.00	1.3300E-01	3.3060E-02	( 1089.76 to 1134.24 )		
1212.80	1.3800E-02	2.8379E-02	( 1188.54 to 1237.06 )		
1299.00	1.6100E-02	2.5307E-02	( 1273.02 to 1324.98 )		
+ 1408.00	2.0800E-01	2.2234E-02	( 1379.84 to 1436.16 )	1423.50	5.8521

Nuclide	Score	T1/2	T1/2_unit	#EmissionInRange	#Matched	Correlation	Comment
92Y	68.28	3.5400E+00	h	5	1	Low	Fiss_Prod

Emission(KeV)	Prob/DK	Detectability	2.00% Energy Window	Peak(KeV)	Norm%_cts
448.50	2.3400E-02	1.8408E-01	( 439.53 to 457.47 )		
561.10	2.4100E-02	1.1836E-01	( 549.88 to 572.32 )		
844.30	2.1500E-02	5.4199E-02	( 827.41 to 861.19 )		
934.46	1.3900E-01	4.5170E-02	( 915.77 to 953.15 )		
+ 1405.40	4.7800E-02	2.2302E-02	( 1377.29 to 1433.51 )	1423.50	5.8521

Nuclide	Score	T1/2	T1/2_unit	#EmissionInRange	#Matched	Correlation	Comment
24Na	64.77	1.5000E+01	h	2	1	Low	n_activ_proc

Emission(KeV)	Prob/DK	Detectability	2.00% Energy Window	Peak(KeV)	Norm%_cts
1368.50	1.0000E+00	2.3303E-02	( 1341.13 to 1395.87 )		
+ 2754.10	9.9900E-01	8.0745E-03	( 2699.02 to 2809.18 )	2779.90	6.6430

Nuclide	Score	T1/2	T1/2_unit	#EmissionInRange	#Matched	Correlation	Comment
56Mn	61.97	2.5800E+00	h	3	1	Low	c

Emission(KeV)	Prob/DK	Detectability	2.00% Energy Window	Peak(KeV)	Norm%_cts
846.75	9.8900E-01	5.3932E-02	( 829.81 to 863.69 )		
+ 1810.70	2.7200E-01	1.5048E-02	( 1774.49 to 1846.91 )	1828.40	3.7506
2113.10	1.4300E-01	1.1769E-02	( 2070.84 to 2155.36 )		

Nuclide	Score	T1/2	T1/2_unit	#EmissionInRange	#Matched	Correlation	Comment
134I	58.39	5.2500E+01	m	25	5	Low	Fiss_Prod

Emission(KeV)	Prob/DK	Detectability	2.00% Energy Window	Peak(KeV)	Norm%_cts
405.45	7.3500E-02	2.2119E-01	( 397.34 to 413.56 )		
433.35	4.1900E-02	1.9645E-01	( 424.68 to 442.02 )		
458.92	1.3000E-02	1.7599E-01	( 449.74 to 468.10 )		
488.88	1.4100E-02	1.5449E-01	( 479.10 to 498.66 )		
514.40	2.3400E-02	1.3982E-01	( 504.11 to 524.69 )		
540.83	7.8200E-02	1.2726E-01	( 530.01 to 551.65 )		
595.36	1.1400E-01	1.0462E-01	( 583.45 to 607.27 )		

621.79	1.0600E-01	9.6945E-02	(	609.35	to	634.23	)		
627.96	2.3700E-02	9.5326E-02	(	615.40	to	640.52	)		
677.34	8.4900E-02	8.3257E-02	(	663.79	to	690.89	)		
730.74	1.9100E-02	7.1844E-02	(	716.13	to	745.35	)		
766.68	4.1000E-02	6.5018E-02	(	751.35	to	782.01	)		
847.02	9.5400E-01	5.3903E-02	(	830.08	to	863.96	)		
857.29	6.9700E-02	5.2799E-02	(	840.14	to	874.44	)		
884.09	6.5300E-01	5.0020E-02	(	866.41	to	901.77	)		
947.86	4.0400E-02	4.3958E-02	(	928.90	to	966.82	)		
+ 974.67	4.6800E-02	4.1625E-02	(	955.18	to	994.16	)	982.70	7.0005
+ 1040.30	1.9100E-02	3.6833E-02	(	1019.49	to	1061.11	)	1048.70	6.1891
1072.60	1.5300E-01	3.5085E-02	(	1051.15	to	1094.05	)		
1136.20	9.7300E-02	3.1873E-02	(	1113.48	to	1158.92	)		
1455.20	2.2900E-02	2.1018E-02	(	1426.10	to	1484.30	)		
+ 1613.80	4.3600E-02	1.7981E-02	(	1581.52	to	1646.08	)	1608.50	15.9419
+ 1741.50	2.6700E-02	1.6021E-02	(	1706.67	to	1776.33	)	1717.70	4.2512
1787.20	1.3400E-02	1.5372E-02	(	1751.46	to	1822.94	)		
+ 1806.80	5.7300E-02	1.5101E-02	(	1770.66	to	1842.94	)	1828.40	3.7506

Nuclide	Score	T1/2	T1/2_unit	#EmissionInRange	#Matched	Correlation	Comment
234Pa	58.10	7.6500E-04	y	44	9	Low	U-238_Daughter
Emission(KeV)	Prob/DK	Detectability	2.00% Energy Window	Peak(KeV)	Norm%_cts		
369.80	2.9600E-02	2.6450E-01	( 362.40 to 377.20 )				
372.40	1.3300E-02	2.6102E-01	( 364.95 to 379.85 )				
458.80	1.5300E-02	1.7609E-01	( 449.62 to 467.98 )				
506.80	1.6300E-02	1.4364E-01	( 496.66 to 516.94 )				
513.70	1.3300E-02	1.4017E-01	( 503.43 to 523.97 )				
565.90	1.4300E-02	1.1634E-01	( 554.58 to 577.22 )				
568.70	3.0600E-02	1.1517E-01	( 557.33 to 580.07 )				
569.50	1.0900E-01	1.1484E-01	( 558.11 to 580.89 )				
574.00	2.0400E-02	1.1300E-01	( 562.52 to 585.48 )				
664.80	1.3300E-02	8.6177E-02	( 651.50 to 678.10 )				
666.70	1.6300E-02	8.5728E-02	( 653.37 to 680.03 )				
669.90	1.4300E-02	8.4978E-02	( 656.50 to 683.30 )				
699.00	4.6900E-02	7.8434E-02	( 685.02 to 712.98 )				
706.10	3.1600E-02	7.6912E-02	( 691.98 to 720.22 )				
733.00	8.7700E-02	7.1395E-02	( 718.34 to 747.66 )				
738.00	1.0200E-02	7.0412E-02	( 723.24 to 752.76 )				
742.81	2.4500E-02	6.9479E-02	( 727.95 to 757.67 )				
755.60	1.4300E-02	6.7053E-02	( 740.49 to 770.71 )				
780.70	1.1200E-02	6.2526E-02	( 765.09 to 796.31 )				
786.27	1.4300E-02	6.1561E-02	( 770.54 to 802.00 )				
793.60	1.5300E-02	6.0314E-02	( 777.73 to 809.47 )				
796.30	3.8800E-02	5.9860E-02	( 780.37 to 812.23 )				
+ 805.60	3.3700E-02	5.8583E-02	( 789.49 to 821.71 )	819.18	12.5980		
+ 819.60	2.6500E-02	5.6959E-02	( 803.21 to 835.99 )	819.18	12.5980		
+ 826.30	4.0800E-02	5.6197E-02	( 809.77 to 842.83 )	819.18	12.5980		
+ 831.60	5.6100E-02	5.5602E-02	( 814.97 to 848.23 )	819.18	12.5980		
876.40	4.0800E-02	5.0803E-02	( 858.87 to 893.93 )				
880.51	1.3220E-01	5.0383E-02	( 862.90 to 898.12 )				
883.24	1.2200E-01	5.0106E-02	( 865.58 to 900.90 )				
899.00	4.1800E-02	4.8535E-02	( 881.02 to 916.98 )				
925.00	2.9600E-02	4.6045E-02	( 906.50 to 943.50 )				
926.00	1.1200E-01	4.5952E-02	( 907.48 to 944.52 )				
926.72	9.1800E-02	4.5885E-02	( 908.19 to 945.25 )				
946.00	1.2200E-01	4.4124E-02	( 927.08 to 964.92 )				
949.00	8.1600E-02	4.3856E-02	( 930.02 to 967.98 )				
955.59	1.0100E-02	4.3273E-02	( 936.48 to 974.70 )				
+ 978.80	1.4300E-02	4.1276E-02	( 959.22 to 998.38 )	982.70	7.0005		
+ 980.50	5.1000E-02	4.1134E-02	( 960.89 to 1000.11 )	982.70	7.0005		
+ 984.00	1.9400E-02	4.0841E-02	( 964.32 to 1003.68 )	982.70	7.0005		
1353.30	1.7300E-02	2.3728E-02	( 1326.23 to 1380.37 )				
1394.10	3.0600E-02	2.2604E-02	( 1366.22 to 1421.98 )				
1452.70	1.0200E-02	2.1081E-02	( 1423.65 to 1481.75 )				
+ 1668.50	1.2200E-02	1.7114E-02	( 1635.13 to 1701.87 )	1676.80	9.3111		
+ 1694.60	1.2200E-02	1.6715E-02	( 1660.71 to 1728.49 )	1676.80	9.3111		

Nuclide	Score	T1/2	T1/2_unit	#EmissionInRange	#Matched	Correlation	Comment
240Np	57.85	6.1900E+01	m	18	2	Low	SNM
Emission(KeV)	Prob/DK	Detectability	2.00% Energy Window	Peak(KeV)	Norm%_cts		
307.00	1.3900E-02	3.6081E-01	( 300.86 to 313.14 )				
448.20	1.6700E-01	1.8432E-01	( 439.24 to 457.16 )				
462.20	1.3900E-02	1.7351E-01	( 452.96 to 471.44 )				
467.40	2.0400E-02	1.6965E-01	( 458.05 to 476.75 )				
507.20	1.8500E-02	1.4343E-01	( 497.06 to 517.34 )				
566.40	2.6900E-01	1.1613E-01	( 555.07 to 577.73 )				
601.10	2.0400E-01	1.0257E-01	( 589.08 to 613.12 )				
606.10	1.5800E-02	1.0118E-01	( 593.98 to 618.22 )				
847.00	4.6400E-02	5.3905E-02	( 830.06 to 863.94 )				
867.40	8.3400E-02	5.1734E-02	( 850.05 to 884.75 )				
884.90	3.7100E-02	4.9938E-02	( 867.20 to 902.60 )				
888.80	1.1100E-02	4.9546E-02	( 871.02 to 906.58 )				
896.50	1.3000E-01	4.8781E-02	( 878.57 to 914.43 )				
915.98	1.3900E-02	4.6895E-02	( 897.66 to 934.30 )				
959.10	2.3200E-02	4.2965E-02	( 939.92 to 978.28 )				
+ 973.90	2.1300E-01	4.1690E-02	( 954.42 to 993.38 )	982.70	7.0005		
+ 987.76	4.6400E-02	4.0530E-02	( 968.00 to 1007.52 )	982.70	7.0005		
1167.60	4.6400E-02	3.0394E-02	( 1144.25 to 1190.95 )				

Nuclide	Score	T1/2	T1/2_unit	#EmissionInRange	#Matched	Correlation	Comment
125Sn	56.70	9.6400E+00	d	7	2	Low	Fiss_Prod
Emission(KeV)	Prob/DK	Detectability	2.00% Energy Window	Peak(KeV)	Norm%_cts		
331.90	1.2900E-02	3.1968E-01	( 325.26 to 338.54 )				
469.70	1.2900E-02	1.6796E-01	( 460.31 to 479.09 )				
+ 822.60	3.7800E-02	5.6617E-02	( 806.15 to 839.05 )	819.18	12.5980		
915.50	3.7800E-02	4.6940E-02	( 897.19 to 933.81 )				
+ 1066.60	8.6000E-02	3.5403E-02	( 1045.27 to 1087.93 )	1048.70	6.1891		
1088.90	4.0400E-02	3.4233E-02	( 1067.12 to 1110.68 )				
2001.70	2.0600E-02	1.2655E-02	( 1961.67 to 2041.73 )				

Nuclide	Score	T1/2	T1/2_unit	#EmissionInRange	#Matched	Correlation	Comment
214Bi	55.28	3.7900E-05	y	21	7	Low	U-238_Daughter
Emission(KeV)	Prob/DK	Detectability	2.00% Energy Window	Peak(KeV)	Norm%_cts		
609.31	4.6300E-01	1.0030E-01	( 597.12 to 621.50 )				
665.45	1.5700E-02	8.6023E-02	( 652.14 to 678.76 )				
768.36	5.0400E-02	6.4714E-02	( 752.99 to 783.73 )				
+ 806.17	1.2300E-02	5.8516E-02	( 790.05 to 822.29 )	819.18	12.5980		
934.06	3.2100E-02	4.5207E-02	( 915.38 to 952.74 )				
1120.30	1.5200E-01	3.2649E-02	( 1097.89 to 1142.71 )				
1155.20	1.7000E-02	3.0970E-02	( 1132.10 to 1178.30 )				
1158.00	3.5100E-02	3.0839E-02	( 1134.84 to 1181.16 )				
1238.10	5.9400E-02	2.7308E-02	( 1213.34 to 1262.86 )				
1281.00	1.4800E-02	2.5852E-02	( 1255.38 to 1306.62 )				
1377.70	4.1100E-02	2.3050E-02	( 1350.15 to 1405.25 )				
+ 1401.50	1.3900E-02	2.2406E-02	( 1373.47 to 1429.53 )	1423.50	5.8521		
+ 1408.00	2.4900E-02	2.2234E-02	( 1379.84 to 1436.16 )	1423.50	5.8521		
+ 1509.20	2.2200E-02	1.9759E-02	( 1479.02 to 1539.38 )	1513.00	11.2602		
+ 1661.30	1.1600E-02	1.7226E-02	( 1628.07 to 1694.53 )	1676.80	9.3111		
+ 1729.60	2.9700E-02	1.6195E-02	( 1695.01 to 1764.19 )	1717.70	4.2512		
1764.50	1.5800E-01	1.5691E-02	( 1729.21 to 1799.79 )				
+ 1847.40	2.0900E-02	1.4555E-02	( 1810.45 to 1884.35 )	1828.40	3.7506		
2118.60	1.1700E-02	1.1732E-02	( 2076.23 to 2160.97 )				
2204.20	4.9800E-02	1.1157E-02	( 2160.12 to 2248.28 )				
2447.90	1.5600E-02	9.6687E-03	( 2398.94 to 2496.86 )				

Nuclide	Score	T1/2	T1/2_unit	#EmissionInRange	#Matched	Correlation	Comment
133Te	52.14	1.2500E+01	m	14	3	Low	Fiss_Prod
Emission(KeV)	Prob/DK	Detectability	2.00% Energy Window	Peak(KeV)	Norm%_cts		
311.99	7.0800E-01	3.5224E-01	( 305.75 to 318.23 )				
407.63	3.0100E-01	2.1916E-01	( 399.48 to 415.78 )				
474.72	1.2000E-02	1.6434E-01	( 465.23 to 484.21 )				
719.65	6.6600E-02	7.4084E-02	( 705.26 to 734.04 )				
786.77	5.5900E-02	6.1476E-02	( 771.03 to 802.51 )				
844.39	3.2600E-02	5.4189E-02	( 827.50 to 861.28 )				
930.67	4.4600E-02	4.5519E-02	( 912.06 to 949.28 )				
+ 1000.80	6.2300E-02	3.9469E-02	( 980.78 to 1020.82 )	982.70	7.0005		
1021.10	2.6900E-02	3.7927E-02	( 1000.68 to 1041.52 )				
+ 1061.80	1.2700E-02	3.5660E-02	( 1040.56 to 1083.04 )	1048.70	6.1891		
1252.20	1.1300E-02	2.6749E-02	( 1227.16 to 1277.24 )				
1333.20	9.9100E-02	2.4301E-02	( 1306.54 to 1359.86 )				
+ 1717.70	3.4000E-02	1.6370E-02	( 1683.35 to 1752.05 )	1717.70	4.2512		
1881.50	0.0000E+00	1.4112E-02	( 1843.87 to 1919.13 )				

## 20<sup>th</sup> 5 min count with scattered scaling factor

```

=====
SmartID-XP
Extended Protocol Synthetic Resolution Identifier
Ver 2.5J
By
G. Sjoden, C. Yi, E. LaVigne, J. Paul
Georgia Institute of Technology
June 2014

Contact: sjoden@gatech.edu
=====

```

Spectrum Name: ../IrradExp/5minSpec/20th5min/20th5min.Spe

29 Peak(s) Identified - Sort by Energy

```

=====

```

keV	Counts	Norm% Cts	Peak Id
406.31	5.1644E+00	1.45805	29
561.22	5.4796E+00	1.54704	28
691.66	1.3893E+01	3.92237	27
741.17	1.6030E+01	4.52571	25
778.67	1.0878E+01	3.07116	26
819.18	2.9069E+01	8.20698	24
850.68	3.0968E+01	8.74312	22
886.69	8.7843E+00	2.48005	23
915.19	2.9952E+01	8.45627	20
951.20	8.7337E+00	2.46576	21
982.70	3.0774E+01	8.68834	17
1036.70	2.2716E+01	6.41335	18
1065.20	4.6785E+00	1.32087	19
1104.20	1.8239E+01	5.14937	15
1141.70	5.7442E+00	1.62175	16
1191.90	7.8767E+00	2.22381	14
1367.40	5.8251E+00	1.64459	13
1423.50	1.2242E+01	3.45625	11
1458.40	6.4509E+00	1.82127	12
1516.00	1.7488E+01	4.93734	9
1560.00	8.5854E+00	2.42389	10
1610.00	1.7273E+01	4.87664	5
1676.80	1.1816E+01	3.33598	6
1717.70	4.4869E+00	1.26677	8
1781.40	2.4019E+00	0.67812	7
1828.40	4.8666E+00	1.37397	4
2708.20	1.8004E+00	0.50830	3
2779.90	5.2930E+00	1.49436	2
2901.00	6.6891E+00	1.88852	1

Most Probable Shielding Settings:

```

=====

```

Shielding material	shielding size(cm)	score
Pb	8.000	7159.1
Pb	5.000	7110.9
Pb	4.000	7051.7
Pb	3.000	6980.2
Pb	6.000	6879.6
Pb	10.000	6772.5
Pb	2.000	6515.6
Fe	10.000	6360.6
Fe	8.000	6105.8
Fe	6.000	5820.9
Pb	1.000	5762.4
Fe	5.000	5661.9
Fe	4.000	5511.5
Pb	0.500	5446.6
Fe	3.000	5394.0

Score Correlation Threshold:

```

=====
High correlation: score > 108.0
Moderate correlation: score in between: [ 99.0, 108.0]

```

Low correlation: score < 99.0 with a cutoff at 50.0

Overall Mean Nuclide Scores (total\_scored=87):  
 [based on integral average of score from each nuclide for all shielding options]

```

=====
Nuclide      Score      Comment      Correlation
234Pa       153.34     U-238_Daughter  High
134I        143.24     Fiss_Prod      High
135I        133.30     Fiss_Prod      High
132I        131.57     Fiss_Prod      High
99Mo        124.89     medical_FP     High
56Mn        116.88     c              High
238Np       116.19     SNM           High
24Na        115.98     n_activ_prod   High
46Sc        111.78     c              High
131mTe      110.23     Fiss_Prod      High
48Sc        108.26     c              High
133mTe      107.44     Fiss_Prod      Moderate
88Rb        106.44     Fiss_Prod      Moderate
140La       101.65     Fiss_Prod      Moderate
97mNb       100.72     Fiss_Prod      Moderate
58Co        100.66     c              Moderate
40K         99.88     NORM          Moderate
97Zr        99.52     Fiss_Prod      Moderate
143La       99.39     Fiss_Prod      Moderate
136Cs       98.99     Fiss_Prod      Low
228Ac       98.60     Th-232_Daughter  Low
91Sr        98.59     Fiss_Prod      Low
141La       98.27     Fiss_Prod      Low
142Ba       96.50     Fiss_Prod      Low
57Co        96.24     c              Low
92Sr        95.80     Fiss_Prod      Low
93Y         95.45     Fiss_Prod      Low
129mTe      95.30     Fiss_Prod      Low
42K         95.00     c              Low
125Sn       93.94     Fiss_Prod      Low
65Zn        93.44     Fiss_Prod      Low
240Np       91.87     SNM           Low
151Pm       91.81     Fiss_Prod      Low
91mY        89.85     Fiss_Prod      Low
110mAg      88.69     Fiss_Prod      Low
152Eu       88.09     Fiss_Prod      Low
82Br        88.02     Fiss_Prod      Low
219Rn       84.51     U-235_Daughter  Low
134Te       84.10     Fiss_Prod      Low
247Cm       84.03     SNM           Low
87Kr        81.38     Fiss_Prod      Low
166mHo      80.86     Fiss_Prod      Low
214Bi       80.27     U-238_Daughter  Low
75Se        78.75     Fiss_Prod      Low
198Au       77.84     c              Low
160Tb       76.14     Fiss_Prod      Low
56Co        75.30     c              Low
156Eu       71.33     Fiss_Prod      Low
89Rb        68.12     Fiss_Prod      Low
143Ce       68.11     Fiss_Prod      Low
52Mn        68.02     c              Low
59Fe        67.74     c              Low
144Pr       67.45     Fiss_Prod      Low
84Br        66.47     Fiss_Prod      Low
187W        58.89     c              Low
126Sb       56.48     Fiss_Prod      Low
148Pm       55.89     Fiss_Prod      Low
57Ni        36.65     c              Low
209Tl       36.22     Np-237_Daughter  Low
212Bi       35.85     Th-232_Daughter  Low
211Pb       34.62     U-235_Daughter  Low
138Cs       34.59     Fiss_Prod      Low
92Y         32.60     Fiss_Prod      Low
124Sb       30.52     Fiss_Prod      Low
  
```

44Sc	29.60	-	c
131Te	29.53	Fiss_Prod	
52Mn	27.80		c
214Pb	26.42	U-238_Daughter	
141Ba	26.30	Fiss_Prod	
48V	26.05	medical_from_Ti-	
138Xe	25.47	Fiss_Prod	
233Pa	25.02	Np-237_Daughter	
130I	21.40	Fiss_Prod	
133Te	15.14	Fiss_Prod	
61Cu	14.72		c
106Ru	14.06	Fiss_Prod	
238U	13.87		SNM
106Rh	11.44	Fiss_Prod	
101Tc	9.70	Fiss_Prod	
140Ba	8.91	Fiss_Prod	
65Ni	4.69		c
97Nb	4.54	Fiss_Prod	
43K	4.51		c
90Y	4.46	Fiss_Prod	
147Nd	4.18	Fiss_Prod	
239Pu	2.84		SNM
105Ru	2.80	Fiss_Prod	

Score Details for Shielding Options:

-----  
Possible Shielding Setting: 1 Total Score: 7159.10  
Shielding Material: Pb Thickness (cm): 8.00

Note:

base score : fuction of (#matched/#emissions), weighted by yield,detectability and matching factor  
bonus I : bonus from number of matched peaks  
bonus II : bonus from relative peak height  
bonus III : bonus from alignment between peakheights and emission yields

Score Summary:

Nuclide	Total	(base + bonus I, II, III)	Comment	Correlation
234Pa	159.63	( 90.1 50.0 19.5 0.0 )	U-238_Daughter	High
134I	151.91	( 97.4 35.8 18.7 0.0 )	Fiss_Prod	High
132I	149.29	( 64.4 50.0 34.9 0.0 )	Fiss_Prod	High
135I	148.04	( 70.7 50.0 27.3 0.0 )	Fiss_Prod	High
140La	136.98	( 94.6 20.6 21.8 0.0 )	Fiss_Prod	High
151Pm	132.47	( 62.2 50.0 20.3 0.0 )	Fiss_Prod	High
46Sc	131.35	( 97.3 1.0 3.0 30.0 )		High
24Na	130.78	( 98.5 1.0 1.3 30.0 )	n_activ_prod	High
99Mo	126.22	( 98.9 10.7 16.6 0.0 )	medical_FP	High
133mTe	123.77	( 80.6 26.7 16.5 0.0 )	Fiss_Prod	High
131mTe	123.57	( 85.9 22.2 15.5 0.0 )	Fiss_Prod	High
110mAg	121.82	( 92.3 16.4 13.2 0.0 )	Fiss_Prod	High
228Ac	120.30	( 94.6 9.7 11.0 5.0 )	Th-232_Daughter	High
142Ba	117.57	( 90.9 16.4 10.3 0.0 )	Fiss_Prod	High
187W	116.52	( 93.0 0.7 2.8 20.0 )		High
238Np	114.33	( 98.3 4.5 9.5 2.0 )		High
97Zr	112.14	( 85.9 3.0 3.2 20.0 )	Fiss_Prod	High
214Bi	110.61	( 77.5 22.5 10.6 0.0 )	U-238_Daughter	High
240Np	108.86	( 81.0 15.4 12.5 0.0 )		High
91Sr	108.50	( 96.0 3.5 9.0 0.0 )	Fiss_Prod	High
134Te	108.46	( 93.5 5.0 10.0 0.0 )	Fiss_Prod	High
152Eu	106.45	( 83.5 12.2 5.7 5.0 )	Fiss_Prod	Moderate
124Sb	105.23	( 87.9 7.1 10.3 0.0 )	Fiss_Prod	Moderate
148Pm	103.62	( 98.7 0.7 4.2 0.0 )	Fiss_Prod	Moderate
143Ce	103.07	( 55.7 30.1 17.3 0.0 )	Fiss_Prod	Moderate
88Rb	102.61	( 98.4 2.5 1.7 0.0 )	Fiss_Prod	Moderate
92Sr	101.74	( 97.2 2.2 2.3 0.0 )	Fiss_Prod	Moderate
57Co	100.87	( 99.3 0.0 1.6 0.0 )		Moderate
166mHo	100.80	( 83.2 6.6 8.9 2.0 )	Fiss_Prod	Moderate
233Pa	100.79	( 99.2 0.0 1.6 0.0 )	Np-237_Daughter	Moderate
97mNb	100.75	( 98.9 0.0 1.8 0.0 )	Fiss_Prod	Moderate

58Co	100.73	( 97.5	0.0	3.3	0.0 )	c	Moderate
42K	100.37	( 98.4	0.0	2.0	0.0 )	c	Moderate
101Tc	100.22	( 98.6	0.0	1.6	0.0 )	Fiss_Prod	Moderate
40K	99.90	( 99.1	0.0	0.7	0.0 )	Fiss_NORM	Moderate
129mTe	99.89	( 98.3	0.0	1.6	0.0 )	Fiss_Prod	Moderate
209Tl	99.59	( 98.6	0.0	1.0	0.0 )	Np-237_Daughter	Moderate
65Zn	99.55	( 97.5	0.0	2.1	0.0 )	Fiss_Prod	Moderate
52mMn	99.43	( 98.0	0.0	1.4	0.0 )	c	Moderate
143La	99.41	( 98.9	0.0	0.5	0.0 )	Fiss_Prod	Moderate
214Pb	98.92	( 97.7	0.0	1.2	0.0 )	U-238_Daughter	Low
140Ba	98.74	( 97.2	0.0	1.6	0.0 )	Fiss_Prod	Low
141La	98.28	( 97.6	0.0	0.7	0.0 )	Fiss_Prod	Low
90Y	98.19	( 96.6	0.0	1.5	0.0 )	Fiss_Prod	Low
44Sc	97.53	( 96.9	0.0	0.6	0.0 )	c	Low
61Cu	96.71	( 91.7	0.7	4.3	0.0 )	c	Low
125Sn	96.68	( 83.8	3.5	9.4	0.0 )	Fiss_Prod	Low
136Cs	94.38	( 82.7	0.7	5.9	5.0 )	Fiss_Prod	Low
57Ni	93.08	( 86.4	0.7	0.9	5.0 )	c	Low
212Bi	92.61	( 83.6	0.8	3.2	5.0 )	Th-232_Daughter	Low
147Nd	91.89	( 90.3	0.0	1.6	0.0 )	Fiss_Prod	Low
131Te	91.53	( 81.6	3.2	6.7	0.0 )	Fiss_Prod	Low
141Ba	91.44	( 81.5	2.9	5.1	2.0 )	Fiss_Prod	Low
130I	89.49	( 83.7	1.7	4.0	0.0 )	Fiss_Prod	Low
106Rh	87.68	( 85.1	0.0	2.5	0.0 )	Fiss_Prod	Low
52Mn	87.50	( 78.9	1.8	6.8	0.0 )	c	Low
106Ru	86.32	( 83.8	0.0	2.5	0.0 )	Fiss_Prod	Low
126Sb	86.11	( 66.8	4.6	9.6	5.0 )	Fiss_Prod	Low
56Mn	85.98	( 81.1	0.8	4.1	0.0 )	c	Low
48Sc	85.12	( 58.2	0.7	6.2	20.0 )	c	Low
82Br	83.38	( 70.4	3.1	7.8	2.0 )	Fiss_Prod	Low
93Y	82.55	( 48.5	25.3	8.8	0.0 )	Fiss_Prod	Low
138Cs	78.71	( 73.1	1.6	4.0	0.0 )	Fiss_Prod	Low
160Tb	73.33	( 63.3	5.1	4.9	0.0 )	Fiss_Prod	Low
92Y	65.14	( 59.5	0.7	4.9	0.0 )	Fiss_Prod	Low
56Co	64.30	( 45.3	7.5	11.5	0.0 )	c	Low
138Xe	61.89	( 56.0	3.0	2.9	0.0 )	Fiss_Prod	Low
156Eu	59.98	( 37.7	14.1	8.2	0.0 )	Fiss_Prod	Low
59Fe	56.70	( 54.6	0.0	2.1	0.0 )	c	Low
89Rb	56.45	( 43.6	3.1	4.8	5.0 )	Fiss_Prod	Low
48V	50.36	( 40.1	0.7	4.6	5.0 )	medical_from_Ti	Low

Scored nuclides details:

Nuclide	Score	T1/2	T1/2_unit	#EmissionInRange	#Matched	Correlation	Comment
234Pa	159.63	7.6500E-04	y	44	29	High	U-238_Daughter
Emission(KeV)	Prob/DK	Detectability	1.50% Energy Window		Peak(KeV)	Norm%_cts	
369.80	2.9600E-02	2.6450E-01	( 364.25 to 375.35 )				
372.40	1.3300E-02	2.6102E-01	( 366.81 to 377.99 )				
458.80	1.5300E-02	1.7609E-01	( 451.92 to 465.68 )				
506.80	1.6300E-02	1.4364E-01	( 499.20 to 514.40 )				
513.70	1.3300E-02	1.4017E-01	( 505.99 to 521.41 )				
+ 565.90	1.4300E-02	1.1634E-01	( 557.41 to 574.39 )		561.22	1.5470	
+ 568.70	3.0600E-02	1.1517E-01	( 560.17 to 577.23 )		561.22	1.5470	
+ 569.50	1.0900E-01	1.1484E-01	( 560.96 to 578.04 )		561.22	1.5470	
574.00	2.0400E-02	1.1300E-01	( 565.39 to 582.61 )				
664.80	1.3300E-02	8.6177E-02	( 654.83 to 674.77 )				
666.70	1.6300E-02	8.5728E-02	( 656.70 to 676.70 )				
669.90	1.4300E-02	8.4978E-02	( 659.85 to 679.95 )				
+ 699.00	4.6900E-02	7.8434E-02	( 688.52 to 709.49 )		691.66	3.9224	
706.10	3.1600E-02	7.6912E-02	( 695.51 to 716.69 )				
+ 733.00	8.7700E-02	7.1395E-02	( 722.01 to 744.00 )		741.17	4.5257	
+ 738.00	1.0200E-02	7.0412E-02	( 726.93 to 749.07 )		741.17	4.5257	
+ 742.81	2.4500E-02	6.9479E-02	( 731.67 to 753.95 )		741.17	4.5257	
755.60	1.4300E-02	6.7053E-02	( 744.27 to 766.93 )				
+ 780.70	1.1200E-02	6.2526E-02	( 768.99 to 792.41 )		778.67	3.0712	
+ 786.27	1.4300E-02	6.1561E-02	( 774.48 to 798.06 )		778.67	3.0712	
793.60	1.5300E-02	6.0314E-02	( 781.70 to 805.50 )				
796.30	3.8800E-02	5.9860E-02	( 784.36 to 808.24 )				
805.60	3.3700E-02	5.8583E-02	( 793.52 to 817.68 )				



+ 819.60	2.6500E-02	5.6959E-02	( 807.31 to 831.89 )	819.18	8.2070
+ 826.30	4.0800E-02	5.6197E-02	( 813.91 to 838.69 )	819.18	8.2070
+ 831.60	5.6100E-02	5.5602E-02	( 819.13 to 844.07 )	819.18	8.2070
+ 876.40	4.0800E-02	5.0803E-02	( 863.25 to 889.55 )	886.69	2.4800
+ 880.51	1.3220E-01	5.0383E-02	( 867.30 to 893.72 )	886.69	2.4800
+ 883.24	1.2200E-01	5.0106E-02	( 869.99 to 896.49 )	886.69	2.4800
+ 899.00	4.1800E-02	4.8535E-02	( 885.52 to 912.48 )	886.69	2.4800
+ 925.00	2.9600E-02	4.6045E-02	( 911.13 to 938.87 )	915.19	8.4563
+ 926.00	1.1200E-01	4.5952E-02	( 912.11 to 939.89 )	915.19	8.4563
+ 926.72	9.1800E-02	4.5885E-02	( 912.82 to 940.62 )	915.19	8.4563
+ 946.00	1.2200E-01	4.4124E-02	( 931.81 to 960.19 )	951.20	2.4658
+ 949.00	8.1600E-02	4.3856E-02	( 934.77 to 963.23 )	951.20	2.4658
+ 955.59	1.0100E-02	4.3273E-02	( 941.26 to 969.92 )	951.20	2.4658
+ 978.80	1.4300E-02	4.1276E-02	( 964.12 to 993.48 )	982.70	8.6883
+ 980.50	5.1000E-02	4.1134E-02	( 965.79 to 995.21 )	982.70	8.6883
+ 984.00	1.9400E-02	4.0841E-02	( 969.24 to 998.76 )	982.70	8.6883
+ 1353.30	1.7300E-02	2.3728E-02	( 1333.00 to 1373.60 )	1367.40	1.6446
1394.10	3.0600E-02	2.2604E-02	( 1373.19 to 1415.01 )		
+ 1452.70	1.0200E-02	2.1081E-02	( 1430.91 to 1474.49 )	1458.40	1.8213
+ 1668.50	1.2200E-02	1.7114E-02	( 1643.47 to 1693.53 )	1676.80	3.3360
+ 1694.60	1.2200E-02	1.6715E-02	( 1669.18 to 1720.02 )	1676.80	3.3360

Nuclide	Score	T1/2	T1/2_unit	#EmissionInRange	#Matched	Correlation	Comment
134I	151.91	5.2500E+01	m	25	14	High	Fiss_Prod
Emission(KeV)	Prob/DK	Detectability	1.50%	Energy Window	Peak(KeV)	Norm%_cts	
+ 405.45	7.3500E-02	2.2119E-01	( 399.37 to 411.53 )	406.31	1.4581		
433.35	4.1900E-02	1.9645E-01	( 426.85 to 439.85 )				
458.92	1.3000E-02	1.7599E-01	( 452.04 to 465.80 )				
488.88	1.4100E-02	1.5449E-01	( 481.55 to 496.21 )				
514.40	2.3400E-02	1.3982E-01	( 506.68 to 522.12 )				
540.83	7.8200E-02	1.2726E-01	( 532.72 to 548.94 )				
595.36	1.1400E-01	1.0462E-01	( 586.43 to 604.29 )				
621.79	1.0600E-01	9.6945E-02	( 612.46 to 631.12 )				
627.96	2.3700E-02	9.5326E-02	( 618.54 to 637.38 )				
677.34	8.4900E-02	8.3257E-02	( 667.18 to 687.50 )				
+ 730.74	1.9100E-02	7.1844E-02	( 719.78 to 741.70 )	741.17	4.5257		
766.68	4.1000E-02	6.5018E-02	( 755.18 to 778.18 )				
+ 847.02	9.5400E-01	5.3903E-02	( 834.31 to 859.73 )	850.68	8.7431		
+ 857.29	6.9700E-02	5.2799E-02	( 844.43 to 870.15 )	850.68	8.7431		
+ 884.09	6.5300E-01	5.0020E-02	( 870.83 to 897.35 )	886.69	2.4800		
+ 947.86	4.0400E-02	4.3958E-02	( 933.64 to 962.08 )	951.20	2.4658		
+ 974.67	4.6800E-02	4.1625E-02	( 960.05 to 989.29 )	982.70	8.6883		
+ 1040.30	1.9100E-02	3.6833E-02	( 1024.70 to 1055.90 )	1036.70	6.4133		
+ 1072.60	1.5300E-01	3.5085E-02	( 1056.51 to 1088.69 )	1065.20	1.3209		
+ 1136.20	9.7300E-02	3.1873E-02	( 1119.16 to 1153.24 )	1141.70	1.6217		
+ 1455.20	2.2900E-02	2.1018E-02	( 1433.37 to 1477.03 )	1458.40	1.8213		
+ 1613.80	4.3600E-02	1.7981E-02	( 1589.59 to 1638.01 )	1610.00	4.8766		
+ 1741.50	2.6700E-02	1.6021E-02	( 1715.38 to 1767.62 )	1717.70	1.2668		
+ 1787.20	1.3400E-02	1.5372E-02	( 1760.39 to 1814.01 )	1781.40	0.6781		
+ 1806.80	5.7300E-02	1.5101E-02	( 1779.70 to 1833.90 )	1828.40	1.3740		

Nuclide	Score	T1/2	T1/2_unit	#EmissionInRange	#Matched	Correlation	Comment
132I	149.29	2.3000E+00	h	147	59	High	Fiss_Prod
Emission(KeV)	Prob/DK	Detectability	1.50%	Energy Window	Peak(KeV)	Norm%_cts	
302.00	1.9700E-04	3.6957E-01	( 297.47 to 306.53 )				
306.70	1.9740E-03	3.6133E-01	( 302.10 to 311.30 )				
310.10	8.8800E-04	3.5547E-01	( 305.45 to 314.75 )				
310.40	8.8800E-04	3.5495E-01	( 305.74 to 315.06 )				
316.70	1.2800E-03	3.4430E-01	( 311.95 to 321.45 )				
343.70	8.8800E-04	3.0158E-01	( 338.54 to 348.86 )				
351.80	7.9000E-04	2.8964E-01	( 346.52 to 357.08 )				
363.34	4.9400E-03	2.7331E-01	( 357.89 to 368.79 )				
387.90	8.8800E-03	2.4105E-01	( 382.08 to 393.72 )				
416.80	4.7400E-03	2.1080E-01	( 410.55 to 423.05 )				
431.80	4.7400E-03	1.9775E-01	( 425.32 to 438.28 )				
445.00	9.8700E-04	1.8688E-01	( 438.33 to 451.68 )				

446.20	6.0200E-03	1.8592E-01	(	439.51	to	452.89	)		
473.60	1.6800E-03	1.6514E-01	(	466.50	to	480.70	)		
478.20	1.6800E-03	1.6187E-01	(	471.03	to	485.37	)		
488.00	8.3000E-03	1.5509E-01	(	480.68	to	495.32	)		
505.79	4.9400E-02	1.4415E-01	(	498.20	to	513.38	)		
522.65	1.6000E-01	1.3578E-01	(	514.81	to	530.49	)		
535.40	5.1300E-03	1.2975E-01	(	527.37	to	543.43	)		
547.20	1.1400E-02	1.2440E-01	(	538.99	to	555.41	)		
+ 559.70	8.8800E-04	1.1895E-01	(	551.30	to	568.10	)	561.22	1.5470
572.50	5.9200E-04	1.1361E-01	(	563.91	to	581.09	)		
591.10	1.3820E-03	1.0624E-01	(	582.23	to	599.97	)		
600.00	2.5600E-03	1.0288E-01	(	591.00	to	609.00	)		
609.80	3.9500E-04	1.0017E-01	(	600.65	to	618.95	)		
621.14	1.9750E-02	9.7118E-02	(	611.82	to	630.46	)		
630.19	1.3300E-01	9.4747E-02	(	620.74	to	639.64	)		
642.20	3.9500E-04	9.1685E-02	(	632.57	to	651.83	)		
650.50	2.5700E-02	8.9624E-02	(	640.74	to	660.26	)		
667.72	9.8700E-01	8.5488E-02	(	657.70	to	677.74	)		
669.80	4.6400E-02	8.5001E-02	(	659.75	to	679.85	)		
671.40	3.4500E-02	8.4628E-02	(	661.33	to	681.47	)		
+ 684.40	7.9000E-04	8.1655E-02	(	674.13	to	694.67	)	691.66	3.9224
+ 687.80	3.9500E-04	8.0894E-02	(	677.48	to	698.12	)	691.66	3.9224
706.40	1.9700E-04	7.6848E-02	(	695.80	to	717.00	)		
727.12	5.3300E-02	7.2568E-02	(	716.21	to	738.03	)		
728.40	1.5800E-02	7.2311E-02	(	717.47	to	739.33	)		
+ 771.70	1.9700E-04	6.4115E-02	(	760.12	to	783.28	)	778.67	3.0712
+ 772.60	7.5600E-01	6.3954E-02	(	761.01	to	784.19	)	778.67	3.0712
+ 780.00	1.1800E-02	6.2648E-02	(	768.30	to	791.70	)	778.67	3.0712
+ 784.40	3.8500E-03	6.1884E-02	(	772.63	to	796.17	)	778.67	3.0712
791.20	9.8700E-04	6.0720E-02	(	779.33	to	803.07	)		
+ 809.50	2.5700E-02	5.8126E-02	(	797.36	to	821.64	)	819.18	8.2070
+ 812.00	5.5300E-02	5.7835E-02	(	799.82	to	824.18	)	819.18	8.2070
+ 831.30	2.4700E-04	5.5635E-02	(	818.83	to	843.77	)	819.18	8.2070
+ 847.90	1.6800E-04	5.3808E-02	(	835.18	to	860.62	)	850.68	8.7431
+ 863.00	5.6300E-03	5.2195E-02	(	850.05	to	875.94	)	850.68	8.7431
866.00	7.1000E-04	5.1880E-02	(	853.01	to	878.99	)		
+ 876.60	1.0400E-02	5.0782E-02	(	863.45	to	889.75	)	886.69	2.4800
+ 886.10	2.4700E-04	4.9817E-02	(	872.81	to	899.39	)	886.69	2.4800
+ 888.70	6.9000E-04	4.9556E-02	(	875.37	to	902.03	)	886.69	2.4800
+ 904.40	1.2800E-04	4.8007E-02	(	890.83	to	917.97	)	915.19	8.4563
+ 910.10	9.2800E-03	4.7456E-02	(	896.45	to	923.75	)	915.19	8.4563
+ 927.40	4.1500E-03	4.5822E-02	(	913.49	to	941.31	)	915.19	8.4563
+ 947.20	4.4400E-04	4.4017E-02	(	932.99	to	961.41	)	951.20	2.4658
+ 954.55	1.7600E-01	4.3364E-02	(	940.23	to	968.87	)	951.20	2.4658
965.80	3.4500E-04	4.2383E-02	(	951.31	to	980.29	)		
+ 984.20	5.9200E-03	4.0825E-02	(	969.44	to	998.96	)	982.70	8.6883
+ 995.80	2.9600E-04	3.9871E-02	(	980.86	to	1010.74	)	982.70	8.6883
1002.50	5.1400E-04	3.9337E-02	(	987.46	to	1017.54	)		
1005.40	1.5800E-04	3.9114E-02	(	990.32	to	1020.48	)		
1009.00	4.6400E-04	3.8839E-02	(	993.87	to	1024.14	)		
+ 1035.00	5.1300E-03	3.7127E-02	(	1019.48	to	1050.53	)	1036.70	6.4133
+ 1049.60	4.6400E-04	3.6321E-02	(	1033.86	to	1065.34	)	1036.70	6.4133
1081.80	3.4500E-04	3.4602E-02	(	1065.57	to	1098.03	)		
1086.20	7.9000E-04	3.4373E-02	(	1069.91	to	1102.49	)		
+ 1096.90	4.4400E-04	3.3823E-02	(	1080.45	to	1113.35	)	1104.20	5.1494
+ 1112.40	6.5100E-04	3.3040E-02	(	1095.71	to	1129.09	)	1104.20	5.1494
+ 1126.50	9.8800E-04	3.2344E-02	(	1109.60	to	1143.40	)	1141.70	1.6217
+ 1136.00	3.0100E-02	3.1883E-02	(	1118.96	to	1153.04	)	1141.70	1.6217
+ 1143.30	1.3500E-02	3.1533E-02	(	1126.15	to	1160.45	)	1141.70	1.6217
+ 1147.80	2.6600E-03	3.1319E-02	(	1130.58	to	1165.02	)	1141.70	1.6217
1172.90	1.0900E-02	3.0150E-02	(	1155.31	to	1190.49	)		
1212.30	1.1800E-04	2.8401E-02	(	1194.12	to	1230.48	)		
1242.60	8.8800E-05	2.7122E-02	(	1223.96	to	1261.24	)		
1254.10	5.9200E-04	2.6689E-02	(	1235.29	to	1272.91	)		
1263.60	2.6600E-04	2.6390E-02	(	1244.65	to	1282.55	)		
1272.80	1.6800E-03	2.6104E-02	(	1253.71	to	1291.89	)		
1290.80	1.1300E-02	2.5554E-02	(	1271.44	to	1310.16	)		
1295.10	1.8800E-02	2.5424E-02	(	1275.67	to	1314.53	)		
1297.91	8.8800E-03	2.5339E-02	(	1278.44	to	1317.38	)		
1314.00	5.9200E-04	2.4861E-02	(	1294.29	to	1333.71	)		

1317.93	1.1800E-03	2.4745E-02	( 1298.16 to 1337.70 )				
+ 1360.00	5.9200E-05	2.3540E-02	( 1339.60 to 1380.40 )	1367.40	1.6446		
+ 1372.07	2.4700E-02	2.3204E-02	( 1351.49 to 1392.65 )	1367.40	1.6446		
1390.70	1.4800E-04	2.2696E-02	( 1369.84 to 1411.56 )				
1398.57	7.0100E-02	2.2484E-02	( 1377.59 to 1419.55 )				
+ 1410.60	4.3400E-04	2.2165E-02	( 1389.44 to 1431.76 )	1423.50	3.4563		
+ 1442.56	1.4000E-02	2.1337E-02	( 1420.92 to 1464.20 )	1458.40	1.8213		
+ 1450.00	7.9000E-05	2.1149E-02	( 1428.25 to 1471.75 )	1458.40	1.8213		
+ 1456.50	4.9400E-04	2.0985E-02	( 1434.65 to 1478.35 )	1458.40	1.8213		
+ 1476.70	1.3000E-03	2.0486E-02	( 1454.55 to 1498.85 )	1458.40	1.8213		
+ 1519.60	7.9000E-04	1.9575E-02	( 1496.81 to 1542.39 )	1516.00	4.9373		
+ 1531.90	5.9200E-05	1.9359E-02	( 1508.92 to 1554.88 )	1516.00	4.9373		
+ 1542.30	1.5800E-04	1.9179E-02	( 1519.17 to 1565.43 )	1560.00	2.4239		
+ 1559.00	8.8800E-05	1.8892E-02	( 1535.62 to 1582.39 )	1560.00	2.4239		
+ 1592.90	4.7400E-04	1.8323E-02	( 1569.01 to 1616.79 )	1610.00	4.8766		
+ 1617.90	9.8700E-05	1.7915E-02	( 1593.63 to 1642.17 )	1610.00	4.8766		
+ 1618.90	6.9100E-05	1.7898E-02	( 1594.62 to 1643.18 )	1610.00	4.8766		
1636.50	2.3600E-04	1.7616E-02	( 1611.95 to 1661.05 )				
1639.10	7.9000E-05	1.7575E-02	( 1614.51 to 1663.69 )				
1644.00	1.2800E-04	1.7497E-02	( 1619.34 to 1668.66 )				
+ 1661.40	1.5800E-04	1.7225E-02	( 1636.48 to 1686.32 )	1676.80	3.3360		
+ 1671.30	2.1700E-04	1.7071E-02	( 1646.23 to 1696.37 )	1676.80	3.3360		
+ 1679.30	5.9200E-05	1.6948E-02	( 1654.11 to 1704.49 )	1676.80	3.3360		
+ 1715.40	5.5300E-04	1.6404E-02	( 1689.67 to 1741.13 )	1717.70	1.2668		
+ 1720.60	5.4300E-04	1.6327E-02	( 1694.79 to 1746.41 )	1717.70	1.2668		
+ 1727.20	6.7100E-04	1.6230E-02	( 1701.29 to 1753.11 )	1717.70	1.2668		
1752.30	2.4700E-04	1.5865E-02	( 1726.02 to 1778.58 )				
+ 1757.40	2.9600E-03	1.5792E-02	( 1731.04 to 1783.76 )	1781.40	0.6781		
+ 1760.40	5.9200E-04	1.5749E-02	( 1733.99 to 1786.81 )	1781.40	0.6781		
+ 1768.50	2.4700E-04	1.5634E-02	( 1741.97 to 1795.03 )	1781.40	0.6781		
+ 1778.50	7.9000E-04	1.5493E-02	( 1751.82 to 1805.18 )	1781.40	0.6781		
+ 1786.50	2.1800E-04	1.5381E-02	( 1759.70 to 1813.30 )	1781.40	0.6781		
+ 1814.00	1.5800E-04	1.5003E-02	( 1786.79 to 1841.21 )	1828.40	1.3740		
+ 1830.10	2.7600E-04	1.4786E-02	( 1802.65 to 1857.55 )	1828.40	1.3740		
1879.20	1.3800E-04	1.4142E-02	( 1851.01 to 1907.39 )				
1913.70	2.9600E-04	1.3705E-02	( 1884.99 to 1942.41 )				
1921.08	1.2300E-02	1.3614E-02	( 1892.26 to 1949.90 )				
1925.70	1.9700E-05	1.3557E-02	( 1896.81 to 1954.59 )				
1939.50	4.9400E-05	1.3388E-02	( 1910.41 to 1968.59 )				
1985.64	1.1800E-04	1.2838E-02	( 1955.86 to 2015.42 )				
2002.20	1.1400E-02	1.2650E-02	( 1972.17 to 2032.23 )				
2086.82	2.5700E-03	1.1952E-02	( 2055.52 to 2118.12 )				
2172.68	2.0700E-03	1.1365E-02	( 2140.09 to 2205.27 )				
2187.00	6.9100E-05	1.1270E-02	( 2154.20 to 2219.80 )				
2204.20	2.9600E-05	1.1157E-02	( 2171.14 to 2237.26 )				
2223.17	1.1800E-03	1.1033E-02	( 2189.82 to 2256.52 )				
2249.10	3.3600E-04	1.0867E-02	( 2215.36 to 2282.84 )				
2290.60	3.5500E-05	1.0605E-02	( 2256.24 to 2324.96 )				
2390.48	1.8800E-03	1.0001E-02	( 2354.62 to 2426.34 )				
2408.60	9.3800E-05	9.8947E-03	( 2372.47 to 2444.73 )				
2416.90	1.3800E-05	9.8465E-03	( 2380.65 to 2453.15 )				
2444.00	5.6300E-05	9.6909E-03	( 2407.34 to 2480.66 )				
2454.80	2.0700E-05	9.6296E-03	( 2417.98 to 2491.62 )				
2487.80	7.9000E-06	9.4445E-03	( 2450.48 to 2525.12 )				
2525.14	3.9500E-04	9.2394E-03	( 2487.26 to 2563.02 )				
2546.50	1.5800E-05	9.1240E-03	( 2508.30 to 2584.70 )				
2569.80	4.9400E-05	8.9998E-03	( 2531.25 to 2608.35 )				
2593.80	1.1800E-05	8.8736E-03	( 2554.89 to 2632.71 )				
2603.20	1.4800E-05	8.8247E-03	( 2564.15 to 2642.25 )				
2607.20	9.8700E-06	8.8039E-03	( 2568.09 to 2646.31 )				
2614.50	3.5500E-05	8.7662E-03	( 2575.28 to 2653.72 )				
2653.80	9.8700E-06	8.5657E-03	( 2613.99 to 2693.61 )				
+ 2690.80	9.8700E-06	8.3811E-03	( 2650.44 to 2731.16 )	2708.20	0.5083		
+ 2717.50	3.4500E-05	8.2504E-03	( 2676.74 to 2758.26 )	2708.20	0.5083		
+ 2757.80	1.2800E-05	8.0569E-03	( 2716.43 to 2799.17 )	2779.90	1.4944		

Nuclide	Score	T1/2	T1/2_unit	#EmissionInRange	#Matched	Correlation	Comment
135I	148.04	6.5900E+00	h	79	31	High	Fiss_Pro

Emission(KeV)	Prob/DK	Detectability	1.50% Energy Window	Peak(KeV)	Norm%_cts
304.91	3.1600E-04	3.6445E-01	( 300.34 to 309.48 )		
305.83	9.5000E-04	3.6285E-01	( 301.24 to 310.42 )		
326.00	2.3000E-05	3.2906E-01	( 321.11 to 330.89 )		
333.60	3.7300E-04	3.1702E-01	( 328.60 to 338.60 )		
342.52	8.6100E-06	3.0335E-01	( 337.38 to 347.66 )		
361.85	1.8700E-03	2.7538E-01	( 356.42 to 367.28 )		
+ 403.03	2.3200E-03	2.2346E-01	( 396.98 to 409.08 )	406.31	1.4581
414.83	3.0100E-03	2.1257E-01	( 408.61 to 421.05 )		
417.63	3.5300E-02	2.1006E-01	( 411.37 to 423.89 )		
429.93	3.0400E-03	1.9934E-01	( 423.48 to 436.38 )		
433.74	5.5400E-03	1.9612E-01	( 427.23 to 440.25 )		
451.63	3.1600E-03	1.8162E-01	( 444.86 to 458.40 )		
530.80	3.1600E-04	1.3190E-01	( 522.84 to 538.76 )		
546.56	7.1500E-02	1.2469E-01	( 538.36 to 554.76 )		
575.97	1.2900E-03	1.1220E-01	( 567.33 to 584.61 )		
588.28	5.1700E-04	1.0733E-01	( 579.46 to 597.10 )		
616.90	3.7300E-04	9.8248E-02	( 607.65 to 626.15 )		
649.85	4.5600E-03	8.9784E-02	( 640.10 to 659.60 )		
656.09	7.4600E-04	8.8261E-02	( 646.25 to 665.93 )		
679.22	5.4500E-04	8.2827E-02	( 669.03 to 689.41 )		
+ 684.60	2.3000E-04	8.1610E-02	( 674.33 to 694.87 )	691.66	3.9224
+ 690.13	1.2900E-03	8.0376E-02	( 679.78 to 700.48 )	691.66	3.9224
707.92	6.6000E-03	7.6526E-02	( 697.30 to 718.54 )		
+ 785.48	1.5200E-03	6.1697E-02	( 773.70 to 797.26 )	778.67	3.0712
795.50	2.3000E-04	5.9994E-02	( 783.57 to 807.43 )		
797.71	1.7200E-03	5.9625E-02	( 785.74 to 809.68 )		
+ 807.20	4.5900E-04	5.8395E-02	( 795.09 to 819.31 )	819.18	8.2070
836.80	6.6900E-02	5.5023E-02	( 824.25 to 849.35 )		
+ 960.29	3.4400E-04	4.2861E-02	( 945.89 to 974.69 )	951.20	2.4658
+ 961.43	1.4600E-03	4.2762E-02	( 947.01 to 975.85 )	951.20	2.4658
+ 971.96	8.9000E-03	4.1855E-02	( 957.38 to 986.54 )	982.70	8.6883
+ 972.62	1.2100E-02	4.1799E-02	( 958.03 to 987.21 )	982.70	8.6883
+ 995.09	1.5500E-03	3.9928E-02	( 980.16 to 1010.02 )	982.70	8.6883
+ 1038.76	7.9500E-02	3.6918E-02	( 1023.18 to 1054.34 )	1036.70	6.4133
+ 1096.86	8.9000E-04	3.3825E-02	( 1080.41 to 1113.31 )	1104.20	5.1494
+ 1101.58	1.6100E-02	3.3585E-02	( 1085.06 to 1118.10 )	1104.20	5.1494
1124.00	3.6200E-02	3.2466E-02	( 1107.14 to 1140.86 )		
+ 1131.51	2.2600E-01	3.2100E-02	( 1114.54 to 1148.48 )	1141.70	1.6217
+ 1151.51	2.8700E-05	3.1143E-02	( 1134.24 to 1168.78 )	1141.70	1.6217
1159.90	1.0300E-03	3.0750E-02	( 1142.50 to 1177.30 )		
1169.04	8.7500E-03	3.0327E-02	( 1151.50 to 1186.58 )		
+ 1180.46	6.3100E-04	2.9807E-02	( 1162.75 to 1198.17 )	1191.90	2.2238
1225.60	4.3100E-04	2.7833E-02	( 1207.22 to 1243.98 )		
1240.47	9.0400E-03	2.7210E-02	( 1221.86 to 1259.08 )		
1254.80	1.1480E-04	2.6666E-02	( 1235.98 to 1273.62 )		
1260.41	2.8700E-01	2.6490E-02	( 1241.50 to 1279.32 )		
1277.83	5.7400E-04	2.5949E-02	( 1258.66 to 1297.00 )		
1308.70	3.4400E-04	2.5017E-02	( 1289.07 to 1328.33 )		
1315.77	6.6000E-04	2.4808E-02	( 1296.03 to 1335.51 )		
1334.80	3.1600E-04	2.4255E-02	( 1314.78 to 1354.82 )		
1343.66	7.7500E-04	2.4001E-02	( 1323.51 to 1363.81 )		
+ 1367.89	6.0800E-03	2.3320E-02	( 1347.37 to 1388.41 )	1367.40	1.6446
+ 1416.30	3.1600E-04	2.2015E-02	( 1395.06 to 1437.54 )	1423.50	3.4563
+ 1441.80	1.7200E-04	2.1356E-02	( 1420.17 to 1463.43 )	1458.40	1.8213
+ 1448.35	3.1600E-03	2.1190E-02	( 1426.62 to 1470.08 )	1458.40	1.8213
+ 1457.56	8.6700E-02	2.0959E-02	( 1435.70 to 1479.42 )	1458.40	1.8213
+ 1502.79	1.0800E-02	1.9874E-02	( 1480.25 to 1525.33 )	1516.00	4.9373
+ 1521.99	3.7300E-04	1.9533E-02	( 1499.16 to 1544.82 )	1516.00	4.9373
+ 1543.70	2.5800E-04	1.9155E-02	( 1520.54 to 1566.86 )	1560.00	2.4239
+ 1566.41	1.2900E-02	1.8766E-02	( 1542.91 to 1589.91 )	1560.00	2.4239
+ 1613.75	2.5800E-04	1.7982E-02	( 1589.54 to 1637.96 )	1610.00	4.8766
+ 1678.03	9.5600E-02	1.6968E-02	( 1652.86 to 1703.20 )	1676.80	3.3360
+ 1706.46	4.1000E-02	1.6537E-02	( 1680.86 to 1732.06 )	1717.70	1.2668
+ 1742.00	1.7200E-04	1.6014E-02	( 1715.87 to 1768.13 )	1717.70	1.2668
+ 1791.20	7.7200E-02	1.5316E-02	( 1764.33 to 1818.07 )	1781.40	0.6781
+ 1830.69	5.8000E-03	1.4778E-02	( 1803.23 to 1858.15 )	1828.40	1.3740
+ 1845.30	5.7400E-05	1.4583E-02	( 1817.62 to 1872.98 )	1828.40	1.3740
1927.30	2.9600E-03	1.3537E-02	( 1898.39 to 1956.21 )		
1948.49	6.3100E-04	1.3279E-02	( 1919.26 to 1977.72 )		

1948.49	6.3100E-04	1.3279E-02	( 1919.26 to 1977.72 )
2045.88	8.7200E-03	1.2243E-02	( 2015.19 to 2076.57 )
2112.40	6.8900E-04	1.1774E-02	( 2080.71 to 2144.09 )
2151.50	2.2400E-04	1.1507E-02	( 2119.23 to 2183.77 )
2179.70	4.0200E-05	1.1318E-02	( 2147.00 to 2212.40 )
2189.40	1.2900E-04	1.1254E-02	( 2156.56 to 2222.24 )
2255.46	6.1400E-03	1.0826E-02	( 2221.63 to 2289.29 )
2408.65	9.5600E-03	9.8944E-03	( 2372.52 to 2444.78 )
2452.80	8.6100E-05	9.6409E-03	( 2416.01 to 2489.59 )
2466.07	7.1800E-04	9.5660E-03	( 2429.08 to 2503.06 )
2477.10	1.4400E-05	9.5041E-03	( 2439.94 to 2514.26 )

Nuclide	Score	T1/2	T1/2_unit	#EmissionInRange	#Matched	Correlation	Comment
140La	136.98	4.0300E+01	h	28	11	High	Fiss_Prod
Emission(KeV)	Prob/DK	Detectability	1.50%	Energy Window	Peak(KeV)	Norm%_cts	
306.90	2.4800E-04	3.6098E-01	(	302.30 to 311.50			
328.76	2.0300E-01	3.2465E-01	(	323.83 to 333.69			
397.52	7.3500E-04	2.2929E-01	(	391.56 to 403.48			
432.49	2.9000E-02	1.9717E-01	(	426.00 to 438.98			
438.50	3.9100E-04	1.9216E-01	(	431.92 to 445.08			
445.50	2.8600E-05	1.8648E-01	(	438.82 to 452.18			
487.02	4.5500E-01	1.5575E-01	(	479.71 to 494.33			
618.12	3.7200E-04	9.7921E-02	(	608.85 to 627.39			
+ 751.64	4.3300E-02	6.7795E-02	(	740.37 to 762.91	741.17	4.5257	
+ 815.77	2.3300E-01	5.7399E-02	(	803.53 to 828.01	819.18	8.2070	
867.85	5.5000E-02	5.1687E-02	(	854.83 to 880.87			
+ 919.55	2.6600E-02	4.6557E-02	(	905.76 to 933.34	915.19	8.4563	
+ 925.19	6.9000E-02	4.6027E-02	(	911.31 to 939.07	915.19	8.4563	
+ 950.99	5.1900E-03	4.3679E-02	(	936.73 to 965.25	951.20	2.4658	
+ 992.90	1.3400E-04	4.0107E-02	(	978.01 to 1007.79	982.70	6.6883	
+ 1045.05	2.4800E-04	3.6570E-02	(	1029.37 to 1060.73	1036.70	6.4133	
+ 1097.20	2.2900E-04	3.3807E-02	(	1080.74 to 1113.66	1104.20	5.1494	
1303.50	4.2000E-04	2.5172E-02	(	1283.95 to 1323.05			
+ 1405.20	5.9100E-04	2.2308E-02	(	1384.12 to 1426.28	1423.50	3.4563	
+ 1596.21	9.5400E-01	1.8269E-02	(	1572.27 to 1620.15	1610.00	4.8766	
1877.29	4.1000E-04	1.4166E-02	(	1849.13 to 1905.45			
1924.62	1.3400E-04	1.3570E-02	(	1895.75 to 1953.49			
2083.20	1.1500E-04	1.1978E-02	(	2051.95 to 2114.45			
2347.88	8.4900E-03	1.0254E-02	(	2312.66 to 2383.10			
2464.10	1.1400E-04	9.5771E-03	(	2427.14 to 2501.06			
2521.40	3.4600E-02	9.2597E-03	(	2483.58 to 2559.22			
2547.34	1.0100E-03	9.1195E-03	(	2509.13 to 2585.55			
+ 2899.61	6.6800E-04	7.4109E-03	(	2856.12 to 2943.10	2901.00	1.8885	

Nuclide	Score	T1/2	T1/2_unit	#EmissionInRange	#Matched	Correlation	Comment
151Pm	132.47	2.8400E+01	h	142	31	High	Fiss_Prod
Emission(KeV)	Prob/DK	Detectability	1.50%	Energy Window	Peak(KeV)	Norm%_cts	
301.80	1.3500E-04	3.6993E-01	(	297.27 to 306.33			
302.50	2.7000E-04	3.6869E-01	(	297.96 to 307.04			
302.80	2.4800E-04	3.6816E-01	(	298.26 to 307.34			
306.74	2.3900E-03	3.6126E-01	(	302.14 to 311.34			
308.97	8.1000E-04	3.5741E-01	(	304.34 to 313.60			
310.80	5.2900E-04	3.5427E-01	(	306.14 to 315.46			
314.94	7.0880E-04	3.4725E-01	(	310.22 to 319.66			
321.87	9.6800E-04	3.3576E-01	(	317.04 to 326.70			
323.94	1.2200E-02	3.3239E-01	(	319.08 to 328.80			
325.20	1.4600E-04	3.3035E-01	(	320.32 to 330.08			
325.80	1.0600E-03	3.2938E-01	(	320.91 to 330.69			
329.00	1.3500E-04	3.2426E-01	(	324.07 to 333.94			
329.75	2.2100E-03	3.2307E-01	(	324.80 to 334.70			
340.08	2.2500E-01	3.0704E-01	(	334.98 to 345.18			
341.00	7.4300E-04	3.0564E-01	(	335.89 to 346.12			
344.90	2.1200E-02	2.9979E-01	(	339.73 to 350.07			
346.10	3.8300E-04	2.9800E-01	(	340.91 to 351.29			
348.80	9.2300E-05	2.9402E-01	(	343.57 to 354.03			
349.81	1.4200E-03	2.9254E-01	(	344.56 to 355.06			
352.30	1.5800E-04	2.8892E-01	(	347.02 to 357.58			

353.32	1.0600E-03	2.8745E-01	(	348.02	to	358.62	)		
356.90	7.8800E-05	2.8233E-01	(	351.55	to	362.25	)		
358.40	1.5300E-04	2.8021E-01	(	353.02	to	363.78	)		
360.90	1.0600E-04	2.7670E-01	(	355.49	to	366.31	)		
369.00	1.6400E-04	2.6558E-01	(	363.47	to	374.54	)		
374.20	2.2100E-04	2.5863E-01	(	368.59	to	379.81	)		
376.90	1.5800E-04	2.5509E-01	(	371.25	to	382.55	)		
378.50	1.0100E-04	2.5300E-01	(	372.82	to	384.18	)		
379.86	9.4500E-03	2.5124E-01	(	374.16	to	385.56	)		
381.20	2.0300E-04	2.4952E-01	(	375.48	to	386.92	)		
390.67	5.4000E-04	2.3761E-01	(	384.81	to	396.53	)		
395.63	4.2800E-04	2.3156E-01	(	389.70	to	401.56	)		
398.90	3.1500E-04	2.2764E-01	(	392.92	to	404.88	)		
+ 400.50	6.9800E-05	2.2586E-01	(	394.49	to	406.51	)	406.31	1.4581
+ 404.74	6.5300E-04	2.2185E-01	(	398.67	to	410.81	)	406.31	1.4581
+ 407.03	1.8700E-03	2.1972E-01	(	400.92	to	413.14	)	406.31	1.4581
+ 410.75	6.3000E-04	2.1628E-01	(	404.59	to	416.91	)	406.31	1.4581
415.70	2.2300E-04	2.1179E-01	(	409.46	to	421.94	)		
416.80	1.5500E-04	2.1080E-01	(	410.55	to	423.05	)		
420.65	5.6300E-04	2.0738E-01	(	414.34	to	426.96	)		
424.55	4.9500E-04	2.0397E-01	(	418.18	to	430.92	)		
425.60	9.9000E-05	2.0306E-01	(	419.22	to	431.98	)		
427.25	6.3000E-04	2.0163E-01	(	420.84	to	433.66	)		
429.10	1.5800E-04	2.0005E-01	(	422.66	to	435.54	)		
440.85	1.5100E-02	1.9024E-01	(	434.24	to	447.46	)		
443.80	2.2500E-04	1.8784E-01	(	437.14	to	450.46	)		
445.68	4.0100E-02	1.8633E-01	(	438.99	to	452.37	)		
448.70	2.0300E-04	1.8393E-01	(	441.97	to	455.43	)		
451.40	2.8800E-03	1.8180E-01	(	444.63	to	458.17	)		
452.20	1.3500E-04	1.8117E-01	(	445.42	to	458.98	)		
454.40	1.3500E-04	1.7946E-01	(	447.58	to	461.22	)		
456.05	3.8300E-04	1.7819E-01	(	449.21	to	462.89	)		
457.50	4.5000E-05	1.7708E-01	(	450.64	to	464.36	)		
462.24	3.6000E-04	1.7348E-01	(	455.31	to	469.17	)		
463.80	9.0000E-05	1.7232E-01	(	456.84	to	470.76	)		
467.20	1.1300E-04	1.6980E-01	(	460.19	to	474.21	)		
470.50	1.8000E-04	1.6738E-01	(	463.44	to	477.56	)		
471.34	3.1500E-04	1.6677E-01	(	464.27	to	478.41	)		
473.80	6.7500E-05	1.6500E-01	(	466.69	to	480.91	)		
477.75	9.4500E-04	1.6218E-01	(	470.58	to	484.92	)		
487.10	1.6900E-04	1.5570E-01	(	479.79	to	494.41	)		
490.26	1.2600E-03	1.5356E-01	(	482.91	to	497.61	)		
494.90	1.1300E-04	1.5047E-01	(	487.48	to	502.32	)		
495.50	1.3500E-04	1.5007E-01	(	488.07	to	502.93	)		
503.70	4.5000E-05	1.4522E-01	(	496.14	to	511.26	)		
507.27	4.7300E-04	1.4340E-01	(	499.66	to	514.88	)		
510.10	8.5500E-05	1.4197E-01	(	502.45	to	517.75	)		
516.25	1.9400E-03	1.3890E-01	(	508.51	to	523.99	)		
521.10	3.1500E-04	1.3653E-01	(	513.28	to	528.92	)		
532.50	3.3800E-04	1.3110E-01	(	524.51	to	540.49	)		
537.65	4.5000E-04	1.2872E-01	(	529.59	to	545.71	)		
550.70	1.5500E-04	1.2285E-01	(	542.44	to	558.96	)		
+ 554.20	1.6200E-04	1.2132E-01	(	545.89	to	562.51	)	561.22	1.5470
+ 562.10	1.9100E-04	1.1793E-01	(	553.67	to	570.53	)	561.22	1.5470
+ 565.00	3.5300E-03	1.1671E-01	(	556.53	to	573.47	)	561.22	1.5470
572.50	5.1800E-04	1.1361E-01	(	563.91	to	581.09	)		
573.20	2.9300E-04	1.1332E-01	(	564.60	to	581.80	)		
574.97	1.1993E-03	1.1260E-01	(	566.35	to	583.60	)		
581.10	4.5000E-05	1.1015E-01	(	572.38	to	589.82	)		
583.10	2.5700E-04	1.0935E-01	(	574.35	to	591.85	)		
584.90	8.5500E-05	1.0865E-01	(	576.13	to	593.67	)		
593.60	1.0100E-04	1.0529E-01	(	584.70	to	602.50	)		
597.73	8.7800E-04	1.0372E-01	(	588.76	to	606.70	)		
599.10	7.6500E-05	1.0321E-01	(	590.11	to	608.09	)		
603.00	1.1300E-04	1.0204E-01	(	593.96	to	612.05	)		
604.00	8.1000E-05	1.0176E-01	(	594.94	to	613.06	)		
605.90	9.6800E-05	1.0124E-01	(	596.81	to	614.99	)		
609.25	4.7300E-04	1.0032E-01	(	600.11	to	618.39	)		
620.60	7.2000E-04	9.7261E-02	(	611.29	to	629.91	)		
636.20	1.4200E-02	9.3203E-02	(	626.66	to	645.74	)		

654.25	2.4100E-03	8.8708E-02	( 644.44 to 664.06 )				
655.60	1.1300E-04	8.8380E-02	( 645.77 to 665.43 )				
661.55	2.2500E-04	8.6949E-02	( 651.63 to 671.47 )				
663.50	9.4500E-04	8.6485E-02	( 653.55 to 673.45 )				
668.70	3.6338E-03	8.5259E-02	( 658.67 to 678.73 )				
669.20	2.9300E-03	8.5141E-02	( 659.16 to 679.24 )				
671.28	9.0000E-03	8.4656E-02	( 661.21 to 681.35 )				
678.30	4.5000E-04	8.3037E-02	( 668.13 to 688.47 )				
+ 699.00	1.9100E-04	7.8434E-02	( 688.52 to 709.49 )	691.66		3.9224	
704.24	3.3800E-03	7.7308E-02	( 693.68 to 714.80 )				
709.25	1.3700E-03	7.6245E-02	( 698.61 to 719.89 )				
712.00	9.4500E-04	7.5668E-02	( 701.32 to 722.68 )				
713.40	9.0000E-05	7.5376E-02	( 702.70 to 724.10 )				
717.72	4.0500E-02	7.4481E-02	( 706.95 to 728.49 )				
719.00	1.1300E-04	7.4218E-02	( 708.21 to 729.78 )				
727.00	6.7500E-05	7.2592E-02	( 716.09 to 737.91 )				
+ 736.12	4.7300E-03	7.0780E-02	( 725.08 to 747.16 )	741.17		4.5257	
+ 740.80	2.2500E-04	6.9867E-02	( 729.69 to 751.91 )	741.17		4.5257	
752.82	1.2800E-02	6.7573E-02	( 741.53 to 764.11 )				
755.00	6.7500E-05	6.7165E-02	( 743.68 to 766.32 )				
758.50	9.0000E-05	6.6515E-02	( 747.12 to 769.88 )				
+ 769.10	1.0600E-03	6.4581E-02	( 757.56 to 780.64 )	778.67		3.0712	
+ 772.76	9.0000E-03	6.3926E-02	( 761.17 to 784.35 )	778.67		3.0712	
+ 785.10	2.2100E-03	6.1763E-02	( 773.32 to 796.88 )	778.67		3.0712	
792.80	2.2500E-05	6.0449E-02	( 780.91 to 804.69 )				
795.74	5.8500E-04	5.9954E-02	( 783.80 to 807.68 )				
+ 807.90	5.6300E-03	5.8313E-02	( 795.78 to 820.02 )	819.18		8.2070	
+ 811.80	6.7500E-04	5.7858E-02	( 799.62 to 823.98 )	819.18		8.2070	
+ 817.70	2.5900E-03	5.7177E-02	( 805.43 to 829.97 )	819.18		8.2070	
+ 822.45	3.3800E-04	5.6634E-02	( 810.11 to 834.79 )	819.18		8.2070	
+ 848.65	2.8100E-03	5.3726E-02	( 835.92 to 861.38 )	850.68		8.7431	
+ 856.20	6.5300E-05	5.2915E-02	( 843.36 to 869.04 )	850.68		8.7431	
+ 859.80	8.3300E-05	5.2533E-02	( 846.90 to 872.70 )	850.68		8.7431	
867.10	2.9300E-05	5.1765E-02	( 854.09 to 880.11 )				
+ 877.70	1.0100E-03	5.0669E-02	( 864.53 to 890.87 )	886.69		2.4800	
+ 883.68	4.5000E-04	5.0061E-02	( 870.42 to 896.94 )	886.69		2.4800	
+ 887.60	2.7000E-05	4.9666E-02	( 874.29 to 900.91 )	886.69		2.4800	
+ 894.10	2.7000E-05	4.9018E-02	( 880.69 to 907.51 )	886.69		2.4800	
+ 898.58	2.4800E-04	4.8576E-02	( 885.10 to 912.06 )	886.69		2.4800	
+ 903.50	3.1500E-05	4.8095E-02	( 889.95 to 917.05 )	915.19		8.4563	
+ 911.25	2.5700E-04	4.7346E-02	( 897.58 to 924.92 )	915.19		8.4563	
+ 919.30	1.8000E-05	4.6580E-02	( 905.51 to 933.09 )	915.19		8.4563	
+ 922.10	1.3500E-05	4.6317E-02	( 908.27 to 935.93 )	915.19		8.4563	
+ 926.10	4.0500E-05	4.5943E-02	( 912.21 to 939.99 )	915.19		8.4563	
933.90	3.8300E-05	4.5221E-02	( 919.89 to 947.91 )				
+ 939.80	3.8300E-05	4.4683E-02	( 925.70 to 953.90 )	951.20		2.4658	
+ 948.72	3.5100E-03	4.3881E-02	( 934.49 to 962.95 )	951.20		2.4658	
+ 953.41	9.6800E-04	4.3465E-02	( 939.11 to 967.71 )	951.20		2.4658	
+ 959.70	6.3000E-04	4.2913E-02	( 945.30 to 974.10 )	951.20		2.4658	
+ 964.40	4.7300E-05	4.2504E-02	( 949.93 to 978.87 )	951.20		2.4658	
+ 968.90	1.4600E-04	4.2117E-02	( 954.37 to 983.43 )	982.70		8.6883	
1012.20	3.6000E-05	3.8595E-02	( 997.02 to 1027.38 )				

Nuclide	Score	T1/2	T1/2_unit	#EmissionInRange	#Matched	Correlation	Comment
46Sc	131.35	2.2900E+01	y	2	2	High	c
Emission(KeV)	Prob/DK	Detectability	1.50% Energy Window		Peak(KeV)	Norm%_cts	
+ 889.25	1.0000E+00	4.9501E-02	( 875.91 to 902.59 )		886.69	2.4800	
+ 1120.50	1.0000E+00	3.2639E-02	( 1103.69 to 1137.31 )		1104.20	5.1494	
Nuclide	Score	T1/2	T1/2_unit	#EmissionInRange	#Matched	Correlation	Comment
24Na	130.78	1.5000E+01	h	2	2	High	n_activ_prod
Emission(KeV)	Prob/DK	Detectability	1.50% Energy Window		Peak(KeV)	Norm%_cts	
+ 1368.50	1.0000E+00	2.3303E-02	( 1347.97 to 1389.03 )		1367.40	1.6446	
+ 2754.10	9.9900E-01	8.0745E-03	( 2712.79 to 2795.41 )		2779.90	1.4944	

Nuclide	Score	T1/2	T1/2_unit	#EmissionInRange	#Matched	Correlation	Comment
99Mo	126.22	6.6000E+01	h	27	8	High	medical_FF
Emission(KeV)	Prob/DK	Detectability	1.50% Energy Window	Peak(KeV)	Norm%_cts		
366.42	1.1900E-02	2.6908E-01	( 360.92 to 371.92 )				
380.13	1.0400E-04	2.5090E-01	( 374.43 to 385.83 )				
391.70	3.1500E-05	2.3634E-01	( 385.82 to 397.58 )				
+ 410.27	1.9400E-05	2.1672E-01	( 404.12 to 416.42 )	406.31	1.4581		
+ 411.49	1.4600E-04	2.1561E-01	( 405.32 to 417.66 )	406.31	1.4581		
455.84	1.3300E-05	1.7835E-01	( 449.00 to 462.68 )				
457.60	8.1300E-05	1.7700E-01	( 450.74 to 464.46 )				
469.63	2.6700E-05	1.6801E-01	( 462.59 to 476.67 )				
490.53	1.0900E-05	1.5338E-01	( 483.17 to 497.89 )				
528.79	5.7000E-04	1.3285E-01	( 520.86 to 536.72 )				
537.79	3.2800E-05	1.2865E-01	( 529.72 to 545.86 )				
580.51	3.1500E-05	1.1038E-01	( 571.80 to 589.22 )				
581.30	9.7000E-06	1.1007E-01	( 572.58 to 590.02 )				
599.60	2.0600E-05	1.0303E-01	( 590.61 to 608.59 )				
620.03	2.3000E-05	9.7412E-02	( 610.73 to 629.33 )				
621.77	2.5800E-04	9.6951E-02	( 612.44 to 631.10 )				
+ 689.60	4.2500E-06	8.0494E-02	( 679.26 to 699.94 )	691.66	3.9224		
+ 739.50	1.2100E-01	7.0120E-02	( 728.41 to 750.59 )	741.17	4.5257		
761.77	4.0000E-06	6.5912E-02	( 750.34 to 773.20 )				
+ 777.92	4.2600E-02	6.3013E-02	( 766.25 to 789.59 )	778.67	3.0712		
+ 822.97	1.3300E-03	5.6575E-02	( 810.63 to 835.31 )	819.18	8.2070		
+ 861.20	7.2800E-05	5.2385E-02	( 848.28 to 874.12 )	850.68	8.7431		
+ 960.75	9.4600E-04	4.2821E-02	( 946.34 to 975.16 )	951.20	2.4658		
+ 986.44	1.4600E-05	4.0639E-02	( 971.64 to 1001.24 )	982.70	8.6883		
1001.34	5.4600E-05	3.9427E-02	( 986.32 to 1016.36 )				
1017.00	6.0700E-06	3.8233E-02	( 1001.75 to 1032.26 )				
+ 1056.20	1.0800E-05	3.5962E-02	( 1040.36 to 1072.04 )	1065.20	1.3209		

Nuclide	Score	T1/2	T1/2_unit	#EmissionInRange	#Matched	Correlation	Comment
133mTe	123.77	5.5400E+01	m	39	13	High	Fiss_Prod
Emission(KeV)	Prob/DK	Detectability	1.50% Energy Window	Peak(KeV)	Norm%_cts		
334.14	5.4300E-02	3.1618E-01	( 329.13 to 339.15 )				
344.50	2.2600E-02	3.0038E-01	( 339.33 to 349.67 )				
347.20	1.1300E-02	2.9637E-01	( 341.99 to 352.41 )				
355.57	1.4800E-02	2.8422E-01	( 350.24 to 360.90 )				
396.96	1.4800E-02	2.2996E-01	( 391.01 to 402.91 )				
429.02	1.2200E-02	2.0012E-01	( 422.58 to 435.46 )				
435.40	1.0400E-02	1.9473E-01	( 428.87 to 441.93 )				
444.90	2.2600E-02	1.8696E-01	( 438.23 to 451.57 )				
462.11	2.0000E-02	1.7358E-01	( 455.18 to 469.04 )				
471.85	2.0000E-02	1.6640E-01	( 464.77 to 478.93 )				
478.59	1.5700E-02	1.6159E-01	( 471.41 to 485.77 )				
534.85	1.7400E-02	1.3001E-01	( 526.83 to 542.87 )				
574.04	2.3500E-02	1.1298E-01	( 565.43 to 582.65 )				
622.03	1.3900E-02	9.6882E-02	( 612.70 to 631.36 )				
647.40	2.9300E-01	9.0389E-02	( 637.69 to 657.11 )				
702.75	3.7400E-02	7.7627E-02	( 692.21 to 713.29 )				
+ 731.69	1.4800E-02	7.1655E-02	( 720.71 to 742.67 )	741.17	4.5257		
+ 733.89	4.6300E-02	7.1219E-02	( 722.88 to 744.90 )	741.17	4.5257		
+ 779.75	5.1500E-02	6.2692E-02	( 768.05 to 791.45 )	778.67	3.0712		
795.70	1.3100E-02	5.9961E-02	( 783.76 to 807.64 )				
800.51	1.9100E-02	5.9184E-02	( 788.50 to 812.52 )				
863.91	1.9500E-01	5.2099E-02	( 850.95 to 876.87 )				
+ 882.83	5.6600E-02	5.0147E-02	( 869.59 to 896.07 )	886.69	2.4800		
+ 912.58	8.7000E-01	4.7219E-02	( 898.89 to 926.27 )	915.19	8.4563		
+ 914.72	1.6500E-01	4.7014E-02	( 901.00 to 928.44 )	915.19	8.4563		
934.40	1.3100E-02	4.5176E-02	( 920.38 to 948.42 )				
+ 978.19	9.4800E-02	4.1328E-02	( 963.52 to 992.86 )	982.70	8.6883		
+ 980.40	2.3500E-02	4.1142E-02	( 965.69 to 995.11 )	982.70	8.6883		
+ 982.90	1.1300E-02	4.0933E-02	( 968.16 to 997.64 )	982.70	8.6883		
1007.50	1.0400E-02	3.8953E-02	( 992.39 to 1022.61 )				
+ 1029.80	1.3100E-02	3.7419E-02	( 1014.35 to 1045.25 )	1036.70	6.4133		
+ 1348.90	2.5200E-02	2.3852E-02	( 1328.67 to 1369.13 )	1367.40	1.6446		
+ 1459.10	2.1800E-02	2.0920E-02	( 1437.21 to 1480.99 )	1458.40	1.8213		



+ 1683.30	5.7400E-02	1.6887E-02	( 1658.05 to 1708.55 )	1676.80	3.3360
1885.70	1.1300E-02	1.4058E-02	( 1857.41 to 1913.99 )		
1887.70	1.3600E-02	1.4033E-02	( 1859.38 to 1916.02 )		
2004.90	3.3100E-02	1.2625E-02	( 1974.83 to 2034.97 )		
2027.70	2.0900E-02	1.2409E-02	( 1997.28 to 2058.12 )		
2049.20	1.0400E-02	1.2219E-02	( 2018.46 to 2079.94 )		

Nuclide	Score	T1/2	T1/2_unit	#EmissionInRange	#Matched	Correlation	Comment
131mTe	123.57	3.2400E+01	h	22	11	High	Fiss_Prod
Emission(KeV)	Prob/DK	Detectability	1.50% Energy Window	Peak(KeV)	Norm%_cts		
334.27	9.5700E-02	3.1598E-01	( 329.26 to 339.28 )				
364.98	1.2000E-02	2.7105E-01	( 359.51 to 370.45 )				
452.32	1.5500E-02	1.8108E-01	( 445.54 to 459.10 )				
462.92	1.8200E-02	1.7297E-01	( 455.98 to 469.86 )				
586.30	1.9800E-02	1.0810E-01	( 577.51 to 595.09 )				
631.94	3.5500E-02	9.4295E-02	( 622.46 to 641.42 )				
665.05	4.3400E-02	8.6117E-02	( 655.07 to 675.03 )				
713.10	1.4300E-02	7.5438E-02	( 702.40 to 723.80 )				
+ 744.20	1.5900E-02	6.9211E-02	( 733.04 to 755.36 )	741.17	4.5257		
+ 773.67	3.8200E-01	6.3764E-02	( 762.06 to 785.28 )	778.67	3.0712		
+ 782.49	7.7900E-02	6.2214E-02	( 770.75 to 794.23 )	778.67	3.0712		
793.75	1.3900E-01	6.0289E-02	( 781.84 to 805.66 )				
+ 822.78	6.1200E-02	5.6596E-02	( 810.44 to 835.12 )	819.18	8.2070		
+ 852.21	2.0700E-01	5.3342E-02	( 839.43 to 864.99 )	850.68	8.7431		
+ 910.00	3.2900E-02	4.7466E-02	( 896.35 to 923.65 )	915.19	8.4563		
+ 920.62	1.2000E-02	4.6456E-02	( 906.81 to 934.43 )	915.19	8.4563		
+ 1059.70	1.5500E-02	3.5773E-02	( 1043.80 to 1075.60 )	1065.20	1.3209		
+ 1125.50	1.1400E-01	3.2393E-02	( 1108.62 to 1142.38 )	1141.70	1.6217		
+ 1148.90	1.5100E-02	3.1267E-02	( 1131.67 to 1166.13 )	1141.70	1.6217		
+ 1206.60	9.7600E-02	2.8648E-02	( 1188.50 to 1224.70 )	1191.90	2.2238		
1646.00	1.2400E-02	1.7466E-02	( 1621.31 to 1670.69 )				
2000.90	2.0200E-02	1.2663E-02	( 1970.89 to 2030.91 )				

Nuclide	Score	T1/2	T1/2_unit	#EmissionInRange	#Matched	Correlation	Comment
110mAg	121.82	6.8400E-01	y	15	9	High	Fiss_Prod
Emission(KeV)	Prob/DK	Detectability	1.50% Energy Window	Peak(KeV)	Norm%_cts		
446.80	3.6400E-02	1.8544E-01	( 440.10 to 453.50 )				
620.35	2.7700E-02	9.7327E-02	( 611.04 to 629.66 )				
657.75	9.4400E-01	8.7860E-02	( 647.88 to 667.62 )				
677.61	1.0700E-01	8.3195E-02	( 667.45 to 687.77 )				
+ 686.99	6.4700E-02	8.1074E-02	( 676.69 to 697.29 )	691.66	3.9224		
706.67	1.6700E-01	7.6791E-02	( 696.07 to 717.27 )				
+ 744.26	4.6400E-02	6.9199E-02	( 733.10 to 755.42 )	741.17	4.5257		
763.93	2.2300E-01	6.5517E-02	( 752.47 to 775.39 )				
+ 818.02	7.2800E-02	5.7140E-02	( 805.75 to 830.29 )	819.18	8.2070		
+ 884.67	7.2600E-01	4.9961E-02	( 871.40 to 897.94 )	886.69	2.4800		
+ 937.48	3.4200E-01	4.4894E-02	( 923.42 to 951.54 )	951.20	2.4658		
+ 1384.30	2.4300E-01	2.2869E-02	( 1363.54 to 1405.06 )	1367.40	1.6446		
+ 1475.80	4.0000E-02	2.0508E-02	( 1453.66 to 1497.94 )	1458.40	1.8213		
+ 1505.00	1.3100E-01	1.9834E-02	( 1482.43 to 1527.58 )	1516.00	4.9373		
+ 1562.30	1.1800E-02	1.8836E-02	( 1538.87 to 1585.73 )	1560.00	2.4239		

Nuclide	Score	T1/2	T1/2_unit	#EmissionInRange	#Matched	Correlation	Comment
228Ac	120.30	7.0000E-04	y	14	7	High	Th-232_Daughter
Emission(KeV)	Prob/DK	Detectability	1.50% Energy Window	Peak(KeV)	Norm%_cts		
327.64	3.2100E-02	3.2643E-01	( 322.73 to 332.55 )				
338.32	1.1400E-01	3.0973E-01	( 333.25 to 343.39 )				
+ 409.51	2.1300E-02	2.1742E-01	( 403.37 to 415.65 )	406.31	1.4581		
463.00	4.4300E-02	1.7291E-01	( 456.06 to 469.95 )				
755.18	1.0500E-02	6.7132E-02	( 743.85 to 766.51 )				
+ 772.17	1.5500E-02	6.4031E-02	( 760.59 to 783.75 )	778.67	3.0712		
794.70	4.6300E-02	6.0129E-02	( 782.78 to 806.62 )				
835.50	1.7500E-02	5.5167E-02	( 822.97 to 848.03 )				
+ 911.07	2.7700E-01	4.7363E-02	( 897.40 to 924.74 )	915.19	8.4563		

+ 947.77	4.1200E-02	4.3966E-02	( 933.55 to 961.99 )	951.20	2.4658
+ 964.60	5.2100E-02	4.2487E-02	( 950.13 to 979.07 )	951.20	2.4658
+ 969.11	1.6600E-01	4.2099E-02	( 954.57 to 983.65 )	982.70	8.6883
+ 1588.00	3.5500E-02	1.8405E-02	( 1564.18 to 1611.82 )	1610.00	4.8766
+ 1630.40	1.8600E-02	1.7714E-02	( 1605.94 to 1654.86 )	1610.00	4.8766

Nuclide	Score	T1/2	T1/2_unit	#EmissionInRange	#Matched	Correlation	Comment
142Ba	117.57	1.0600E+01	m	15	9	High	Fiss_Prod
Emission(KeV)	Prob/DK	Detectability	1.50% Energy Window	Peak(KeV)	Norm%_cts		
309.02	2.2600E-02	3.5732E-01	( 304.38 to 313.66 )				
334.80	1.2500E-02	3.1515E-01	( 329.78 to 339.82 )				
363.80	3.9200E-02	2.7268E-01	( 358.34 to 369.26 )				
425.03	4.9800E-02	2.0355E-01	( 418.65 to 431.41 )				
599.84	1.6000E-02	1.0294E-01	( 590.84 to 608.84 )				
+ 840.23	3.0300E-02	5.4645E-02	( 827.63 to 852.83 )	850.68	8.7431		
+ 894.90	1.1000E-01	4.8939E-02	( 881.48 to 908.32 )	886.69	2.4800		
+ 948.75	8.9000E-02	4.3878E-02	( 934.52 to 962.98 )	951.20	2.4658		
1000.90	7.8300E-02	3.9461E-02	( 985.89 to 1015.91 )				
+ 1078.50	9.2600E-02	3.4774E-02	( 1062.32 to 1094.68 )	1065.20	1.3209		
+ 1093.60	2.2100E-02	3.3991E-02	( 1077.20 to 1110.00 )	1104.20	5.1494		
+ 1126.50	1.5300E-02	3.2344E-02	( 1109.60 to 1143.40 )	1141.70	1.6217		
+ 1202.20	5.3400E-02	2.8840E-02	( 1184.17 to 1220.23 )	1191.90	2.2238		
+ 1204.10	1.3700E-01	2.8757E-02	( 1186.04 to 1222.16 )	1191.90	2.2238		
+ 1379.90	3.4000E-02	2.2989E-02	( 1359.20 to 1400.60 )	1367.40	1.6446		

Nuclide	Score	T1/2	T1/2_unit	#EmissionInRange	#Matched	Correlation	Comment
187W	116.52	2.3900E+01	h	6	2	High	c
Emission(KeV)	Prob/DK	Detectability	1.50% Energy Window	Peak(KeV)	Norm%_cts		
479.53	2.3400E-01	1.6093E-01	( 472.34 to 486.72 )				
551.55	5.4400E-02	1.2248E-01	( 543.28 to 559.82 )				
618.37	6.7100E-02	9.7854E-02	( 609.09 to 627.65 )				
625.52	1.1600E-02	9.5963E-02	( 616.14 to 634.90 )				
+ 685.81	2.9200E-01	8.1338E-02	( 675.52 to 696.10 )	691.66	3.9224		
+ 772.87	4.4000E-02	6.3906E-02	( 761.28 to 784.46 )	778.67	3.0712		

Nuclide	Score	T1/2	T1/2_unit	#EmissionInRange	#Matched	Correlation	Comment
238Np	114.33	2.1200E+00	d	4	4	High	SNM
Emission(KeV)	Prob/DK	Detectability	1.50% Energy Window	Peak(KeV)	Norm%_cts		
+ 923.98	2.4800E-02	4.6140E-02	( 910.12 to 937.84 )	915.19	8.4563		
+ 984.45	2.3800E-01	4.0804E-02	( 969.68 to 999.22 )	982.70	8.6883		
+ 1025.90	8.2100E-02	3.7638E-02	( 1010.51 to 1041.29 )	1036.70	6.4133		
+ 1028.50	1.7400E-01	3.7492E-02	( 1013.07 to 1043.93 )	1036.70	6.4133		

Nuclide	Score	T1/2	T1/2_unit	#EmissionInRange	#Matched	Correlation	Comment
97Zr	112.14	1.6900E+01	h	11	4	High	Fiss_Prod
Emission(KeV)	Prob/DK	Detectability	1.50% Energy Window	Peak(KeV)	Norm%_cts		
355.39	2.2800E-02	2.8448E-01	( 350.06 to 360.72 )				
507.64	5.0300E-02	1.4321E-01	( 500.03 to 515.25 )				
602.37	1.3800E-02	1.0222E-01	( 593.33 to 611.41 )				
703.76	1.0100E-02	7.7410E-02	( 693.20 to 714.32 )				
+ 743.36	9.3100E-01	6.9373E-02	( 732.21 to 754.51 )	741.17	4.5257		
1021.20	1.0100E-02	3.7919E-02	( 1005.88 to 1036.52 )				
+ 1147.97	2.6200E-02	3.1311E-02	( 1130.75 to 1165.19 )	1141.70	1.6217		
1276.07	9.4000E-03	2.6003E-02	( 1256.93 to 1295.21 )				
+ 1361.00	6.5100E-03	2.3512E-02	( 1340.59 to 1381.42 )	1367.40	1.6446		
+ 1362.68	1.0200E-02	2.3465E-02	( 1342.24 to 1383.12 )	1367.40	1.6446		
1750.24	1.0900E-02	1.5895E-02	( 1723.99 to 1776.49 )				

Nuclide	Score	T1/2	T1/2_unit	#EmissionInRange	#Matched	Correlation	Comment
214Bi	110.61	3.7900E-05	y	21	11	High	U-238_Daughter

Emission(KeV)	Prob/DK	Detectability	1.50% Energy Window	Peak(KeV)	Norm%_cts
609.31	4.6300E-01	1.0030E-01	( 600.17 to 618.45 )		
665.45	1.5700E-02	8.6023E-02	( 655.47 to 675.43 )		
+ 768.36	5.0400E-02	6.4714E-02	( 756.83 to 779.89 )	778.67	3.0712
806.17	1.2300E-02	5.8516E-02	( 794.08 to 818.26 )		
934.06	3.2100E-02	4.5207E-02	( 920.05 to 948.07 )		
+ 1120.30	1.5200E-01	3.2649E-02	( 1103.50 to 1137.10 )	1104.20	5.1494
+ 1155.20	1.7000E-02	3.0970E-02	( 1137.87 to 1172.53 )	1141.70	1.6217
+ 1158.00	3.5100E-02	3.0839E-02	( 1140.63 to 1175.37 )	1141.70	1.6217
1238.10	5.9400E-02	2.7308E-02	( 1219.53 to 1256.67 )		
1281.00	1.4800E-02	2.5852E-02	( 1261.79 to 1300.22 )		
+ 1377.70	4.1100E-02	2.3050E-02	( 1357.03 to 1398.37 )	1367.40	1.6446
1401.50	1.3900E-02	2.2406E-02	( 1380.48 to 1422.52 )		
+ 1408.00	2.4900E-02	2.2234E-02	( 1386.88 to 1429.12 )	1423.50	3.4563
+ 1509.20	2.2200E-02	1.9759E-02	( 1486.56 to 1531.84 )	1516.00	4.9373
+ 1661.30	1.1600E-02	1.7226E-02	( 1636.38 to 1686.22 )	1676.80	3.3360
+ 1729.60	2.9700E-02	1.6195E-02	( 1703.66 to 1755.54 )	1717.70	1.2668
+ 1764.50	1.5800E-01	1.5691E-02	( 1738.03 to 1790.97 )	1781.40	0.6781
+ 1847.40	2.0900E-02	1.4555E-02	( 1819.69 to 1875.11 )	1828.40	1.3740
2118.60	1.1700E-02	1.1732E-02	( 2086.82 to 2150.38 )		
2204.20	4.9800E-02	1.1157E-02	( 2171.14 to 2237.26 )		
2447.90	1.5600E-02	9.6687E-03	( 2411.18 to 2484.62 )		

---

Nuclide	Score	T1/2	T1/2_unit	#EmissionInRange	#Matched	Correlation	Comment
240Np	108.86	6.1900E+01	m	18	9	High	SNM

Emission(KeV)	Prob/DK	Detectability	1.50% Energy Window	Peak(KeV)	Norm%_cts
307.00	1.3900E-02	3.6081E-01	( 302.40 to 311.61 )		
448.20	1.6700E-01	1.8432E-01	( 441.48 to 454.92 )		
462.20	1.3900E-02	1.7351E-01	( 455.27 to 469.13 )		
467.40	2.0400E-02	1.6965E-01	( 460.39 to 474.41 )		
507.20	1.8500E-02	1.4343E-01	( 499.59 to 514.81 )		
+ 566.40	2.6900E-01	1.1613E-01	( 557.90 to 574.90 )	561.22	1.5470
601.10	2.0400E-01	1.0257E-01	( 592.08 to 610.12 )		
606.10	1.5800E-02	1.0118E-01	( 597.01 to 615.19 )		
+ 847.00	4.6400E-02	5.3905E-02	( 834.30 to 859.70 )	850.68	8.7431
867.40	8.3400E-02	5.1734E-02	( 854.39 to 880.41 )		
+ 884.90	3.7100E-02	4.9938E-02	( 871.63 to 898.17 )	886.69	2.4800
+ 888.80	1.1100E-02	4.9546E-02	( 875.47 to 902.13 )	886.69	2.4800
+ 896.50	1.3000E-01	4.8781E-02	( 883.05 to 909.95 )	886.69	2.4800
+ 915.98	1.3900E-02	4.6895E-02	( 902.24 to 929.72 )	915.19	8.4563
+ 959.10	2.3200E-02	4.2965E-02	( 944.71 to 973.49 )	951.20	2.4658
+ 973.90	2.1300E-01	4.1690E-02	( 959.29 to 988.51 )	982.70	8.6883
+ 987.76	4.6400E-02	4.0530E-02	( 972.94 to 1002.58 )	982.70	8.6883
1167.60	4.6400E-02	3.0394E-02	( 1150.09 to 1185.11 )		

---

Nuclide	Score	T1/2	T1/2_unit	#EmissionInRange	#Matched	Correlation	Comment
91Sr	108.50	9.6300E+00	h	7	4	High	Fiss_Pro

Emission(KeV)	Prob/DK	Detectability	1.50% Energy Window	Peak(KeV)	Norm%_cts
620.10	1.7200E-02	9.7394E-02	( 610.80 to 629.40 )		
652.30	2.8900E-02	8.9183E-02	( 642.52 to 662.08 )		
652.90	7.8000E-02	8.9037E-02	( 643.11 to 662.69 )		
+ 749.80	2.3000E-01	6.8143E-02	( 738.55 to 761.05 )	741.17	4.5257
+ 776.34	1.1900E-02	6.3291E-02	( 764.69 to 787.99 )	778.67	3.0712
+ 925.80	3.7400E-02	4.5970E-02	( 911.91 to 939.69 )	915.19	8.4563
+ 1024.30	3.2500E-01	3.7729E-02	( 1008.94 to 1039.66 )	1036.70	6.4133

---

Nuclide	Score	T1/2	T1/2_unit	#EmissionInRange	#Matched	Correlation	Comment
134Te	108.46	4.1800E+01	m	11	5	High	Fiss_Pro

Emission(KeV)	Prob/DK	Detectability	1.50% Energy Window	Peak(KeV)	Norm%_cts
435.06	1.8600E-01	1.9502E-01	( 428.53 to 441.59 )		
461.00	1.0800E-01	1.7442E-01	( 454.09 to 467.92 )		
464.64	5.1000E-02	1.7169E-01	( 457.67 to 471.61 )		
+ 565.99	1.8900E-01	1.1630E-01	( 557.50 to 574.48 )	561.22	1.5470
636.26	1.7100E-02	9.3187E-02	( 626.72 to 645.80 )		

665.85	1.2000E-02	8.5928E-02	( 655.86 to 675.84 )				
712.97	4.2000E-02	7.5466E-02	( 702.28 to 723.66 )				
+ 742.59	1.4700E-01	6.9521E-02	( 731.45 to 753.73 )	741.17	4.5257		
+ 767.20	3.0000E-01	6.4923E-02	( 755.69 to 778.71 )	778.67	3.0712		
+ 844.06	1.2000E-02	5.4225E-02	( 831.40 to 856.72 )	850.68	8.7431		
+ 925.55	1.6500E-02	4.5994E-02	( 911.67 to 939.43 )	915.19	8.4563		

---

Nuclide	Score	T1/2	T1/2_unit	#EmissionInRange	#Matched	Correlation	Comment
152Eu	106.45	1.3400E+01	y	12	5	Moderate	Fiss_Prod

Emission(KeV)	Prob/DK	Detectability	1.50% Energy Window	Peak(KeV)	Norm%_cts		
344.27	2.6500E-01	3.0073E-01	( 339.11 to 349.43 )				
+ 411.11	2.2100E-02	2.1595E-01	( 404.94 to 417.28 )	406.31	1.4581		
443.98	2.8100E-02	1.8770E-01	( 437.32 to 450.64 )				
+ 778.89	1.2700E-01	6.2842E-02	( 767.21 to 790.57 )	778.67	3.0712		
867.32	4.1600E-02	5.1742E-02	( 854.31 to 880.33 )				
+ 964.01	1.4400E-01	4.2538E-02	( 949.55 to 978.47 )	951.20	2.4658		
1085.80	9.9600E-02	3.4394E-02	( 1069.51 to 1102.09 )				
+ 1089.70	1.6800E-02	3.4192E-02	( 1073.35 to 1106.05 )	1104.20	5.1494		
+ 1112.00	1.3300E-01	3.3060E-02	( 1095.32 to 1128.68 )	1104.20	5.1494		
1212.80	1.3800E-02	2.8379E-02	( 1194.61 to 1230.99 )				
1299.00	1.6100E-02	2.5307E-02	( 1279.52 to 1318.49 )				
+ 1408.00	2.0800E-01	2.2234E-02	( 1386.88 to 1429.12 )	1423.50	3.4563		

---

Nuclide	Score	T1/2	T1/2_unit	#EmissionInRange	#Matched	Correlation	Comment
124Sb	105.23	1.6500E-01	y	13	6	Moderate	Fiss_Prod

Emission(KeV)	Prob/DK	Detectability	1.50% Energy Window	Peak(KeV)	Norm%_cts		
602.71	9.7900E-01	1.0212E-01	( 593.67 to 611.75 )				
645.85	7.2600E-02	9.0773E-02	( 636.16 to 655.54 )				
709.31	1.4200E-02	7.6233E-02	( 698.67 to 719.95 )				
713.82	2.3800E-02	7.5288E-02	( 703.11 to 724.53 )				
722.78	1.1100E-01	7.3445E-02	( 711.94 to 733.62 )				
+ 968.20	1.9200E-02	4.2177E-02	( 953.68 to 982.72 )	982.70	8.6883		
+ 1045.20	1.8600E-02	3.6562E-02	( 1029.52 to 1060.88 )	1036.70	6.4133		
+ 1208.30	1.3400E-02	2.8574E-02	( 1190.18 to 1226.42 )	1191.90	2.2238		
1325.50	1.5000E-02	2.4524E-02	( 1305.62 to 1345.38 )				
+ 1368.20	2.5100E-02	2.3311E-02	( 1347.68 to 1388.72 )	1367.40	1.6446		
+ 1436.60	1.1400E-02	2.1489E-02	( 1415.05 to 1458.15 )	1423.50	3.4563		
+ 1691.00	4.9000E-01	1.6770E-02	( 1665.64 to 1716.37 )	1676.80	3.3360		
2091.00	5.7300E-02	1.1923E-02	( 2059.64 to 2122.37 )				

---

Nuclide	Score	T1/2	T1/2_unit	#EmissionInRange	#Matched	Correlation	Comment
148Pm	103.62	5.3700E+00	d	4	2	Moderate	Fiss_Prod

Emission(KeV)	Prob/DK	Detectability	1.50% Energy Window	Peak(KeV)	Norm%_cts		
550.27	2.2000E-01	1.2304E-01	( 542.02 to 558.52 )				
611.26	1.0200E-02	9.9770E-02	( 602.09 to 620.43 )				
+ 914.85	1.1500E-01	4.7002E-02	( 901.13 to 928.57 )	915.19	8.4563		
+ 1465.10	2.2200E-01	2.0771E-02	( 1443.12 to 1487.08 )	1458.40	1.8213		

---

Nuclide	Score	T1/2	T1/2_unit	#EmissionInRange	#Matched	Correlation	Comment
143Ce	103.07	3.3000E+01	h	45	14	Moderate	Fiss_Prod

Emission(KeV)	Prob/DK	Detectability	1.50% Energy Window	Peak(KeV)	Norm%_cts		
338.30	8.5600E-06	3.0976E-01	( 333.23 to 343.37 )				
350.62	3.2300E-02	2.9136E-01	( 345.36 to 355.88 )				
357.80	5.9900E-06	2.8106E-01	( 352.43 to 363.17 )				
371.29	2.4800E-04	2.6250E-01	( 365.72 to 376.86 )				
389.64	3.6400E-04	2.3888E-01	( 383.80 to 395.48 )				
416.57	6.8500E-05	2.1101E-01	( 410.32 to 422.82 )				
433.00	1.5900E-03	1.9674E-01	( 426.51 to 439.49 )				
438.43	4.2800E-05	1.9222E-01	( 431.85 to 445.01 )				
446.02	1.5000E-04	1.8606E-01	( 439.33 to 452.71 )				
447.45	5.9900E-04	1.8492E-01	( 440.74 to 454.16 )				
490.37	2.1600E-02	1.5348E-01	( 483.01 to 497.73 )				

497.81	4.4500E-04	1.4856E-01	(	490.34	to	505.28	)		
523.00	1.7100E-05	1.3561E-01	(	515.16	to	530.85	)		
+ 556.87	3.1700E-04	1.2017E-01	(	548.52	to	565.22	)	561.22	1.5470
569.91	5.1400E-05	1.1467E-01	(	561.36	to	578.46	)		
587.20	2.6700E-03	1.0775E-01	(	578.39	to	596.01	)		
594.50	2.1400E-05	1.0494E-01	(	585.58	to	603.42	)		
614.22	1.2000E-04	9.8968E-02	(	605.01	to	623.43	)		
664.57	5.6900E-02	8.6231E-02	(	654.60	to	674.54	)		
670.12	8.1300E-05	8.4926E-02	(	660.07	to	680.17	)		
675.50	8.5600E-06	8.3679E-02	(	665.37	to	685.63	)		
+ 692.82	8.5600E-05	8.2011E-02	(	672.58	to	693.06	)	691.66	3.9224
709.59	8.5600E-05	7.6174E-02	(	698.95	to	720.23	)		
721.93	5.3900E-02	7.3618E-02	(	711.10	to	732.76	)		
729.87	3.0000E-05	7.2017E-02	(	718.92	to	740.82	)		
+ 767.70	3.1700E-05	6.4833E-02	(	756.18	to	779.22	)	778.67	3.0712
+ 787.40	2.5700E-05	6.1368E-02	(	775.59	to	799.21	)	778.67	3.0712
791.07	1.3300E-04	6.0742E-02	(	779.20	to	802.94	)		
806.34	2.8700E-04	5.8496E-02	(	794.24	to	818.44	)		
+ 809.98	3.1200E-04	5.8070E-02	(	797.83	to	822.13	)	819.18	8.2070
+ 890.46	1.0300E-02	5.0388E-02	(	867.25	to	893.67	)	886.69	2.4800
+ 891.47	8.1300E-05	4.9279E-02	(	878.10	to	904.84	)	886.69	2.4800
+ 907.10	1.2800E-05	4.7746E-02	(	893.49	to	920.71	)	915.19	8.4563
+ 937.82	2.6100E-04	4.4863E-02	(	923.75	to	951.89	)	951.20	2.4658
+ 956.90	1.2800E-05	4.3158E-02	(	942.55	to	971.25	)	951.20	2.4658
1002.85	7.5300E-04	3.9310E-02	(	987.81	to	1017.89	)		
1014.30	1.2800E-05	3.8436E-02	(	999.09	to	1029.51	)		
+ 1031.22	2.0100E-04	3.7339E-02	(	1015.75	to	1046.69	)	1036.70	6.4133
+ 1046.78	1.2000E-04	3.6475E-02	(	1031.08	to	1062.48	)	1036.70	6.4133
+ 1060.22	3.6400E-04	3.5745E-02	(	1044.32	to	1076.12	)	1065.20	1.3209
+ 1103.25	4.1500E-03	3.3500E-02	(	1086.70	to	1119.80	)	1104.20	5.1494
1160.58	2.4000E-05	3.0719E-02	(	1143.17	to	1177.99	)		
1324.48	1.5800E-05	2.4553E-02	(	1304.61	to	1344.35	)		
1340.10	3.0800E-05	2.4102E-02	(	1320.00	to	1360.20	)		
+ 1382.00	3.8500E-06	2.2932E-02	(	1361.27	to	1402.73	)	1367.40	1.6446

Nuclide	Score	T1/2	T1/2_unit	#EmissionInRange	#Matched	Correlation	Comment
88Rb	102.61	1.7800E+01	m	3	3	Moderate	Fiss_Prod
Emission(KeV)	Prob/DK	Detectability	1.50%	Energy Window	Peak(KeV)	Norm%_cts	
+ 898.02	1.4000E-01	4.8631E-02	(	884.55 to 911.49	886.69	2.4800	
+ 1836.00	2.1400E-01	1.4707E-02	(	1808.46 to 1863.54	1828.40	1.3740	
+ 2677.90	1.9600E-02	8.4450E-03	(	2637.73 to 2718.07	2708.20	0.5083	

Nuclide	Score	T1/2	T1/2_unit	#EmissionInRange	#Matched	Correlation	Comment
92Sr	101.74	2.7100E+00	h	4	3	Moderate	Fiss_Prod
Emission(KeV)	Prob/DK	Detectability	1.50%	Energy Window	Peak(KeV)	Norm%_cts	
430.56	3.3300E-02	1.9880E-01	(	424.10 to 437.02			
+ 953.32	3.6000E-02	4.3473E-02	(	939.02 to 967.62	951.20	2.4658	
+ 1142.30	2.8800E-02	3.1580E-02	(	1125.17 to 1159.43	1141.70	1.6217	
+ 1383.90	9.0000E-01	2.2880E-02	(	1363.14 to 1404.66	1367.40	1.6446	

Nuclide	Score	T1/2	T1/2_unit	#EmissionInRange	#Matched	Correlation	Comment
57Co	100.87	7.4400E-01	y	1	1	Moderate	c
Emission(KeV)	Prob/DK	Detectability	1.50%	Energy Window	Peak(KeV)	Norm%_cts	
+ 692.41	1.5800E-03	7.9873E-02	(	682.02 to 702.80	691.66	3.9224	

Nuclide	Score	T1/2	T1/2_unit	#EmissionInRange	#Matched	Correlation	Comment
166mHo	100.80	1.2000E+03	y	16	6	Moderate	Fiss_Prod
Emission(KeV)	Prob/DK	Detectability	1.50%	Energy Window	Peak(KeV)	Norm%_cts	
300.74	3.7200E-02	3.7181E-01	(	296.23 to 305.25			
365.78	2.4200E-02	2.6995E-01	(	360.29 to 371.27			
+ 410.94	1.1100E-01	2.1611E-01	(	404.78 to 417.10	406.31	1.4581	
451.52	2.9200E-02	1.8171E-01	(	444.75 to 458.29			

464.83	1.2000E-02	1.7155E-01	(	457.86	to	471.80	)				
529.81	9.5100E-02	1.3236E-01	(	521.86	to	537.76	)				
571.00	5.4700E-02	1.1422E-01	(	562.44	to	579.56	)				
611.52	1.4200E-02	9.9699E-02	(	602.35	to	620.69	)				
670.51	5.3500E-02	8.4835E-02	(	660.45	to	680.57	)				
+ 691.21	1.3600E-02	8.0137E-02	(	680.84	to	701.58	)	691.66		3.9224	
711.69	5.4100E-01	7.5733E-02	(	701.01	to	722.37	)				
+ 752.27	1.2100E-01	6.7677E-02	(	740.99	to	763.55	)	741.17		4.5257	
+ 778.82	3.0300E-02	6.2855E-02	(	767.14	to	790.50	)	778.67		3.0712	
+ 810.31	5.7100E-01	5.8032E-02	(	798.16	to	822.46	)	819.18		8.2070	
+ 830.56	9.6600E-02	5.5718E-02	(	818.10	to	843.02	)	819.18		8.2070	
+ 950.94	2.6900E-02	4.3683E-02	(	936.68	to	965.20	)	951.20		2.4658	
-----											
Nuclide	Score	T1/2	T1/2_unit	#EmissionInRange	#Matched	Correlation	Comment				
233Pa	100.79	7.3900E-02	y	6	1	Moderate	Np-237_Daughter				
Emission(KeV)	Prob/DK	Detectability		1.50% Energy Window	Peak(KeV)	Norm%_cts					
300.12	6.6400E-02	3.7291E-01	(	295.62	to	304.62	)				
311.98	3.8600E-01	3.5226E-01	(	307.30	to	316.66	)				
340.50	4.5200E-02	3.0640E-01	(	335.39	to	345.61	)				
398.62	1.2700E-02	2.2798E-01	(	392.64	to	404.60	)				
415.76	1.6200E-02	2.1174E-01	(	409.52	to	422.00	)				
+ 692.70	1.5300E-02	7.9809E-02	(	682.31	to	703.09	)	691.66		3.9224	
-----											
Nuclide	Score	T1/2	T1/2_unit	#EmissionInRange	#Matched	Correlation	Comment				
97mNb	100.75	5.2700E+01	s	1	1	Moderate	Fiss_Prod				
Emission(KeV)	Prob/DK	Detectability		1.50% Energy Window	Peak(KeV)	Norm%_cts					
+ 743.36	9.8000E-01	6.9373E-02	(	732.21	to	754.51	)	741.17		4.5257	
-----											
Nuclide	Score	T1/2	T1/2_unit	#EmissionInRange	#Matched	Correlation	Comment				
58Co	100.73	1.9400E-01	y	1	1	Moderate	c				
Emission(KeV)	Prob/DK	Detectability		1.50% Energy Window	Peak(KeV)	Norm%_cts					
+ 810.76	9.9400E-01	5.7979E-02	(	798.60	to	822.92	)	819.18		8.2070	
-----											
Nuclide	Score	T1/2	T1/2_unit	#EmissionInRange	#Matched	Correlation	Comment				
42K	100.37	1.2400E+01	h	2	1	Moderate	c				
Emission(KeV)	Prob/DK	Detectability		1.50% Energy Window	Peak(KeV)	Norm%_cts					
312.70	3.1900E-03	3.5103E-01	(	308.01	to	317.39	)				
+ 1524.70	1.7900E-01	1.9485E-02	(	1501.83	to	1547.57	)	1516.00		4.9373	
-----											
Nuclide	Score	T1/2	T1/2_unit	#EmissionInRange	#Matched	Correlation	Comment				
101Tc	100.22	1.4200E+01	m	4	1	Moderate	Fiss_Prod				
Emission(KeV)	Prob/DK	Detectability		1.50% Energy Window	Peak(KeV)	Norm%_cts					
306.81	8.7500E-01	3.6114E-01	(	302.21	to	311.41	)				
531.49	1.0100E-02	1.3158E-01	(	523.52	to	539.46	)				
545.14	5.9500E-02	1.2532E-01	(	536.96	to	553.32	)				
+ 694.70	1.1400E-02	7.9370E-02	(	684.28	to	705.12	)	691.66		3.9224	
-----											
Nuclide	Score	T1/2	T1/2_unit	#EmissionInRange	#Matched	Correlation	Comment				
40K	99.90	1.2800E+09	y	1	1	Moderate	NORM				
Emission(KeV)	Prob/DK	Detectability		1.50% Energy Window	Peak(KeV)	Norm%_cts					
+ 1460.83	1.0700E-01	2.0877E-02	(	1438.92	to	1482.74	)	1458.40		1.8213	
-----											
Nuclide	Score	T1/2	T1/2_unit	#EmissionInRange	#Matched	Correlation	Comment				
129mTe	99.89	3.3600E+01	d	1	1	Moderate	Fiss_Prod				
Emission(KeV)	Prob/DK	Detectability		1.50% Energy Window	Peak(KeV)	Norm%_cts					
+ 695.88	3.2700E-02	7.9112E-02	(	685.44	to	706.32	)	691.66		3.9224	

Nuclide	Score	T1/2	T1/2_unit	#EmissionInRange	#Matched	Correlation	Comment
209Tl	99.59	4.1900E-06	y	2	1	Moderate	Np-237_Daughter
Emission(KeV)	Prob/DK	Detectability	1.50% Energy Window	Peak(KeV)	Norm%_cts		
465.07	9.6600E-01	1.7137E-01	( 458.09 to 472.05 )				
+ 1567.00	9.9700E-01	1.8756E-02	( 1543.50 to 1590.51 )	1560.00	2.4239		
Nuclide	Score	T1/2	T1/2_unit	#EmissionInRange	#Matched	Correlation	Comment
65Zn	99.55	6.6700E-01	y	2	1	Moderate	Fiss_Prod
Emission(KeV)	Prob/DK	Detectability	1.50% Energy Window	Peak(KeV)	Norm%_cts		
511.00	2.8300E-02	1.4151E-01	( 503.34 to 518.67 )				
+ 1115.55	5.0800E-01	3.2884E-02	( 1098.82 to 1132.28 )	1104.20	5.1494		
Nuclide	Score	T1/2	T1/2_unit	#EmissionInRange	#Matched	Correlation	Comment
52Mn	99.43	2.1100E+01	m	3	1	Moderate	c
Emission(KeV)	Prob/DK	Detectability	1.50% Energy Window	Peak(KeV)	Norm%_cts		
377.74	1.6800E-02	2.5399E-01	( 372.07 to 383.41 )				
511.00	1.9300E+00	1.4151E-01	( 503.34 to 518.67 )				
+ 1434.10	9.8200E-01	2.1553E-02	( 1412.59 to 1455.61 )	1423.50	3.4563		
Nuclide	Score	T1/2	T1/2_unit	#EmissionInRange	#Matched	Correlation	Comment
143La	99.41	1.4200E+01	m	1	1	Moderate	Fiss_Prod
Emission(KeV)	Prob/DK	Detectability	1.50% Energy Window	Peak(KeV)	Norm%_cts		
+ 1722.90	1.6800E-02	1.6293E-02	( 1697.06 to 1748.74 )	1717.70	1.2668		
Nuclide	Score	T1/2	T1/2_unit	#EmissionInRange	#Matched	Correlation	Comment
214Pb	98.92	5.1000E-05	y	2	1	Low	U-238_Daughter
Emission(KeV)	Prob/DK	Detectability	1.50% Energy Window	Peak(KeV)	Norm%_cts		
351.92	3.7200E-01	2.8947E-01	( 346.64 to 357.20 )				
+ 785.91	1.1000E-02	6.1623E-02	( 774.12 to 797.70 )	778.67	3.0712		
Nuclide	Score	T1/2	T1/2_unit	#EmissionInRange	#Matched	Correlation	Comment
140Ba	98.74	1.2000E+01	d	8	1	Low	Fiss_Prod
Emission(KeV)	Prob/DK	Detectability	1.50% Energy Window	Peak(KeV)	Norm%_cts		
304.85	4.2900E-02	3.6456E-01	( 300.28 to 309.42 )				
418.44	3.6600E-05	2.0934E-01	( 412.16 to 424.72 )				
423.72	3.1500E-02	2.0469E-01	( 417.36 to 430.08 )				
437.58	1.9300E-02	1.9292E-01	( 431.02 to 444.14 )				
467.50	1.9500E-05	1.6957E-01	( 460.49 to 474.51 )				
537.26	2.4400E-01	1.2890E-01	( 529.20 to 545.32 )				
551.08	3.1200E-05	1.2269E-01	( 542.81 to 559.35 )				
+ 699.89	8.2900E-06	7.8242E-02	( 689.39 to 710.39 )	691.66	3.9224		
Nuclide	Score	T1/2	T1/2_unit	#EmissionInRange	#Matched	Correlation	Comment
141La	98.28	3.9200E+00	h	1	1	Low	Fiss_Prod
Emission(KeV)	Prob/DK	Detectability	1.50% Energy Window	Peak(KeV)	Norm%_cts		
+ 1354.50	2.6200E-02	2.3694E-02	( 1334.18 to 1374.82 )	1367.40	1.6446		
Nuclide	Score	T1/2	T1/2_unit	#EmissionInRange	#Matched	Correlation	Comment
90Y	98.19	3.1900E+00	h	2	1	Low	Fiss_Prod
Emission(KeV)	Prob/DK	Detectability	1.50% Energy Window	Peak(KeV)	Norm%_cts		
479.51	9.0800E-01	1.6094E-01	( 472.32 to 486.70 )				
+ 681.80	3.1900E-03	8.2241E-02	( 671.57 to 692.03 )	691.66	3.9224		

Nuclide	Score	T1/2	T1/2_unit	#EmissionInRange	#Matched	Correlation	Comment
44Sc	97.53	3.9300E+00	h	2	1	Low	c
Emission(KeV)	Prob/DK	Detectability	1.50% Energy Window	Peak(KeV)	Norm%_cts		
511.00	1.8900E+00	1.4151E-01	( 503.34 to 518.67 )				
+ 1157.00	9.9900E-01	3.0886E-02	( 1139.65 to 1174.36 )	1141.70	1.6217		
Nuclide	Score	T1/2	T1/2_unit <th>#EmissionInRange</th> <th>#Matched</th> <th>Correlation</th> <th>Comment</th>	#EmissionInRange	#Matched	Correlation	Comment
61Cu	96.71	3.3300E+00	h	6	2	Low	c
Emission(KeV)	Prob/DK	Detectability	1.50% Energy Window	Peak(KeV)	Norm%_cts		
373.05	2.1200E-02	2.6016E-01	( 367.45 to 378.65 )				
511.00	1.2300E+00	1.4151E-01	( 503.34 to 518.67 )				
588.60	1.1800E-02	1.0721E-01	( 579.77 to 597.43 )				
656.01	1.0500E-01	8.8281E-02	( 646.17 to 665.85 )				
+ 908.63	1.1900E-02	4.7598E-02	( 895.00 to 922.26 )	915.19	8.4563		
+ 1185.20	3.6300E-02	2.9593E-02	( 1167.42 to 1202.98 )	1191.90	2.2238		
Nuclide	Score	T1/2	T1/2_unit <th>#EmissionInRange</th> <th>#Matched</th> <th>Correlation</th> <th>Comment</th>	#EmissionInRange	#Matched	Correlation	Comment
125Sn	96.68	9.6400E+00	d	7	4	Low	Fiss_Prod
Emission(KeV)	Prob/DK	Detectability	1.50% Energy Window	Peak(KeV)	Norm%_cts		
331.90	1.2900E-02	3.1968E-01	( 326.92 to 336.88 )				
469.70	1.2900E-02	1.6796E-01	( 462.65 to 476.75 )				
+ 822.60	3.7800E-02	5.6617E-02	( 810.26 to 834.94 )	819.18	8.2070		
+ 915.50	3.7800E-02	4.6940E-02	( 901.77 to 929.23 )	915.19	8.4563		
+ 1066.60	8.6000E-02	3.5403E-02	( 1050.60 to 1082.60 )	1065.20	1.3209		
+ 1088.90	4.0400E-02	3.4233E-02	( 1072.57 to 1105.23 )	1104.20	5.1494		
2001.70	2.0600E-02	1.2655E-02	( 1971.67 to 2031.73 )				
Nuclide	Score	T1/2	T1/2_unit <th>#EmissionInRange</th> <th>#Matched</th> <th>Correlation</th> <th>Comment</th>	#EmissionInRange	#Matched	Correlation	Comment
136Cs	94.38	1.3100E+01	d	4	2	Low	Fiss_Prod
Emission(KeV)	Prob/DK	Detectability	1.50% Energy Window	Peak(KeV)	Norm%_cts		
340.57	4.8500E-01	3.0630E-01	( 335.46 to 345.68 )				
+ 818.50	9.9700E-01	5.7085E-02	( 806.22 to 830.78 )	819.18	8.2070		
+ 1048.10	7.9600E-01	3.6403E-02	( 1032.38 to 1063.82 )	1036.70	6.4133		
1235.30	1.9700E-01	2.7425E-02	( 1216.77 to 1253.83 )				
Nuclide	Score	T1/2	T1/2_unit <th>#EmissionInRange</th> <th>#Matched</th> <th>Correlation</th> <th>Comment</th>	#EmissionInRange	#Matched	Correlation	Comment
57Ni	93.08	3.5600E+01	h	4	2	Low	c
Emission(KeV)	Prob/DK	Detectability	1.50% Energy Window	Peak(KeV)	Norm%_cts		
511.00	8.0200E-01	1.4151E-01	( 503.34 to 518.67 )				
+ 1377.60	7.7900E-01	2.3052E-02	( 1356.94 to 1398.26 )	1367.40	1.6446		
+ 1757.50	7.0900E-02	1.5791E-02	( 1731.14 to 1783.86 )	1781.40	0.6781		
1919.40	1.4700E-01	1.3635E-02	( 1890.61 to 1948.19 )				
Nuclide	Score	T1/2	T1/2_unit <th>#EmissionInRange</th> <th>#Matched</th> <th>Correlation</th> <th>Comment</th>	#EmissionInRange	#Matched	Correlation	Comment
212Bi	92.61	1.1500E-04	y	3	2	Low	Th-232_Daughter
Emission(KeV)	Prob/DK	Detectability	1.50% Energy Window	Peak(KeV)	Norm%_cts		
727.17	1.1800E-01	7.2558E-02	( 716.26 to 738.08 )				
+ 785.46	1.9700E-02	6.1701E-02	( 773.68 to 797.24 )	778.67	3.0712		
+ 1620.60	2.7500E-02	1.7871E-02	( 1596.29 to 1644.91 )	1610.00	4.8766		
Nuclide	Score	T1/2	T1/2_unit <th>#EmissionInRange</th> <th>#Matched</th> <th>Correlation</th> <th>Comment</th>	#EmissionInRange	#Matched	Correlation	Comment
147Nd	91.89	1.1000E+01	d	10	1	Low	Fiss_Prod
Emission(KeV)	Prob/DK	Detectability	1.50% Energy Window	Peak(KeV)	Norm%_cts		
319.41	1.9500E-02	3.3980E-01	( 314.62 to 324.20 )				
398.16	8.7000E-03	2.2853E-01	( 392.19 to 404.13 )				
+ 410.48	1.4000E-03	2.1653E-01	( 404.32 to 416.64 )	406.31	1.4581		



439.90	1.2000E-02	1.9101E-01	(	433.30	to	446.50	)		
489.24	1.5300E-03	1.5425E-01	(	481.90	to	496.58	)		
531.02	1.3100E-01	1.3180E-01	(	523.05	to	538.99	)		
589.35	4.5800E-04	1.0692E-01	(	580.51	to	598.19	)		
594.80	2.6500E-03	1.0483E-01	(	585.88	to	603.72	)		
680.52	1.9500E-04	8.2532E-02	(	670.31	to	690.73	)		
+ 685.90	8.1200E-03	8.1318E-02	(	675.61	to	696.19	)	691.66	3.9224

Nuclide	Score	T1/2	T1/2_unit	#EmissionInRange	#Matched	Correlation	Comment		
131Te	91.53	2.5000E+01	m	9	4	Low	Fiss_Prod		
Emission(KeV)	Prob/DK	Detectability	1.50%	Energy Window	Peak(KeV)	Norm%_cts			
452.32	1.8200E-01	1.8108E-01	(	445.54	to	459.10	)		
492.66	4.8400E-02	1.5195E-01	(	485.27	to	500.05	)		
602.04	4.2000E-02	1.0231E-01	(	593.01	to	611.07	)		
654.26	1.5300E-02	8.8705E-02	(	644.45	to	664.07	)		
+ 696.01	1.1900E-02	7.9084E-02	(	685.57	to	706.45	)	691.66	3.9224
+ 948.54	2.2600E-02	4.3897E-02	(	934.31	to	962.77	)	951.20	2.4658
+ 997.25	3.3400E-02	3.9753E-02	(	982.29	to	1012.21	)	982.70	8.6883
+ 1147.00	4.9600E-02	3.1357E-02	(	1129.80	to	1164.21	)	1141.70	1.6217
1881.50	1.4200E-02	1.4112E-02	(	1853.28	to	1909.72	)		

Nuclide	Score	T1/2	T1/2_unit	#EmissionInRange	#Matched	Correlation	Comment		
141Ba	91.44	1.8300E+01	m	14	4	Low	Fiss_Prod		
Emission(KeV)	Prob/DK	Detectability	1.50%	Energy Window	Peak(KeV)	Norm%_cts			
304.24	2.6600E-01	3.6563E-01	(	299.68	to	308.80	)		
343.71	1.5000E-01	3.0156E-01	(	338.55	to	348.87	)		
389.78	1.4000E-02	2.3871E-01	(	383.93	to	395.63	)		
457.58	5.0500E-02	1.7702E-01	(	450.72	to	464.44	)		
462.15	5.0500E-02	1.7355E-01	(	455.22	to	469.08	)		
467.26	5.7800E-02	1.6975E-01	(	460.25	to	474.27	)		
625.23	3.4500E-02	9.6039E-02	(	615.85	to	634.61	)		
647.88	5.9300E-02	9.0270E-02	(	638.16	to	657.60	)		
+ 739.10	4.5200E-02	7.0198E-02	(	728.01	to	750.19	)	741.17	4.5257
831.72	1.6000E-02	5.5588E-02	(	819.24	to	844.20	)		
+ 876.29	3.6000E-02	5.0814E-02	(	863.15	to	889.43	)	886.69	2.4800
+ 1197.50	4.8000E-02	2.9046E-02	(	1179.54	to	1215.46	)	1191.90	2.2238
1252.00	1.7300E-02	2.6755E-02	(	1233.22	to	1270.78	)		
+ 1682.40	1.4100E-02	1.6901E-02	(	1657.16	to	1707.64	)	1676.80	3.3360

Nuclide	Score	T1/2	T1/2_unit	#EmissionInRange	#Matched	Correlation	Comment		
130I	89.49	1.2400E+01	h	8	3	Low	Fiss_Prod		
Emission(KeV)	Prob/DK	Detectability	1.50%	Energy Window	Peak(KeV)	Norm%_cts			
418.01	3.4200E-01	2.0972E-01	(	411.74	to	424.28	)		
536.09	9.9000E-01	1.2944E-01	(	528.05	to	544.13	)		
539.10	1.4000E-02	1.2805E-01	(	531.01	to	547.19	)		
586.05	1.6900E-02	1.0820E-01	(	577.26	to	594.84	)		
668.54	9.6100E-01	8.5296E-02	(	658.51	to	678.57	)		
+ 685.99	1.0700E-02	8.1298E-02	(	675.70	to	696.28	)	691.66	3.9224
+ 734.80	8.2300E-01	7.1040E-02	(	723.78	to	745.82	)	741.17	4.5257
+ 1157.50	1.1300E-01	3.0862E-02	(	1140.14	to	1174.86	)	1141.70	1.6217

Nuclide	Score	T1/2	T1/2_unit	#EmissionInRange	#Matched	Correlation	Comment		
106Rh	87.68	1.0000E+00	y	3	1	Low	Fiss_Prod		
Emission(KeV)	Prob/DK	Detectability	1.50%	Energy Window	Peak(KeV)	Norm%_cts			
512.00	2.0600E-01	1.4101E-01	(	504.32	to	519.68	)		
621.84	9.8100E-02	9.6932E-02	(	612.51	to	631.17	)		
+ 1050.50	1.7300E-02	3.6272E-02	(	1034.74	to	1066.26	)	1036.70	6.4133

Nuclide	Score	T1/2	T1/2_unit	#EmissionInRange	#Matched	Correlation	Comment
52Mn	87.50	5.5900E+00	d	7	3	Low	c

Emission(KeV)	Prob/DK	Detectability	1.50% Energy Window	Peak(KeV)	Norm%_cts
511.00	5.8800E-01	1.4151E-01	( 503.34 to 518.67 )		
+ 744.21	9.0000E-01	6.9209E-02	( 733.05 to 755.37 )	741.17	4.5257
+ 848.13	3.3200E-02	5.3783E-02	( 835.41 to 860.85 )	850.68	8.7431
935.52	9.4500E-01	4.5073E-02	( 921.49 to 949.55 )		
1246.20	4.2100E-02	2.6974E-02	( 1227.51 to 1264.89 )		
1333.60	5.0700E-02	2.4289E-02	( 1313.60 to 1353.60 )		
+ 1434.10	1.0000E+00	2.1553E-02	( 1412.59 to 1455.61 )	1423.50	3.4563

---

Nuclide	Score	T1/2	T1/2_unit	#EmissionInRange	#Matched	Correlation	Comment
106Ru	86.32	1.0000E+00	y	2	1	Low	Fiss_Prod

Emission(KeV)	Prob/DK	Detectability	1.50% Energy Window	Peak(KeV)	Norm%_cts
622.20	9.9500E-02	9.6837E-02	( 612.87 to 631.53 )		
+ 1050.50	1.5600E-02	3.6272E-02	( 1034.74 to 1066.26 )	1036.70	6.4133

---

Nuclide	Score	T1/2	T1/2_unit	#EmissionInRange	#Matched	Correlation	Comment
126Sb	86.11	2.9800E+02	h	14	5	Low	Fiss_Prod

Emission(KeV)	Prob/DK	Detectability	1.50% Energy Window	Peak(KeV)	Norm%_cts
414.70	8.3300E-01	2.1269E-01	( 408.48 to 420.92 )		
+ 555.20	1.6900E-02	1.2089E-01	( 546.87 to 563.53 )	561.22	1.5470
573.80	6.6800E-02	1.1308E-01	( 565.19 to 582.41 )		
593.00	7.4700E-02	1.0551E-01	( 584.11 to 601.90 )		
656.30	2.1900E-02	8.8210E-02	( 646.46 to 666.14 )		
666.33	9.9600E-01	8.5815E-02	( 656.34 to 676.32 )		
675.00	3.6900E-02	8.3795E-02	( 664.88 to 685.13 )		
+ 695.00	9.9600E-01	7.9304E-02	( 684.58 to 705.43 )	691.66	3.9224
+ 697.00	2.8900E-01	7.8868E-02	( 686.55 to 707.45 )	691.66	3.9224
720.50	5.3800E-01	7.3910E-02	( 709.69 to 731.31 )		
+ 856.80	1.7600E-01	5.2851E-02	( 843.95 to 869.65 )	850.68	8.7431
+ 954.00	1.2000E-02	4.3413E-02	( 939.69 to 968.31 )	951.20	2.4658
+ 989.30	6.7700E-02	4.0403E-02	( 974.46 to 1004.14 )	982.70	8.6883
1213.00	2.3900E-02	2.8371E-02	( 1194.81 to 1231.20 )		

---

Nuclide	Score	T1/2	T1/2_unit	#EmissionInRange	#Matched	Correlation	Comment
56Mn	85.98	2.5800E+00	h	3	2	Low	c

Emission(KeV)	Prob/DK	Detectability	1.50% Energy Window	Peak(KeV)	Norm%_cts
+ 846.75	9.8900E-01	5.3932E-02	( 834.05 to 859.45 )	850.68	8.7431
+ 1810.70	2.7200E-01	1.5048E-02	( 1783.54 to 1837.86 )	1828.40	1.3740
2113.10	1.4300E-01	1.1769E-02	( 2081.40 to 2144.80 )		

---

Nuclide	Score	T1/2	T1/2_unit	#EmissionInRange	#Matched	Correlation	Comment
48Sc	85.12	4.3700E+01	h	4	2	Low	c

Emission(KeV)	Prob/DK	Detectability	1.50% Energy Window	Peak(KeV)	Norm%_cts
+ 983.50	1.0000E+00	4.0883E-02	( 968.75 to 998.25 )	982.70	8.6883
+ 1037.50	9.7500E-01	3.6988E-02	( 1021.94 to 1053.06 )	1036.70	6.4133
1212.80	2.3800E-02	2.8379E-02	( 1194.61 to 1230.99 )		
1312.10	1.0000E+00	2.4917E-02	( 1292.42 to 1331.78 )		

---

Nuclide	Score	T1/2	T1/2_unit	#EmissionInRange	#Matched	Correlation	Comment
82Br	83.38	3.5300E+01	h	10	4	Low	Fiss_Prod

Emission(KeV)	Prob/DK	Detectability	1.50% Energy Window	Peak(KeV)	Norm%_cts
+ 554.32	7.0600E-01	1.2127E-01	( 546.01 to 562.63 )	561.22	1.5470
606.30	1.1700E-02	1.0113E-01	( 597.21 to 615.39 )		
613.83	2.8200E-01	9.9073E-02	( 604.62 to 623.04 )		
619.07	4.3100E-01	9.7668E-02	( 609.78 to 628.36 )		
+ 776.49	8.3300E-01	6.3264E-02	( 764.84 to 788.14 )	778.67	3.0712
+ 827.81	2.4200E-01	5.6027E-02	( 815.39 to 840.23 )	819.18	8.2070
1007.60	1.2700E-02	3.8945E-02	( 992.49 to 1022.71 )		
+ 1044.00	2.7300E-01	3.6628E-02	( 1028.34 to 1059.66 )	1036.70	6.4133
1317.50	2.6900E-01	2.4758E-02	( 1297.74 to 1337.26 )		

+ 1474.80 1.6600E-01 2.0532E-02 ( 1452.68 to 1496.92 ) 1458.40 1.8213

Nuclide	Score	T1/2	T1/2_unit	#EmissionInRange	#Matched	Correlation	Comment
93Y	82.55	1.0200E+01	h	26	12	Low	Fiss_Prod
Emission(KeV)	Prob/DK	Detectability	1.50%	Energy Window	Peak(KeV)	Norm%_cts	
341.50	4.4300E-04	3.0489E-01	(	336.38 to 346.62)			
387.50	7.5000E-05	2.4154E-01	(	381.69 to 393.31)			
680.20	6.5800E-03	8.2604E-02	(	670.00 to 690.40)			
714.40	1.7300E-04	7.5168E-02	(	703.68 to 725.12)			
+ 947.10	2.0900E-02	4.4026E-02	(	932.89 to 961.31)	951.20	2.4658	
+ 962.30	1.2000E-04	4.2686E-02	(	947.87 to 976.73)	951.20	2.4658	
+ 971.00	6.7500E-05	4.1937E-02	(	956.43 to 985.56)	982.70	8.6883	
+ 987.70	1.0500E-04	4.0535E-02	(	972.88 to 1002.52)	982.70	8.6883	
+ 1158.50	3.0000E-04	3.0815E-02	(	1141.12 to 1175.88)	1141.70	1.6217	
1168.60	1.0500E-04	3.0348E-02	(	1151.07 to 1186.13)			
+ 1183.50	4.8000E-04	2.9670E-02	(	1165.75 to 1201.25)	1191.90	2.2238	
+ 1184.70	1.9500E-04	2.9616E-02	(	1166.93 to 1202.47)	1191.90	2.2238	
+ 1203.30	1.0700E-03	2.8792E-02	(	1185.25 to 1221.35)	1191.90	2.2238	
1237.40	2.9300E-04	2.7338E-02	(	1218.84 to 1255.96)			
+ 1425.40	2.4500E-03	2.1778E-02	(	1404.02 to 1446.78)	1423.50	3.4563	
+ 1450.50	3.2700E-03	2.1136E-02	(	1428.74 to 1472.26)	1458.40	1.8213	
+ 1470.10	6.5300E-04	2.0648E-02	(	1448.05 to 1492.15)	1458.40	1.8213	
1642.70	5.1800E-04	1.7518E-02	(	1618.06 to 1667.34)			
1651.70	2.3300E-04	1.7376E-02	(	1626.92 to 1676.48)			
+ 1827.80	2.3300E-04	1.4816E-02	(	1800.38 to 1855.22)	1828.40	1.3740	
1917.80	1.5500E-02	1.3655E-02	(	1889.03 to 1946.57)			
2184.60	1.5700E-03	1.1286E-02	(	2151.83 to 2217.37)			
2190.80	1.6900E-03	1.1245E-02	(	2157.94 to 2223.66)			
2457.30	6.7500E-05	9.6154E-03	(	2420.44 to 2494.16)			
2473.80	1.1300E-04	9.5226E-03	(	2436.69 to 2510.91)			
2605.00	1.1300E-04	8.8153E-03	(	2565.93 to 2644.07)			

Nuclide	Score	T1/2	T1/2_unit	#EmissionInRange	#Matched	Correlation	Comment
138Cs	78.71	3.3400E+01	m	11	3	Low	Fiss_Prod
Emission(KeV)	Prob/DK	Detectability	1.50%	Energy Window	Peak(KeV)	Norm%_cts	
+ 408.98	4.6600E-02	2.1791E-01	(	402.85 to 415.11)	406.31	1.4581	
462.79	3.0800E-01	1.7307E-01	(	455.85 to 469.73)			
546.94	1.0800E-01	1.2452E-01	(	538.74 to 555.14)			
871.80	5.1100E-02	5.1277E-02	(	858.72 to 884.88)			
1009.80	2.9800E-01	3.8778E-02	(	994.65 to 1024.95)			
+ 1147.20	1.2400E-02	3.1347E-02	(	1129.99 to 1164.41)	1141.70	1.6217	
1343.60	1.1500E-02	2.4003E-02	(	1323.45 to 1363.75)			
+ 1435.90	7.6300E-01	2.1507E-02	(	1414.36 to 1457.44)	1423.50	3.4563	
+ 1613.20	1.6200E-02	1.7991E-02	(	1589.00 to 1637.40)	1610.00	4.8766	
2218.00	1.5200E-01	1.1067E-02	(	2184.73 to 2251.27)			
2639.60	7.6300E-02	8.6376E-03	(	2600.01 to 2679.19)			

Nuclide	Score	T1/2	T1/2_unit	#EmissionInRange	#Matched	Correlation	Comment
160Tb	73.33	1.9800E-01	y	10	5	Low	Fiss_Prod
Emission(KeV)	Prob/DK	Detectability	1.50%	Energy Window	Peak(KeV)	Norm%_cts	
392.49	1.2800E-02	2.3538E-01	(	386.60 to 398.38)			
765.28	1.9300E-02	6.5271E-02	(	753.80 to 776.76)			
+ 879.36	2.8500E-01	5.0500E-02	(	866.17 to 892.55)	886.69	2.4800	
+ 962.29	9.0300E-02	4.2687E-02	(	947.86 to 976.72)	951.20	2.4658	
966.15	2.4200E-01	4.2353E-02	(	951.66 to 980.64)			
+ 1115.10	1.5000E-02	3.2906E-02	(	1098.37 to 1131.83)	1104.20	5.1494	
+ 1177.90	1.4400E-01	2.9923E-02	(	1160.23 to 1195.57)	1191.90	2.2238	
+ 1199.90	2.3600E-02	2.8941E-02	(	1181.90 to 1217.90)	1191.90	2.2238	
1271.90	7.0300E-02	2.6132E-02	(	1252.82 to 1290.98)			
1312.20	2.8500E-02	2.4914E-02	(	1292.52 to 1331.88)			

Nuclide	Score	T1/2	T1/2_unit	#EmissionInRange	#Matched	Correlation	Comment
92Y	65.14	3.5400E+00	h	5	2	Low	Fiss_Prod

Emission(KeV)	Prob/DK	Detectability	1.50% Energy Window	Peak(KeV)	Norm%_cts
448.50	2.3400E-02	1.8408E-01	( 441.77 to 455.23 )		
+ 561.10	2.4100E-02	1.1836E-01	( 552.68 to 569.52 )	561.22	1.5470
+ 844.30	2.1500E-02	5.4199E-02	( 831.64 to 856.96 )	850.68	8.7431
934.46	1.3900E-01	4.5170E-02	( 920.44 to 948.48 )		
+ 1405.40	4.7800E-02	2.2302E-02	( 1384.32 to 1426.48 )	1423.50	3.4563

---

Nuclide	Score	T1/2	T1/2_unit	#EmissionInRange	#Matched	Correlation	Comment
<sup>56</sup> Co	64.30	2.1200E-01	y	11	6	Low	c

Emission(KeV)	Prob/DK	Detectability	1.50% Energy Window	Peak(KeV)	Norm%_cts
511.00	3.9500E-01	1.4151E-01	( 503.34 to 518.67 )		
+ 846.75	1.0000E+00	5.3932E-02	( 834.05 to 859.45 )	850.68	8.7431
+ 977.42	1.4300E-02	4.1393E-02	( 962.76 to 992.08 )	982.70	8.6883
+ 1037.80	1.4000E-01	3.6971E-02	( 1022.23 to 1053.37 )	1036.70	6.4133
+ 1175.10	2.2800E-02	3.0050E-02	( 1157.47 to 1192.73 )	1191.90	2.2238
1238.30	6.7000E-01	2.7300E-02	( 1219.73 to 1256.87 )		
+ 1360.20	4.2900E-02	2.3534E-02	( 1339.80 to 1380.60 )	1367.40	1.6446
+ 1771.40	1.5500E-01	1.5593E-02	( 1744.83 to 1797.97 )	1781.40	0.6781
2015.40	3.0300E-02	1.2525E-02	( 1985.17 to 2045.63 )		
2034.90	7.7800E-02	1.2341E-02	( 2004.38 to 2065.42 )		
2598.50	1.6900E-01	8.8491E-03	( 2559.52 to 2637.48 )		

---

Nuclide	Score	T1/2	T1/2_unit	#EmissionInRange	#Matched	Correlation	Comment
<sup>138</sup> Xe	61.89	1.4100E+01	m	11	4	Low	Fiss_Prod

Emission(KeV)	Prob/DK	Detectability	1.50% Energy Window	Peak(KeV)	Norm%_cts
396.43	6.3000E-02	2.3060E-01	( 390.48 to 402.38 )		
+ 401.36	2.1700E-02	2.2504E-01	( 395.34 to 407.38 )	406.31	1.4581
434.49	2.0300E-01	1.9549E-01	( 427.97 to 441.01 )		
+ 1114.30	1.4700E-02	3.2946E-02	( 1097.59 to 1131.01 )	1104.20	5.1494
+ 1118.60	2.6600E-02	3.2732E-02	( 1101.82 to 1135.38 )	1104.20	5.1494
+ 1768.30	1.6700E-01	1.5637E-02	( 1741.78 to 1794.82 )	1781.40	0.6781
+ 1850.90	1.4200E-02	1.4509E-02	( 1823.14 to 1878.66 )	1828.40	1.3740
2004.80	5.3600E-02	1.2626E-02	( 1974.73 to 2034.87 )		
2015.80	1.2300E-01	1.2521E-02	( 1985.56 to 2046.04 )		
2079.20	1.4400E-02	1.2006E-02	( 2048.01 to 2110.39 )		
2252.30	2.2900E-02	1.0846E-02	( 2218.52 to 2286.08 )		

---

Nuclide	Score	T1/2	T1/2_unit	#EmissionInRange	#Matched	Correlation	Comment
<sup>156</sup> Eu	59.98	1.5200E+01	d	24	9	Low	Fiss_Prod

Emission(KeV)	Prob/DK	Detectability	1.50% Energy Window	Peak(KeV)	Norm%_cts
599.47	2.3100E-02	1.0307E-01	( 590.48 to 608.46 )		
646.29	7.0900E-02	9.0664E-02	( 636.60 to 655.98 )		
723.47	6.0200E-02	7.3305E-02	( 712.62 to 734.32 )		
+ 811.77	1.0400E-01	5.7862E-02	( 799.59 to 823.95 )	819.18	8.2070
867.01	1.4000E-02	5.1775E-02	( 854.00 to 880.02 )		
+ 944.35	1.3900E-02	4.4272E-02	( 930.18 to 958.52 )	951.20	2.4658
+ 960.50	1.6200E-02	4.2843E-02	( 946.09 to 974.91 )	951.20	2.4658
+ 1065.10	5.2400E-02	3.5483E-02	( 1049.12 to 1081.08 )	1065.20	1.3209
+ 1079.20	4.8900E-02	3.4738E-02	( 1063.01 to 1095.39 )	1065.20	1.3209
+ 1102.70	1.5900E-02	3.3528E-02	( 1086.16 to 1119.24 )	1104.20	5.1494
+ 1153.50	7.1800E-02	3.1050E-02	( 1136.20 to 1170.80 )	1141.70	1.6217
+ 1154.10	5.3000E-02	3.1021E-02	( 1136.79 to 1171.41 )	1141.70	1.6217
1230.70	8.9400E-02	2.7618E-02	( 1212.24 to 1249.16 )		
1242.40	6.7600E-02	2.7130E-02	( 1223.76 to 1261.04 )		
1277.40	3.2100E-02	2.5963E-02	( 1258.24 to 1296.56 )		
+ 1366.40	1.7600E-02	2.3361E-02	( 1345.90 to 1386.90 )	1367.40	1.6446
1877.00	1.7300E-02	1.4170E-02	( 1848.85 to 1905.16 )		
1937.70	2.1400E-02	1.3410E-02	( 1908.63 to 1966.77 )		
1966.00	4.2000E-02	1.3069E-02	( 1936.51 to 1995.49 )		
2026.60	3.5400E-02	1.2419E-02	( 1996.20 to 2057.00 )		
2097.70	4.2700E-02	1.1876E-02	( 2066.23 to 2129.17 )		
2180.90	2.4300E-02	1.1310E-02	( 2148.19 to 2213.61 )		
2186.70	3.9500E-02	1.1272E-02	( 2153.90 to 2219.50 )		

Nuclide	Score	T1/2	T1/2_unit	#EmissionInRange	#Matched	Correlation	Comment
59Fe	56.70	4.4500E+01	d	2	1	Low	c
Emission(KeV)	Prob/DK	Detectability	1.50% Energy Window		Peak(KeV)	Norm%_cts	
+ 1099.20	5.6500E-01	3.3705E-02	( 1082.71 to 1115.69 )		1104.20	5.1494	
1291.60	4.3200E-01	2.5530E-02	( 1272.23 to 1310.97 )				

Nuclide	Score	T1/2	T1/2_unit	#EmissionInRange	#Matched	Correlation	Comment
89Rb	56.45	1.5200E+01	m	10	4	Low	Fiss_Prod
Emission(KeV)	Prob/DK	Detectability	1.50% Energy Window		Peak(KeV)	Norm%_cts	
657.71	9.9800E-02	8.7870E-02	( 647.84 to 667.58 )				
+ 947.69	9.2200E-02	4.3973E-02	( 933.47 to 961.91 )		951.20	2.4658	
+ 1031.90	5.8000E-01	3.7301E-02	( 1016.42 to 1047.38 )		1036.70	6.4133	
1248.10	4.2300E-01	2.6896E-02	( 1229.38 to 1266.82 )				
+ 1538.10	2.5500E-02	1.9251E-02	( 1515.03 to 1561.17 )		1560.00	2.4239	
1950.30	1.1800E-02	1.3257E-02	( 1921.05 to 1979.55 )				
2007.50	2.3800E-02	1.2600E-02	( 1977.39 to 2037.61 )				
2196.00	1.3300E-01	1.1211E-02	( 2163.06 to 2228.94 )				
2570.10	9.8600E-02	8.9982E-03	( 2531.55 to 2608.65 )				
+ 2707.20	2.0300E-02	8.3006E-03	( 2666.59 to 2747.81 )		2708.20	0.5083	

Nuclide	Score	T1/2	T1/2_unit	#EmissionInRange	#Matched	Correlation	Comment
48V	50.36	1.6000E+01	d	5	2	Low	medical_from_Ti-48
Emission(KeV)	Prob/DK	Detectability	1.50% Energy Window		Peak(KeV)	Norm%_cts	
511.00	1.0000E+00	1.4151E-01	( 503.34 to 518.67 )				
+ 944.10	7.7600E-02	4.4295E-02	( 929.94 to 958.26 )		951.20	2.4658	
+ 983.50	1.0000E+00	4.0883E-02	( 968.75 to 998.25 )		982.70	8.6883	
1312.10	9.7500E-01	2.4917E-02	( 1292.42 to 1331.78 )				
2240.30	2.4100E-02	1.0923E-02	( 2206.70 to 2273.90 )				

## APPENDIX E

### NEW SMARTID LIBRARY FOR SPENT FUEL ATTRIBUTION

idx	jdx	E(keV)	Nuclide	T1/2	T1/2_unit	Prob/DK	lib-freq	comment
25	3	3.6	126Sn	1.00E+05	y	1.12E-01	9	Fiss_Prod
22	10	3.77	125Sb	2.76E+00	y	4.95E-02	13	Fiss_Prod
34	27	3.77	131mTe	3.24E+01	h	1.67E-02	36	Fiss_Prod
30	3	3.94	129Te	3.36E+01	d	6.16E-02	4	Fiss_Prod
34	36	3.94	131mTe	3.24E+01	h	1.11E-02	36	Fiss_Prod
36	12	3.94	131Te	2.50E+01	m	1.45E-02	14	Fiss_Prod
50	5	4.11	135mXe	1.53E+01	m	1.66E-02	5	Fiss_Prod
44	5	4.29	133Xe	5.24E+00	d	6.14E-02	10	Fiss_Prod
52	14	4.47	136Cs	1.31E+01	d	2.82E-02	14	Fiss_Prod
54	5	4.47	137mBa	2.55E+00	m	1.04E-02	5	Fiss_Prod
59	2	4.65	140Ba	1.20E+01	d	1.47E-01	20	Fiss_Prod
76	93	4.82	151Pm	2.84E+01	h	6.08E-04	234	Fiss_Prod
73	18	5.64	148mPm	4.13E+01	d	1.07E-02	18	Fiss_Prod
79	4	5.85	153Sm	4.63E+01	h	1.19E-01	5	Fiss_Prod
82	9	6.06	156Eu	1.52E+01	d	5.44E-02	29	Fiss_Prod
84	6	6.5	160Tb	1.98E-01	y	1.07E-01	17	Fiss_Prod
193	3	8.03	65Zn	6.67E-01	y	1.15E-01	5	Fiss_Prod
193	2	8.05	65Zn	6.67E-01	y	2.26E-01	5	Fiss_Prod
193	4	8.91	65Zn	6.67E-01	y	4.61E-02	5	Fiss_Prod
204	11	13.34	88Kr	2.84E+00	h	2.37E-02	20	Fiss_Prod
204	6	13.4	88Kr	2.84E+00	h	4.59E-02	20	Fiss_Prod
140	1	13.6	238Pu	8.77E+01	y	1.16E-01	7	SNM
143	1	13.6	239Pu	2.41E+04	y	4.41E-02	83	SNM
145	1	13.6	240Pu	6.54E+03	y	1.10E-01	5	SNM
138	12	13.81	237U	1.62E+02	h	9.90E-04	24	237Np_Parent
59	8	13.85	140Ba	1.20E+01	d	1.22E-02	20	Fiss_Prod
147	1	13.9	241Am	4.32E+02	y	4.27E-01	28	SNM
139	1	14.3	238Np	2.12E+00	d	3.74E-01	5	SNM
149	2	14.3	242Am	1.60E+01	h	1.27E-01	5	SNM
208	2	14.96	91mY	4.97E+01	m	1.65E-02	2	Fiss_Prod
149	1	15	242Am	1.60E+01	h	1.97E-01	5	SNM
204	19	15	88Kr	2.84E+00	h	1.20E-02	20	Fiss_Prod
25	9	21.65	126Sn	1.00E+05	y	1.24E-02	9	Fiss_Prod
25	7	23.28	126Sn	1.00E+05	y	6.40E-02	9	Fiss_Prod
60	37	24.6	140La	4.03E+01	h	2.86E-05	38	Fiss_Prod
76	21	25.69	151Pm	2.84E+01	h	9.68E-03	234	Fiss_Prod

25	6	26.11	126Sn	1.00E+05	y	8.33E-02	9	Fiss_Prod
147	3	26.34	241Am	4.32E+02	y	2.40E-02	28	SNM
138	4	26.35	237U	1.62E+02	h	2.43E-02	24	237Np_Parent
25	2	26.36	126Sn	1.00E+05	y	1.56E-01	9	Fiss_Prod
22	4	27.2	125Sb	2.76E+00	y	1.28E-01	13	Fiss_Prod
27	1	27.2	127Te	9.35E+00	h	1.04E-01	1	Fiss_Prod
34	17	27.2	131mTe	3.24E+01	h	3.59E-02	36	Fiss_Prod
22	2	27.47	125Sb	2.76E+00	y	2.39E-01	13	Fiss_Prod
34	11	27.47	131mTe	3.24E+01	h	6.70E-02	36	Fiss_Prod
204	14	27.51	88Kr	2.84E+00	h	2.06E-02	20	Fiss_Prod
30	1	27.77	129Te	3.36E+01	d	1.63E-01	4	Fiss_Prod
34	20	28.32	131mTe	3.24E+01	h	2.83E-02	36	Fiss_Prod
36	7	28.32	131Te	2.50E+01	m	3.68E-02	14	Fiss_Prod
34	13	28.61	131mTe	3.24E+01	h	5.27E-02	36	Fiss_Prod
36	3	28.61	131Te	2.50E+01	m	6.85E-02	14	Fiss_Prod
33	6	29.46	131I	8.02E+00	d	1.35E-02	6	Fiss_Prod
50	3	29.46	135mXe	1.53E+01	m	3.84E-02	5	Fiss_Prod
25	8	29.7	126Sn	1.00E+05	y	5.34E-02	9	Fiss_Prod
33	4	29.78	131I	8.02E+00	d	2.50E-02	6	Fiss_Prod
50	2	29.78	135mXe	1.53E+01	m	7.13E-02	5	Fiss_Prod
59	3	29.97	140Ba	1.20E+01	d	1.41E-01	20	Fiss_Prod
44	3	30.63	133Xe	5.24E+00	d	1.36E-01	10	Fiss_Prod
51	4	30.63	135Xe	9.14E+00	h	1.45E-02	4	Fiss_Prod
44	2	30.97	133Xe	5.24E+00	d	2.23E-01	10	Fiss_Prod
51	3	30.97	135Xe	9.14E+00	h	2.68E-02	4	Fiss_Prod
22	7	31	125Sb	2.76E+00	y	8.28E-02	13	Fiss_Prod
34	21	31	131mTe	3.24E+01	h	2.32E-02	36	Fiss_Prod
52	11	31.82	136Cs	1.31E+01	d	4.95E-02	14	Fiss_Prod
54	3	31.82	137mBa	2.55E+00	m	2.07E-02	5	Fiss_Prod
52	8	32.19	136Cs	1.31E+01	d	9.12E-02	14	Fiss_Prod
54	2	32.19	137mBa	2.55E+00	m	3.82E-02	5	Fiss_Prod
34	24	32.3	131mTe	3.24E+01	h	1.85E-02	36	Fiss_Prod
36	9	32.3	131Te	2.50E+01	m	2.40E-02	14	Fiss_Prod
138	10	33.2	237U	1.62E+02	h	1.30E-03	24	237Np_Parent
50	4	33.6	135mXe	1.53E+01	m	2.54E-02	5	Fiss_Prod
44	4	35	133Xe	5.24E+00	d	9.06E-02	10	Fiss_Prod
76	116	35.2	151Pm	2.84E+01	h	3.38E-04	234	Fiss_Prod
22	11	35.49	125Sb	2.76E+00	y	4.17E-02	13	Fiss_Prod
52	13	36.4	136Cs	1.31E+01	d	3.32E-02	14	Fiss_Prod
54	4	36.4	137mBa	2.55E+00	m	1.39E-02	5	Fiss_Prod
72	4	38.17	147Nd	1.10E+01	d	1.30E-01	18	Fiss_Prod
138	17	38.54	237U	1.62E+02	h	2.10E-04	24	237Np_Parent
143	3	38.66	239Pu	2.41E+04	y	1.05E-04	83	SNM

72	2	38.72	147Nd	1.10E+01	d	2.36E-01	18	Fiss_Prod
73	15	38.72	148mPm	4.13E+01	d	1.32E-02	18	Fiss_Prod
73	14	39.52	148mPm	4.13E+01	d	1.67E-02	18	Fiss_Prod
74	4	40.12	148Pm	5.37E+00	d	3.03E-02	5	Fiss_Prod
143	23	40.41	239Pu	2.41E+04	y	1.62E-06	83	SNM
222	6	40.58	99Mo	6.60E+01	h	1.05E-02	35	medical_FP
79	3	40.9	153Sm	4.63E+01	h	1.73E-01	5	Fiss_Prod
79	1	41.54	153Sm	4.63E+01	h	3.12E-01	5	Fiss_Prod
143	22	42.06	239Pu	2.41E+04	y	1.65E-06	83	SNM
82	16	42.31	156Eu	1.52E+01	d	3.83E-02	29	Fiss_Prod
82	6	43	156Eu	1.52E+01	d	6.91E-02	29	Fiss_Prod
138	15	43.42	237U	1.62E+02	h	2.40E-04	24	237Np_Parent
140	2	43.48	238Pu	8.77E+01	y	3.93E-04	7	SNM
59	14	43.8	140Ba	1.20E+01	d	1.95E-05	20	Fiss_Prod
72	5	43.8	147Nd	1.10E+01	d	9.06E-02	18	Fiss_Prod
148	4	44.2	241Pu	1.44E+01	y	4.90E-08	6	SNM
142	12	44.66	239Np	5.66E+01	h	1.30E-03	37	239Pu_Parent
148	6	44.86	241Pu	1.44E+01	y	8.36E-09	6	SNM
84	9	45.21	160Tb	1.98E-01	y	6.03E-02	17	Fiss_Prod
145	2	45.24	240Pu	6.54E+03	y	4.50E-04	5	SNM
73	16	45.4	148mPm	4.13E+01	d	1.18E-02	18	Fiss_Prod
84	5	46	160Tb	1.98E-01	y	1.08E-01	17	Fiss_Prod
143	11	46.21	239Pu	2.41E+04	y	7.37E-06	83	SNM
143	38	46.69	239Pu	2.41E+04	y	5.80E-07	83	SNM
82	19	48.7	156Eu	1.52E+01	d	2.73E-02	29	Fiss_Prod
142	13	49.41	239Np	5.66E+01	h	1.30E-03	37	239Pu_Parent
138	9	51.01	237U	1.62E+02	h	3.40E-03	24	237Np_Parent
143	2	51.63	239Pu	2.41E+04	y	2.70E-04	83	SNM
84	11	52.1	160Tb	1.98E-01	y	4.32E-02	17	Fiss_Prod
148	5	56	241Pu	1.44E+01	y	3.43E-08	6	SNM
143	9	56.84	239Pu	2.41E+04	y	1.13E-05	83	SNM
142	14	57.28	239Np	5.66E+01	h	1.30E-03	37	239Pu_Parent
142	26	57.3	239Np	5.66E+01	h	4.80E-05	37	239Pu_Parent
67	2	57.36	143Ce	3.30E+01	h	1.17E-01	52	Fiss_Prod
226	1	58	W_Kalpha2	0.00E+00	u	1.00E-08	1	c
138	1	59.54	237U	1.62E+02	h	3.45E-01	24	237Np_Parent
147	2	59.54	241Am	4.32E+02	y	3.59E-01	28	SNM
76	130	59.93	151Pm	2.84E+01	h	2.48E-04	234	Fiss_Prod
76	207	61	151Pm	2.84E+01	h	6.98E-05	234	Fiss_Prod
142	8	61.46	239Np	5.66E+01	h	1.29E-02	37	239Pu_Parent
76	51	62.91	151Pm	2.84E+01	h	2.07E-03	234	Fiss_Prod
59	19	63.17	140Ba	1.20E+01	d	2.93E-07	20	Fiss_Prod
143	42	64.04	239Pu	2.41E+04	y	3.20E-07	83	SNM



60	31	64.14	140La	4.03E+01	h	1.43E-04	38	Fiss_Prod
25	4	64.28	126Sn	1.00E+05	y	9.58E-02	9	Fiss_Prod
138	6	64.83	237U	1.62E+02	h	1.28E-02	24	237Np_Parent
76	11	64.88	151Pm	2.84E+01	h	1.89E-02	234	Fiss_Prod
76	19	65.83	151Pm	2.84E+01	h	1.15E-02	234	Fiss_Prod
52	7	66.91	136Cs	1.31E+01	d	1.25E-01	14	Fiss_Prod
142	16	67.86	239Np	5.66E+01	h	9.20E-04	37	239Pu_Parent
60	19	68.92	140La	4.03E+01	h	7.54E-04	38	Fiss_Prod
79	5	69.67	153Sm	4.63E+01	h	5.17E-02	5	Fiss_Prod
76	34	69.7	151Pm	2.84E+01	h	4.73E-03	234	Fiss_Prod
138	23	69.76	237U	1.62E+02	h	9.50E-06	24	237Np_Parent
76	52	76.22	151Pm	2.84E+01	h	2.03E-03	234	Fiss_Prod
44	6	79.62	133Xe	5.24E+00	d	2.70E-03	10	Fiss_Prod
44	1	81	133Xe	5.24E+00	d	3.80E-01	10	Fiss_Prod
34	16	81.14	131mTe	3.24E+01	h	4.07E-02	36	Fiss_Prod
52	10	86.29	136Cs	1.31E+01	d	6.28E-02	14	Fiss_Prod
84	4	86.79	160Tb	1.98E-01	y	1.33E-01	17	Fiss_Prod
25	5	86.94	126Sn	1.00E+05	y	8.92E-02	9	Fiss_Prod
25	1	87.57	126Sn	1.00E+05	y	3.70E-01	9	Fiss_Prod
142	23	88.06	239Np	5.66E+01	h	6.00E-05	37	239Pu_Parent
76	169	88.8	151Pm	2.84E+01	h	1.24E-04	234	Fiss_Prod
82	2	88.96	156Eu	1.52E+01	d	9.05E-02	29	Fiss_Prod
222	22	89.4	99Mo	6.60E+01	h	3.03E-05	35	medical_FP
72	1	91.11	147Nd	1.10E+01	d	2.79E-01	18	Fiss_Prod
76	214	91.7	151Pm	2.84E+01	h	5.63E-05	234	Fiss_Prod
76	117	92.97	151Pm	2.84E+01	h	3.38E-04	234	Fiss_Prod
140	6	94.66	238Pu	8.77E+01	y	1.05E-06	7	SNM
143	5	94.66	239Pu	2.41E+04	y	4.22E-05	83	SNM
143	48	96.13	239Pu	2.41E+04	y	2.23E-07	83	SNM
147	8	97.07	241Am	4.32E+02	y	1.18E-05	28	SNM
76	36	98.05	151Pm	2.84E+01	h	3.60E-03	234	Fiss_Prod
140	5	98.44	238Pu	8.77E+01	y	1.69E-06	7	SNM
73	13	98.48	148mPm	4.13E+01	d	2.47E-02	18	Fiss_Prod
76	95	98.74	151Pm	2.84E+01	h	5.85E-04	234	Fiss_Prod
143	8	98.78	239Pu	2.41E+04	y	1.22E-05	83	SNM
147	4	98.95	241Am	4.32E+02	y	2.03E-04	28	SNM
59	20	99.49	140Ba	1.20E+01	d	1.95E-07	20	Fiss_Prod
149	4	99.55	242Am	1.60E+01	h	3.66E-02	5	SNM
140	3	99.86	238Pu	8.77E+01	y	7.24E-05	7	SNM
76	9	100.02	151Pm	2.84E+01	h	2.54E-02	234	Fiss_Prod
76	172	100.6	151Pm	2.84E+01	h	1.19E-04	234	Fiss_Prod
138	2	101.07	237U	1.62E+02	h	2.63E-01	24	237Np_Parent
147	7	101.07	241Am	4.32E+02	y	1.90E-05	28	SNM

76	16	101.93	151Pm	2.84E+01	h	1.28E-02	234	Fiss_Prod
142	35	101.97	239Np	5.66E+01	h	8.00E-06	37	239Pu_Parent
34	7	102.06	131mTe	3.24E+01	h	7.94E-02	36	Fiss_Prod
76	120	102.7	151Pm	2.84E+01	h	3.15E-04	234	Fiss_Prod
147	5	102.97	241Am	4.32E+02	y	1.95E-04	28	SNM
138	20	102.98	237U	1.62E+02	h	6.40E-05	24	237Np_Parent
143	19	103.02	239Pu	2.41E+04	y	2.17E-06	83	SNM
79	2	103.18	153Sm	4.63E+01	h	2.83E-01	5	Fiss_Prod
148	2	103.68	241Pu	1.44E+01	y	1.02E-06	6	SNM
142	2	103.76	239Np	5.66E+01	h	2.37E-01	37	239Pu_Parent
149	3	103.76	242Am	1.60E+01	h	5.89E-02	5	SNM
145	3	104.24	240Pu	6.54E+03	y	7.08E-05	5	SNM
76	8	104.84	151Pm	2.84E+01	h	3.51E-02	234	Fiss_Prod
142	1	106.12	239Np	5.66E+01	h	2.72E-01	37	239Pu_Parent
142	19	106.47	239Np	5.66E+01	h	4.90E-04	37	239Pu_Parent
60	16	109.42	140La	4.03E+01	h	2.19E-03	38	Fiss_Prod
76	80	109.56	151Pm	2.84E+01	h	8.55E-04	234	Fiss_Prod
49	82	112.78	135I	6.59E+00	h	1.26E-04	93	Fiss_Prod
76	186	113.1	151Pm	2.84E+01	h	9.68E-05	234	Fiss_Prod
49	85	113.15	135I	6.59E+00	h	6.89E-05	93	Fiss_Prod
59	11	113.51	140Ba	1.20E+01	d	1.61E-04	20	Fiss_Prod
143	10	116	239Pu	2.41E+04	y	1.06E-05	83	SNM
149	5	117	242Am	1.60E+01	h	2.77E-02	5	SNM
59	10	118.84	140Ba	1.20E+01	d	6.10E-04	20	Fiss_Prod
72	11	120.48	147Nd	1.10E+01	d	3.96E-03	18	Fiss_Prod
147	28	121.2	241Am	4.32E+02	y	6.85E-09	28	SNM
76	77	121.77	151Pm	2.84E+01	h	9.00E-04	234	Fiss_Prod
67	28	122.4	143Ce	3.30E+01	h	8.56E-05	52	Fiss_Prod
147	9	123.01	241Am	4.32E+02	y	1.00E-05	28	SNM
80	1	123.07	154Eu	8.50E+00	y	4.05E-01	13	Fiss_Prod
143	49	123.62	239Pu	2.41E+04	y	1.97E-07	83	SNM
142	22	124.4	239Np	5.66E+01	h	1.00E-04	37	239Pu_Parent
143	37	124.51	239Pu	2.41E+04	y	6.13E-07	83	SNM
76	170	125.2	151Pm	2.84E+01	h	1.22E-04	234	Fiss_Prod
76	171	125.2	151Pm	2.84E+01	h	1.22E-04	234	Fiss_Prod
143	34	125.21	239Pu	2.41E+04	y	7.11E-07	83	SNM
147	6	125.29	241Am	4.32E+02	y	4.08E-05	28	SNM
76	226	126.8	151Pm	2.84E+01	h	2.93E-05	234	Fiss_Prod
143	4	129.29	239Pu	2.41E+04	y	6.31E-05	83	SNM
76	85	130.43	151Pm	2.84E+01	h	6.75E-04	234	Fiss_Prod
60	13	131.12	140La	4.03E+01	h	4.67E-03	38	Fiss_Prod
59	9	132.69	140Ba	1.20E+01	d	2.02E-03	20	Fiss_Prod
76	140	134.22	151Pm	2.84E+01	h	2.03E-04	234	Fiss_Prod

76	219	134.9	151Pm	2.84E+01	h	4.05E-05	234	Fiss_Prod
37	74	136.7	132I	2.30E+00	h	7.90E-04	173	Fiss_Prod
76	109	138.38	151Pm	2.84E+01	h	4.05E-04	234	Fiss_Prod
76	125	138.9	151Pm	2.84E+01	h	2.70E-04	234	Fiss_Prod
76	33	139.28	151Pm	2.84E+01	h	4.95E-03	234	Fiss_Prod
67	12	139.74	143Ce	3.30E+01	h	7.70E-04	52	Fiss_Prod
222	3	140.51	99Mo	6.60E+01	h	4.52E-02	35	medical_FP
143	43	141.66	239Pu	2.41E+04	y	3.20E-07	83	SNM
76	181	141.7	151Pm	2.84E+01	h	1.01E-04	234	Fiss_Prod
76	50	143.17	151Pm	2.84E+01	h	2.14E-03	234	Fiss_Prod
76	182	143.2	151Pm	2.84E+01	h	1.01E-04	234	Fiss_Prod
143	50	143.35	239Pu	2.41E+04	y	1.73E-07	83	SNM
143	17	144.21	239Pu	2.41E+04	y	2.83E-06	83	SNM
143	26	146.08	239Pu	2.41E+04	y	1.19E-06	83	SNM
76	150	146.2	151Pm	2.84E+01	h	1.67E-04	234	Fiss_Prod
147	12	146.56	241Am	4.32E+02	y	4.61E-06	28	SNM
37	52	147.4	132I	2.30E+00	h	2.37E-03	173	Fiss_Prod
76	60	147.53	151Pm	2.84E+01	h	1.53E-03	234	Fiss_Prod
76	98	148.5	151Pm	2.84E+01	h	5.40E-04	234	Fiss_Prod
148	1	148.57	241Pu	1.44E+01	y	1.85E-06	6	SNM
6	12	149.2	105Ru	4.44E+00	h	1.67E-02	17	Fiss_Prod
34	14	149.72	131mTe	3.24E+01	h	5.08E-02	36	Fiss_Prod
36	1	149.72	131Te	2.50E+01	m	6.89E-01	14	Fiss_Prod
76	189	150.1	151Pm	2.84E+01	h	9.00E-05	234	Fiss_Prod
147	18	150.11	241Am	4.32E+02	y	7.40E-07	28	SNM
140	4	152.68	238Pu	8.77E+01	y	9.37E-06	7	SNM
52	9	153.22	136Cs	1.31E+01	d	7.46E-02	14	Fiss_Prod
72	16	154	147Nd	1.10E+01	d	5.58E-04	18	Fiss_Prod
76	131	155.5	151Pm	2.84E+01	h	2.48E-04	234	Fiss_Prod
76	61	156.18	151Pm	2.84E+01	h	1.49E-03	234	Fiss_Prod
143	80	158.1	239Pu	2.41E+04	y	1.00E-08	83	SNM
222	11	158.78	99Mo	6.60E+01	h	1.89E-04	35	medical_FP
148	3	159.96	241Pu	1.44E+01	y	6.54E-08	6	SNM
143	61	160.19	239Pu	2.41E+04	y	6.20E-08	83	SNM
145	4	160.28	240Pu	6.54E+03	y	4.02E-06	5	SNM
44	7	160.61	133Xe	5.24E+00	d	6.60E-04	10	Fiss_Prod
143	24	161.45	239Pu	2.41E+04	y	1.23E-06	83	SNM
222	13	162.37	99Mo	6.60E+01	h	1.19E-04	35	medical_FP
49	83	162.65	135I	6.59E+00	h	9.76E-05	93	Fiss_Prod
59	4	162.66	140Ba	1.20E+01	d	6.22E-02	20	Fiss_Prod
76	26	162.94	151Pm	2.84E+01	h	8.78E-03	234	Fiss_Prod
76	13	163.58	151Pm	2.84E+01	h	1.55E-02	234	Fiss_Prod
52	12	163.89	136Cs	1.31E+01	d	4.61E-02	14	Fiss_Prod

147	19	164.6	241Am	4.32E+02	y	6.67E-07	28	SNM
138	5	164.61	237U	1.62E+02	h	1.86E-02	24	237Np_Parent
49	70	165.74	135I	6.59E+00	h	3.13E-04	93	Fiss_Prod
147	26	165.93	241Am	4.32E+02	y	2.32E-07	28	SNM
204	10	165.98	88Kr	2.84E+00	h	3.10E-02	20	Fiss_Prod
142	20	166.39	239Np	5.66E+01	h	1.70E-04	37	239Pu_Parent
76	2	167.75	151Pm	2.84E+01	h	8.33E-02	234	Fiss_Prod
76	23	168.39	151Pm	2.84E+01	h	9.23E-03	234	Fiss_Prod
143	28	171.3	239Pu	2.41E+04	y	1.10E-06	83	SNM
60	17	173.54	140La	4.03E+01	h	1.27E-03	38	Fiss_Prod
22	8	176.33	125Sb	2.76E+00	y	6.89E-02	13	Fiss_Prod
76	28	176.52	151Pm	2.84E+01	h	8.55E-03	234	Fiss_Prod
52	5	176.55	136Cs	1.31E+01	d	1.36E-01	14	Fiss_Prod
76	6	177.16	151Pm	2.84E+01	h	3.83E-02	234	Fiss_Prod
143	36	179.2	239Pu	2.41E+04	y	6.60E-07	83	SNM
222	2	181.07	99Mo	6.60E+01	h	5.99E-02	35	medical_FP
142	17	181.7	239Np	5.66E+01	h	8.10E-04	37	239Pu_Parent
37	59	183.6	132I	2.30E+00	h	1.38E-03	173	Fiss_Prod
59	16	183.83	140Ba	1.20E+01	d	9.76E-06	20	Fiss_Prod
49	74	184.49	135I	6.59E+00	h	2.35E-04	93	Fiss_Prod
76	56	186.59	151Pm	2.84E+01	h	1.80E-03	234	Fiss_Prod
143	32	189.3	239Pu	2.41E+04	y	8.30E-07	83	SNM
73	17	189.63	148mPm	4.13E+01	d	1.10E-02	18	Fiss_Prod
76	205	192.9	151Pm	2.84E+01	h	7.43E-05	234	Fiss_Prod
76	126	195.5	151Pm	2.84E+01	h	2.70E-04	234	Fiss_Prod
143	29	195.7	239Pu	2.41E+04	y	1.07E-06	83	SNM
204	2	196.32	88Kr	2.84E+00	h	2.60E-01	20	Fiss_Prod
72	13	196.64	147Nd	1.10E+01	d	2.04E-03	18	Fiss_Prod
84	10	197.04	160Tb	1.98E-01	y	4.90E-02	17	Fiss_Prod
49	65	197.19	135I	6.59E+00	h	3.27E-04	93	Fiss_Prod
67	40	197.6	143Ce	3.30E+01	h	2.57E-05	52	Fiss_Prod
34	10	200.63	131mTe	3.24E+01	h	7.56E-02	36	Fiss_Prod
76	27	201.96	151Pm	2.84E+01	h	8.78E-03	234	Fiss_Prod
143	12	203.54	239Pu	2.41E+04	y	5.69E-06	83	SNM
147	27	204.06	241Am	4.32E+02	y	2.90E-08	28	SNM
216	2	204.12	95Nb	3.50E+01	d	2.33E-02	3	Fiss_Prod
76	64	204.17	151Pm	2.84E+01	h	1.31E-03	234	Fiss_Prod
76	190	205.7	151Pm	2.84E+01	h	9.00E-05	234	Fiss_Prod
76	113	206.7	151Pm	2.84E+01	h	3.60E-04	234	Fiss_Prod
76	206	207	151Pm	2.84E+01	h	7.43E-05	234	Fiss_Prod
138	3	208	237U	1.62E+02	h	2.12E-01	24	237Np_Parent
147	10	208	241Am	4.32E+02	y	7.91E-06	28	SNM
76	12	209	151Pm	2.84E+01	h	1.73E-02	234	Fiss_Prod

142	5	209.75	239Np	5.66E+01	h	3.42E-02	37	239Pu_Parent
76	191	215.3	151Pm	2.84E+01	h	9.00E-05	234	Fiss_Prod
84	12	215.65	160Tb	1.98E-01	y	3.72E-02	17	Fiss_Prod
49	13	220.5	135I	6.59E+00	h	1.75E-02	93	Fiss_Prod
197	9	221.45	82Br	3.53E+01	h	2.26E-02	11	Fiss_Prod
138	16	221.8	237U	1.62E+02	h	2.12E-04	24	237Np_Parent
44	10	223.23	133Xe	5.24E+00	d	1.20E-06	10	Fiss_Prod
24	17	223.8	126Sb	2.98E+02	h	1.40E-02	18	Fiss_Prod
143	52	225.4	239Pu	2.41E+04	y	1.51E-07	83	SNM
142	11	226.38	239Np	5.66E+01	h	2.80E-03	37	239Pu_Parent
76	40	227.18	151Pm	2.84E+01	h	3.38E-03	234	Fiss_Prod
76	101	227.81	151Pm	2.84E+01	h	4.95E-04	234	Fiss_Prod
142	10	227.83	239Np	5.66E+01	h	5.10E-03	37	239Pu_Parent
142	4	228.18	239Np	5.66E+01	h	1.08E-01	37	239Pu_Parent
76	134	229.01	151Pm	2.84E+01	h	2.25E-04	234	Fiss_Prod
49	35	229.72	135I	6.59E+00	h	2.41E-03	93	Fiss_Prod
67	7	231.55	143Ce	3.30E+01	h	2.05E-02	52	Fiss_Prod
76	20	232.43	151Pm	2.84E+01	h	1.04E-02	234	Fiss_Prod
76	79	232.7	151Pm	2.84E+01	h	8.78E-04	234	Fiss_Prod
37	112	234.3	132I	2.30E+00	h	2.96E-04	173	Fiss_Prod
138	18	234.4	237U	1.62E+02	h	2.05E-04	24	237Np_Parent
76	73	236.2	151Pm	2.84E+01	h	9.45E-04	234	Fiss_Prod
76	59	236.6	151Pm	2.84E+01	h	1.60E-03	234	Fiss_Prod
76	53	236.7	151Pm	2.84E+01	h	1.94E-03	234	Fiss_Prod
76	32	237.1	151Pm	2.84E+01	h	5.18E-03	234	Fiss_Prod
143	53	237.4	239Pu	2.41E+04	y	1.44E-07	83	SNM
76	7	240.09	151Pm	2.84E+01	h	3.83E-02	234	Fiss_Prod
210	4	241.52	92Sr	2.71E+00	h	2.97E-02	5	Fiss_Prod
60	15	241.93	140La	4.03E+01	h	4.14E-03	38	Fiss_Prod
222	24	242.29	99Mo	6.60E+01	h	2.55E-05	35	medical_FP
143	46	243.4	239Pu	2.41E+04	y	2.53E-07	83	SNM
12	2	245.39	111Ag	7.45E+00	d	1.23E-02	2	Fiss_Prod
76	145	247.1	151Pm	2.84E+01	h	1.80E-04	234	Fiss_Prod
49	71	247.5	135I	6.59E+00	h	2.87E-04	93	Fiss_Prod
76	123	247.8	151Pm	2.84E+01	h	2.93E-04	234	Fiss_Prod
80	7	247.94	154Eu	8.50E+00	y	6.60E-02	13	Fiss_Prod
222	18	249.03	99Mo	6.60E+01	h	3.88E-05	35	medical_FP
51	1	249.79	135Xe	9.14E+00	h	8.99E-01	4	Fiss_Prod
34	9	249.93	131mTe	3.24E+01	h	7.59E-02	36	Fiss_Prod
76	192	250.5	151Pm	2.84E+01	h	9.00E-05	234	Fiss_Prod
37	128	250.8	132I	2.30E+00	h	1.78E-04	173	Fiss_Prod
37	129	250.8	132I	2.30E+00	h	1.78E-04	173	Fiss_Prod
221	6	254.17	97Zr	1.69E+01	h	1.15E-02	12	Fiss_Prod

76	57	254.28	151Pm	2.84E+01	h	1.69E-03	234	Fiss_Prod
142	15	254.4	239Np	5.66E+01	h	1.10E-03	37	239Pu_Parent
49	75	254.74	135I	6.59E+00	h	2.30E-04	93	Fiss_Prod
37	53	255.1	132I	2.30E+00	h	2.37E-03	173	Fiss_Prod
37	124	255.1	132I	2.30E+00	h	1.97E-04	173	Fiss_Prod
143	33	255.4	239Pu	2.41E+04	y	8.00E-07	83	SNM
76	30	258.11	151Pm	2.84E+01	h	5.63E-03	234	Fiss_Prod
76	173	261.4	151Pm	2.84E+01	h	1.13E-04	234	Fiss_Prod
6	5	262.9	105Ru	4.44E+00	h	7.20E-02	17	Fiss_Prod
37	22	262.9	132I	2.30E+00	h	1.28E-02	173	Fiss_Prod
143	44	263.9	239Pu	2.41E+04	y	2.65E-07	83	SNM
49	38	264.26	135I	6.59E+00	h	1.84E-03	93	Fiss_Prod
60	14	266.54	140La	4.03E+01	h	4.66E-03	38	Fiss_Prod
214	1	266.9	93Y	1.02E+01	h	7.32E-02	29	Fiss_Prod
138	8	267.54	237U	1.62E+02	h	7.12E-03	24	237Np_Parent
147	25	267.6	241Am	4.32E+02	y	2.63E-07	28	SNM
76	86	270.72	151Pm	2.84E+01	h	6.75E-04	234	Fiss_Prod
206	10	272.45	89Rb	1.52E+01	m	1.42E-02	12	Fiss_Prod
142	18	272.84	239Np	5.66E+01	h	7.70E-04	37	239Pu_Parent
67	29	272.9	143Ce	3.30E+01	h	8.56E-05	52	Fiss_Prod
214	11	273	93Y	1.02E+01	h	7.13E-04	29	Fiss_Prod
52	6	273.65	136Cs	1.31E+01	d	1.27E-01	14	Fiss_Prod
209	8	274.7	91Sr	9.63E+00	h	1.00E-02	8	Fiss_Prod
59	18	275.18	140Ba	1.20E+01	d	3.66E-06	20	Fiss_Prod
76	3	275.21	151Pm	2.84E+01	h	6.75E-02	234	Fiss_Prod
72	10	275.37	147Nd	1.10E+01	d	8.01E-03	18	Fiss_Prod
142	3	277.6	239Np	5.66E+01	h	1.44E-01	37	239Pu_Parent
76	94	277.62	151Pm	2.84E+01	h	6.08E-04	234	Fiss_Prod
76	201	278.2	151Pm	2.84E+01	h	7.88E-05	234	Fiss_Prod
37	99	278.4	132I	2.30E+00	h	3.95E-04	173	Fiss_Prod
37	100	278.4	132I	2.30E+00	h	3.95E-04	173	Fiss_Prod
34	26	278.56	131mTe	3.24E+01	h	1.78E-02	36	Fiss_Prod
24	13	278.6	126Sb	2.98E+02	h	2.39E-02	18	Fiss_Prod
76	47	280.09	151Pm	2.84E+01	h	2.32E-03	234	Fiss_Prod
33	3	284.3	131I	8.02E+00	d	6.05E-02	6	Fiss_Prod
37	32	284.9	132I	2.30E+00	h	7.11E-03	173	Fiss_Prod
76	231	285	151Pm	2.84E+01	h	2.25E-05	234	Fiss_Prod
142	9	285.46	239Np	5.66E+01	h	7.90E-03	37	239Pu_Parent
214	10	287	93Y	1.02E+01	h	7.50E-04	29	Fiss_Prod
73	7	288.11	148mPm	4.13E+01	d	1.26E-01	18	Fiss_Prod
49	12	288.45	135I	6.59E+00	h	3.10E-02	93	Fiss_Prod
49	31	290.27	135I	6.59E+00	h	3.04E-03	93	Fiss_Prod
76	29	290.75	151Pm	2.84E+01	h	8.33E-03	234	Fiss_Prod

76	174	292.4	151Pm	2.84E+01	h	1.13E-04	234	Fiss_Prod
138	21	292.7	237U	1.62E+02	h	2.50E-05	24	237Np_Parent
67	1	293.27	143Ce	3.30E+01	h	4.28E-01	52	Fiss_Prod
76	162	294.8	151Pm	2.84E+01	h	1.35E-04	234	Fiss_Prod
76	153	295.2	151Pm	2.84E+01	h	1.58E-04	234	Fiss_Prod
24	11	296.5	126Sb	2.98E+02	h	4.48E-02	18	Fiss_Prod
24	10	297.3	126Sb	2.98E+02	h	4.98E-02	18	Fiss_Prod
143	41	297.5	239Pu	2.41E+04	y	4.98E-07	83	SNM
76	110	297.8	151Pm	2.84E+01	h	3.83E-04	234	Fiss_Prod
76	213	298.6	151Pm	2.84E+01	h	6.08E-05	234	Fiss_Prod
76	163	301.8	151Pm	2.84E+01	h	1.35E-04	234	Fiss_Prod
37	125	302	132I	2.30E+00	h	1.97E-04	173	Fiss_Prod
76	127	302.5	151Pm	2.84E+01	h	2.70E-04	234	Fiss_Prod
76	132	302.8	151Pm	2.84E+01	h	2.48E-04	234	Fiss_Prod
44	8	302.85	133Xe	5.24E+00	d	4.80E-05	10	Fiss_Prod
143	63	302.9	239Pu	2.41E+04	y	5.10E-08	83	SNM
59	5	304.85	140Ba	1.20E+01	d	4.29E-02	20	Fiss_Prod
49	66	304.91	135I	6.59E+00	h	3.16E-04	93	Fiss_Prod
49	46	305.83	135I	6.59E+00	h	9.50E-04	93	Fiss_Prod
37	66	306.7	132I	2.30E+00	h	9.87E-04	173	Fiss_Prod
37	67	306.7	132I	2.30E+00	h	9.87E-04	173	Fiss_Prod
76	46	306.74	151Pm	2.84E+01	h	2.39E-03	234	Fiss_Prod
60	27	306.9	140La	4.03E+01	h	2.48E-04	38	Fiss_Prod
143	62	307.8	239Pu	2.41E+04	y	5.50E-08	83	SNM
76	81	308.97	151Pm	2.84E+01	h	8.10E-04	234	Fiss_Prod
138	24	309.1	237U	1.62E+02	h	2.70E-06	24	237Np_Parent
37	70	310.1	132I	2.30E+00	h	8.88E-04	173	Fiss_Prod
37	71	310.4	132I	2.30E+00	h	8.88E-04	173	Fiss_Prod
76	114	310.8	151Pm	2.84E+01	h	3.60E-04	234	Fiss_Prod
76	148	310.8	151Pm	2.84E+01	h	1.69E-04	234	Fiss_Prod
73	12	311.63	148mPm	4.13E+01	d	3.92E-02	18	Fiss_Prod
143	45	311.7	239Pu	2.41E+04	y	2.58E-07	83	SNM
76	89	314.92	151Pm	2.84E+01	h	6.30E-04	234	Fiss_Prod
76	202	315.1	151Pm	2.84E+01	h	7.88E-05	234	Fiss_Prod
142	7	315.88	239Np	5.66E+01	h	1.60E-02	37	239Pu_Parent
143	54	316.4	239Pu	2.41E+04	y	1.32E-07	83	SNM
6	4	316.5	105Ru	4.44E+00	h	1.17E-01	17	Fiss_Prod
37	61	316.7	132I	2.30E+00	h	1.28E-03	173	Fiss_Prod
72	6	319.41	147Nd	1.10E+01	d	1.95E-02	18	Fiss_Prod
143	39	320.9	239Pu	2.41E+04	y	5.42E-07	83	SNM
76	71	321.87	151Pm	2.84E+01	h	9.68E-04	234	Fiss_Prod
142	25	322.26	239Np	5.66E+01	h	5.20E-05	37	239Pu_Parent
143	40	323.8	239Pu	2.41E+04	y	5.39E-07	83	SNM

76	18	323.94	151Pm	2.84E+01	h	1.22E-02	234	Fiss_Prod
76	160	325.2	151Pm	2.84E+01	h	1.46E-04	234	Fiss_Prod
76	67	325.8	151Pm	2.84E+01	h	1.06E-03	234	Fiss_Prod
49	91	326	135I	6.59E+00	h	2.30E-05	93	Fiss_Prod
6	15	326.1	105Ru	4.44E+00	h	1.18E-02	17	Fiss_Prod
60	4	328.76	140La	4.03E+01	h	2.03E-01	38	Fiss_Prod
76	164	329	151Pm	2.84E+01	h	1.35E-04	234	Fiss_Prod
76	48	329.75	151Pm	2.84E+01	h	2.21E-03	234	Fiss_Prod
23	6	331.9	125Sn	9.64E+00	d	1.29E-02	7	Fiss_Prod
147	16	332.3	241Am	4.32E+02	y	1.49E-06	28	SNM
138	7	332.36	237U	1.62E+02	h	1.20E-02	24	237Np_Parent
143	14	332.8	239Pu	2.41E+04	y	4.94E-06	83	SNM
49	60	333.6	135I	6.59E+00	h	3.73E-04	93	Fiss_Prod
34	6	334.27	131mTe	3.24E+01	h	9.57E-02	36	Fiss_Prod
142	6	334.31	239Np	5.66E+01	h	2.07E-02	37	239Pu_Parent
138	13	335.38	237U	1.62E+02	h	9.51E-04	24	237Np_Parent
147	11	335.41	241Am	4.32E+02	y	4.96E-06	28	SNM
143	27	336.11	239Pu	2.41E+04	y	1.12E-06	83	SNM
138	19	337.7	237U	1.62E+02	h	8.90E-05	24	237Np_Parent
67	49	338.3	143Ce	3.30E+01	h	8.56E-06	52	Fiss_Prod
76	1	340.08	151Pm	2.84E+01	h	2.25E-01	234	Fiss_Prod
138	22	340.45	237U	1.62E+02	h	1.65E-05	24	237Np_Parent
52	3	340.57	136Cs	1.31E+01	d	4.85E-01	14	Fiss_Prod
76	83	341	151Pm	2.84E+01	h	7.43E-04	234	Fiss_Prod
214	15	341.5	93Y	1.02E+01	h	4.43E-04	29	Fiss_Prod
143	35	341.51	239Pu	2.41E+04	y	6.62E-07	83	SNM
12	1	342.13	111Ag	7.45E+00	d	6.68E-02	2	Fiss_Prod
49	93	342.52	135I	6.59E+00	h	8.61E-06	93	Fiss_Prod
37	72	343.7	132I	2.30E+00	h	8.88E-04	173	Fiss_Prod
76	10	344.9	151Pm	2.84E+01	h	2.12E-02	234	Fiss_Prod
143	13	345.01	239Pu	2.41E+04	y	5.56E-06	83	SNM
76	111	346.1	151Pm	2.84E+01	h	3.83E-04	234	Fiss_Prod
76	188	348.8	151Pm	2.84E+01	h	9.23E-05	234	Fiss_Prod
76	62	349.81	151Pm	2.84E+01	h	1.42E-03	234	Fiss_Prod
6	16	350.2	105Ru	4.44E+00	h	1.10E-02	17	Fiss_Prod
67	5	350.62	143Ce	3.30E+01	h	3.23E-02	52	Fiss_Prod
37	75	351.8	132I	2.30E+00	h	7.90E-04	173	Fiss_Prod
76	154	352.3	151Pm	2.84E+01	h	1.58E-04	234	Fiss_Prod
76	68	353.32	151Pm	2.84E+01	h	1.06E-03	234	Fiss_Prod
221	4	355.39	97Zr	1.69E+01	h	2.28E-02	12	Fiss_Prod
76	203	356.9	151Pm	2.84E+01	h	7.88E-05	234	Fiss_Prod
67	51	357.8	143Ce	3.30E+01	h	5.99E-06	52	Fiss_Prod
76	159	358.4	151Pm	2.84E+01	h	1.53E-04	234	Fiss_Prod



76	180	360.9	151Pm	2.84E+01	h	1.06E-04	234	Fiss_Prod
49	37	361.85	135I	6.59E+00	h	1.87E-03	93	Fiss_Prod
143	55	361.9	239Pu	2.41E+04	y	1.22E-07	83	SNM
204	12	362.23	88Kr	2.84E+00	h	2.25E-02	20	Fiss_Prod
37	38	363.34	132I	2.30E+00	h	4.94E-03	173	Fiss_Prod
33	1	364.48	131I	8.02E+00	d	8.12E-01	6	Fiss_Prod
34	34	364.98	131mTe	3.24E+01	h	1.20E-02	36	Fiss_Prod
222	5	366.42	99Mo	6.60E+01	h	1.19E-02	35	medical_FP
143	30	367.05	239Pu	2.41E+04	y	8.90E-07	83	SNM
138	14	368.59	237U	1.62E+02	h	3.92E-04	24	237Np_Parent
143	31	368.6	239Pu	2.41E+04	y	8.80E-07	83	SNM
147	14	368.61	241Am	4.32E+02	y	2.17E-06	28	SNM
76	151	369	151Pm	2.84E+01	h	1.64E-04	234	Fiss_Prod
147	21	370.93	241Am	4.32E+02	y	5.23E-07	28	SNM
138	11	370.94	237U	1.62E+02	h	1.07E-03	24	237Np_Parent
67	22	371.29	143Ce	3.30E+01	h	2.48E-04	52	Fiss_Prod
76	139	374.2	151Pm	2.84E+01	h	2.21E-04	234	Fiss_Prod
143	6	375.04	239Pu	2.41E+04	y	1.55E-05	83	SNM
147	17	376.6	241Am	4.32E+02	y	1.38E-06	28	SNM
76	155	376.9	151Pm	2.84E+01	h	1.58E-04	234	Fiss_Prod
76	183	378.5	151Pm	2.84E+01	h	1.01E-04	234	Fiss_Prod
76	22	379.86	151Pm	2.84E+01	h	9.45E-03	234	Fiss_Prod
222	14	380.13	99Mo	6.60E+01	h	1.04E-04	35	medical_FP
143	16	380.17	239Pu	2.41E+04	y	3.05E-06	83	SNM
22	13	380.44	125Sb	2.76E+00	y	1.50E-02	13	Fiss_Prod
76	141	381.2	151Pm	2.84E+01	h	2.03E-04	234	Fiss_Prod
143	18	382.75	239Pu	2.41E+04	y	2.59E-06	83	SNM
147	24	383.74	241Am	4.32E+02	y	2.82E-07	28	SNM
44	9	383.85	133Xe	5.24E+00	d	2.40E-05	10	Fiss_Prod
214	27	387.5	93Y	1.02E+01	h	7.50E-05	29	Fiss_Prod
37	46	387.9	132I	2.30E+00	h	2.96E-03	173	Fiss_Prod
37	47	387.9	132I	2.30E+00	h	2.96E-03	173	Fiss_Prod
37	48	387.9	132I	2.30E+00	h	2.96E-03	173	Fiss_Prod
67	16	389.64	143Ce	3.30E+01	h	3.64E-04	52	Fiss_Prod
76	99	390.67	151Pm	2.84E+01	h	5.40E-04	234	Fiss_Prod
222	20	391.7	99Mo	6.60E+01	h	3.15E-05	35	medical_FP
142	29	392.4	239Np	5.66E+01	h	1.60E-05	37	239Pu_Parent
84	17	392.49	160Tb	1.98E-01	y	1.28E-02	17	Fiss_Prod
143	20	392.5	239Pu	2.41E+04	y	2.05E-06	83	SNM
143	15	393.1	239Pu	2.41E+04	y	3.48E-06	83	SNM
6	6	393.4	105Ru	4.44E+00	h	4.20E-02	17	Fiss_Prod
76	108	395.63	151Pm	2.84E+01	h	4.28E-04	234	Fiss_Prod
60	20	397.52	140La	4.03E+01	h	7.35E-04	38	Fiss_Prod

72	8	398.16	147Nd	1.10E+01	d	8.70E-03	18	Fiss_Prod
76	121	398.9	151Pm	2.84E+01	h	3.15E-04	234	Fiss_Prod
76	208	400.5	151Pm	2.84E+01	h	6.98E-05	234	Fiss_Prod
49	36	403.03	135I	6.59E+00	h	2.32E-03	93	Fiss_Prod
76	88	404.74	151Pm	2.84E+01	h	6.53E-04	234	Fiss_Prod
76	55	407.03	151Pm	2.84E+01	h	1.87E-03	234	Fiss_Prod
222	27	410.27	99Mo	6.60E+01	h	1.94E-05	35	medical_FP
72	15	410.48	147Nd	1.10E+01	d	1.40E-03	18	Fiss_Prod
76	90	410.75	151Pm	2.84E+01	h	6.30E-04	234	Fiss_Prod
143	59	411.2	239Pu	2.41E+04	y	6.80E-08	83	SNM
222	12	411.49	99Mo	6.60E+01	h	1.46E-04	35	medical_FP
6	8	413.5	105Ru	4.44E+00	h	2.48E-02	17	Fiss_Prod
143	7	413.71	239Pu	2.41E+04	y	1.47E-05	83	SNM
73	5	414.07	148mPm	4.13E+01	d	1.87E-01	18	Fiss_Prod
24	3	414.7	126Sb	2.98E+02	h	8.33E-01	18	Fiss_Prod
49	33	414.83	135I	6.59E+00	h	3.01E-03	93	Fiss_Prod
76	138	415.7	151Pm	2.84E+01	h	2.23E-04	234	Fiss_Prod
67	34	416.57	143Ce	3.30E+01	h	6.85E-05	52	Fiss_Prod
37	39	416.8	132I	2.30E+00	h	4.74E-03	173	Fiss_Prod
76	157	416.8	151Pm	2.84E+01	h	1.55E-04	234	Fiss_Prod
49	11	417.63	135I	6.59E+00	h	3.53E-02	93	Fiss_Prod
31	4	418.01	130I	1.24E+01	h	3.42E-01	8	Fiss_Prod
59	12	418.44	140Ba	1.20E+01	d	3.66E-05	20	Fiss_Prod
76	97	420.65	151Pm	2.84E+01	h	5.63E-04	234	Fiss_Prod
143	25	422.6	239Pu	2.41E+04	y	1.22E-06	83	SNM
59	6	423.72	140Ba	1.20E+01	d	3.15E-02	20	Fiss_Prod
76	102	424.55	151Pm	2.84E+01	h	4.95E-04	234	Fiss_Prod
76	185	425.6	151Pm	2.84E+01	h	9.90E-05	234	Fiss_Prod
143	47	426.7	239Pu	2.41E+04	y	2.33E-07	83	SNM
76	91	427.25	151Pm	2.84E+01	h	6.30E-04	234	Fiss_Prod
22	1	427.89	125Sb	2.76E+00	y	2.93E-01	13	Fiss_Prod
76	156	429.1	151Pm	2.84E+01	h	1.58E-04	234	Fiss_Prod
142	27	429.5	239Np	5.66E+01	h	3.90E-05	37	239Pu_Parent
49	32	429.93	135I	6.59E+00	h	3.04E-03	93	Fiss_Prod
143	66	430.1	239Pu	2.41E+04	y	4.30E-08	83	SNM
210	3	430.56	92Sr	2.71E+00	h	3.33E-02	5	Fiss_Prod
37	40	431.8	132I	2.30E+00	h	4.74E-03	173	Fiss_Prod
60	9	432.49	140La	4.03E+01	h	2.90E-02	38	Fiss_Prod
73	11	432.78	148mPm	4.13E+01	d	5.35E-02	18	Fiss_Prod
67	11	433	143Ce	3.30E+01	h	1.59E-03	52	Fiss_Prod
49	27	433.74	135I	6.59E+00	h	5.54E-03	93	Fiss_Prod
142	21	434.7	239Np	5.66E+01	h	1.30E-04	37	239Pu_Parent
59	7	437.58	140Ba	1.20E+01	d	1.93E-02	20	Fiss_Prod

67	36	438.43	143Ce	3.30E+01	h	4.28E-05	52	Fiss_Prod
60	25	438.5	140La	4.03E+01	h	3.91E-04	38	Fiss_Prod
72	7	439.9	147Nd	1.10E+01	d	1.20E-02	18	Fiss_Prod
76	14	440.85	151Pm	2.84E+01	h	1.51E-02	234	Fiss_Prod
76	135	443.8	151Pm	2.84E+01	h	2.25E-04	234	Fiss_Prod
37	68	445	132I	2.30E+00	h	9.87E-04	173	Fiss_Prod
60	38	445.5	140La	4.03E+01	h	2.86E-05	38	Fiss_Prod
76	5	445.68	151Pm	2.84E+01	h	4.01E-02	234	Fiss_Prod
143	57	445.7	239Pu	2.41E+04	y	8.80E-08	83	SNM
67	24	446.02	143Ce	3.30E+01	h	1.50E-04	52	Fiss_Prod
37	33	446.2	132I	2.30E+00	h	6.02E-03	173	Fiss_Prod
11	13	446.8	110mAg	6.84E-01	y	3.64E-02	15	Fiss_Prod
67	14	447.45	143Ce	3.30E+01	h	5.99E-04	52	Fiss_Prod
142	37	447.6	239Np	5.66E+01	h	2.60E-06	37	239Pu_Parent
76	142	448.7	151Pm	2.84E+01	h	2.03E-04	234	Fiss_Prod
76	43	451.4	151Pm	2.84E+01	h	2.88E-03	234	Fiss_Prod
143	21	451.5	239Pu	2.41E+04	y	1.89E-06	83	SNM
49	29	451.63	135I	6.59E+00	h	3.16E-03	93	Fiss_Prod
76	165	452.2	151Pm	2.84E+01	h	1.35E-04	234	Fiss_Prod
34	29	452.32	131mTe	3.24E+01	h	1.55E-02	36	Fiss_Prod
36	2	452.32	131Te	2.50E+01	m	1.82E-01	14	Fiss_Prod
142	34	454.2	239Np	5.66E+01	h	8.20E-06	37	239Pu_Parent
76	166	454.4	151Pm	2.84E+01	h	1.35E-04	234	Fiss_Prod
222	29	455.84	99Mo	6.60E+01	h	1.33E-05	35	medical_FP
76	112	456.05	151Pm	2.84E+01	h	3.83E-04	234	Fiss_Prod
76	216	457.5	151Pm	2.84E+01	h	4.50E-05	234	Fiss_Prod
143	77	457.6	239Pu	2.41E+04	y	1.49E-08	83	SNM
222	15	457.6	99Mo	6.60E+01	h	8.13E-05	35	medical_FP
30	2	459.6	129Te	3.36E+01	d	7.10E-02	4	Fiss_Prod
143	72	461.3	239Pu	2.41E+04	y	2.27E-08	83	SNM
142	30	461.9	239Np	5.66E+01	h	1.60E-05	37	239Pu_Parent
76	115	462.24	151Pm	2.84E+01	h	3.60E-04	234	Fiss_Prod
34	25	462.92	131mTe	3.24E+01	h	1.82E-02	36	Fiss_Prod
22	6	463.38	125Sb	2.76E+00	y	1.04E-01	13	Fiss_Prod
76	193	463.8	151Pm	2.84E+01	h	9.00E-05	234	Fiss_Prod
76	175	467.2	151Pm	2.84E+01	h	1.13E-04	234	Fiss_Prod
59	15	467.5	140Ba	1.20E+01	d	1.95E-05	20	Fiss_Prod
6	2	469.4	105Ru	4.44E+00	h	1.75E-01	17	Fiss_Prod
222	23	469.63	99Mo	6.60E+01	h	2.67E-05	35	medical_FP
23	7	469.7	125Sn	9.64E+00	d	1.29E-02	7	Fiss_Prod
142	31	469.8	239Np	5.66E+01	h	1.10E-05	37	239Pu_Parent
6	13	470	105Ru	4.44E+00	h	1.30E-02	17	Fiss_Prod
76	146	470.5	151Pm	2.84E+01	h	1.80E-04	234	Fiss_Prod

76	147	471.3	151Pm	2.84E+01	h	1.80E-04	234	Fiss_Prod
76	167	471.4	151Pm	2.84E+01	h	1.35E-04	234	Fiss_Prod
37	56	473.6	132I	2.30E+00	h	1.68E-03	173	Fiss_Prod
76	209	473.8	151Pm	2.84E+01	h	6.75E-05	234	Fiss_Prod
45	8	475.35	134Cs	5.24E+00	d	1.46E-02	9	Fiss_Prod
76	74	477.75	151Pm	2.84E+01	h	9.45E-04	234	Fiss_Prod
37	57	478.2	132I	2.30E+00	h	1.68E-03	173	Fiss_Prod
143	65	481.5	239Pu	2.41E+04	y	4.60E-08	83	SNM
142	32	484.3	239Np	5.66E+01	h	1.00E-05	37	239Pu_Parent
60	2	487.02	140La	4.03E+01	h	4.55E-01	38	Fiss_Prod
76	149	487.1	151Pm	2.84E+01	h	1.69E-04	234	Fiss_Prod
30	4	487.39	129Te	3.36E+01	d	1.31E-02	4	Fiss_Prod
37	41	488	132I	2.30E+00	h	4.15E-03	173	Fiss_Prod
37	42	488	132I	2.30E+00	h	4.15E-03	173	Fiss_Prod
72	14	489.24	147Nd	1.10E+01	d	1.53E-03	18	Fiss_Prod
76	65	490.26	151Pm	2.84E+01	h	1.26E-03	234	Fiss_Prod
67	6	490.37	143Ce	3.30E+01	h	2.16E-02	52	Fiss_Prod
222	30	490.53	99Mo	6.60E+01	h	1.09E-05	35	medical_FP
142	24	492.3	239Np	5.66E+01	h	6.00E-05	37	239Pu_Parent
36	5	492.66	131Te	2.50E+01	m	4.84E-02	14	Fiss_Prod
76	176	494.9	151Pm	2.84E+01	h	1.13E-04	234	Fiss_Prod
76	168	495.5	151Pm	2.84E+01	h	1.35E-04	234	Fiss_Prod
4	1	497.08	103Ru	3.94E+01	d	8.89E-01	2	Fiss_Prod
142	28	497.8	239Np	5.66E+01	h	3.20E-05	37	239Pu_Parent
67	15	497.81	143Ce	3.30E+01	h	4.45E-04	52	Fiss_Prod
142	33	498.7	239Np	5.66E+01	h	1.00E-05	37	239Pu_Parent
6	9	499.2	105Ru	4.44E+00	h	2.40E-02	17	Fiss_Prod
73	9	501.26	148mPm	4.13E+01	d	6.75E-02	18	Fiss_Prod
76	217	503.7	151Pm	2.84E+01	h	4.50E-05	234	Fiss_Prod
142	36	504.2	239Np	5.66E+01	h	7.80E-06	37	239Pu_Parent
37	8	505.79	132I	2.30E+00	h	4.94E-02	173	Fiss_Prod
76	103	507.27	151Pm	2.84E+01	h	4.73E-04	234	Fiss_Prod
221	2	507.64	97Zr	1.69E+01	h	5.03E-02	12	Fiss_Prod
76	197	510.1	151Pm	2.84E+01	h	8.55E-05	234	Fiss_Prod
40	4	510.53	133I	2.08E+01	h	1.81E-02	7	Fiss_Prod
83	1	511	15O	1.22E+02	s	2.00E+00	1	c
143	81	511	239Pu	2.41E+04	y	1.00E-08	83	SNM
193	5	511	65Zn	6.67E-01	y	2.83E-02	5	Fiss_Prod
7	1	512	106Rh	1.00E+00	y	2.06E-01	3	Fiss_Prod
76	54	516.25	151Pm	2.84E+01	h	1.94E-03	234	Fiss_Prod
76	122	521.1	151Pm	2.84E+01	h	3.15E-04	234	Fiss_Prod
37	4	522.65	132I	2.30E+00	h	1.60E-01	173	Fiss_Prod
67	44	523	143Ce	3.30E+01	h	1.71E-05	52	Fiss_Prod

50	1	526.56	135mXe	1.53E+01	m	8.10E-01	5	Fiss_Prod
222	9	528.79	99Mo	6.60E+01	h	5.70E-04	35	medical_FP
40	1	529.87	133I	2.08E+01	h	8.63E-01	7	Fiss_Prod
49	67	530.8	135I	6.59E+00	h	3.16E-04	93	Fiss_Prod
72	3	531.02	147Nd	1.10E+01	d	1.31E-01	18	Fiss_Prod
76	118	532.5	151Pm	2.84E+01	h	3.38E-04	234	Fiss_Prod
37	36	535.4	132I	2.30E+00	h	5.13E-03	173	Fiss_Prod
31	1	536.09	130I	1.24E+01	h	9.90E-01	8	Fiss_Prod
59	1	537.26	140Ba	1.20E+01	d	2.44E-01	20	Fiss_Prod
76	105	537.65	151Pm	2.84E+01	h	4.50E-04	234	Fiss_Prod
222	19	537.79	99Mo	6.60E+01	h	3.28E-05	35	medical_FP
31	7	539.1	130I	1.24E+01	h	1.40E-02	8	Fiss_Prod
49	7	546.56	135I	6.59E+00	h	7.15E-02	93	Fiss_Prod
37	25	547.2	132I	2.30E+00	h	1.14E-02	173	Fiss_Prod
73	1	550.27	148mPm	4.13E+01	d	9.49E-01	18	Fiss_Prod
74	2	550.27	148Pm	5.37E+00	d	2.20E-01	5	Fiss_Prod
76	158	550.7	151Pm	2.84E+01	h	1.55E-04	234	Fiss_Prod
59	13	551.08	140Ba	1.20E+01	d	3.12E-05	20	Fiss_Prod
76	152	554.2	151Pm	2.84E+01	h	1.62E-04	234	Fiss_Prod
197	2	554.32	82Br	3.53E+01	h	7.06E-01	11	Fiss_Prod
24	16	555.2	126Sb	2.98E+02	h	1.69E-02	18	Fiss_Prod
67	18	556.87	143Ce	3.30E+01	h	3.17E-04	52	Fiss_Prod
208	1	557.57	91mY	4.97E+01	m	9.51E-01	2	Fiss_Prod
37	73	559.7	132I	2.30E+00	h	8.88E-04	173	Fiss_Prod
216	3	561.88	95Nb	3.50E+01	d	1.30E-04	3	Fiss_Prod
76	143	562.1	151Pm	2.84E+01	h	1.91E-04	234	Fiss_Prod
45	5	563.23	134Cs	5.24E+00	d	8.38E-02	9	Fiss_Prod
76	38	565	151Pm	2.84E+01	h	3.53E-03	234	Fiss_Prod
45	3	569.32	134Cs	5.24E+00	d	1.54E-01	9	Fiss_Prod
67	35	569.91	143Ce	3.30E+01	h	5.14E-05	52	Fiss_Prod
37	84	572.5	132I	2.30E+00	h	5.92E-04	173	Fiss_Prod
76	100	572.5	151Pm	2.84E+01	h	5.18E-04	234	Fiss_Prod
76	124	573.2	151Pm	2.84E+01	h	2.93E-04	234	Fiss_Prod
24	9	573.8	126Sb	2.98E+02	h	6.68E-02	18	Fiss_Prod
76	66	574.97	151Pm	2.84E+01	h	1.17E-03	234	Fiss_Prod
76	227	575.1	151Pm	2.84E+01	h	2.93E-05	234	Fiss_Prod
6	17	575.3	105Ru	4.44E+00	h	1.07E-02	17	Fiss_Prod
49	43	575.97	135I	6.59E+00	h	1.29E-03	93	Fiss_Prod
222	21	580.51	99Mo	6.60E+01	h	3.15E-05	35	medical_FP
76	218	581.1	151Pm	2.84E+01	h	4.50E-05	234	Fiss_Prod
222	32	581.3	99Mo	6.60E+01	h	9.70E-06	35	medical_FP
76	128	583.1	151Pm	2.84E+01	h	2.57E-04	234	Fiss_Prod
76	198	584.9	151Pm	2.84E+01	h	8.55E-05	234	Fiss_Prod

31	6	586.05	130I	1.24E+01	h	1.69E-02	8	Fiss_Prod
34	23	586.3	131mTe	3.24E+01	h	1.98E-02	36	Fiss_Prod
67	10	587.2	143Ce	3.30E+01	h	2.67E-03	52	Fiss_Prod
49	57	588.28	135I	6.59E+00	h	5.17E-04	93	Fiss_Prod
72	17	589.35	147Nd	1.10E+01	d	4.58E-04	18	Fiss_Prod
37	80	591.1	132I	2.30E+00	h	6.91E-04	173	Fiss_Prod
37	81	591.1	132I	2.30E+00	h	6.91E-04	173	Fiss_Prod
80	8	591.81	154Eu	8.50E+00	y	4.83E-02	13	Fiss_Prod
24	7	593	126Sb	2.98E+02	h	7.47E-02	18	Fiss_Prod
76	184	593.6	151Pm	2.84E+01	h	1.01E-04	234	Fiss_Prod
67	43	594.5	143Ce	3.30E+01	h	2.14E-05	52	Fiss_Prod
72	12	594.8	147Nd	1.10E+01	d	2.65E-03	18	Fiss_Prod
76	82	597.7	151Pm	2.84E+01	h	7.88E-04	234	Fiss_Prod
76	194	598	151Pm	2.84E+01	h	9.00E-05	234	Fiss_Prod
143	75	598	239Pu	2.41E+04	y	1.67E-08	83	SNM
76	204	599.1	151Pm	2.84E+01	h	7.65E-05	234	Fiss_Prod
82	21	599.47	156Eu	1.52E+01	d	2.31E-02	29	Fiss_Prod
222	26	599.6	99Mo	6.60E+01	h	2.06E-05	35	medical_FP
73	8	599.74	148mPm	4.13E+01	d	1.25E-01	18	Fiss_Prod
37	62	600	132I	2.30E+00	h	1.28E-03	173	Fiss_Prod
37	63	600	132I	2.30E+00	h	1.28E-03	173	Fiss_Prod
22	3	600.56	125Sb	2.76E+00	y	1.78E-01	13	Fiss_Prod
36	6	602.04	131Te	2.50E+01	m	4.20E-02	14	Fiss_Prod
221	5	602.37	97Zr	1.69E+01	h	1.38E-02	12	Fiss_Prod
19	1	602.71	124Sb	1.65E-01	y	9.79E-01	13	Fiss_Prod
76	177	603	151Pm	2.84E+01	h	1.13E-04	234	Fiss_Prod
76	200	604	151Pm	2.84E+01	h	8.10E-05	234	Fiss_Prod
45	1	604.7	134Cs	2.06E+00	y	9.76E-01	9	Fiss_Prod
76	187	605.9	151Pm	2.84E+01	h	9.68E-05	234	Fiss_Prod
197	11	606.3	82Br	3.53E+01	h	1.17E-02	11	Fiss_Prod
22	9	606.64	125Sb	2.76E+00	y	5.02E-02	13	Fiss_Prod
51	2	608.19	135Xe	9.14E+00	h	2.90E-02	4	Fiss_Prod
76	104	609.25	151Pm	2.84E+01	h	4.73E-04	234	Fiss_Prod
37	101	609.8	132I	2.30E+00	h	3.95E-04	173	Fiss_Prod
4	2	610.33	103Ru	3.94E+01	d	5.60E-02	2	Fiss_Prod
73	10	611.26	148mPm	4.13E+01	d	5.48E-02	18	Fiss_Prod
74	5	611.26	148Pm	5.37E+00	d	1.02E-02	5	Fiss_Prod
197	4	613.83	82Br	3.53E+01	h	2.82E-01	11	Fiss_Prod
67	26	614.22	143Ce	3.30E+01	h	1.20E-04	52	Fiss_Prod
49	61	616.9	135I	6.59E+00	h	3.73E-04	93	Fiss_Prod
143	78	617.1	239Pu	2.41E+04	y	1.34E-08	83	SNM
60	26	618.12	140La	4.03E+01	h	3.72E-04	38	Fiss_Prod
143	74	618.3	239Pu	2.41E+04	y	2.04E-08	83	SNM

147	20	619.01	241Am	4.32E+02	y	5.94E-07	28	SNM
197	3	619.07	82Br	3.53E+01	h	4.31E-01	11	Fiss_Prod
143	79	619.2	239Pu	2.41E+04	y	1.21E-08	83	SNM
222	25	620.03	99Mo	6.60E+01	h	2.30E-05	35	medical_FP
209	6	620.1	91Sr	9.63E+00	h	1.72E-02	8	Fiss_Prod
11	14	620.35	110mAg	6.84E-01	y	2.77E-02	15	Fiss_Prod
76	84	620.6	151Pm	2.84E+01	h	7.20E-04	234	Fiss_Prod
37	44	620.9	132I	2.30E+00	h	3.95E-03	173	Fiss_Prod
37	18	621.2	132I	2.30E+00	h	1.58E-02	173	Fiss_Prod
222	10	621.77	99Mo	6.60E+01	h	2.58E-04	35	medical_FP
7	2	621.84	106Rh	1.00E+00	y	9.81E-02	3	Fiss_Prod
8	1	622.2	106Ru	1.00E+00	y	9.95E-02	2	Fiss_Prod
73	2	629.97	148mPm	4.13E+01	d	8.90E-01	18	Fiss_Prod
37	5	630.19	132I	2.30E+00	h	1.33E-01	173	Fiss_Prod
34	18	631.94	131mTe	3.24E+01	h	3.55E-02	36	Fiss_Prod
143	71	633.15	239Pu	2.41E+04	y	2.53E-08	83	SNM
22	5	635.89	125Sb	2.76E+00	y	1.13E-01	13	Fiss_Prod
76	15	636.2	151Pm	2.84E+01	h	1.42E-02	234	Fiss_Prod
33	2	636.97	131I	8.02E+00	d	7.26E-02	6	Fiss_Prod
143	70	637.84	239Pu	2.41E+04	y	2.56E-08	83	SNM
143	58	640.08	239Pu	2.41E+04	y	8.20E-08	83	SNM
37	102	642.2	132I	2.30E+00	h	3.95E-04	173	Fiss_Prod
145	5	642.48	240Pu	6.54E+03	y	1.30E-07	5	SNM
19	4	645.85	124Sb	1.65E-01	y	7.26E-02	13	Fiss_Prod
143	51	645.97	239Pu	2.41E+04	y	1.52E-07	83	SNM
82	5	646.29	156Eu	1.52E+01	d	7.09E-02	29	Fiss_Prod
49	28	649.85	135I	6.59E+00	h	4.56E-03	93	Fiss_Prod
143	82	650	239Pu	2.41E+04	y	1.00E-08	83	SNM
37	13	650.5	132I	2.30E+00	h	2.57E-02	173	Fiss_Prod
143	60	652.07	239Pu	2.41E+04	y	6.55E-08	83	SNM
209	5	652.3	91Sr	9.63E+00	h	2.89E-02	8	Fiss_Prod
209	3	652.9	91Sr	9.63E+00	h	7.80E-02	8	Fiss_Prod
147	22	653.02	241Am	4.32E+02	y	3.77E-07	28	SNM
76	45	654.25	151Pm	2.84E+01	h	2.41E-03	234	Fiss_Prod
36	11	654.26	131Te	2.50E+01	m	1.53E-02	14	Fiss_Prod
143	73	654.88	239Pu	2.41E+04	y	2.25E-08	83	SNM
76	178	655.6	151Pm	2.84E+01	h	1.13E-04	234	Fiss_Prod
49	49	656.09	135I	6.59E+00	h	7.46E-04	93	Fiss_Prod
6	10	656.1	105Ru	4.44E+00	h	2.40E-02	17	Fiss_Prod
24	15	656.3	126Sb	2.98E+02	h	2.19E-02	18	Fiss_Prod
206	4	657.71	89Rb	1.52E+01	m	9.98E-02	12	Fiss_Prod
10	1	657.75	110Ag	2.46E+01	s	4.49E-02	1	Fiss_Prod
11	1	657.75	110mAg	6.84E-01	y	9.44E-01	15	Fiss_Prod

219	1	657.9	97Nb	7.21E+01	m	9.81E-01	2	Fiss_Prod
143	56	658.93	239Pu	2.41E+04	y	9.69E-08	83	SNM
76	136	661.55	151Pm	2.84E+01	h	2.25E-04	234	Fiss_Prod
53	1	661.6	137Cs	3.02E+01	y	8.51E-01	1	Fiss_Prod
54	1	661.65	137mBa	2.55E+00	m	9.00E-01	5	Fiss_Prod
147	13	662.42	241Am	4.32E+02	y	3.64E-06	28	SNM
76	75	663.5	151Pm	2.84E+01	h	9.45E-04	234	Fiss_Prod
67	3	664.57	143Ce	3.30E+01	h	5.69E-02	52	Fiss_Prod
143	76	664.59	239Pu	2.41E+04	y	1.66E-08	83	SNM
34	15	665.05	131mTe	3.24E+01	h	4.34E-02	36	Fiss_Prod
24	1	666.33	126Sb	2.98E+02	h	9.96E-01	18	Fiss_Prod
37	1	667.72	132I	2.30E+00	h	9.87E-01	173	Fiss_Prod
76	224	668.5	151Pm	2.84E+01	h	3.38E-05	234	Fiss_Prod
31	2	668.54	130I	1.24E+01	h	9.61E-01	8	Fiss_Prod
76	37	668.7	151Pm	2.84E+01	h	3.60E-03	234	Fiss_Prod
76	42	669.2	151Pm	2.84E+01	h	2.93E-03	234	Fiss_Prod
37	9	669.8	132I	2.30E+00	h	4.64E-02	173	Fiss_Prod
67	32	670.12	143Ce	3.30E+01	h	8.13E-05	52	Fiss_Prod
76	24	671.28	151Pm	2.84E+01	h	9.00E-03	234	Fiss_Prod
37	10	671.4	132I	2.30E+00	h	3.45E-02	173	Fiss_Prod
22	12	671.41	125Sb	2.76E+00	y	1.81E-02	13	Fiss_Prod
24	12	675	126Sb	2.98E+02	h	3.69E-02	18	Fiss_Prod
67	50	675.5	143Ce	3.30E+01	h	8.56E-06	52	Fiss_Prod
6	3	676.4	105Ru	4.44E+00	h	1.67E-01	17	Fiss_Prod
11	8	677.61	110mAg	6.84E-01	y	1.07E-01	15	Fiss_Prod
76	106	678.3	151Pm	2.84E+01	h	4.50E-04	234	Fiss_Prod
49	56	679.22	135I	6.59E+00	h	5.45E-04	93	Fiss_Prod
214	4	680.2	93Y	1.02E+01	h	6.58E-03	29	Fiss_Prod
72	18	680.52	147Nd	1.10E+01	d	1.95E-04	18	Fiss_Prod
67	30	682.82	143Ce	3.30E+01	h	8.56E-05	52	Fiss_Prod
37	76	684.4	132I	2.30E+00	h	7.90E-04	173	Fiss_Prod
49	76	684.6	135I	6.59E+00	h	2.30E-04	93	Fiss_Prod
72	9	685.9	147Nd	1.10E+01	d	8.12E-03	18	Fiss_Prod
31	8	685.99	130I	1.24E+01	h	1.07E-02	8	Fiss_Prod
11	10	686.99	110mAg	6.84E-01	y	6.47E-02	15	Fiss_Prod
37	103	687.8	132I	2.30E+00	h	3.95E-04	173	Fiss_Prod
147	23	688.7	241Am	4.32E+02	y	3.25E-07	28	SNM
222	34	689.6	99Mo	6.60E+01	h	4.25E-06	35	medical_FP
49	44	690.13	135I	6.59E+00	h	1.29E-03	93	Fiss_Prod
80	11	692.41	154Eu	8.50E+00	y	1.69E-02	13	Fiss_Prod
24	2	695	126Sb	2.98E+02	h	9.96E-01	18	Fiss_Prod
36	14	696.01	131Te	2.50E+01	m	1.19E-02	14	Fiss_Prod
71	1	696.49	144Pr	7.79E-01	y	1.48E-02	3	Fiss_Prod



24	5	697	126Sb	2.98E+02	h	2.89E-01	18	Fiss_Prod
76	144	699	151Pm	2.84E+01	h	1.91E-04	234	Fiss_Prod
59	17	699.89	140Ba	1.20E+01	d	8.29E-06	20	Fiss_Prod
143	67	703.7	239Pu	2.41E+04	y	3.95E-08	83	SNM
221	9	703.76	97Zr	1.69E+01	h	1.01E-02	12	Fiss_Prod
76	41	704.24	151Pm	2.84E+01	h	3.38E-03	234	Fiss_Prod
37	126	706.4	132I	2.30E+00	h	1.97E-04	173	Fiss_Prod
40	5	706.58	133I	2.08E+01	h	1.49E-02	7	Fiss_Prod
11	6	706.67	110mAg	6.84E-01	y	1.67E-01	15	Fiss_Prod
6	14	707.36	105Ru	4.44E+00	h	1.28E-02	17	Fiss_Prod
49	23	707.92	135I	6.59E+00	h	6.60E-03	93	Fiss_Prod
76	63	709.25	151Pm	2.84E+01	h	1.37E-03	234	Fiss_Prod
19	11	709.31	124Sb	1.65E-01	y	1.42E-02	13	Fiss_Prod
67	31	709.59	143Ce	3.30E+01	h	8.56E-05	52	Fiss_Prod
80	12	710.54	154Eu	8.50E+00	y	1.59E-02	13	Fiss_Prod
76	76	712	151Pm	2.84E+01	h	9.45E-04	234	Fiss_Prod
34	32	713.1	131mTe	3.24E+01	h	1.43E-02	36	Fiss_Prod
76	195	713.4	151Pm	2.84E+01	h	9.00E-05	234	Fiss_Prod
19	7	713.82	124Sb	1.65E-01	y	2.38E-02	13	Fiss_Prod
214	21	714.4	93Y	1.02E+01	h	1.73E-04	29	Fiss_Prod
76	4	717.72	151Pm	2.84E+01	h	4.05E-02	234	Fiss_Prod
143	68	718	239Pu	2.41E+04	y	2.80E-08	83	SNM
76	179	719	151Pm	2.84E+01	h	1.13E-04	234	Fiss_Prod
24	4	720.5	126Sb	2.98E+02	h	5.38E-01	18	Fiss_Prod
67	4	721.93	143Ce	3.30E+01	h	5.39E-02	52	Fiss_Prod
147	15	722	241Am	4.32E+02	y	1.96E-06	28	SNM
19	3	722.78	124Sb	1.65E-01	y	1.11E-01	13	Fiss_Prod
33	5	722.89	131I	8.02E+00	d	1.80E-02	6	Fiss_Prod
80	3	723.3	154Eu	8.50E+00	y	1.97E-01	13	Fiss_Prod
82	8	723.47	156Eu	1.52E+01	d	6.02E-02	29	Fiss_Prod
217	2	724.2	95Zr	1.75E-01	y	4.42E-01	2	Fiss_Prod
6	1	724.5	105Ru	4.44E+00	h	4.90E-01	17	Fiss_Prod
73	3	725.7	148mPm	4.13E+01	d	3.28E-01	18	Fiss_Prod
37	16	727	132I	2.30E+00	h	2.17E-02	173	Fiss_Prod
76	210	727	151Pm	2.84E+01	h	6.75E-05	234	Fiss_Prod
37	11	727.2	132I	2.30E+00	h	3.16E-02	173	Fiss_Prod
37	19	728.4	132I	2.30E+00	h	1.58E-02	173	Fiss_Prod
67	39	729.87	143Ce	3.30E+01	h	3.00E-05	52	Fiss_Prod
31	3	734.8	130I	1.24E+01	h	8.23E-01	8	Fiss_Prod
76	35	736.12	151Pm	2.84E+01	h	4.73E-03	234	Fiss_Prod
222	1	739.5	99Mo	6.60E+01	h	1.21E-01	35	medical_FP
76	137	740.8	151Pm	2.84E+01	h	2.25E-04	234	Fiss_Prod
218	1	743.36	97mNb	5.27E+01	s	9.80E-01	1	Fiss_Prod

221	1	743.36	97Zr	1.69E+01	h	9.31E-01	12	Fiss_Prod
34	28	744.2	131mTe	3.24E+01	h	1.59E-02	36	Fiss_Prod
11	11	744.26	110mAg	6.84E-01	y	4.64E-02	15	Fiss_Prod
209	2	749.8	91Sr	9.63E+00	h	2.30E-01	8	Fiss_Prod
60	7	751.64	140La	4.03E+01	h	4.33E-02	38	Fiss_Prod
76	17	752.82	151Pm	2.84E+01	h	1.28E-02	234	Fiss_Prod
76	211	755	151Pm	2.84E+01	h	6.75E-05	234	Fiss_Prod
143	69	756.4	239Pu	2.41E+04	y	2.80E-08	83	SNM
217	1	756.73	95Zr	1.75E-01	y	5.45E-01	2	Fiss_Prod
80	9	756.87	154Eu	8.50E+00	y	4.33E-02	13	Fiss_Prod
76	196	758.5	151Pm	2.84E+01	h	9.00E-05	234	Fiss_Prod
222	35	761.77	99Mo	6.60E+01	h	4.00E-06	35	medical_FP
11	5	763.93	110mAg	6.84E-01	y	2.23E-01	15	Fiss_Prod
84	15	765.28	160Tb	1.98E-01	y	1.93E-02	17	Fiss_Prod
216	1	765.81	95Nb	3.50E+01	d	9.98E-01	3	Fiss_Prod
140	7	766.41	238Pu	8.77E+01	y	2.20E-07	7	SNM
67	37	767.7	143Ce	3.30E+01	h	3.17E-05	52	Fiss_Prod
76	69	769.1	151Pm	2.84E+01	h	1.06E-03	234	Fiss_Prod
143	64	769.4	239Pu	2.41E+04	y	5.10E-08	83	SNM
37	127	771.7	132I	2.30E+00	h	1.97E-04	173	Fiss_Prod
37	2	772.6	132I	2.30E+00	h	7.56E-01	173	Fiss_Prod
76	25	772.76	151Pm	2.84E+01	h	9.00E-03	234	Fiss_Prod
34	1	773.67	131mTe	3.24E+01	h	3.82E-01	36	Fiss_Prod
209	7	776.34	91Sr	9.63E+00	h	1.19E-02	8	Fiss_Prod
197	1	776.49	82Br	3.53E+01	h	8.33E-01	11	Fiss_Prod
222	4	777.92	99Mo	6.60E+01	h	4.26E-02	35	medical_FP
37	24	780	132I	2.30E+00	h	1.18E-02	173	Fiss_Prod
34	8	782.49	131mTe	3.24E+01	h	7.79E-02	36	Fiss_Prod
37	45	784.4	132I	2.30E+00	h	3.85E-03	173	Fiss_Prod
76	49	785.1	151Pm	2.84E+01	h	2.21E-03	234	Fiss_Prod
49	41	785.48	135I	6.59E+00	h	1.52E-03	93	Fiss_Prod
67	41	787.4	143Ce	3.30E+01	h	2.57E-05	52	Fiss_Prod
67	25	791.07	143Ce	3.30E+01	h	1.33E-04	52	Fiss_Prod
37	69	791.2	132I	2.30E+00	h	9.87E-04	173	Fiss_Prod
76	232	792.8	151Pm	2.84E+01	h	2.25E-05	234	Fiss_Prod
34	3	793.75	131mTe	3.24E+01	h	1.39E-01	36	Fiss_Prod
49	77	795.5	135I	6.59E+00	h	2.30E-04	93	Fiss_Prod
76	96	795.74	151Pm	2.84E+01	h	5.85E-04	234	Fiss_Prod
45	2	795.84	134Cs	2.06E+00	y	8.54E-01	9	Fiss_Prod
49	39	797.71	135I	6.59E+00	h	1.72E-03	93	Fiss_Prod
45	4	801.93	134Cs	2.06E+00	y	8.73E-02	9	Fiss_Prod
67	20	806.34	143Ce	3.30E+01	h	2.87E-04	52	Fiss_Prod
49	58	807.2	135I	6.59E+00	h	4.59E-04	93	Fiss_Prod

76	31	807.9	151Pm	2.84E+01	h	5.63E-03	234	Fiss_Prod
143	83	808.4	239Pu	2.41E+04	y	1.21E-09	83	SNM
37	14	809.5	132I	2.30E+00	h	2.57E-02	173	Fiss_Prod
67	19	809.98	143Ce	3.30E+01	h	3.12E-04	52	Fiss_Prod
82	1	811.77	156Eu	1.52E+01	d	1.04E-01	29	Fiss_Prod
76	87	811.8	151Pm	2.84E+01	h	6.75E-04	234	Fiss_Prod
37	7	812	132I	2.30E+00	h	5.53E-02	173	Fiss_Prod
60	3	815.77	140La	4.03E+01	h	2.33E-01	38	Fiss_Prod
76	58	817.7	151Pm	2.84E+01	h	1.69E-03	234	Fiss_Prod
76	78	817.7	151Pm	2.84E+01	h	9.00E-04	234	Fiss_Prod
11	9	818.02	110mAg	6.84E-01	y	7.28E-02	15	Fiss_Prod
52	1	818.5	136Cs	1.31E+01	d	9.97E-01	14	Fiss_Prod
76	119	822.45	151Pm	2.84E+01	h	3.38E-04	234	Fiss_Prod
23	3	822.6	125Sn	9.64E+00	d	3.78E-02	7	Fiss_Prod
34	12	822.78	131mTe	3.24E+01	h	6.12E-02	36	Fiss_Prod
222	7	822.97	99Mo	6.60E+01	h	1.33E-03	35	medical_FP
197	7	827.81	82Br	3.53E+01	h	2.42E-01	11	Fiss_Prod
37	119	831.3	132I	2.30E+00	h	2.47E-04	173	Fiss_Prod
204	4	834.83	88Kr	2.84E+00	h	1.30E-01	20	Fiss_Prod
49	8	836.8	135I	6.59E+00	h	6.69E-02	93	Fiss_Prod
37	130	847.9	132I	2.30E+00	h	1.68E-04	173	Fiss_Prod
76	44	848.65	151Pm	2.84E+01	h	2.81E-03	234	Fiss_Prod
34	2	852.21	131mTe	3.24E+01	h	2.07E-01	36	Fiss_Prod
76	212	856.2	151Pm	2.84E+01	h	6.53E-05	234	Fiss_Prod
40	7	856.28	133I	2.08E+01	h	1.23E-02	7	Fiss_Prod
24	6	856.8	126Sb	2.98E+02	h	1.76E-01	18	Fiss_Prod
76	199	859.8	151Pm	2.84E+01	h	8.33E-05	234	Fiss_Prod
222	16	861.2	99Mo	6.60E+01	h	7.28E-05	35	medical_FP
37	35	863	132I	2.30E+00	h	5.63E-03	173	Fiss_Prod
37	105	866	132I	2.30E+00	h	3.55E-04	173	Fiss_Prod
37	106	866	132I	2.30E+00	h	3.55E-04	173	Fiss_Prod
82	27	867.01	156Eu	1.52E+01	d	1.40E-02	29	Fiss_Prod
76	228	867.1	151Pm	2.84E+01	h	2.93E-05	234	Fiss_Prod
60	6	867.85	140La	4.03E+01	h	5.50E-02	38	Fiss_Prod
80	5	873.19	154Eu	8.50E+00	y	1.15E-01	13	Fiss_Prod
40	2	875.33	133I	2.08E+01	h	4.47E-02	7	Fiss_Prod
6	7	875.8	105Ru	4.44E+00	h	3.40E-02	17	Fiss_Prod
37	29	876.6	132I	2.30E+00	h	1.04E-02	173	Fiss_Prod
76	70	877.7	151Pm	2.84E+01	h	1.01E-03	234	Fiss_Prod
84	1	879.36	160Tb	1.98E-01	y	2.85E-01	17	Fiss_Prod
67	8	880.46	143Ce	3.30E+01	h	1.03E-02	52	Fiss_Prod
76	107	883.68	151Pm	2.84E+01	h	4.50E-04	234	Fiss_Prod
11	2	884.67	110mAg	6.84E-01	y	7.26E-01	15	Fiss_Prod

37	120	886.1	132I	2.30E+00	h	2.47E-04	173	Fiss_Prod
76	229	887.6	151Pm	2.84E+01	h	2.70E-05	234	Fiss_Prod
37	107	888.7	132I	2.30E+00	h	3.45E-04	173	Fiss_Prod
37	108	888.7	132I	2.30E+00	h	3.45E-04	173	Fiss_Prod
67	33	891.47	143Ce	3.30E+01	h	8.13E-05	52	Fiss_Prod
76	230	894.1	151Pm	2.84E+01	h	2.70E-05	234	Fiss_Prod
205	2	898.02	88Rb	1.78E+01	m	1.40E-01	3	Fiss_Prod
76	133	898.58	151Pm	2.84E+01	h	2.48E-04	234	Fiss_Prod
76	225	903.5	151Pm	2.84E+01	h	3.15E-05	234	Fiss_Prod
37	137	904.4	132I	2.30E+00	h	1.28E-04	173	Fiss_Prod
67	46	907.1	143Ce	3.30E+01	h	1.28E-05	52	Fiss_Prod
34	19	910	131mTe	3.24E+01	h	3.29E-02	36	Fiss_Prod
37	30	910.1	132I	2.30E+00	h	9.28E-03	173	Fiss_Prod
76	129	911.25	151Pm	2.84E+01	h	2.57E-04	234	Fiss_Prod
74	3	914.85	148Pm	5.37E+00	d	1.15E-01	5	Fiss_Prod
73	6	915.33	148mPm	4.13E+01	d	1.72E-01	18	Fiss_Prod
23	4	915.5	125Sn	9.64E+00	d	3.78E-02	7	Fiss_Prod
76	233	919.3	151Pm	2.84E+01	h	1.80E-05	234	Fiss_Prod
60	10	919.55	140La	4.03E+01	h	2.66E-02	38	Fiss_Prod
34	35	920.62	131mTe	3.24E+01	h	1.20E-02	36	Fiss_Prod
76	234	922.1	151Pm	2.84E+01	h	1.35E-05	234	Fiss_Prod
139	5	923.98	238Np	2.12E+00	d	2.48E-02	5	SNM
60	5	925.19	140La	4.03E+01	h	6.90E-02	38	Fiss_Prod
209	4	925.8	91Sr	9.63E+00	h	3.74E-02	8	Fiss_Prod
76	220	926.1	151Pm	2.84E+01	h	4.05E-05	234	Fiss_Prod
37	43	927.4	132I	2.30E+00	h	4.15E-03	173	Fiss_Prod
76	221	933.9	151Pm	2.84E+01	h	3.83E-05	234	Fiss_Prod
11	3	937.48	110mAg	6.84E-01	y	3.42E-01	15	Fiss_Prod
67	21	937.82	143Ce	3.30E+01	h	2.61E-04	52	Fiss_Prod
76	222	939.8	151Pm	2.84E+01	h	3.83E-05	234	Fiss_Prod
82	28	944.35	156Eu	1.52E+01	d	1.39E-02	29	Fiss_Prod
214	2	947.1	93Y	1.02E+01	h	2.09E-02	29	Fiss_Prod
37	96	947.2	132I	2.30E+00	h	4.44E-04	173	Fiss_Prod
206	6	947.69	89Rb	1.52E+01	m	9.22E-02	12	Fiss_Prod
36	10	948.54	131Te	2.50E+01	m	2.26E-02	14	Fiss_Prod
76	39	948.72	151Pm	2.84E+01	h	3.51E-03	234	Fiss_Prod
60	12	950.99	140La	4.03E+01	h	5.19E-03	38	Fiss_Prod
210	2	953.32	92Sr	2.71E+00	h	3.60E-02	5	Fiss_Prod
76	72	953.41	151Pm	2.84E+01	h	9.68E-04	234	Fiss_Prod
24	18	954	126Sb	2.98E+02	h	1.20E-02	18	Fiss_Prod
37	3	954.55	132I	2.30E+00	h	1.76E-01	173	Fiss_Prod
67	47	956.9	143Ce	3.30E+01	h	1.28E-05	52	Fiss_Prod
76	92	959.7	151Pm	2.84E+01	h	6.30E-04	234	Fiss_Prod

49	63	960.29	135I	6.59E+00	h	3.44E-04	93	Fiss_Prod
82	25	960.5	156Eu	1.52E+01	d	1.62E-02	29	Fiss_Prod
222	8	960.75	99Mo	6.60E+01	h	9.46E-04	35	medical_FP
49	42	961.43	135I	6.59E+00	h	1.46E-03	93	Fiss_Prod
84	7	962.29	160Tb	1.98E-01	y	9.03E-02	17	Fiss_Prod
214	22	962.3	93Y	1.02E+01	h	1.20E-04	29	Fiss_Prod
76	215	964.4	151Pm	2.84E+01	h	4.73E-05	234	Fiss_Prod
37	109	965.8	132I	2.30E+00	h	3.45E-04	173	Fiss_Prod
84	2	966.15	160Tb	1.98E-01	y	2.42E-01	17	Fiss_Prod
19	8	968.2	124Sb	1.65E-01	y	1.92E-02	13	Fiss_Prod
76	161	968.9	151Pm	2.84E+01	h	1.46E-04	234	Fiss_Prod
6	11	969.4	105Ru	4.44E+00	h	2.34E-02	17	Fiss_Prod
214	28	971	93Y	1.02E+01	h	6.75E-05	29	Fiss_Prod
49	20	971.96	135I	6.59E+00	h	8.90E-03	93	Fiss_Prod
49	16	972.62	135I	6.59E+00	h	1.21E-02	93	Fiss_Prod
37	34	984.2	132I	2.30E+00	h	5.92E-03	173	Fiss_Prod
139	2	984.45	238Np	2.12E+00	d	2.38E-01	5	SNM
204	17	985.78	88Kr	2.84E+00	h	1.32E-02	20	Fiss_Prod
222	28	986.44	99Mo	6.60E+01	h	1.46E-05	35	medical_FP
214	25	987.7	93Y	1.02E+01	h	1.05E-04	29	Fiss_Prod
24	8	989.3	126Sb	2.98E+02	h	6.77E-02	18	Fiss_Prod
60	32	992.9	140La	4.03E+01	h	1.34E-04	38	Fiss_Prod
49	40	995.09	135I	6.59E+00	h	1.55E-03	93	Fiss_Prod
37	113	995.8	132I	2.30E+00	h	2.96E-04	173	Fiss_Prod
80	6	996.32	154Eu	8.50E+00	y	1.03E-01	13	Fiss_Prod
36	8	997.25	131Te	2.50E+01	m	3.34E-02	14	Fiss_Prod
204	15	1000.1	88Kr	2.84E+00	h	1.89E-02	20	Fiss_Prod
222	17	1001.34	99Mo	6.60E+01	h	5.46E-05	35	medical_FP
37	117	1002.5	132I	2.30E+00	h	2.57E-04	173	Fiss_Prod
37	118	1002.5	132I	2.30E+00	h	2.57E-04	173	Fiss_Prod
67	13	1002.85	143Ce	3.30E+01	h	7.53E-04	52	Fiss_Prod
80	4	1004.8	154Eu	8.50E+00	y	1.79E-01	13	Fiss_Prod
37	131	1005.4	132I	2.30E+00	h	1.58E-04	173	Fiss_Prod
197	10	1007.6	82Br	3.53E+01	h	1.27E-02	11	Fiss_Prod
37	94	1009	132I	2.30E+00	h	4.64E-04	173	Fiss_Prod
76	223	1012.2	151Pm	2.84E+01	h	3.60E-05	234	Fiss_Prod
73	4	1013.8	148mPm	4.13E+01	d	2.03E-01	18	Fiss_Prod
67	48	1014.3	143Ce	3.30E+01	h	1.28E-05	52	Fiss_Prod
222	33	1017	99Mo	6.60E+01	h	6.07E-06	35	medical_FP
221	10	1021.2	97Zr	1.69E+01	h	1.01E-02	12	Fiss_Prod
209	1	1024.3	91Sr	9.63E+00	h	3.25E-01	8	Fiss_Prod
219	2	1024.5	97Nb	7.21E+01	m	1.08E-02	2	Fiss_Prod
139	4	1025.9	238Np	2.12E+00	d	8.21E-02	5	SNM

139	3	1028.5	238Np	2.12E+00	d	1.74E-01	5	SNM
67	23	1031.22	143Ce	3.30E+01	h	2.01E-04	52	Fiss_Prod
37	37	1035	132I	2.30E+00	h	5.13E-03	173	Fiss_Prod
45	9	1038.6	134Cs	2.06E+00	y	1.00E-02	9	Fiss_Prod
49	5	1038.76	135I	6.59E+00	h	7.95E-02	93	Fiss_Prod
197	5	1044	82Br	3.53E+01	h	2.73E-01	11	Fiss_Prod
60	28	1045.05	140La	4.03E+01	h	2.48E-04	38	Fiss_Prod
19	9	1045.2	124Sb	1.65E-01	y	1.86E-02	13	Fiss_Prod
67	27	1046.78	143Ce	3.30E+01	h	1.20E-04	52	Fiss_Prod
52	2	1048.1	136Cs	1.31E+01	d	7.96E-01	14	Fiss_Prod
37	95	1049.6	132I	2.30E+00	h	4.64E-04	173	Fiss_Prod
7	3	1050.5	106Rh	1.00E+00	y	1.73E-02	3	Fiss_Prod
8	2	1050.5	106Ru	1.00E+00	y	1.56E-02	2	Fiss_Prod
222	31	1056.2	99Mo	6.60E+01	h	1.08E-05	35	medical_FP
34	30	1059.7	131mTe	3.24E+01	h	1.55E-02	36	Fiss_Prod
67	17	1060.22	143Ce	3.30E+01	h	3.64E-04	52	Fiss_Prod
82	11	1065.1	156Eu	1.52E+01	d	5.24E-02	29	Fiss_Prod
23	1	1066.6	125Sn	9.64E+00	d	8.60E-02	7	Fiss_Prod
82	12	1079.2	156Eu	1.52E+01	d	4.89E-02	29	Fiss_Prod
37	110	1081.8	132I	2.30E+00	h	3.45E-04	173	Fiss_Prod
37	77	1086.2	132I	2.30E+00	h	7.90E-04	173	Fiss_Prod
23	2	1088.9	125Sn	9.64E+00	d	4.04E-02	7	Fiss_Prod
49	47	1096.86	135I	6.59E+00	h	8.90E-04	93	Fiss_Prod
37	97	1096.9	132I	2.30E+00	h	4.44E-04	173	Fiss_Prod
60	30	1097.2	140La	4.03E+01	h	2.29E-04	38	Fiss_Prod
49	14	1101.58	135I	6.59E+00	h	1.61E-02	93	Fiss_Prod
82	26	1102.7	156Eu	1.52E+01	d	1.59E-02	29	Fiss_Prod
67	9	1103.25	143Ce	3.30E+01	h	4.15E-03	52	Fiss_Prod
37	83	1112.4	132I	2.30E+00	h	6.51E-04	173	Fiss_Prod
84	16	1115.1	160Tb	1.98E-01	y	1.50E-02	17	Fiss_Prod
193	1	1115.55	65Zn	6.67E-01	y	5.08E-01	5	Fiss_Prod
49	10	1124	135I	6.59E+00	h	3.62E-02	93	Fiss_Prod
34	4	1125.5	131mTe	3.24E+01	h	1.14E-01	36	Fiss_Prod
37	90	1126.5	132I	2.30E+00	h	4.94E-04	173	Fiss_Prod
37	91	1126.5	132I	2.30E+00	h	4.94E-04	173	Fiss_Prod
49	2	1131.51	135I	6.59E+00	h	2.26E-01	93	Fiss_Prod
37	12	1136	132I	2.30E+00	h	3.01E-02	173	Fiss_Prod
204	18	1141.3	88Kr	2.84E+00	h	1.28E-02	20	Fiss_Prod
210	5	1142.3	92Sr	2.71E+00	h	2.88E-02	5	Fiss_Prod
37	21	1143.3	132I	2.30E+00	h	1.35E-02	173	Fiss_Prod
36	4	1147	131Te	2.50E+01	m	4.96E-02	14	Fiss_Prod
37	50	1147.8	132I	2.30E+00	h	2.66E-03	173	Fiss_Prod
221	3	1147.97	97Zr	1.69E+01	h	2.62E-02	12	Fiss_Prod

34	31	1148.9	131mTe	3.24E+01	h	1.51E-02	36	Fiss_Prod
49	90	1151.51	135I	6.59E+00	h	2.87E-05	93	Fiss_Prod
82	4	1153.5	156Eu	1.52E+01	d	7.18E-02	29	Fiss_Prod
82	10	1154.1	156Eu	1.52E+01	d	5.30E-02	29	Fiss_Prod
31	5	1157.5	130I	1.24E+01	h	1.13E-01	8	Fiss_Prod
214	16	1158.5	93Y	1.02E+01	h	3.00E-04	29	Fiss_Prod
49	45	1159.9	135I	6.59E+00	h	1.03E-03	93	Fiss_Prod
67	42	1160.58	143Ce	3.30E+01	h	2.40E-05	52	Fiss_Prod
45	7	1167.9	134Cs	2.06E+00	y	1.80E-02	9	Fiss_Prod
214	26	1168.6	93Y	1.02E+01	h	1.05E-04	29	Fiss_Prod
49	21	1169.04	135I	6.59E+00	h	8.75E-03	93	Fiss_Prod
37	28	1172.9	132I	2.30E+00	h	1.09E-02	173	Fiss_Prod
84	3	1177.9	160Tb	1.98E-01	y	1.44E-01	17	Fiss_Prod
49	53	1180.46	135I	6.59E+00	h	6.31E-04	93	Fiss_Prod
214	14	1183.5	93Y	1.02E+01	h	4.80E-04	29	Fiss_Prod
214	20	1184.7	93Y	1.02E+01	h	1.95E-04	29	Fiss_Prod
84	14	1199.9	160Tb	1.98E-01	y	2.36E-02	17	Fiss_Prod
214	9	1203.3	93Y	1.02E+01	h	1.07E-03	29	Fiss_Prod
34	5	1206.6	131mTe	3.24E+01	h	9.76E-02	36	Fiss_Prod
19	12	1208.3	124Sb	1.65E-01	y	1.34E-02	13	Fiss_Prod
37	139	1212.3	132I	2.30E+00	h	1.18E-04	173	Fiss_Prod
24	14	1213	126Sb	2.98E+02	h	2.39E-02	18	Fiss_Prod
49	59	1225.6	135I	6.59E+00	h	4.31E-04	93	Fiss_Prod
82	3	1230.7	156Eu	1.52E+01	d	8.94E-02	29	Fiss_Prod
52	4	1235.3	136Cs	1.31E+01	d	1.97E-01	14	Fiss_Prod
40	6	1236.4	133I	2.08E+01	h	1.49E-02	7	Fiss_Prod
214	17	1237.4	93Y	1.02E+01	h	2.93E-04	29	Fiss_Prod
49	19	1240.47	135I	6.59E+00	h	9.04E-03	93	Fiss_Prod
82	7	1242.4	156Eu	1.52E+01	d	6.76E-02	29	Fiss_Prod
37	147	1242.6	132I	2.30E+00	h	8.88E-05	173	Fiss_Prod
204	20	1250.7	88Kr	2.84E+00	h	1.12E-02	20	Fiss_Prod
37	85	1254.1	132I	2.30E+00	h	5.92E-04	173	Fiss_Prod
49	86	1254.8	135I	6.59E+00	h	5.74E-05	93	Fiss_Prod
49	87	1254.8	135I	6.59E+00	h	5.74E-05	93	Fiss_Prod
49	1	1260.41	135I	6.59E+00	h	2.87E-01	93	Fiss_Prod
37	116	1263.6	132I	2.30E+00	h	2.66E-04	173	Fiss_Prod
84	8	1271.9	160Tb	1.98E-01	y	7.03E-02	17	Fiss_Prod
37	58	1272.8	132I	2.30E+00	h	1.68E-03	173	Fiss_Prod
80	2	1274.5	154Eu	8.50E+00	y	3.55E-01	13	Fiss_Prod
221	11	1276.07	97Zr	1.69E+01	h	9.40E-03	12	Fiss_Prod
82	18	1277.4	156Eu	1.52E+01	d	3.21E-02	29	Fiss_Prod
49	55	1277.83	135I	6.59E+00	h	5.74E-04	93	Fiss_Prod
37	27	1290.8	132I	2.30E+00	h	1.13E-02	173	Fiss_Prod

37	17	1295.1	132I	2.30E+00	h	1.88E-02	173	Fiss_Prod
37	31	1297.91	132I	2.30E+00	h	8.88E-03	173	Fiss_Prod
40	3	1298.2	133I	2.08E+01	h	2.33E-02	7	Fiss_Prod
60	23	1303.5	140La	4.03E+01	h	4.20E-04	38	Fiss_Prod
49	64	1308.7	135I	6.59E+00	h	3.44E-04	93	Fiss_Prod
84	13	1312.2	160Tb	1.98E-01	y	2.85E-02	17	Fiss_Prod
37	86	1314	132I	2.30E+00	h	5.92E-04	173	Fiss_Prod
49	52	1315.77	135I	6.59E+00	h	6.60E-04	93	Fiss_Prod
197	6	1317.5	82Br	3.53E+01	h	2.69E-01	11	Fiss_Prod
37	64	1317.93	132I	2.30E+00	h	1.18E-03	173	Fiss_Prod
67	45	1324.48	143Ce	3.30E+01	h	1.58E-05	52	Fiss_Prod
19	10	1325.5	124Sb	1.65E-01	y	1.50E-02	13	Fiss_Prod
49	68	1334.8	135I	6.59E+00	h	3.16E-04	93	Fiss_Prod
67	38	1340.1	143Ce	3.30E+01	h	3.08E-05	52	Fiss_Prod
49	48	1343.66	135I	6.59E+00	h	7.75E-04	93	Fiss_Prod
63	1	1354.5	141La	3.92E+00	h	2.62E-02	1	Fiss_Prod
37	153	1360	132I	2.30E+00	h	5.92E-05	173	Fiss_Prod
221	12	1361	97Zr	1.69E+01	h	6.51E-03	12	Fiss_Prod
221	8	1362.68	97Zr	1.69E+01	h	1.02E-02	12	Fiss_Prod
45	6	1365.2	134Cs	2.06E+00	y	3.04E-02	9	Fiss_Prod
82	23	1366.4	156Eu	1.52E+01	d	1.76E-02	29	Fiss_Prod
49	25	1367.89	135I	6.59E+00	h	6.08E-03	93	Fiss_Prod
19	6	1368.2	124Sb	1.65E-01	y	2.51E-02	13	Fiss_Prod
204	16	1369.5	88Kr	2.84E+00	h	1.48E-02	20	Fiss_Prod
37	15	1372.07	132I	2.30E+00	h	2.47E-02	173	Fiss_Prod
67	52	1382	143Ce	3.30E+01	h	3.85E-06	52	Fiss_Prod
210	1	1383.9	92Sr	2.71E+00	h	9.00E-01	5	Fiss_Prod
11	4	1384.3	110mAg	6.84E-01	y	2.43E-01	15	Fiss_Prod
37	135	1390.7	132I	2.30E+00	h	1.48E-04	173	Fiss_Prod
37	6	1398.57	132I	2.30E+00	h	7.01E-02	173	Fiss_Prod
60	22	1405.2	140La	4.03E+01	h	5.91E-04	38	Fiss_Prod
37	98	1410.6	132I	2.30E+00	h	4.34E-04	173	Fiss_Prod
49	69	1416.3	135I	6.59E+00	h	3.16E-04	93	Fiss_Prod
214	6	1425.4	93Y	1.02E+01	h	2.45E-03	29	Fiss_Prod
19	13	1436.6	124Sb	1.65E-01	y	1.14E-02	13	Fiss_Prod
49	79	1441.8	135I	6.59E+00	h	1.72E-04	93	Fiss_Prod
37	20	1442.56	132I	2.30E+00	h	1.40E-02	173	Fiss_Prod
49	30	1448.35	135I	6.59E+00	h	3.16E-03	93	Fiss_Prod
37	149	1450	132I	2.30E+00	h	7.90E-05	173	Fiss_Prod
214	5	1450.5	93Y	1.02E+01	h	3.27E-03	29	Fiss_Prod
37	92	1456.5	132I	2.30E+00	h	4.94E-04	173	Fiss_Prod
49	4	1457.56	135I	6.59E+00	h	8.67E-02	93	Fiss_Prod
74	1	1465.1	148Pm	5.37E+00	d	2.22E-01	5	Fiss_Prod



214	12	1470.1	93Y	1.02E+01	h	6.53E-04	29	Fiss_Prod
197	8	1474.8	82Br	3.53E+01	h	1.66E-01	11	Fiss_Prod
11	12	1475.8	110mAg	6.84E-01	y	4.00E-02	15	Fiss_Prod
37	60	1476.7	132I	2.30E+00	h	1.30E-03	173	Fiss_Prod
71	3	1489	144Pr	7.79E-01	y	2.78E-03	3	Fiss_Prod
49	17	1502.79	135I	6.59E+00	h	1.08E-02	93	Fiss_Prod
11	7	1505	110mAg	6.84E-01	y	1.31E-01	15	Fiss_Prod
204	13	1518.4	88Kr	2.84E+00	h	2.15E-02	20	Fiss_Prod
37	78	1519.6	132I	2.30E+00	h	7.90E-04	173	Fiss_Prod
49	62	1521.99	135I	6.59E+00	h	3.73E-04	93	Fiss_Prod
204	5	1529.8	88Kr	2.84E+00	h	1.09E-01	20	Fiss_Prod
37	154	1531.9	132I	2.30E+00	h	5.92E-05	173	Fiss_Prod
37	132	1542.3	132I	2.30E+00	h	1.58E-04	173	Fiss_Prod
49	72	1543.7	135I	6.59E+00	h	2.58E-04	93	Fiss_Prod
37	148	1559	132I	2.30E+00	h	8.88E-05	173	Fiss_Prod
11	15	1562.3	110mAg	6.84E-01	y	1.18E-02	15	Fiss_Prod
49	15	1566.41	135I	6.59E+00	h	1.29E-02	93	Fiss_Prod
37	93	1592.9	132I	2.30E+00	h	4.74E-04	173	Fiss_Prod
80	13	1593	154Eu	8.50E+00	y	1.03E-02	13	Fiss_Prod
60	1	1596.21	140La	4.03E+01	h	9.54E-01	38	Fiss_Prod
80	10	1596.5	154Eu	8.50E+00	y	1.85E-02	13	Fiss_Prod
49	73	1613.75	135I	6.59E+00	h	2.58E-04	93	Fiss_Prod
37	145	1617.9	132I	2.30E+00	h	9.87E-05	173	Fiss_Prod
37	151	1618.9	132I	2.30E+00	h	6.91E-05	173	Fiss_Prod
37	140	1636.5	132I	2.30E+00	h	1.18E-04	173	Fiss_Prod
37	141	1636.5	132I	2.30E+00	h	1.18E-04	173	Fiss_Prod
37	150	1639.1	132I	2.30E+00	h	7.90E-05	173	Fiss_Prod
214	13	1642.7	93Y	1.02E+01	h	5.18E-04	29	Fiss_Prod
37	138	1644	132I	2.30E+00	h	1.28E-04	173	Fiss_Prod
34	33	1646	131mTe	3.24E+01	h	1.24E-02	36	Fiss_Prod
214	18	1651.7	93Y	1.02E+01	h	2.33E-04	29	Fiss_Prod
37	133	1661.4	132I	2.30E+00	h	1.58E-04	173	Fiss_Prod
37	123	1671.3	132I	2.30E+00	h	2.17E-04	173	Fiss_Prod
49	3	1678.03	135I	6.59E+00	h	9.56E-02	93	Fiss_Prod
37	155	1679.3	132I	2.30E+00	h	5.92E-05	173	Fiss_Prod
19	2	1691	124Sb	1.65E-01	y	4.90E-01	13	Fiss_Prod
49	9	1706.46	135I	6.59E+00	h	4.10E-02	93	Fiss_Prod
37	88	1715.4	132I	2.30E+00	h	5.53E-04	173	Fiss_Prod
37	89	1720.6	132I	2.30E+00	h	5.43E-04	173	Fiss_Prod
37	82	1727.2	132I	2.30E+00	h	6.71E-04	173	Fiss_Prod
49	80	1742	135I	6.59E+00	h	1.72E-04	93	Fiss_Prod
221	7	1750.24	97Zr	1.69E+01	h	1.09E-02	12	Fiss_Prod
37	121	1752.3	132I	2.30E+00	h	2.47E-04	173	Fiss_Prod

37	49	1757.4	132I	2.30E+00	h	2.96E-03	173	Fiss_Prod
37	87	1760.4	132I	2.30E+00	h	5.92E-04	173	Fiss_Prod
37	122	1768.5	132I	2.30E+00	h	2.47E-04	173	Fiss_Prod
37	79	1778.5	132I	2.30E+00	h	7.90E-04	173	Fiss_Prod
37	143	1786.5	132I	2.30E+00	h	1.09E-04	173	Fiss_Prod
37	144	1786.5	132I	2.30E+00	h	1.09E-04	173	Fiss_Prod
49	6	1791.2	135I	6.59E+00	h	7.72E-02	93	Fiss_Prod
37	134	1814	132I	2.30E+00	h	1.58E-04	173	Fiss_Prod
214	19	1827.8	93Y	1.02E+01	h	2.33E-04	29	Fiss_Prod
37	115	1830.1	132I	2.30E+00	h	2.76E-04	173	Fiss_Prod
49	26	1830.69	135I	6.59E+00	h	5.80E-03	93	Fiss_Prod
205	1	1836	88Rb	1.78E+01	m	2.14E-01	3	Fiss_Prod
49	88	1845.3	135I	6.59E+00	h	5.74E-05	93	Fiss_Prod
82	24	1877	156Eu	1.52E+01	d	1.73E-02	29	Fiss_Prod
60	24	1877.29	140La	4.03E+01	h	4.10E-04	38	Fiss_Prod
37	136	1879.2	132I	2.30E+00	h	1.38E-04	173	Fiss_Prod
36	13	1881.5	131Te	2.50E+01	m	1.42E-02	14	Fiss_Prod
37	114	1913.7	132I	2.30E+00	h	2.96E-04	173	Fiss_Prod
214	3	1917.8	93Y	1.02E+01	h	1.55E-02	29	Fiss_Prod
37	23	1921.08	132I	2.30E+00	h	1.23E-02	173	Fiss_Prod
60	33	1924.62	140La	4.03E+01	h	1.34E-04	38	Fiss_Prod
37	164	1925.7	132I	2.30E+00	h	1.97E-05	173	Fiss_Prod
49	34	1927.3	135I	6.59E+00	h	2.96E-03	93	Fiss_Prod
82	22	1937.7	156Eu	1.52E+01	d	2.14E-02	29	Fiss_Prod
37	157	1939.5	132I	2.30E+00	h	4.94E-05	173	Fiss_Prod
49	54	1948.49	135I	6.59E+00	h	6.31E-04	93	Fiss_Prod
82	14	1966	156Eu	1.52E+01	d	4.20E-02	29	Fiss_Prod
37	142	1985.64	132I	2.30E+00	h	1.18E-04	173	Fiss_Prod
34	22	2000.9	131mTe	3.24E+01	h	2.02E-02	36	Fiss_Prod
23	5	2001.7	125Sn	9.64E+00	d	2.06E-02	7	Fiss_Prod
37	26	2002.2	132I	2.30E+00	h	1.14E-02	173	Fiss_Prod
82	17	2026.6	156Eu	1.52E+01	d	3.54E-02	29	Fiss_Prod
204	7	2029.8	88Kr	2.84E+00	h	4.53E-02	20	Fiss_Prod
204	8	2035.4	88Kr	2.84E+00	h	3.74E-02	20	Fiss_Prod
49	22	2045.88	135I	6.59E+00	h	8.72E-03	93	Fiss_Prod
60	34	2083.2	140La	4.03E+01	h	1.15E-04	38	Fiss_Prod
37	51	2086.82	132I	2.30E+00	h	2.57E-03	173	Fiss_Prod
19	5	2091	124Sb	1.65E-01	y	5.73E-02	13	Fiss_Prod
82	13	2097.7	156Eu	1.52E+01	d	4.27E-02	29	Fiss_Prod
49	51	2112.4	135I	6.59E+00	h	6.89E-04	93	Fiss_Prod
49	78	2151.5	135I	6.59E+00	h	2.24E-04	93	Fiss_Prod
37	54	2172.68	132I	2.30E+00	h	2.07E-03	173	Fiss_Prod
49	89	2179.7	135I	6.59E+00	h	4.02E-05	93	Fiss_Prod

82	20	2180.9	156Eu	1.52E+01	d	2.43E-02	29	Fiss_Prod
214	8	2184.6	93Y	1.02E+01	h	1.57E-03	29	Fiss_Prod
71	2	2186	144Pr	7.79E-01	y	6.94E-03	3	Fiss_Prod
82	15	2186.7	156Eu	1.52E+01	d	3.95E-02	29	Fiss_Prod
37	152	2187	132I	2.30E+00	h	6.91E-05	173	Fiss_Prod
49	81	2189.4	135I	6.59E+00	h	1.29E-04	93	Fiss_Prod
214	7	2190.8	93Y	1.02E+01	h	1.69E-03	29	Fiss_Prod
204	3	2195.8	88Kr	2.84E+00	h	1.32E-01	20	Fiss_Prod
37	162	2204.2	132I	2.30E+00	h	2.96E-05	173	Fiss_Prod
37	65	2223.17	132I	2.30E+00	h	1.18E-03	173	Fiss_Prod
225	1	2224	H-1_n-g	3.17E-17	y	1.00E-08	1	n_irrad=SNM
204	9	2231.8	88Kr	2.84E+00	h	3.39E-02	20	Fiss_Prod
37	111	2249.1	132I	2.30E+00	h	3.36E-04	173	Fiss_Prod
49	24	2255.46	135I	6.59E+00	h	6.14E-03	93	Fiss_Prod
82	29	2269.9	156Eu	1.52E+01	d	1.12E-02	29	Fiss_Prod
37	159	2290.6	132I	2.30E+00	h	3.55E-05	173	Fiss_Prod
60	11	2347.88	140La	4.03E+01	h	8.49E-03	38	Fiss_Prod
37	55	2390.48	132I	2.30E+00	h	1.88E-03	173	Fiss_Prod
204	1	2392.1	88Kr	2.84E+00	h	3.46E-01	20	Fiss_Prod
37	146	2408.6	132I	2.30E+00	h	9.38E-05	173	Fiss_Prod
49	18	2408.65	135I	6.59E+00	h	9.56E-03	93	Fiss_Prod
37	167	2416.9	132I	2.30E+00	h	1.38E-05	173	Fiss_Prod
37	156	2444	132I	2.30E+00	h	5.63E-05	173	Fiss_Prod
49	84	2452.8	135I	6.59E+00	h	8.61E-05	93	Fiss_Prod
37	163	2454.8	132I	2.30E+00	h	2.07E-05	173	Fiss_Prod
214	29	2457.3	93Y	1.02E+01	h	6.75E-05	29	Fiss_Prod
60	35	2464.1	140La	4.03E+01	h	1.14E-04	38	Fiss_Prod
49	50	2466.07	135I	6.59E+00	h	7.18E-04	93	Fiss_Prod
214	23	2473.8	93Y	1.02E+01	h	1.13E-04	29	Fiss_Prod
49	92	2477.1	135I	6.59E+00	h	1.44E-05	93	Fiss_Prod
37	173	2487.8	132I	2.30E+00	h	7.90E-06	173	Fiss_Prod
60	8	2521.4	140La	4.03E+01	h	3.46E-02	38	Fiss_Prod
37	104	2525.14	132I	2.30E+00	h	3.95E-04	173	Fiss_Prod
37	165	2546.5	132I	2.30E+00	h	1.58E-05	173	Fiss_Prod
60	18	2547.34	140La	4.03E+01	h	1.01E-03	38	Fiss_Prod
37	158	2569.8	132I	2.30E+00	h	4.94E-05	173	Fiss_Prod
37	169	2593.8	132I	2.30E+00	h	1.18E-05	173	Fiss_Prod
37	166	2603.2	132I	2.30E+00	h	1.48E-05	173	Fiss_Prod
214	24	2605	93Y	1.02E+01	h	1.13E-04	29	Fiss_Prod
37	170	2607.2	132I	2.30E+00	h	9.87E-06	173	Fiss_Prod
37	160	2614.5	132I	2.30E+00	h	3.55E-05	173	Fiss_Prod
37	171	2653.8	132I	2.30E+00	h	9.87E-06	173	Fiss_Prod
205	3	2677.9	88Rb	1.78E+01	m	1.96E-02	3	Fiss_Prod

37	172	2690.8	132I	2.30E+00	h	9.87E-06	173	Fiss_Prod
37	161	2717.5	132I	2.30E+00	h	3.45E-05	173	Fiss_Prod
37	168	2757.8	132I	2.30E+00	h	1.28E-05	173	Fiss_Prod
60	21	2899.61	140La	4.03E+01	h	6.68E-04	38	Fiss_Prod
60	29	3118.51	140La	4.03E+01	h	2.48E-04	38	Fiss_Prod
60	36	3320.4	140La	4.03E+01	h	3.82E-05	38	Fiss_Prod
75	1	5000	151mPm	5.37E+00	d	1.79E-02	1	Fiss_Prod

## APPENDIX F

### ADJOINT IMPORTANCES PER FUEL PIN

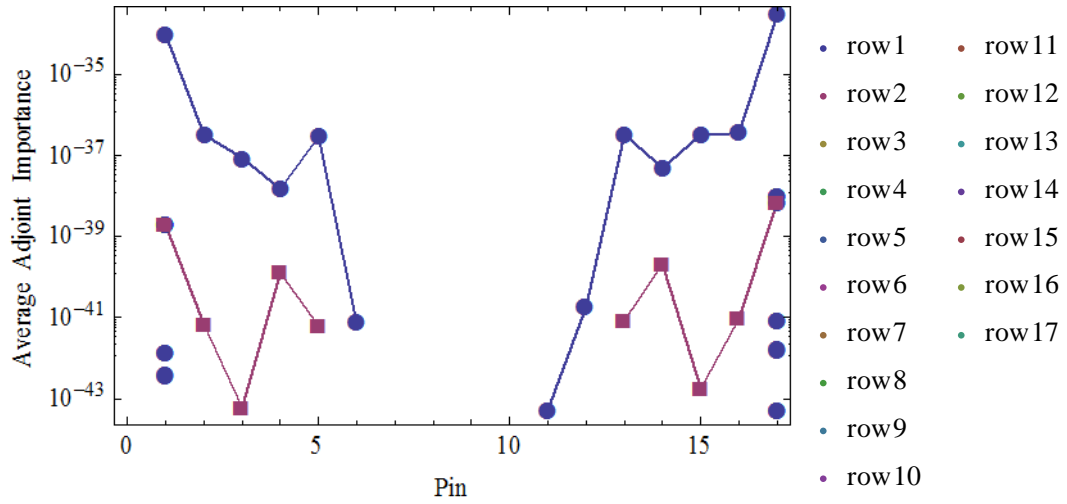


Figure F.1. Adjoint group 1 (0 – 0.3 MeV) adjoint importances per fuel pin in a Westinghouse 17x17 PWR fuel assembly.

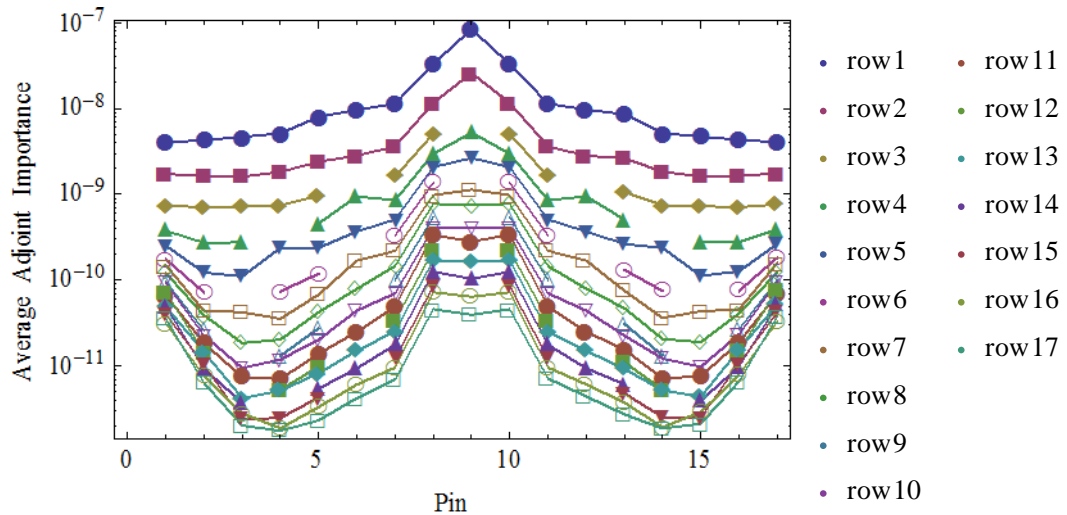


Figure F.2. Adjoint group 2 (0.3 – 0.741 MeV) adjoint importances per fuel pin in a Westinghouse 17x17 PWR fuel assembly.

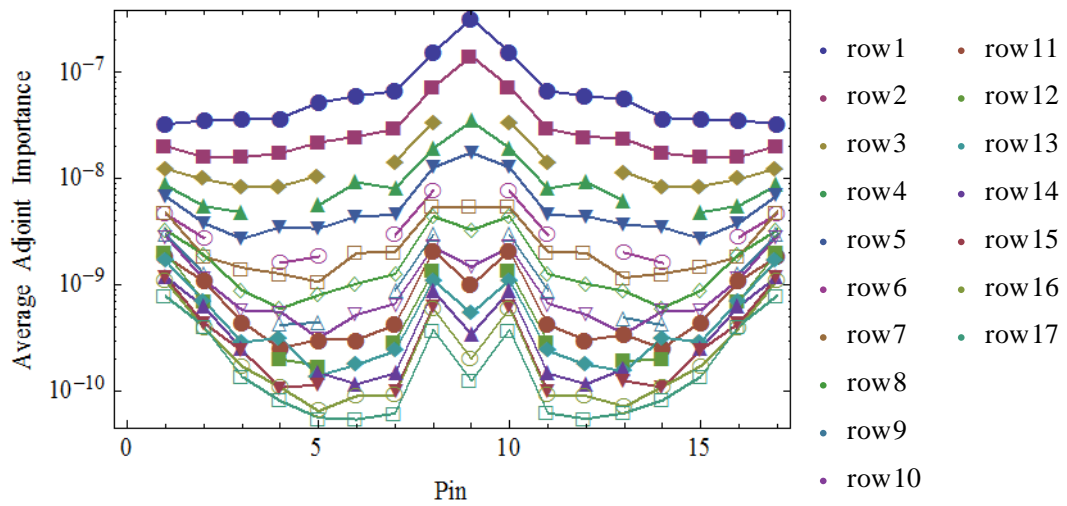


Figure F.3. Adjoint group 3 (0.741 – 0.743 MeV) adjoint importances per fuel pin in a Westinghouse 17x17 PWR fuel assembly.

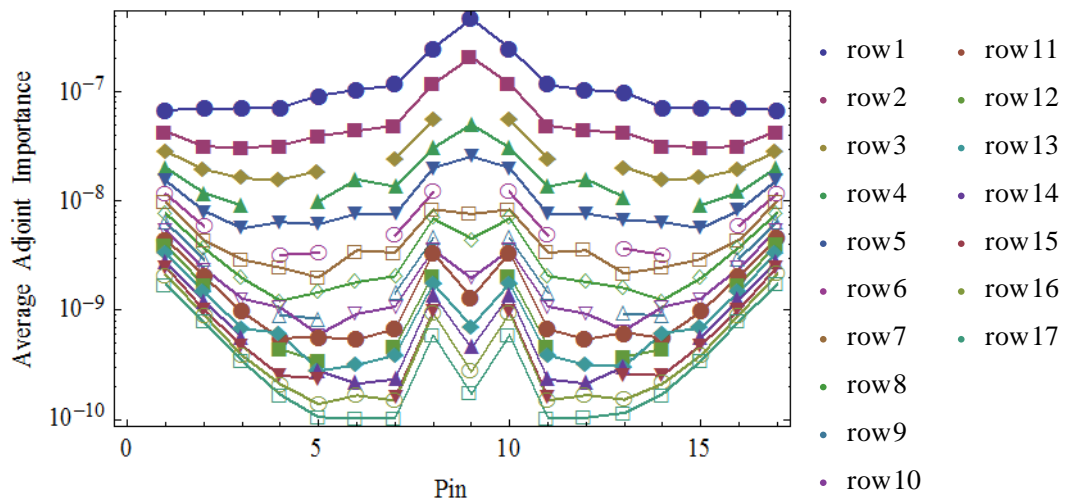


Figure F.4. Adjoint group 4 (0.743 – 0.765 MeV) adjoint importances per fuel pin in a Westinghouse 17x17 PWR fuel assembly.

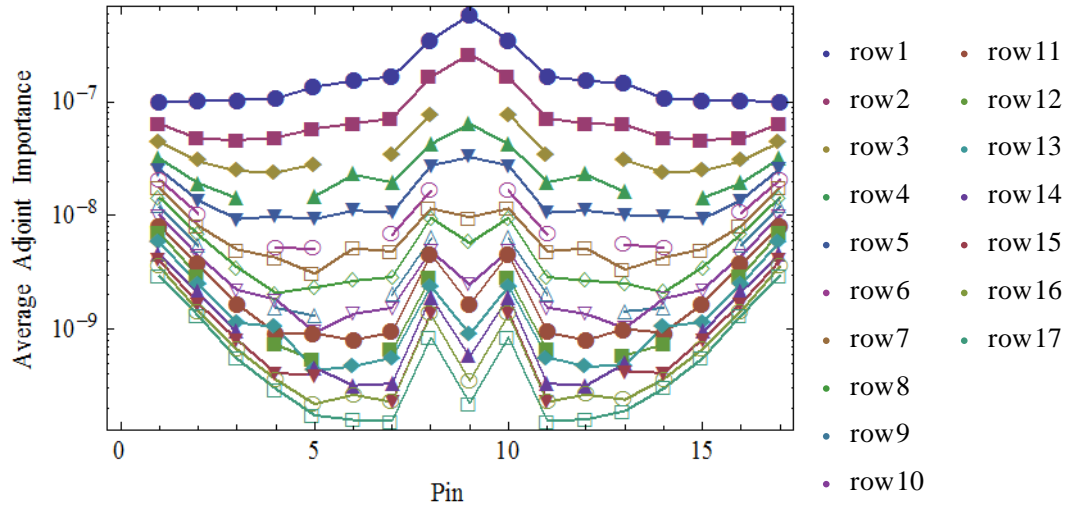


Figure F.5. Adjoint group 5 (0.765 – 0.767 MeV) adjoint importances per fuel pin in a Westinghouse 17x17 PWR fuel assembly.

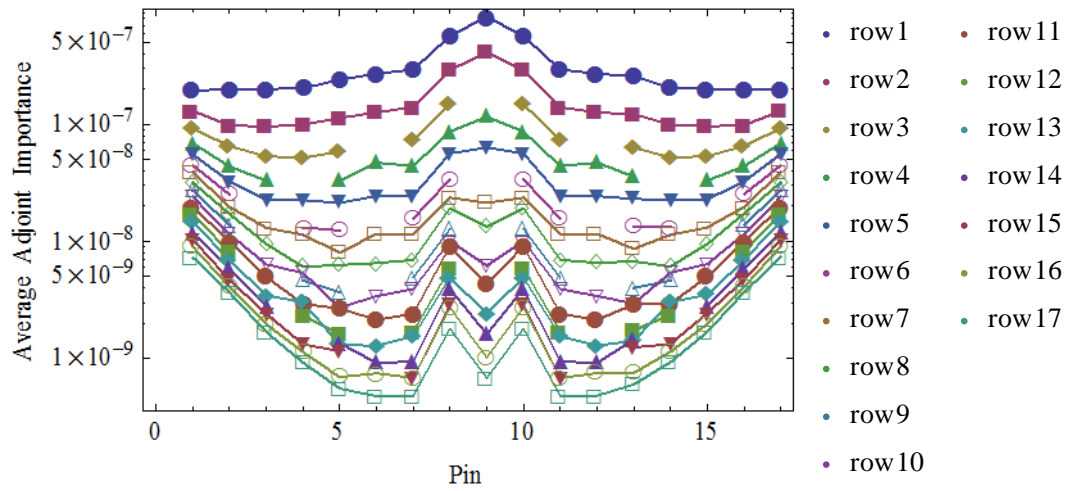


Figure F.6. Adjoint group 6 (0.767 – 0.954 MeV) adjoint importances per fuel pin in a Westinghouse 17x17 PWR fuel assembly.

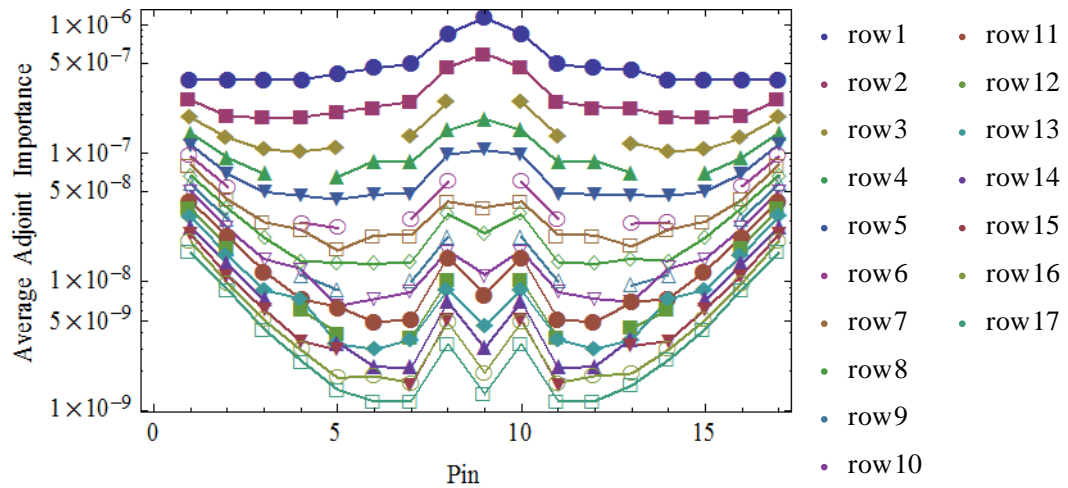


Figure F.7. Adjoint group 7 (0.954 – 0.956 MeV) adjoint importances per fuel pin in a Westinghouse 17x17 PWR fuel assembly.

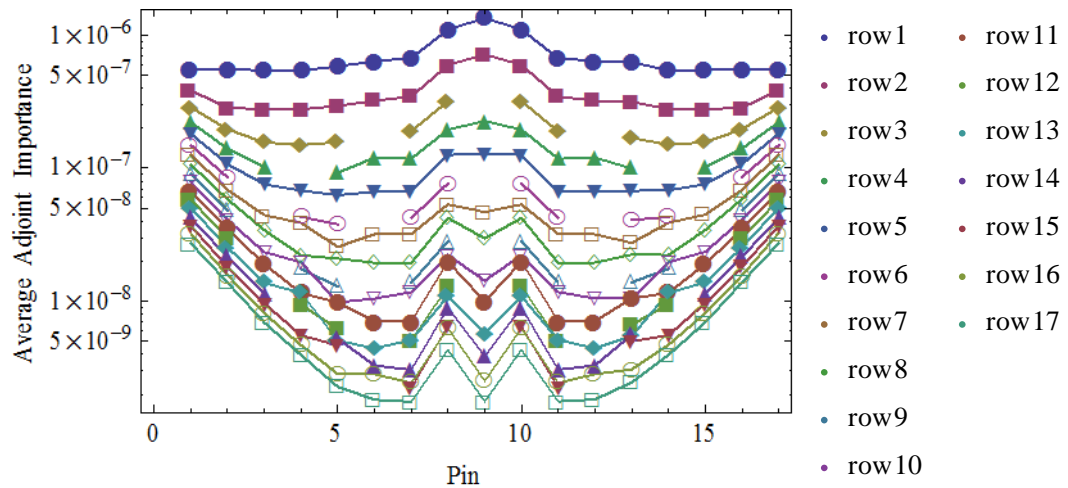


Figure F.8. Adjoint group 8 (0.956 – 0.999 MeV) adjoint importances per fuel pin in a Westinghouse 17x17 PWR fuel assembly.



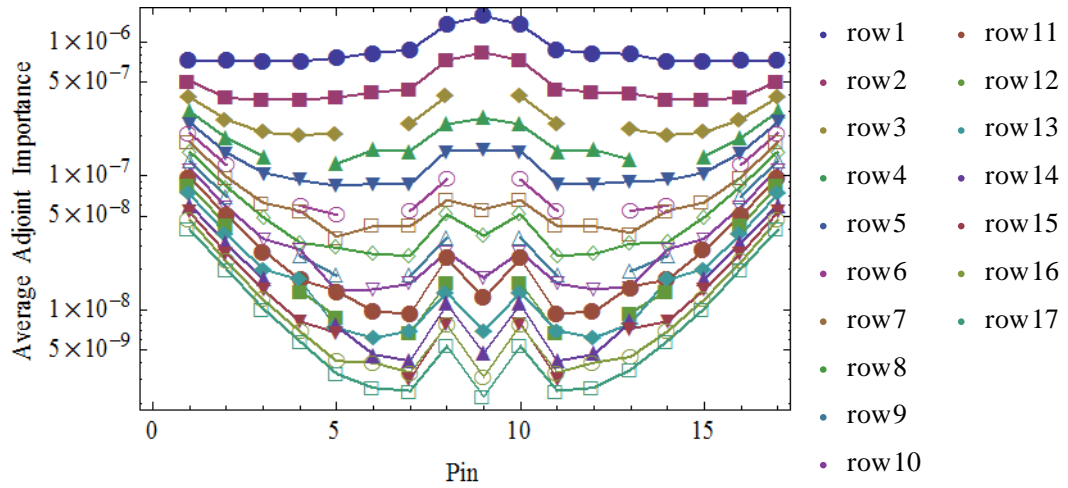


Figure F.9. Adjoint group 9 (0.999 – 1.002 MeV) adjoint importances per fuel pin in a Westinghouse 17x17 PWR fuel assembly.

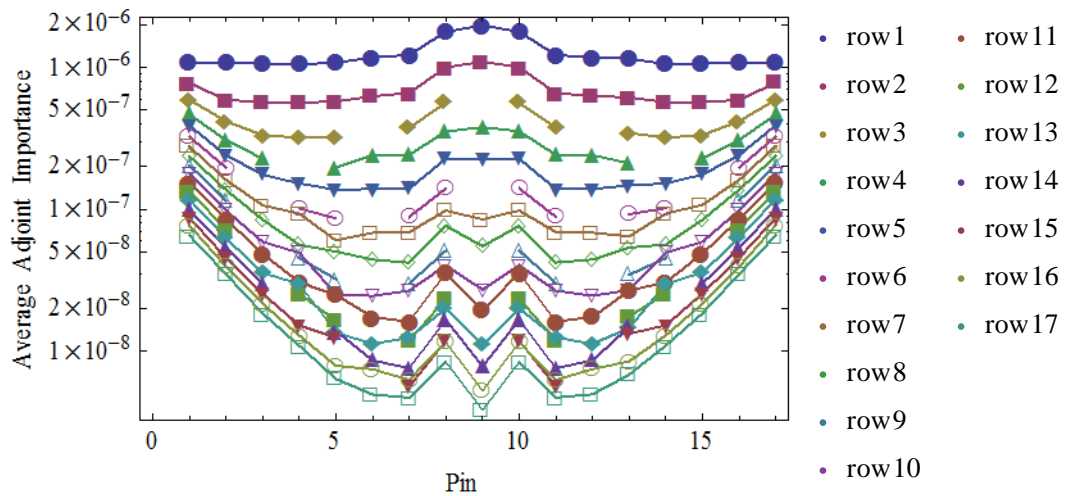


Figure F.10. Adjoint group 10 (1.002 – 1.18 MeV) adjoint importances per fuel pin in a Westinghouse 17x17 PWR fuel assembly.

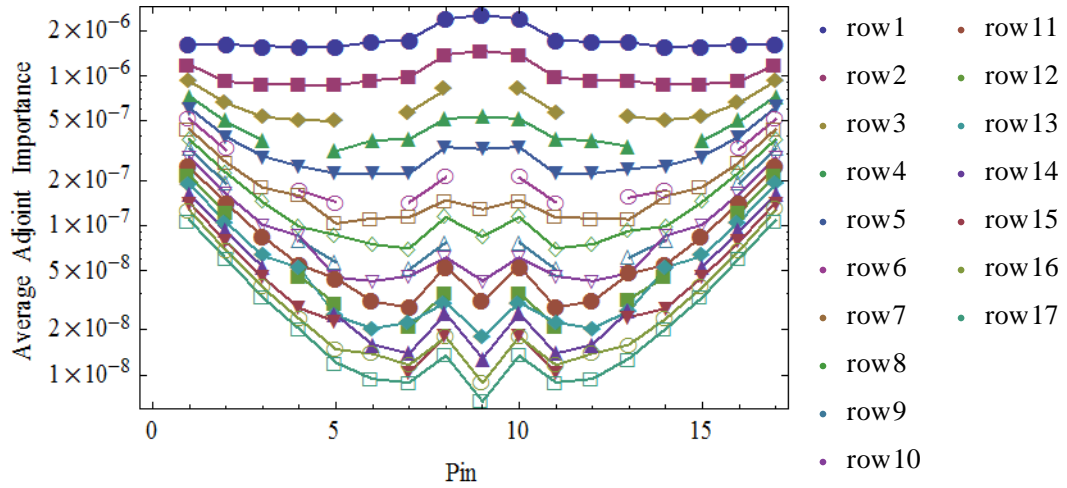


Figure F.11. Adjoint group 11 (1.18 – 1.2 MeV) adjoint importances per fuel pin in a Westinghouse 17x17 PWR fuel assembly.

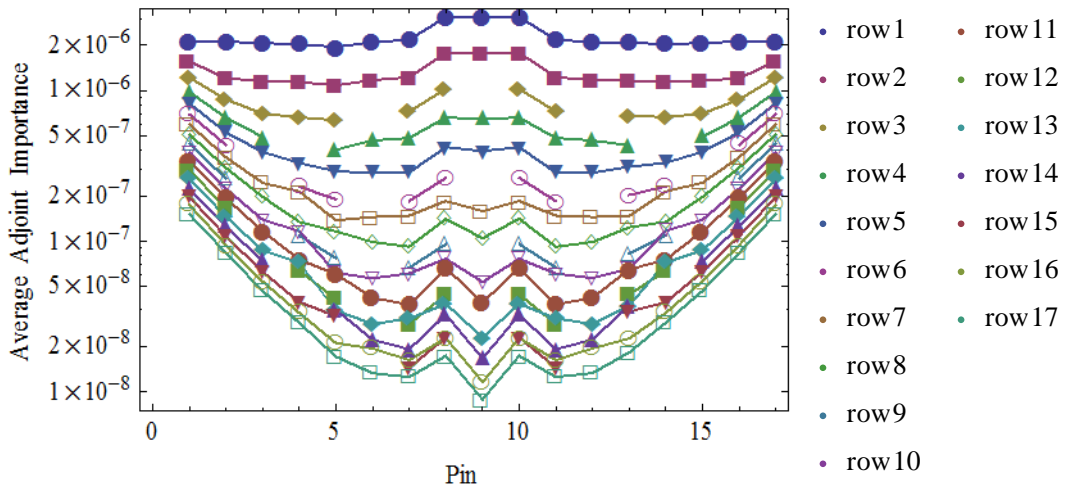


Figure F.12. Adjoint group 12 (1.2 – 1.24 MeV) adjoint importances per fuel pin in a Westinghouse 17x17 PWR fuel assembly.

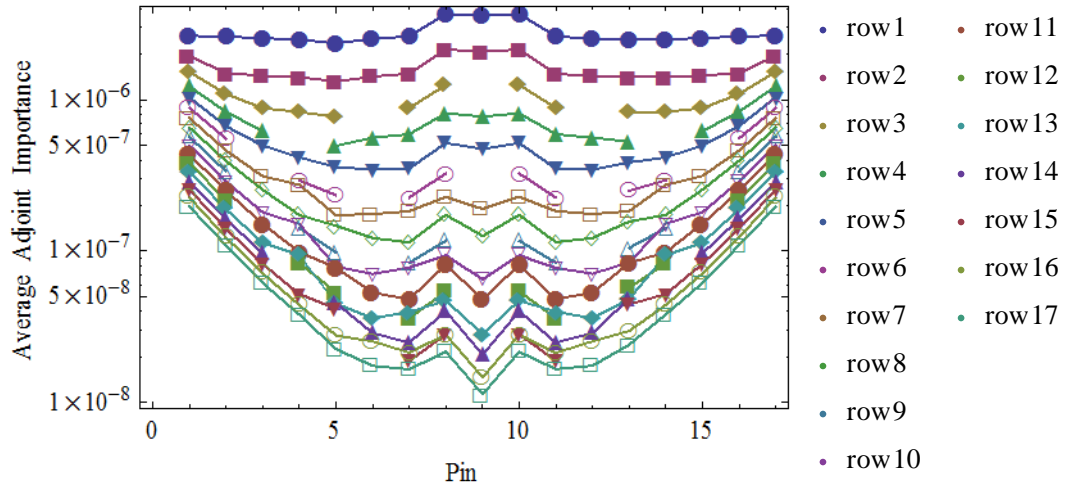


Figure F.13. Adjoint group 13 (1.24 – 1.26 MeV) adjoint importances per fuel pin in a Westinghouse 17x17 PWR fuel assembly.

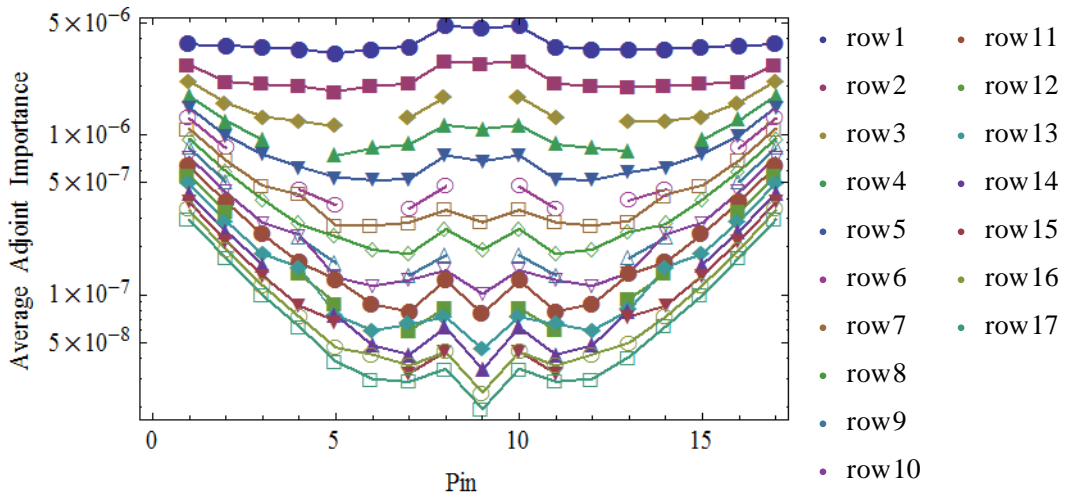


Figure F.14. Adjoint group 14 (1.26 – 1.5 MeV) adjoint importances per fuel pin in a Westinghouse 17x17 PWR fuel assembly.

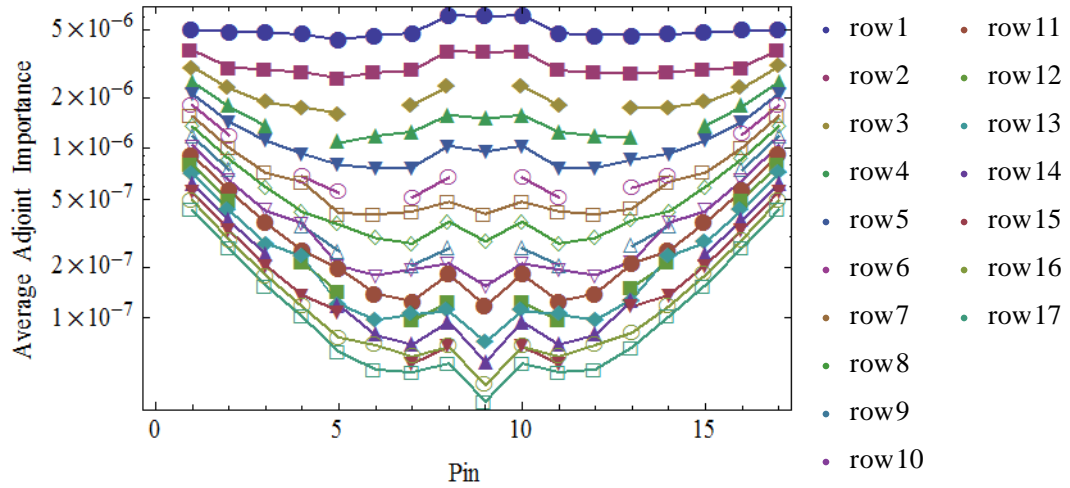


Figure F.15. Adjoint group 15 (1.5 – 1.52 MeV) adjoint importances per fuel pin in a Westinghouse 17x17 PWR fuel assembly.

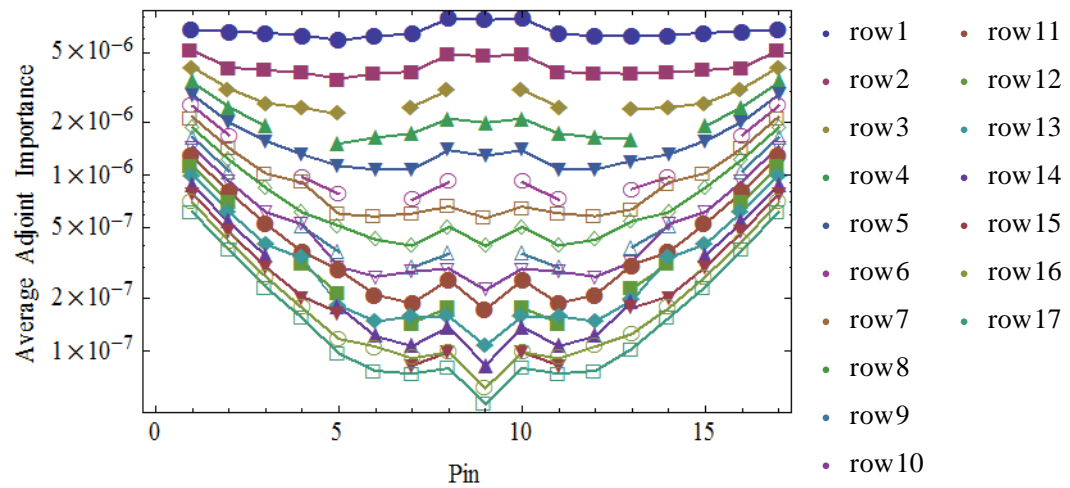


Figure F.16. Adjoint group 16 (1.52 – 1.736 MeV) adjoint importances per fuel pin in a Westinghouse 17x17 PWR fuel assembly.

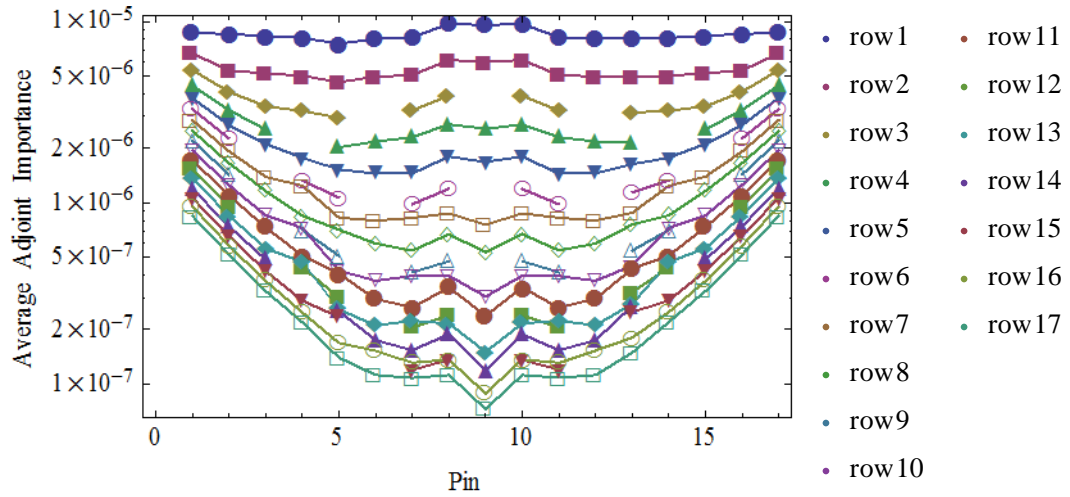


Figure F.17. Adjoint group 17 (1.736 – 1.74 MeV) adjoint importances per fuel pin in a Westinghouse 17x17 PWR fuel assembly.

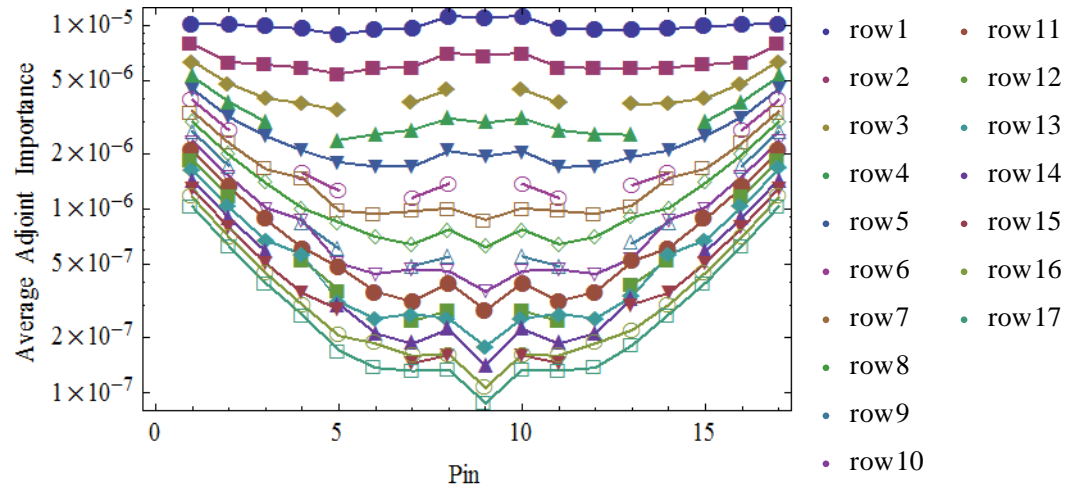


Figure F.18. Adjoint group 1 (1.74 – 1.76 MeV) adjoint importances per fuel pin in a Westinghouse 17x17 PWR fuel assembly.

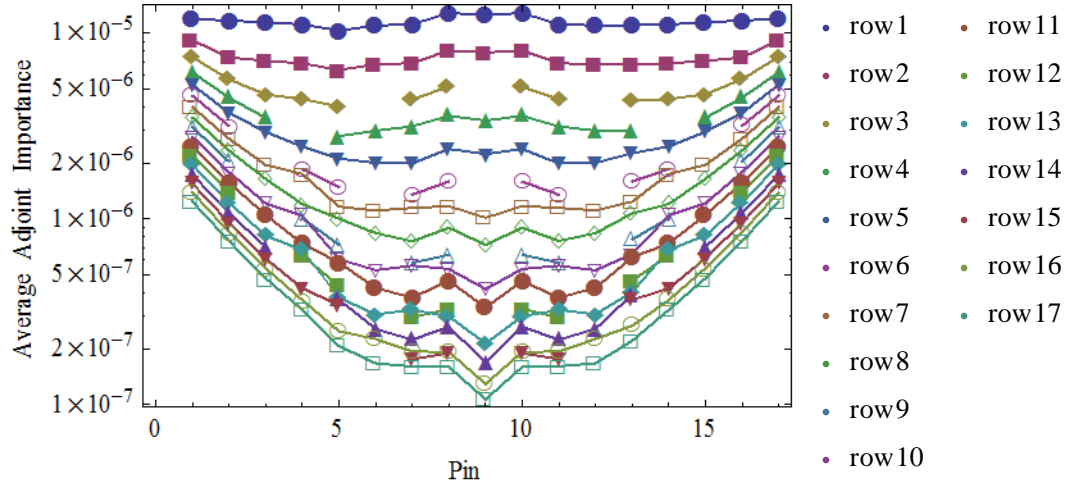


Figure F.19. Adjoint group 19 (1.76 – 1.83 MeV) adjoint importances per fuel pin in a Westinghouse 17x17 PWR fuel assembly.

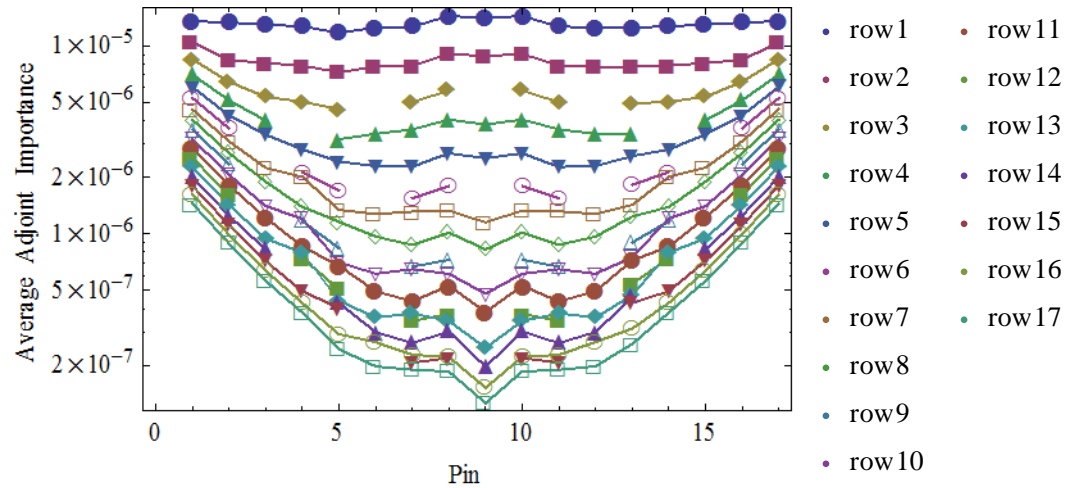


Figure F.20. Adjoint group 20 (1.83 – 1.832 MeV) adjoint importances per fuel pin in a Westinghouse 17x17 PWR fuel assembly.

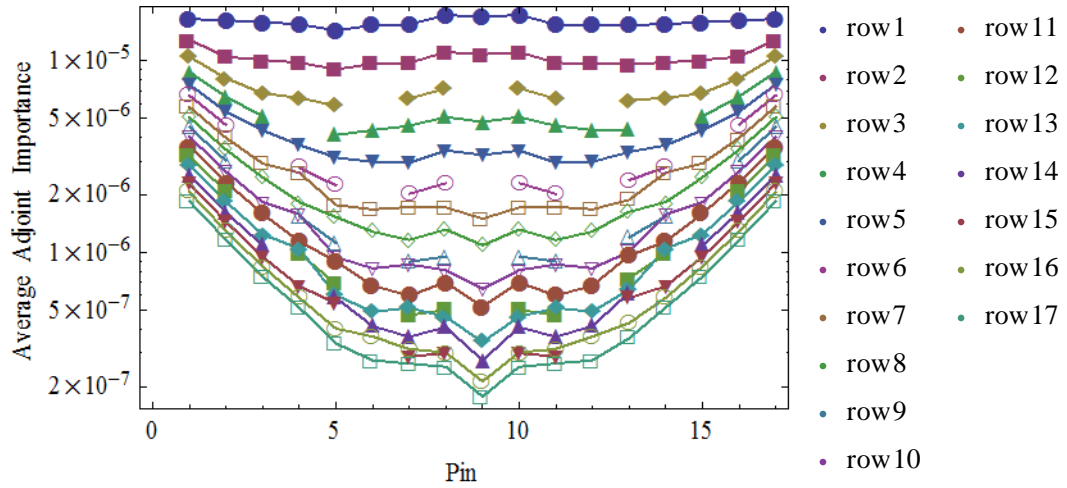


Figure F.21. Adjoint group 21 (1.832 – 2.21 MeV) adjoint importances per fuel pin in a Westinghouse 17x17 PWR fuel assembly.

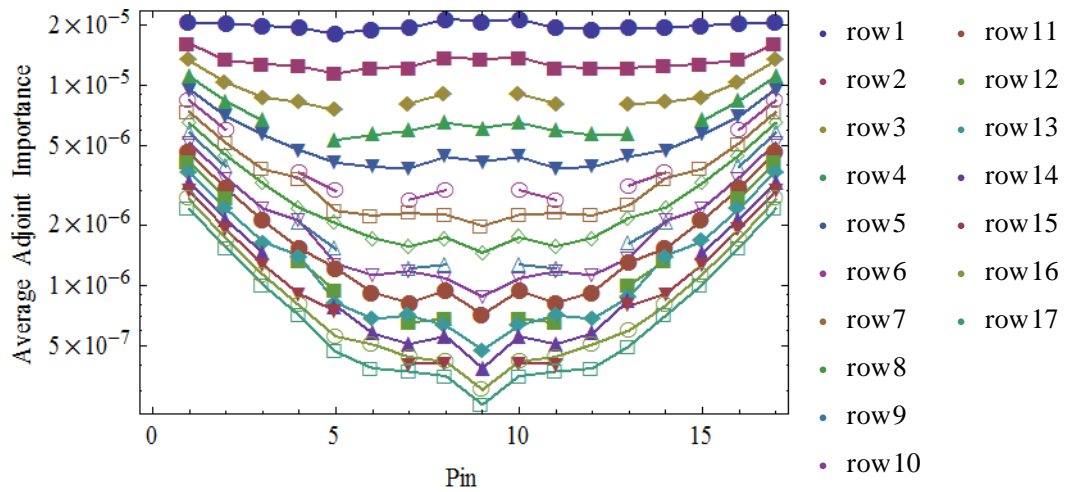


Figure F.22. Adjoint group 22 (2.21 – 2.25 MeV) adjoint importances per fuel pin in a Westinghouse 17x17 PWR fuel assembly.

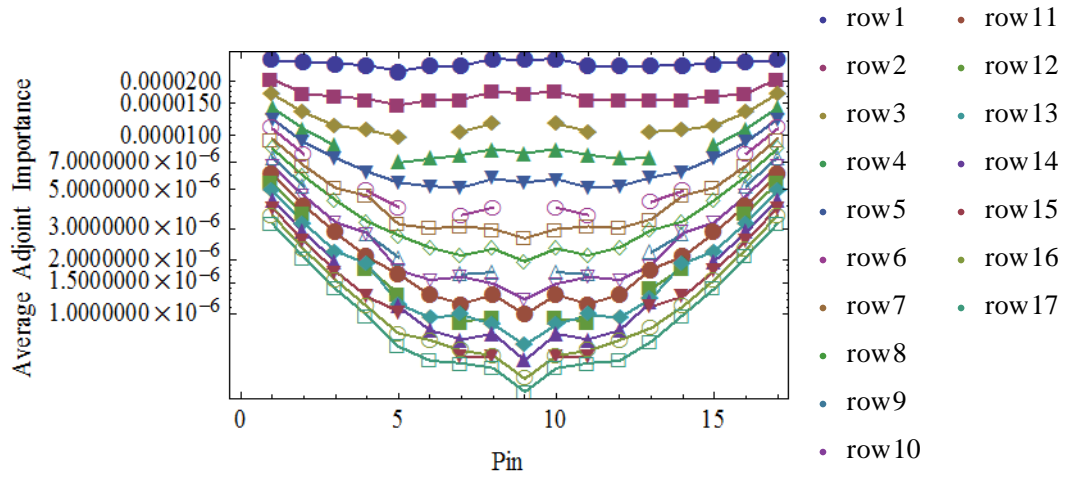


Figure F.23. Adjoint group 23 (2.25 – 2.749 MeV) adjoint importances per fuel pin in a Westinghouse 17x17 PWR fuel assembly.

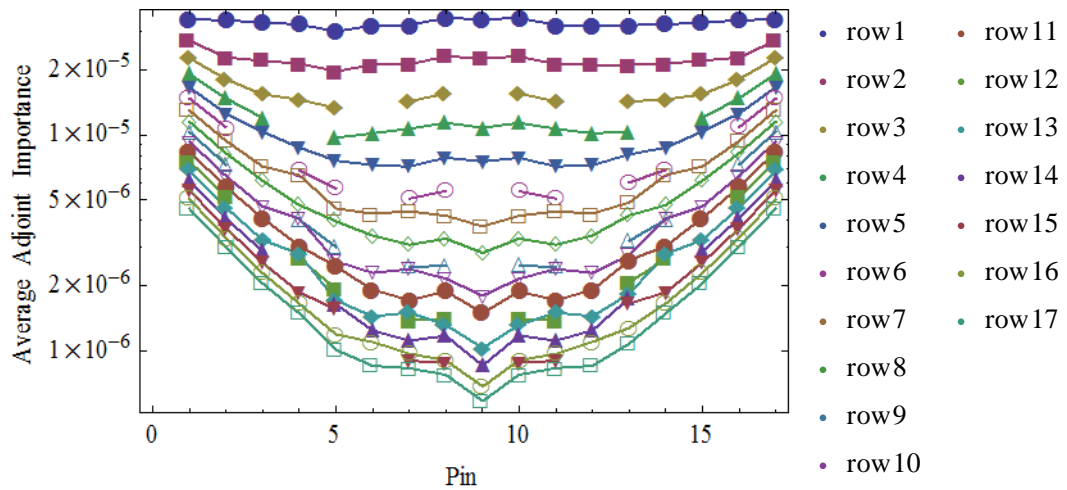


Figure F.24. Adjoint group 24 (2.749 – 3 MeV) adjoint importances per fuel pin in a Westinghouse 17x17 PWR fuel assembly.



## APPENDIX G

### CODE FOR DETERMINING ADJOINT IMPORTANCES PER FUEL

#### PIN

```
!  
PROGRAM MassEstimate  
!  
IMPLICIT REAL (A-H,O-Z)  
IMPLICIT INTEGER (I-N)  
!  
! MAIN PROGRAM  
!  
!////////////////////  
!  
CALL HEADER  
!  
CALL PEAKACTIVITY  
!  
STOP  
!  
END  
!  
!-----  
!  
! SUB HEADER  
!  
!  
SUBROUTINE HEADER  
!  
!
```

```

WRITE(*,'(A2)') '
WRITE(*,'(2X,A48)') Nuclide Concentration Estimator '
WRITE(*,'(A2)') '
WRITE(*,'(2X,A48)') Version 1.0 SINGLE PRECISION '
WRITE(*,'(A2)') '
WRITE(*,'(2X,A48)') J.N.Paul '
WRITE(*,'(A2)') '
WRITE(*,'(2X,A48)') Feb 2015 '
WRITE(*,'(A2)') '
!
END
!
!-----
!
! SUB PEAKACTIVITY
!
!
SUBROUTINE PEAKACTIVITY
!
CHARACTER*64 infile, infile2, fname, outfname
CHARACTER*104 dummy
CHARACTER*28, DIMENSION(200,50) :: Window
CHARACTER*8, DIMENSION(200) :: isotope
CHARACTER*5, DIMENSION(200) :: unit
CHARACTER*18, DIMENSION(200) :: corr
CHARACTER*18, DIMENSION(200) :: comment
CHARACTER*7 nuclideExp
CHARACTER*1 Plus,sign
INTEGER Percent,ID,icount,isonum,peakcount,pkct
INTEGER, DIMENSION(200) :: numemiss, nummatch
REAL, DIMENSION(200,50) :: Emission, ProbDk, Detect, Peak,
& NormCts,Importance,Pins,Activity,Mass,Curies,CiErrorp,Aerrorp,
& ImpErrorp,Errorp, CiErrorm,Aerrorm,ImpErrorm,Errorm

```

```

REAL, DIMENSION(200) :: score,hlfife
REAL Erg,Cts,NormCts1,TotCts,Time,Time2,Error
!
Plus='+ '
peakcount=0
pkct=0
TotCts=0
!
WRITE(*,*) 'SmartID output file for analysis: '
READ(*,*) infile
WRITE(*,*) ' '
WRITE(*,*) 'Spectrum file for analysis (.Spe): '
READ(*,*) infile2
WRITE(*,*) ' '
WRITE(*,*) 'Input % for the number of pins contributing to signal'
WRITE(*,*) 'Options (90, 95, 99)%'
READ(*,*) Percent
WRITE(*,*) 'Input % error from energy emission'
READ(*,*) Error
Error=Error/100
!
OPEN(1, FILE=infile, ACCESS='SEQUENTIAL')
OPEN(2, FILE=infile2, ACCESS='SEQUENTIAL')
OPEN(3, FILE='isoMass.txt', STATUS='NEW', ACCESS='SEQUENTIAL')
WRITE(3,*) 'Files read: ',infile, ' and ',infile2
WRITE(3,*) '% for number of pins contributing to signal: ',Percent
WRITE(3,*) 'Nuclide  Emission(MeV)  half life (s)',
&      ' Activity (Ci)      Error Window      ',
&      ' Importance  # of Pins'
!
DO iskip=1, 13
READ(1,'(A)',END=1000) dummy
END DO

```

```

!
DO jskip=1,9
READ(2,'(A)') dummy
END DO
!
READ(2,'(F9.0,F10.0)')Time,Time2
READ(1,'(A15,A20)') dummy,fname
WRITE(*,*) 'Spectrum File Read: '
WRITE(*,*) fname
! WRITE(*,*) ' TIME: ',Time
!
READ(1,'(A)',END=1000) dummy
!
READ(1,'(I3,A38)') numPeaks, dummy
!
READ(1,'(A)',END=1000) dummy
READ(1,'(A)',END=1000) dummy
!
! ADD TOTAL NUMBER OF COUNTS
Do ipeak=1, numPeaks
READ(1,'(F9.2,F15.4,F14.5,I8)') Erg,Cts,NormCts1,ID
TotCts=TotCts+Cts/Time
! WRITE(*,*) Erg,Cts,NormCts,ID
END DO
! WRITE(*,*)'TotCts: ',TotCts
! WRITE(*,*)'TIME: ',Time
! PAUSE
!
100 CONTINUE
READ(1,'(A)') dummy
isearch=INDEX(dummy,'Nuclide')
!
IF(isearch.EQ.0) THEN

```

```

        GOTO 100
ELSE IF(isearch.GT.0) THEN
    isonum=-1
200  CONTINUE
    isonum=isonum+1
    IF(isonum.GT.0)THEN
!    READ(1,*) dummy
!    WRITE(*,*)'line: ',dummy
    READ(1,'(A8,F11.2,F14.4,A5,2I15,A18,A18)')isotope(isonum),
&    score(isonum),hlflfe(isonum),unit(isonum),numemiss(isonum),
&    nummatch(isonum),corr(isonum),comment(isonum)
    IF(unit(isonum).EQ.' y')THEN
        hlflfe(isonum)=hlflfe(isonum)*86400*365.25
    ELSE IF(unit(isonum).EQ.' d')THEN
        hlflfe(isonum)=hlflfe(isonum)*86400
    ELSE IF (unit(isonum).EQ.' h')THEN
        hlflfe(isonum)=hlflfe(isonum)*3600
    ELSE IF(unit(isonum).EQ.' m')THEN
        hlflfe(isonum)=hlflfe(isonum)*60
    END IF
    WRITE(*,*)'isotope: ',isotope(isonum), 'half life: ',
&    hlflfe(isonum)
    END IF
    pkct=0
300  CONTINUE
    READ(1,'(A)')sign
    jsearch=INDEX(sign,plus)
    IF(jsearch.GT.0)THEN
        BACKSPACE(1)
        pkct=pkct+1
        READ(1,'(A1,F8.2,F15.4,F13.4,A28,F10.2,F14.4)')sign,
&    Emission(isonum,pkct),ProbDK(isonum,pkct),Detect(isonum,pkct),
&    Window(isonum,pkct),Peak(isonum,pkct),NormCts(isonum,pkct)

```

```

! WRITE(*,'(A1,F8.2,F15.4,F13.4,A28,F10.2,F14.4)'sign,
! & Emission(isonum,pkct),ProbDK(isonum,pkct),Detect(isonum,pkct),
! & Window(isonum,pkct),Peak(isonum,pkct),NormCts(isonum,pkct)
! WRITE(*,*)'isonum: ',isonum,' pkct: ',pkct
!
i=isonum
j=pkct
IF(Percent.EQ.90) THEN
  Emission(i,j)=0.001*Emission(i,j)
  Eerrorm(i,j)=Emission(i,j)*(1-Error)
  Eerrorp(i,j)=Emission(i,j)*(1+Error)
  IF(Emission(i,j).LT.1.095)THEN
    Importance(i,j)=2.8228E-7*Emission(i,j)**5.91
!   ImpErrorp(i,j)=2.8228E-7*Eerrorp(i,j)**5.91
!   ImpErrorm(i,j)=2.8228E-7*Eerrorm(i,j)**5.91
    ImpErrorp(i,j)=1.3*2.8228E-7*Emission(i,j)**5.91
    ImpErrorm(i,j)=0.7*2.8228E-7*Eerrorm(i,j)**5.91
    Pins(i,j)=-8.1792+44.0168*Emission(i,j)+
&       137.2431*Emission(i,j)**2-
&       68.9146*Emission(i,j)**3
    Activity(i,j)=NormCts(i,j)*TotCts*.01
    Aerrorp(i,j)=(Activity(i,j)*264)/(ImpErrorp(i,j)
&       *Pins(i,j))
    Aerrorm(i,j)=(Activity(i,j)*264)/(ImpErrorm(i,j)
&       *Pins(i,j))
    Activity(i,j)=Activity(i,j)/Importance(i,j)
    Activity(i,j)=Activity(i,j)/Pins(i,j)
    Activity(i,j)=Activity(i,j)*264
!   WRITE(*,*)'Activity: ',Activity(i,j)
    Curies(i,j)=Activity(i,j)/(3.7E10*ProbDK(i,j))
    CiErrorp(i,j)=Aerrorp(i,j)/3.7E10/ProbDK(i,j)
    CiErrorm(i,j)=Aerrorm(i,j)/3.7E10/ProbDK(i,j)
    Mass(i,j)=Activity(i,j)/hlflfe(i)/ProbDK(i,j)

```

```

WRITE(*,*)'Imp: ',Importance(i,j),'Pins: ',Pins(i,j)
WRITE(*,*)'Activity: ',Activity(i,j),' Mass: ',Mass(i,j)
WRITE(*,*)'
WRITE(*,*)'Curies: ',Curies(i,j)
WRITE(*,*)'
WRITE(3,*)isotope(i),' ',Emission(i,j),' ',hflfe(i),' ',
&      Curies(i,j),' ( ',CiErrorp(i,j),' ',
&      CiErrorm(i,j),' ) ',
&      Importance(i,j),' ',Pins(i,j)
ELSE IF(Emission(i,j).GE.1.095)THEN
      Importance(i,j)=8.1077E-6-1.7859E-5*Emission(i,j)+
&      1.1867E-5*Emission(i,j)**2-
&      1.7594E-6*Emission(i,j)**3
!      ImpErrorp(i,j)=8.1077E-6-1.7859E-5*Eerrorm(i,j)+
! &      1.1867E-5*Eerrorm(i,j)**2-
! &      1.7594E-6*Eerrorm(i,j)**3
!      ImpErrorm(i,j)=8.1077E-6-1.7859E-5*Eerrorm(i,j)+
! &      1.1867E-5*Eerrorm(i,j)**2-
! &      1.7594E-6*Eerrorm(i,j)**3
      ImpErrorp(i,j)=1.3*(8.1077E-6-1.7859E-5*Emission(i,j)+
&      1.1867E-5*Emission(i,j)**2-
&      1.7594E-6*Emission(i,j)**3)
      ImpErrorm(i,j)=0.7*(8.1077E-6-1.7859E-5*Emission(i,j)+
&      1.1867E-5*Emission(i,j)**2-
&      1.7594E-6*Emission(i,j)**3)
      Pins(i,j)=-35.9819+227.5443*Emission(i,j)-
&      109.9411*Emission(i,j)**2+
&      24.4343*Emission(i,j)**3-
&      2.0076*Emission(i,j)**4
      Activity(i,j)=NormCts(i,j)*TotCts*.01
      Aerrorp(i,j)=(Activity(i,j)*264)/(ImpErrorp(i,j)
&      *Pins(i,j))
      Aerrorm(i,j)=(Activity(i,j)*264)/(ImpErrorm(i,j)

```

```

&          *Pins(i,j))
Activity(i,j)=(Activity(i,j)*264)/(Importance(i,j)*
&          Pins(i,j))
Curies(i,j)=Activity(i,j)/3.7E10/ProbDK(i,j)
CiErrorp(i,j)=Aerrorp(i,j)/3.7E10/ProbDK(i,j)
CiErrorm(i,j)=Aerrorm(i,j)/3.7E10/ProbDK(i,j)
Mass(i,j)=Activity(i,j)/(hlflfe(i)*ProbDK(i,j))
WRITE(*,*)'Imp: ',Importance(i,j),'Pins: ',Pins(i,j)
WRITE(*,*)'Activity: ',Activity(i,j),' Mass: ',Mass(i,j)
WRITE(*,*)' '
WRITE(*,*)'Curies: ',Curies(i,j)
WRITE(*,*)' '
WRITE(3,*)isotope(i),' ',Emission(i,j),' ',hlflfe(i),' ',
&          Curies(i,j),' ( ',CiErrorp(i,j),' ',
&          CiErrorm(i,j),' ) ',
&          Importance(i,j),' ',Pins(i,j)
END IF
ELSE IF(Percent.EQ.95) THEN
Emission(i,j)=0.001*Emission(i,j)
Eerrorm(i,j)=Emission(i,j)*(1-Error)
Eerrorp(i,j)=Emission(i,j)*(1+Error)
IF(Emission(i,j).LT.1.095)THEN
Importance(i,j)=2.8228E-7*Emission(i,j)**5.91
ImpErrorp(i,j)=2.8228E-7*Eerrorp(i,j)**5.91
ImpErrorm(i,j)=2.8228E-7*Eerrorm(i,j)**5.91
Pins(i,j)=-8.1792+44.0168*Emission(i,j)+
&          137.2431*Emission(i,j)**2-
&          68.9146*Emission(i,j)**3
Activity(i,j)=NormCts(i,j)*TotCts*.01
Aerrorp(i,j)=(Activity(i,j)*264)/(ImpErrorp(i,j)
&          *Pins(i,j))
Aerrorm(i,j)=(Activity(i,j)*264)/(ImpErrorm(i,j)
&          *Pins(i,j))

```



```

Activity(i,j)=Activity(i,j)/Importance(i,j)
Activity(i,j)=Activity(i,j)/Pins(i,j)
Activity(i,j)=Activity(i,j)*264
!   WRITE(*,*)'Activity: ',Activity(i,j)
Curies(i,j)=Activity(i,j)/3.7E10
CiErrorp(i,j)=Aerrorp(i,j)/3.7E10
CiErrorm(i,j)=Aerrorm(i,j)/3.7E10
Mass(i,j)=Activity(i,j)/hlflfe(i)/ProbDK(i,j)
WRITE(*,*)'Imp: ',Importance(i,j),'Pins: ',Pins(i,j)
WRITE(*,*)'Activity: ',Activity(i,j),' Mass: ',Mass(i,j)
WRITE(*,*) '
WRITE(*,*)'Curies: ',Curies(i,j)
WRITE(*,*) '
WRITE(3,*)isotope(i),' ',Emission(i,j),' ',hlflfe(i),' ',
&         Curies(i,j),' ( ',CiErrorp(i,j),' ',
&         CiErrorm(i,j),' ) ',
&         Importance(i,j),' ',Pins(i,j)
ELSE IF(Emission(i,j).GE.1.095)THEN
    Importance(i,j)=8.1077E-6-1.7859E-5*Emission(i,j)+
&         1.1867E-5*Emission(i,j)**2-
&         1.7594E-6*Emission(i,j)**3
    ImpErrorp(i,j)=8.1077E-6-1.7859E-5*Eerrorm(i,j)+
&         1.1867E-5*Eerrorm(i,j)**2-
&         1.7594E-6*Eerrorm(i,j)**3
    ImpErrorm(i,j)=8.1077E-6-1.7859E-5*Eerrorm(i,j)+
&         1.1867E-5*Eerrorm(i,j)**2-
&         1.7594E-6*Eerrorm(i,j)**3
    Pins(i,j)=-35.9819+227.5443*Emission(i,j)-
&         109.9411*Emission(i,j)**2+
&         24.4343*Emission(i,j)**3-
&         2.0076*Emission(i,j)**4
    Activity(i,j)=NormCts(i,j)*TotCts*.01
    Aerrorp(i,j)=(Activity(i,j)*264)/(ImpErrorp(i,j)

```

```

&          *Pins(i,j))
Aerrorm(i,j)=(Activity(i,j)*264)/(ImpErrorm(i,j)
&          *Pins(i,j))
Activity(i,j)=(Activity(i,j)*264)/(Importance(i,j)*
&          Pins(i,j))
Curies(i,j)=Activity(i,j)/3.7E10
CiErrorp(i,j)=Aerrorp(i,j)/3.7E10
CiErrorm(i,j)=Aerrorm(i,j)/3.7E10
Mass(i,j)=Activity(i,j)/(hflfe(i)*ProbDK(i,j))
WRITE(*,*)'Imp: ',Importance(i,j),'Pins: ',Pins(i,j)
WRITE(*,*)'Activity: ',Activity(i,j),' Mass: ',Mass(i,j)
WRITE(*,*)' '
WRITE(*,*)'Curies: ',Curies(i,j)
WRITE(*,*)' '
WRITE(3,*)isotope(i),' ',Emission(i,j),' ',hflfe(i),' ',
&          Curies(i,j),' ( ',CiErrorp(i,j),' ',
&          CiErrorm(i,j),' ) ',
&          Importance(i,j),' ',Pins(i,j)
END IF
ELSE IF(Percent.EQ.99) THEN
Emission(i,j)=0.001*Emission(i,j)
Eerrorm(i,j)=Emission(i,j)*(1-Error)
Eerrorp(i,j)=Emission(i,j)*(1+Error)
IF(Emission(i,j).LT.1.095)THEN
Importance(i,j)=2.8228E-7*Emission(i,j)**5.91
ImpErrorp(i,j)=2.8228E-7*Eerrorp(i,j)**5.91
ImpErrorm(i,j)=2.8228E-7*Eerrorm(i,j)**5.91
Pins(i,j)=-8.1792+44.0168*Emission(i,j)+
&          137.2431*Emission(i,j)**2-
&          68.9146*Emission(i,j)**3
Activity(i,j)=NormCts(i,j)*TotCts*.01
Aerrorp(i,j)=(Activity(i,j)*264)/(ImpErrorp(i,j)
&          *Pins(i,j))

```

```

Aerrorm(i,j)=(Activity(i,j)*264)/(ImpErrorm(i,j)
&          *Pins(i,j))
Activity(i,j)=Activity(i,j)/Importance(i,j)
Activity(i,j)=Activity(i,j)/Pins(i,j)
Activity(i,j)=Activity(i,j)*264
!  WRITE(*,*)'Activity: ',Activity(i,j)
Curies(i,j)=Activity(i,j)/3.7E10
CiErrorp(i,j)=Aerrorp(i,j)/3.7E10
CiErrorm(i,j)=Aerrorm(i,j)/3.7E10
Mass(i,j)=Activity(i,j)/hlflfe(i)/ProbDK(i,j)
WRITE(*,*)'Imp: ',Importance(i,j),'Pins: ',Pins(i,j)
WRITE(*,*)'Activity: ',Activity(i,j),' Mass: ',Mass(i,j)
WRITE(*,*)' '
WRITE(*,*)'Curies: ',Curies(i,j)
WRITE(*,*)' '
WRITE(3,*)isotope(i),' ',Emission(i,j),' ',hlflfe(i),' ',
&          Curies(i,j),' ( ',CiErrorp(i,j),' ',
&          CiErrorm(i,j),' ) ',
&          Importance(i,j),' ',Pins(i,j)
ELSE IF(Emission(i,j).GE.1.095)THEN
Importance(i,j)=8.1077E-6-1.7859E-5*Emission(i,j)+
&          1.1867E-5*Emission(i,j)**2-
&          1.7594E-6*Emission(i,j)**3
ImpErrorp(i,j)=8.1077E-6-1.7859E-5*Eerrorm(i,j)+
&          1.1867E-5*Eerrorm(i,j)**2-
&          1.7594E-6*Eerrorm(i,j)**3
ImpErrorm(i,j)=8.1077E-6-1.7859E-5*Eerrorm(i,j)+
&          1.1867E-5*Eerrorm(i,j)**2-
&          1.7594E-6*Eerrorm(i,j)**3
Pins(i,j)=-35.9819+227.5443*Emission(i,j)-
&          109.9411*Emission(i,j)**2+
&          24.4343*Emission(i,j)**3-
&          2.0076*Emission(i,j)**4

```

```

        Activity(i,j)=NormCts(i,j)*TotCts*.01
        Aerrorp(i,j)=(Activity(i,j)*264)/(ImpErrorp(i,j)
&            *Pins(i,j))
        Aerrorm(i,j)=(Activity(i,j)*264)/(ImpErrorm(i,j)
&            *Pins(i,j))
        Activity(i,j)=(Activity(i,j)*264)/(Importance(i,j)*
&            Pins(i,j))
        Curies(i,j)=Activity(i,j)/3.7E10
        CiErrorp(i,j)=Aerrorp(i,j)/3.7E10
        CiErrorm(i,j)=Aerrorm(i,j)/3.7E10
        Mass(i,j)=Activity(i,j)/(hflfe(i)*ProbDK(i,j))
        WRITE(*,*)'Imp: ',Importance(i,j),'Pins: ',Pins(i,j)
        WRITE(*,*)'Activity: ',Activity(i,j),' Mass: ',Mass(i,j)
        WRITE(*,*) '
        WRITE(*,*)'Curies: ',Curies(i,j)
        WRITE(*,*) '
        WRITE(3,*)isotope(i),' ',Emission(i,j),' ',hflfe(i),' ',
&            Curies(i,j),' ( ',CiErrorp(i,j),',',
&            CiErrorm(i,j),') ',
&            Importance(i,j),' ',Pins(i,j)
        END IF
    END IF
!
    GOTO 300
ELSE IF(jsearch.EQ.0)THEN
    Backspace(1)
    READ(1,(A))nuclideExp
    IF(nuclideExp.EQ.'Nuclide') THEN
        GOTO 200
    ELSE IF (nuclideExp.EQ.'End of ')THEN
        GOTO 400
    ELSE
        GOTO 300

```

```
        END IF
    END IF
END IF
!
400 CONTINUE
!
!
    CLOSE(1)
    CLOSE(2)
    CLOSE(3)
!
1000 END
```

## APPENDIX E

### CALCULATING BURNUP FROM $^{137}\text{CS}$ ACTIVITY

The basic understanding of burnup is described by

$$\text{Burnup} = Pt = E$$

where  $P$  is the reactor power,  $t$  is time and  $E$  is energy. The units for burnup are typically represented by Megawatts multiplied by days. Since energy is typically represented by MeV in nuclear physics applications, conversion factors are necessary to transform all units into Joules. The constant  $6.022 \times 10^{-13} \frac{J}{\text{MeV}}$  is multiplied to transform MeV to Joules, and the constant  $86,400 \frac{s}{d}$  transforms days into seconds. Therefore, the burnup equation can be rewritten as

$$\begin{aligned} \text{Burnup}[\text{MWd}] \cdot 86400 \left[ \frac{s}{d} \right] \cdot 10^6 \left[ \frac{W}{\text{MW}} \right] &= P[\text{MW}]t[\text{s}] \\ &= \overline{\phi}_T \left[ \frac{n}{\text{cm}^2\text{s}} \right] \overline{\Sigma}_f \left[ \frac{1}{\text{cm}} \right] V_{\text{Fuel}}[\text{cm}^3]t[\text{s}] \cdot 200 \left[ \frac{\text{MeV}}{\text{fiss}} \right] \cdot 6.022 \\ &\times 10^{-13} \left[ \frac{J}{\text{MeV}} \right] = N_{\text{fiss}} \cdot 200 \left[ \frac{\text{MeV}}{\text{fiss}} \right] \cdot 6.022 \times 10^{-13} \left[ \frac{J}{\text{MeV}} \right] \end{aligned}$$

where  $\overline{\phi}_T$  is the average thermal flux in the assembly,  $\overline{\Sigma}_f$  is the average macroscopic fission cross section in the fuel,  $V_{\text{Fuel}}$  is the volume of the fuel in the assembly, and  $N_{\text{fiss}}$  is the number of fissions that took place in the assembly.  $N_{\text{fiss}}$  for a given isotope that has a fission yield that is similar across all fissile isotopes can be calculated by

$$N_{fiss} = \frac{A}{f_{yield} \cdot \lambda}$$

where  $A$  is the activity of the given nuclide,  $f_{yield}$  is the fission yield for the given nuclide, and  $\lambda$  is the decay probability for the given nuclide.

I can show that the activity of  $^{137}\text{Cs}$  can be directly attributed to the burnup of a fuel assembly. I show how I can match the predetermined activity for a 33,000 MWD/MTU burned assembly from the isotope depletion code ORIGEN. My assumption is that an activity of  $1.0604 \times 10^5 \text{ Ci}$  is measured for the fuel assembly after 1 day since removal from the reactor. From this, I determine the activity at the time of discharge using the relationship

$$N(t) = N(0)e^{-\lambda t} \Rightarrow A(t) = A(0)e^{-\lambda t}$$

And find that

$$A(0) = A(t)e^{\lambda t} = 1.0604 \times 10^5 \text{ Ci} \cdot e^{\frac{\ln(2)}{30.02\text{y}} 1\text{d} \frac{1\text{y}}{365.25\text{d}}} = 1.0605 \times 10^5 \text{ Ci}$$

From this activity, I solved for the number of fissions that occurred in the fuel

$$N_{fiss} = \frac{1.0605 \times 10^5 \text{ Ci} \frac{3.7 \times 10^{10} \text{ Bq}}{\text{Ci}}}{0.0622 \frac{\ln(2)}{30.02\text{y}} \frac{1\text{y}}{365.25\text{d}} \frac{1\text{d}}{86400\text{s}}} = 8.6235 \times 10^{25} \text{ fissions}$$

Now that I know the number of fissions, I directly relate that to the energy released in the fuel. I assume that each fission results in a release of 200 MeV. From this, I see that

$$E = 8.6235 \times 10^{25} \text{ fission} \cdot 200 \frac{\text{MeV}}{\text{fission}} \cdot 6.022 \times 10^{-13} \frac{\text{J}}{\text{MeV}} = 2.7633 \times 10^{15} \text{ J}$$

However, burnup is in units of MWd, so this becomes

$$2.7633 \times 10^{15} \text{ J} \cdot \frac{d}{86400 \text{ s}} = 3.198 \times 10^{10} \frac{\text{J}}{\text{s}} d = 3.198 \times 10^{10} \text{ W} \cdot d = 31,982 \text{ MWD}$$

Comparing this result to the desired burnup of 33,000 MWD, I see that this falls within a percent error of 3.08 %.



## **VITA**

### **JESSICA N. PAUL**

PAUL was born in 1989, and graduated from Olentangy Liberty High School in Powell, OH in 2007. Following high school, she enrolled at the University of Florida. She graduated from the University of Florida receiving a B.S. in Nuclear Engineering in 2011. In the fall of 2011, she was awarded the Nuclear Forensics Graduate Fellowship and began her graduate school education at the Georgia Institute of Technology. She completed her Master's degree in Nuclear Engineering in December 2013, before beginning her doctoral work.

She has accepted the National Nuclear Security Administration Graduate Fellowship, and will be working in Washington, DC upon completion of her doctoral program at the Georgia Institute of Technology.